



Universitat de Girona

# BIOINSPIRED IRON AND MANGANESE CATALYSTS FOR THE EFFECTIVE AND SELECTIVE OXIDATION OF ALKANES AND ALKENES

Laura GÓMEZ MARTÍN

ISBN: 978-84-693-6117-7

Dipòsit legal: GI-877-2010

<http://www.tesisenxarxa.net/TDX-0812110-124637/>

**ADVERTIMENT.** La consulta d'aquesta tesi queda condicionada a l'acceptació de les següents condicions d'ús: La difusió d'aquesta tesi per mitjà del servei TDX ([www.tesisenxarxa.net](http://www.tesisenxarxa.net)) ha estat autoritzada pels titulars dels drets de propietat intel·lectual únicament per a usos privats emmarcats en activitats d'investigació i docència. No s'autoritza la seva reproducció amb finalitats de lucre ni la seva difusió i posada a disposició des d'un lloc aliè al servei TDX. No s'autoritza la presentació del seu contingut en una finestra o marc aliè a TDX (framing). Aquesta reserva de drets afecta tant al resum de presentació de la tesi com als seus continguts. En la utilització o cita de parts de la tesi és obligat indicar el nom de la persona autora.

**ADVERTENCIA.** La consulta de esta tesis queda condicionada a la aceptación de las siguientes condiciones de uso: La difusión de esta tesis por medio del servicio TDR ([www.tesisenred.net](http://www.tesisenred.net)) ha sido autorizada por los titulares de los derechos de propiedad intelectual únicamente para usos privados enmarcados en actividades de investigación y docencia. No se autoriza su reproducción con finalidades de lucro ni su difusión y puesta a disposición desde un sitio ajeno al servicio TDR. No se autoriza la presentación de su contenido en una ventana o marco ajeno a TDR (framing). Esta reserva de derechos afecta tanto al resumen de presentación de la tesis como a sus contenidos. En la utilización o cita de partes de la tesis es obligado indicar el nombre de la persona autora.

**WARNING.** On having consulted this thesis you're accepting the following use conditions: Spreading this thesis by the TDX ([www.tesisenxarxa.net](http://www.tesisenxarxa.net)) service has been authorized by the titular of the intellectual property rights only for private uses placed in investigation and teaching activities. Reproduction with lucrative aims is not authorized neither its spreading and availability from a site foreign to the TDX service. Introducing its content in a window or frame foreign to the TDX service is not authorized (framing). This rights affect to the presentation summary of the thesis as well as to its contents. In the using or citation of parts of the thesis it's obliged to indicate the name of the author.



Universitat de Girona

Doctoral dissertation

**BIOINSPIRED IRON AND MANGANESE CATALYSTS  
FOR THE EFFECTIVE AND SELECTIVE OXIDATION OF  
ALKANES AND ALKENES**

**LAURA GÓMEZ MARTÍN**

March 2010



Universitat de Girona

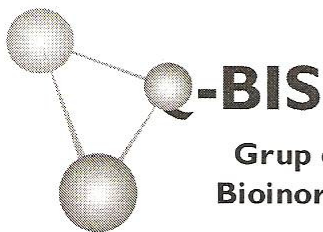
**Doctoral dissertation**

**BIOINSPIRED IRON AND MANGANESE CATALYSTS  
FOR THE EFFECTIVE AND SELECTIVE OXIDATION OF  
ALKANES AND ALKENES**

Presented by: **LAURA GÓMEZ MARTÍN**

Girona, March 2010. Programa de doctorat Catàlisis Homogènia  
Directed by: Dr. Miquel Costas Salgueiro and Dr. Xavi Ribas Salamaña

**In candidacy for the degree of  
Doctor of Philosophy in Chemistry**



Grup de Recerca de Química  
Bioinorgànica i Supramolecular



Universitat de Girona  
Departament de Química  
Àrea de Química Inorgànica

Els sotasignants Dr. **Miquel Costas Salgueiro** i Dr. **Xavi Ribas Salamaña**, Professors Titulars del Departament de Química de la Universitat de Girona, CERTIFIQUEN que:

La memòria que porta per títol "*Bioinspired iron and manganese catalysts for the effective and selective oxidation of alkanes and alkenes*" recull el treball realitzat sota la seva direcció per la **Laura Gómez Martín**, Llicenciada en Química per la Universitat de Girona, i que constitueix la seva memòria de Tesi Doctoral per aspirar al grau de Doctora en Ciències, especialitat Química.

I perquè així consti, signen aquest certificat el dia 1 de març de 2010.

Dr. Miquel Costas Salgueiro

Dr. Xavi Ribas Salamaña

# Table of contents

---

Abstract (p. 1).

Abbreviations (p. 3).

Supplementary digital material (p.5).

Acknowledgements (p. 6).

---

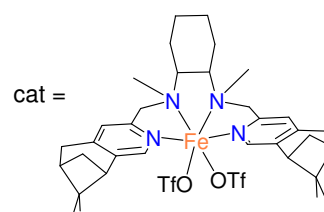
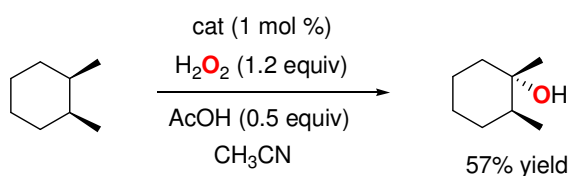
**Chapter I.** General introduction. Alkane and alkene oxidation: biological precedents and functional models (p. 7).

---

**Chapter II.** Main objectives (p. 53).

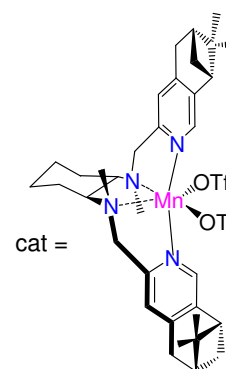
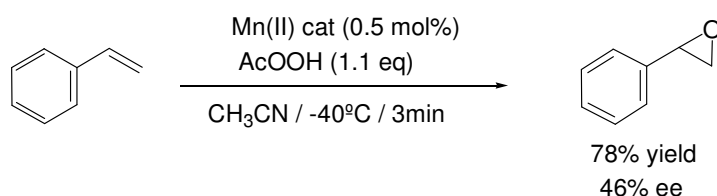
---

**Chapter III.** Stereospecific C-H and C=C oxidation with H<sub>2</sub>O<sub>2</sub> catalyzed by a new family of chemically robust site-isolated iron catalysts (p. 57).



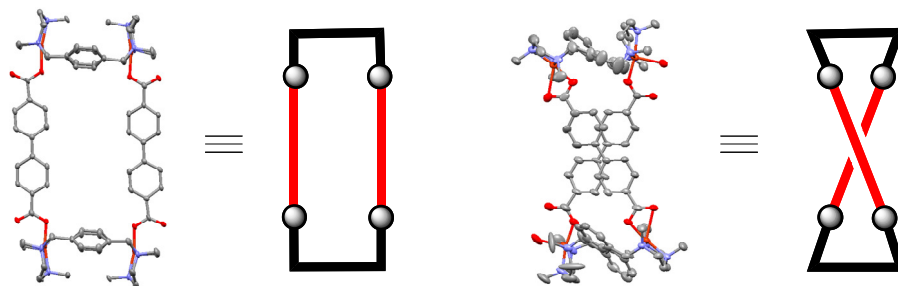
---

**Chapter IV.** Chiral manganese complexes with pinene appended tetradentate ligands as stereoselective epoxidation catalysts (p. 125).



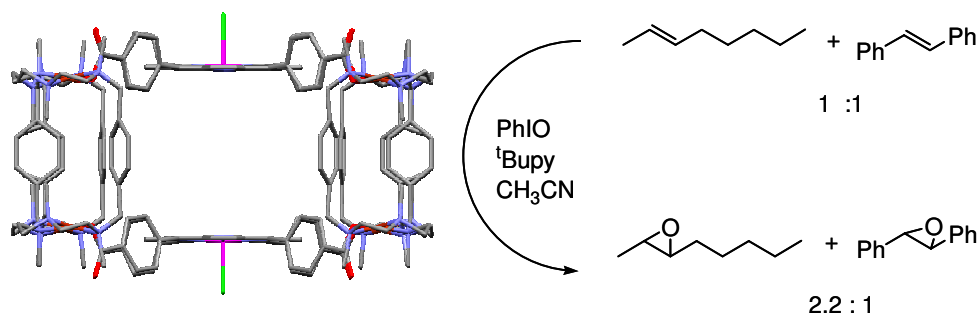
---

**Chapter V.** Self-assembling of nanoscopic molecular rectangles, extended helicates and porous-like materials based on macrocyclic dicopper building blocks under fine supramolecular control (p. 143).



---

**Chapter VI.** A self-assembled nanoreactor with porphyrinic building blocks as a catalyst for the selective oxidation of olefins (p. 165).



---

**Chapter VII.** General conclusions (p. 183).

---

## Abstract

The high efficiency, selectivity and mild conditions exhibited by the reactions that take place in the active site of metalloxygenases are the source of inspiration of the present dissertation. With the aim of designing efficient oxidation catalysts, in this thesis we make use of two different strategies: the first one is the design of low molecular weight complexes inspired by structural aspects of the first coordination sphere of the metal active site of non-heme iron and manganese enzymes. These complexes are studied as catalysts for the selective oxidation of alkanes and alkenes using green oxidants such as  $H_2O_2$  (or peracetic acid). The second strategy is based on the use of supramolecular chemistry to develop self-assembled molecular structures with desired shape and chemical properties. Particularly, the construction of cavity-containing 3D nanovessels with an oxidation catalyst embedded in their structures would allow us to perform more selective reactions, analogously to the reactions taking place in the active site of enzymes.

In the first part (Chapter III and IV), we describe the introduction of sterically bulky pinene groups at the 4<sup>th</sup>-5<sup>th</sup> position of the pyridine rings of a series of nitrogen based tetradentate ligands. The corresponding mononuclear iron(II) complexes are prepared, spectroscopically and structurally characterized, and have been studied in catalytic alkane and alkene oxidation reactions. The sterically bulky catalysts are more efficient in the oxidation of alkanes than their homologues lacking the steric pinene groups (Chapter III). The electrodonating properties of the pinene groups along with the steric protection that they confer to the metal centre are suggested to be responsible for the increase in the activity by stabilizing species implicated in the catalysis.

In the Chapter IV, two mononuclear manganese(II) complexes derived from the aforementioned ligands are employed as stereoselective epoxidation catalysts.

The second part of the dissertation (Chapter V and VI) starts with the development of control parameters for the formation of 2D self-assembled molecular structures (rectangles and helicates) with the desired shape (Chapter V). Three levels of molecular control are studied. Evolution of the system to a 3D nanovessel with catalytic properties is developed in Chapter VI. Finally, the performance and selectivity of this system in alkene epoxidation is studied.

## Resum

La gran eficiència, selectivitat i les condicions suaus exhibides per les reaccions que tenen lloc al centre actiu de metal·looxigenases són la font d'inspiració per la present dissertació. Amb l'objectiu de dissenyar catalitzadors d'oxidació eficients, en aquesta tesi doctoral hem fet ús de dues estratègies: la primera consisteix en el disseny de complexos amb baix pes molecular inspirats en aspectes estructurals de la primera esfera de coordinació del centre metàl·lic d'enzims de ferro i de manganès. Aquests complexos són estudiats com a catalitzadors en l'oxidació selectiva d'alcans i d'alquens fent servir oxidants "verds" com l' $\text{H}_2\text{O}_2$  (o l'àcid peracètic). La segona estratègia està basada en la utilització de la química supramolecular per tal de desenvolupar estructures moleculars auto-acoblades amb la forma i propietats químiques desitjades. Concretament, la construcció de nanocontenidors amb un catalitzador d'oxidació incrustat a la seva estructura ens permetria dur a terme reaccions més selectives, tal com passa en les reaccions que tenen lloc al centre actiu dels enzims.

En la primera part de la tesi (Chapter III i IV), es descriu la introducció de grups voluminosos com són els pinens a la posició 4-5 dels anells de piridina d'una sèrie de lligands nitrogen donadors tetradentats. Es varen preparar i caracteritzar espectroscòpicament i estructuralment els corresponents complexos mononuclears de ferro(II), i es varen estudiar com a catalitzadors en reaccions d'oxidació d'alcans i d'alquens. Aquests catalitzadors resulten ser més eficients en l'oxidació d'alcans que els seus homòlegs mancats dels anells de pinè (Chapter III). Les propietats electrodonadores dels grups de pinè juntament amb la protecció espacial que aquests confereixen al centre metàl·lic es proposen com a responsables de l'augment en l'activitat mitjançant l'estabilització de les espècies implicades en la catàlisi.

En el Chapter IV, dos complexos mononuclears de manganès(II) derivats dels lligands anteriorment esmentats s'han emprat com a catalitzadors estereoselectius d'epoxidació d'olefines.

La segona part de la dissertació (Chapter V i VI) comença amb el desenvolupament de paràmetres de control per a la formació d'estructures moleculars 2D auto-acoblades (rectangles i doble-hèlixs) amb la forma desitjada (Chapter V). S'han estudiat tres nivells de control molecular. L'evolució del sistema cap a nanocontenidors 3D amb propietats catalítiques s'ha desenvolupat al Chapter VI. Per acabar, el sistema s'ha estudiat en termes d'eficiència i selectivitat en l'epoxidació d'alquens.



## Abbreviations

2<sup>o</sup>: secondary.

3<sup>o</sup>: tertiary.

A/K: Alcohol/ketone ratio.

AcOEt: Ethyl acetate.

AcOH: Acetic acid.

AcOOH: Peracetic acid.

approx.: Approximately.

aq: Aqueous.

Asp: Asparagine.

BArF: [B{3,5-(CF<sub>3</sub>)<sub>2</sub>-C<sub>6</sub>H<sub>3</sub>}<sub>4</sub>].

bisPB: 4,5-pinene-2,2'-bipyridine.

bpbp: *N,N*-bis(2-pyridylmethyl)-2,2'-bipyrrolidine.

bpmcn: *N,N'*-dimethyl-*N,N'*-bis(2-pyridylmethyl)cyclohexane-*trans*-1,2-diamine.

bpmen: *N,N'*-dimethyl-*N,N'*-bis(2-pyridylmethyl)ethane-1,2-diamine.

bpy: 2,2'-Bipyridine.

*c*-C<sub>6</sub>H<sub>12</sub>: Cyclohexane.

*c*-C<sub>6</sub>D<sub>12</sub>: Cyclohexane-D<sub>12</sub>.

cat: Catalyst.

Cc: Catalytic cycles.

cHx: Cyclohexane.

*cis*-1,2-DMCH: *cis*-1,2-dimethylcyclohexane.

Conv.: Conversion.

CV: Cyclic voltammetry.

Cyt P450: Cytochrome P450.

de: Diastereomeric excess.

diol: *cis*-diol product in alkene oxidation.

DMF: *N,N*-dimethylformamide.

ee: Enantiomeric excess.

Eff.: Efficiency.

epox: Epoxide product in alkene oxidation.

Equiv: Equivalentents.

ESI-MS: ElectroSpray Ionization Mass Spectroscopy.

FT-IR: Fourier Transform Infrared Spectroscopy.

GC: Gas Chromatography.

Glu: Glutamine.

His: Histidine.

HPCD: 3,4-dihydroxyphenylacetate 2,3-dioxygenase from *Brevibacterium fuscum*.

Kcal: Kilocalorie.

KIE: Kinetic isotope effect.

L: Ligand.  
mCPBA: 3-chloroperbenzoic acid.  
min: Minutes.  
MndD: 3,4-dihydroxyphenylacetate 2,3-dioxygenase from *Arthrobacter globiformis*.  
MW: Molecular weight.  
n.d.: Not determined.  
n.m.: Not measured.  
NAD(P)H: Nicotinamide adenine dinucleotide(phosphate).  
NDO: Naphthalene 1,2-dioxygenase.  
NMR: Nuclear Magnetic Resonance.  
ol: Alcohol product in alkane oxidation.  
one: Ketone product in alkane oxidation.  
OTf: Trifluoromethanesulfonate anion.  
[Ox]: Oxidant.  
p.: Page.  
PAA<sub>R</sub>: Peracetic acid prepared with strongly acidic resins.  
PhIO: Iodosylbenzene.  
py: Pyridine.  
RC: Retention of configuration in the oxidation of the tertiary C-H bonds of *cis*-1,2-dimethylcyclohexane, expressed as the ratio of the tertiary alcohols:  $[(1R,2R + 1S,2S) - (1R,2S + 1S,2R)] / [(1R,2R + 1S,2S) - (1R,2S + 1S,2R)]$ .  
RT: Room temperature.  
SCE: Saturated Calomel Electrode.  
T: Temperature.  
T<sub>1</sub>: Spin-lattice relaxation time.  
TACN: 1,4,7-triazacyclononane.  
<sup>t</sup>Bupy: 4-*tert*-butylpyridine.  
THF: Tetrahydrofuran.  
TN: Turnover Number.  
tpa = tris(2-pyridylmethyl)amine.  
Triflate: Trifluoromethanesulfonate.  
UV-Vis: Ultraviolet-Visible.

## Supplementary digital material

The material listed below can be found in the attached CD:

- pdf file of the PhD dissertation.
- pdf file of the Annex containing all ESI-MS, NMR, FT-IR (ATR) spectra and CVs.
- cif files for each crystal structure presented within this thesis

| Chapter            | Crystal structure                                                                                                                                                      | File name               |
|--------------------|------------------------------------------------------------------------------------------------------------------------------------------------------------------------|-------------------------|
| <b>Chapter III</b> | $\Delta$ -[Fe(CF <sub>3</sub> SO <sub>3</sub> ) <sub>2</sub> (bpmenp)]                                                                                                 | <b>1OTf</b>             |
|                    | $\Lambda$ -[FeCl <sub>2</sub> (( <i>S,S,R</i> )-(bpmcnp))]                                                                                                             | <b>2Cl</b>              |
|                    | $\Lambda$ -[Fe(CF <sub>3</sub> SO <sub>3</sub> ) <sub>2</sub> (( <i>S,S,R</i> )-(bpmcnp))]                                                                             | <b>2OTf</b>             |
|                    | $\Delta$ -[FeCl <sub>2</sub> (( <i>R,R,R</i> )-(bpmcnp))]                                                                                                              | <b>3Cl</b>              |
|                    | $\Lambda$ -[Fe(CF <sub>3</sub> SO <sub>3</sub> ) <sub>2</sub> (( <i>S,S,R</i> )-(bpbpp))]                                                                              | <b>4OTf</b>             |
|                    | $\Lambda$ -[Fe(CF <sub>3</sub> SO <sub>3</sub> ) <sub>2</sub> (( <i>R,R,R</i> )-(bpbpp))]                                                                              | <b>5OTf</b>             |
| <b>Chapter IV</b>  | $\Lambda$ -[Mn(CF <sub>3</sub> SO <sub>3</sub> ) <sub>2</sub> (( <i>S,S,R</i> )-(bpmcnp))]                                                                             | <b>2Mn</b>              |
| <b>Chapter V</b>   | [(Cu <sub>2</sub> (Me2p)) <sub>2</sub> (O <sub>2</sub> CC <sub>12</sub> H <sub>8</sub> CO <sub>2</sub> ) <sub>2</sub> ](CF <sub>3</sub> SO <sub>3</sub> ) <sub>4</sub> | <b>3OTf</b>             |
|                    | [(Cu <sub>2</sub> (Me2m)) <sub>2</sub> (O <sub>2</sub> CC <sub>12</sub> H <sub>8</sub> CO <sub>2</sub> ) <sub>2</sub> ](ClO <sub>4</sub> ) <sub>4</sub>                | <b>4ClO<sub>4</sub></b> |
|                    | [(Cu <sub>2</sub> (Me2p)) <sub>2</sub> (O <sub>2</sub> CC <sub>10</sub> H <sub>6</sub> CO <sub>2</sub> ) <sub>2</sub> ](CF <sub>3</sub> SO <sub>3</sub> ) <sub>4</sub> | <b>5OTf</b>             |
|                    | [(Cu <sub>2</sub> (Me2p)) <sub>2</sub> (O <sub>2</sub> CC <sub>10</sub> H <sub>6</sub> CO <sub>2</sub> ) <sub>2</sub> ](BArF) <sub>4</sub>                             | <b>5BArF</b>            |
|                    | [(Cu <sub>2</sub> (Me2m)) <sub>2</sub> (O <sub>2</sub> CC <sub>10</sub> H <sub>6</sub> CO <sub>2</sub> ) <sub>2</sub> ](CF <sub>3</sub> SO <sub>3</sub> ) <sub>4</sub> | <b>6OTf</b>             |
| <b>Chapter VI</b>  | [(Cu <sub>2</sub> (Me2p)) <sub>4</sub> (PorphMnCl) <sub>2</sub> ](ClO <sub>4</sub> ) <sub>8</sub> <sup>a</sup>                                                         | <b>1ClO<sub>4</sub></b> |

<sup>a</sup> Provisional structure (.res file).

## Acknowledgements

This work would not have been possible without the following collaborations:

- Dr. Jordi-Benet Buchholz from *Institut Català d'Investigació Química (ICIQ)* and Xavier Fontrodona from Serveis Tècnics de Recerca of the *Universitat de Girona* for the X-Ray studies.
- Professor Stephane Menage and Dr. Caroline Marchi-Delapierre from *CEA/Université de Grenoble-UJF/CNRS* for the ee's measurements.
- Susana Delgado from *ICIQ research support unit* and Dr. Xavi Sala from *Institut Català d'Investigació Química (ICIQ)* for the ee's measurements.
- Professor Alfons Polo from *Universitat de Girona* for the help in the synthesis of bipyrrolidine synthons.
- Dr. Bert Klein Gebbink from *Utrecht University* for hosting a scientific visit within the context of the development of supramolecular nanocatalysts presented in Chapter VI.
- COST Action D40-WG1 for financial support of the aforementioned short stay.
- Dr. Cees Versluis from Utrecht Institute for Pharmaceutical Sciences of *Utrecht University* for the ESI-MS experiments.
- Serveis Tècnics de Recerca from *Universitat de Girona* for technical support
- MCYT of Spain for financial support through projects CTQ2006-05367/BQU and CTQ2009-08464/BQU and MEC for PhD-FPU grant. Generalitat de Catalunya for project 2009 SGR-637.

# CHAPTER I

---

**General introduction.**

**Alkane and alkene oxidation:**

**Biological precedents and functional models**

---

**Abstract**

Selective oxidation of alkanes and alkenes in environmentally sustainable manner represents an important challenge for chemists. Moreover, the development of those methods can enable the synthesis of complex molecules in a more efficient way. Nature represents an important source of inspiration for catalyst design. This chapter provides a concise background to recent biological and bioinspired developments in the field.

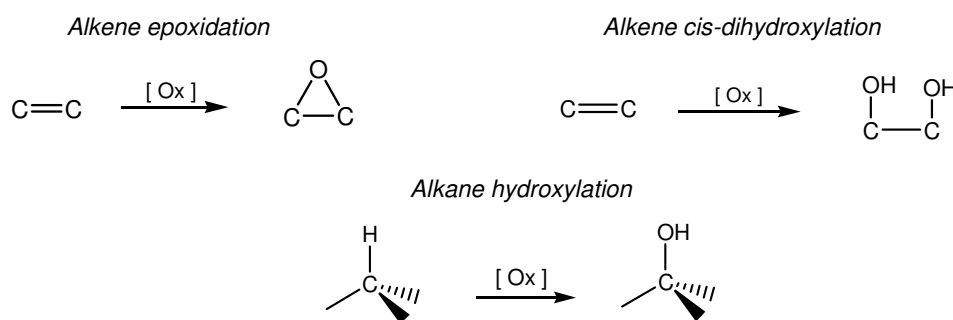


# Contents

|                                                                                                  |           |
|--------------------------------------------------------------------------------------------------|-----------|
| <b>I.1. MODERN CHALLENGES IN ALKANE AND ALKENE OXIDATION.....</b>                                | <b>10</b> |
| I.1.1. EPOXIDATION AND <i>CIS</i> -DIHYDROXYLATION OF ALKENES: SEEKING A GREENER METHODOLOGY     | 10        |
| I.1.2. ALKANE OXIDATION: AN ATTRACTIVE BUT CHALLENGING SYNTHETIC TOOL.....                       | 11        |
| <b>I.2. METALLOENZYMES AND MODEL COMPOUNDS.....</b>                                              | <b>13</b> |
| <b>I.3. BIOLOGICAL PRECEDENTS .....</b>                                                          | <b>14</b> |
| I.3.1. BIOLOGICAL ROLE OF IRON.....                                                              | 14        |
| I.3.1.1. Oxidative iron proteins .....                                                           | 14        |
| <i>I.3.1.1.1. Cytochrome P450 .....</i>                                                          | <i>16</i> |
| <i>I.3.1.1.2. Rieske dioxygenases .....</i>                                                      | <i>17</i> |
| <i>I.3.1.1.3. Apocarotene dioxygenase.....</i>                                                   | <i>19</i> |
| I.3.2. BIOLOGICAL ROLE OF MANGANESE .....                                                        | 20        |
| I.3.2.1. Oxidative manganese proteins .....                                                      | 20        |
| <i>I.3.2.1.1. Catechol dioxygenases .....</i>                                                    | <i>21</i> |
| <b>I.4. IRON AND MANGANESE BIOINSPIRED COMPLEXES .....</b>                                       | <b>22</b> |
| I.4.1. SIMPLE COORDINATION COMPLEXES AS BIOINSPIRED OXIDATION CATALYSTS .....                    | 22        |
| I.4.1.1. Cytochrome P450–inspired oxidation catalysts .....                                      | 22        |
| I.4.1.2. Oxidation of alkanes (C-H bonds) by non-heme iron complexes .....                       | 24        |
| I.4.1.3. Oxidation of alkenes (C=C double bonds) by non-heme iron complexes .....                | 28        |
| <i>I.4.1.3.1. Epoxidation .....</i>                                                              | <i>28</i> |
| <i>I.4.1.3.2. Cis-dihydroxylation.....</i>                                                       | <i>30</i> |
| I.4.1.4. Oxidation of alkanes (C-H bonds) by non-porphyrinic manganese complexes.....            | 33        |
| I.4.1.5. Oxidation of alkenes (C=C double bonds) by non-porphyrinic manganese<br>complexes ..... | 34        |
| I.4.2. SUPRAMOLECULAR STRATEGIES FOR BIOINSPIRED OXIDATION CATALYSTS.....                        | 36        |
| I.4.2.1 Design approaches to supramolecular catalysis .....                                      | 37        |
| <i>I.4.2.1.1. Covalent approach.....</i>                                                         | <i>37</i> |
| <i>I.4.2.1.2. Non covalent approach .....</i>                                                    | <i>40</i> |
| <b>I.5. REFERENCES.....</b>                                                                      | <b>44</b> |

## I.1. Modern challenges in alkane and alkene oxidation

Oxidation reactions play an important role in organic chemistry;<sup>1-4</sup> among them, hydroxylation of alkanes and dihydroxylation and epoxidation of alkenes are highly interesting reactions from a synthetic point of view (see scheme 1). Despite the fact that great strides in oxidation technologies have developed over the last century, an important remaining challenge is to achieve efficient, but more significantly, selective incorporation of oxidized functionalities into organic frameworks using environmentally friendly conditions. That could expand the use of oxidation technologies in complex organic synthesis.



**Scheme 1.** Challenging oxidation reactions.

### I.1.1. Epoxidation and *cis*-dihydroxylation of alkenes: seeking a greener methodology

Among the different feedstocks, olefins are one of the most important starting materials for organic synthesis. Their oxidation leads to various value-added products. Among them, epoxides constitute an important and extremely versatile class of intermediate organic compounds to obtain more elaborated chemical products both in organic synthesis and in industrial production of bulk and fine chemicals, as well as pharmaceuticals. For this reason, epoxidation of olefins is an ongoing important field of research in industry and academia. Nevertheless, epoxidation methods still include *chlorohydrin* process (chlorine in combination with sodium hydroxide) for industrial formation of epoxides of simple olefins and the use of *meta*-chloroperbenzoic acid in the production of fine chemicals via epoxides.<sup>4-6</sup>

Similarly, 1,2-diols also have a wide variety of applications. At present 1,2-diols are manufactured industrially by a two step sequence consisting of epoxidation of an olefin followed by hydrolysis of the resulting epoxide. Instead, the dihydroxylation of C=C bonds constitutes a more atom-efficient and shorter route to 1,2-diols. In general, osmium, ruthenium or manganese oxo species are employed to catalyze the dihydroxylation of olefins. The osmium-catalyzed variant is the most reliable and efficient method for the synthesis of *cis*-1,2-diols.<sup>7-9</sup> Moreover, the discovery of Sharpless method for catalytic asymmetric dihydroxylation opened the door for numerous applications in organic synthesis.<sup>10,11</sup> The main disadvantage of the Sharpless



procedure is the high toxicity associated with the osmium metal in the asymmetric dihydroxylation mixtures.

From ecological and economic points of view, today there is considerable pressure to employ more environmentally benign reaction conditions. While significant advances have been made, important challenges remain; these include substrate conversion with high selectivity, and the use of inexpensive and environmentally friendly metals. Moreover, most oxidants have the disadvantage that, in addition to the oxidized products, stoichiometric amounts of waste products are formed. Therefore, there is special interest on the use of environmentally friendly oxidants ("green" oxidants) to minimize the amount of waste.<sup>12</sup> Among the environmentally benign oxidants, aside from air and O<sub>2</sub>, the most efficient are peroxides. In particular, hydrogen peroxide is a suitable "green" oxidant since the only side product after an oxidation reaction is water. Furthermore, it exhibits good atom efficiency and it is relatively cheap and easier to handle than dioxygen. Despite hydrogen peroxide has advantages, it also presents some disadvantages: its use in high concentrations can be dangerous to handle and in the presence of metals, it easily generates highly reactive hydroxyl radicals ( $\cdot\text{OH}$ ) giving rise to non selective oxidation reactions. Finally, H<sub>2</sub>O<sub>2</sub> often undergoes self-disproportionation reactions in the presence of transition metals.<sup>13</sup>

Indeed state of the art heterogeneous catalysts make use of benign oxidants such as hydrogen peroxide or molecular oxygen, but require relatively harsh reaction conditions. Hence, there is an ongoing interest in the discovery of more active and selective catalysts. On the other hand, known homogeneous metal complexes that make use of hydrogen peroxide are mainly based on ruthenium, rhenium, molybdenum, manganese and more recently iron.<sup>14,15</sup> With regard to catalysts, the use of iron or manganese based complexes is attractive due to their low price and low toxicity.

### **I.1.2. Alkane oxidation: an attractive but challenging synthetic tool**

From the point of view of synthetic organic chemistry, one-step selective transformation of ubiquitous C-H bonds of organic compounds, a process that often needs several steps, is a very interesting class of reaction. With those methods, minimal functional group manipulations would enable the rapid build-up of molecular complexity from inert functionalities, unlocking opportunities for markedly different synthetic strategies.

Particularly challenging is the selective transformation of C-H bonds into alcohols or ketones. Due to the lack of selective and efficient methods, modern synthetic planning often centers on the use and maintenance of preexisting oxidized functionalities, making necessary the use of protecting groups and lengthening synthetic routes. Oxidation reactions for isolated, unactivated sp<sup>3</sup> C-H bonds capable of operating selectivity hold special promise for streamlining syntheses. Such reactions would provide a general way to introduce oxidized functionalities at a late stage, thereby reducing unproductive chemical manipulations. A few methods are available, but many of these are unselective, yielding complicated mixture of products (such as Gif processes),<sup>16</sup> using difficult to handle oxidants (have to be prepared in situ, such as

dioxiranes),<sup>17</sup> or generating non acceptable toxic waste (such as permanganate).<sup>6</sup> The reason is four major challenges interfering with selective and efficient C-H oxidation:

**Reactivity:** While most oxidation reactions are thermodynamically downhill, there is generally a large kinetic barrier associated with the C-H bond cleavage event required prior to/during functionalization.

**Chemoselectivity:** A second major challenge is the ability to stop functionalization at the required oxidation state, as the over-oxidation of functionalized products is often highly thermodynamically downhill.

**Regioselectivity:** Most organic molecules contain many different types of C-H bonds, and usually there is very little difference in reactivity between the various C-H bonds in alkanes; therefore, developing transformations that regioselectively functionalize a single C-H bond within a complex structure remains a challenge in this field.

**Stereoselectivity:** The functionalization of C-H bonds to generate new stereogenic centers in a highly diastereoselective and/or enantioselective fashion represents a fourth challenge in this field. Notably, the stereospecific oxidative functionalization of C-H bonds at existing stereocenters represents another attractive method for the construction of chiral molecules.

## I.2. Metalloenzymes and model compounds

Enzymes are “biological catalysts” and are responsible for the acceleration of reactions in living organisms. A common cofactor found in the active site of these proteins is metal ions that, even though accounting for less than 1% of the total protein weight, are essential for the biological activity. Metals in enzymes promote complex biochemical reactions and participate in highly specialized biological functions such as oxygen activation (see below)<sup>18</sup> thanks to their ability to exist in multiple oxidation states and different geometries. Several factors modulate the reactivity of the active center, such as: the nature of the metal and the ligand, the coordination geometry of the metal center, the relative disposition of the metal centers in polynuclear systems and the tridimensional configuration of the polypeptidic chain, among others.

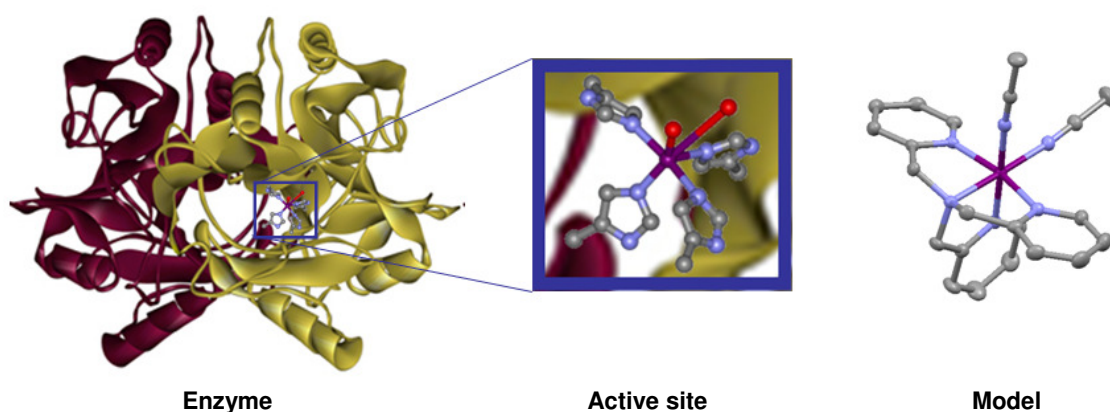


**Figure 1.** Bioinorganic chemistry gain inspiration from metal active site of enzymes to design structural or functional model compounds.

One of the most important topics in bioinorganic chemistry focuses on the role of metals in biology. Particularly, one important area is the structural characterization of enzyme’s active sites and the study of their reactivity. One of the strategies to study these biological systems takes advantage of synthetic model chemistry (biomimetic studies).<sup>19</sup> Model chemistry is based in designing and studying low weight synthetic complexes that could reproduce structural, spectroscopic and/or chemical properties of an enzyme (figure 1). In model chemistry, the accomplishment of these objectives often begins with the preparation of a suitable ligand (organic synthesis) and continues through several steps towards the ultimate goal of understanding and/or reproducing the catalytic reactivity of enzymes.

In this thesis we take advantage of the model chemistry approach in order to develop bioinspired oxidation catalysts for the selective oxidation of C-H and C=C bonds. Two strategies are employed: the development of simple coordination complexes of Fe or Mn inspired in structural aspects of the first coordination sphere of the active site of mononuclear iron or manganese enzymes, and secondly, the development of a supramolecular strategy to emulate not only the first coordination sphere but also weak interactions with substrates in the active site.

### I.3. Biological precedents

Nature has developed many remarkable transition metal-dependent oxidative enzymes, which are capable of activating dioxygen and catalyzing the stereospecific oxidation of C-H (alkane hydroxylation) or C=C bonds (olefin epoxidation and olefin *cis*-dihydroxylation) (see below). The first two transformations are carried out by enzymes with either heme (e.g. cytochrome P450)<sup>20-23</sup> or non-heme iron (and sometimes manganese) centers (e.g. Rieske dioxygenases).<sup>24-28</sup> On the other hand, *cis*-dihydroxylation is so far an activity only characteristic of non-heme iron-containing Rieske dioxygenases, which attack arene double bonds in the first step of the biodegradation of arenes by soil bacteria.<sup>29</sup> Remarkable examples of oxidases relevant to this research work are described in the following pages. Understanding their structure and activity serves as inspiration for the work presented in this dissertation.

#### I.3.1. Biological role of iron

Iron is spread in all forms of life: from bacteria to mammals. Its versatility is unique, Fe participates in oxygen transport and electron transfer and it is found in the active center of a variety of metalloenzymes such as oxidases, hydrogenases, reductases, dehydrogenases and deoxygenases.<sup>30</sup>

In the earth's crust, iron is the 4<sup>th</sup> most abundant element (after oxygen, silicon and aluminum), and it has two readily interconverting oxidation states: Fe<sup>II</sup> and Fe<sup>III</sup>. In addition, in order to explain some biological processes in natural systems, the presence of iron centers in higher oxidation states, such as Fe<sup>IV</sup> or Fe<sup>V</sup>, and lower oxidation states such as Fe<sup>I</sup>, has been postulated.<sup>19</sup> In fact, Fe<sup>IV</sup> intermediate species have been directly detected in selected natural systems.<sup>31-34</sup>

Its high availability and its various attainable oxidation states most likely have led to the evolutionary selection of iron in many life processes.

##### I.3.1.1. Oxidative iron proteins

Iron proteins implicated in oxidation processes via O<sub>2</sub> activation are present in nature in a wide range of configurations. They can be classified in three different superfamilies depending on the structure of their active site: heme proteins, mononuclear non-heme systems and dinuclear non-heme enzymes. Table 1 shows the most representative O<sub>2</sub>-activating iron proteins that take part in oxidative processes and the reactions they catalyze.

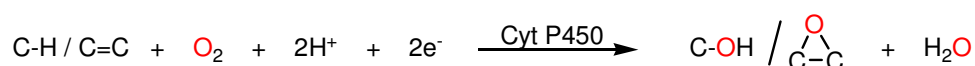
In this introduction, only three examples will be described in detail as they constitute relevant examples of iron enzymes.

**Table 1.** Iron proteins implicated in oxidation reactions by oxygen activation.<sup>19,25,35</sup>

| PROTEIN                                                        | CATALYTIC REACTION                                                                                                                                                                          |
|----------------------------------------------------------------|---------------------------------------------------------------------------------------------------------------------------------------------------------------------------------------------|
| <b>Heme proteins</b>                                           |                                                                                                                                                                                             |
| Cytochrome P450                                                | $\text{C-H or C=C} \xrightarrow[2 e^-, 2\text{H}^+]{\text{O}_2} \text{R-OH or } \begin{array}{c} \text{O} \\ \diagup \quad \diagdown \\ \text{C}-\text{C} \end{array} + \text{H}_2\text{O}$ |
| <b>Non-heme proteins</b>                                       |                                                                                                                                                                                             |
| <b>Mononuclear center</b>                                      |                                                                                                                                                                                             |
| <b>Enzymes with the 2-His-1-Carboxylate facial triad motif</b> |                                                                                                                                                                                             |
| Extradiol-cleaving catechol dioxygenases                       |                                                                                                                                                                                             |
| Rieske dioxygenases                                            |                                                                                                                                                                                             |
| $\alpha$ -ketoglutarate dependent hydroxylases                 | $\text{R-H} + \text{R}'\text{COCOOH} + \text{O}_2 \rightarrow \text{R-OH} + \text{R}'\text{COOH} + \text{CO}_2$                                                                             |
| Pterin-dependent enzymes                                       |                                                                                                                                                                                             |
| <b>Other Iron(III) and Iron(II) dioxygenases</b>               |                                                                                                                                                                                             |
| Intradiol-cleaving catechol dioxygenases (Fe <sup>III</sup> )  |                                                                                                                                                                                             |
| Lipoxygenases (Fe <sup>III</sup> )                             |                                                                                                                                                                                             |
| Apocarotene dioxygenase (Fe <sup>II</sup> )                    |                                                                                                                                                                                             |
| <b>Dinuclear center</b>                                        |                                                                                                                                                                                             |
| Methane monooxygenase (soluble)                                | $\text{CH}_4 + \text{O}_2 + 2\text{H}^+ + 2e^- \rightarrow \text{CH}_3\text{OH} + \text{H}_2\text{O}$                                                                                       |

### I.3.1.1.1. Cytochrome P450

The cytochrome P450 (Cyt P450) is an important family of iron enzymes ubiquitous in life forms ranging from bacteria to humans.<sup>20-23</sup> Cyt P450 enzymes were first identified and purified approximately 50 years ago and they have been thoroughly studied. They are oxidoreductases that catalyze the oxidation of a wide variety of biological substrates by means of dioxygen activation. Cyt P450 is known to catalyze hydroxylations, epoxidations (scheme 2), N-, S- and O-dealkylations, N-oxidations, sulfoxidations and dehalogenations. These oxygenation reactions play a central role in biosynthesis, metabolism and detoxification of harmful substances.



**Scheme 2.** Hydroxylation and epoxidation reactions catalyzed by cytochrome P450.

The active site of Cyt P450-camphor is known in detail from several X-ray crystal structures (figure 2).<sup>23</sup> It contains a single ferric heme coordinated to a cysteinyl sulfur and to a sixth ligand assigned either as water or hydroxide.

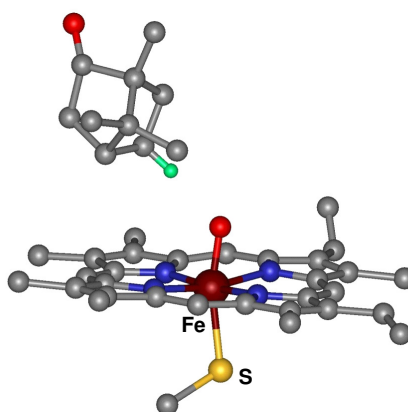
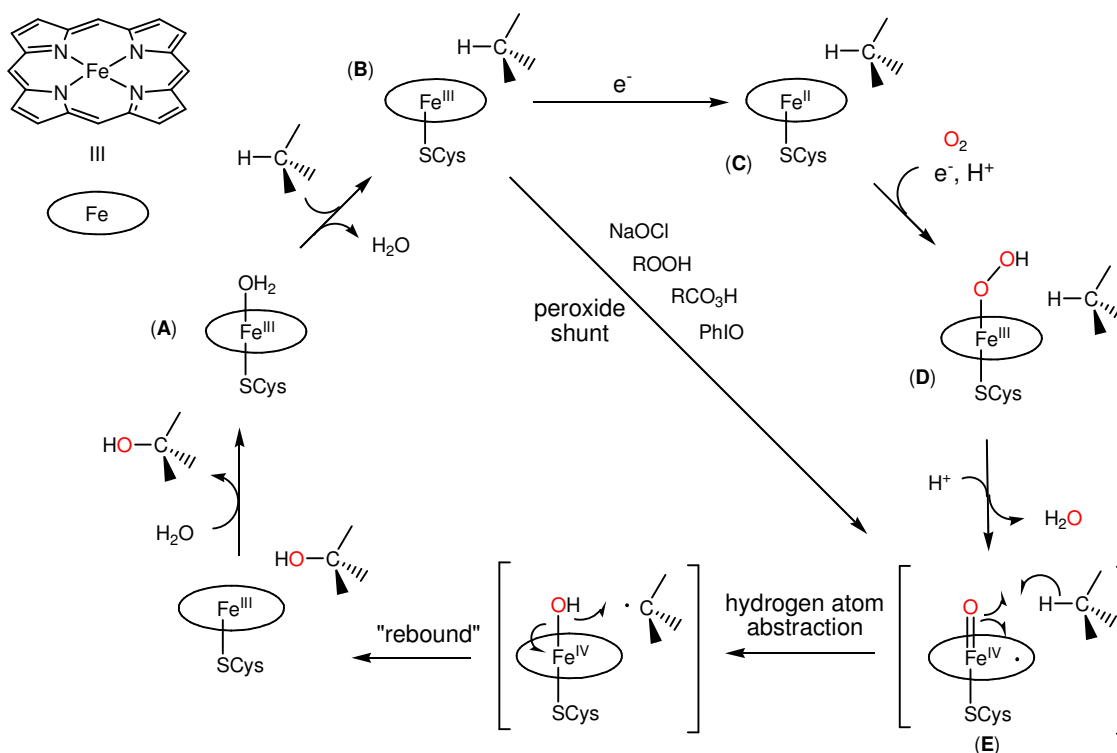


**Figure 2.** The active site of cytochrome P450-camphor from *Pseudomonas putida*.

The Cyt P450 family is considered to be the paradigm for oxygen activation and hydrocarbon oxidation by an iron center due to their versatility and efficiency. For this reason, extensive efforts have been devoted to understand its catalytic mechanism over the past 30 years. The principal features of the catalytic cycle of Cyt P450 are nowadays well-established.<sup>21-23</sup> As shown in scheme 3, the first step entails the binding of the alkane substrate to the active site (A → B), which triggers the one-electron reduction of the Fe<sup>III</sup> (C). The subsequent binding of O<sub>2</sub> to the Fe<sup>II</sup> center gives a ferric Cyt P450-superoxide complex. A second electron is transferred to this complex to afford a peroxyiron(III) complex, which is further protonated to generate a hydroperoxyiron(III) complex (D). This species undergoes proton assisted heterolytic cleavage of the O-O bond to generate a high-valent oxo-Fe<sup>IV</sup>-porphyrin radical cation (E) and a water molecule. The oxygen atom is transferred from this oxo complex to the nearby substrate through a two-step process known as “oxygen rebound”.<sup>36</sup> Dissociation of the product

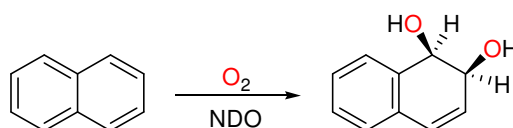
completes the catalytic cycle. Direct cycling between the ferric resting state (B) and the high valent oxidant species (E) can be done by using oxidants such as hydro and alkylperoxides, NaOCl, PhIO and peracids. This shortcut is known as the "peroxide shunt" (scheme 3) and receives use in catalysis.<sup>37</sup>



**Scheme 3.** The reaction mechanism of alkane hydroxylation proposed for cytochrome P450.

### I.3.1.1.2. Rieske dioxygenases

Great strides have been made in the past 15 years towards the understanding of mononuclear non-heme iron(II) enzymes. Among them, Rieske dioxygenases are specially efficient and versatile, even more than the heme-containing Cyt P450. Rieske dioxygenases are the only among both heme and non-heme iron enzymes that are capable of carrying out stereospecific and enantioselective *cis*-dihydroxylation of arene and olefin double bonds (scheme 4).<sup>25,28,29,38,39</sup> This is a novel transformation not observed so far in synthetic organic chemistry, therefore there is strong interest in these enzymes as biotechnological tools.<sup>40,41</sup> Apart from *cis*-dihydroxylation, Rieske dioxygenases also catalyze a number of oxidations such as benzylic hydroxylation, desaturation, sulfoxidation, and O- and N-dealkylation.<sup>38</sup> Such versatility has led to consider Rieske dioxygenases as the non-heme analog of Cyt P450.



**Scheme 4.** Arene *cis*-dihydroxylation reaction of naphthalene catalyzed by naphthalene 1,2-dioxygenase (NDO).

One of the best studied examples of the Rieske dioxygenases family is naphthalene 1,2-dioxygenase (NDO).<sup>38,42</sup> NDO catalyzes the *cis*-dihydroxylation of naphthalene (scheme 4) and it is known that in the course of catalysis, both atoms of O<sub>2</sub> are incorporated into the *cis*-diol product. NDO is representative of other *cis*-dihydroxylating enzymes such as benzoate 1,2-dioxygenase,<sup>43</sup> toluene 2,3-dioxygenase,<sup>44</sup> benzene dioxygenase<sup>45</sup> and phthalate dioxygenase<sup>46</sup>. The structure of the active site of NDO from *Pseudomonas putida* shows the characteristic structure of the Rieske dioxygenases: an oxygenase component (a mononuclear non-heme iron(II) center in the high spin) where O<sub>2</sub> activation and substrate dihydroxylation occur and a reductase component (Rieske-type Fe<sub>2</sub>S<sub>2</sub> cluster) that mediates electron transfer from NAD(P)H (figure 3).<sup>42</sup>

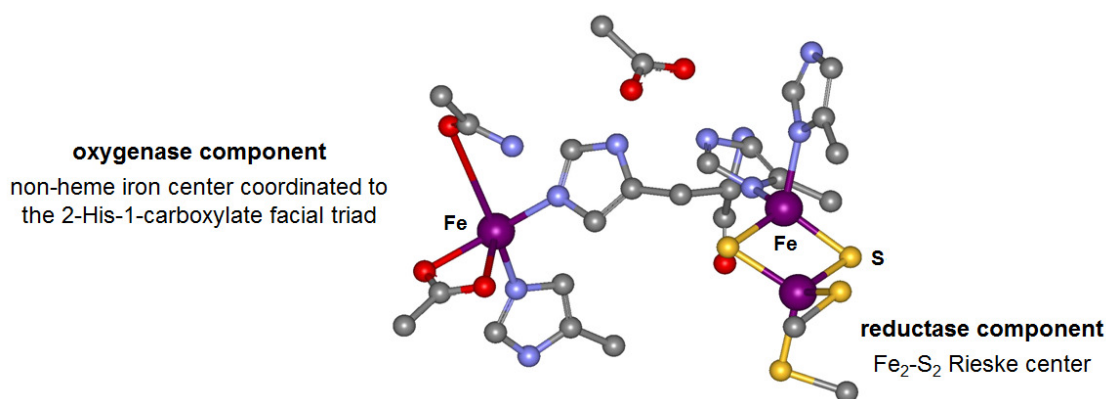
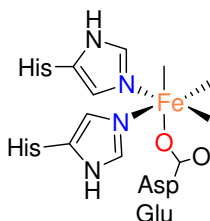


**Figure 3.** Active center of Rieske dioxygenase showing the oxygenase and reductase component.

Moreover, Rieske dioxygenases belong to a superfamily of enzymes that contain in their active site (oxygenase component) an iron(II) center coordinated by the so called 2-His-1-carboxylate facial triad.<sup>28,47,48</sup> It consists in three protein residues (two His and a bidentate Asp or Glu) that leave three *cis* sites available for exogenous ligands binding (scheme 5). In the isolated enzymes, these sites are usually occupied by solvent molecules but they can accommodate both substrate (or co-substrate) and O<sub>2</sub>, bringing them into close proximity for subsequent reaction, thereby accounting in large part for its versatility.<sup>27</sup>

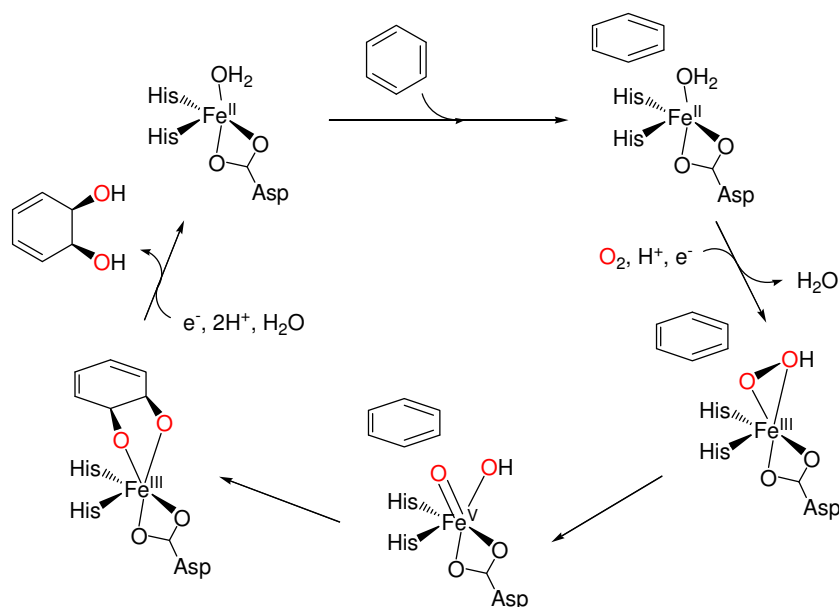


**Scheme 5.** Schematic representation of the 2-His-1-carboxylate facial triad found in some mononuclear non-heme iron enzymes.

Time resolved cryo-crystallography on frozen crystals of NDO exposed to O<sub>2</sub> indicate that a side-on bound peroxo (or hydroperoxo)-iron(III) species is the last detectable intermediate before substrate oxidation occurs.<sup>49</sup> Recent experiments also reveal that phthalate dioxygenase



can elicit catalytic chemistry when  $\text{H}_2\text{O}_2$  is used as oxidant thus resembling the “peroxide-shunt” of Cyt P450.<sup>50</sup> Overall, a number of evidences point towards a common mechanistic landscape operating in Cyt P450 and Rieske dioxygenases and suggesting that high-valent iron species are responsible for the catalysis (scheme 6).



**Scheme 6.** Catalytic cycle proposed for Rieske dioxygenases.

### I.3.1.1.3. Apocarotene dioxygenase

Retinal-forming carotenoid oxygenases constitute a sequence-related family of more than 100 currently known members. A prominent family member is  $\beta$ -carotene-15,15'-oxygenase found in animals, which cleaves  $\beta$ -carotene symmetrically to generate two molecules of retinal.<sup>51</sup> A very recent crystallographic characterization reveals that  $\beta$ -carotene-15,15'-oxygenase is a monomeric iron(II)-containing oxygenase where  $\text{Fe}^{\text{II}}$  ion presents an almost perfect octahedral coordination to four histidines and two water molecules (figure 4).<sup>52</sup> Comparisons within the carotenoid oxygenase family show that the environment of the active center is well conserved and contain four histidines in all cases.

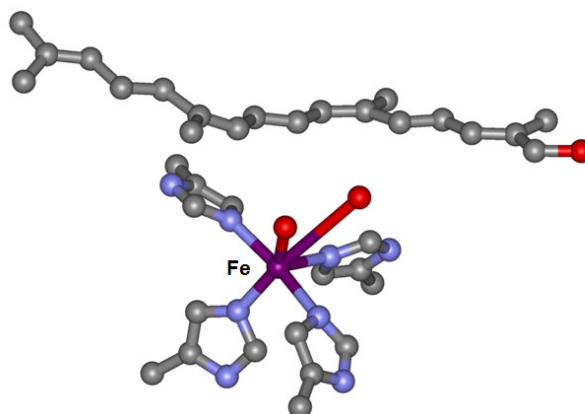
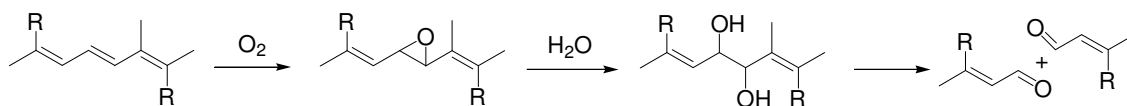


**Figure 4.** Active site of  $\beta$ -carotene-15,15'-oxygenase.

The catalyzed reaction requires dioxygen and the central cleavage proceeds stoichiometrically to yield two moles of aldehyde from one mole of carotenoid (scheme 7). Experimental evidence suggests that olefin cleavage is initiated in a monooxygenase-type mechanism, in which the first step is the epoxidation of the central double bond of the carotenoid. This is followed by unselective ring opening with water and final diol cleavage to yield two molecules of aldehyde (scheme 7).<sup>51</sup>



**Scheme 7.** Proposed mechanism for the formation of two molecules of retinal from  $\beta$ -carotene by  $\beta$ -carotene-15-15'-oxygenase through the cleavage at the central 15-15' bond.

### I.3.2. Biological role of manganese

Manganese is an essential trace nutrient in all forms of life.  $Mn^{II}$  ions serve as cofactors for a number of enzymes in living organisms. Its high availability (manganese is the 3<sup>rd</sup> most abundant transition metal, after Fe and Ti, in the Earth's crust) and various attainable oxidation states (manganese has access to three oxidation states of relevance to biology,  $Mn^{II}$ ,  $Mn^{III}$  and  $Mn^{IV}$ ) have likely led to the evolutionary selection of manganese. One of the most remarkable features of manganese-dependent enzymes is their very wide range of functionality. Enzymes containing manganese cofactors include oxidoreductases, transferases, hydrolases, oxygenases, lyases, isomerases, ligases, lectins, integrins and the oxygen evolving center of photosystem II.<sup>30</sup>

In most cases, the role of this metal ion is directly related to two basic functions: in +2 oxidation state, as a Lewis acid used in living organisms for essential functions, which should be intermediate between that of  $Mg^{II}$  and  $Ca^{II}$  and  $Zn^{II}$ , and the second, in higher oxidation states as powerful oxidizing agent.

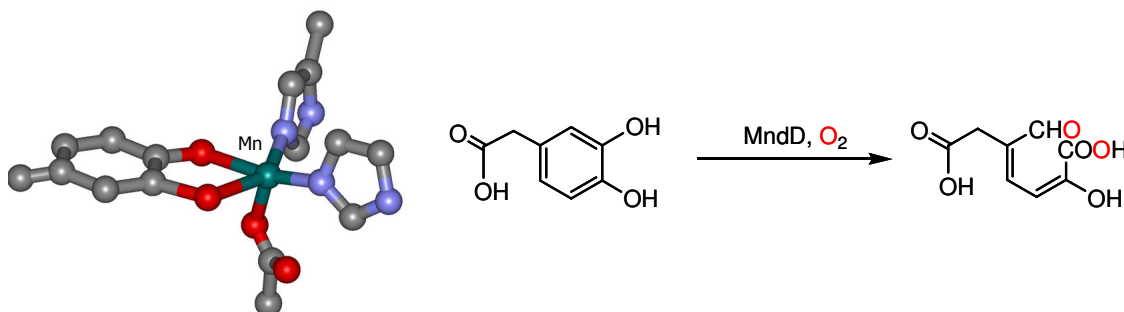
#### I.3.2.1. Oxidative manganese proteins

Nature has taken advantage of the manganese oxidation power (comparable to iron and copper) and employed it as cofactor for many oxidative enzymes. A major difference with other redox active metals, such as iron, is that manganese has less reducing potential than iron under most biological conditions. While  $Fe^{III}$  is stabilized with respect to  $Fe^{II}$ ,  $Mn^{II}$  is stabilized relative to  $Mn^{III}$ . This is because in both cases the half-filled  $d^5$  shell of both  $Fe^{III}$  and  $Mn^{II}$  confers thermodynamic stability. Two important consequences of this redox chemistry are that  $Mn^{II}$  can participate in redox catalysis on many similar substrates to  $Fe^{III}$  and whereas the higher redox potential of  $Mn^{II}$  makes free  $Mn^{II}$  innocuous under conditions where free  $Fe^{III}$  would wreak havoc through the generation of hydroxyl radicals.

In this introduction, only catechol dioxygenase will be described in detail as it constitutes a relevant example of oxidative manganese enzymes.

### I.3.2.1.1. Catechol dioxygenases

The extradiol cleavage of dihydroxybenzenes represents the more common pathway for the biodegradation of aromatic molecules in the soil by bacteria (scheme 8). Few of the extradiol-cleaving enzymes utilize a manganese(II) active site,<sup>53</sup> but the extradiol-cleaving enzymes typically use iron(II). The 3,4-dihydroxyphenylacetate 2,3-dioxygenases from *Brevibacterium fuscum* and *Arthrobacter globiformis* represent an interesting pair of enzymes.<sup>54</sup> These two enzymes bear 82% sequence identity but they have distinct metal ion requirements: the *B. fuscum* enzyme (HPCD) has an iron(II) in the active site, while the *A. globiformis* enzyme (MndD) requires manganese(II). Crystallographic data for both enzymes shows that the metal center is placed in a square pyramidal active site with a 2-His-1-carboxylate facial triad (scheme 8). While there is no insight into the reasons for the different metal ion requirements, it is clear that both enzymes can catalyze extradiol cleavage of the same substrate.



**Scheme 8.** Structure of the active center of manganese-dependent extradiol-cleaving catechol dioxygenase (MndD) (left). Reaction of MndD towards 2-(3,4-dihydroxyphenyl)acetic acid (right).

On the other hand, very recently Que and co-workers demonstrated that in the case of homoprotocatechuate 2,3-dioxygenase from *Brevibacterium fuscum* (containing Fe) and from *Arthrobacter globiformis* (containing Mn), swapping of Mn and Fe do not induce substantial changes in the activity and structure.<sup>55</sup>

Structural and functional homology between iron and manganese dependent enzymes is not exclusive of this family of enzymes but it is also found in Fe and Mn-dependent superoxide dismutases,<sup>56,57</sup> and lipoxygenases.<sup>58-60</sup> Overall, this homology suggests that Mn enzymes may play a more prominent role than currently known in O<sub>2</sub> metabolism.

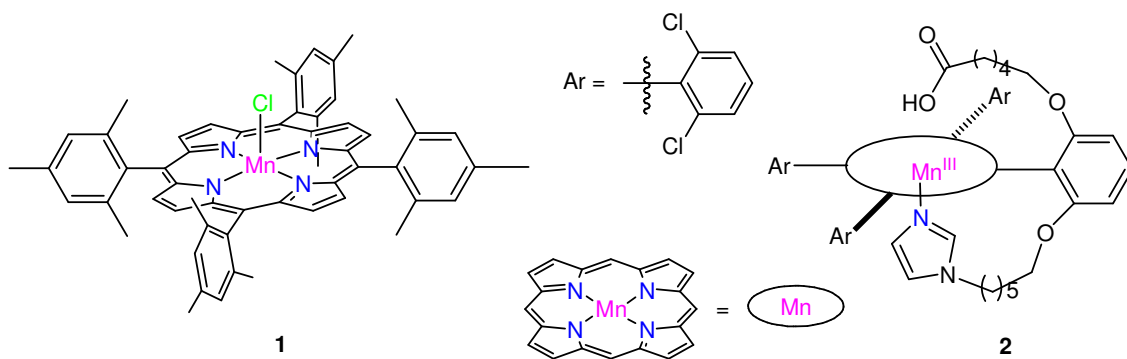
## I.4. Iron and manganese bioinspired complexes

Inspired by the active site of iron and manganese oxidation enzymes, chemists have designed a wide variety of complexes that functionally mimic these metalloenzymes, with the aim of designing oxidation catalysts. In the following pages prominent examples of these alkane and alkene oxidation catalysts are reviewed.

### I.4.1. Simple coordination complexes as bioinspired oxidation catalysts

#### I.4.1.1. Cytochrome P450–inspired oxidation catalysts

The active site of cytochrome P450 monooxygenase has been and still is source of inspiration for catalyst design. In this context, porphyrins have been widely studied as chemical models.<sup>61</sup> Groves and co-workers were the first to demonstrate cytochrome P450-like activity in a model system using iron *meso*-tetraphenylporphyrin chloride and iodosylbenzene (PhIO) as the oxidant.<sup>62</sup> In their study it was shown that cyclohexene was converted to its epoxide and cyclohexane to cyclohexanol. Other metalloporphyrins (including Cr, Mn, and Ru) were also shown to catalyze both epoxidation of olefins and hydroxylation of unactivated hydrocarbons mimicking the natural reactions. This first generation of porphyrin complexes, however, was prone to oxidative decomposition and therefore synthetic applications were hampered by rapid catalyst deactivation. This problem was overcome by attaching alkyl or halogen substituents at the *ortho*, *meta*, or *para* positions of the phenyl groups located at the macrocycle *meso* positions (second generation, catalyst 1, scheme 9 left), in order to (i) provide steric effects to avoid the formation of catalytically inactive oxo complexes and/or (ii) enhance the electrophilicity of the metal-oxo entity by electron withdrawing substituents on phenyl rings. In a third generation,  $\beta$ -pyrrole positions were halogenated generating considerable electronic activation of the catalyst, which showed exceptional stabilities and efficiencies in epoxidation and hydroxylation reactions. Moreover, the stereoscrumbling in the oxidation of *cis*-olefins showed by previous generations of porphyrins was also limited pointing to an enhanced preference for a concerted pathway.



**Scheme 9.** Examples of porphyrinic Mn complexes that catalyze epoxidation.

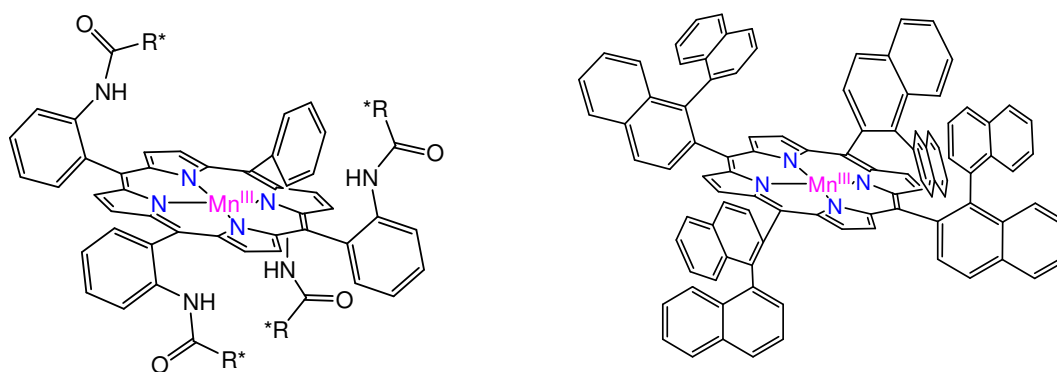
A variety of oxidants such as iodosylarenes, alkylhydroperoxides, peracids and hypochlorite, in addition to  $\text{H}_2\text{O}_2$ , have been employed.<sup>61,63</sup> Initial attempts to use  $\text{H}_2\text{O}_2$  as oxidant for alkene epoxidation with porphyrin based catalysts were unsuccessful due to dismutation of  $\text{H}_2\text{O}_2$ . Mansuy and coworkers demonstrated that the catalytic system could be greatly improved by performing the oxidation reaction in the presence of large amounts of imidazole.<sup>64</sup> This catalytic system provides epoxides in yields up to 99%. The amount of axial ligand could be significantly reduced by the addition of catalytic amounts of a carboxylic acid (see table 2).<sup>65</sup>

**Table 2.** Manganese-porphyrin catalyzed epoxidation of *cis*-cyclooctene using aqueous  $\text{H}_2\text{O}_2$  (see scheme 9 for catalysts code number).

| Entry | Catalyst     | Additive                                                 | Temp. | Time   | Yield |
|-------|--------------|----------------------------------------------------------|-------|--------|-------|
| 1     | 1 (2.5 mol%) | imidazole (0.6 equiv)                                    | 20°C  | 45 min | 90%   |
| 2     | 1 (0.5 mol%) | N-hexyl-imidazole (0.5 mol%) and benzoic acid (0.5% mol) | 0°C   | 15 min | 100%  |
| 3     | 2 (0.1 mol%) | -                                                        | 0°C   | 3 min  | 100%  |

Enhanced epoxidation rates were observed by using a modified Mn-porphyrin complex in which the carboxylic acid and imidazole groups are both covalently linked to the ligand (see table 2 and scheme 9 right).<sup>66,67</sup> Employing 0.1 mol% of the manganese complex and 2 equiv of  $\text{H}_2\text{O}_2$ , cyclooctene was converted in only 3 min to the corresponding epoxide with 100% conversion and selectivity, with turnover numbers up to 1000.

The epoxidation systems using hydrogen peroxide as the terminal oxidant were reported to be stereospecific for *cis*-alkenes, whereas *trans*-alkenes are poor substrates with these catalysts.<sup>65</sup> Moreover, carboxylic acids and nitrogen containing additives are considered to facilitate the heterolytic cleavage of the O-O bond. It is known that the competing homolytic cleavage of the O-O bond leads to the formation of hydroxyl radicals and unselective oxidation reactions, which is a serious problem when using  $\text{H}_2\text{O}_2$  in numerous metal-catalyzed oxidations.



**Scheme 10.** Selected examples of chiral porphyrins.

On the other hand, porphyrins were also used for asymmetric oxidation reactions. Following the first report by Groves and Myers<sup>68</sup> using a chiral metalloporphyrin, a wide variety of porphyrin ligands linked to chiral appendages have been introduced (scheme 10).<sup>69-72</sup>

Although high enantioselectivities were observed with iodosylbenzene as oxidant, the use of  $\text{H}_2\text{O}_2$  has only resulted in moderate enantiomeric excess (ee) so far.

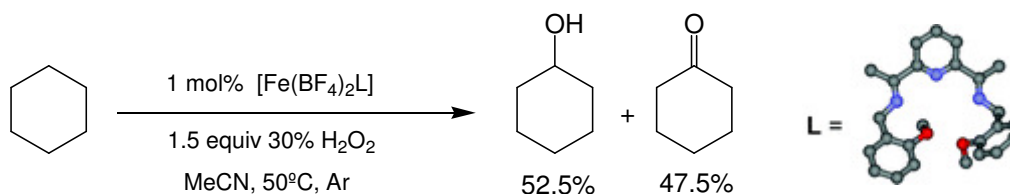
#### I.4.1.2. Oxidation of alkanes (C-H bonds) by non-heme iron complexes

Gaining inspiration from nature, chemists have combined first row metals, especially  $\text{Fe}^{\text{II}}$  but also  $\text{Cu}^{\text{I}}$ ,  $\text{Mn}^{\text{II}}$  and  $\text{Co}^{\text{II}}$ , with peroxides to perform oxidation of organic compounds (Fenton's reagent).<sup>73,74</sup> In this "bioinspired" approach, the combination of  $\text{O}_2$  and  $2\text{e}^-$  is replaced by peroxides, which can be understood as a  $2\text{e}^-$  reduced version of  $\text{O}_2$ . However, after extensive disputes for more than a century over the reaction mechanisms, the current understanding is that Fenton's chemistry is related to non selective reactions and free-diffusing radicals (scheme 11).<sup>75</sup>



**Scheme 11.** Fenton's reaction involves free diffusing radicals.

Introduction of appropriate ligands into the system exert dramatic changes in the chemistry and afford more selective reactions.<sup>76</sup> Gif systems constitute a more elaborated approach. The most prominent example of Gif chemistry involve the reaction of iron salts and  $\text{H}_2\text{O}_2$  in pyridine in the presence of acetic acid and/or picolinic acid.<sup>16,77</sup> This method functionalizes saturated hydrocarbons to ketones, preferentially at secondary positions. Other approaches involve the use of polynuclear oxo-bridged iron compounds as catalysts with good results, such the hexanuclear iron carboxylate with a  $[\text{Fe}_6(\mu_3\text{-O})_3(\mu_2\text{-OH})]^{+11}$  core reported by Smith and Arion<sup>78</sup> or the tetrairon complex  $[\text{Fe}_4(\text{L}_A)_4(\mu\text{-O})_2]^{+4}$  ( $\text{L}_A$  = 1-carboxymethyl-4,7-dimethyl-1,4,7-triazacyclononane) reported by Shul'pin.<sup>79</sup> On the other hand, Reedijk and co-workers reported an iron(III) complex with a pentadentate ligand that converted cyclohexane quantitatively to a mixture of cyclohexanol and cyclohexanone (scheme 12). The system uses  $\text{H}_2\text{O}_2$  as oxidant and works at  $50^\circ\text{C}$  under argon atmosphere.<sup>80,81</sup>

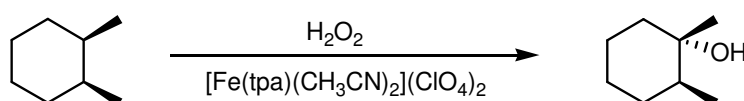


**Scheme 12.** Cyclohexane oxidation catalyzed by Reedijk and co-workers system.<sup>81</sup>

However, performing stereospecific alkane hydroxylation reactions to give alcohols by selective metal based oxidant analogous to those used in biological systems (scheme 13), rather than  $\text{HO}\cdot$  or  $\text{RO}\cdot$  radicals, has demonstrated to be more challenging, and the number of reported examples are much more limited. Because it is often difficult to observe the actual reagent that carries out the key oxidative transformation, indirect probes have been useful to



The first system that performed stereospecific hydroxylation of alkanes with  $\text{H}_2\text{O}_2$  was reported by Que and co-workers in 1997 using a tpa iron(II) complex (scheme 14 and 15).<sup>83</sup> Since then, several non-heme mononuclear iron complexes capable of performing stereospecific alkane oxidation to give alcohols have been described, and a schematic representation of the most relevant ones is depicted in scheme 14. Common features in these non-heme iron catalysts are the use of tetradentate N-donor ligands and two *cis* labile co-ligands. The importance of the presence of two *cis* labile sites available for coordination with exogenous ligands (the oxidant and/or the substrate) was first studied by Menage and co-workers.<sup>84</sup> This study concluded that weakly coordinating triflate anions or acetonitrile molecules in combination with non-coordinating anions, led to metal based pathways while coordinating ligands, such as chloride, led to Fenton type reactions.



**Scheme 15.** Stereospecific oxidation of *cis*-1,2-dimethylcyclohexane (*cis*-DMCH) by tpa iron(II) complex reported by Que and co-workers.

Two main families of complexes bearing tetradentate ligands have been studied in the oxidation of alkanes: tpa (tripodal) and bpmen (linear) families.<sup>85</sup> Mononuclear iron(II) complexes derived from these ligands are quite efficient catalysts and the mechanistic probes clearly point towards the mediation of metal based oxidants (table 3).<sup>86</sup> More recently, our research group reported a new family of tetradentate ligands derived from 1,4,7-triazacyclononane (TACN) which showed remarkable efficiencies and evidences of metal based oxidants (table 3).<sup>87,88</sup>

**Table 3.** Oxidation of alkanes with  $\text{H}_2\text{O}_2$  catalyzed by different iron(II) complexes.

| ligand                | cyclohexane              |     | <i>cis</i> -1,2-DMCH | adamantane                                  | Ref |
|-----------------------|--------------------------|-----|----------------------|---------------------------------------------|-----|
|                       | A + K (A/K) <sup>a</sup> | KIE | RC (%) <sup>b</sup>  | 3 <sup>o</sup> /2 <sup>o</sup> <sup>c</sup> |     |
| tpa                   | 3.2 (6)                  | 3.5 | 100                  | 17                                          | 86  |
| 5Me <sub>3</sub> -tpa | 4.0 (5)                  | 3.8 | 100                  | 21                                          | 86  |
| 6Me <sub>3</sub> -tpa | 2.9 (2)                  | 3.3 | 54                   | 15                                          | 86  |
| bpmen                 | 6.3 (5)                  | 3.2 | 96                   | 15                                          | 86  |
| bqen                  | 5.1 (5)                  | -   | -                    | -                                           | 89  |
| α-bpmcn               | 5.9 (9)                  | 3.2 | >99                  | 15                                          | 90  |
| β-bpmcn               | 1.9 (0.9)                | 4.0 | 68                   | 17                                          | 90  |
| <sup>H</sup> PyTACN   | 6.5 (12)                 | 4.3 | 93                   | 30                                          | 88  |
| <sup>Me</sup> PyTACN  | 7.6 (10)                 | 3.4 | 94                   | 20                                          | 88  |

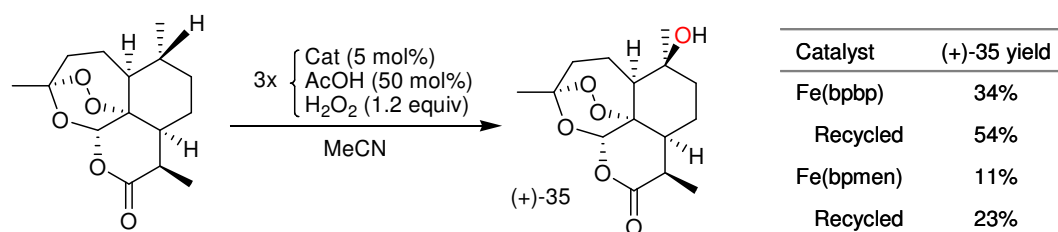
Catalyst: $\text{H}_2\text{O}_2$ :alkane = 1:10:1000. <sup>a</sup>Turnover number (TN, mols of product / mols of catalyst), A = cyclohexanol, K = cyclohexanone. A/K = (mols A / mols K). <sup>b</sup>Retention of configuration in the oxidation of *cis*-1,2-DMCH. <sup>c</sup>3<sup>o</sup>/2<sup>o</sup> = 3x(1-adamantanol)/(2-adamantanol+2-adamantanone).



Designing suitable ligands is essential to obtain efficient catalysts. In a series of papers, Britovsek's and Que's groups showed that minor modifications in the ligand architecture can cause important changes in the catalytic performance (table 3). Steric effects were investigated introducing methyl substituents in the  $\alpha$  position of the pyridine ring of tpa ligand.<sup>86</sup> Differently to tpa, 6Me<sub>3</sub>-tpa generates a catalyst with some non-metal based character as evidenced by the low percentage of retention of configuration (RC) in the oxidation of *cis*-1,2-DMCH and the large percentage of O<sub>2</sub> incorporation into products.<sup>86</sup> The latter originates from diffusion controlled O<sub>2</sub> trapping of carbon centered radical intermediates. Electronic effects have been investigated by the introduction of substituents in the pyridyl *para*-positions<sup>86,91</sup> or changing the number of pyridines in tripodal ligands.<sup>92</sup> In all cases, similar or lower activity was observed. The effect of the structure and atom donor nature of the backbond was studied for the linear bpmen and bqen ligands.<sup>89-91,93,94</sup> Rigidity of the ligand backbond appears to be an important factor, since a too flexible backbonds leads to a mixture of coordination modes, leading to less active catalysts. Exquisite example of the dramatic differences in the catalytic outcome of an iron complex depending on its coordination structure is the comparison between the *cis*- $\alpha$  and *cis*- $\beta$  topological isomeric forms of [Fe(CF<sub>3</sub>SO<sub>3</sub>)<sub>2</sub>(bpmcn)] (table 3 and figure 14 for ligand structure). The former is an efficient catalyst for stereospecific C-H hydroxylation, the latter give rise to carbon center diffusing radicals.<sup>90</sup>

As shown by the aforementioned studies, catalyst stability under the harsh oxidizing conditions required to oxidize alkanes is a major factor in determining the catalytic efficiency of a given catalyst. As proof of concept, the more efficient iron(II) catalyst reported so far are based on the very robust ligands bpmen and PyTACN.

However, the application of those systems in synthetic organic chemistry is hampered by low substrate conversions. In contrast, In a recent work, Chen and White reported the hydroxylation of aliphatic tertiary C-H bonds achieving high yields and selectivities using a combination of H<sub>2</sub>O<sub>2</sub> and acetic acid as the oxidant.<sup>95</sup> In this study the catalyst is a mononuclear iron complex with the bpbp ligand (see scheme 14), a chiral version of bpmen. Impressively, this system showed predictable selectivity based in steric and electronic factors, making it very interesting from a synthetic point of view. Moreover, selective oxidation in complex molecules was achieved obtaining synthetically useful yields (scheme 16).



**Scheme 16.** Selective hydroxylation of (+)-artemisin by bpbp and bpmen iron complexes (see scheme 14 for ligands' structures). The oxidation occurs preferentially at the most electron-rich and the least sterically hindered 3<sup>o</sup> C-H bond.<sup>95</sup>

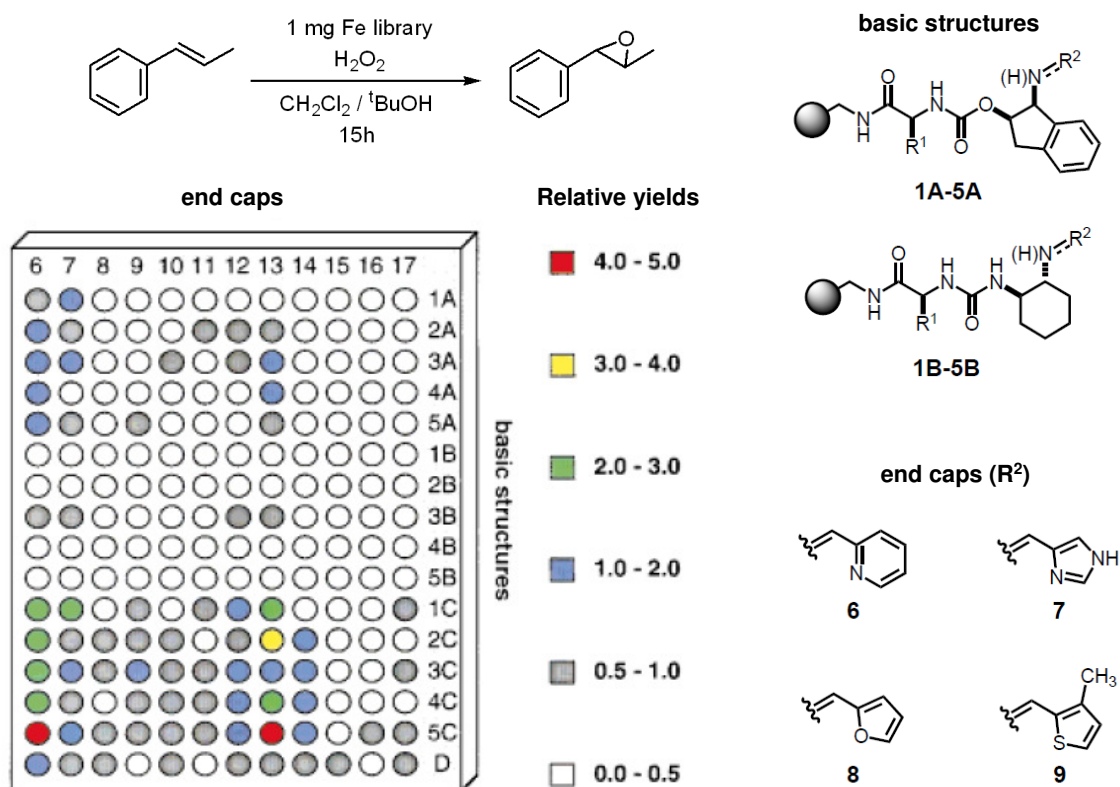
White and Chen landmark system uses 15% catalyst loadings, and even though it affords very modest turnover numbers (3–6), efficiencies were substantially better than in any previously reported non-heme catalyst. Indeed, in their work, Chen *et al.* compare the activity of their catalyst with  $[\text{Fe}(\text{bpmen})(\text{CH}_3\text{CN})_2](\text{SbF}_6)_2$ , at this time the most efficient iron catalyst, showing that *bbbp*'s iron complex is more efficient in the same conditions (scheme 16).

### I.4.1.3. Oxidation of alkenes (C=C double bonds) by non-heme iron complexes

#### I.4.1.3.1. Epoxidation

Several iron complexes have been studied for the selective epoxidation of alkenes. One of the first examples of selective epoxidation at a non-heme catalyst was reported by Valentine and co-workers using a mononuclear iron complex of TMC (1,4,8,11-tetraazacyclotetradecane, see scheme 20 for ligand structure) with  $\text{H}_2\text{O}_2$  as oxidant.<sup>96</sup>

On the other hand, Francis and Jacobsen used combinatorial chemistry for the screening of a 5760 metal-ligand complexes' library for finding highly efficient catalysts for *trans*- $\beta$ -methylstyrene oxidation.<sup>97</sup> They found that iron complexes led to clean epoxide product formation using  $\text{H}_2\text{O}_2$  as the terminal oxidant (scheme 17). Moreover, parallel libraries were used to determine ligand features important for high catalytic activity and to identify enantioselective catalyst structures.

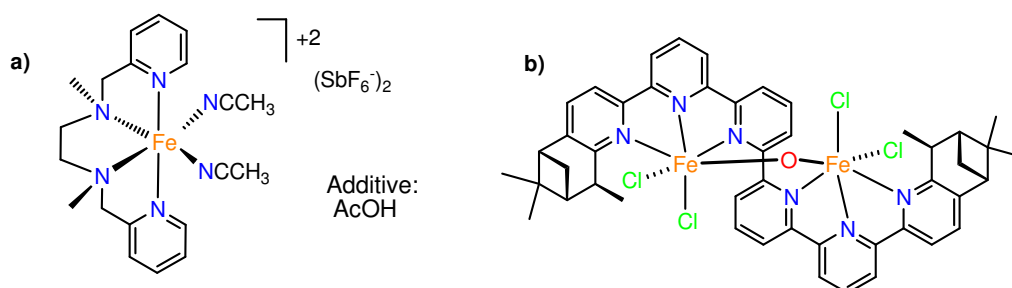


**Scheme 17.** *trans*- $\beta$ -methylstyrene epoxidation activity in a parallel library of iron complexes along with some of the structures of the ligands.

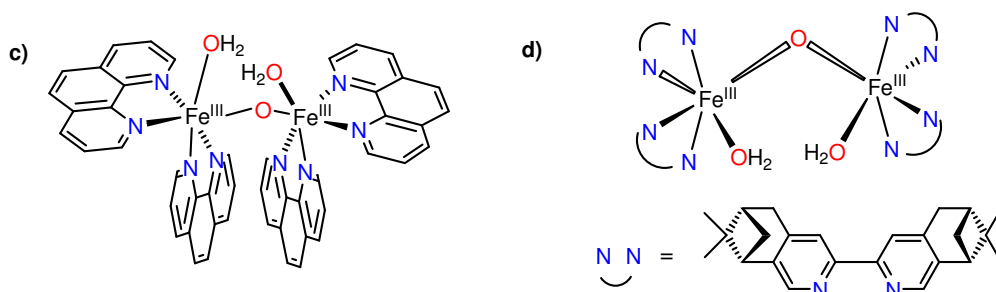
Many other examples have been reported, some of them are capable to epoxidize alkenes efficiently, but only few achieve synthetically useful yields and high substrate conversion.

In this sense, Jacobsen group also reported a mononuclear iron(II) complex based on the bpmen ligand (scheme 18a), which could perform the epoxidation of alkenes using a combination of  $\text{H}_2\text{O}_2$  and acetic acid as the oxidant.<sup>98</sup> Aliphatic olefins were rapidly (less than 5 min) epoxidized in high yields (60 – 90%). Nowadays this methodology constitutes one of the first examples of a bioinspired catalyst used as a synthetic tool for the synthesis of epoxides. The role of the acetic acid in these reactions has been recently studied by Que and co-workers, suggesting that it plays a key role in promoting fast O-O bond cleavage.<sup>99</sup> Moreover, acetic acid increases the efficiency and switches the selectivity affording the epoxide product almost selectively in the cases studied (tpa and bpmen iron(II) complexes).

#### $\text{H}_2\text{O}_2$ as oxidant:



#### $\text{CH}_3\text{CO}_3\text{H}$ as oxidant:

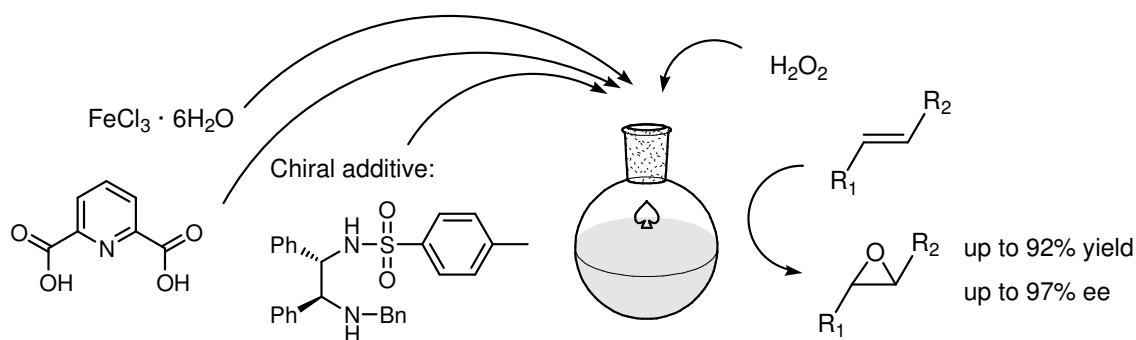


**Scheme 18.** Schematic representation of the most relevant iron catalysts for olefin oxidation. a) bpmen iron complex reported by Jacobsen.<sup>98</sup> b) Chiral iron sexipyridine reported by Kwong.<sup>100</sup> c) Dimeric phenanthroline based complex reported by Stack.<sup>101</sup> d) Chiral dimeric complex reported by Menage.<sup>102</sup>

Diiron complexes have also been used for alkene epoxidation. Stack and co-workers reported a  $\mu$ -oxo-iron(III) dimer also based on nitrogen-donor ligands.<sup>101</sup> Phenanthroline in combination with iron salts produced an efficient epoxidation catalyst for a wide range of olefins, including terminal alkenes, using commercially available 32% peracetic acid as the oxidant (scheme 18c). Low catalyst loadings, in situ catalyst preparation from common reagents, fast reaction times (<5 min at 0°C) and enhanced reaction performance at high substrate concentrations combine to create a synthetically efficient procedure for alkene epoxidation. A structurally related approach has been pursued by Menage and coworkers,<sup>102</sup> who have

synthesized a dinuclear oxo-bridged diiron complex using chiral bipyridine type of ligands (scheme 18d), that enantioselectively catalyzed the conversion of alkenes into epoxides. Unsymmetrical alkenes were oxidized rapidly into their epoxides with high conversions and enantiomeric excesses (ee's) ranging from 9 to 63%. Finally, in a recent report Kwong and co-workers described an iron sexipyridine complex capable of performing efficient epoxidation with  $\text{H}_2\text{O}_2$  (scheme 18b), and obtaining moderate ee's in the oxidation of aromatic olefins (up to 43% was achieved for the case of styrene).

With a completely different structural approach, Beller and co-workers have developed a simple process (room temperature, aerobic atmosphere) to epoxidize alkenes: commercially available  $\text{FeCl}_3 \cdot 3\text{H}_2\text{O}$  as iron source, pyridine-2,6-dicarboxylic acid as ligand and pyrrolidine as additive, are combined in-situ to generate a non characterized catalyst that epoxidizes aromatic alkenes using  $\text{H}_2\text{O}_2$  as a terminal oxidant.<sup>103</sup> Improvement of the system, aliphatic alkene oxidation<sup>104</sup> and chiral version<sup>105,106</sup> were achieved by the addition of benzylamines instead of pyrrolidine (scheme 19). The system achieves good yields and moderate to good ee. Unfortunately, this system suffers from relatively high catalyst loadings (typically, 5 mol%).

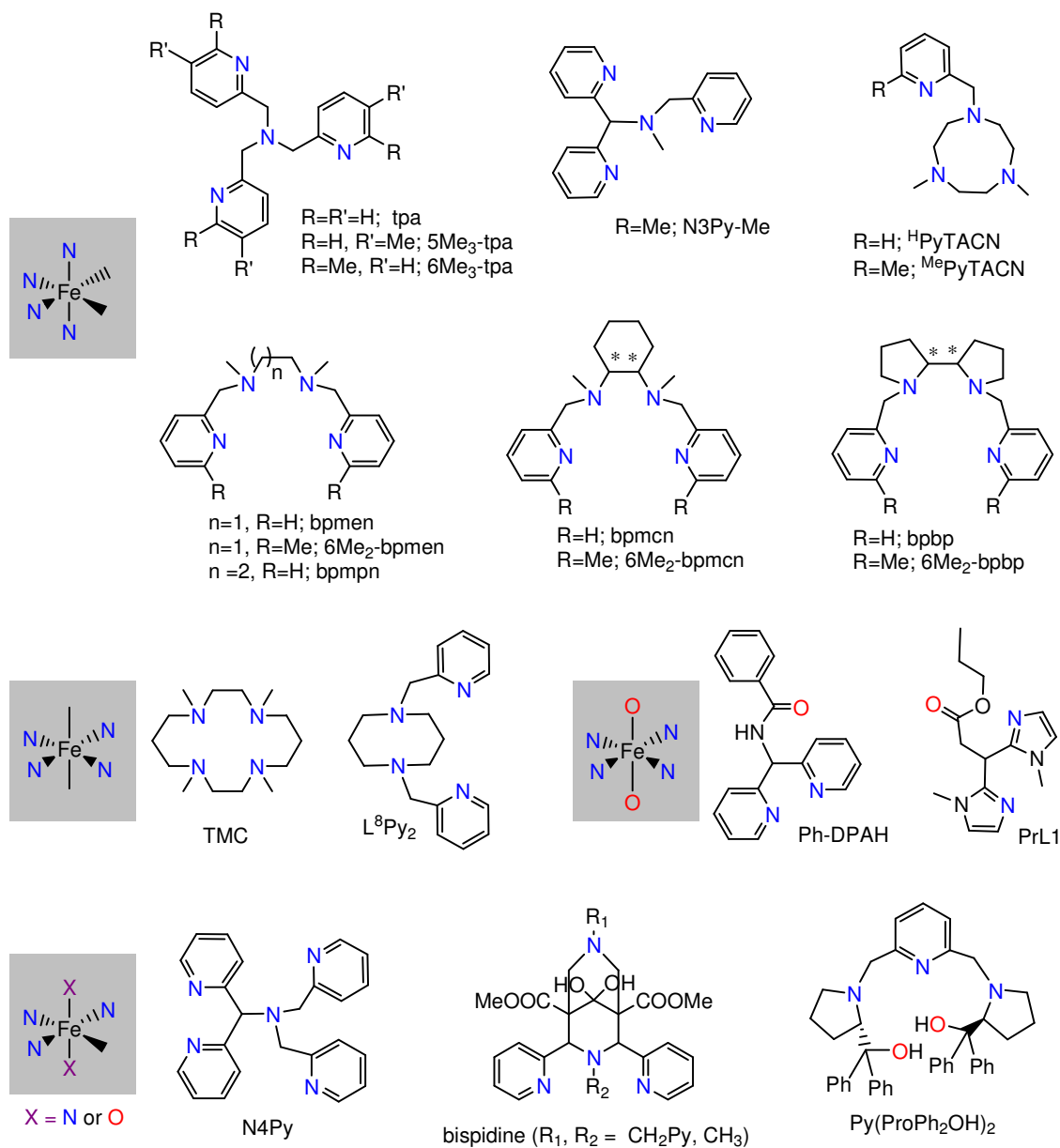


**Scheme 19.** In situ generated catalyst reported by Beller.<sup>105,106</sup>

More recently, the same group reported in-situ formation of imidazole iron complexes<sup>107</sup> that epoxidize aliphatic and aromatic olefins with high chemoselectivity and moderate to good yields.

#### I.4.1.3.2. *Cis*-dihydroxylation

Concomitantly with the studies of alkane oxidation, the same bioinspired non-heme iron catalysts were tested in the oxidation of olefins using  $\text{H}_2\text{O}_2$ . These complexes differ from previously discussed iron systems in their ability to catalyze not only epoxidation but also olefin *cis*-dihydroxylation, analogously to the reaction performed by Rieske dioxygenases.<sup>108</sup> Concurrently to alkane oxidation, the first reported examples of non-heme iron catalysts capable of eliciting olefin epoxidation and *cis*-dihydroxylation are those containing ligands of the tpa and bpmn family.<sup>109</sup> Later, other mononuclear complexes based on N4 ligands such as bpmcn,<sup>90</sup> bpbp,<sup>110</sup> bispidine<sup>111</sup> and PyTACN<sup>88</sup> have also shown to elicit the same catalytic activity (scheme 20).



**Scheme 20.** Schematic representation of the most relevant ligands used to prepare mononuclear iron(II) complexes to perform olefin oxidations along with the coordination they adopt around the metal center.

Table 4 collects results in the epoxidation of olefins by different non-heme catalysts. It shows that conversion of the oxidant in *cis*-cyclooctene oxidation can be as high as 84%, and diol:epoxide ratios range from 0.1 to 16.8. Diol product does not derive from the epoxide, as both products are formed at the same time, and the use of epoxide as a potential substrate under the same reaction conditions does not afford *cis*-diol. It is clear from the results that the ligand structure exerts a significant control on the diol:epoxide ratio. A general trend is that the presence of methyl groups in the  $\alpha$  position of the pyridine ring results in an increase in the diol:epoxide ratio. In most cases, high retention of configuration is observed in the epoxidation and *cis*-dihydroxylation of *cis*-2-heptene. This observation, together with the incorporation of

oxygen from water into oxidation products (isotopic labeling studies),<sup>90,109,112</sup> clearly indicates that a metal based oxidant is operating in these reactions.

**Table 4.** Oxidation of *cis*-cyclooctene with H<sub>2</sub>O<sub>2</sub> catalyzed by different iron(II) complexes.<sup>a</sup>

| ligand                              | D + E <sup>d</sup> | (D/E) <sup>e</sup> | ref. |
|-------------------------------------|--------------------|--------------------|------|
| tpa                                 | 7.4                | 1.2                | 109  |
| 5Me <sub>3</sub> -tpa               | 6.7                | 1.4                | 109  |
| 6Me <sub>3</sub> -tpa               | 7.1                | 16.8               | 109  |
| N3Py-Me <sup>c</sup>                | 37                 | 1.6                | 113  |
| <sup>H</sup> PyTACN                 | 8.1                | 1.0                | 88   |
| <sup>Me</sup> PyTACN                | 7.1                | 5.5                | 88   |
| bpmen                               | 8.4                | 0.1                | 112  |
| 6Me <sub>2</sub> -bpmen             | 7.9                | 4.3                | 114  |
| bpmpn                               | 6                  | 0.7                | 115  |
| α-bpmcn                             | 6.5                | 0.1                | 90   |
| β-bpmcn                             | 7.7                | 1.9                | 90   |
| 6-Me <sub>2</sub> -bpmcn            | 9.3                | 1.7                | 90   |
| bpbp <sup>b</sup>                   | 4.3                | 0.7                | 110  |
| 6Me <sub>2</sub> -bpbp <sup>b</sup> | 6.5                | 64.0               | 110  |
| TMC                                 | 3.5                | 0.03               | 115  |
| L <sup>8</sup> Py <sub>2</sub>      | 3.9                | 0.1                | 115  |
| Ph-DPAH                             | 7.5                | 14                 | 116  |
| PrL1                                | 4.3                | 1.7                | 117  |

<sup>a</sup> Catalyst:H<sub>2</sub>O<sub>2</sub>:*cis*-cyclooctene = 1:10:1000. <sup>b</sup> 1-octene was used instead of cyclooctene. <sup>c</sup> 50 equiv of H<sub>2</sub>O<sub>2</sub> instead of 10. <sup>d</sup> Turnover number (TN, mols of product / mols of catalyst), E = epoxide, D = diol. <sup>e</sup> D/E = (mols of D / mols of E).

Pentadentate ligands that only leave one labile coordination site at the metal have also been used, but resulted less efficient systems.<sup>118-120</sup> On the other hand, tetradentate ligands that adopt an equatorial coordination and leave two labile sites in a relative *trans* disposition, as TMC and L<sup>8</sup>Py<sub>2</sub>, have also been applied to these catalytic transformations but no *cis*-diol is formed.<sup>115,120</sup> It seems clear from these results that the availability of two labile sites in a *cis* configuration is necessary to model the *cis*-dihydroxylation reaction catalyzed by Rieske dioxygenases in biological systems.

However, all ligands employed in these studies provide the metal centre with an all-N donor set, that does not accurately reflect the N,N,O ligand environment found at the active site of the enzymes. For this reason, attention has been recently devoted to the development of iron complexes with mixed donor ligands. Oldenburg *et al.* used the ligand Ph-DPAH to obtain a very selective *cis*-dihydroxylation catalyst<sup>116</sup> and in a related contribution Klein Gebbink and co-workers, reported that iron complexes of PrL1 also show epoxidation and enzyme like *cis*-dihydroxylation activity (see table 4 and scheme 20).<sup>117</sup>

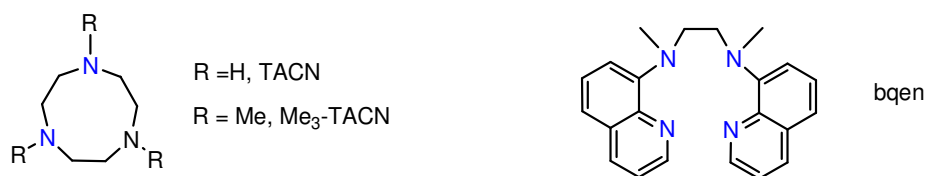
It was not until very recently that Que and co-workers reported complex  $[\text{Fe}(\text{tpa})(\text{CH}_3\text{CN})_2]^{+2}$  as the first authentic functional model of naphthalene dioxygenase.<sup>121</sup> The oxidation of naphthalene using  $\text{H}_2\text{O}_2$  as oxidant afforded four products, *cis*-1,2-dihydro-1,2-naphthalenediol, 1-naphtol, 2-naphtol and 1,4-naphthoquinone, being the former the major product as in NDO-catalyzed reaction.

The main limitation of the aforementioned systems is the relatively low TN and substrate conversion obtained. An exception is  $^{\text{Me}}\text{PyTACN}$  (see scheme 20) which afford 141 TN of diol vs 4.9 TN of epoxide in the oxidation of cyclooctane using 0.3% of catalyst and achieving 50% of efficiency in the conversion of  $\text{H}_2\text{O}_2$  into the oxygenated products.<sup>88</sup> Still, the weakness of this system is low conversions of substrate. Instead,  $5\text{Me}_3\text{-tpa}$  can catalyze the oxidation of olefins to *cis*-diols (D/E ratio around 3 in most of cases) under conditions of limiting substrate with high conversion and efficiency, but 3% of catalyst and 4 equivalents of  $\text{H}_2\text{O}_2$  were needed.<sup>122</sup> On the other hand, chiral ligands have been used for the development of asymmetric systems capable of giving diols with high enantiomeric excess and with high selectivity.<sup>110,114</sup> Overall, these mononuclear non-heme iron(II) systems may constitute an attractive environmentally benign alternative to the traditional toxic and more expensive osmium reagents used for *cis*-dihydroxylation, though significant improvement in reaction efficiencies is highly required to achieve this goal.

#### **I.4.1.4. Oxidation of alkanes (C-H bonds) by non-porphyrinic manganese complexes**

Manganese complexes have been traditionally less applied in the oxidation of alkanes than their iron homologues. However, some prominent systems exist.

The trioxo bridged dimanganese complex of TACN and  $\text{Me}_3\text{-TACN}$  (see scheme 21) were first studied for modeling the oxygen evolving centre of photosystem II.<sup>123</sup> Since the disclosure that these complexes were potent low-temperature bleaching catalysts,<sup>124</sup> considerable effort has focused on their development towards the efficient catalytic oxidation of other substrates, principally using the environmentally benign oxidant  $\text{H}_2\text{O}_2$  (for alkene oxidation see section I.4.1.5).<sup>125,126</sup> In an extensive series of reports, Lindsay Smith and Shul'pin showed the application of dimanganese complexes of TACN and their derivatives in the C–H oxidation of a variety of substrates.<sup>127-130</sup> The  $\text{Me}_3\text{-TACN}$  catalyst oxidizes alkanes in acetonitrile solution with TN up to 3300 for cyclohexane after 2h, yielding 46% of oxygenated products based on the alkane. It is important to emphasize that no alkane oxidation occurs in the absence of acetic acid, thus this co-catalyst allows the suppression of catalase activity. The process was demonstrated to proceed *via* the initial formation of alkyl hydroperoxides, which later in the course of the reaction decompose to produce the corresponding ketones. Some regioselectivity and considerable preference for the oxidation of tertiary centers was observed. Overall these findings were interpreted as being largely inconsistent with a radical pathway involving  $\cdot\text{OH}$ , although such species may be involved during the induction period. Remarkably, the system is also capable to oxidize light gaseous alkanes at modest pressures (up to 3100 TN for propane).



**Scheme 21.** Schematic representation of TACN, Me<sub>3</sub>-TACN and bqen ligands used to prepare manganese(II) complexes to perform alkane oxidation.

A more sophisticated system based on a dimanganese-bis- $\mu$ -oxo modified-terpyridine complex was reported by Crabtree and co-workers (see scheme 27, section I.4.2.1.1).<sup>131</sup> The terpyridine ligand includes a carboxylic acid group for the recognition of substrates that contain also this same group. H-bonding mediated molecular recognition and oriented the substrate towards the catalyst active site. The oxygenation of saturated C-H bonds occurred with oxone as the primary oxidant in very high (<98%) regioselectivity and stereospecificity with multi-hundred turnovers.

It was not since three years ago that Nam and co-workers reported a series of manganese mononuclear complexes derived from the bpmen family that were capable to oxidize alkanes with good yields (ligands employed: bpmen, bpmcn and bqen, for ligand structure see scheme 20 and 21).<sup>132</sup> Using peracetic acid as oxidant, the system catalyzed the stereospecific and regioselective oxidation of alkanes. The best results were obtained with the bqen manganese(II) complex. Up to 60% of substrate was converted to the desired product in the oxidation of *cis*-1,2-DMCH.

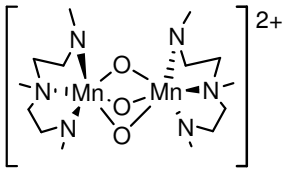
#### I.4.1.5. Oxidation of alkenes (C=C double bonds) by non-porphyrinic manganese complexes

While Mn ions are less commonly found than iron in oxidative enzymes, selective manganese complexes are emerging as very remarkable olefin oxidation catalysts. Manganese salts have been described as simple epoxidation agents in combination with H<sub>2</sub>O<sub>2</sub> in bicarbonate buffered solutions.<sup>133-135</sup> In selected cases, the use of nitrogen based ligands results in an enhanced catalytic activity. A very remarkable example is the family of TACN manganese complexes. In combination with H<sub>2</sub>O<sub>2</sub> and using oxalate as additive, the dinuclear catalyst [(Me<sub>3</sub>-TACN)<sub>2</sub>Mn<sub>2</sub>( $\mu$ -O)<sub>3</sub>]<sup>+2</sup> is a highly active and selective epoxidation catalyst.<sup>124,136,137</sup> Oxalate, not only suppressed the catalase activity in acetonitrile but also reduced the *cis*- and *trans*- isomerisation. In addition, various functional groups including electron withdrawing groups and alcohols are tolerated. The system was further improved by additives such as ascorbic acid;<sup>138</sup> nearly quantitative yields of epoxides with retention of the olefinic configuration were found employing catalyst loadings as low as 0.03%.

More recently, Feringa and co-workers<sup>139,140</sup> studied dimanganese complexes based on the same Me<sub>3</sub>TACN ligand for *cis*-dihydroxylation and epoxidation of alkenes employing H<sub>2</sub>O<sub>2</sub> as the oxidant (see scheme 22). The formation of different carboxylate-bridged dinuclear manganese complexes in the reaction mixture controls the selectivity and activity toward *cis*-



dihydroxylation and epoxidation. Moreover, modest but remarkable enantioselectivity was achieved using chiral carboxylate ligands.<sup>141</sup>

|                                                                                                                                                      | Additive                                   | conversion | D/E  |
|------------------------------------------------------------------------------------------------------------------------------------------------------|--------------------------------------------|------------|------|
| <br>$[(\text{Me}_3\text{-TACN})_2\text{Mn}_2(\mu\text{-O})_3]^{2+}$ | $\text{CCl}_3\text{CO}_2\text{H}$ (1 mol%) | 91%        | 2:1  |
|                                                                                                                                                      | salicylic acid (1 mol %)                   | 82%        | 1:11 |
|                                                                                                                                                      | 2,6-dichlorobenzoic acid (3 mol%)          | 67%        | 7:1  |

**Scheme 22.** Schematic representation of  $[(\text{Me}_3\text{-TACN})_2\text{Mn}_2(\mu\text{-O})_3]^{2+}$  (left). Carboxylate promoted selectivity in the oxidation of cyclooctane (right).

As for the corresponding iron analogue catalyst, tetradentate N4 ligands also afforded good results. Stack and co-workers<sup>142</sup> reported a highly selective and efficient manganese complex with a nitrogen rich (*R,R*)-bpmcn ligand (see scheme 20). The catalyst rapidly (<5min) performed the epoxidation of a wide range of olefins at room temperature with low catalyst loadings using 1.2 equivalents of commercially available peracetic acid as a terminal oxidant. The reactions were readily scaled up from 5 mg to 25 g within minimal solvent volume, and the isolated yields were generally > 85%. However, only modest diastereoselectivity of the terminal olefin epoxidation was observed (15% is found in 8,9-monoepoxide from *R*-(-)-carvone).

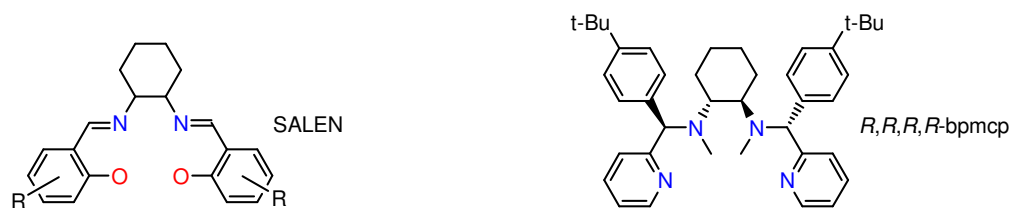
Very recently, our group reported a very robust and selective manganese catalyst based on a tetradentate ligand derived from triazacyclononane (<sup>H</sup>PyTACN, see scheme 20) that achieved up to 4500 TN using  $\text{H}_2\text{O}_2/\text{AcOH}$  for the epoxidation of styrene.<sup>143</sup>

On the other hand, state of the art metal catalyzed asymmetric epoxidation of olefins include Mn-SALEN,<sup>144-148</sup> (scheme 23) Mo-bishydroxamic acid,<sup>149</sup> Ru-oxazine catalysts systems<sup>150,151</sup> and Ti-SALAN/SALALEN complexes.<sup>152-155</sup>

The best example in asymmetric epoxidation by manganese catalysts are manganese-SALEN (see scheme 23) complexes developed simultaneously by Jacobsen and Katsuki.<sup>156</sup> Early inspired as simple and easy to prepare porphyrin-analogues complexes<sup>156</sup>, manganese-SALEN complexes<sup>144,145</sup> catalyze alkene epoxidation reactions in moderate to good yields (63-96%) with high enantioselectivities (>90% ee). Compared with chiral manganese porphyrin complexes, the use of Mn-SALEN catalyst generally results in higher ee's and yields. As for porphyrins, prominent chemoselectivity for *cis*-olefins over *trans*-olefins is observed for this catalyst, due to the near-planar geometry adopted by the ligand. The typical terminal oxidant is NaOCl, although other oxidants can be used. In most cases, using hydrogen peroxide as oxidant led to the formation of hydroxyl radicals ( $\cdot\text{OH}$ ), causing catalyst deactivation. However, urea/ $\text{H}_2\text{O}_2$  or  $\text{Ph}_3\text{P}(\text{O})/\text{H}_2\text{O}_2$  systems minimized this decomposition.<sup>4</sup> The main limitations of Mn-SALEN complexes are the relatively limited substrate scope, relatively high catalyst loading required (5-10%) and easily catalyst degradation, leaving many opportunities for improvement.

Enantioselective olefin epoxidation with non-SALEN manganese complexes results very challenging. One of the strategies employed oxazoline-derived ligands, however poor results

were obtained.<sup>157,158</sup> In the case reported by Pfaltz and co-workers modest stereoselectivity (up to 21%) was observed using a family of selected N4 diamino-bisoxazoline manganese complexes.<sup>158</sup>



**Scheme 23.** Schematic representation of the SALEN and *R,R,R,R*-bpmcp ligands used to prepare mononuclear manganese(II) complexes to perform olefin oxidations.

Asymmetric epoxidation reactions catalyzed by TACN-based chiral derivatives systems have also been explored,<sup>159-161</sup> but the catalysts somewhat suffer from low activity and modest stereoselectivity.

More recently, after the publication of our results with bpmcn-pinene ligands that promote asymmetric epoxidation with peracetic acid (see chapter IV), Xia and co-workers described the asymmetric epoxidation of alkenes with moderate to good enantiomeric excess,<sup>162</sup> by using bpmcn derivatives (*R,R,R,R*-bpmcp, see scheme 23) and  $\text{H}_2\text{O}_2/\text{AcOH}$ , achieving good ee's (70-80%) in the epoxidation of  $\alpha,\beta$ -enones. Enantiomeric excess are only moderate for other alkenes, similar to those reported by our group.

## 1.4.2. Supramolecular strategies for bioinspired oxidation catalysts

Chemist have developed a wide range of synthetic bioinspired catalysts (*vide supra*). Nonetheless, when compared to enzymes, these new systems are rather limited in performance, in particular with respect to substrate-, regio- and enantioselectivity. This is a direct consequence of the fact that in synthetic catalysts the second coordination sphere is generally ill-defined, whereas one of the enzymes' key features is their precisely defined substrate binding pocket. It allows selective binding of the substrate and stabilization of the transition state and the reaction intermediates for a particular transformation.

Therefore, to be an efficient enzyme mimic, the designed molecule needs to possess a binding cavity or site able to selectively recognize and bind a desired substrate with a particular proper orientation, which in the next step has to be converted at the catalytic center placed in direct proximity. Following this strategy, over the past few years, promising advances in the application of supramolecular chemistry in catalysis have been achieved.<sup>163</sup> Attempts have been made to merge synthetic catalysts with synthetic hosts to create artificial metalloenzymes with beneficial characteristics of both worlds. The basic concept of this is outlined in figure 5. A synthetic transition metal catalyst is connected to an anchor group, the anchor allowing immobilization of the metal catalysts within a binding pocket via covalent or noncovalent interactions.

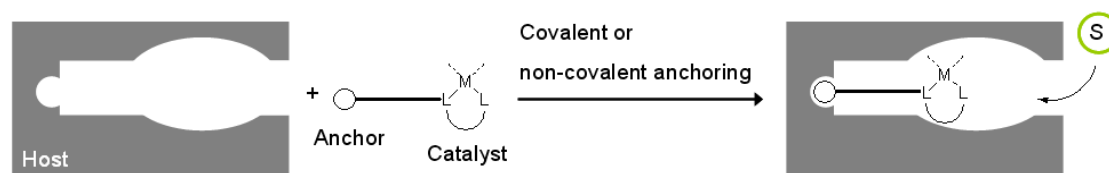


**Figure 5.** Synthesis of an artificial metalloenzyme by immobilization of a transition metal catalyst within the binding site of a host (S = substrate).

When the reacting functionalities are brought in close proximity, e.g., by binding a template/receptor or by inclusion into a molecular vessel, one of the observed benefits is rate acceleration due to an increase in the effective local concentration. In principle, cavities could be also used to bind reactants selectively, control reaction stereochemistry or protect highly active catalytic sites from interaction with species other than intended substrates.<sup>163</sup>

The design of supramolecular systems is challenging. First, it needs to recognize the reagents (which requires sufficiently strong binding) and second, needs to correctly orient the two reagents and bring them together. If the host has a higher affinity for the product than for the reagents, an additional problem comes into play: inhibition of turnover of the catalyst by the product. Although a host can not be regarded as truly catalytic if this occurs (stoichiometric amounts of host are required to achieve full conversion), the host can still accelerate the rate of the reaction and, interestingly may even influence the outcome of the reaction.

#### I.4.2.1 Design approaches to supramolecular catalysis

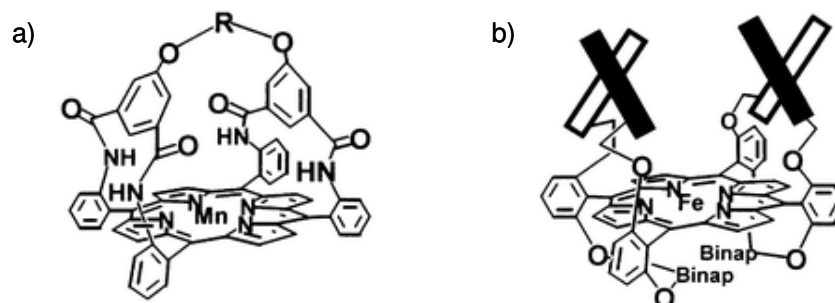
##### I.4.2.1.1. Covalent approach: Molecular receptors as substrate binding site irreversibly connected to the catalytic center

Inspired by the high efficiency displayed by enzymes, many scientists started in this research area by connecting known active sites (metal centers and other active groups) to known binding sites, anticipating that bringing them together would provide better catalysts in terms of selectivity and activity.<sup>163</sup> In this context, supramolecular catalysis is largely equivalent to mimicking enzymes via host-guest catalysis. Occasionally, enormous accelerations and changes in selectivity were noted but applications in synthetic chemistry remain elusive.<sup>163</sup>

Many approaches to synthesize low molecular weight oxidation catalysts, which contain a substrate covalently linked binding site that recognizes substrates next to the active site, have been described in the literature. Some examples are given in the next pages.

An extensively explored approach consists in using metalloporphyrins as the catalytic centre with modifications at its periphery to confer substrate recognition and selectivity. One of the first successful systems was developed by Collman's group with the so-called "picnic basket porphyrins" (scheme 24a).<sup>164-166</sup> These systems possess a rigid cavity on one face of the macrocycle that mimics the protein structure surrounding the active sites of enzymes. The unhindered face of manganese "picnic basket porphyrins" is blocked by 3,5-di-tert-butylphenoxide, an axial ligand too bulky to be coordinated inside the cavity. Selectivity in the

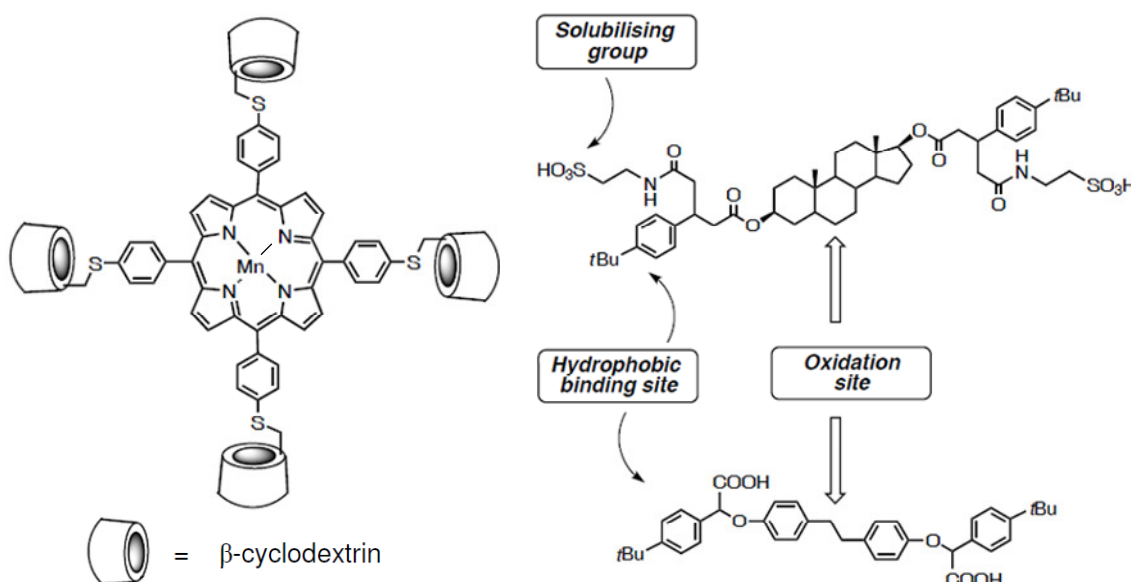
oxidation of olefins with different sizes was achieved. For example, “picnic basket porphyrins” are 60 to 1000 times more selective in competitive epoxidations of *cis*-2-octene and *cis*-cyclooctene (1:1) than MnTPP (TPP = *meso*-tetraphenylporphyrin). Chiral versions of those “picnic basket porphyrins” achieved moderate to good enantioselectivity (scheme 24b).<sup>166,70</sup>



**Scheme 24.** a) “Picnic basket” porphyrin model developed by Collman.<sup>164</sup> b) Eclipsed iron “bitetralins twin coronet porphyrin” epoxidize 3,5-dinitrostyrene with 96% ee.<sup>70</sup>

In contrast, Bhyrappa and co-workers prepared a new class of oxidatively robust dendrimer-metalloporphyrins as sterically hindered, shape-selective oxidation catalysts. The attached dendrimers favor the oxidation of less sterically hindered linear alkenes over cyclic alkenes.<sup>167</sup>

On the other hand, cyclodextrins (CDs) are naturally abundant cavity molecules that have been extensively used as binding sites in supramolecular catalysts. Breslow took advantage of their hydrophobic binding properties to design a selective supramolecular system, in which a manganese porphyrin was equipped with four covalently linked peripheral  $\beta$ -CDs (scheme 25).<sup>168,169</sup>

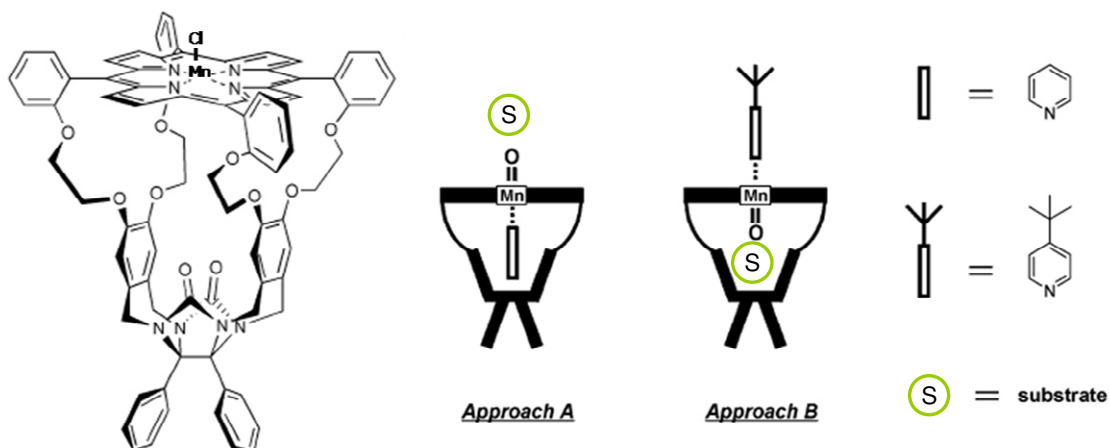


**Scheme 25.** Breslow manganese tetra- $\beta$ -cyclodextrin porphyrin (left) along with key aspects of substrate recognition and oxidation (right).<sup>168</sup>

In the presence of iodosyl benzene, this complex was capable of performing 650 TN of the selective hydroxylation of a dihydrostilbene derivative. Its superior selectivity is best illustrated by the fact that it can regio- and stereoselectively oxidize unactivated C-H bonds of an steroid derivative. The selectivity relies on a precise positioning of this C-H bond directly over the porphyrin metal center, caused by the encapsulation of the two *tert*-butylphenyl groups of the substrate by two *trans*-positioned CD cavities, as was concluded from molecular modeling calculations (scheme 25).

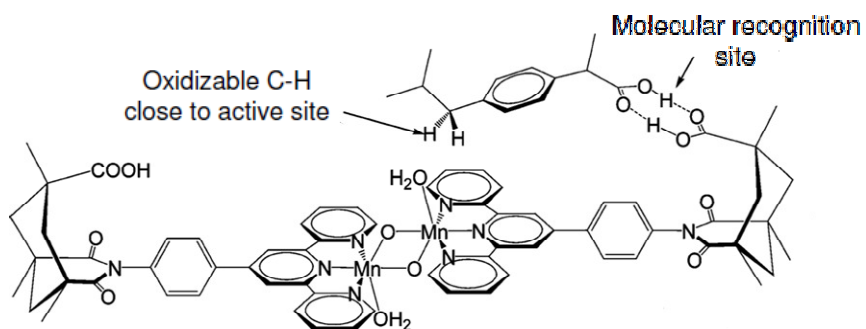
More recently, Nolte, Rowan and co-workers described a catalyst which consists of a substrate-binding cavity incorporating a manganese(III) porphyrin complex acting as the catalytic center (scheme 26).<sup>172</sup> A bulky axial ligand is attached at the outer face of the porphyrin catalyst, both activating the porphyrin complex and allowing a preferential (80%) oxidation of alkenes inside the cavity.

Moreover, the system was found to epoxidize the double bonds of a polybutadiene polymer strand when the polymer threaded into the catalyst cavity.<sup>173</sup> Thereby, it mimics the ability of processive enzymes to catalyze multiple rounds of reaction while the polymer substrate remains bound.



**Scheme 26.** Cavity containing manganese porphyrinic catalyst reported by Nolte, along with the catalytic approaches when it is combined with pyridine and *tert*-butylpyridine as the axial ligand.<sup>172</sup>

Crabtree and co-workers reported an innovative approach to the design of a bioinspired catalyst for the highly selective oxidation of C-H bonds. H-bonding mediates molecular recognition between substrate and ligand -COOH pending groups orienting the substrate towards the catalyst active site. Their system consist on a dimanganese-bis- $\mu$ -oxo terpyridine complex bearing a modified terpyridine ligand containing a molecular recognition group capable of binding carboxylic acid substrates (scheme 27). The oxygenation of saturated C-H bonds occurred with oxone as the primary oxidant in very high (<98%) regio and stereoselectivity with multi-hundred turnovers.<sup>131</sup> Surprisingly, oxidation of olefins was accomplished with much poorer regioselectivity.<sup>170</sup>



**Scheme 27.** Representation of substrate recognition by a dimanganese- $\mu$ -oxo terpyridine complex reported by Crabtree.<sup>131</sup>

A similar strategy was used by Schalz, Mirkin and co-workers, using one catalyst that combines a  $Mn^{III}$ -SALEN epoxidation catalysts with an amidopyridine receptor. In this case, hydrogen bonding between the amidopyridine receptor and the 4-vinylbenzoic acid favors the epoxidation of the latter in front of styrene, achieving inversion on product selectivity.<sup>171</sup> Remarkably, in this case they made use of coordination driven supramolecular assembly to bring together the catalyst and the recognition motive.

#### I.4.2.1.2. Non covalent approach: binding site of catalyst via reversible interactions

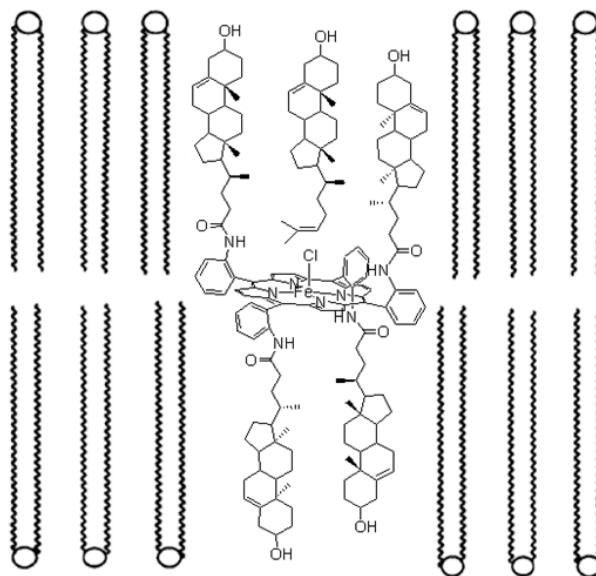
Covalently built structures with supramolecular recognition properties have proven their value as catalysts with impressive efficiencies and selectivities in several cases. However, as the scale and complexity of the target products increase, designing and preparing these catalysts in a covalent fashion rapidly becomes a very complex and time-consuming process. Moreover, the resulting catalysts are not so versatile because they are often highly specific to only a limited number of reactions. It is for this reason that in the past decade a shift has been observed in the approach to construct these catalysts, from traditional covalent chemistry to multicomponent self-assembly of relatively small complementary building blocks.

With the advances in supramolecular chemistry it is possible to construct a system in which all recognition motifs, both between the catalyst subunits and between substrate and the catalyst, are kinetically labile.

Noncovalent interactions normally lead to the rapid formation of bonds in an effective, reversible and strikingly apparently simple way. Typically, assembling through hydrogen-bonding and metal-ligand interactions is used. Hydrogen-bonding interactions are highly directional and specific, whereas metal-ligand bonds are generally much stronger, yielding more robust self-assembled structures. Chemists have exploited these features and have elegantly used reversible interactions to easily generate structurally diverse supramolecular ligands, compared to the use of standard covalent chemistry.<sup>163</sup> Some examples exist where the self-assembled systems display similar efficiencies and selectivities as those of their natural counterparts.

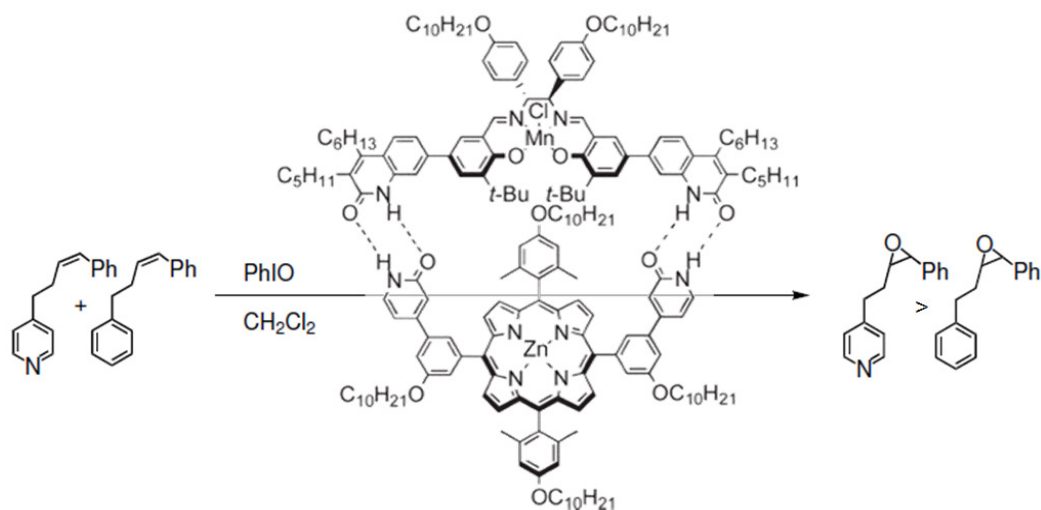
One of the most distinct examples of how nature uses self assembly of relatively simple building blocks to create organized structures is probably the cell membrane. The major constituents of the cell membrane are the phospholipids, amphiphilic molecules that self-assemble in water driven by the hydrophobic effect. Cytochrome P450 is a membrane-bound enzyme, a feature which prompted numerous research groups to design model systems in which metal porphyrins are incorporated in the bilayers of vesicle membranes.<sup>166</sup>

For example, Groves and Newmann reported a steroidal porphyrin intercalated to the center of the phospholipid bilayer, with the porphyrin ring orientated perpendicular to the phospholipids bilayer (scheme 28). In this configuration, iron tetra(*o*-cholonylamidophenyl)porphyrin obtained regioselectivity in the epoxidation at the side chain of steroids.<sup>174,175</sup> The double bond more distant from the hydroxyl group is selectively epoxidized, while Fe<sup>III</sup>TPPCI in CH<sub>2</sub>Cl<sub>2</sub> showed 3-4 fold preference for the nearest double bond from the hydroxyl group. A more complex self-assembled system was developed by Groves and improved by Nolte, in which the reductive activation of molecular oxygen by a Mn<sup>III</sup> porphyrin in an amphiphile bilayer is performed with the assistance of an assembled reductive agent.<sup>176,177</sup>



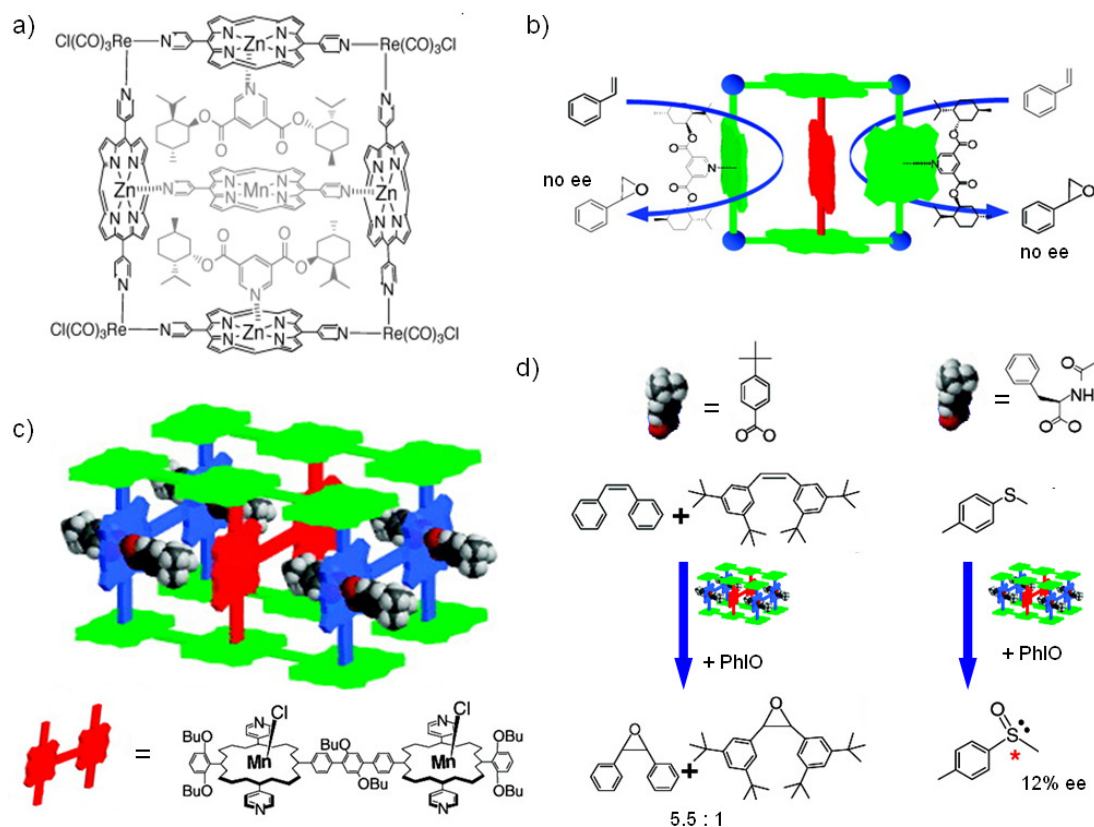
**Scheme 28.** Idealized molecular assembly of iron tetra-(*o*-cholonylamidophenyl)porphyrin and the phospholipid bilayer.<sup>174</sup>

A very different strategy was used by Wärnmark and co-workers. The formation of a dynamic supramolecular catalytic system involved a hydrogen bonding complex between a Mn<sup>III</sup>-SALEN catalyst and a Zn<sup>II</sup> porphyrin receptor (scheme 29).<sup>178</sup> The system exhibits only low selectivity for pyridine-appended styrene derivatives over phenyl-appended derivatives in a catalytic epoxidation reaction. Although not high, the observed selectivities serve as a proof of concept, thus weak, kinetically labile interactions can in fact be successfully applied to the design of supramolecular catalysts.



**Scheme 29.** Dynamic supramolecular assembly formed by hydrogen bonding interactions between a manganese SALEN catalyst and a zinc porphyrin receptor along with the reaction catalyzed.<sup>178</sup>

Using a very elegant concept, Nguyen and Hupp have demonstrated the self-assembly and encapsulation of both the catalysts and the substrate within a molecular nanosquare.<sup>179</sup> The system is constructed in a single step and in quantitative yield by coordination of four zinc porphyrins via their pyridyl ligands to four tris(carbonyl)rhenium chloride centers.



**Scheme 30.** a) Self-assembled protective encapsulation of Hupp and Nguyen catalyst in the presence of a chiral and cavity size control additive. b) More realistic representation of the chiral environment inside the pentaporphyrin catalyst assembly. c) Supramolecular rigid catalytic box reported by the same group. d) Size selective catalytic oxidation of alkanes and enantioselective oxidation of methyl *p*-tolyl sulfide.<sup>179,180</sup>



Protective encapsulation of the manganese porphyrin (scheme 30a) moiety was found to stabilize the catalyst, extending its lifetime for olefin epoxidation by an order of magnitude or more. Moreover, the molecular nanosquare also induced substrate size selectivity by preventing access of bulky substrates to the active site. Dilution of the catalysts with respect to the capsules resulted in impressive turnover numbers of up to 21000 (<500 TN for non encapsulated porphyrin) as a result of enhanced protective encapsulation. The effective cavity size of the system could be further tuned by the coordination of pyridine derived axial ligands to the zinc ions in the cavities of the capsule. It allows tailor substrate size selectivity but enantioselectivity is not achieved. A plausible explanation is ligand binding at the outer face of the cavity (rather than within), the cavity and torsional freedom of the cavity walls and the encapsulated catalyst (scheme 30b).

Those limitations were avoided by the same group with the design of porphyrin building blocks that can assemble into rigid cavity-tailored catalytic supramolecular boxes in order to form highly stable assemblies (scheme 30c and 30d).<sup>180</sup> These assemblies readily effect size selective olefin epoxidation. Furthermore, when the cavity is modified with a chiral amino acid ligand, asymmetric catalysis via through-space control of the chiral cavity in sulfoxidation was achieved.

## I.5. References

1. Mijs, W. J.; de Jonge, C. R. H. I. *Organic Synthesis by Oxidation with Metal Compounds*; Plenum Press: New York, 1986.
2. Sheldon, R. A.; Kochi, J. A. *Metal-Catalyzed Oxidations of Organic Compounds*; Academic Press: New York, 1981.
3. Hudlicky, M. *Oxidation in Organic Chemistry*; ACS Monograph Ser. 186, American Chemical Society: Washington D.C., 1990.
4. Bäckvall, J. E. *Modern oxidation Methods*; Wiley-VCH: Weinheim, 2004.
5. Kirk-Othmer *Encyclopedia of Chemical Technology*, 3rd ed.; John Wiley & Sons: New York, 1980; Vol. 9, pp 251-274.
6. March, J. *Advanced Organic Chemistry*, 3rd ed.: New York, 1985.
7. Schröder, M. *Chem. Rev.* **1980**, *80*, 187-213.
8. Kolb, H. C.; VanNieuwenhze, M. S.; Sharpless, K. B. *Chem. Rev.* **1994**, *94*, 2483-2547.
9. Beller, M.; Sharpless, K. B. *Applied Homogeneous Catalysis*; VCH: Weinheim, 1996.
10. Hentges, S. G.; Sharpless, K. B. *J. Am. Chem. Soc.* **1980**, *102*, 4263-4265.
11. Sharpless, K. B.; Amberg, W.; Bennani, Y. L.; Crispino, G. A.; Hartung, J.; Jeong, K.-S.; Kwong, H.-L.; Morikawa, K.; Wang, Z.-M.; Xu, D.; Zhang, X.-L. *J. Org. Chem.* **1992**, *57*, 2768-2771.
12. Sheldon, R. A. In *Biomimetic Oxidations Catalyzed by Transition Metal Complexes*; Meunier, B. Ed.; Imperial College Press: London, 2000; pp. 613-662.
13. Noyori, R.; Aoki, M.; Sato, K. *Chem. Commun.* **2003**, 1977–1986.
14. Lane, B. S.; Burgess, K. *Chem. Rev.* **2003**, *103*, 2457-2474.
15. Sheldon, R. A., Kochi, J. A. *Metal-Catalyzed Oxidations of Organic Compounds*; Academic Press: New York, 1981.
16. Barton, D. H. R.; Doller, D. *Acc. Chem. Res.* **1992**, *25*, 504-512.
17. Curci, R.; d'Accolti, L.; Fusco, C. *Acc. Chem. Res.* **2006**, *39*, 1-9.
18. Bertini, I.; Gray, H. B.; Stiefel, E. I.; Valentine, S. J. *Biological inorganic Chemistry: structure & reactivity*; University Science Books: Sausalito, California, 2007.
19. Kraatz, H.-B.; Metzler-Nolte, N. *Concepts and Models in Bioinorganic Chemistry*; Wiley-VCH: Weinheim, 2006.
20. Meunier, B.; Bernadou, J. *Struct. Bonding* **2000**, *97*, 1-35.
21. Meunier, B.; de Visser, S. P.; Shaik, S. *Chem. Rev.* **2004**, *104*, 3947-3980.

22. Montellano, P. O. d. *Cytochrome P450 : Structure, Mechanism, and Biochemistry*, 3rd ed.; Springer ed.: New York, 2005.
23. Schlichting, I.; Berendzen, J.; Chu, K.; Stock, A. M.; Maves, S. A.; Benson, D. E.; Sweet, R. M.; Ringe, D.; Petsko, G. A.; Sligar, S. G. *Science* **2000**, *287*, 1615-1622.
24. Tshuva, E. Y.; Lippard, S. J. *Chem. Rev.* **2004**, *104*, 987-1012.
25. Costas, M.; Mehn, M. P.; Jensen, M. P.; Que Jr., L. *Chem. Rev.* **2004**, *104*, 939-986.
26. Abu-Omar, M. M.; Loaiza, A.; Hontzeas, N. *Chem. Rev.* **2005**, *105*, 2227-2252.
27. Solomon, E. I.; Brunold, T. C.; Davis, M. I.; Kemsley, J. N.; Lee, S.-K.; Lehnert, N.; Neese, F.; Skulan, A. J.; Yang, Y.-S.; Zhou, J. *Chem. Rev.* **2000**, *100*, 235-349.
28. Bruijninx, P. C. A.; van Koten, G.; Klein Gebbink, R. J. M. *Chem. Soc. Rev.* **2008**, *37*, 2716 - 2744.
29. Gibson, D. T.; Subramanian, V. In *Microbial Degradation of Aromatic Hydrocarbons*; Gibson, D. T. Ed.; Marcel Dekker: New York, 1984; pp. 181-251.
30. Cotton, F. A.; Wilkinson, G.; Murillo, C. A.; Bochmann, M. In *Advanced Inorganic Chemistry*; John Wiley & Sons: New York, 1999.
31. Price, J. C.; Barr, E. W.; Tirupati, B.; Bollinger Jr., J. M.; Krebs, C. *Biochemistry* **2003**, *42*, 7497-7508.
32. Hoffart, L. M.; Barr, E. W.; Guyer, R. B.; Bollinger Jr., J. M.; Krebs, C. *Proc. Natl. Acad. Sci. USA* **2006**, *103*, 14738-14743.
33. Eser, B. E.; Barr, E. W.; Frantom, P. A.; Saleh, L.; Bollinger Jr., J. M.; Krebs, C.; Fitzpatrick, P. F. *J. Am. Chem. Soc.* **2007**, *129*, 11334-11335.
34. Galonic, D. P.; Barr, E. W.; Walsh, C. T.; Bollinger Jr., J. M.; Krebs, C. *Nat. Chem. Biol.* **2007**, *3*, 113-116.
35. Wallar, B. J.; Lipscomb, J. D. *Chem. Rev.* **1996**, *96*, 2625-2658.
36. Groves, J. T.; McCluskey, G. A. *J. Am. Chem. Soc.* **1976**, *98*, 859-861.
37. Sono, M.; Roach, M. P.; Coulter, E. D.; Dawson, J. H. *Chem. Rev.* **1996**, *96*, 2841-2887.
38. Gibson, D. T.; Resnick, S. M.; Lee, K.; Brand, J. M.; Torok, D. S.; Wackett, L. P.; Schocken, M. J.; Haigler, B. E. *J. Bacteriol.* **1995**, *177*, 2615-2621.
39. Wolfe, M. D.; Parales, J. V.; Gibson, D. T.; Lipscomb, J. D. *J. Biol. Chem.* **2001**, *276*, 1945-1953.
40. Gibson, D. T.; Parales, R. E. *Curr. Opin. Biotechnol.* **2000**, *11*, 236-243.
41. Hudlicky, T.; Gonzalez, D.; Gibson, D. T. *Aldrichimica Acta* **1999**, *32*, 35-62.

42. Kauppi, B.; Lee, K.; Carredano, E.; Parales, R. E.; Gibson, D. T.; Eklund, H.; Ramaswamy, S. *Structure* **1998**, *6*, 571-586.
43. Wolfe, M. D.; Altier, D. J.; Stubna, A.; Popescu, C. V.; Münck, E.; Lipscomb, J. D. *Biochemistry* **2002**, *41*, 9611-9626.
44. Gibson, D. T.; Yeh, W.-K.; Liu, T.-N.; Subramanian, V. In *Oxygenases and Oxygen Metabolism* Ed. Academic: New York, 1982; pp. 51-62.
45. Crutcher, S. E.; Geary, P. J. *Biochem. J.* **1979**, *177*, 393-400.
46. Pavel, E. G.; Martins, L. J.; Ellis, W. R., Jr.; Solomon, E. I. *Chem. Biol.* **1994**, *1*, 173-183.
47. Hegg, E. L.; Que Jr., L. *Eur. J. Biochem.* **1997**, *250*, 625-629.
48. Koehntop, K., D.; Emerson, J. P.; Que Jr., L. *J. Biol. Inorg. Chem.* **2005**, *10*, 87-93.
49. Karlsson, A.; Parales, J. V.; Parales, R. E.; Gibson, D. T.; Eklund, H.; Ramaswamy, S. *Science* **2003**, *299*, 1039-1042.
50. Wolfe, M. D.; Lipscomb, J. D. *J. Biol. Chem.* **2003**, *278*, 829-835.
51. Leuenberger, M. G.; Engeloch-Jarret, C.; Woggon, W. D. *Angew. Chem. Int. Ed.* **2001**, *40*, 2613-2617.
52. Kloer, D. P.; Ruch, S.; Al-Babili, S.; Beyer, P.; Schulz, G. E. *Science* **2005**, *308*, 267-269.
53. Whiting, A. K.; Boldt, Y. R.; Hendrich, M. P.; Wackett, L. P.; Que Jr., L. *Biochemistry* **1996**, *35*, 160-170.
54. Vetting, M. W.; Wackett, L. P.; Que Jr., L.; Lipscomb, J. D.; Ohlendorf, D. H. *J. Bacteriol.* **2004**, *186*, 1945-1958.
55. Emerson, J. P.; Kovaleva, E. G.; Farquhar, E. R.; Lipscomb, J. D.; Que Jr., L. *PNAS* **2008**, *105*, 7347-7352.
56. Lah, M. S.; Dixon, M. M.; Patridge, K. A.; Stallings, W. C.; Fee, J. A.; Ludwig, M. L. *Biochemistry* **1995**, *34*, 1646-1660.
57. Vance, C. K.; Miller, A.-F. *J. Am. Chem. Soc.* **1998**, *120*, 461-467.
58. Boyington, J. C.; Gaffney, B. J.; Amzel, L. M. *Science* **1993**, *260*, 1482-1486.
59. Skrzypczak-Jankun, E.; Bross, R. A.; Carroll, R. T.; Dunham, W. R.; Funk, M. O., Jr. *J. Am. Chem. Soc.* **2001**, *123*, 10814-10820.
60. Su, C. O.; H., E. *J. Biol. Chem.* **1998**, *273*, 13072-13079.
61. Meunier, B. *Chem. Rev.* **1992**, *92*, 1411-1456.
62. Groves, J. T.; Nemo, T. E.; Myers, R. S. *J. Am. Chem. Soc.* **1979**, *101*, 1032-1033.

63. Katsuki, T. *Coord. Chem. Rev.* **1995**, *143*, 189-214.
64. Renaud, J.-P.; Battioni, P.; Bartoli, J.-F.; Mansuy, D. *Chem. Comm.* **1985**, 888-889.
65. Anelli, P. L.; Banfi, S.; Montari, F.; Quici, S. *Chem. Commun.* **1989**, 779-7780.
66. Banfi, S.; Legramandi, F.; Montari, F.; Pozzi, G.; Quici, S. *Chem. Comm.* **1991**, 1285-1287.
67. Anelli, P. L.; Banfi, L.; Legramandi, F.; Montari, F.; Pozzi, G.; Quici, S. *J. Chem. Soc. Perkin Trans. 1* **1993**, 1345-1357.
68. Groves, J. T.; Myers, R. S. *J. Am. Chem. Soc.* **1983**, *105*, 5791-5796.
69. Campbell, L. A.; Kodadek, T. *J. Mol. Cat. A: Chem.* **1996**, *113*, 293-310.
70. Collman, J. P.; Zhang, X.; Lee, V. J.; Uffelman, E. S.; Brauman, J. I. *Science* **1993**, *261*, 1404-1411.
71. Naruta, Y.; Sasayama, M.-a.; Sadaki, T. *Angew. Chem. Int. Ed. Engl.* **1994**, *33*, 1839-1841.
72. Collman, J. P.; Wang, Z.; Straumanis, A.; Quejquejeu, M. *J. Am. Chem. Soc.* **1999**, *121*, 460-461.
73. Sawyer, D. T.; Sobkowiak, A.; Matsushita, T. *Acc. Chem. Res.* **1996**, *29*, 409-416.
74. MacFaul, P. A.; Wayner, D. D. M.; Ingold, K. U. *Acc. Chem. Res.* **1998**, *31*, 159-162.
75. Walling, C. *Acc. Chem. Res.* **1998**, *31*, 155-157.
76. Groves, J. T.; Van Der Puy, M. *J. Am. Chem. Soc.* **1976**, *98*, 5290-5297.
77. Stavropoulos, P.; Celenligil-Cetin, R.; Tapper, A. E. *Acc. Chem. Res.* **2001**, *34*, 745-752.
78. Trettenhahn, G.; Nagl, M.; Neuwirth, N.; Arion, V. B.; Jary, W.; Pöchlauer, P.; Schmid, W. *Angew. Chem. Int. Ed.* **2006**, *45*, 2794-2798.
79. Romakh, V. B.; Therrien, B.; Süss-Fink, G.; Shul'pin, G. B. *Inorg. Chem.* **2007**, *46*, 3166-3175.
80. Retcher, B.; Sánchez Costa, J.; Tang, J.; Hage, R.; Gamez, P.; Reedijk, J. *J. Mol. Cat. A: Chem.* **2008**, *286*, 1-5.
81. Tang, J.; Gamez, P.; Reedijk, J. *Dalton Trans.* **2007**, *41*, 4644-4646.
82. Costas, M.; Chen, K.; Que Jr., L. *Coord. Chem. Rev.* **2000**, *200-202*, 517-544.
83. Kim, C.; Chen, K.; Kim, J.; Que Jr., L. *J. Am. Chem. Soc.* **1997**, *119*, 5964-5965.
84. Mekmouche, Y.; Ménage, S.; Pécaut, J.; Lebrun, C.; Reilly, L.; Schuenemann, V.; Trautwein, A.; Fontecave, M. *Eur. J. Inorg. Chem.* **2004**, 3163-3171.
85. Chen, K.; Que Jr., L. *Chem. Commun.* **1999**, 1375-1376.

86. Chen, K.; Que Jr., L. *J. Am. Chem. Soc.* **2001**, *123*, 6327-6337.
87. Company, A.; Gómez, L.; Güell, M.; Ribas, X.; Luis, J. M.; Que Jr., L.; Costas, M. *J. Am. Chem. Soc.* **2007**, *129*, 15766-15767.
88. Company, A.; Gómez, L.; Fontrodona, X.; Ribas, X.; Costas, M. *Chem. Eur. J.* **2008**, *14*, 5727-5731.
89. England, J.; Britovsek, G. J. P.; Rabadia, N.; White, A. J. P. *Inorg. Chem.* **2007**, *46*, 3752-3767.
90. Costas, M.; Que Jr., L. *Angew Chem. Int. Ed.* **2002**, *41*, 2179-2181.
91. England, J.; Gondhia, R.; Bigorra-Lopez, L.; Petersen, A. R.; White, A. J. P.; Britovsek, G. J. P. *Dalton Trans.* **2009**, *27*, 5319-5334.
92. Britovsek, G. J. P.; England, J.; Spitzmesser, S. K.; White, A. J. P.; Williams, D. J. *Dalton Trans.* **2005**, 945-955.
93. Britovsek, G. J. P.; England, J.; White, A. J. P. *Dalton Trans.* **2006**, *11*, 1399-1408.
94. England, J.; Davies, C. R.; Banaru, M.; White, A. J. P.; Britovsek, G. J. P. *Adv. Synth. Catal.* **2008**, *350*, 883-897.
95. Chen, M. S.; White, M. C. *Science* **2007**, *318*, 783-787.
96. Nam, W.; Ho, R. Y. N.; Valentine, J. S. *J. Am. Chem. Soc.* **1991**, *113*, 7052-7054.
97. Francis, M. B.; Jacobsen, E. N. *Angew. Chem. Int. Ed.* **1999**, *38*, 937 - 941.
98. White, M. C.; Doyle, A. G.; Jacobsen, E. N. *J. Am. Chem. Soc.* **2001**, *123*, 7194-7195.
99. Mas-Balleste, R.; Que Jr., L. *J. Am. Chem. Soc.* **2007**, *129*, 15964-15972.
100. Yeung, H.-L.; Sham, K.-C.; Tsang, C.-S.; Lau, T.-C.; Kwong, H.-L. *Chem. Commun.* **2008**, 3801-3803.
101. Dubois, G.; Murphy, A.; Stack, T. D. P. *Org. Lett.* **2003**, *5*, 2469-2472.
102. Marchi-Delapierre, C.; Jorge-Robin, A.; Thibon, A.; Ménage, S. *Chem. Commun.* **2007**, 1166-1168.
103. Anilkumar, G.; Bitterlich, B.; Gelalcha, F. G.; Tse, M. K.; Beller, M. *Chem. Commun.* **2007**, 289-291.
104. Bitterlich, B.; Schröder, K.; Tse, M. K.; Beller, M. *Eur. J. Org. Chem.* **2008**, 4867-4870.
105. Gelalcha, F. G.; Bitterlich, B.; Anilkumar, G.; Tse, M. K.; Beller, M. *Angew Chem. Int. Ed.* **2007**, *46*, 7293-7296.
106. Gelalcha, F. G.; Anilkumar, G.; Tse, M. K.; Brückner, A.; Beller, M. *Chem. Eur. J.* **2008**, *14*, 7687-7698.

107. Schröder, K.; Enthaler, S.; Bitterlich, B.; Schulz, T.; Spannenberg, A.; Tse, M. K.; Junge, K.; Beller, M. *Chem. Eur. J.* **2009**, *15*, 5471-5481.
108. Oldenburg, P. D.; Que Jr., L. *Catal. Today* **2006**, *117*, 15-21.
109. Chen, K.; Costas, M.; Kim, J.; Tipton, A. K.; Que Jr., L. *J. Am. Chem. Soc.* **2002**, *124*, 3026-3035.
110. Suzuki, K.; Oldenburg, P. D.; Que Jr., L. *Angew. Chem. Int. Ed.* **2008**, *47*, 1887-1889.
111. Bautz, J.; Comba, P.; Lopez de Laorden, C.; Menzel, M.; Rajaraman, G. *Angew. Chem. Int. Ed.* **2007**, *46*, 8067-8070.
112. Quiñonero, D.; Morokuma, K.; Musaev, D. G.; Mas-Balleste, R.; Que, J., L. *J. Am. Chem. Soc.* **2005**, *127*, 6548-6549.
113. Klopstra, M.; Roelfes, G.; Hage, R.; Kellogg, B. H.; Feringa, B. L. *European Journal of Inorganic Chemistry* **2004**, 846-856.
114. Costas, M.; Tipton, A. K.; Chen, K.; Jo, D.-H.; Que Jr., L. *J. Am. Chem. Soc.* **2001**, *123*, 6722-6723.
115. Mas-Ballesté, R.; Costas, M.; Berg, T. v. d.; Que Jr., L. *Chem. Eur. J.* **2006**, *12*, 7489-7500.
116. Oldenburg, P. D.; Shteinman, A. A.; Que Jr., L. *J. Am. Chem. Soc.* **2005**, *127*, 15672-15673.
117. Bruijninx, P. C. A.; Buurmans, I. L. C.; Gosiewska, S.; Moelands, M. A. H.; Lutz, M.; Spek, A. L.; Koten, G. v.; Klein Gebbink, R. J. M. *Chem. Eur. J.* **2008**, *14*, 1228 – 1237.
118. Gosiewska, S.; Lutz, M.; Spek, A. L.; Gebbink, R. J. M. *Inorganica Chimica Acta* **2007**, *360*, 405-417.
119. Bukowski, M. R.; Comba, P.; Lienke, A.; Limberg, C.; Lopez de Laorden, C.; Mas-Ballesté, R.; Merz, M.; Que Jr., L. *Angew. Chem. Int. Ed.* **2006**, *45*, 3446-3449.
120. Chen, K.; Que Jr., L. *Angew. Chem. Int. Ed.* **1999**, *38*, 2227-2229.
121. Feng, Y.; Ke, C.; Xue, G.; Que Jr., L. *Chem. Comm.* **2009**, 50-52.
122. Ryu, J. Y.; Kim, J.; Costas, M.; Chen, K.; Nam, W.; Que Jr., L. *Chem. Commun.* **2002**, *12*, 1288-1289.
123. Wieghardt, K.; Bossek, U.; Nuber, B.; Weiss, J.; Bonvoison, J.; Corbella, M.; Vitols, S. E.; Girerd, J. J. *J. Am. Chem. Soc.* **1988**, *110*, 7398-7411 and references cited therein.
124. Hage, R.; Iburg, J. E.; Kerschner, J.; Koek, J. H.; Lempers, E. L. M.; Martens, R. J.; Racherla, U. S.; Russell, S. W.; Swarthoff, T.; van Vliet, M. R. P.; Warnaar, J. B.; van der Wolf, L.; Krijnen, B. *Nature* **1994**, *369*, 637.

125. Brinksma, J.; de Boer, J. W.; Hage, R.; Feringa, B. L. In *Manganese-based Oxidation with Hydrogen Peroxide*; Wiley-VCH, 2004.
126. Sibbons, K. F.; Shastri, K.; Watkinson, M. *Dalton Trans.* **2006**, 645-661.
127. Smith, J. R. L.; Shul'pin, G. B. *Tetrahedron Lett.* **1998**, *39*, 4909-4912.
128. Shul'pin, G. B.; Smith, J. R. L. *Russ. Chem. Bull* **1998**, *47*, 2379-2386.
129. Shul'pin, G. B.; Süss-Fink, G.; Smith, J. R. L. *Tetrahedron* **1999**, *55*, 5345-5358.
130. Shul'pin, G. B.; Süss-Fink, G.; Shul'pina, L. S. *J. Mol. Catal. A: Chem.* **2001**, *170*, 17-34.
131. Das, S.; Incarvito, C. D.; Crabtree, R. H.; Brudvig, G. W. *Science* **2006**, *312*, 1941-1943.
132. Nehru, K.; Kim, S. J.; Kim, I. Y.; Seo, M. S.; Kim, Y.; Kim, S.-J.; Kim, J.; Nam, W. *Chem. Comm.* **2007**, 4623-4625.
133. Lane, B. S.; Burgess, K. *J. Am. Chem. Soc.* **2001**, *123*, 2933-2934.
134. Lane, B. S.; Vogt, M.; DeRose, J.; Burgess, K. *J. Am. Chem. Soc.* **2002**, *124*, 11946-11954.
135. Tong, K.-H.; Wong, K.-Y.; Chan, T. H. *Org. Lett.* **2003**, *5*, 3423-3425.
136. Quee-Smith, V. C.; Delpizzo, L.; Jureller, S. H.; Kerschner, J. L.; Hage, R. *Inorg. Chem.* **1996**, *35*, 6461-6455.
137. De Vos, D. E.; Sels, B. F.; Reynaers, M.; Subba Rao, Y. V.; Jacobs, P. A. *Tetrahedron Lett.* **1998**, *39*, 3221-3224.
138. de Boer, J. W.; Alsters, P. L.; Meetsma, A.; Hage, R.; Browne, W. R.; Feringa, B. L. *Dalton Trans.* **2008**, *44*, 6283-6295.
139. de Boer, J. W.; Brinksma, J.; Browne, W. R.; Meetsma, A.; Alsters, P. L.; Hage, R.; Feringa, B. L. *J. Am. Chem. Soc.* **2005**, *127*, 7990-7991.
140. de Boer, J. W.; Browne, W. R.; Brinksma, J.; Alsters, P. L.; Hage, R.; Feringa, B. L. *Inorg. Chem.* **2007**, *46*, 6353-6372.
141. de Boer, J. W.; Browne, W. R.; Harutyunyan, S. R.; Bini, L.; Tiemersma-Wegman, T. D.; Alsters, P. L.; Hage, R.; Feringa, B. L. *Chem. Comm.* **2008**, *32*, 3747-3749.
142. Murphy, A.; Dubois, G.; Stack, T. D. P. *J. Am. Chem. Soc.* **2003**, *125*, 5250-5251.
143. Garcia-Bosch, I.; Ribas, X.; Costas, M. *Adv. Synth. Catal.* **2009**, *351*, 348-352.
144. Jacobsen, E. N.; Zhang, W.; Muci, A. R.; Ecker, J. R.; Deng, L. *J. Am. Chem. Soc.* **1991**, *113*, 7063-7064.
145. Zhang, W.; Loebach, J. L.; Wilson, S. R.; Jacobsen, E. N. *J. Am. Chem. Soc.* **1990**, *112*, 2801-2803.



146. Palucki, M.; Pospisil, P. J.; Zhang, W.; Jacobsen, E. N. *J. Am. Chem. Soc.* **1994**, *116*, 9333-9334.
147. Palucki, M.; McCormick, G. J.; Jacobsen, E. N. *Tetrahedron Lett.* **1995**, *36*, 5457-5460.
148. Palucki, M.; Finney, N. S.; Pospisil, O. J.; Güler, M. L.; Ishida, T. T.; Jacobsen, E. N. *J. Am. Chem. Soc.* **1998**, *120*, 948-954.
149. Barlan, A. U.; Basak, A.; Yamamoto, H. *Angew. Chem. Int. Ed.* **2006**, *45*, 5849-5852.
150. Tse, M. K.; Bhor, S.; Klawonn, M.; Anilkumar, G.; Jiao, H.; Döbler, C.; Spannenberg, A.; Mägerlein, W.; Hugl, H.; Beller, M. *Chem. Eur. J.* **2006**, *12*, 1855-1874.
151. Tse, M. K.; Bhor, S.; Klawonn, M.; Anilkumar, G.; Jiao, H.; Spannenberg, A.; Döbler, C.; Mägerlein, W.; Hugl, H.; Beller, M. *Chem. Eur. J.* **2006**, *12*, 1875-1888.
152. Matsumoto, K.; Sawada, Y.; Saito, B.; Sakai, K.; Katsuki, T. *Angew. Chem. Int. Ed.* **2005**, *44*, 4935-4939.
153. Sawada, Y.; Matsumoto, K.; Kondo, S.; Watanabe, H.; Ozawa, T.; Suzuki, K.; Saito, B.; Katsuki, T. *Angew. Chem. Int. Ed.* **2006**, *45*, 3478-3480.
154. Sawada, Y.; Matsumoto, K.; Katsuki, T. *Angew. Chem. Int. Ed.* **2007**, *46*, 4559-4561.
155. Matsumoto, K.; Oguma, T.; Katsuki, T. *Angew. Chem. Int. Ed.* **2009**, 7432-7435.
156. Ojima, I., Ed. *Catalytic Asymmetric Synthesis*, 2nd ed.; Wiley-VCH: New York, 2000.
157. Godbole, M. D.; Hotze, A. C. G.; Hage, R.; Mills, A. M.; Kooijman, H.; Spek, A. L.; Bouwman, E. *Inorg. Chem.* **2005**, *44*.
158. Guillemot, G.; Neuburger, M.; Pfaltz, A. *Chem. Eur. J.* **2007**, *13*, 8960-8970.
159. Bolm, C.; Kadereit, D.; Valacchi, M. *Synlett* **1997**, 687-688.
160. Bolm, C.; Meyer, N.; Raabe, G.; Weyhermüller, T.; Bothe, E. *Chem. Comm.* **2000**, 2435-2436.
161. Romakh, V. B.; Therrien, B.; Suss-Fink, G.; Shul'pin, G. B. *Inorg. Chem.* **2007**, *46*, 1315-1331.
162. Wu, M.; Wang, B.; Wang, S.; Xia, C.; Sun, W. *Org. Lett.* **2009**, *11*, 3622-3625.
163. Leeuwen, P. W. N. M. v., Ed. *Supramolecular Catalysis*; WILEY-VCH: Weinheim, 2008.
164. Collman, J. P.; Brauman, J. I.; Fitzgerald, J. P.; Hampton, P. D.; Maruta, Y.; Michida, T. *Bull. Chem. Soc. Jpn.* **1988**, *61*, 47-57.
165. Collman, J. P.; Lee, V. J.; Zhang, X.; Ibers, J. A.; Brauman, J. I. *J. Am. Chem. Soc.* **1993**, *115*, 3834-3835.
166. Feiters, M. C.; Rowan, A. E.; Nolte, R. J. M. *Chem. Soc. Rev.* **2000**, *29*, 375-384.

167. Bhyrappa, P.; Young, J. K.; Moore, J. S.; Suslick, K. S. *J. Am. Chem. Soc.* **1996**, *118*, 5708-5711.
168. Breslow, R.; Huang, Y.; Zhang, X.; Yang, J. *Proc. Acad. Sci. USA* **1997**, *94*, 11156-11158.
169. Breslow, R.; Gabriele, B.; Yang, J. *Tetrahedron Letters* **1998**, *39*, 2887-2890.
170. Hull, J. F.; Sauer, E. L. O.; Incarvito, C. D.; Faller, J. W.; Brudvig, G. W.; Crabtree, R. H. *Inorg. Chem.* **2008**, *48*, 488-495.
171. Ulmann, P. A.; Braunschweig, A. B.; Lee, O.-S.; Wiester, M. J.; Schatz, G. C.; Mirkin, C. A. *Chem. Comm.* **2009**, *34*, 5121-5123.
172. Elemans, J. A. A. W.; Bijsterveld, E. J. A.; Rowan, A. E.; Nolte, R. J. M. *Chem. Commun.* **2000**, 2443-2444.
173. Thordarson, P.; Bijsterveld, E. J. A.; Rowan, A. E.; Nolte, R. J. M. *Nature* **2003**, *424*, 915-918.
174. Groves, J. T.; Neumann, R. *J. Am. Chem. Soc.* **1987**, *109*, 5045-5047.
175. Groves, J. T.; Neumann, R. *J. Am. Chem. Soc.* **1989**, *111*, 2900-2909.
176. Groves, J. T.; Ungashe, S. B. *J. Am. Chem. Soc.* **1990**, *112*, 7796-7797.
177. Schenning, A. P. H. J.; Hubert, D. H. W.; van Esch, J. H.; Feiters, M. C.; Nolte, R. J. M. *Angew. Chem. Int. Ed.* **1994**, *33*, 2468-2470.
178. Jonsson, S.; Odille, F. G. J.; Norrby, P.-O.; Warnmark, K. *Chem. Comm.* **2005**, 549-551.
179. Merlau, M. L.; Mejia, M. d. P.; Nguyen, S. T.; Hupp, J. T. *Angew Chem. Int. Ed.* **2001**, *40*, 4239-4242.
180. Lee, S. J.; Cho, S.-H.; Mulfort, K. L.; Tiede, D. M.; Hupp, J. T.; Nguyen, S. T. *J. Am. Chem. Soc.* **2008**, *130*, 16828-16829.

## **CHAPTER II**

---

### **Main Objectives**

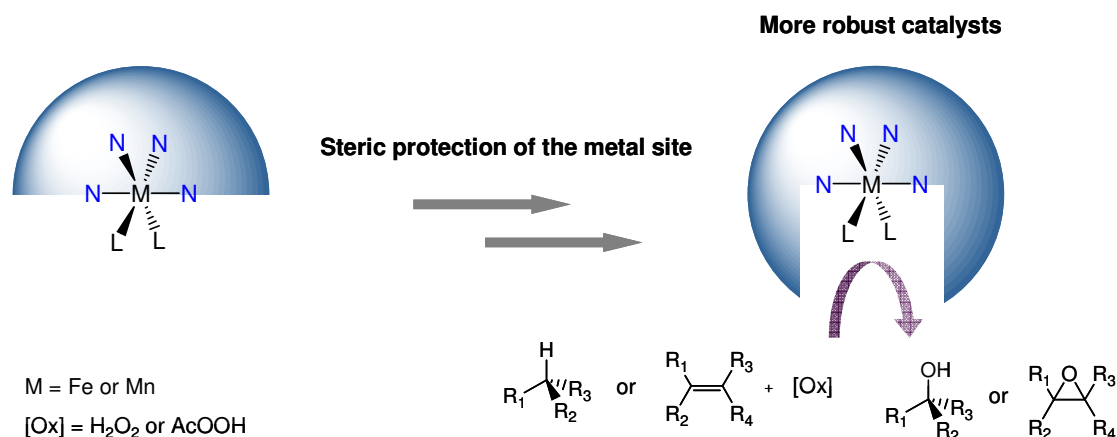
---



## II. Main objectives

Inspired by the efficiency, selectivity and mild conditions of oxidation reactions that take place in nature and are catalyzed by metalloenzymes, two strategies for the design of selective oxidation catalysts are developed in this dissertation.

In the first part of this thesis (Chapter III and IV) we aim to design iron and manganese low molecular weight complexes as catalysts for the oxidation of alkanes and alkenes. Our design strategy is inspired by the first coordination sphere of iron and manganese active centres found in oxidative enzymes, such as apocarotene dioxygenase. In addition, we have taken advantage of well-established principles of ligand design established from studies with porphyrin catalysts. It is well known that steric protection of the metal via ligand design is very important for obtaining selective and robust catalysts. In this sense, we focus in the development of a new family of ligands based in well known tetradentate N-based ligands whose iron and manganese complexes have been previously described as robust catalysts in bioinspired oxidation reactions. We envisioned that introduction of a bulky alkyl group such as a pinene in the 4<sup>th</sup> and 5<sup>th</sup> position of the pyridine rings of those ligands will increase the electronic density on the metal stabilizing high oxidation states and it will sterically protect the metal site.



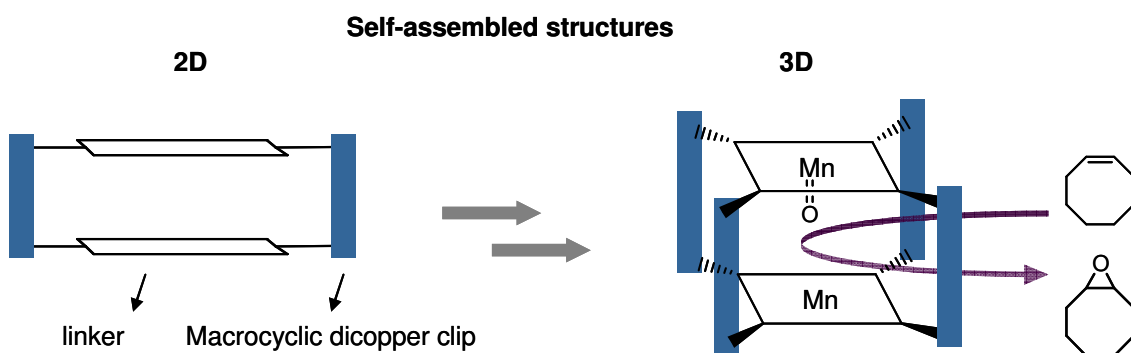
The catalytic performance of the resulting iron and manganese complexes will be examined in the oxidation of alkenes and, in the case of iron complexes, catalytic alkane oxidation will be also studied. The combination of low-toxic metals such as iron and manganese with hydrogen peroxide (or peracetic acid) as oxidant, would make this system a “green” alternative for the current methods. Moreover, the mechanism of the oxidation will be examined in order to gain insight into the active species responsible for the catalysis.

On the other hand, the introduction of the chiral pinene ring prompts us to explore the stereoselectivity in epoxidation catalysis by the corresponding iron and manganese complexes.

In the second part of this dissertation (Chapter V and VI), supramolecular chemistry is employed to assembly superstructures under shape and dimensions control. Our ultimate goal

is the construction of self-assembled nanoreactors with catalytic properties. This approach is inspired by the very selective reactions occurring at the binding site of enzymes.

The first step will consist in enlarging the dimensions of molecular rectangles earlier reported by our group. Those rectangles are based on the coordination driven assembly of macrocyclic dicopper complexes, acting as supramolecular clips, and dicarboxylate linkers. We will focus on developing and understanding parameters that control the construction of desired shaped structures. Interpretation of the different levels of control that define the final structure will let us to jump from 2D to 3D structures with the aim of creating well-defined cavities and increase their possible applications. We will explore the possibility of performing catalysis within the space of the cavity, analogously to enzymatic processes taking place in active sites.



For this reason, in order to create a self-assembled nanoreactor for oxidation reactions, we will embed metalloporphyrin reactive sites in the structure of a metal driven self-assembled prism. The structural rigidity of porphyrins allows for their use as convenient building blocks in the construction of a self-assembled 3D structure. Moreover, their well known properties as oxidation catalysts, in combination with substrate recognition and/or exclusion events that may be dictated by the structural and chemical properties of well-defined cavities, convert them in potential selective oxidation catalysts. As proof of concept, we will study the performance of the system in the epoxidation of alkenes.

---

# Stereospecific C-H and C=C Oxidation with H<sub>2</sub>O<sub>2</sub> Catalyzed by a New Family of Chemically Robust Site-Isolated Iron Catalysts

---

### Abstract

Herein is described the rational design of a family of robust iron catalysts (**1OTf-5OTf**, see scheme 2) for the stereospecific and site selective hydroxylation of alkanes and epoxidation of alkenes with H<sub>2</sub>O<sub>2</sub>. Complexes **1OTf-5OTf** contain lineal tetradentate bis-pyridyl bis-amine N4 ligands based on bpmen, bpmcn and bpbp scaffolds, whose iron complexes have been reported as very active catalysts (scheme 1).<sup>1-6</sup> Introduction of a pinene group in 4<sup>th</sup>-5<sup>th</sup> position of the pyridine rings isolate the active site and increase the chemical stability leading to very robust catalysts. Moreover, control over the reactivity and selectivity of the catalyst is achieved by the structure and the chirality of the diamine backbone. Stereospecific and very selective oxidation of alkanes is achieved with this family of complexes under environmentally benign conditions. Hydrogen peroxide as oxidant is employed in substrate limiting conditions to afford up to 69% of substrate conversion to the tertiary alcohol using no more than 3% of catalyst loading. In addition, epoxidation of alkenes is achieved in moderate to good yields.





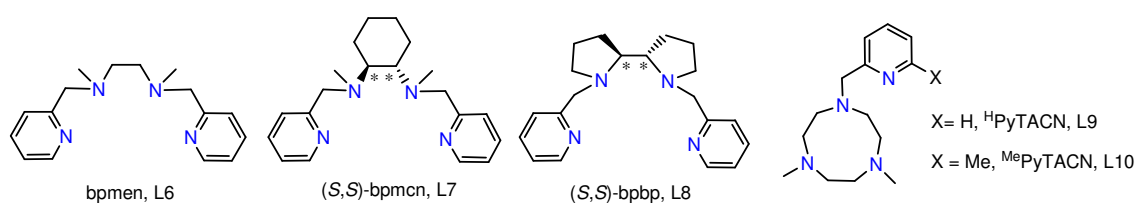
# Contents

|                                                                            |           |
|----------------------------------------------------------------------------|-----------|
| <b>III.1. INTRODUCTION</b> .....                                           | <b>61</b> |
| <b>III.2. RESULTS</b> .....                                                | <b>62</b> |
| III.2.1. SYNTHESIS OF LIGANDS AND IRON COMPLEXES .....                     | 62        |
| III.2.2. CHARACTERIZATION OF COMPLEXES.....                                | 64        |
| III.2.2.1. Solid state structures .....                                    | 64        |
| III.2.2.2. Solution behavior.....                                          | 68        |
| III.2.2.2.1. ESI-MS .....                                                  | 68        |
| III.2.2.2.2. UV-Vis spectroscopy .....                                     | 68        |
| III.2.2.2.3. <sup>1</sup> H-NMR spectroscopy .....                         | 69        |
| III.2.2.2.4. Electrochemical properties.....                               | 73        |
| III.2.3. CATALYTIC STUDIES.....                                            | 74        |
| III.2.3.1. Alkane oxidation .....                                          | 74        |
| III.2.3.1.1. Substrate excess conditions .....                             | 74        |
| III.2.3.1.2. Substrate limiting conditions .....                           | 77        |
| III.2.3.2. Alkene oxidation .....                                          | 82        |
| III.2.4. KINETIC STUDIES .....                                             | 84        |
| III.2.4.1. GC monitoring of catalyst activity .....                        | 84        |
| III.2.4.2. ESI-MS monitoring of catalyst stability .....                   | 85        |
| <b>III.3. DISCUSSION</b> .....                                             | <b>87</b> |
| III.3.1. A NEW FAMILY OF COMPLEXES WITH PYRIDINE-PINENE PENDANT ARMS ..... | 87        |
| III.3.2. OXIDATION OF ALKANES .....                                        | 89        |
| III.3.2.1. A family of efficient stereospecific oxidation catalysts.....   | 89        |
| III.3.2.1.1. Mechanistic considerations.....                               | 89        |
| III.3.2.2. Synthetically useful conditions in alkane oxidation.....        | 90        |
| III.3.2.2.1. Selectivity considerations.....                               | 90        |
| III.3.2.2.2. Catalyst stability.....                                       | 92        |
| III.3.3. OXIDATION OF ALKENES .....                                        | 92        |
| <b>III.4. CONCLUDING REMARKS</b> .....                                     | <b>93</b> |
| <b>III.5. EXPERIMENTAL SECTION</b> .....                                   | <b>93</b> |
| III.5.1. INSTRUMENTATION .....                                             | 93        |
| III.5.2. MATERIALS .....                                                   | 94        |
| III.5.3. SYNTHESIS OF LIGANDS .....                                        | 94        |
| III.5.4. SYNTHESIS OF COMPLEXES .....                                      | 103       |
| III.5.5. UV-VIS SPECTRA.....                                               | 107       |
| III.5.6. CRYSTAL DATA .....                                                | 107       |
| III.5.7. SYNTHESIS OF SUBSTRATES.....                                      | 109       |
| III.5.8. REACTION CONDITIONS FOR CATALYSIS .....                           | 110       |
| III.5.8.1. Alkanes .....                                                   | 110       |

|                                                           |            |
|-----------------------------------------------------------|------------|
| III.5.8.1.1. <i>Standard conditions</i> .....             | 110        |
| III.5.8.1.2. <i>Conditions of limited substrate</i> ..... | 111        |
| III.5.8.1.3. <i>Procedure for product isolation</i> ..... | 116        |
| III.5.8.2. Alkenes .....                                  | 119        |
| III.5.9. KINETIC STUDIES .....                            | 120        |
| <b>III.6. REFERENCES</b> .....                            | <b>120</b> |

### III.1. Introduction

Alkane functionalization stands as the bottleneck for the chemical transformation of hydrocarbon feedstocks, and methodologies for stereospecific C-H bond oxidation can also open novel and straighter synthetic strategies towards complex organic molecules.<sup>7-11</sup> However, the inert nature of non activated C-H bonds poses incomparable difficulties related to selectivity, and most common methodologies require the use of large excesses of substrate relative to oxidant in order to minimize overoxidation reactions. Not surprisingly, only few systems capable of affording synthetically useful yields have been described.<sup>5,12-22</sup> Olefin epoxidation is also a very interesting reaction because epoxides are excellent building blocks for a number of ulterior transformations. Of particular interest is the development of novel environmentally benign epoxidation technologies.<sup>23-25</sup>



**Scheme 1.** Selected ligands used to prepare mononuclear iron(II) complexes to perform alkane and alkene oxidation catalysis.

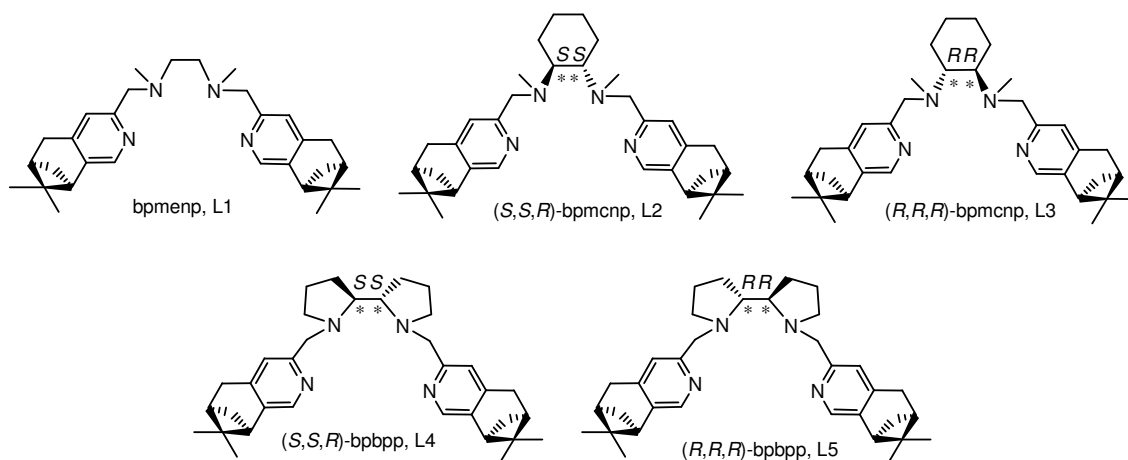
Selected bioinspired non-heme iron complexes such as  $[\text{Fe}(\text{CH}_3\text{CN})_2(\text{bpmen})]^{+2}$  (**6**, scheme 1) are particularly attractive oxidation catalysts because they use  $\text{H}_2\text{O}_2$  as oxidant and operate under mild conditions. Jacobsen *et al.* first discovered that **6** is an excellent epoxidation catalyst,<sup>3</sup> and stereospecific hydroxylation of alkanes was described by Que and co-workers, although in the latter case, very modest product yields were commonly obtained.<sup>20-22</sup> However, Chen and White recently reported that in the presence of acetic acid **6** and  $[\text{Fe}(\text{CH}_3\text{CN})_2((S,S)\text{-bpbp})]^{+2}$  (**8**, scheme 1) catalyze the hydroxylation of complex organic molecules in a predictable manner and with synthetically useful yields.<sup>5</sup> White's landmark system uses 15% catalyst loadings, and even though it affords very modest turnover numbers (3-6), efficiencies are substantially better than in any previously reported non-heme catalyst. A challenging dramatic dependence between catalytic efficiency and small changes in the architecture of related catalysts is being put forward,<sup>2,5,26-31</sup> and strategies for improvement remain to be developed. Our strategy is based on well-established principles in oxidation catalysis with heme complexes.<sup>32,33</sup> Introduction of aryl groups at the porphyrin *meso* positions isolates the metal site, which in turn limits bimolecular self-decomposition pathways and enhances the catalytic activity of the complexes by precluding formation of catalytically non competent oxo-dimers. We reasoned that analogous principles may be applied to non-heme iron complexes. As simple as it looks, this strategy is rapidly challenged by the known counterproductive modifications on the 6<sup>th</sup> position of the pyridine rings in polypyridyl iron complexes.<sup>2</sup> Consequently, we targeted modification at a more remote position of the pyridine with a bulky hydrocarbon as a general

strategy towards the design of a catalyst, where the iron site will be embedded in an oxidatively robust cavity.

## III.2. Results

### III.2.1. Synthesis of ligands and iron complexes

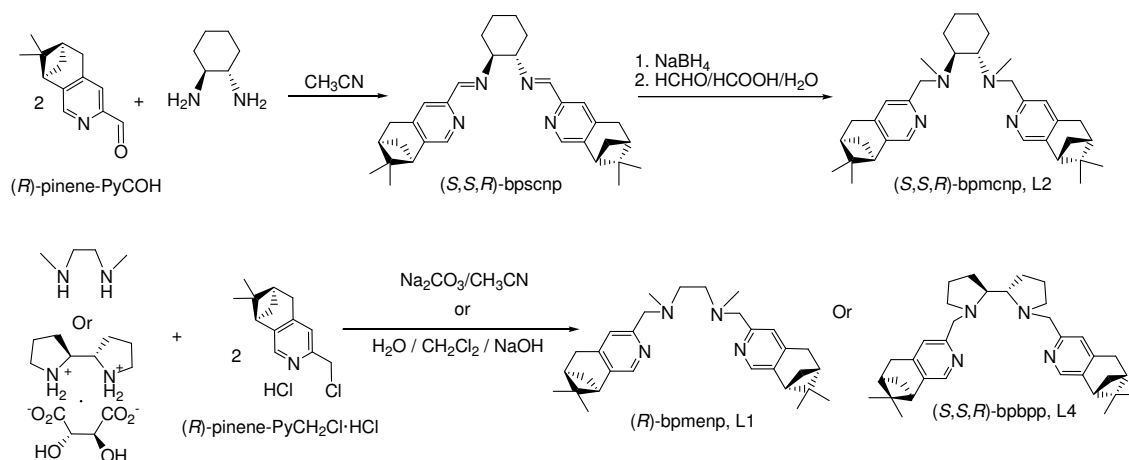
A new family of asymmetric tetradentate ligands (L1-L5, see scheme 2) that contain two aliphatic amino groups and two pyridines fused to a chiral pinene ring has been prepared. These ligands are an extension of the bpmen (L6) and bpmcn (L7) (scheme 1), whose iron complexes were reported as robust and efficient oxidation catalysts.<sup>1-4</sup> More recently, iron complexes of the related bpbp (L8, scheme 1) were reported as an excellent catalyst for alkane<sup>5</sup> and alkene<sup>6</sup> oxidation. It was originally expected that the introduction of the pinene rings into the pyridine rings of those ligands would substantially modify the chiral discrimination of these complexes in asymmetric catalysis and would create a hydrophobic core that could isolate the metal site, thus preventing oligomerization via formation of iron-oxo bridges. In addition, the electron-donating nature of the pinene ring was expected to increase the basicity of the pyridine ring and thus somewhat modify the reactivity of the complexes. Furthermore, the use of different aliphatic diamino backbones with distinctive rigidity, basicity and chirality would allow for fine tuning of the catalyst.



**Scheme 2.** Representation of the new family of pinene-derived ligands.

L2 and L3 were synthesized following a three-step synthetic method involving aldehyde-diamine condensation, hydrogenation and permethylation with yields ranging from moderate to good (see scheme 3). The addition of two equivalents of (*R*)-4,5-pinene-2-picolylaldehyde ((*R*)-pinene-PyOH) to a solution of chiral 1,2-*trans*-diaminocyclohexane (*S,S* and *R,R*) in acetonitrile yielded Schiff base ligands (*S,S,R*)-bpscnp and (*R,R,R*)-bpscnp in nearly quantitative yields (> 99% and 96%, respectively). (*S,S,R*)- and (*R,R,R*)-bpscnp were hydrogenated to (*S,S,R*)- and (*R,R,R*)-bphcnp, respectively by treatment with NaBH<sub>4</sub> in methanol. Finally, reaction of (*S,S,R*)- and (*R,R,R*)-bphcnp with HCHO/HCOOH/H<sub>2</sub>O under reflux afforded methylated ligands (*S,S,R*)-

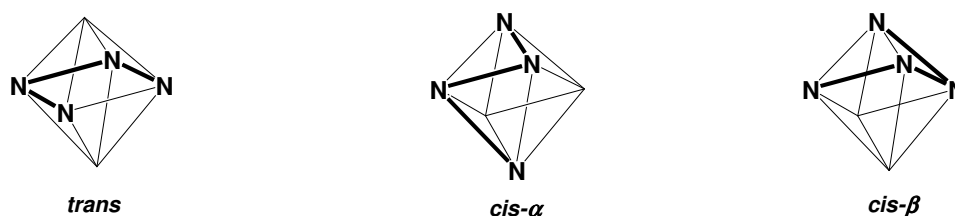
and (*R,R,R*)-bpmcnp (L2 and L3, respectively; scheme 2) as pale yellow oils in 56% and 75% respective yields after chromatographic purification.



**Scheme 3.** Synthesis of ligands employed in this work.

On the other hand, L1, L4 and L5 were synthesized by nucleophilic substitution of the (*R*)-4,5-pinene-2-picolylchloride hydrochloride ((*R*)-pinene-PyCH<sub>2</sub>Cl·HCl) with the corresponding diamine (see scheme 3). L1 was prepared from ethylene diamine and (*R*)-pinene-PyCH<sub>2</sub>·HCl in CH<sub>3</sub>CN and using Na<sub>2</sub>CO<sub>3</sub> as the base. In the case of L4 and L5, the reaction between the adequate tartrate salt of the bipyrrrolidine ((*S,S*) and (*R,R*), respectively) and (*R*)-pinene-PyCH<sub>2</sub>Cl·HCl took place in biphasic CH<sub>2</sub>Cl<sub>2</sub>/H<sub>2</sub>O 1:1 mixture and NaOH was used as the base. In all cases pale yellow oils were obtained after column chromatography purification in 90% for L1 and 37% yield for L4 and L5.

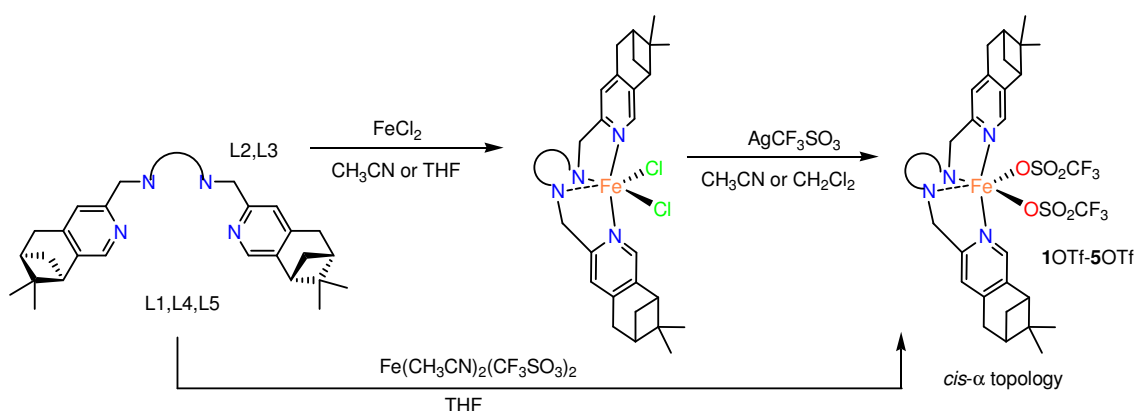
Linear tetradentate ligands can form three isomerically related octahedral complexes depending on the way they wrap around the metal centre: *cis*- $\alpha$ , *cis*- $\beta$  and *trans* topologies (scheme 4).<sup>28,34-37</sup> Our original target was the selective preparation of complexes adopting a *cis*- $\alpha$  topological geometry, because recent studies have demonstrated they are specially efficient oxidation catalysts.<sup>3,28,34,38</sup>



**Scheme 4.** Three different topologies that can be adopted by lineal tetradentate ligands.

Reaction of the pinene fused ligands L2 and L3 with Fe(OTf)<sub>2</sub>(CH<sub>3</sub>CN)<sub>2</sub> (OTf= trifluoromethanesulfonate anion) in acetonitrile afforded a mixture of products, as evidenced by <sup>1</sup>H-NMR spectroscopy, and separation of the *cis*- $\alpha$  isomer proved impossible. However, a two-step route for the selective preparation of this isomer was devised via reaction of the tetradentate ligand with iron(II) chloride and subsequent reaction with 2 equiv of AgOTf;  $\Lambda$ -

[FeCl<sub>2</sub>(L2)], **2Cl** was obtained as a yellow powder from reaction of equimolar amounts of L2 and FeCl<sub>2</sub> in acetonitrile (scheme 5). Attempts to form Δ-[FeCl<sub>2</sub>(L3)], **3Cl** by this route were unsuccessful, yielding only impure brown sticky solids. In contrast, reaction of L3 with FeCl<sub>2</sub> in THF led, upon stirring overnight, to precipitation of the desired complex. Subsequent reaction of **2Cl** and **3Cl** with two equiv of AgOTf yielded Λ-[Fe(CF<sub>3</sub>SO<sub>3</sub>)<sub>2</sub>(L2)] and Δ-[Fe(CF<sub>3</sub>SO<sub>3</sub>)<sub>2</sub>(L3)], **2OTf** and **3OTf**, respectively (in the case of **3OTf**, pure complex and better yield were obtained using CH<sub>2</sub>Cl<sub>2</sub> as solvent instead of CH<sub>3</sub>CN). After solvent removal, **2OTf-3OTf** were easily obtained as crystalline solids, from dichloromethane:ether mixtures. On the other hand, Δ-[Fe(CF<sub>3</sub>SO<sub>3</sub>)<sub>2</sub>(L1)], Λ-[Fe(CF<sub>3</sub>SO<sub>3</sub>)<sub>2</sub>(L4)] and Δ-[Fe(CF<sub>3</sub>SO<sub>3</sub>)<sub>2</sub>(L5)] (**1OTf**, **4OTf** and **5OTf**, respectively) were obtained as *cis-α* complexes by using directly Fe(OTf)<sub>2</sub>(CH<sub>3</sub>CN)<sub>2</sub> as iron source as the analogous complexes described by Que and co-workers (scheme 5).<sup>1,6</sup>



**Scheme 5.** Preparation of complexes **1OTf-5OTf**.

### III.2.2. Characterization of complexes

Metal complexes have been characterized by combustion analysis, CV, ESI-MS spectrometry, FT-IR, UV-Vis and <sup>1</sup>H-NMR spectroscopy and X-Ray diffraction analysis.

#### III.2.2.1. Solid state structures

The solid state structure of **2Cl**, **3Cl**, **1OTf**, **2OTf**, **4OTf** and **5OTf** could be established by X-Ray diffraction analysis. Figure 1 shows the Mercury diagrams of the complexes and table 1 gathers selected bond lengths and angles for the six crystallographically determined structures. The experimental details of the crystal structure determination of complexes are collected in table 12 (in section III.5.6). **2Cl** and **1OTf** crystallize in space group C2 and **3Cl**, **2OTf**, **4OTf** and **5OTf** in chiral space group P2<sub>1</sub>2<sub>1</sub>2<sub>1</sub>. All complexes have C<sub>2</sub> pseudo-symmetry about an axis that passes through the metal centre and bisects the aliphatic diamine of the ligand, what ensures that the complex has two equivalent parts. The complexes are neutral and the Fe<sup>II</sup> coordination geometry is distorted octahedral. Four coordination sites are occupied by the N atoms of the ligand and the coordination environment is completed by two anionic ligands, either Cl<sup>-</sup> or triflate.

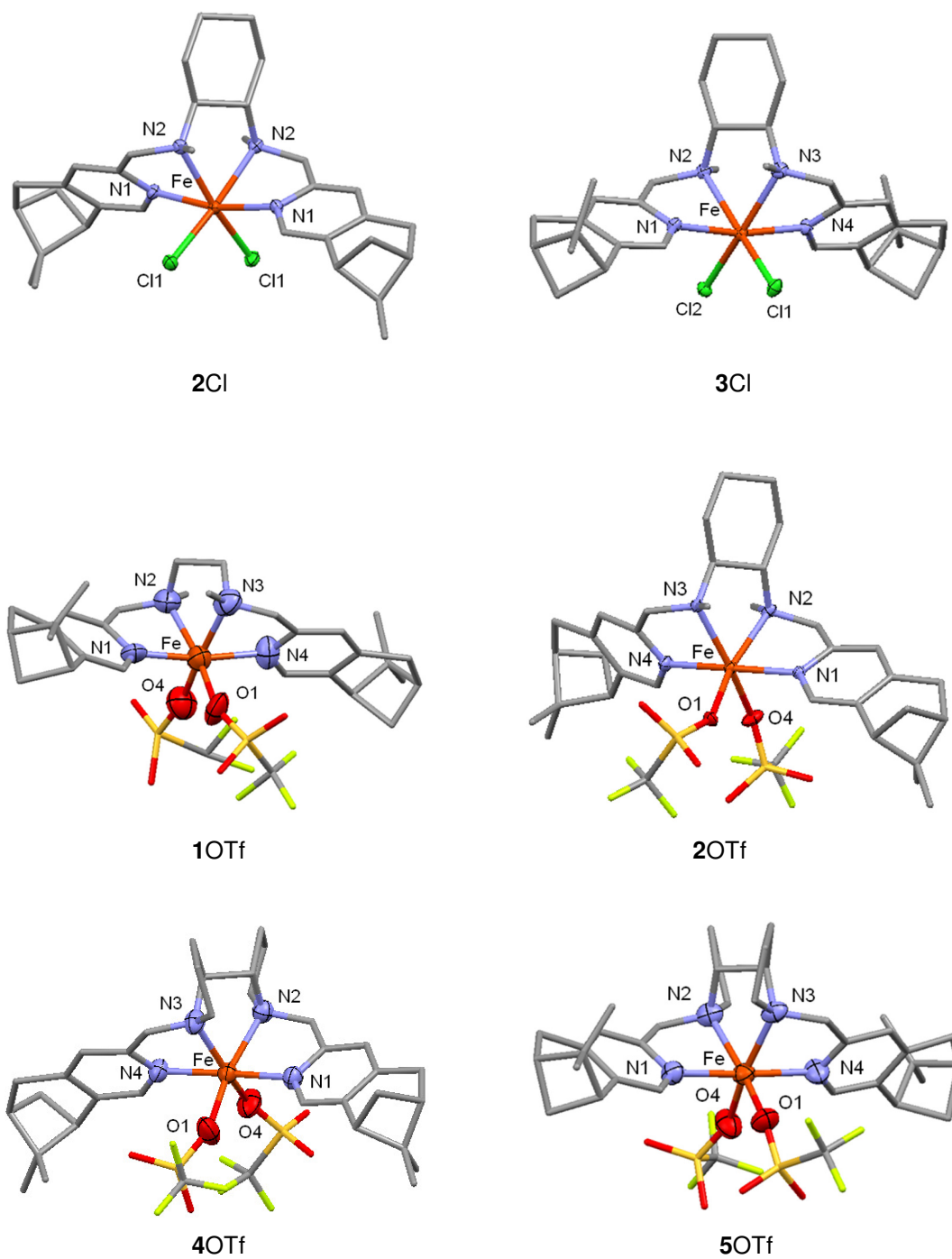


**Figure 1.** X-Ray structures of **2Cl**, **3Cl**, **1OTf**, **2OTf**, **4OTf** and **5OTf**. Hydrogen atoms and solvents of crystallization are omitted for clarity.

**Table 1.** Selected bond lengths [Å] and angles [°] for **2Cl**, **3Cl**, **1OTf**, **2OTf**, **4OTf** and **5OTf**.

| 2Cl         |            | 3Cl         |            | 1OTf      |            | 2OTf      |            | 4OTf        |            | 5OTf      |            |
|-------------|------------|-------------|------------|-----------|------------|-----------|------------|-------------|------------|-----------|------------|
| Fe1 N1      | 2.179(3)   | Fe1 N1      | 2.1812(17) | Fe1 N1    | 2.161(5)   | Fe1 N1    | 2.1885(9)  | Fe1 N1      | 2.176(3)   | Fe1 N1    | 2.180(3)   |
| Fe1 N2      | 2.285(3)   | Fe1 N2      | 2.2780(17) | Fe1 N2    | 2.237(6)   | Fe1 N2    | 2.2312(11) | Fe1 N2      | 2.220(3)   | Fe1 N2    | 2.218(3)   |
| Fe1 N2      | 2.285(3)   | Fe1 N3      | 2.2686(19) | Fe1 N3    | 2.240(6)   | Fe1 N3    | 2.2426(10) | Fe1 N3      | 2.210(3)   | Fe1 N3    | 2.228(3)   |
| Fe1 N1      | 2.179(3)   | Fe1 N4      | 2.1796(18) | Fe1 N4    | 2.178(5)   | Fe1 N4    | 2.1695(11) | Fe1 N4      | 2.184(3)   | Fe1 N4    | 2.175(3)   |
| Fe1 Cl1     | 2.4266(11) | Fe1 Cl1     | 2.4026(7)  | Fe1 O1    | 2.120(4)   | Fe1 O1    | 2.1482(11) | Fe1 O1A     | 2.132(3)   | Fe1 O1    | 2.121(3)   |
| Fe1 Cl1     | 2.4266(11) | Fe1 Cl2     | 2.4298(6)  | Fe1 O4    | 2.126(5)   | Fe1 O4    | 2.1071(10) | Fe1 O1B     | 2.116(3)   | Fe1 O4    | 2.127(3)   |
| N1 Fe1 N2   | 75.37(12)  | N1 Fe1 N2   | 75.80(6)   | N1 Fe1 N2 | 77.7(2)    | N1 Fe1 N2 | 77.31(4)   | N1 Fe1 N2   | 77.49(11)  | N1 Fe1 N2 | 77.79(12)  |
| N1 Fe1 N2   | 94.78(12)  | N1 Fe1 N3   | 97.59(7)   | N1 Fe1 N3 | 93.87(19)  | N1 Fe1 N3 | 105.86(4)  | N1 Fe1 N3   | 99.18(11)  | N1 Fe1 N3 | 98.47(11)  |
| N1 Fe1 N1   | 167.57(17) | N1 Fe1 N4   | 169.14(7)  | N1 Fe1 N4 | 169.3(2)   | N1 Fe1 N4 | 174.09(5)  | N1 Fe1 N4   | 172.96(11) | N1 Fe1 N4 | 175.75(12) |
| N2 Fe1 N2   | 77.06(16)  | N2 Fe1 N3   | 78.23(6)   | N2 Fe1 N3 | 80.6(2)    | N2 Fe1 N3 | 79.63(4)   | N2 Fe1 N3   | 80.80(12)  | N2 Fe1 N3 | 79.93(12)  |
| N1 Fe1 N1   | 94.78(12)  | N2 Fe1 N4   | 94.74(6)   | N2 Fe1 N4 | 97.9(2)    | N2 Fe1 N4 | 99.15(4)   | N2 Fe1 N4   | 107.20(11) | N2 Fe1 N4 | 102.19(13) |
| N1 Fe1 N2   | 75.37(12)  | N3 Fe1 N4   | 74.93(7)   | N3 Fe1 N4 | 75.7(2)    | N3 Fe1 N4 | 77.90(4)   | N3 Fe1 N4   | 76.75(11)  | N3 Fe1 N4 | 77.38(11)  |
| N1 Fe1 Cl1  | 97.88(9)   | N1 Fe1 Cl1  | 93.92(5)   | N1 Fe1 O1 | 90.36(17)  | N1 Fe1 O1 | 85.95(4)   | O1B Fe1 N1  | 86.46(11)  | N1 Fe1 O1 | 88.46(12)  |
| N2 Fe1 Cl1  | 166.47(8)  | N2 Fe1 Cl1  | 165.03(5)  | N2 Fe1 O1 | 166.77(19) | N2 Fe1 O1 | 162.12(4)  | O1B Fe1 N2  | 162.98(11) | N2 Fe1 O1 | 161.73(12) |
| N2 Fe1 Cl1  | 92.07(9)   | N3 Fe1 Cl1  | 92.66(5)   | N3 Fe1 O1 | 94.77(18)  | N3 Fe1 O1 | 99.27(4)   | O1B Fe1 N3  | 96.42(14)  | N3 Fe1 O1 | 90.42(11)  |
| N1 Fe1 Cl1  | 90.14(9)   | N4 Fe1 Cl1  | 94.29(5)   | N4 Fe1 O1 | 92.86(19)  | N4 Fe1 O1 | 98.03(4)   | O1B Fe1 N4  | 88.28(11)  | N4 Fe1 O1 | 90.64(13)  |
| N1 Fe1 Cl1  | 90.14(9)   | N1 Fe1 Cl2  | 91.96(5)   | N1 Fe1 O4 | 98.8(2)    | N1 Fe1 O4 | 88.10(4)   | O1A Fe1 N1  | 95.94(12)  | N1 Fe1 O4 | 96.35(11)  |
| N2 Fe1 Cl1  | 92.07(9)   | N2 Fe1 Cl2  | 91.08(5)   | N2 Fe1 O4 | 94.3(2)    | N2 Fe1 O4 | 91.97(5)   | O1A Fe1 N2  | 85.23(13)  | N2 Fe1 O4 | 92.48(13)  |
| N2 Fe1 Cl1  | 166.47(8)  | N3 Fe1 Cl2  | 163.39(5)  | N3 Fe1 O4 | 165.05(19) | N3 Fe1 O4 | 161.47(4)  | O1A Fe1 N3  | 156.62(12) | N3 Fe1 O4 | 161.49(11) |
| N1 Fe1 Cl1  | 97.88(9)   | N4 Fe1 Cl2  | 93.57(5)   | N4 Fe1 O4 | 91.2(2)    | N4 Fe1 O4 | 87.29(5)   | O1A Fe1 N4  | 89.75(11)  | N4 Fe1 O4 | 87.90(12)  |
| Cl1 Fe1 Cl1 | 99.74(6)   | Cl1 Fe1 Cl2 | 100.25(2)  | O1 Fe1 O4 | 93.1(2)    | O1 Fe1 O4 | 93.73(5)   | O1B Fe1 O1A | 102.24(15) | O1 Fe1 O4 | 101.04(13) |



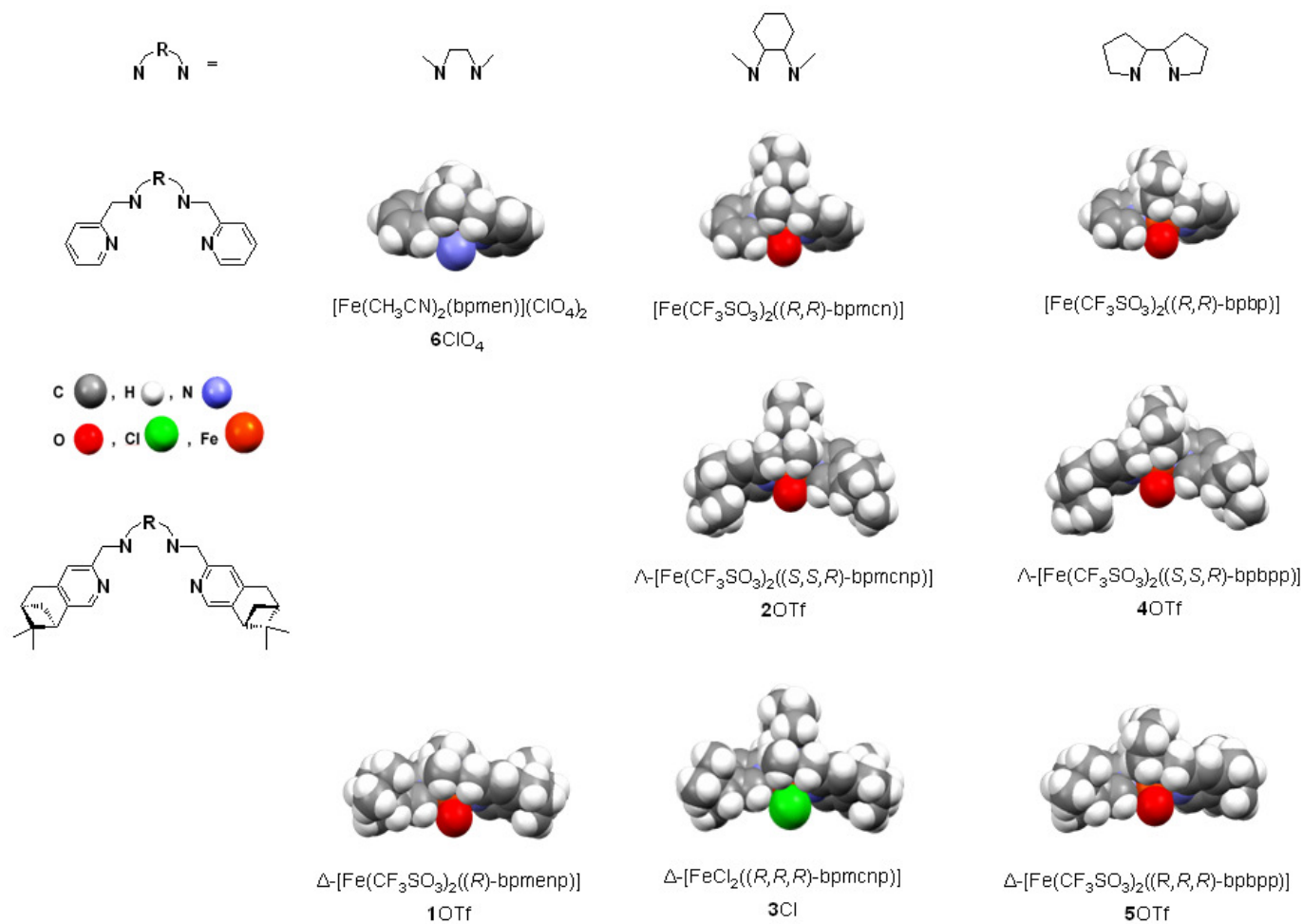


**Figure 2.** Space filling diagrams of 6ClO<sub>4</sub>,<sup>1</sup>  $[\text{Fe}(\text{CF}_3\text{SO}_3)_2((R,R)\text{-bpmcn})]$ ,<sup>39</sup>  $[\text{Fe}(\text{CF}_3\text{SO}_3)_2((R,R)\text{-bpbp})]$ ,<sup>6</sup> 1OTf, 2OTf, 3Cl, 4OTf and 5OTf. CF<sub>3</sub>SO<sub>3</sub> and CH<sub>3</sub>CN molecules have been omitted for clarity, except for the atom directly bound to the iron center. Perchlorate anions and solvent of crystallization are also omitted.

X-Ray analyses reveal that all of the complexes adopt a *cis-α* geometric topology. The two nitrogen atoms pyridine rings are mutually *trans*, with the  $N_{py}$ -Fe- $N_{py}$  angle ranging from  $167.57(17)^\circ$  for **2Cl** to  $175.75(12)^\circ$  for **5OTf**, while the two aliphatic nitrogen atoms (R'RN-Fe-NRR') are mutually *cis*. Because of the formation of five member chelate-rings, the R'RM-Fe-NRR' and R'RN-Fe- $N_{py}$  angles are all smaller than  $90^\circ$ . Fe-N distances measured in **2Cl**, **3Cl**, **1OTf**, **2OTf**, **4OTf** and **5OTf** are characteristic of high spin  $Fe^{II}$  complexes ( $\approx 2.1$ - $2.2$  Å).<sup>2,40</sup> Fe- $N_{py}$  distances are similar in all those complexes but the Fe-NRR' distances are approximately 0.04 Å shorter in triflate complexes than in chloride complexes, presumably a consequence of the varying *trans* influences exerted by triflate and chloride ligands.

The X-Ray structures show that **2Cl**, **2OTf** and **4OTf** present  $\Lambda$  topological chirality while **3Cl**, **1OTf**, **3OTf** and **5OTf** present  $\Delta$  topological chirality. Moreover, in the former group of complexes the methyl groups of the pinene rings are pointing at the anionic ligands ( $Cl^-$  or  $CF_3SO_3^-$ ; figure 1), creating a closed cavity around the *cis* labile positions. The contrary happens in the  $\Delta$  complexes, in which the methyl groups are pointing at the opposite direction of the anionic ligands and the ligand adopts a more open conformation. Interestingly, the topology showed by the complexes is determined by the chirality of the diamine backbone. In the case of **1OTf**, containing an achiral diamine, the conformation is induced by the pinene.  $^1H$ -NMR and X-Ray diffraction analyses show that one unique product is formed with  $\Delta$  topological chirality. That is a nice example where a remote chiral orientation of the ligand determines the chirality at the metal (topological chirality).<sup>37</sup>

Comparison between the solid state structures of **1-5** and those of previously reported  $[Fe(CH_3CN)_2(bpmen)](ClO_4)_2$ ,<sup>1</sup>  $[Fe(CF_3SO_3)_2((R,R)\text{-}bpmcn)]$ ,<sup>39</sup> and  $[Fe(CF_3SO_3)_2((R,R)\text{-}bpbp)]$ <sup>6</sup> indicates only minor differences between their respective structural parameters of the first coordination sphere. Major differences are most obvious in a space filling diagram which shows a deep well-defined cavity around the *cis* labile positions (figure 2) in **1-5**. The cavity is particularly well-defined in complexes with  $\Lambda$  topological chirality, which a priori suggests that better stereodiscrimination and metal site isolation should be accomplished by these catalysts.

### III.2.2.2. Solution behavior

#### III.2.2.2.1. ESI-MS

ESI-MS analyses of the complexes described in this work indicate that they retain their integrity in solution. The spectra of **1Cl-5Cl** in methanol show a major peak at  $m/z$  549.2, 603.2, 603.2, 601.3 and 601.3 assigned to  $[FeCl(L)]^+$  ( $L = L1$ - $L5$ ), respectively. On the other hand, ESI-MS analysis of **1OTf-5OTf** in acetonitrile solution exhibit a peak at  $m/z$  663.2, 717.2, 717.2, 715.3 and 715.3, respectively assigned to  $[Fe(OTf)(L)]^+$  ( $L = L1$ - $L5$ ).

#### III.2.2.2.2. UV-Vis spectroscopy

The visible region of the electronic spectra of chloride complexes (**1Cl-5Cl**) in acetonitrile displays a band around 400 nm which causes their yellow color (table 2 and figure

13 in section III.5.6). This band is presumably due to a metal-to-pyridine charge transfer process.<sup>41</sup>

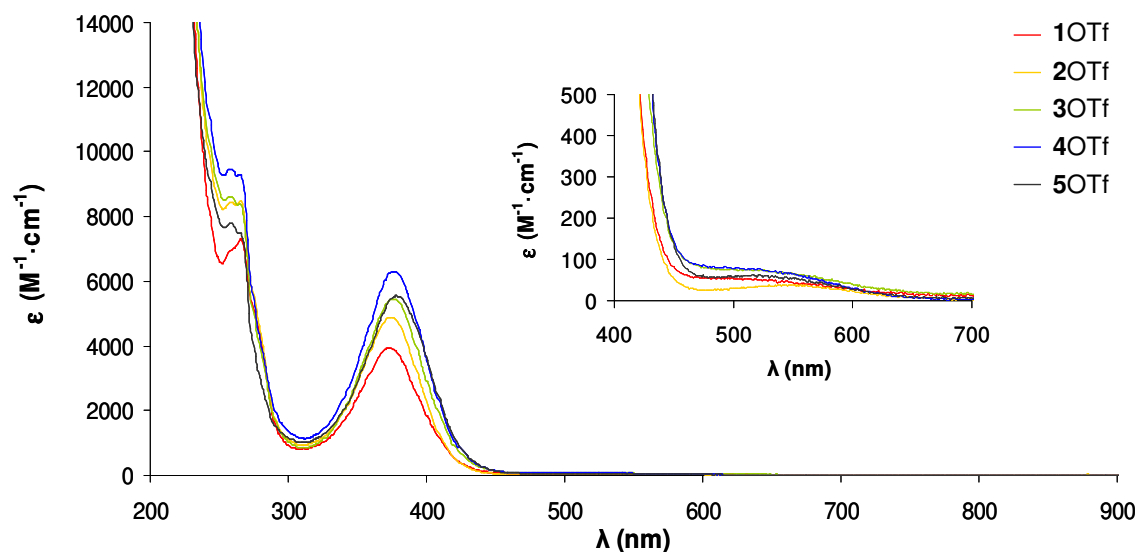


**Figure 3.** UV-Vis spectra (298K) in acetonitrile of the complexes and 1OTf-5OTf.

**Table 2.** Spectroscopic data for complexes 1-5Cl and 1-5OTf in CH<sub>3</sub>CN.

| Complex | $\lambda_{\text{max}}$ , nm ( $\epsilon$ , M <sup>-1</sup> cm <sup>-1</sup> ) | Complex | $\lambda_{\text{max}}$ , nm ( $\epsilon$ , M <sup>-1</sup> cm <sup>-1</sup> ) |
|---------|-------------------------------------------------------------------------------|---------|-------------------------------------------------------------------------------|
| 1Cl     | 269 (8700), 403 (1800)                                                        | 1OTf    | 375 (3900)                                                                    |
| 2Cl     | 268 (7400), 411 (1381)                                                        | 2OTf    | 374 (4884)                                                                    |
| 3Cl     | 270 (5500), 419 (1100)                                                        | 3OTf    | 377 (5500)                                                                    |
| 4Cl     | 265 (6000), 402 (1200)                                                        | 4OTf    | 376 (6300)                                                                    |
| 5Cl     | 269 (5600), 420 (1170)                                                        | 5OTf    | 378 (5600)                                                                    |

The UV-Vis spectra of triflate complexes (1OTf-5OTf) in acetonitrile solution at room temperature exhibit a band around 375 nm that reflects a metal-to-ligand charge transfer process (MLCT) and a relatively weak band ( $\epsilon < 100 \text{ M}^{-1}\cdot\text{cm}^{-1}$ ) at  $\approx 540 \text{ nm}$ , responsible for the pink-reddish color of the solution, which suggests partial population of the low spin configuration, and thus the onset of a spin-crossover process (figure 3 and table 2).<sup>41-43</sup> That band corresponds to a d-d transition of the octahedral iron(II) low spin complex.

### III.2.2.2.3. <sup>1</sup>H-NMR spectroscopy

The structure of 1Cl-5Cl and 1OTf-5OTf in solution was studied by <sup>1</sup>H-NMR spectroscopy. All complexes have high-spin Fe<sup>II</sup> centers ( $S = 2$ ) in CD<sub>2</sub>Cl<sub>2</sub>, as is indicated by paramagnetically shifted <sup>1</sup>H-NMR signals expanding from -25 ppm to 155 ppm (figure 4). The spectrum of each complex only shows one set of signals for the two symmetric parts of the ligand consistent with C<sub>2</sub> symmetry and indicative of the presence of unique species with *cis*- $\alpha$  conformation.

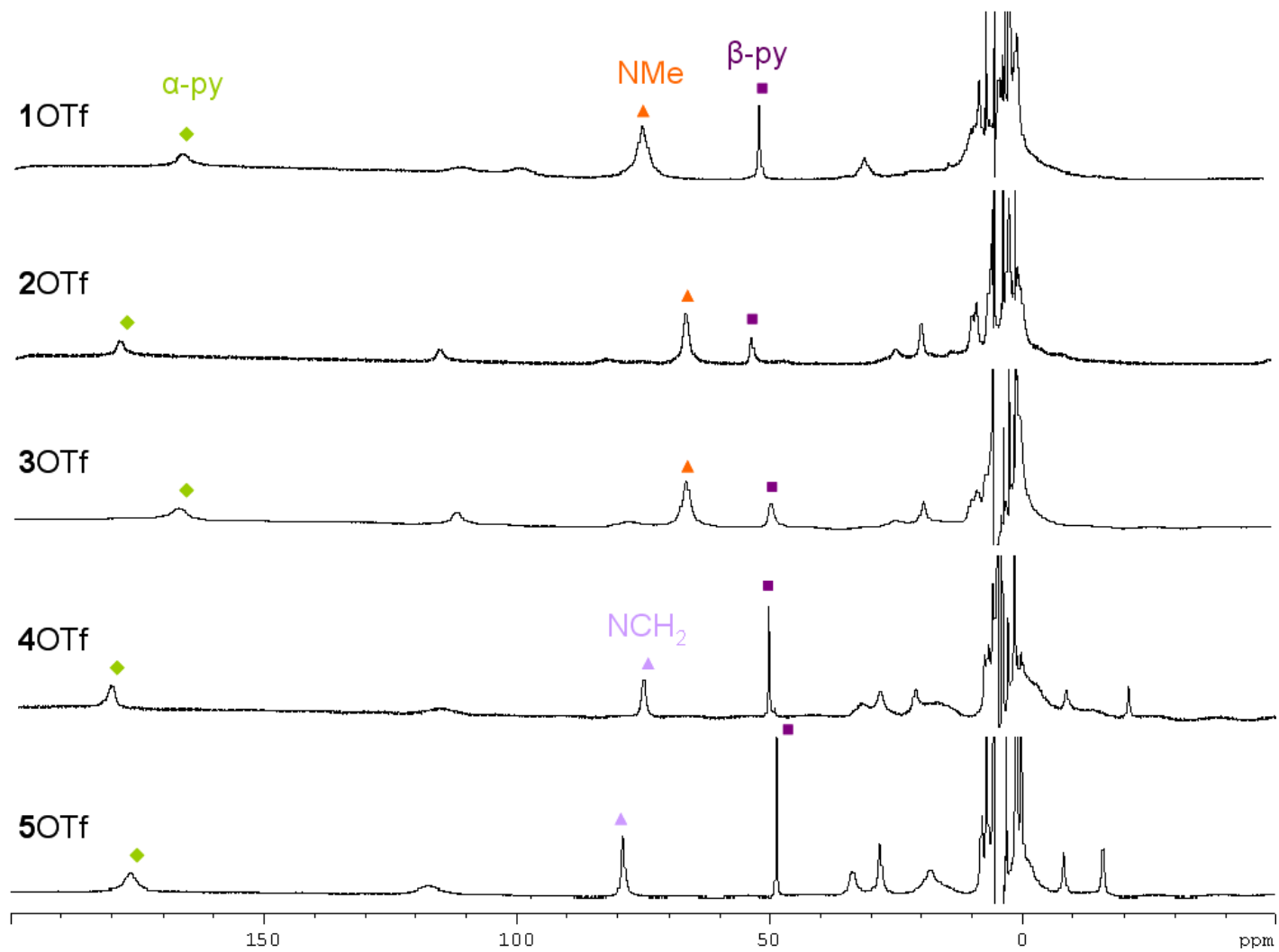


**Figure 4.**  $^1\text{H-NMR}$  spectra of triflate complexes 1OTf-5OTf in  $\text{CD}_2\text{Cl}_2$  at 300K.

Full assignment of the spectra resulted impossible, but the most characteristic peaks could be assigned. The resonance at ~170 ppm was assigned to the  $\alpha$ -py proton due to the large isotropic shift and relative integration (2H). Because of the same reasons and comparing with other earlier reported complexes,<sup>44</sup> the peak at ~50 ppm was assigned to  $\beta$ -py (2H). The signal at ~65 ppm in the  $^1\text{H}$ -RMN spectra of complexes **1OTf-3OTf** was assigned to NMe on the basis of its integration (6H). In the case of **4OTf** and **5OTf** the corresponding  $\text{NCH}_2$  signal appears at ~80 ppm and its integration is 4H.

$^1\text{H}$ -NMR spectra of **1OTf-5OTf** in  $\text{CD}_3\text{CN}$  at 298K show severely broadened peaks that expand from -1 to 110 ppm, difficulting the interpretation of the spectrum (figure 5). Such broad peaks are the result of a chemical exchange between triflate and acetonitrile molecules and have been documented in related iron(II) high spin complexes.<sup>28,42</sup>

Variable temperature  $^1\text{H}$ -NMR spectra of **2OTf** in acetonitrile exhibit dramatic changes indicative of a spin crossover process. This behavior is observed in figure 6 where different temperature spectrums for **2OTf** are collected. The 100 ppm-wide room temperature spectrum undergoes compression of the spectral window upon cooling down, and at 220K, the spectrum expands from 0 to 18 ppm. Therefore, at high temperatures the spectrum is typical for high-spin  $\text{Fe}^{\text{II}}$  complexes ( $t_{2g}^4e_g^2$ ), but approaches the low-spin diamagnetic state ( $t_{2g}^6e_g^0$ ) at low temperature. The observed chemical shift of paramagnetically shifted protons is not lineally related to  $1/T$  (figure 7). The lack of Curie behavior strongly suggests the presence of a spin crossover process in this system.

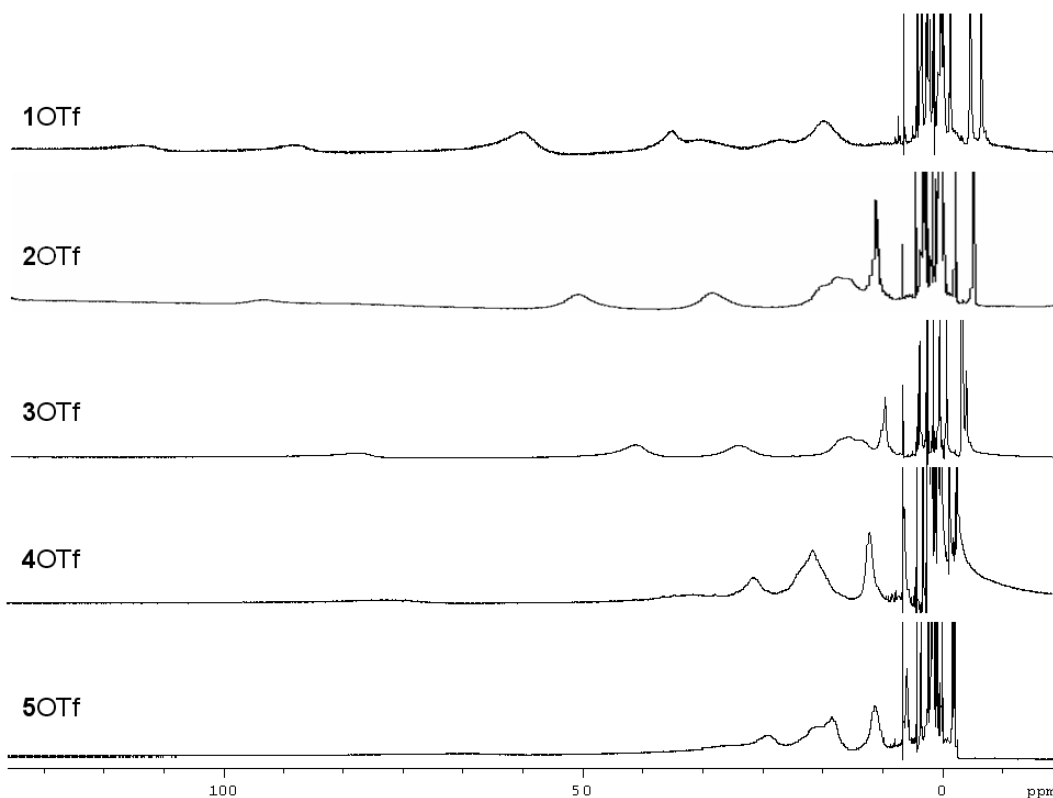


**Figure 5.**  $^1\text{H}$ NMR spectra of triflate complexes **1OTf-5OTf** in  $\text{CD}_3\text{CN}$  at 300K.

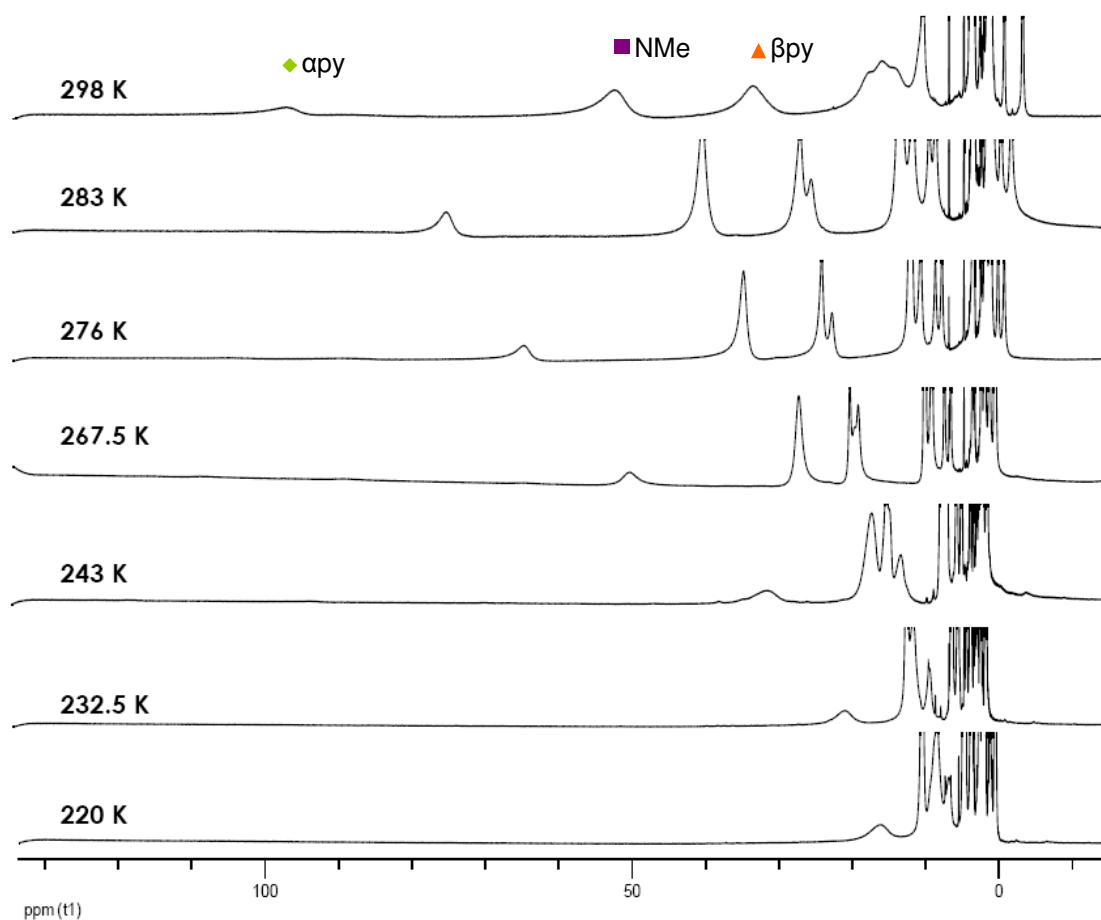


**Figure 6.**  $^1\text{H}$ -NMR spectra of 2OTf in  $\text{CD}_3\text{CN}$  at 298K, 283K, 276K, 267.5K, 243K, 232.5K and 220K.

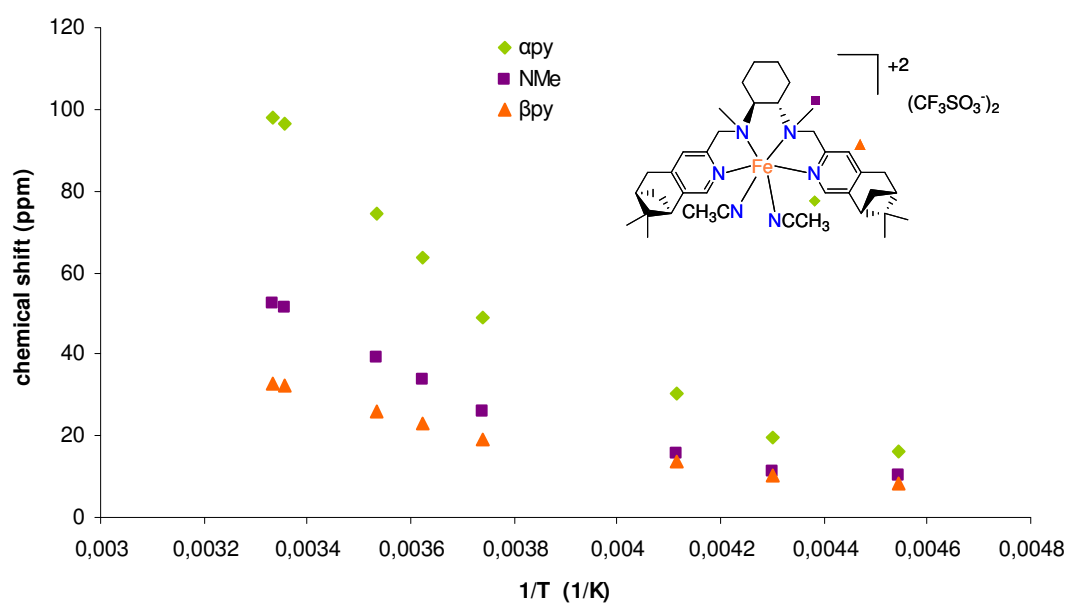


**Figure 7.** Variation of chemical shift of  $\alpha\text{py}$ , NMe and  $\beta\text{py}$  protons of 2OTf in  $\text{CD}_3\text{CN}$  with temperature, showing the onset of the population of the low spin configuration.

### III.2.2.2.4. Electrochemical properties.

Comparison between the electronic properties exerted by the different ligands can be studied by cyclic voltammetry (CV) of the chloride complexes. Analogous analyses with triflate complexes were precluded by their chemically irreversible redox behavior. The complexes exhibit an electrochemically quasireversible ( $\Delta E \sim 92\text{-}119$  mV, scan rate = 100 mV/s), chemically reversible ( $I_{pa}/I_{pc} \sim 1$ )  $1e^-$  process that is assigned to the  $Fe^{III}/Fe^{II}$  redox couple. The redox potential appears to be related to the structure of the ligand (figure 8 and table 3). Introduction of pinene ring fused to the 4<sup>th</sup>-5<sup>th</sup> position of the pyridine, in all cases, decrease the redox potential by approximately 62 mV (table 3), indicating that the pinene ring increases the basicity of the pyridine ligands, thus lowering the redox potential of the  $Fe^{III}/Fe^{II}$  couple. On the other hand, comparison between complexes that only differ in the diamine backbone shows that the donation of the diamine to the metal is related to the inductive effect of its substituents and the accessibility to the electron pair of the nitrogen. The latter is dictated by the rigidity of the aliphatic diamine moiety, being the bipyrrolidine the most rigid. In a series of complexes,  $E_{1/2}$  values decrease in the following order: ethylene diamine > cyclohexane diamine > bipyrrolidine.

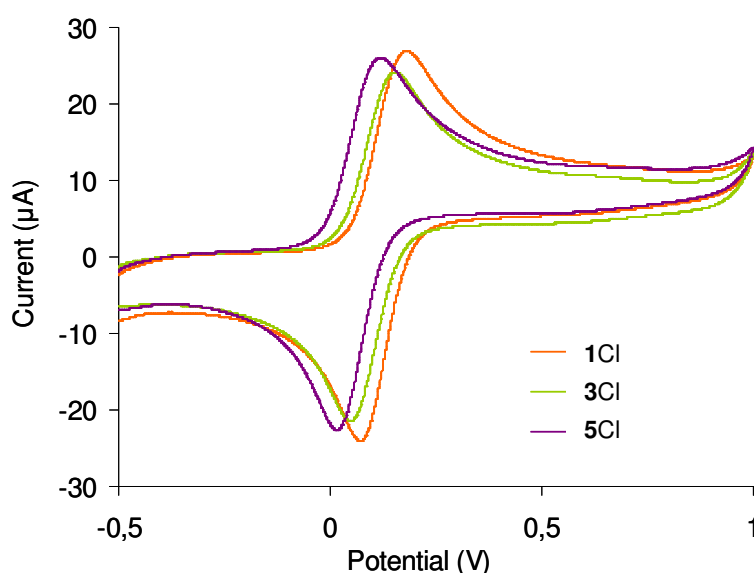


**Figure 8.** Cyclic voltammetry of complexes **1Cl**, **3Cl** and **5Cl** in  $CH_3CN$  (*versus* SCE (Saturated Calomel Electrode)).

**Table 3.**  $E_{1/2}$  values *versus* SCE in mV of complexes **1Cl**-**8Cl** in  $CH_3CN$ .

|  | 125 ( <b>1Cl</b> ) | 98 ( <b>2Cl</b> )<br>101 ( <b>3Cl</b> ) | 61 ( <b>4Cl</b> )<br>67 ( <b>5Cl</b> ) |
|--|--------------------|-----------------------------------------|----------------------------------------|
|  | 187 ( <b>6Cl</b> ) | 163 ( <b>7Cl</b> )                      | 125 ( <b>8Cl</b> )                     |

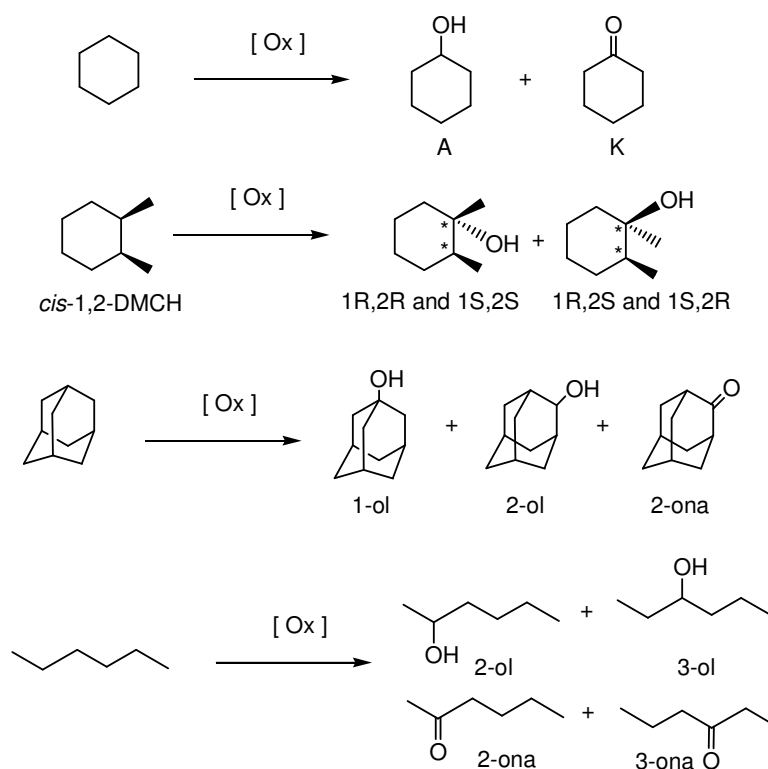
### III.2.3. Catalytic studies

#### III.2.3.1. Alkane oxidation

##### III.2.3.1.1. Substrate excess conditions

The family of complexes **1OTf-5OTf** was tested as catalysts for the oxidation of alkanes and alkenes using  $\text{H}_2\text{O}_2$  as oxidant. Selected alkane oxidation reactions were carried out under standard conditions of large excess of substrate in order to minimize overoxidation reactions and to compare the results with previously reported data. The most extensive study was done exclusively for **2OTf**, which proved to be the most efficient among the pinene derived family of complexes (*vide infra*). For comparative purposes, the structurally related  $[\text{Fe}(\text{CF}_3\text{SO}_3)_2((S,S)\text{-bpmcn})]$  (**7OTf**) was also studied under analogous conditions.

In a typical alkane oxidation experiment, 10-100 equiv of  $\text{H}_2\text{O}_2$  diluted in acetonitrile were delivered via syringe pump during 30 min into an acetonitrile solution of catalysts (1 equiv) and substrate (100-1000 equiv). No peroxide remained at the end of the reaction, as indicated by iodometry. Under these conditions,  $\text{H}_2\text{O}_2$  is the limiting reagent and because of that, yields described are based on the amount of oxidant ( $\text{H}_2\text{O}_2$ ) converted into oxygenated products.



**Scheme 6.** Selected alkane oxidation reactions.

The oxidation of cyclohexane ( $c\text{-C}_6\text{H}_{12}$ ) with 10 equiv of peroxide (table 4, scheme 6) by **2OTf** is performed with remarkably high efficiency (70%) and large alcohol/ketone (A/K) ratio ( $\approx 11$ ), accomplishing better results than the structurally related  $[\text{Fe}(\text{CF}_3\text{SO}_3)_2(\text{bpmen})]$  (**6OTf**) and  $[\text{Fe}(\text{CF}_3\text{SO}_3)_2((S,S)\text{-bpmcn})]$  (**7OTf**) (63% and 59% yield; 8 and 9 A/K, respectively). The high



activity showed for **2OTf** resemble that showed for the most efficient catalyst reported so far, [Fe(CF<sub>3</sub>SO<sub>3</sub>)<sub>2</sub>(<sup>Me</sup>PyTACN)] (**10OTf**, 76% yield, 10.2 A/K).

**Table 4.** Alkane hydroxylation reactions catalyzed by **2OTf**, **6OTf**, **7OTf** and **10OTf** at room temperature.

| Entry | Catalyst                   | Substrate (equiv)                       | H <sub>2</sub> O <sub>2</sub> | Products (TN)                                                                           | Eff. (%) | A/K <sup>a</sup> |
|-------|----------------------------|-----------------------------------------|-------------------------------|-----------------------------------------------------------------------------------------|----------|------------------|
| 1     | <b>10OTf</b> <sup>27</sup> | c-C <sub>6</sub> H <sub>12</sub> (1000) | 10                            | A(6.7)/K (0.9)                                                                          | 76       | 10.2             |
| 2     | <b>6OTf</b> <sup>2</sup>   | c-C <sub>6</sub> H <sub>12</sub> (1000) | 10                            | A(5.6)/K (0.7)                                                                          | 63       | 8.0              |
| 3     | <b>7OTf</b> <sup>2</sup>   | c-C <sub>6</sub> H <sub>12</sub> (1000) | 10                            | A(5.3)/K(0.6)                                                                           | 59       | 9                |
| 4     | <b>2OTf</b>                | c-C <sub>6</sub> H <sub>12</sub> (1000) | 10                            | A(6.4)/K (0.6)                                                                          | 70       | 11               |
| 5     | <b>2OTf</b> <sup>b</sup>   | c-C <sub>6</sub> H <sub>12</sub> (1000) | 10                            | A(7.0)/K (0.2)                                                                          | 72       | 29               |
| 6     | <b>10OTf</b> <sup>27</sup> | c-C <sub>6</sub> H <sub>12</sub> (1000) | 100                           | A(51.9)/K (12.1)                                                                        | 64       | 4.3              |
| 7     | <b>6OTf</b> <sup>2</sup>   | c-C <sub>6</sub> H <sub>12</sub> (1000) | 100                           | A(34.3)/K (13.7)                                                                        | 48       | 2.5              |
| 8     | <b>7OTf</b> <sup>2</sup>   | c-C <sub>6</sub> H <sub>12</sub> (1000) | 100                           | A(36.5)/K (11.0)                                                                        | 48       | 3.5              |
| 9     | <b>2OTf</b>                | c-C <sub>6</sub> H <sub>12</sub> (1000) | 100                           | A(59)/K (13.6)                                                                          | 73       | 4.3              |
| 10    | <b>7OTf</b>                | c-C <sub>6</sub> H <sub>12</sub> (100)  | 100                           | A(6.4)/K (15.9)                                                                         | 22       | 0.40             |
| 11    | <b>2OTf</b>                | c-C <sub>6</sub> H <sub>12</sub> (100)  | 100                           | A(7.2)/K (20.4)                                                                         | 28       | 0.35             |
| 12    | <b>2OTf</b>                | c-C <sub>5</sub> H <sub>10</sub> (1000) | 100                           | c-C <sub>5</sub> H <sub>9</sub> OH (21.4)<br>c-C <sub>5</sub> H <sub>8</sub> O (8.4)    | 30       | 2.5              |
| 13    | <b>2OTf</b>                | c-C <sub>7</sub> H <sub>14</sub> (1000) | 100                           | c-C <sub>7</sub> H <sub>15</sub> OH (44.0)<br>c-C <sub>7</sub> H <sub>12</sub> O (10.3) | 54       | 4.3              |
| 14    | <b>2OTf</b>                | c-C <sub>8</sub> H <sub>16</sub> (1000) | 100                           | c-C <sub>8</sub> H <sub>17</sub> OH (44.1)<br>c-C <sub>8</sub> H <sub>14</sub> O (7.4)  | 52       | 5.9              |
| 15    | <b>2OTf</b>                | n-hexane (1000)                         | 100                           | 2-ol (13.5)<br>3-ol (8.7)<br>2-one (7.0)<br>3-one (4.7)                                 | 34       | 1.9              |
| 17    | <b>2OTf</b>                | 2,3-dimethylbutane<br>(1000)            | 100                           | 2-ol (14.0)                                                                             | 14       | -                |

<sup>a</sup> A/K = (mols A / mols K). <sup>b</sup> Additive: 50 equiv of AcOH, temperature: 0°C.

Increasing of the H<sub>2</sub>O<sub>2</sub> concentration up to 100 equiv afforded a high conversion of H<sub>2</sub>O<sub>2</sub> oxidant into oxidation products (73%) for catalysis with **2OTf**. Significant decrease of the A/K ratio is also observed (4.3), presumably originated from alcohol to ketone oxidation. Noticeably, under these conditions **2OTf** is significantly more efficient than **6OTf** and **7OTf** (48% yield) and slightly better than **10OTf** (64% yield). The large conversion of H<sub>2</sub>O<sub>2</sub> into products as well as the number of catalytic cycles, qualifies **2OTf** as a very efficient non-heme iron catalyst similar to the state of the art catalysts. In order to test the scope of the system, cyclohexane was oxidized under conditions of limited substrate concentration. Remarkably, in these reactions **2OTf** afforded 7.2 turnovers (TN) of cyclohexanol and 20.4 TN of cyclohexanone, with an overall 48%

(2OTf) yield (relative to H<sub>2</sub>O<sub>2</sub>) and 28% conversion of substrate into products. Under these conditions, the alcohol was further oxidized to the ketone because alcohol and alkane concentrations are of the same order. For this reason, efficiency of the transformation of H<sub>2</sub>O<sub>2</sub> into products can be also calculated assuming that each ketone molecule originates from 2 H<sub>2</sub>O<sub>2</sub> molecules.

Other cycloalkanes were tested affording moderate yields (cyclopentane, cycloheptane and cyclooctane; 30, 54 and 52% yield, respectively). Finally, the ability of 2OTf to perform enantiospecific C-H bond hydroxylation was tested towards the hydroxylation of n-hexane. Unfortunately, only marginal enantioselectivity ( $\leq 10\%$  ee) was observed.

**Table 5.** Alkane oxidation reactions catalyzed by 2OTf.

| T (°C) | Substrate (equiv)                                                         | H <sub>2</sub> O <sub>2</sub> (equiv) | AcOH (equiv) | Products (TN)                                                                                                    | Eff. (%) |                                                   |
|--------|---------------------------------------------------------------------------|---------------------------------------|--------------|------------------------------------------------------------------------------------------------------------------|----------|---------------------------------------------------|
| 25     | c-C <sub>6</sub> H <sub>12</sub> /c-C <sub>6</sub> D <sub>12</sub> (1000) | 10                                    | 0            | A (D) (2.6)<br>A (H) (3.2)<br>K (D) (0.1)<br>K (H) (0.3)                                                         | 62       | KIE<br>3.6                                        |
| 0      | c-C <sub>6</sub> H <sub>12</sub> /c-C <sub>6</sub> D <sub>12</sub> (1000) | 10                                    | 50           | A (D) (2.8)<br>A (H) (3.4)<br>K (D) (0.1)<br>K (H) (0.3)                                                         | 66       | KIE<br>3.6                                        |
| 25     | Adamantane (10)                                                           | 10                                    | 0            | 1-ol (3.8)<br>2-ol (0.3)<br>2-one (0.2)                                                                          | 43       | 3 <sup>o</sup> /2 <sup>o</sup> <sup>a</sup><br>23 |
| 0      | Adamantane (10)                                                           | 10                                    | 50           | 1-ol (4.3)<br>2-ol (0.3)<br>2-one (0.2)                                                                          | 48       | 3 <sup>o</sup> /2 <sup>o</sup> <sup>a</sup><br>27 |
| 25     | <i>cis</i> -1,2-DMCH (1000)                                               | 10                                    | 0            | 1 <i>R</i> ,2 <i>R</i> + 1 <i>S</i> ,2 <i>S</i> (4)<br>1 <i>R</i> ,2 <i>S</i> + 1 <i>S</i> ,2 <i>R</i><br>(0.03) | 41       | RC <sup>b</sup><br>> 99                           |
| 25     | n-hexane (1000)                                                           | 10                                    | 0            | 2-ol (1.9)<br>3-ol (1.2)<br>2-one (0.1)                                                                          | 32       |                                                   |

<sup>a</sup> 3<sup>o</sup>/2<sup>o</sup> ratio in adamantane oxidation = 3 x (1-adamantanol)/(2-adamantanol + 2-adamantanone). <sup>b</sup> RC = retention of configuration in the oxidation of the tertiary C-H bonds of *cis*-1,2-dimethylcyclohexane, expressed as the ratio of the tertiary alcohols: [(1*R*,2*R* + 1*S*,2*S*) - (1*R*,2*S* + 1*S*,2*R*)] / [(1*R*,2*R* + 1*S*,2*S*) - (1*R*,2*S* + 1*S*,2*R*)].

On the other hand, insight into the nature of the active species was obtained by the use of several mechanistic probes. Comparable active species are expected for complexes 1OTf-5OTf due to the similar structure, therefore mechanistic study was performed only for 2OTf.

Apart from the remarkable high A/K ratio found in the oxidation of cyclohexane (A/K = 11, table 4 entry 4), 2OTf also exhibited high selectivity for the oxidation of tertiary C-H bonds compared to secondary ones as was pointed out in the oxidation of adamantane (3<sup>o</sup>/2<sup>o</sup>

normalized selectivity =  $3 \times (1\text{-adamantanol}) / (2\text{-adamantanol} + 2\text{-adamantanone})$ : 23, table 5, scheme 6). Moreover, kinetic isotope effect (KIE) evaluated in competition oxidation reaction of a 1:3 mixture of cyclohexane and cyclohexane- $D_{12}$  was 3.6, indicating that the strength of the C-H bond plays a major role in dictating C-H site selectivity. Most remarkably, the hydroxylation of *cis*-1,2-DMCH to the corresponding tertiary alcohol affords almost exclusively the epimer with *cis*-dimethyl groups, indicating large degree of stereoretention of configuration (> 99%) and that no long lived radical or carbocationic type of intermediates are formed along the reaction.

In conclusion, selective metal centered species are responsible for the oxidation ability of these complexes and free diffusing radicals do not significantly operate in the reactions.

On the other hand, acetic acid (AcOH) has been reported as a key additive in oxidation with iron catalysts,<sup>45</sup> and a decrease of the reaction temperature has been used to achieve better selectivities. The influence of acetic acid and temperature on the selectivity of the reactions was evaluated, in order to gain some experimental evidence for a change in the nature of the active species. Working conditions of no acetic acid at room temperature were compared with the addition of 50 equiv of acetic acid at 0°C (table 5). Efficiency and selectivity were just slightly improved or not modified in all evaluated cases (oxidation of cyclohexane: A+K (A/K), 7.0 (11) and 7.2 (29) respectively; KIE (TN), 3.6 (6.2) and 3.6 (6.6) respectively. Oxidation of adamantane: 2<sup>o</sup>/3<sup>o</sup> (TN), 23 (4.3) and 27 (4.8)) when temperature was 0°C and 50 equiv of AcOH were added. All these data strongly suggest that very similar, or the same, active species are responsible for the oxidation under both experimental conditions. As we will show later on (see discussion on section III.3.2.1), we propose that the role of acetic acid is the stabilization of the resting state of the catalyst.

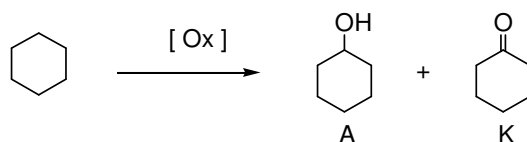
#### III.2.3.1.2. Substrate limiting conditions

Despite the great efficiency showed by 2OTf in the above mentioned conditions, low conversion of substrate makes the system not useful for synthetic chemistry. In 2007, Chen and White described the first non-heme catalyst capable to perform efficient alkane oxidation in preparative way (limiting substrate conditions).<sup>5</sup> Moreover their catalyst showed unprecedented predictable selectivity, making the system a useful tool for synthetic chemistry. Acetic acid is used in that system as a key additive to improve product yields. Taking in consideration this precedent, a new procedure for alkane oxidation with substrate limiting conditions was planned. Under standard conditions, 1.2 equivalents of H<sub>2</sub>O<sub>2</sub> were delivered over 6 minutes to a stirred solution cooled at 0°C with an ice-water bath containing 1 equivalent of substrate, 1% of catalyst and 50 equiv of AcOH. Depending on the substrate, after stirring for 10 minutes, a second and third simultaneous addition of solutions, containing H<sub>2</sub>O<sub>2</sub> in one syringe and catalyst and acetic acid in a parallel syringe, delivered over 6 minutes, could be required.

The first scan of this new conditions was done for the oxidation of cyclohexane and catalyst 7OTf (table 6, cat:H<sub>2</sub>O<sub>2</sub>:cyclohexane:AcOH ratio was 1:120:100:50 at 0°C), obtaining 17% total yield, showing not improvement versus initial conditions (cat:H<sub>2</sub>O<sub>2</sub>:CHx:AcOH, 1:100:100:0 at room temperature; 22% yield). Increasing the AcOH equivalents up to 1000, the yield was raised to 43%, whereas increasing initial catalyst loading afforded a 36% yield. A

second addition of catalyst, H<sub>2</sub>O<sub>2</sub> and AcOH (see experimental section) increased the total yield to 60%, obtaining almost selectively cyclohexanone as a product. A third and fourth addition of catalyst, H<sub>2</sub>O<sub>2</sub> and AcOH improved the yield up to 74% and 82%, respectively.

**Table 6.** Oxidation of cyclohexane under substrate limiting conditions.



| Catalyst          | Conditions<br>(cat:H <sub>2</sub> O <sub>2</sub> :cHx:AcOH) | A (TN) | K (TN) | Yield <sup>a</sup> |
|-------------------|-------------------------------------------------------------|--------|--------|--------------------|
| 7OTf <sup>c</sup> | 1:100:100:0                                                 | 6.4    | 15.9   | 22                 |
| 7OTf              | 1:120:100:50                                                | 6.9    | 10.6   | 17                 |
| 7OTf              | 1:120:100:1000                                              | 6.5    | 36.3   | 43                 |
| 7OTf              | 5:120:100:1000                                              | 1.8    | 5.4    | 36                 |
| 7OTf              | (1)x2:(120)x2:100:(1000)x2                                  | 1.8    | 28.2   | 60                 |
| 7OTf              | (1)x3:(120)x3:100:(1000)x3                                  | 1.1    | 23.3   | 74                 |
| 7OTf              | (1)x4:(120)x4:100:(1000)x4                                  | 0,4    | 20.1   | 82                 |
| 2OTf              | 1:100:100:0                                                 | 7.2    | 20.4   | 28                 |
| 2OTf              | 1:120:100:50                                                | 5.4    | 36.1   | 42                 |
| 2OTf              | 1:120:100:200                                               | 6.3    | 40.3   | 46                 |
| 2OTf              | 1:120:100:1000                                              | 10.1   | 32.7   | 44                 |
| 2OTf              | 1:150:100:50                                                | 6.3    | 42.7   | 49                 |
| 2OTf              | (1)x2:(120)x2:100:(50)x2                                    | 0.7    | 36.2   | 71                 |
| 2OTf              | (1)x3:(120)x3:100:(50)x3                                    | -      | 24.1   | 47                 |

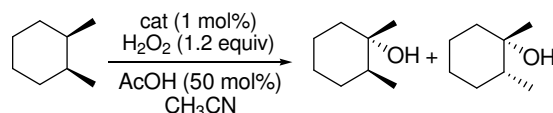
<sup>a</sup> GC yields based on product converted.

In the case of 2OTf, similar yields were obtained with 50, 200 and 1000 equivalents of AcOH (42, 46, 44% respectively) and only moderate improvement was achieved with respect to conditions in absence of AcOH at room temperature (28% yield). Increasing the number of H<sub>2</sub>O<sub>2</sub> equivalents from 120 to 150, the yield was slightly improved (49%). In contrast, a second addition of cat:H<sub>2</sub>O<sub>2</sub>:AcOH gave a 71% yield. A third addition caused a decrease in yield (47%), presumably due to the oxidation of the desired product. 2OTf exhibits a higher efficiency and robustness in the same conditions as for 7OTf. While two additions were necessary to achieve 71% yield with 2OTf, four were necessary to achieve 82% in the case of 7OTf. These data suggest that the addition of AcOH and the introduction of the pinene rings increase the efficiency of the catalyst. Combination of the two strategies led to a remarkably efficient reaction.

As a result of the experimental optimization, 1:120:100:50 were the selected conditions and the number of extra additions of cat:H<sub>2</sub>O<sub>2</sub>:AcOH required was evaluated for each substrate.

The oxidation of *cis*-1,2-DMCH was the first test in order to compare the activity of the different catalysts of the pinene-containing family. The complexes were tested as catalysts (1 mol%) for the hydroxylation of *cis*-1,2-DMCH using H<sub>2</sub>O<sub>2</sub> (1.2 equiv) as oxidant (table 7). Confirming our expectations, **1OTf-5OTf** proved to be very efficient catalysts, affording the corresponding tertiary alcohol in 54-63% yield with excellent stereoretention (> 99% *cis*). This yield is significantly better than those obtained with structurally related complexes **6OTf** and **7OTf** lacking the pinene arms (38 and 36%, respectively). TACN-based iron complex [Fe(CF<sub>3</sub>SO<sub>3</sub>)<sub>2</sub>(<sup>H</sup>PyTACN)] (**9OTf**) afforded a very low yield (2%), but **10OTf** and bipyrrolidine based [Fe(CH<sub>3</sub>CN)<sub>2</sub>((*S,S*)-bpbp)](CF<sub>3</sub>SO<sub>3</sub>)<sub>2</sub> (**8OTf**) which have been reported as exceptionally active catalysts<sup>5,27</sup> provided the corresponding alcohol in 45 and 47% yield respectively. Finally, since selective C-H hydroxylation reactions have been reported for manganese based complexes,<sup>46,47</sup> [Mn(CF<sub>3</sub>SO<sub>3</sub>)<sub>2</sub>((L7))]<sup>48</sup> and [Mn(CF<sub>3</sub>SO<sub>3</sub>)<sub>2</sub>(<sup>H</sup>PyTACN)]<sup>49,50</sup> were also tested, but proved non efficient (table 7, entries 12 and 13).

**Table 7.** Oxidation of *cis*-1,2-DMCH by various catalysts.<sup>a</sup>



| Entry | Catalyst                                                                   | Conversion | Yield(%) <sup>b</sup> | RC <sup>d</sup> |
|-------|----------------------------------------------------------------------------|------------|-----------------------|-----------------|
| 1     | <b>1OTf</b>                                                                | 68         | 54                    | > 99            |
| 2     | <b>2OTf</b>                                                                | 76         | 57                    | > 99            |
| 3     | <b>3OTf</b>                                                                | 77         | 63                    | > 99            |
| 4     | <b>4OTf</b>                                                                | 82         | 60                    | > 99            |
| 5     | <b>5OTf</b>                                                                | 78         | 63                    | > 99            |
| 6     | <b>6OTf</b>                                                                | 46         | 38                    | > 99            |
| 7     | <b>7OTf</b>                                                                | 59         | 36                    | > 99            |
| 8     | <b>8OTf</b>                                                                | 68         | 47                    | > 99            |
| 9     | <b>8SbF<sub>6</sub></b> <sup>c</sup>                                       | 67         | 54                    | > 99            |
| 10    | <b>9OTf</b>                                                                | 30         | 2                     | 90              |
| 11    | <b>10OTf</b>                                                               | 70         | 45                    | > 99            |
| 12    | [Mn(CF <sub>3</sub> SO <sub>3</sub> ) <sub>2</sub> ((L7))]                 | 16         | 1                     | 90              |
| 13    | [Mn(CF <sub>3</sub> SO <sub>3</sub> ) <sub>2</sub> ( <sup>H</sup> PyTACN)] | 30         | 8                     | 90              |

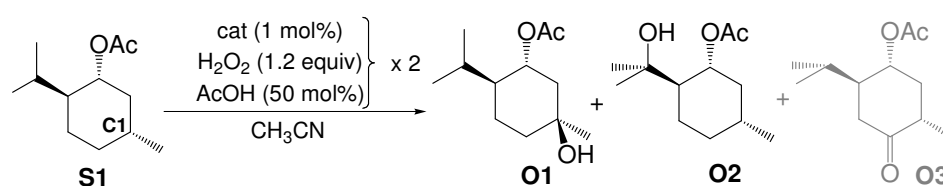
<sup>a</sup> Cat:H<sub>2</sub>O<sub>2</sub>:substrate:AcOH 1:120:100:50. <sup>b</sup> GC yields based on product converted. <sup>c</sup> [Fe(CH<sub>3</sub>CN)<sub>2</sub>((*S,S*)-bpbp)](SbF<sub>6</sub>)<sub>2</sub>. <sup>d</sup> RC = retention of configuration in the oxidation of the tertiary C-H bonds of *cis*-1,2-DMCH, expressed as the ratio of the tertiary alcohols: [(1*R*,2*R* + 1*S*,2*S*) - (1*R*,2*S* + 1*S*,2*R*)] / [(1*R*,2*R* + 1*S*,2*S*) - (1*R*,2*S* + 1*S*,2*R*)].

The selectivity of the complexes was tested using (–)-menthyl acetate (**S1**, table 8). This substrate contains two tertiary C-H bonds at the same distance of an acetate group, but C1 is

sterically less hindered.<sup>5</sup> In all cases hydroxylation preferentially occurs in the more accessible tertiary (C1)-H bond giving product **O1** as the main product while **O2** is obtained in lower yields. This resulted to be a more challenging substrate, and larger catalytic activity differences between complexes with and without pinene rings were found. **2OTf** proved to be the most efficient and selective one obtaining **O1** in 64% GC yield (50% isolated yield) and 17/1 **O1/O2** selectivity, followed by **4OTf** with 56% yield and 12.5/1 **O1/O2**. Moreover, **4OTf** was able to perform up to 224 TN of the desired product (28% **O1** yield) when low catalyst loading (0.125%) was used indicating the robustness of the catalyst.

In contrast, **1OTf**, **5OTf**, **8SbF<sub>6</sub>** and **10OTf** achieved moderate yields (26, 36, 33 and 34% respectively) and **3OTf** (5%), **6OTf** (6%) and **7OTf** (6%; up to 37% (**O1/O2** =9/1) if (cat:H<sub>2</sub>O<sub>2</sub>:AcOH 5:120:50)x3 are used) were poor catalysts for this reaction. On the other hand, a third product assigned as a ketone (**O3**, see table 8), was obtained in significant ratio when the topological chirality of the catalyst is  $\Delta$  (complexes **1OTf**, **3OTf** and **5OTf**; see figure 2) or when using catalyst **10OTf**. That suggests that the chiral topology adopted for the complex can determine efficiency and selectivity in selected substrates (see section III.3.2.2. for further discussion). The structure of the complex also plays an important role in selectivity, since the TACN based catalyst **10OTf** presented significantly lower 3° alcohol/ketone selectivity than the complexes containing linear ligands (**1-8**).

**Table 8.** Regioselective oxidation of (–)-menthyl acetate, **S1**.<sup>a</sup>



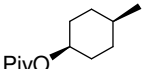
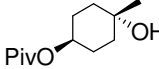
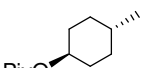
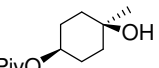
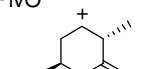
| Entry          | Catalyst                | Conversion | O1 Yield(%) <sup>b</sup> | O2 Yield(%) <sup>c</sup> | O3 Yield(%) <sup>b</sup> | O1/O2 <sup>d</sup> |
|----------------|-------------------------|------------|--------------------------|--------------------------|--------------------------|--------------------|
| 1              | <b>1OTf</b>             | 38         | 26                       | 5                        | 7                        | 4.8/1              |
| 2              | <b>2OTf</b>             | 85         | 64 (50) <sup>e</sup>     | 4                        | >1                       | 17/1               |
| 3              | <b>3OTf</b>             | 7          | 5                        | n.m.                     | n.m.                     | n.m.               |
| 4              | <b>4OTf</b>             | 72         | 56                       | 5                        | 7                        | 12.5/1             |
| 5 <sup>f</sup> | <b>4OTf</b>             | 53         | 48                       | n.m.                     | n.m.                     | n.m.               |
| 6 <sup>g</sup> | <b>4OTf</b>             | 33         | 28                       | n.m.                     | n.m.                     | n.m.               |
| 7              | <b>5OTf</b>             | 52         | 36                       | 7                        | 9                        | 5.2/1              |
| 8              | <b>6OTf</b>             | 8          | 6                        | n.m.                     | n.m.                     | n.m.               |
| 9              | <b>7OTf</b>             | 9          | 6                        | n.m.                     | n.m.                     | n.m.               |
| 10             | <b>8SbF<sub>6</sub></b> | 45         | 33                       | 4                        | 5                        | 8.9/1              |
| 11             | <b>10OTf</b>            | 67         | 34                       | 6                        | 15                       | 5.8/1              |

<sup>a</sup> Cat:H<sub>2</sub>O<sub>2</sub>:substrate:AcOH 1:120:100:50 followed by a second addition of cat:H<sub>2</sub>O<sub>2</sub>:AcOH 1:120:50. <sup>b</sup> GC yields based on product converted. <sup>c</sup> <sup>1</sup>H-NMR yield. <sup>d</sup> <sup>1</sup>H-NMR. <sup>e</sup> Isolated yield. <sup>f</sup> 1 mol% cat, 1 addition of 1.2 equiv. of H<sub>2</sub>O<sub>2</sub>. <sup>g</sup> 0.125 mol% cat, 1 addition of 1.2 equiv. of H<sub>2</sub>O<sub>2</sub>. n.m. = no measured.

The good results obtained by **2OTf** prompted us to further study its catalytic performance with other substrates. Several substrates with tertiary C-H bonds were oxidized achieving moderate to good yields (35-69%, tables 9 and 10). A particular interesting example is the difference in the selectivity in the oxidation of *cis*- and *trans*-4-methoxycyclohexyl pivalate. *cis*-4-methoxycyclohexyl pivalate is selectively hydroxylated at the 3° C-H bond, while *trans*-4-methoxycyclohexyl pivalate is oxidized to a mixture of 3° alcohol and ketone resulting from oxidation at 2° positions.

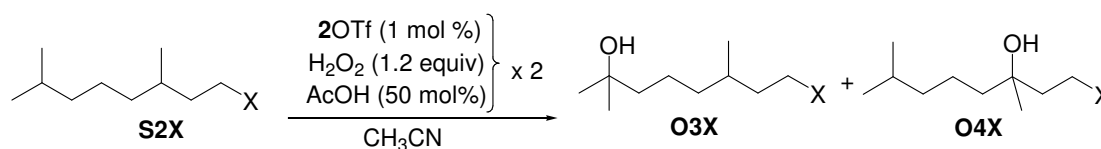
Site selectivity directed by electronic parameters was evaluated by using substrates with two 3° C-H bonds with the same or different electronic properties (table 10). In the oxidation of 2,6-dimethyloctane (**S2H**), both tertiary positions are oxidized, but noticeable selectivity for the more distant 3° C-H bond to the acetate (**S2OAc**) or bromide (**S2Br**) group is present.

**Table 9.** Alkane oxidation reactions catalyzed by **2OTf**.<sup>a</sup>

| Entry          | Substrate                                                                           | Products                                                                            | Yield (%) <sup>b</sup>                 |
|----------------|-------------------------------------------------------------------------------------|-------------------------------------------------------------------------------------|----------------------------------------|
| 1              | <i>c</i> -C <sub>6</sub> H <sub>12</sub>                                            | <i>c</i> -C <sub>6</sub> H <sub>10</sub> O                                          | 71                                     |
| 2              | <i>c</i> -C <sub>6</sub> D <sub>12</sub>                                            | <i>c</i> -C <sub>6</sub> D <sub>10</sub> O                                          | 63                                     |
| 3              | <i>c</i> -C <sub>7</sub> D <sub>14</sub>                                            | <i>c</i> -C <sub>7</sub> D <sub>12</sub> O                                          | 59                                     |
| 4              | <i>c</i> -C <sub>8</sub> D <sub>16</sub>                                            | <i>c</i> -C <sub>8</sub> D <sub>14</sub> O                                          | 55                                     |
| 5 <sup>c</sup> |  |  | 69(57 <sup>d</sup> )(51 <sup>e</sup> ) |
| 6              |  |  | 50(39 <sup>d</sup> )                   |
|                |                                                                                     |  | 19(16 <sup>d</sup> )                   |

<sup>a</sup> Cat:H<sub>2</sub>O<sub>2</sub>:substrate:AcOH 1:120:100:50 followed by a second addition of cat:H<sub>2</sub>O<sub>2</sub>:AcOH 1:120:50. <sup>b</sup> GC yields based on product converted. <sup>c</sup> Third addition of cat:H<sub>2</sub>O<sub>2</sub>:AcOH 1:120:50. <sup>d</sup> Isolated yield. <sup>e</sup> GC yield for **8OTf** under same conditions (analogous yield was obtained when **8SbF<sub>6</sub>** was used as catalyst).

**Table 10.** Electronic discrimination in the oxidation of substrates with multiple tertiary C-H bonds.



|                   | Isolated Yield (%) | GC Yield (%) | O3X/O4X |
|-------------------|--------------------|--------------|---------|
| X= H <sup>a</sup> |                    | 35           | 1/1     |
| Br                | 48                 | 51           | 7/1     |
| OAc               | 46                 | 49           | 5/1     |

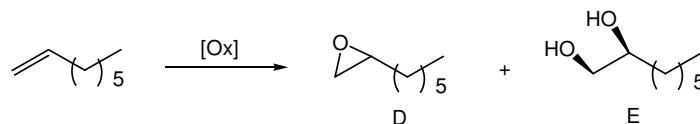
<sup>a</sup>One addition of 1.8 equiv of H<sub>2</sub>O<sub>2</sub>.

### III.2.3.2. Alkene oxidation

The oxidation of alkenes was also studied. Reaction conditions were not optimized but directly taken from a previous study by Jacobsen et al.<sup>3</sup> (reaction conditions: olefin (0.16M in CH<sub>3</sub>CN), catalyst (3.0 mol%), CH<sub>3</sub>CO<sub>2</sub>H (10 equiv relative to catalyst), H<sub>2</sub>O<sub>2</sub> (1.5 equiv relative to olefin, 1.5M in CH<sub>3</sub>CN added dropwise over 2 min), 0°C, 5 min). However, because of the higher activity of **2OTf**, preliminary experiments with 1-octene showed that better yields were obtained when 1.1 equiv of H<sub>2</sub>O<sub>2</sub> (instead of 1.5 equiv as Jacobsen originally reported) were used (82% and 76%, respectively), probably minimizing overoxidation of the product.<sup>3</sup> The oxidation of 1-octene with **1OTf-5OTf** showed in all cases strong preference for the epoxide *versus* the *cis*-diol product, obtaining the former in good yields ranging from 69 to 82%. The introduction of the pinene did not influence remarkably on the reactivity of the complexes (see table 11).

Oxidation of carvone was regioselective in all cases, affording almost exclusively the 8,9-monoepoxide in 71 to 80% yield (<sup>1</sup>H-NMR of crude reaction revealed that aldehyde (up to 10%) was formed) (scheme 7 and table 11). Most remarkably, the reaction exhibited a significant degree of diastereoselectivity. The impact of the introduction of the pinene ring in the diastereoselectivity of the reaction was positive in all cases but the extent of it was different depending on the diamine backbond. Small influence was observed between **7OTf** and **2OTf-3OTf** (18 and 24-26% de, respectively) and medium between **8OTf** and **4OTf-5OTf** (13 and 25% de, respectively). The introduction of the pinene ring to the achiral catalyst **6OTf** induced 21% of de. The latter case shows that the chirality of the pinene ring itself is capable of inducing chirality to the complex as was shown by X-ray (see section III.2.2). Moreover, modification of the diamine, whether chiral or achiral, does not influence deeply the obtained de. On the other hand, the sign of the major diastereoisomer obtained is determined by the topology of the helix, being (-) for  $\Delta$  complexes (**1OTf**, **3OTf** and **5OTf**) and (+) for  $\Lambda$  complexes (**2OTf** and **4OTf**). Although still far from practical utility, the stereoselectivity for non aromatic substrates exhibited by **1OTf-5OTf** is significantly better than any previously reported non-heme iron catalyst. For example, Menage and coworkers have recently reported the first example of a dinuclear iron-oxo complex containing pinene-bipyridine ligands [Fe<sub>2</sub>O(bisPB)<sub>4</sub>(H<sub>2</sub>O)<sub>2</sub>](ClO<sub>4</sub>)<sub>4</sub> (bisPB = 4,5-pinene-2,2'-bipyridine) that catalyzes the enantioselective conversion of alkenes into epoxides, and they reported 19% de in the oxidation of carvone.<sup>51</sup> Although structurally related, it is very likely that the better stereo discrimination exhibited by **1OTf-5OTf** is due to complete control of the topological isomerism, as [Fe<sub>2</sub>O(bisPB)<sub>4</sub>(H<sub>2</sub>O)<sub>2</sub>](ClO<sub>4</sub>)<sub>4</sub> catalysts is likely to be a mixture of diastereoisomers. Unfortunately, epoxidation of aromatic substrates, which commonly afford better enantioselectivities, by **1OTf-5OTf** is not possible as the substrates are somehow destroyed under the reaction conditions.



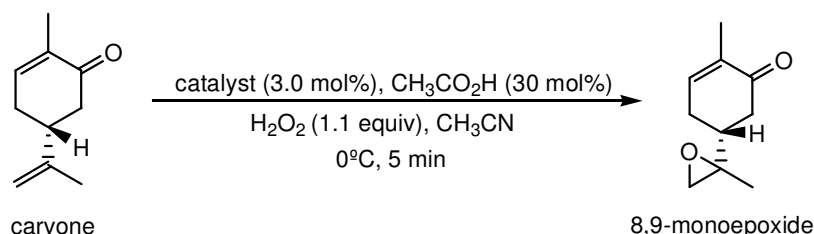
**Table 11.** Selected olefin epoxidation reactions by various catalysts.<sup>a</sup>

| Entry | Complex           | Substrate               | Conv. (%) | Products (TN) | Epoxide yield | de <sup>b</sup> | Cc <sup>c</sup> |
|-------|-------------------|-------------------------|-----------|---------------|---------------|-----------------|-----------------|
|       |                   |                         |           | E/D           | (%)           |                 |                 |
| 1     | 1OTf              | 1-octene                | 100       | 24.5/1.1      | 77            |                 | 26              |
| 2     | 2OTf <sup>d</sup> | 1-octene                | 100       | 29.1/0.8      | 76            |                 | 30              |
| 3     | 2OTf              | 1-octene                | 98        | 30.1/1.2      | 82            |                 | 31              |
| 4     | 2OTf <sup>e</sup> | 1-octene                | 95        | 24.2/0.7      | 72            |                 | 25              |
| 5     | 2OTf <sup>f</sup> | 1-octene                | n.d.      | 81.0/3.5      | 81            |                 | 84.5            |
| 6     | 3OTf              | 1-octene                | 96        | 28.0/1.1      | 82            |                 | 29              |
| 7     | 4OTf              | 1-octene                | 91        | 25.1/1.2      | 69            |                 | 26              |
| 8     | 5OTf              | 1-octene                | 100       | 28.5/1.6      | 78            |                 | 30              |
| 9     | 7OTf <sup>d</sup> | 1-octene                | 100       | 28.6/1.3      | 86            |                 | 30              |
| 10    | 8OTf              | 1-octene                | 100       | 26.9/1.9      | 81            |                 | 29              |
| 11    | 1OTf              | carvone                 | 95        | 25.4          | 77            | -21             | 25              |
| 12    | 2OTf              | carvone                 | 98        | 29.3          | 80            | +24             | 29              |
| 13    | 3OTf              | carvone                 | 96        | 23.8          | 71            | -26             | 24              |
| 14    | 4OTf              | carvone                 | 91        | 21.0          | 63            | +25             | 21              |
| 15    | 5OTf              | carvone                 | 95        | 25.6          | 77            | -25             | 26              |
| 16    | 6OTf              | carvone                 | 91        | 25.9          | 78            | 0               | 26              |
| 17    | 7OTf <sup>d</sup> | carvone                 | 100       | 19.4          | 59            | +18             | 19              |
| 18    | 8OTf              | carvone                 | 96        | 25.2          | 75            | +13             | 25              |
| 19    | 2OTf              | <i>cis</i> -2-heptene   | n.d.      | 25.2/0.4      | 76            |                 | 26              |
| 20    | 2OTf              | <i>trans</i> -2-heptene | n.d.      | 19.8/0.3      | 60            |                 | 20              |
| 21    | 2OTf              | <i>trans</i> -3-octene  | 96        | 28.2/0.2      | 85            |                 | 28              |
| 22    | 2OTf <sup>f</sup> | <i>trans</i> -4-octene  | n.d.      | 76.9/2.1      | 77            |                 | 79              |
| 23    | 2OTf              | <i>cis</i> -cyclooctene | 100       | 28.0/0.8      | 87            |                 | 29              |
| 24    | 2OTf              | vinylcyclohexane        | 100       | 26.9/0.3      | 80            |                 | 27              |
| 25    | 2OTf <sup>f</sup> | vinylcyclohexane        | 87        | 78.5/2.7      | 79            |                 | 81              |

<sup>a</sup> Reaction conditions: olefin (0.16M in CH<sub>3</sub>CN), catalyst (3.0 mol%), CH<sub>3</sub>CO<sub>2</sub>H (10 equiv relative to catalyst), H<sub>2</sub>O<sub>2</sub> (1.1 equiv relative to olefin, 1.5M in CH<sub>3</sub>CN added dropwise over 2 min), 0°C, 5 min. <sup>b</sup> Diastereomeric excess (the sign of the major diastereoisomer was not determined, but was assigned randomly). <sup>c</sup> Catalytic cycles. <sup>d</sup> 1.5 equiv of H<sub>2</sub>O<sub>2</sub>. <sup>e</sup> 1 equiv of H<sub>2</sub>O<sub>2</sub>. <sup>f</sup> 1% of catalyst. n.d = not determined.

As similar results were obtained for the five 1OTf-5OTf complexes, the scope of the reaction was determined only for 2OTf. Oxidation of *trans*-4-octene, *trans*-3-octene, *cis*-cyclooctene and vinylcyclohexane under these conditions afforded epoxide products in moderate to good yield (60-87%, table 11). No significant amounts of diols were observed.

Oxidation of *cis*-2-heptene and *trans*-2-heptene were stereospecific, affording exclusively the corresponding *cis*-epoxide and *trans*-epoxide, respectively. Finally, two tests with 1% of catalyst were done obtaining the same results as previously (1-octene 81% and vinylcyclohexane 79%, table 11 entries 3, 5, 25 and 26), indicating that the catalyst is robust and that smaller catalyst loading can be used without significant decrease of the catalytic activity.



**Scheme 7.** Regioselective oxidation of carvone.

## III.2.4. Kinetic studies

### III.2.4.1. GC monitoring of catalyst activity

The profound effect that the bulky pinene groups have in the efficiency and stability of the catalysts is evidenced by performing a time profile analysis of the oxidation of (-)-menthyl acetate, **S1** (see table 8 and figure 9). The formation of **O1** was followed over time by GC for catalysts **7OTf**, **8SbF<sub>6</sub>** and **2OTf**. This analysis shows that **7OTf** has a much lower catalytic activity than **8SbF<sub>6</sub>** and **2OTf** during all H<sub>2</sub>O<sub>2</sub> addition (addition of oxidant during the initial 6 minutes). This is in agreement with the lower yields observed for **7OTf**. In sharp contrast, the structurally related pinene containing **2OTf** consume more rapidly and efficiently the H<sub>2</sub>O<sub>2</sub> oxidant. Moreover, **2OTf** showed maintenance of the very high activity during all the addition of oxidant. **8SbF<sub>6</sub>** instead, exhibit comparable profile as **2OTf** in the initial two minutes of H<sub>2</sub>O<sub>2</sub> addition, but activity decreases quickly after that time, indicating deactivation of the catalyst.

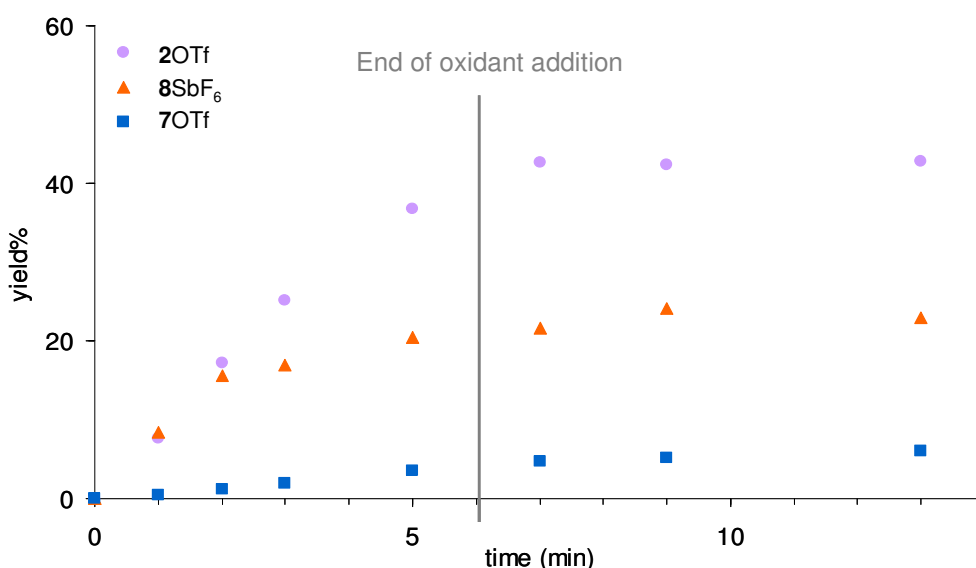


**Figure 9.** **O1** yield versus time in the catalytic oxidation of **S1** by **2OTf**, **8SbF<sub>6</sub>** and **7OTf** (Cat:H<sub>2</sub>O<sub>2</sub>:substrate:AcOH 1:120:100:50 at 0°C, addition of H<sub>2</sub>O<sub>2</sub> during the 6 initial minutes followed for 10 additional minutes of stirring at 0°C).

To gain more insight into the stability of the complexes, a second addition of oxidant was performed in presence of excess of substrate, in order to minimize overoxidation of the product that could mask the real activity. **2OTf**, **4OTf**, **5OTf**, **7OTf** and **8OTf** were compared (see figure 10). Only **2OTf** and **4OTf**, the pinene-containing complexes with  $\Lambda$  topological chirality, maintained its activity after the first  $\text{H}_2\text{O}_2$  addition, while **5OTf** ( $\Delta$  isomer) or complexes without pinene groups were completely deactivated (**7OTf** and **8OTf**). Indeed, for the particular case of **2OTf**, the number of TN of **O1** product obtained in the first and second  $\text{H}_2\text{O}_2$  addition are comparable (50 TN and 45 TN, respectively). These observations thus demonstrate that both the presence of the pinene rings, the proper combination of the topological chirality ( $\Lambda/\Delta$ ) and the chirality of the pinene rings exert a profound influence in the efficiency and stability of the catalysts.

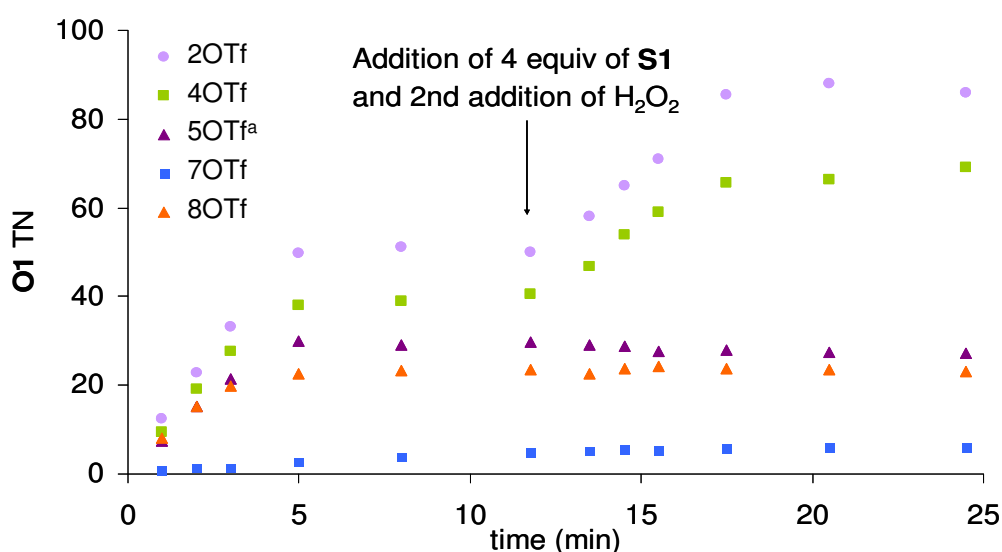


**Figure 10.** The **O1** formation in the hydroxylation of **S1** versus time in two-step addition of  $\text{H}_2\text{O}_2$  in presence of large excess of substrate, show the relative stability of the catalysts **2OTf**, **4OTf**, **5OTf**, **7OTf** and **8OTf**. <sup>a</sup> For **5OTf**, **O1+O2** TN is represented. (Cat: $\text{H}_2\text{O}_2$ :substrate:AcOH 1:120:100:50 at  $0^\circ\text{C}$ , addition of  $\text{H}_2\text{O}_2$  during the 6 initial minutes followed for 6 additional minutes of stirring at  $0^\circ\text{C}$ . Addition of 4 equiv of substrate and immediately second addition of  $\text{H}_2\text{O}_2$  over 6 minutes).

#### III.2.4.2. ESI-MS monitoring of catalyst stability

In order to obtain experimental evidence of the species present in solution during the catalytic reactions that could help to understand the role of the bulky pinene rings, reactions were followed by ESI-MS spectrometry. Oxidation of **S1** (1 equiv) with  $\text{H}_2\text{O}_2$  (1.2 equiv over 6 min) and **2OTf** or **7OTf** as catalyst (1 mol%) in the presence of 50% mol of AcOH at  $0^\circ\text{C}$  was performed and samples were analyzed after 3 minutes since beginning of  $\text{H}_2\text{O}_2$  addition and at the end of the  $\text{H}_2\text{O}_2$  addition. In general, the ESI-MS spectra of these catalytic reactions are quite complex and exhibit a number of peaks that have eluded complete characterization. Nevertheless, key observations are derived from the experiments.

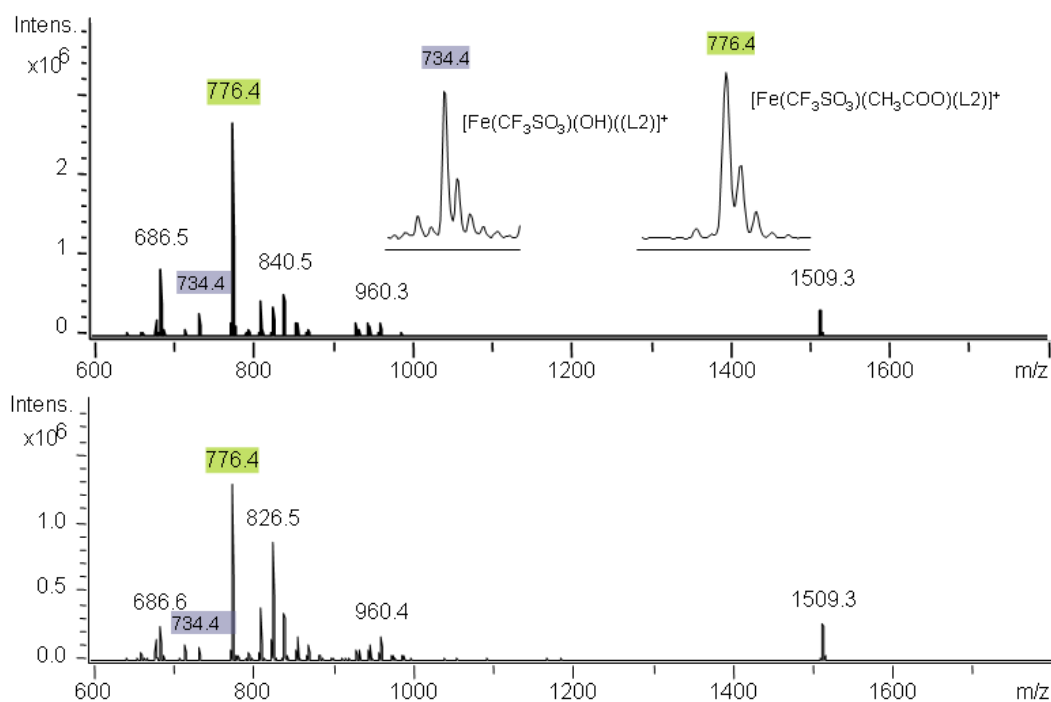


**Figure 11.** ESI-MS spectrum obtained during  $\text{H}_2\text{O}_2$  addition (at time = 3 min) in the catalytic oxidation of **S1** by **2OTf** (up). Amplified peaks corresponding to  $[\text{Fe}(\text{CF}_3\text{SO}_3)(\text{OH})(\text{L2})]^+$  and  $[\text{Fe}(\text{CF}_3\text{SO}_3)(\text{CH}_3\text{COO})(\text{L2})]^+$  (inset). ESI-MS spectrum obtained after  $\text{H}_2\text{O}_2$  addition in the catalytic oxidation of **S1** by **2OTf** (down).

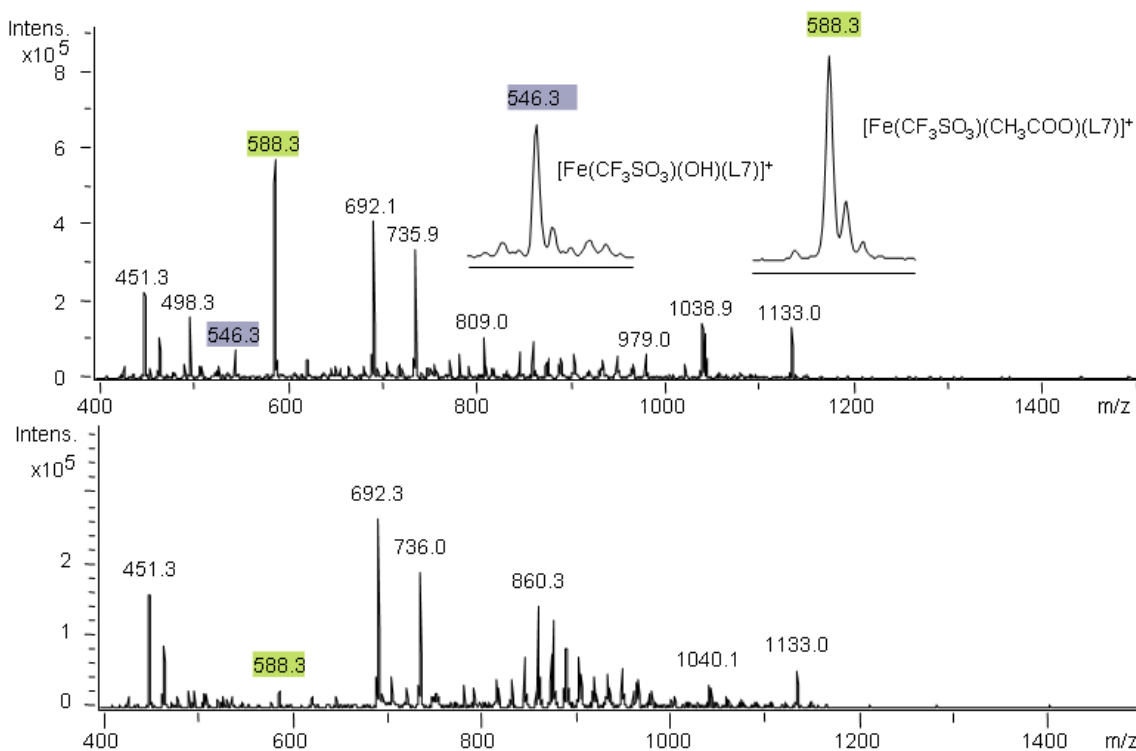


**Figure 12.** ESI-MS spectrum obtained during  $\text{H}_2\text{O}_2$  addition (3 min since beginning of addition) in the catalytic oxidation of **S1** by **7OTf** (up). Amplified and simulated peaks corresponding to  $[\text{Fe}(\text{CF}_3\text{SO}_3)(\text{OH})(\text{L7})]^+$  and  $[\text{Fe}(\text{CF}_3\text{SO}_3)(\text{CH}_3\text{COO})(\text{L7})]^+$  (inset). ESI-MS spectrum obtained after  $\text{H}_2\text{O}_2$  addition in the catalytic oxidation of **S1** by **7OTf** (down).

In particular, ESI-MS analyses (figures 11 and 12) show that monomeric  $[\text{Fe}^{\text{III}}(\text{OR})(\text{CF}_3\text{SO}_3)\text{L}]^+$  (OR = OH, OAc) species (L = L2,  $m/z$  = 734.4 and 776.4, respectively; L = L7,  $m/z$  = 546.3 and 588.3, respectively) are rapidly formed upon reaction of **2OTf** and **7OTf** with  $\text{H}_2\text{O}_2$  in presence of AcOH and **S1**. These species are presumed to be the precursors of the mononuclear high-valent iron-oxo species responsible for catalytic activity.<sup>2,27,29,45</sup> Most remarkably, such species still remain in final reaction solutions of **2OTf**, whereas they have rapidly disappeared during  $\text{H}_2\text{O}_2$  addition when **7OTf** is used. We conclude that the pinene rings play a key role in stabilizing such mononuclear species, most likely via steric encumbrance.

### III.3. Discussion

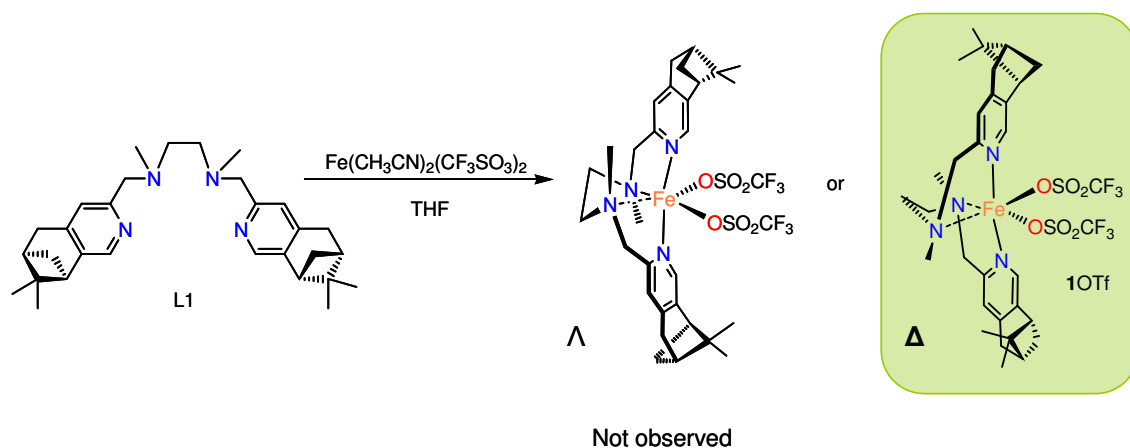
#### III.3.1. A new family of complexes with pyridine-pinene pendant arms

A new family of non-heme monoiron complexes has been prepared. The complexes contain tetradentate  $\text{N}_4$  ligands with two pyridine rings pendant from an aliphatic diamine. They are structurally related to the earlier reported bpmn, bpmcn and bpbp ligands and contain bulky pinene groups fused at 4<sup>th</sup> and 5<sup>th</sup> positions of the pyridine rings that help to isolate the iron site without perturbing the stability of the complexes. In addition, the chirality and structure of the diamine backbone allows predetermination of the topological chirality ( $\Delta$  or  $\Lambda$ ) and determines the relative orientation of the robust pinene  $\text{CH}_3$  groups with respect to the metal site. Moreover, these very simple modifications let us fine tuning the properties of the resulting complexes. For example, the basicity of this family of ligands is modulated by these structural variations. This is clearly evidenced in the  $\text{Fe}^{\text{III}}/\text{Fe}^{\text{II}}$  redox potential of the corresponding **1Cl-5Cl** complexes which expand from 61 to 125 mV (all  $E_{1/2}$  values are measured *versus* SCE, table 3). The redox potential decreases depending on the aliphatic diamine backbone nature in the following order: ethylenediamine > cyclohexanediamine > bipyrrrolidine. Moreover, the presence of the pinene ring fused to the pyridine causes a decrease in the redox potential with respect to complexes **6Cl-8Cl** that lack the pinene group. It is also interesting to notice that complex **4Cl** exhibits a  $E_{1/2}$  redox potential for  $\text{Fe}^{\text{III}}/\text{Fe}^{\text{II}}$  pair ( $E_{1/2}$  = 61 mV) at lower potentials than analogous  $[\text{FeCl}_2(\text{tpa})]$  ( $E_{1/2}$  = 200 mV, tpa = tris(2-pyridylmethyl)amine),<sup>2</sup> and  $[\text{FeCl}_2(\text{}^{\text{H}}\text{PyTACN})]$  ( $E_{1/2}$  = 138 mV)<sup>52</sup> thus indicating that L4 is more basic than tpa and  ${}^{\text{H}}\text{PyTACN}$  (see scheme 1 for ligands' structures). High-valent iron species have been established as key elements on tpa,<sup>2,53</sup> PyTACN<sup>27,29</sup> and bpmcn<sup>4</sup> families in the catalytic oxidation of alkanes and alkenes with  $\text{H}_2\text{O}_2$ ; consequently, the major basicity of the pinene derivate ligand, strongly suggests that high oxidation states are also accessible for this system under analogous reaction conditions.

Complexes **1OTf-5OTf** were prepared as catalysts' precursors as they are straightforward synthesized and isolated in pure crystalline form (scheme 5). Compounds **1OTf-5OTf** were obtained exclusively in *cis- $\alpha$*  conformation as indicated by the presence of one set of signals for the two symmetric parts of the complexes in the  ${}^1\text{H-NMR}$  spectrum. This observation was corroborated by X-Ray analysis.  $\text{Fe}^{\text{II}}$  ( $3d^6$ ) compounds **1OTf-5OTf** are high spin in non coordinating solvents as  $\text{CH}_2\text{Cl}_2$  as ascertained by their paramagnetically shifted  ${}^1\text{H-NMR}$

spectra, and also in the solid state as proven by the Fe-N distances ( $\sim 2.2 \text{ \AA}$ ) in the single crystal X-Ray structures. On the other hand, upon dissolving in acetonitrile, **1OTf-5OTf** undergo fast substitution reactions to give complexes of the type  $[\text{Fe}(\text{CH}_3\text{CN})_2(\text{L})](\text{OTf})_2$ , which can exist in a spin crossover regime.<sup>54</sup> The rapid interconversion between paramagnetic high spin (HS) and diamagnetic low spin (LS) complexes, combined with the exchange of coordinated and free acetonitrile and triflate ligands, results in very broad  $^1\text{H-NMR}$  signals that expand from -1 to 120 ppm at room temperature, making interpretation of the spectrum not straightforward. Moreover, complex **2OTf** presented temperature-dependent  $^1\text{H-NMR}$  behavior as is shown in figure 6. Upon lowering the temperature, the more paramagnetically shifted signals tend to collapse due to the increasing population of the diamagnetic (LS) state. This is evidenced by the lack of linearity in variation of chemical shift of more paramagnetically shifted protons *versus*  $1/T$  (see figure 7).

From the X-Ray analyses several interesting observations arise. Complexes **1OTf**, **3OTf** and **5OTf** show  $\Delta$  topological chirality and, unlike **2OTf** and **4OTf** (figure 2), do not create a well defined closed cavity around the metal ion. On the other hand, **2OTf** and **4OTf** exhibit  $\Lambda$  topological chirality and the ligand form a well defined cavity around the metal ion that improves its isolation. Interestingly, X-Ray and  $^1\text{H-NMR}$  analyses indicate that **1OTf** was obtained selectively in a unique topological chirality even though the ligand contains an achiral diamine backbone, indicating that the  $\Delta$  topology is the more stable structure. This is a very remarkable observation as it indicates that the chirality of the rather remote pinene ring dictates its topology and thus it determines the chirality “at the metal” (see scheme 8). This was reversed in the case of **2OTf** and **4OTf** which contain a (*S,S*) chiral diamine. These differences in conformation and in the relative orientation of the pinene-Me groups (towards the triflate ligands inside of the cavity or the opposite direction outside of the cavity) can be controlled just by changing the chirality of the diamine backbone and are related with the differences in selectivity observed among the members of this family of complexes in catalytic oxidation reactions (*vide infra*).



**Scheme 8.** Stereospecific synthesis of **1OTf**.

## III.3.2. Oxidation of alkanes

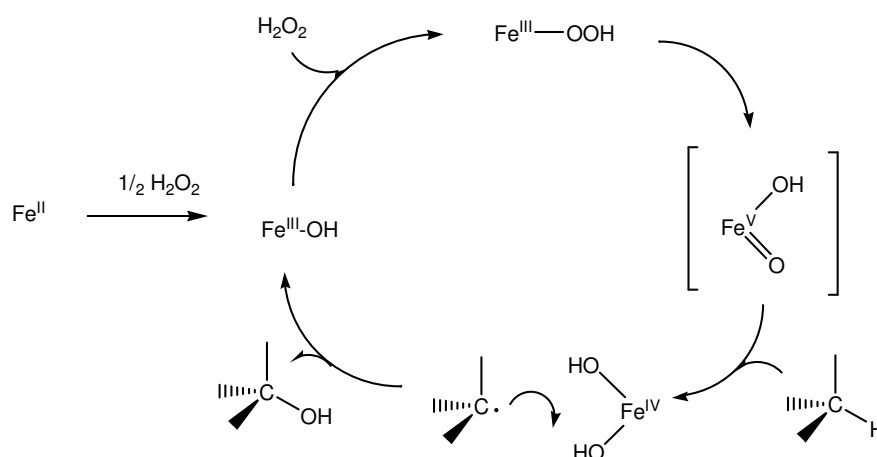
### III.3.2.1. A family of efficient stereospecific oxidation catalysts

Large excess of substrate conditions were initially employed in the catalytic oxidation of selected alkanes in order to compare the efficiency of **2OTf** with non-heme iron catalysts reported in the literature. The very close structure of complexes **1OTf-5OTf** justifies the use of **2OTf** as starting model for the whole family. The oxidation of cyclohexane with 10 and 100 equivalents of H<sub>2</sub>O<sub>2</sub> showed that **2OTf** (7.0TN (A+K), 11 (A/K); 73TN (A+K), 4.3 (A/K); respectively) is a very efficient catalyst, comparable with state of the art non-heme iron catalysts evaluated under analogous conditions; **10OTf** (7.6TN (A+K), 10.2 (A/K); 64TN (A+K), 4.3 (A/K); respectively; table 4). Interestingly, comparison of **2OTf** with **7OTf** showed that the latter exhibits a significant decrease in catalytic efficiency and A/K ratios (5.9TN (A+K), 9(A/K); 48TN (A+K), 3.5 (A/K); respectively).

#### III.3.2.1.1. Mechanistic considerations

Insight into the nature of the species responsible for the C-H oxidation was evaluated by making use of different mechanistic probes. The high stereoretention in *cis*-1,2-DMCH oxidation, large KIE values in the oxidation of cyclohexane and normalized  $3^{\circ}/2^{\circ}$  adamantane selectivities (table 5) are clearly different from hydroxyl radical initiated reactions, and they are indicative of the involvement of a highly selective metal centered oxidant in these reactions. In the presence of various accessible C-H positions, the strength of the C-H bond is a major factor in determining C-H selectivity, which strongly suggests the involvement of the C-H bond cleavage in the rate determining step of the hydrocarbon functionalization and suggesting the formation of a metal based selective oxidant. Most remarkably, the high stereoretention observed in the hydroxylation of *cis*-1,2-DMCH is consistent with a mechanism where long lived radical and/or carbocationic intermediates do not mediate the formation of the C-OH bond. If this was the case, epimerization and subsequent low retention of configuration would be detected in the oxidized products. On the other hand, the impact of the addition of acetic acid at 0°C were evaluated by means of different mechanistic probes. The data obtained was compared with more common standard conditions that did not include AcOH and where reactions were run at room temperature. Neither significant changes in terms of selectivity (KIE for C<sub>6</sub>H<sub>10</sub>/C<sub>6</sub>D<sub>10</sub>,  $3^{\circ}/2^{\circ}$  for adamantane) nor stereospecificity (*cis*-1,2-DMCH) were observed, strongly suggesting that the nature of the C-H hydroxylating active species is the same under both experimental conditions. On the basis of literature precedents, the reaction mechanism proposed for the present systems is showed in scheme 9. The mechanism is initiated by the oxidation of the starting Fe<sup>II</sup> complex to Fe<sup>III</sup>-OH species. Such species further reacts with H<sub>2</sub>O<sub>2</sub> to generate Fe<sup>III</sup>-OOH species that undergoes heterolytic O-O bond cleavage to form Fe<sup>V</sup>=O species that is responsible for the hydroxylation of the C-H bond and epoxidation of olefins. In this mechanism, the role of AcOH in olefin epoxidation reactions has been recently proposed to assist the O-O bond cleavage event. Moreover, one catalyst deactivation path is the formation

of oxo-bridged oligomeric species, a very facile reaction because of the high Lewis acidity of the  $\text{Fe}^{\text{III}}$  center. Most likely, the decrease in the pH caused by the AcOH addition also plays a beneficial role by limiting the Lewis acid driven dimerization.



**Scheme 9.** Proposed reaction mechanism for alkane hydroxylation with  $\text{Fe}^{\text{II}}$  complexes and  $\text{H}_2\text{O}_2$  as oxidant.

### III.3.2.2. Synthetically useful conditions in alkane oxidation

Under the previous experimental conditions of large excess of substrate, good efficiencies in the stereospecific hydroxylation of unactivated  $\text{sp}^3$  C-H bonds are achieved using  $\text{H}_2\text{O}_2$ , an inexpensive and environmentally friendly oxidant, and **2OTf** as catalyst. But the aforementioned conditions are useless from a synthetic point of view because of the large excess of substrate required. For this reason we optimized the conditions reported by Chen and White, in which the substrate is the limiting reactive. Iterative additions of catalyst,  $\text{H}_2\text{O}_2$  and AcOH were employed. Importantly, only 1 to 3% of catalyst loadings were necessary to obtain moderate to good yields, compared to the 15-20% reported by White, what is attributed to a higher activity of our catalysts.

#### III.3.2.2.1. Selectivity considerations

Oxidation of *cis*-1,2-DMCH was stereospecific (table 7), indicating that also in these conditions long lived carbocationic and/or radical type of intermediates are not involved. Moreover, only one addition of  $\text{H}_2\text{O}_2$  was required for optimal results in the stereospecific oxidation of *cis*-1,2-DMCH, and similar results were obtained for all the pinene-substituted complexes **1OTf-5OTf** (54-63% yield). Such yields represent an improvement of up to 27% if compared with the respective catalyst without pinene rings (**1OTf** vs **6OTf**, **2OTf-3OTf** vs **7OTf** and **4OTf-5OTf** vs **8OTf-8SbF<sub>6</sub>**).

Electronic and/or steric factors play a role in discriminating between different C-H bonds, thus making site-selective oxidation predictable. The role of steric factors was established by performing the oxidation of (–)-menthyl acetate (**S1**, table 8). This substrate presents two tertiary C-H bonds at the same distance to an acetate group, are electronically equivalent,<sup>5</sup> but C1 is less sterically hindered (table 8). All of the catalysts explored afforded the



C1-hydroxylated alcohol as the major product, **O1**, but product yields and the extent of site selectivity were dependent on the specific nature of the catalyst. (-)-menthyl acetate demonstrates to be a challenging substrate; two iterative additions were necessary for optimal results and more differences between catalysts arose. With the single exception of **3OTf**, product yields of a given catalyst containing pinene rings were better than with the respective catalyst without pinene rings (table 8, compare **1OTf** with **6OTf**, **2OTf** with **7OTf**, and **4OTf** and **5OTf** with and **8SbF<sub>6</sub>**). The chiral conformation adopted by the ligand appears to be crucial in the selectivity and activity of the catalyst. **2OTf** and **4OTf** with  $\Lambda$  conformation, proved to be the most selective and efficient catalysts (yield,%(**O1/O2**), 64(17/1) and 54(12,5/1), respectively). Such results are significantly better than those obtained by **8SbF<sub>6</sub>** under analogous conditions. On the other hand, **5OTf**, which only differs from **4OTf** in the configuration of the diamine backbone and presented a  $\Delta$  conformation, showed completely different selectivity. Not only **O2** was formed in 7% yield but a second side product corresponding to ketone **O3** was formed in 9% yield. Moreover the overall yield obtained with **5OTf** is significantly lower than with **4OTf**. This is also observed for **1OTf**, which affords a better yield than **6OTf**, (albeit not as high as with **2OTf**), while the site selectivity exhibited was similar as in the case of **5OTf**. All these observations point to the enhancement of the selectivity and yields when a proper disposition of the pinene rings is forced by the ligand backbone. In this respect, robustness of catalyst **4OTf** was demonstrated performing 224TN with high selectivity in the oxidation of **S1** (**O1** in 28% yield) when only using 0.125% of catalyst loading. On the other hand the ligand structure is also a crucial factor in the selectivity since TACN based complex **10OTf** presented lower selectivity for the tertiary alcohol than the pinene-containing family of complexes.

**2OTf** proved to be the most efficient as well as the most selective catalyst among the studied complexes. Thus, its catalytic activity was further studied against a series of substrates. The stereospecific hydroxylation of tertiary C-H bonds was explored, since it opens an entry to trisubstituted chiral alcohols, which are not amenable for free diffusing radical type of reactions. A series of substrates (tables 7-10) were oxidized to the corresponding tertiary alcohol. In general, the catalyst exhibits good selectivity for tertiary C-H bonds, even in the presence of statistically more abundant secondary C-H sites. This preference for 3<sup>o</sup> positions indicates that the strength of the C-H bond is a major factor dictating site selectivity and, it is consistent with an oxidant that operates via hydrogen atom abstraction.

Site selectivity directed by electronic parameters was clearly evidenced when the oxidation of substrates containing multiple C-H bonds was attempted (table 10). Oxidation of 2,6-dimethyloctane (**S2H**) afforded a 1:1 mixture of tertiary alcohol products (**O3H** and **O4H**), while functionalization of **S2Br** and **S2OAc**, occurred selectively at the distal C-H bond. In all cases examined, hydroxylation occurred preferentially at the most electron-rich tertiary C-H bond, despite the fact that secondary C-H bond have a significant statistical advantage.

The oxidation of *trans*-4-methoxycyclohexyl pivalate occurred in 69% yield obtaining 2.6/1 3<sup>o</sup> alcohol/ketone ratio. On the other hand, *cis*-4-methoxycyclohexyl pivalate was selectively oxidated in the tertiary C-H bond distant to the pivalate group in 69%. This observation can be reasoned by the fact that equatorial C-H bonds react more rapidly than

those oriented axially. The rate enhancement in these reactions is attributed to a release of strain in the 1,3-diaxial interactions, as was recently pointed out by Baran and co-workers<sup>55</sup> and exemplified by White and co-workers in the oxidation of *cis* and *trans*-1,2-DMCH.<sup>56</sup> Furthermore, hydroxylation occurred with complete retention of stereochemistry in both cases (figures 14 and 15 in experimental section).

Besides, simple alkanes were also oxidized to obtain the corresponding ketones in moderate to good yields (56-71%), which compare favorably with metal based systems that work under free-diffusing radical conditions.<sup>57-60</sup>

#### III.3.2.2.2. Catalyst stability

In order to demonstrate the influence of the introduction of the pinene and the chirality of the complexes on the robustness of the catalyst, the product formation in the oxidation of **S1** was monitored. Those experiments clearly showed that the proper disposition of the pinene rings, controlled by the chirality ( $\Lambda$  or  $\Delta$ ) of the complex, not only increases the efficiency of  $H_2O_2$  transformation into products and the selectivity but also the catalyst stability (figure 10). While catalysts lacking of pinene (**7OTf** and **8OTf**) or with  $\Delta$  configuration (**5OTf**) showed deactivation after the first addition of  $H_2O_2$ ,  $\Lambda$  complexes (**2OTf** and **4OTf**) displayed high activities in the second addition of oxidant.

Moreover, ESI-MS monitoring of the reaction showed that the resting state of the catalytic cycle can be detected at the end of addition of  $H_2O_2$  in the case of complex **2OTf**, but not in the case of **7OTf** (figure 11 and 12).

Those observations are in agreement with the very high efficiencies in catalysis observed for complex **2OTf** and **4OTf**, demonstrating that the well defined ligand cavity around the iron ion in those complexes increases their robustness protecting them from deactivation pathways.

### III.3.3. Oxidation of alkenes

The catalytic ability of **1-5OTf** in the oxidation of olefins with  $H_2O_2$  was also explored and the main results are showed in table 11. In this case, all complexes showed good yields expanding from 59 to 87 for the formation of the corresponding epoxide as main product. Remarkably, results are good even for challenging olefins like terminal ones (table 11). These results are comparable to those showed by the related system reported by Jacobsen and co-workers.<sup>3</sup> Noticeably, our system exhibits higher efficiency in the transformation of the oxidant into products than the above mentioned related system. These results along with the low catalyst loading required show the high efficiency of our system, specially remarkable if compare with other epoxidation systems based in iron complexes that showed low substrate conversion<sup>4,34,39,53,61-63</sup> or good results for aromatic olefins but showed problems in the oxidation of aliphatic olefins.<sup>64-67</sup>

Moreover, remarkable regioselectivity for the 8,9-monoepoxide was achieved in the oxidation of carvone. In addition, the reaction showed moderate diastereoselectivity. While the diastereoselectivity exhibited by this family of catalysts is still far from satisfactory, it is

remarkable for a non-heme iron system with non-aromatic substrates and is comparable with that reported with a diiron pinene-derived complex.<sup>51</sup> However, the oxidation of aromatic olefins, which usually afford better enantioselectivities was precluded due to the deactivation of the catalyst.<sup>51,68-70</sup>

### III.4. Concluding remarks

A new family of pinene-derived ligands have been designed (L1-L5) and the corresponding iron(II) complexes (**1OTf-5OTf**) have been synthesized and characterized. Their catalytic performance in oxidation of alkanes and alkenes has been evaluated. While previous studies have demonstrated that small modifications in the pyridine ring of the bpmcn family resulted in a dramatic loss of efficiency, the introduction of a pinene ring in the 4<sup>th</sup>-5<sup>th</sup> position of the pyridine rings of the bpmcn, bpmcn and bbbp ligands led to more stable catalysts. Moreover, chirality in these complexes arises from the combination of the stereochemistry of the diamino backbone and from the pinene ring, defining  $\Delta$  or  $\Lambda$  configuration of the overall molecule. In all cases, a hydrophobic pocket around the metal ion is created by the ligand, being more defined in the case of  $\Lambda$  complexes (**2OTf** and **4OTf**) and increasing the robustness and the selectivity of this catalyst in comparison with the  $\Delta$  isomers (**1OTf**, **3OTf** and **5OTf**) or the complexes lacking the pinene (**6OTf-8OTf**). In consequence **2OTf** and **4OTf** demonstrated the more robust and selective non-heme iron enzymes to date for the stereospecific hydroxylation of tertiary C-H bonds. The impressive TN and efficiencies achieved with this system makes it a synthetic tool for the stereoselective introduction of tertiary alcohols. Furthermore, mechanistic studies point towards the implication of selective metal-based oxidants and the lack of implication of free diffusing radicals.

In alkene oxidation low catalyst loadings were required and H<sub>2</sub>O<sub>2</sub> was efficiently used. Moreover, moderate diastereoselectivity was achieved.

We envision that further use of the principle of steric isolation, combined with an oxidatively robust site, may lead to the design of even more active catalysts that could open the door to environmentally benign synthetic strategies based on C-H hydroxylation.

### III.5. Experimental section

#### III.5.1. Instrumentation

IR spectra were taken in a Mattson-Galaxy Satellite FT-IR spectrophotometer using a MKII Golden Gate single reflection ATR system. UV-Vis spectroscopy was performed on a Cary 50 Scan (Varian) UV-Vis spectrophotometer with 1 cm quartz cells. Cyclic voltammetry (CV) experiments were performed in an IJ-Cambria IH-660 potentiostat using a three electrode cell. Glassy carbon disk electrodes (3 mm diameter) from BAS were used as working electrode, platinum wire was used as auxiliary and SCE was used as the reference electrode (all the potentials given in this work are always with regard to this reference electrode). Unless explicitly

mentioned, all cyclic voltammograms presented in this work were recorded at 100 mV/s scan rate under nitrogen atmosphere and complex concentration was approximately 1 mM. The complexes were dissolved in previously degassed solvents containing the necessary amount of  $n\text{-Bu}_4\text{NPF}_6$  (TBAH) as supporting electrolyte to yield a 0.1 M ionic strength solution. All  $E_{1/2}$  values reported in this work were estimated from cyclic voltammetric experiments as the average of the oxidative and reductive peak potentials  $(E_{pa} + E_{pc})/2$ . NMR spectra were taken on a Bruker DPX 200 MHz, Bruker DPX 400 MHz and Bruker DRX 500 MHz spectrometers.  $^1\text{H}$ -NMR spectra of paramagnetic compounds were performed with the following special parameters; relaxation delay = 0.03 s, acquisition time = 0.064 s, line broadening = 30 Hz, sweep width = 100-250 ppm.  $^1\text{H}$ -NMR spin-lattice relaxation times ( $T_1$ ) were obtained with the standard inversion-recovery method. Spectra were referenced to the residual proto solvents peaks or TMS (tetramethylsilane) for  $^1\text{H}$ . Elemental analyses were performed using a CHNS-O EA-1108 elemental analyzer from Fisons or FlashEA1112 elemental analyzer from ThermoFinnigan. ESI-MS experiments were performed on a Navigator LC/MS chromatograph from Thermo Quest Finnigan or a Bruker Daltonics Esquire 3000 Spectrometer, using methanol or acetonitrile as a mobile phase. Product analyses were performed on a Shimadzu GC-2010 gas chromatograph (Cyclodex-B 30 m column or Astec CHIRALDEXTM G-TA capillary column 10 m x 0.25 mm) and a flame ionization detector. GC-MS spectral analyses were performed on a ThermoQuest Trace GC 2000 Series chromatograph interfaced with a Finnigan ThermoQuest Trace MS mass spectrometer.

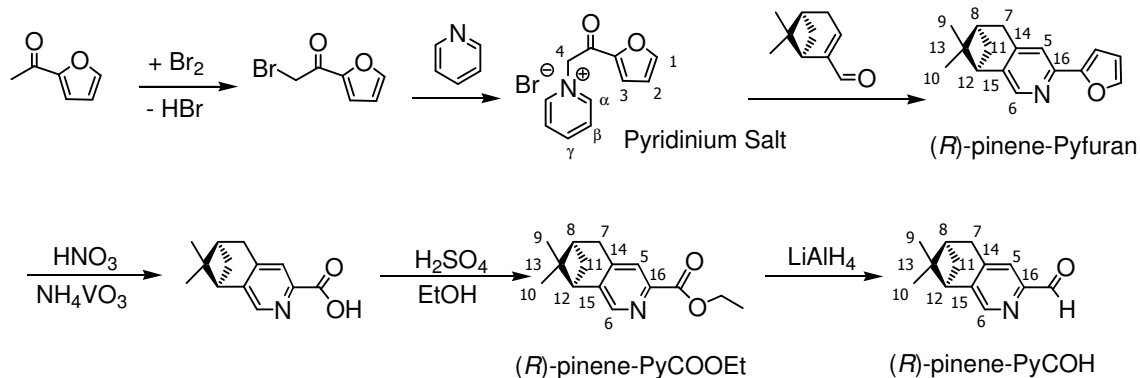
### III.5.2. Materials

Reagents and solvents used were commercially available reagent quality unless otherwise stated. Solvents were purchased from SDS and Scharlab. Solvents were purified and dried by passing through and activated alumina purification system (MBraun SPS-800) or by conventional distillation techniques. Acetonitrile was distilled over  $\text{P}_2\text{O}_5$ . Diethyl ether was distilled over Na/benzophenone.  $\text{CH}_2\text{Cl}_2$  was distilled over  $\text{CaH}_2$ . Preparation and handling of air-sensitive materials were carried out in a  $\text{N}_2$  drybox (mBraun UNIlab) with  $\text{O}_2$  and  $\text{H}_2\text{O}$  concentrations < 1 ppm.  $[\text{Fe}(\text{CF}_3\text{SO}_3)_2(\text{bpmen})]$  (**6OTf**),<sup>1</sup>  $[\text{Fe}(\text{CF}_3\text{SO}_3)_2((S,S)\text{-bpmcn})]$  (**7OTf**),<sup>71</sup>  $[\text{Fe}(\text{CF}_3\text{SO}_3)_2((S,S)\text{-bpbp})]$  (**8OTf**),<sup>6</sup>  $[\text{Fe}(\text{CH}_3\text{CN})_2((S,S)\text{-bpbp})](\text{SbF}_6)_2$  (**8SbF<sub>6</sub>**),<sup>5</sup>  $[\text{Fe}(\text{CF}_3\text{SO}_3)_2(^H\text{PyTACN})]$  (**9OTf**),<sup>29</sup>  $[\text{Fe}(\text{CF}_3\text{SO}_3)_2(^{\text{Me}}\text{PyTACN})]$  (**10OTf**),<sup>27</sup>  $[\text{Mn}(\text{CF}_3\text{SO}_3)_2((S,S)\text{-bpmcn})]$ <sup>48</sup> and  $[\text{Mn}(\text{CF}_3\text{SO}_3)_2(^H\text{PyTACN})]$ <sup>49</sup> were prepared according to published procedures.

### III.5.3. Synthesis of ligands

**Pyridinium Salt** was synthesized similar as described in literature.<sup>72</sup> A solution of 2-acetylfuran (25 g, 0.23 mol) in chloroform (190 mL) and a pinch of steel wool was charged in a three-neck round-bottom flask with a slow addition flask charged with a solution of bromide (36 g, 0.23 mol) in chloroform (115 mL). The system was purged with  $\text{N}_2$  and maintained over  $\text{N}_2$  atmosphere during all the reaction. The 2-acetylfuran solution was heated to 60°C and then the bromide solution was added slowly and the reaction mixture was stirred for 3h at 60°C. The

reaction mixture was then filtered through a plug of silica gel, concentrated to approximately 200 mL on a rotary evaporator and cooled to 0°C. Pyridine (39 mL) was added slowly and the reaction mixture was stirred at room temperature overnight. The formed precipitate was filtered and washed with cold ether to obtain 40 g (0.15 mol, 65%) of a grey-brown solid. <sup>1</sup>H-NMR (400 MHz, D<sub>2</sub>O, 300 K) δ, ppm: 8.85-8.83 (m, 2H (α-Py)); 8.73 (tt, 1H, J = 1.4, 8.0 Hz (γ-Py)); 8.23–8.19 (m, 2H, β-Py); 8.0 (d, 1H, J = 1.7 Hz (1 or 3)); 7.73 (d, 1H, J = 3.8 Hz (1 or 3)); 6.85 (dd, 1H, J = 3.8, 1.7 Hz (2)); 6.25 (s, 2H (4)).



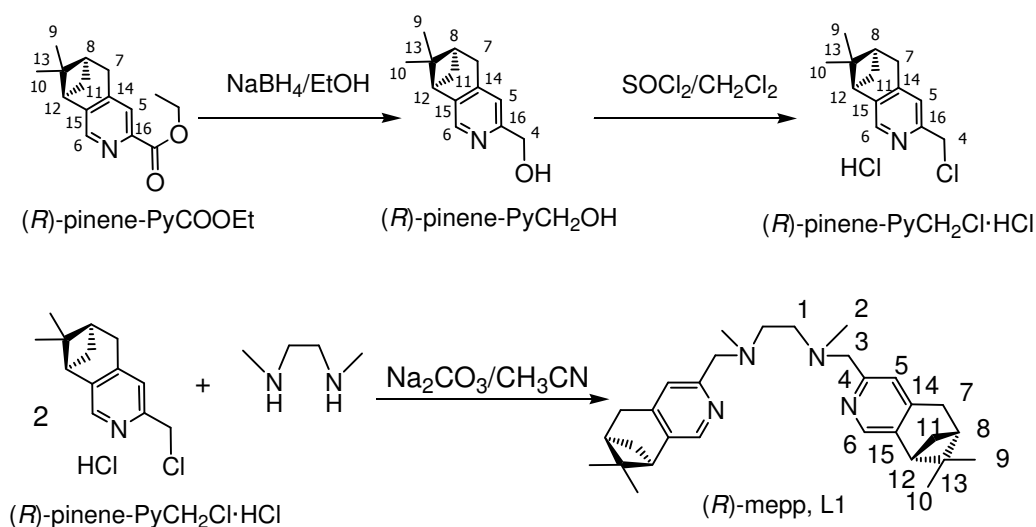
**Scheme 10.** Synthetic scheme for the preparation of (*R*)-pinene-PyCOH along with the numeric code used in the NMR assignment.

(*R*)-4,5-pinene-2-(furan-2-yl)-pyridine, (*R*)-pinene-Pyfuran, was synthesized following the procedure described in literature.<sup>72</sup> 1*R*-(-)-Myrtenal (22.7 g, 0.15 mol) was added to a solution containing **pyridinium salt** (39.7g, 0.15 mols) and ammonium acetate (92.6 g, 1.20 mol) in 238 mL of acetic acid and the reaction mixture was stirred at 120°C overnight. The reaction mixture was then poured into water (100mL) and extracted with hexanes (3 x 200 mL). The combined organic layers were washed with water (2 x 150 mL), dried over MgSO<sub>4</sub> and concentrated on a rotary evaporator to yield 25.4 g (0.11 mol, 71%) of a brown oil. FT-IR (ATR)  $\nu$ , cm<sup>-1</sup>: 2977 - 2869 (C-H)sp<sup>3</sup>, 1608, 1548, 1497, 1478, 1377, 1002, 884, 815, 734, 593. <sup>1</sup>H-NMR (CDCl<sub>3</sub>, 400 MHz, 300 K) δ, ppm: 8.13 (s, 1H (6)), 7.49 (s.a., 2H (5 and furan)), 6.97 (d, 1H, J=3.41 (furan)), 6.51-6.50 (m, 1H (furan), 3.00 (d, J = 2.6 Hz, 2H (7)), 2.84-2.81 (m, 1H (12)), 2.67-2.67 (m, 1H (11 exo)), 2.31-2.29 (m, 1H (8), 1.41 (s, 3H (10)), 1.22 (d, 2H, J = 9.6 Hz (11 endo)), 0.65 (s, 6H (9)). <sup>13</sup>C-NMR (CDCl<sub>3</sub>, 100 MHz, 300 K) δ, ppm: 145.8 (6); 154.1, 147.7, 145.2, 141.2 (Cquaternary furan, 14, 15 and 16); 118.2 (5); 142.7, 111.9, 107.4 (furan); 44.5 (12); 40.05 (8); 39.3 (13); 32.9 (7); 31.9 (11); 26.0 (9); 21.4 (10). ESI-MS (m/z): 240.1 [M+H]<sup>+</sup>.

(*R*)-4,5-pinene-2-picolyl ethyl ester, (*R*)-pinene-PyCOOEt was synthesized as previously described.<sup>72</sup> To a suspension of (*R*)-pinene-Pyfuran (10.9 g, 46 mmol) and ammonium metavanadate (0.76 g, 6.4 mmols. Caution!! Very toxic) in water (220 mL) was added concentrated nitric acid (145 mL) and the mixture was stirred and refluxed for 4 h. The water and nitric acid were removed by distillation at 106°C applying just the necessary vacuum to let the mixture distillate dropwise. At the end the collector flask was changed for a clean one and vacuum was applied to ensure dryness of the reaction mixture. An ethanolic (88 mL)

solution of sulfuric acid (22 mL) was prepared in a water-ice bath. This solution was added to the reaction flask and the mixture was stirred at reflux overnight. The reaction mixture was let cooled to room temperature and poured into hexanes (150 mL) and neutralized with an aqueous solution of saturated sodium bicarbonate (250 mL) and solid  $\text{NaHCO}_3$ . The aqueous layer was extracted with hexanes (4 x 100 mL) and the combined organic layers were then washed with water (3 x 100 mL), dried over magnesium sulfate and concentrated on a rotary evaporator to yield 7 g (28.5 mmol, 62.6%) of brown oil.  $^1\text{H-NMR}$  ( $\text{CDCl}_3$ , 400 MHz, 300 K)  $\delta$ , ppm: 8.28 (s, 1H (6)), 7.93 (s, 1H (5)), 4.47 (q, 2H,  $J = 7.1$  Hz ( $\text{CH}_3\text{-CH}_2\text{-O-}$ )), 3.04 (d,  $J = 2.6$  Hz, 2H (7)), 2.92-2.89 (m, 1H (12)), 2.70-2.75 (m, 1H (11 exo)), 2.32-2.35 (m, 1H (8)), 1.42-1.46 (m, 6H (10 and  $\text{CH}_3\text{-CH}_2\text{-O-}$ )), 1.20 (d, 1H,  $J = 9.4$  Hz (11 endo)), 0.62 (s, 3H (9)).  $^{13}\text{C-NMR}$  ( $\text{CDCl}_3$ , 50 MHz, 300 K)  $\delta$ , ppm: 146.4 (6); 166.2, 146.6, 146.5, 145.5 (C=O, 14, 15 and 16); 124.6 (5); 61.7 ( $\text{CH}_3\text{-CH}_2\text{-O-}$ ); 44.7 (12), 39.9 (8); 39.0 (13); 32.8 (7), 31.5 (11); 25.9 (9); 21.3 (10); 12.4 ( $\text{CH}_3\text{-CH}_2\text{-O-}$ ).

**(*R*)-4,5-pinene-2-picolylaldehyde, (*R*)-pinene-PyCOH** was synthesized as described in literature.<sup>72</sup> A solution of **(*R*)-pinene-PyCOOEt** (6.8 g, 27.7 mmol) in tetrahydrofuran (150 mL) was cooled to  $-78^\circ\text{C}$ , under nitrogen. A lithium aluminum hydride solution (34 mL, 1M, in diethyl ether, 34 mmol) was then added slowly and the resulting dark brown solution was stirred at  $-78^\circ\text{C}$  for 1 hour. Acetic acid (15 mL) was added to the reaction mixture at  $-78^\circ\text{C}$  and the resulting solution was added to hexanes (300 mL). The mixture was then poured into water (300 mL) and extracted with hexanes (3 x 300 mL). The combined organic layers were washed with water (2 x 100 mL), dried over magnesium sulfate and concentrated on a rotary evaporator: yield 4.1 g (20.4 mmol, 74%) reddish-orange oil.  $^1\text{H-NMR}$  ( $\text{CDCl}_3$ , 200 MHz, 300 K)  $\delta$ , ppm: 10.05 (s, 1H (aldehyde)), 8.35 (s, 1H (6)), 7.80 (s, 1H (5)), 3.07 (d,  $J = 2.4$  Hz, 2H (7)), 2.96-2.89 (m, 1H (12)), 2.79-2.75 (m, 1H (11 exo)), 2.45-2.35 (m, 1H (8)), 1.46 (s, 3H (10)), 1.24 (d, 1H,  $J = 9.6$  Hz (11 endo)), 0.66 (s, 3H (9)).



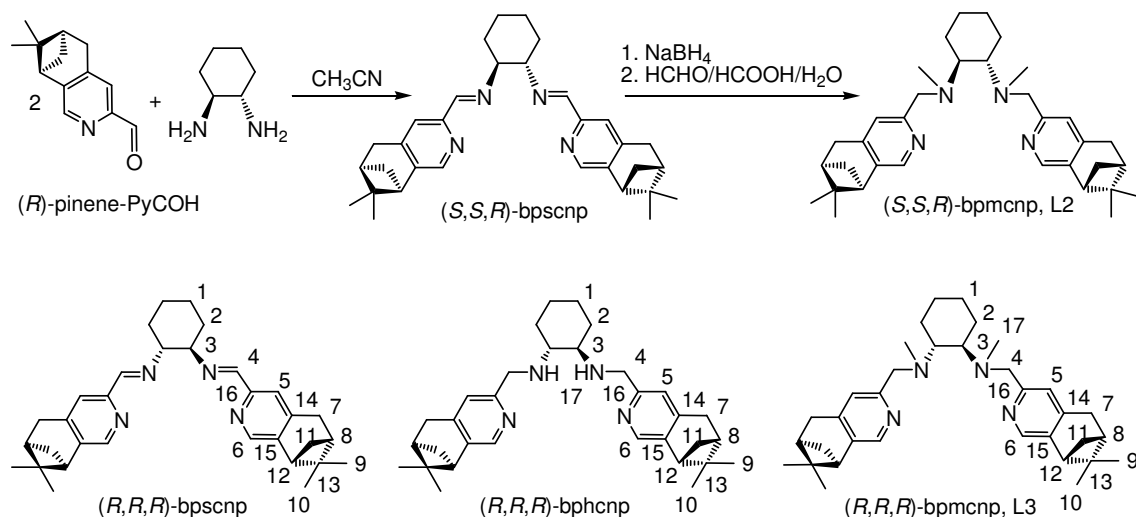
**Scheme 11.** Synthetic scheme for the preparation of **(*R*)-bpmenp** ligand along with the numeric code used in the NMR assignment.

**(R)-4,5-pinene-2-picolylalcohol, (R)-pinene-PyCH<sub>2</sub>OH.** (R)-4,5-pinene-2-picolyl ethyl ester, **(R)-pinene-PyCOOEt** (3.65 g, 14.9 mmol) was dissolved in absolute ethanol (60 mL). NaBH<sub>4</sub> (2.15 g, 50.7 mmol) was added as a solid and the solution was placed under N<sub>2</sub> and refluxed for 3h. The dark orange reaction mixture was then cooled to room temperature and H<sub>2</sub>O (10 mL) and HCl 2 M (10 mL) were added. The mixture was stirred for 10 min and it was basified to pH = 14 with concentrated NaOH solution (12 M). The mixture was extracted with CHCl<sub>3</sub> (3 x 100 mL). The organic phases were combined and washed with H<sub>2</sub>O (100 mL), dried over MgSO<sub>4</sub> and filtered. The solvent was removed under reduced pressure to obtain 2.8 g (13.8 mmol, 97%) of the alcohol product as a dark brown oil that was directly used for the next step. <sup>1</sup>H-NMR (CDCl<sub>3</sub>, 400 MHz, 300 K) δ, ppm: 8.06 (s, 1H, (6)), 7.04 (s, 1H (5)), 4.70 (s, 2H (4)), 2.96 (d, 2H, J = 2.8 Hz (7)), 2.83-2.80 (m, 1H (12)), 2.70-2.66 (m, 1H (11 exo)), 2.32-2.27 (m, 1H (8)), 1.40 (s, 3H (10)), 1.19 (d, 1H, J = 9.5 Hz (11 endo)), 0.62 (s, 3H (0)). <sup>13</sup>C-NMR (CDCl<sub>3</sub>, 50 MHz, 300 K) δ, ppm: 144.4 (6); 156.9, 145.4, 141.3 (14, 15 and 16); 119.8 (5); 64.1 (4); 44.3 (12); 40.0 (8); 39.2 (13); 32.7 (7); 31.8 (11); 25.9 (9); 21.3(10).

**(R)-4,5-pinene-2-picolylchloride hydrochloride, (R)-pinene-PyCH<sub>2</sub>Cl·HCl.** Alcohol **(R)-pinene-PyCH<sub>2</sub>OH** (2.8 g, 13.8 mmol) was dissolved in anhydrous CH<sub>2</sub>Cl<sub>2</sub> (60 mL). Thionyl chloride (10 mL, 135.7 mmol) dissolved in CH<sub>2</sub>Cl<sub>2</sub> (10 mL) was added dropwise and the resulting mixture was stirred overnight. The solvent was removed under a stream of N<sub>2</sub>. The residue was washed with ether (100 mL) and then dissolved in EtOH (60 mL) and stirred for 24 hours. The solvent was removed under vacuum to afford a dark brown oil that crystallized upon standing in the fridge. The product was used in the next step without additional purification (3.5 g, 13.6 mmol, 98%). <sup>1</sup>H-NMR (CDCl<sub>3</sub>, 200 MHz, 400 K) δ, ppm: 8.10 (s, 1H (6)), 7.24 (s, 1H (5)), 4.69 (s, 2H (4)), 2.98 (d, 2H, J = 2.8 Hz (7)), 2.84-2.81 (t, 1H, J = 5.4 Hz (12)), 2.72-2.67 (m, 1H (11 exo)), 2.32-2.28 (m, 1H (8)), 1.41 (s, 3H (10)), 1.19 (d, 1H, J = 9.8 Hz (11 endo)), 0.63 (s, 3H (9)). <sup>13</sup>C-NMR (CDCl<sub>3</sub>, 50 MHz, 300 K) δ, ppm: 157.9, 149.0, 146.5, 135.5, 125.8, 44.3, 39.6, 39.0, 38.8, 34.2, 30.9, 25.3, 21.4.

**(R)-bpmenp (L1).** *N,N'*-dimethyl-ethanediamine (0.182 g, 2.07 mmol), **(R)-pinene-PyCH<sub>2</sub>Cl·HCl** (1.07 g, 4.14 mmol) and anhydrous acetonitrile (20 mL) were mixed in a 50 mL flask. Na<sub>2</sub>CO<sub>3</sub> (2.0 g) and tetrabutylammonium bromide, TBABr (0.04 g), were added directly as solids and the resulting mixture was heated at reflux under N<sub>2</sub> for 20 hours. After cooling to room temperature, the resulting yellow mixture was filtered and the filter cake was washed with CH<sub>3</sub>CN. The solvent from the combined filtrates was evaporated under reduced pressure. Hexanes (50 mL) were added to the resulting residue and the mixture was stirred for 1 h. The clear and yellow hexanes layer was decanted. The remaining residue was further extracted with hexanes (2 x 50 mL). The combined extracts were evaporated under vacuum to obtain the product as a yellow oil that was further dried under high vacuum for 2 h. 0.85 g of a pale yellow oil (1.85 mmol, 89.5 %) were obtained. FT-IR (ATR) ν, cm<sup>-1</sup>: 2922 – 2759 (C-H)sp<sup>3</sup>, 1739, 1604, 1557, 1483, 1465, 1453, 1366, 1238, 1122, 1028, 948, 653, 625. <sup>1</sup>H-NMR (CDCl<sub>3</sub>, 200 MHz, 300 K) δ, ppm: 8.07 (s, 2H (6)), 7.23 (s, 2H (5)), 3.64 (s, 4H (3)), 2.95 (d, 4H, J = 2.6 Hz (7)), 2.83-2.79 (m, 2H (12)), 2.70-2.65 (m, 2H (11 exo)), 2.68 (s, 4H (1)), 2.29 (s broad, 8H (2 and

8)), 1.41 (s, 6H (10)), 1.20 (d, 2H, J = 9.4 Hz (11 endo)), 0.62 (s, 6H (9)).  $^{13}\text{C-NMR}$  ( $\text{CDCl}_3$ , 50 MHz, 300 K)  $\delta$ , ppm: 145.1 (6); 157.2, 144.8, 140.7 (4, 14 and 15); 122.3 (5); 64.3, 55.6 (1 and 3); 44.3, 40.1 (CH pinene); 42.9 (2); 39.16 (13); 32.7, 31.8 ( $\text{CH}_2$  pinene); 25.9 (9); 21.3 (10). ESI-MS ( $m/z$ ): 459.3  $[\text{M}+\text{H}]^+$ .



**Scheme 12.** Synthetic scheme for the preparation of **bpmcnp** ligands employed in this work along with the numeric code used in the NMR assignment.

**(S,S,R)-bpscnp.** To a solution of  $(1S,2S)\text{-}(+)\text{-1,2-diaminocyclohexane}$  (245 mg, 2.1 mmol) in  $\text{CH}_3\text{CN}$  (10 mL), **(R)-pinene-PyCOH** (841 mg, 4.2 mmol) was added and the suspension was stirred for 3 hours at room temperature. The solvent was removed under reduced pressure affording 999 mg (2.1 mmol, 99%) of a yellow oil corresponding to **(S,S,R)-bpscnp**. FT-IR (ATR)  $\nu$ ,  $\text{cm}^{-1}$ : 2827-2985 (C-H) $_{\text{sp}^3}$ , 1651 (C=N), 1601, 1556, 1481, 1489, 1445, 1423, 1373, 1268, 1246, 1144, 1101, 1026, 946, 864.  $^1\text{H-NMR}$  ( $\text{CDCl}_3$ , 200 MHz, 300 K)  $\delta$ , ppm: 8.29 (s, 2H (6)), 8.07 (s, 2H (4)), 7.71 (s, 2H (5)), 3.48-3.51 (m, 2H (3)), 2.94 (d, 4H, J = 2 Hz (7)), 2.71-2.80 (m, 2H (12)), 2.63-2.71 (m, 2H (11 $_{\text{exo}}$ )), 2.25-2.29 (m, 2H (8)), 1.41-1.84 (m, 8H (1 and 2)), 1.37 (s, 6H (10)), 1.14 (d, 2H, J = 9 Hz (11 endo)), 0.54 (s, 6H (9)).  $^{13}\text{C-NMR}$  (50 MHz,  $\text{CDCl}_3$ , 300 K)  $\delta$ , ppm: 161.8 (4); 145.4 (6); 153.1, 145.0, 144.0 (14, 15 and 16); 120.4 (5); 73.5 (3); 44.6 (12), 39.9 (8); 39.1 (13); 32.9, 32.6, 31.6 ( $\text{CH}_2$  pinene and 2); 25.9 (9); 24.4 (1); 21.3 (10). ESI-MS ( $m/z$ ): 481.4 (100)  $[\text{M}+\text{H}]^+$ , 298.2 (21)  $[\text{C}_{19}\text{H}_{28}\text{N}_3]^+$ .

**(R,R,R)-bpscnp** was prepared in analogous manner to **(S,S,R)-bpscnp** starting from  $(1R,2R)\text{-}(-)\text{-1,2-diaminocyclohexane}$ . (971 mg, 2.0 mmol, 96.2%). FT-IR (ATR)  $\nu$ ,  $\text{cm}^{-1}$ : 2860-2972 (C-H) $_{\text{sp}^3}$ ; 1648 (C=N), 1599, 1552, 1481, 1447, 1424, 1362, 1263, 1246, 1141, 1086, 1031, 945, 859.  $^1\text{H-NMR}$  ( $\text{CDCl}_3$ , 200 MHz, 300 K)  $\delta$ , ppm: 8.29 (s, 2H, (6)), 8.07 (s, 2H, (4)), 7.73 (s, 2H, (5)), 3.49-3.46 (m, 2H, (3)), 2.95 (d, 4H, J= 2 Hz, (7)), 2.70-2.81 (m, 2H, (12)), 2.62-2.70 (m, 2H, (11 exo)), 2.25-2.29 (m, 2H, (8)), 1.41-1.85 (m, 8H, (1 and 2)), 1.38 (s, 6H, (10)), 1.15 (d, 2H, J = 9 Hz, (11 endo)), 0.59 (s, 6H, (9)).  $^{13}\text{C-NMR}$  ( $\text{CDCl}_3$ , 50 MHz, 300 K)  $\delta$ , ppm: 161.8 (4); 145.3 (6); 153.1, 145.0, 144.0 (14, 15 and 16); 120.34 (5); 73.5 (3); 44.6 (12); 39.9



(8); 39.1 (13); 32.9, 32.6, 31.5 (CH<sub>2</sub> pinene and 2); 25.9 (9); 24.4 (1); 21.3 (10). ESI-MS (m/z): 481.4 (100) [M+H]<sup>+</sup>, 298.2 (21) [C<sub>19</sub>H<sub>28</sub>N<sub>3</sub>]<sup>+</sup>.

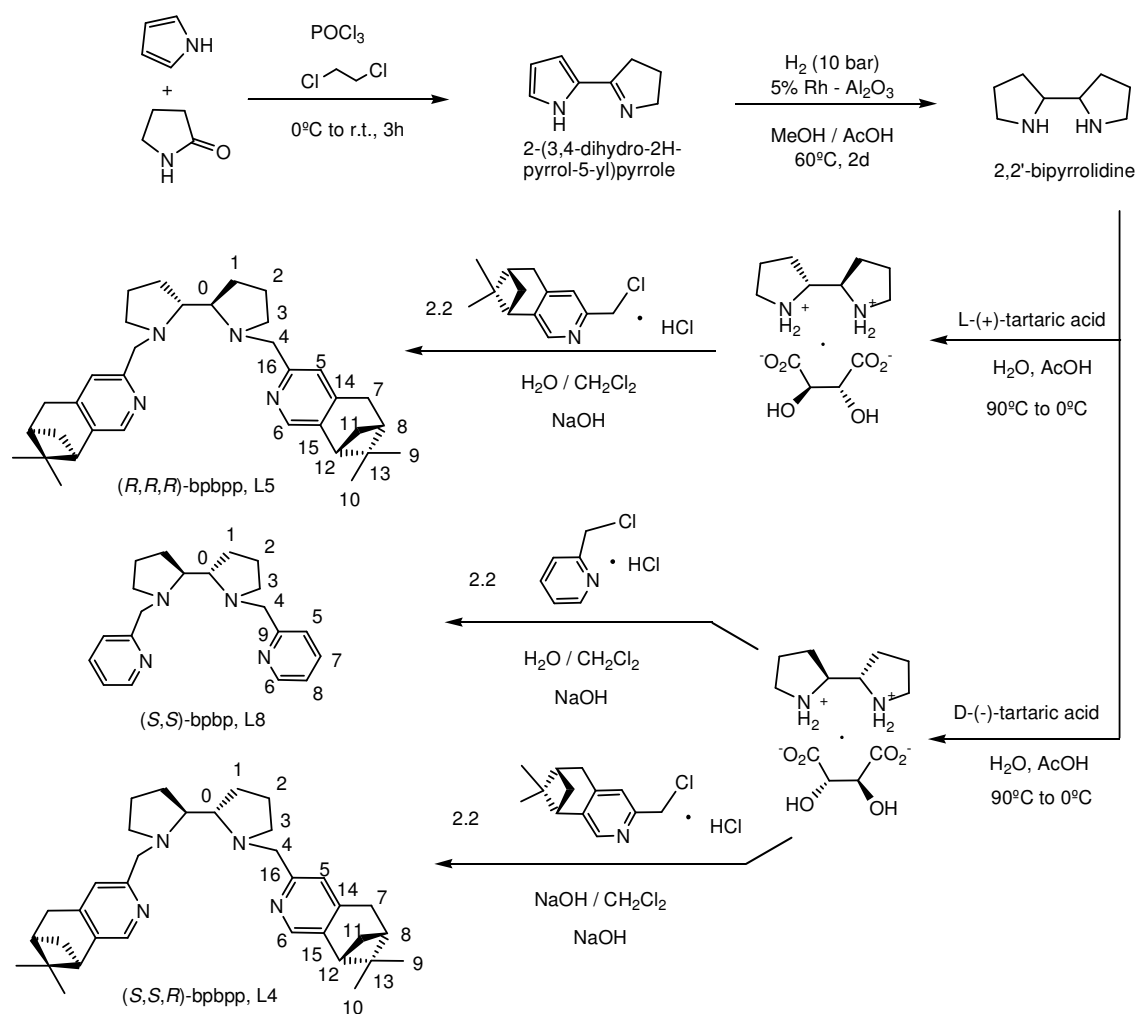
**(S,S,R)-bphcnp.** NaBH<sub>4</sub> (284 mg, 7.5 mmol) was slowly added to a stirred solution of **(S,S,R)-bpscnp** (913 mg, 1.9 mmol) in methanol (15 mL). The mixture was stirred for 4 hours at room temperature. The solvent was removed under reduced pressure and the resulting mixture was treated with 7 mL of water and 12 mL of CH<sub>2</sub>Cl<sub>2</sub>. The aqueous phase was extracted with 2 x 12 mL of CH<sub>2</sub>Cl<sub>2</sub>. The organic layers were dried over MgSO<sub>4</sub> and the solvent was removed under reduced pressure to give 911 mg (1.9 mmol, 99%) of a white solid. FT-IR (ATR)  $\nu$ , cm<sup>-1</sup>: 3295 (N-H), 2978-2856 (C-H)sp<sup>3</sup>, 1605, 1557, 1483, 1461, 1448, 1426, 1396, 1367, 1138, 1112, 948, 850. <sup>1</sup>H-NMR (CDCl<sub>3</sub>, 200 MHz, 300 K)  $\delta$ , ppm: 8.07 (s, 2H (6)), 7.21 (s, 2H (5)), 4.01 (d, 2H, J = 13.6 Hz (4)), 3.80 (d, 2H, J = 13.8 Hz (4)), 2.95 (d, 4H, J = 2.6 Hz (7)), 2.75-2.84 (m, 2H (12)), 2.67-2.75 (m, 2H (11 exo)), 2.15-2.42 (m, 6H (8, 3 and 17)), 1.42 (s, 6H (10)), 1.73 and 1.19-1.29 (m, 10H (11 endo, 1 and 2)), 0.64 (s, 6H (9)). <sup>13</sup>C-NMR (CDCl<sub>3</sub>, 50 MHz, 300 K)  $\delta$ , ppm: 145.1 (6); 158.4, 144.7, 140.4 (14, 15 and 16); 121.6 (5); 61.5 (3); 52.5 (4); 44.3 (12); 40.1 (8); 39.2 (13); 32.7, 31.9; 31.59 (CH<sub>2</sub> pinene and 2); 25.98 (9); 24.99 (1); 21.31 (10). ESI-MS (m/z): 485.4 (100) [M+H]<sup>+</sup>.

**(R,R,R)-bphcnp** was prepared in analogous manner to **(S,S,R)-bphcnp** (801 mg, 1.6 mmol, 87%). FT-IR (ATR)  $\nu$ , cm<sup>-1</sup>: 3289 (N-H); 2971-2862 (C-H)sp<sup>3</sup>, 1606, 1558, 1484, 1448, 1426, 1395, 1367, 1138, 1112, 948, 853. <sup>1</sup>H-NMR (CDCl<sub>3</sub>, 200 MHz, 300 K)  $\delta$ , ppm: 8.03 (s, 2H (6)), 7.18 (s, 2H (5)), 3.97 (d, 2H, J = 12 Hz (4)), 3.77 (d, 2H, J = 12 Hz (4)), 2.91 (d, 4H, J = 2 Hz (7)), 2.75-2.84 (m, 2H (12)), 2.63-2.75 (m, 2H (11 exo)), 2.13-2.39 (m, 6H (8, 3 and 17)), 1.39 (s, 6H (10)), 1.68 and 1.15-1.26 (m, 10H (11 endo, 1 and 2)), 0.61 (s, 6H (9)). <sup>13</sup>C-NMR (CDCl<sub>3</sub>, 50 MHz, 300 K)  $\delta$ , ppm: 145.0 (6); 157.5, 145.1, 140.7 (14, 15 and 16); 121.7 (5); 61.2 (3); 52.0 (4); 44.3 (12); 40.0 (8); 39.1 (13); 32.7, 31.8, 31.2 (CH<sub>2</sub> pinene and 2); 25.9 (9); 24.9 (1); 21.3 (10). ESI-MS (m/z): 485.4 (100) [M+H]<sup>+</sup>, 300.1 (15) [C<sub>20</sub>H<sub>30</sub>N<sub>2</sub>+H]<sup>+</sup>.

**(S,S,R)-bpmcnp (L2).** A mixture of **(S,S,R)-bphcnp** (780 mg, 1.6 mmol), water (5 mL), HCHO (37%, 1.1 mL, 14.5 mmol) and HCO<sub>2</sub>H (97%, 0.56 mL, 14.5 mmol) were refluxed for 10 h. The solution was then cooled and an aqueous solution of NaOH 6M was added (5.5 mL). The resulting suspension was extracted with CH<sub>2</sub>Cl<sub>2</sub> (2 x 20 mL). The organic layers were dried over MgSO<sub>4</sub> and the solvent was removed to dryness to give 788 mg of a yellow oil. The product was purified over a short alumina chromatographic column eluting with hexane/ethyl acetate 5/95 followed by a silica chromatographic column eluting with dichloromethane/methanol/NH<sub>4</sub>OH 94:5:1 to give 462 mg (0.9 mmol, 56%) of the pure product as a yellow oil. FT-IR (ATR)  $\nu$ , cm<sup>-1</sup>: 2972 - 2786 (C-H)sp<sup>3</sup>, 1605, 1557, 1482, 1466, 1448, 1426, 1384, 1367, 1264, 1238, 1136, 1122, 1050, 1027, 948, 877, 852. <sup>1</sup>H-NMR (200 MHz, CDCl<sub>3</sub>, 300 K)  $\delta$ , ppm: 8.01 (s, 2H (6)), 7.39 (s, 2H (5)), 3.87 (d, 2H, J = 14 Hz (4)), 3.76 (d, 2H, J = 14 Hz (4)), 2.87 (d, 4H, J = 2.6 Hz (7)), 2.81-2.72 (m, 2H (12)), 2.72-2.61 (m, 4H (11 exo and 3)), 2.28 (s, 6H (17)), 2.16-2.15 (m, 2H (8)), 2.04-1.95 and 1.77-1.73 (m, 4H (2)), 1.30-1.14 (m, 6H (11 endo and 1)), 1.39 (s, 6H (10)), 0.61 (s, 6H (9)). <sup>13</sup>C-NMR (50 MHz, CDCl<sub>3</sub>, 300 K)  $\delta$ , ppm: 145.2 (6); 159.0; 144.6; 140.3

(14, 15 and 16); 122.2 (5); 64.0 (3); 60.3 (4); 44.3 (12); 40.1 (8); 39.2 (13); 36.8 (17); 32.7 (7); 31.8 (11); 26.0 (9); 25.8 (1 and 2); 21.3 (10). ESI-MS ( $m/z$ ): 513.3 (100)  $[M+H]^+$ , 342.2 (15)  $[C_{22}H_{35}N_3 + H]^+$ .

**(*R,R,R*)-bpmcnp (L3)** was prepared following a procedure analogous to **(*S,S,R*)-bpmcnp** (6.19 mg, 1.2 mmol, 75%). FT-IR (ATR)  $\nu$ ,  $cm^{-1}$ : 2986 - 2774 (C-H) $sp^3$ , 1605, 1556, 1482, 1466, 1448, 1426, 1384, 1367, 1265, 1237, 1136, 1123, 1049, 1027, 948, 879, 851.  $^1H$ -NMR (400 MHz,  $CDCl_3$ , 300 K)  $\delta$ , ppm: 8.01 (s, 2H (6)), 7.40 (s, 2H (5)) 3.85 (d, 2H,  $J = 14$  Hz (4)), 3.76 (d, 2H,  $J = 14$  Hz (4)), 2.88 (d, 4H,  $J = 2.4$  Hz (7)), 2.80-2.77 (m, 2H (12)), 2.68-2.62 (m, 4H (11 exo and 3)), 2.29 (s, 6H (17)), 2.28-2.22 (m, 2H (8)), 2.01-1.97 and 1.75-1.74 (m, 4H (2)), 1.38 (s, 6H (10)), 1.28-1.23 (m, 6H (11 endo and 1)), 0.61 (s, 6H (9)).  $^{13}C$ -NMR (50 MHz,  $CDCl_3$ , 300 K)  $\delta$ , ppm: 144.7 (6); 159.1, 144.6; 140.3 (14, 15 and 16); 122.2 (5); 63.9 (3); 60.2 (4); 44.3 (12); 40.1 (8); 39.2 (13); 36.9 (17); 32.8 (7); 31.9 (11); 25.8 (9); 25.6 (1 and 2); 21.3 (10). ESI-MS ( $m/z$ ): 513.5 (100)  $[M+H]^+$ .



**Scheme 13.** Synthetic scheme for the preparation of **(*S,S*)-bpbp**, **(*R,R,R*)-bpbpp** and **(*S,S,R*)-bpbpp** ligand along with numeric code used in the NMR assignment.

**2-(3,4-dihydro-2H-pyrrol-5-yl)pyrrole** was obtained exactly following the published procedure<sup>73</sup> in 35% yield (8.4 g, 63 mmol). FT-IR (ATR)  $\nu$ ,  $\text{cm}^{-1}$ : 3186 – 2865, 1617, 1423, 1349, 1310, 1145, 1113, 1064, 1030, 975, 870, 845, 724, 605.  $^1\text{H-NMR}$  (400 MHz,  $\text{CDCl}_3$ , 300 K)  $\delta$ , ppm: 6.93 (dd,  $J = 2.6, 1.4$  Hz, 1H), 6.52 (dd,  $J = 3.6$  Hz, 1.4 Hz, 1H), 6.22 (dd,  $J = 3.6, 2.6$  Hz, 1H), 4.03 – 3.99 (m, 2H), 2.92 - 2.87 (m, 2H), 2.05-1.97 (m, 2H).  $^{13}\text{C-NMR}$  ( $\text{CDCl}_3$ , 100 MHz, 300 K)  $\delta$ , ppm: 166.2, 127.9, 121.9, 112.9, 109.2, 60.5, 34.9, 22.7. ESI-MS ( $m/z$ ): 135.1 (100)  $[\text{M}+\text{H}]^+$ .

**2,2'-bipyrrolidine** was synthesized following a slight modification of a previously published procedure.<sup>73</sup> A methanol/acetic acid v/v 1:1 (82 mL) solution of **2-(3,4-dihydro-2H-pyrrol-5-yl)pyrrole** (8.4 g, 63 mmol) prepared under a nitrogen atmosphere, was introduced into an evacuated reactor Berghof HR-200 containing the solid hydrogenation catalyst (0.7 g of 5% Rh on activated alumina) and heated to 60 °C with stirring. Once the system reached thermal equilibrium, hydrogen gas was introduced to reach the working pressure (10 bar). During the reaction, the pressure was maintained constant by introducing hydrogen gas from a gas ballast. The pressure drop in the ballast was monitored using a pressure transducer connected to an electronic measurement. The evolution of the reaction was checked every 24h by  $^1\text{H-NMR}$  (see Annex). After 2 days, the reaction was completed and the reactor was cooled, the mixture was filtered through Celite® and the filtrate concentrated to 30 mL and diluted with  $\text{Et}_2\text{O}$  (100 mL). Under vigorous stirring at 0°C, 10 M aqueous KOH solution (21 mL) was added and further basified to pH 11 with KOH pellets. The organic layer was separated and the aqueous layer was extracted with  $\text{Et}_2\text{O}$  (4 x 100 mL). The combined extracts were dried with  $\text{MgSO}_4$ , filtered and the solvent was removed under reduced pressure. The resulting residue was distilled under reduced pressure to give a mixture of (*R,R*), (*S,S*) and *meso*-2,2'-bipyrrolidine; to prevent solidifying, the condenser of the distillation apparatus was not cooled by water but the receiver flasks were cooled with an ice-water bath. 52% yield (4.6 g, 33 mmol).

**Resolution of 2,2'-bipyrrolidine** was done as described in literature.<sup>74</sup>

**(*S,S*)-2,2'-bipyrrolidine D-tartrate.** To a solution of the 1:1 mixture of *meso*-2,2'-bipyrrolidine and dl-2,2'-bipyrrolidine (4.6 g, 33 mmol) in  $\text{H}_2\text{O}$  (18 mL), D-(-)-tartaric acid (2.5 g, 16.5 mmol) and glacial AcOH (1.9 mL, 33 mmol) were added. The stirred mixture was heated to 90°C and the homogeneous solution is allowed to cool to room temperature slowly before it was placed in an ice bath. If the initial precipitation takes too much time the process can be facilitated by stirring the mixture with glass rod. After the solid precipitation the mixture was kept in an ice bath for another 2h. The precipitate was filtered and washed with ice-cold water. The orange mother liquor was saved for the recovery of the (*R,R*)-2,2'-bipyrrolidine. The crystals were recrystallized twice with hot water yielding 1.5 g (5.2 mmol, 63% yield based on isomer content) of colorless crystals corresponding to (*S,S*)-2,2'-bipyrrolidine D-tartrate. The enantiomeric purity was determined to be >99% by chiral GC: small sample of crystals (10 mg) were dissolved in 20M KOH aqueous solution (1 mL) and extracted with ether (3 x 3 mL). The combined organic phases were dried with  $\text{MgSO}_4$  and filtered. The resulting solution was analyzed by chiral GC (Astec CHIRALDEXTM G-TA capillary column 10 m x 0.25 mm). FT-IR

(ATR)  $\nu$ ,  $\text{cm}^{-1}$ : 3132, 3000, 2882, 2706, 2515, 1691, 1573, 1384, 1125, 1073, 703. Anal. Calcd for  $\text{C}_{12}\text{H}_{22}\text{N}_2\text{O}_6 \cdot 3.2 \text{H}_2\text{O}$  (MW = 347.9 g/mol): N, 8.05; C, 41.42; H, 8.23%. Found: N, 7.77; C, 41.66; H, 7.92%.  $^1\text{H-NMR}$  (400 MHz,  $\text{D}_2\text{O}$ , 300 K)  $\delta$ , ppm: 4.37 (s, 2H), 3.91 - 3.88 (m, 2H), 3.59 - 3.45 (m, 4H), 2.42 - 2.34 (m, 2H), 2.22-2.01 (m, 4H), 1.92 - 1.81 (m, 2H). ESI-MS (m/z): 141.1 (100)  $[\text{M} - \text{C}_4\text{H}_5\text{O}_6]^+$ .

**(R,R)-2,2'-bipyrrolidine L-tartrate.** The mother liquor from initial resolution was cooled to  $0^\circ\text{C}$  and KOH pellets (9 g) were added slowly. The mixture was stirred vigorously at  $0^\circ\text{C}$  for 10 min. To this solution diethyl ether (70 mL) was added and the mixture was stirred at room temperature for 20 min. The aqueous layer was separated and then was extracted with diethyl ether (4 x 70 mL). The diethyl ether extracts were combined, dried ( $\text{K}_2\text{CO}_3$ ), filtrated and then were concentrated under vacuum to give 2.5 g of a yellow oil. The oil was dissolved in water (12 mL), then L-tartaric acid (2.5 g) and acetic acid (2 mL) were added. The mixture was heated to  $90^\circ\text{C}$  and the homogeneous solution was allowed to cool to room temperature slowly before it was cool in an ice bath. After the solid precipitation, the mixture was kept in an ice bath for another 2 hours. The precipitate was filtered and the solid washed with ice-cold water. The solid was recrystallized twice with hot water obtaining 0.6 g of white crystals (2.1 mmol, 25% yield based on isomer content). The enantiomeric purity was determined to be >99% by chiral GC (Astec CHIRALDEXTM G-TA capillary column 10 m x 0.25 mm): small sample of crystals (10mg) were dissolved in 20M KOH aqueous solution (1 mL) and extracted with ether (3 x 3 mL). The combined organic phases were dried with  $\text{MgSO}_4$  and filtered. The resulting solution was analyzed by chiral GC. Anal. Calcd for  $\text{C}_{12}\text{H}_{22}\text{N}_2\text{O}_6 \cdot 3.1 \text{H}_2\text{O}$  (MW = 346.1 g/mol): N, 8.09; C, 41.64; H, 8.21%. Found: N, 7.83; C, 41.75; H, 7.95%.  $^1\text{H-NMR}$  (400 MHz,  $\text{D}_2\text{O}$ , 300 K)  $\delta$ , ppm: 4.31 (s, 2H), 3.85 - 3.81 (m, 2H), 3.42 - 3.39 (m, 4H), 2.35 - 2.27 (m, 2H), 2.15-1.94 (m, 4H), 1.85 - 1.75 (m, 2H).

**(S,S)-bpbp (L8)** was prepared according to a modification of the procedure described by White et. al.<sup>5</sup>. A 10 mL round bottom flask was charged with a stir bar, **(S,S)-2,2'-bipyrrolidine D-tartrate** (1 eq, 0.40 g, 1.4 mmol),  $\text{H}_2\text{O}$  (3 mL) and  $\text{CH}_2\text{Cl}_2$  (3 mL). Solid NaOH pellets (6.4 eq, 0.35 g, 8.5 mmol), followed by 2-picolychloride-HCl (2.2 eq, 0.51 g, 3.1 mmol) were added leading to a pink-orange solution. After 48h stirring at room temperature, the yellow reaction mixture was diluted with 1N NaOH (3 mL). The aqueous layer was extracted with  $\text{CH}_2\text{Cl}_2$  (3 x 5 mL) and the organic extracts were combined, dried over  $\text{MgSO}_4$  and concentrated in vacuum obtaining a brown oil that was purified through silica gel chromatography ( $\text{CH}_2\text{Cl}_2$ :MeOH: $\text{NH}_3$  97:2:1). The collected fractions were combined, concentrated, washed with 1M NaOH, dried over  $\text{MgSO}_4$  and concentrated in vacou to provide 0.32 g of (S,S)-BPBP (1.0 mmol, 72% yield). FT-IR (ATR)  $\nu$ ,  $\text{cm}^{-1}$ : 2999 - 2760 (C-H) $\text{sp}^3$ , 1589, 1569, 1474, 1432, 1371, 1207, 1146, 1120, 1046, 993, 891, 758.  $^1\text{H-NMR}$  (400 MHz,  $\text{CDCl}_3$ , 300 K)  $\delta$ , ppm: 8.50 (ddd, J = 4.9, 1.9, 0.9 Hz, 2H (6)), 7.60 (dt, J = 7.8, 7.3, 1.9 Hz, 2H (8)), 7.40 (d, J = 7.8 Hz, 2H (5)), 7.11 (dd, J = 7.3, 4.9 Hz, 2H (7)), 4.20 (d, J = 14.0 Hz, 2H (4)), 3.51 (d, J = 14.0 Hz, 2H (4)), 3.00 (m, 2H (3)), 2.80 (m, 2H (0)), 2,24 (appq, J = 9.0 Hz, 2H (3)), 1.83 - 1.68 (m, 8H (1 and 2)).

$^{13}\text{C}$ -NMR ( $\text{CDCl}_3$ , 75 MHz, 300 K)  $\delta$ , ppm: 160.5, 148.8, 136.3, 122.7, 121.7, 65.4, 61.2, 55.3, 26.0, 23.6. ESI-MS ( $m/z$ ): 323.2 (100)  $[\text{M}+\text{H}]^+$ , 162.1 (10)  $[\text{M}+2\text{H}]^{+2}$ .

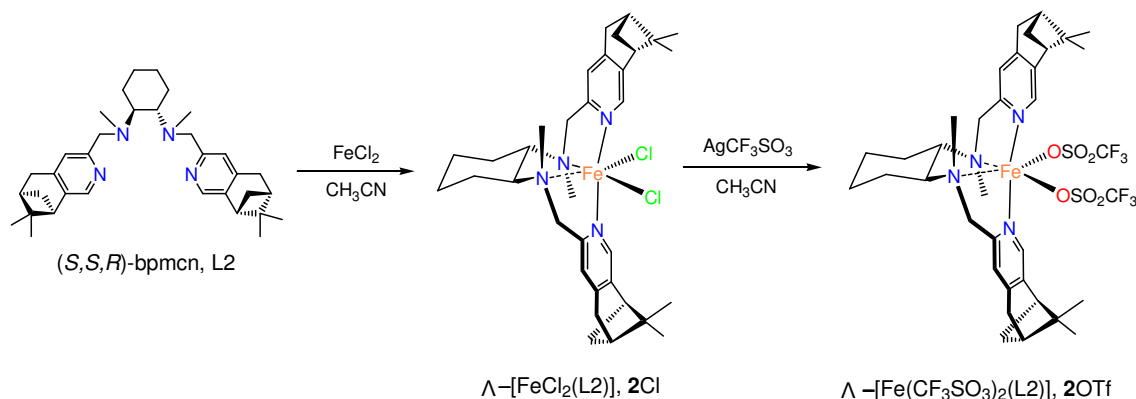
**(S,S,R)-bpbpp (L4)**. A solution containing **(S,S)-2,2'-bipyrrolidine D-tartrate** (0.35 g, 1.2 mmol),  $\text{H}_2\text{O}$  (2.6 mL),  $\text{CH}_2\text{Cl}_2$  (4 mL) was added to a 10 mL round bottom flask charged with a stir bar and **(R)-pinene-PyCH<sub>2</sub>Cl·HCl**. The aqueous phase was extracted with  $\text{CH}_2\text{Cl}_2$  (3 x 5 mL), the organic fractions were combined, dried over  $\text{MgSO}_4$  and the solvent was eliminated to vacuo. The brown oil was purified over silica column ( $\text{CH}_2\text{Cl}_2$ : $\text{MeOH}$ : $\text{NH}_3$  97:2:1) and the collected fractions were combined and concentrated to 5 mL. This fraction was washed with 1M  $\text{NaOH}$  (1 mL), dried over  $\text{MgSO}_4$  and the solvent was removed under reduced pressure to provide 230 mg (0.45 mmol, 37%) of a yellow oil that turns solid after vacuum application. FT-IR (ATR)  $\nu$ ,  $\text{cm}^{-1}$ : 2921 – 2806 (C-H) $_{\text{sp}^3}$ , 1695, 1605, 1557, 1483, 1466, 1444, 1426, 1368, 1266, 1211, 1116, 1026, 948- 865.  $^1\text{H}$ -NMR (300 MHz,  $\text{CDCl}_3$ , 300 K)  $\delta$ , ppm: 8.02 (s, 2H (6)); 7.17 (s, 2H (5)); 4.10 (d, 2H,  $J = 14$  Hz, (4)); 3.40 (d, 2H,  $J = 14$  Hz, (4)); 3.04-3.00 (m, 2H (3)); 2.94-2.92 (m, 4H (7)); 2.80-2.76 (m, 2H (12)); 2.71-2.63 (m, 4H (11 exo and 0)); 2.30-2.18 (m, 4H (3 and 8)); 1.84-1.67 (m, 8H (1 and 2)); 1.39 (s, 6H (10)); 1.15 (d, 2H  $J = 7.2$  Hz, (11 endo)); 0.61 (s, 6H (9)).  $^{13}\text{C}$ -NMR (75 MHz,  $\text{CDCl}_3$ , 300 K)  $\delta$ , ppm: 145.1 (6); 158.2, 145.1, 140.8 (14, 15 and 16); 122.5 (5); 65.6 (0); 61.7 (4); 55.8 (3); 44.5 (12); 40.3 (8); 39.4 (13); 32.9 (7); 32.1 (11); 26.2 (9); 26.0, 23.6 (1 and 2); 21.6 (10). ESI-MS ( $m/z$ ): 511.5 (100)  $[\text{M}+\text{H}]^+$ .

**(R,R,R)-bpbpp (L5)**. was prepared in analogous manner to **(S,S,R)-bpbpp** starting from **(R,R)-2,2'-bipyrrolidine L-tartrate**. (230 mg, 0.45 mmol, 37%). FT-IR (ATR)  $\nu$ ,  $\text{cm}^{-1}$ : 2968 - 2806 (C-H) $_{\text{sp}^3}$ .  $^1\text{H}$ -NMR (300 MHz,  $\text{CDCl}_3$ , 300 K)  $\delta$ , ppm: 8.02 (s, 2H (6)); 7.15 (s, 2H (5)); 4.13 (d, 2H,  $J = 14$  Hz, (4)); 3.43 (d, 2H,  $J = 14$  Hz, (4)); 3.03-2.99 (m, 2H (3)); 2.92-2.91 (m, 4H (7)); 2.78-2.71 (m, 4H (12 and 0)); 2.68-2.63 (m, 2H (11 exo)); 2.29-2.19 (m, 4H (3 and 8)); 1.87-1.68 (m, 8H (1 and 2)); 1.39 (s, 6H (10)); 1.15 (d, 2H  $J = 8.8$  Hz, (11 endo)); 0.61 (s, 6H (9)).  $^{13}\text{C}$ -NMR (75 MHz,  $\text{CDCl}_3$ , 300 K)  $\delta$ , ppm: 144.9 (6); 158.1, 144.7, 140.5 (14, 15 and 16); 122.0 (5); 65.6 (0); 61.4 (4); 55.4 (3); 44.3 (12); 40.1 (8); 39.2 (13); 32.8 (7); 31.9 (11); 26.0 (9); 25.9, 23.4 (1 and 2); 21.4 (10). ESI-MS ( $m/z$ ): 511.5 (100)  $[\text{M}+\text{H}]^+$ .

### III.5.4. Synthesis of complexes

**$\Delta$ -[FeCl<sub>2</sub>(L1)] (1Cl)**. Under a  $\text{N}_2$  atmosphere,  $\text{FeCl}_2$  (57 mg, 0.045 mmol) was added to a **(R)-bpmenp (L1)** (206 mg, 0.045 mmol) solution in  $\text{CH}_3\text{CN}$  (3 mL). The dark mixture was stirred for 2 hours and then left standing overnight. The yellow precipitate formed was filtered and dried under vacuum (160 mg, 61%). Anal. Calcd for  $\text{C}_{30}\text{H}_{42}\text{Cl}_2\text{FeN}_4 \cdot 1\text{H}_2\text{O}$  (MW = 603.45 g/mol): N, 9.28; C, 59.71; H, 7.35%. Found: N, 9.27; C, 59.67; H, 6.95%. FT-IR (ATR)  $\nu$ ,  $\text{cm}^{-1}$ : 2987 – 2871 (C-H) $_{\text{sp}^3}$ , 1736, 1615, 1558, 1487, 1470, 1456, 1422, 1361, 1265, 1081, 1021, 990, 953, 929, 809, 735.  $^1\text{H}$ -NMR (400 MHz,  $\text{CD}_3\text{CN}$ , 300 K)  $\delta$ , ppm: 142.2 (s), 140.0 (s), 107.7 (s), 107.4 (s), 90.3 (s), 89.7 (s), 57.2 (s), 55.6 (s), 48.1 (s), 47.6 (s), 10.2 to -3.5 (m), -18.3 (s), -19.4 (s). ESI-MS ( $m/z$ ): 549.2 (100)  $[\text{M}-\text{Cl}]^+$ . UV( $\text{CH}_3\text{CN}$ ):  $\lambda_{\text{max}}$ , nm ( $\epsilon$ ,  $\text{M}^{-1}\text{cm}^{-1}$ ): 269 (8672), 334 (sh) and 403 (1810). CV:  $E_{1/2}$  ( $\Delta E$ ): 125 mV (108).

**$\Delta$ -[Fe(CF<sub>3</sub>SO<sub>3</sub>)<sub>2</sub>(L1)] (1OTf)**. A suspension of Fe(CH<sub>3</sub>CN)<sub>2</sub>(CF<sub>3</sub>SO<sub>3</sub>)<sub>2</sub> (65 mg, 0.15 mmol) in THF (1.5 mL) was added dropwise to a vigorously stirred solution of L1 (69 mg, 0.15 mmol) in THF (1 mL). The pale yellow precipitate formed after stirring overnight was filtered. Diethyl ether was added to the resulting solution to ensure the complete precipitation of the product. This solid was added to the previously filtered, redissolved in CH<sub>2</sub>Cl<sub>2</sub> (2 mL) and filtered again. Slow diethyl ether diffusion over the solution afforded, after a couple of days, the product as pale yellow needles suitable for X-ray diffraction (77 mg, 0.095 mmol, 63%). Anal. Calcd for C<sub>32</sub>H<sub>42</sub>F<sub>6</sub>FeN<sub>4</sub>O<sub>6</sub>S<sub>2</sub>·1.2 CH<sub>2</sub>Cl<sub>2</sub> (MW = 612.66 g/mol): N, 6.13; C, 43.60; H, 4.89; S, 7.01%. Found: N, 6.10; C, 43.40; H, 4.77; S, 7.54%. FT-IR (ATR)  $\nu$ , cm<sup>-1</sup>: 2985 - 2876 (C-H)<sub>sp3</sub>, 1308 (Py), 1235, 1214, 1181, 1153, 1029, 634 (CF<sub>3</sub>SO<sub>3</sub>). <sup>1</sup>H-NMR (400 MHz, CD<sub>2</sub>Cl<sub>2</sub>, 300 K)  $\delta$ , ppm: 165 (s), 110 (s), 98 (s), 74 (s), 50.5 (s), 29 (s), 8.3 to -0.8 (m). ESI-MS (m/z): 663.2 (33) [M-CF<sub>3</sub>SO<sub>3</sub>]<sup>+</sup> and 257.0 (100) [M-2CF<sub>3</sub>SO<sub>3</sub>]<sup>+2</sup>. UV(CH<sub>3</sub>CN):  $\lambda_{max}$ , nm ( $\epsilon$ , M<sup>-1</sup>cm<sup>-1</sup>): 257 (sh), 265 (sh) and 373 (3932). X-ray analysis indicates that the complex adopts a  $\Delta$  chiral topology.



**Scheme 14.** Schematic view of the stereoselective preparation of the complexes with **(S,S,R)-bpmcnp** (L2) ligand.

**$\Lambda$ -[FeCl<sub>2</sub>(L2)] (2Cl)**. Under a N<sub>2</sub> atmosphere, FeCl<sub>2</sub> (62.7 mg, 0.5 mmol) was added to a stirred solution of **(S,S,R)-bpmcnp** (L2) (253 mg, 0.5 mmol) in CH<sub>3</sub>CN (5 mL). The reaction mixture was stirred for 2 hours to allow the complete precipitation of a yellow solid which corresponds to **2Cl**. The solution was filtered and the resulting solid washed with CH<sub>3</sub>CN and dried under vacuum to give 145 mg (0.23 mmol, 46%) of a yellow powder. Single crystals were grown from slow diffusion of diethyl ether in a CH<sub>2</sub>Cl<sub>2</sub> solution of the compound. Anal. Calcd for C<sub>34</sub>H<sub>48</sub>Cl<sub>2</sub>FeN<sub>4</sub>·1.75 H<sub>2</sub>O (MW = 671.06 g/mol): N, 8.35; C, 60.86; H, 7.74%. Found: N, 8.50; C, 60.98; H, 8.04%. FT-IR (ATR)  $\nu$ , cm<sup>-1</sup>: 2970 - 2867 (C-H)<sub>sp3</sub>, 1618, 1559, 1489, 1469, 1458, 1425, 1361, 1274, 1255, 1116, 1028, 977, 955, 926, 886, 782. <sup>1</sup>H-NMR (200 MHz, CD<sub>2</sub>Cl<sub>2</sub>, 300 K)  $\delta$ , ppm: 105 (s), 50 (s), 46 (s), 17(s), 9.53-1.16 (m), -5.8 (s), -25 (s). ESI-MS (m/z): 603.2 (100) [M-Cl]<sup>+</sup>. UV(CH<sub>3</sub>CN):  $\lambda_{max}$ , nm ( $\epsilon$ , M<sup>-1</sup>cm<sup>-1</sup>): 268 (7403), 333 (sh) and 411 (1381). CV: E<sub>1/2</sub> ( $\Delta E$ ): 98 mV (119). X-Ray analysis indicates that the complex adopts a  $\Lambda$  topological chirality.

**$\Lambda$ -[Fe(CF<sub>3</sub>SO<sub>3</sub>)<sub>2</sub>(L2)] (2OTf)**. Under a N<sub>2</sub> atmosphere, to a stirred mixture of **2Cl** (50 mg, 0.08 mmol) in CH<sub>3</sub>CN (1.5 mL) was added a solution of AgCF<sub>3</sub>SO<sub>3</sub> (40 mg, 0.16 mmol) in CH<sub>3</sub>CN (1 mL). The mixture was stirred for 1 hour and then filtered through Celite® to remove precipitated AgCl. The solvent was removed under vacuum and the compound was redissolved

in  $\text{CH}_2\text{Cl}_2$ . Slow diffusion of diethyl ether into this solution afforded 60 mg (0.069 mmol, 88%) of yellow crystals suitable for X-Ray analysis. Anal. Calcd for  $\text{C}_{36}\text{H}_{48}\text{F}_6\text{FeN}_4\text{O}_6\text{S}_2 \cdot 0.25\text{CH}_2\text{Cl}_2$  (MW = 887.93 g/mol): N, 6.31; C, 49.04; H, 5.51; S, 7.22%. Found: N, 6.33; C, 49.36; H, 5.58; S, 6.75%. FT-IR (ATR)  $\nu$ ,  $\text{cm}^{-1}$ : 2933 - 2874 (C-H)<sub>sp3</sub>, 1306 (Py), 1233, 1216, 1156, 1029, 632 ( $\text{CF}_3\text{SO}_3$ ).  $^1\text{H-NMR}$  (400 MHz,  $\text{CD}_2\text{Cl}_2$ , 300 K)  $\delta$ , ppm: 179 (s), 116 (s), 67 (s), 54 (s), 25 (s), 20 (s), 9.7 (s), 8.8 (s), 6.7 - 0.7 (m). ESI-MS (m/z): 717.2 (100)  $[\text{M-CF}_3\text{SO}_3]^+$ . UV( $\text{CH}_3\text{CN}$ ):  $\lambda_{\text{max}}$ , nm ( $\epsilon$ ,  $\text{M}^{-1}\text{cm}^{-1}$ ): 257 (sh), 265 (sh) and 374 (4884).  $\mu_{\text{eff}}$  in  $\text{CD}_2\text{Cl}_2$ : 5.37 MB, 4.46 unpaired electrons.  $\mu_{\text{eff}}$  in  $\text{CD}_3\text{CN}$ : 4.17 MB, 3.29 unpaired electrons. X-Ray analysis indicates that the complex adopts a  $\Lambda$  topological chirality.

**$\Delta$ -[FeCl<sub>2</sub>(L3)] (3Cl)**. Under a  $\text{N}_2$  atmosphere,  $\text{FeCl}_2$  (25 mg, 0.198 mmol) was added to a stirred solution of (*R,R,R*)-bpmcnp (L3) (100 mg, 0.198 mmol) in THF (5 mL). The reaction was stirred overnight to obtain an orange jelly. The solvent was evaporated under reduced pressure and the resulting solid was redissolved with  $\text{CH}_2\text{Cl}_2$  and filtered. Slow diffusion of diethyl ether to the solution led to the formation of 40 mg (0.062 mmol, 63%) of orange crystals after 2 days. Anal. Calcd for  $\text{C}_{34}\text{H}_{48}\text{Cl}_2\text{FeN}_4 \cdot 0.6 \text{CH}_2\text{Cl}_2$  (MW = 639.53 g/mol): N, 8.11; C, 60.19; H, 7.18. %. Found: N, 8.44; C, 59.61; H, 7.03%. FT-IR (ATR)  $\nu$ ,  $\text{cm}^{-1}$ : 2969 - 2867 (C-H)<sub>sp3</sub>, 1736, 1616, 1560, 1489, 1473, 1454, 1422, 1356, 1270, 1253, 1107, 1020, 975, 956, 925, 873, 724.  $^1\text{H-NMR}$  (400 MHz,  $\text{CD}_3\text{CN}$ , 300 K)  $\delta$ , ppm: 138 (s), 107 (s), 48.4 (s), 47.5 (s), 16.8 (s), 9.98-0.89 (m), -6.0 (s), -23.5 (s). ESI-MS (m/z): 603.3 (100)  $[\text{M-Cl}]^+$ , 284.1 (25)  $[\text{M-2Cl}]^{+2}$ . UV( $\text{CH}_3\text{CN}$ ):  $\lambda_{\text{max}}$ , nm ( $\epsilon$ ,  $\text{M}^{-1}\text{cm}^{-1}$ ): 270 (5518), 330 (sh) and 419 (1114). CV:  $E_{1/2}$  ( $\Delta E$ ): 101 mV (106). X-Ray analysis indicates that the complex adopts a  $\Delta$  topological chirality.

**$\Delta$ -[Fe( $\text{CF}_3\text{SO}_3$ )<sub>2</sub>(L3)] (3OTf)**. Under a  $\text{N}_2$  atmosphere, to a stirred mixture of 3Cl (50 mg, 0.08 mmol) in  $\text{CH}_2\text{Cl}_2$  (1.5 mL) was added a suspension of  $\text{AgCF}_3\text{SO}_3$  (40.7 mg, 0.16 mmol) in  $\text{CH}_2\text{Cl}_2$  (1.5 mL). The mixture was stirred for 1 hour and then filtered through Celite® to remove the precipitated  $\text{AgCl}$ . The solvent was removed under reduced pressure and the resulting solid redissolved in 1 mL of  $\text{CH}_2\text{Cl}_2$ . Slow diffusion of diethyl ether to the solution led to the formation of 41 mg (0.048 mmol, 60%) of yellow crystals after 2 days. Anal. Calcd for  $\text{C}_{36}\text{H}_{48}\text{F}_6\text{FeN}_4\text{O}_6\text{S}_2 \cdot 0.15 \text{CH}_2\text{Cl}_2$  (MW = 879.44 g/mol): N, 6.37; C, 49.37; H, 5.54; S, 7.29%. Found: N, 6.71; C, 49.08; H, 5.61; S, 7.04%. FT-IR (ATR)  $\nu$ ,  $\text{cm}^{-1}$ : 2935 - 2875 (C-H)<sub>sp3</sub>, 1289 (Py), 1236, 1217, 1160, 1026, 634 ( $\text{CF}_3\text{SO}_3$ ).  $^1\text{H-NMR}$  (400 MHz,  $\text{CD}_2\text{Cl}_2$ , 300 K)  $\delta$ , ppm: 167 (s), 112 (s), 66.5 (s), 50 (s), 25 (s), 19 (s), 9.7-0.1 (m). ESI-MS (m/z): 717.2 (100)  $[\text{M-CF}_3\text{SO}_3]^+$ , 284.9 (20)  $[\text{M-2CF}_3\text{SO}_3]^{+2}$ . UV( $\text{CH}_3\text{CN}$ ):  $\lambda_{\text{max}}$ , nm ( $\epsilon$ ,  $\text{M}^{-1}\text{cm}^{-1}$ ): 256 (sh), 265 (sh) and 377 (5448).

**$\Lambda$ -[FeCl<sub>2</sub>(L4)] (4Cl)**. The same procedure as for complex 2Cl gave 4Cl as a yellow powder (57%). Anal. Calcd for  $\text{C}_{34}\text{H}_{46}\text{Cl}_2\text{FeN}_4 \cdot 1.65 \text{CH}_2\text{Cl}_2$  (MW = 777.65 g/mol): N, 7.20; C, 55.06; H, 7.20%. Found: N, 7.55; C, 54.80; H, 6.15%. FT-IR (ATR)  $\nu$ ,  $\text{cm}^{-1}$ : 3045 - 2898 (C-H)<sub>sp3</sub>, 1736, 1615, 1559, 1488, 1468, 1420, 1357, 1299, 1258, 1101, 1024, 954, 908, 899, 855, 726, 696.  $^1\text{H-NMR}$  (400 MHz,  $\text{CD}_3\text{CN}$ , 300 K)  $\delta$ , ppm: 154 (s), 120 (s), 80 (s), 46.5 (s), 22.5 (s), 21.7 (s), 11.6-0.8 (m), -11.6 (s), -12.4 (s), -20 (s). ESI-MS (m/z): 601.2 (100)  $[\text{M-Cl}]^+$ , 283.1 (33)

$[M-2Cl]^{+2}$ . UV(CH<sub>3</sub>CN):  $\lambda_{max}$ , nm ( $\epsilon$ , M<sup>-1</sup>cm<sup>-1</sup>): 265 (5990), 337 (sh) and 402 (1172). CV: E<sub>1/2</sub> ( $\Delta E$ ): 61 mV (96).

**$\Lambda$ -[Fe(CF<sub>3</sub>SO<sub>3</sub>)<sub>2</sub>(L4)] (4OTf).** The same procedure as for complex 1OTf gave 4OTf as yellow crystals (59%). Anal. Calcd for C<sub>36</sub>H<sub>46</sub>F<sub>6</sub>FeN<sub>4</sub>O<sub>6</sub>S<sub>2</sub>·0.1 Et<sub>2</sub>O (MW = 872.15 g/mol): N, 6.42; C, 50.13; H, 5.43; S, 7.35%. Found: N, 6.72; C, 50.36; H, 5.25; S, 7.55%. FT-IR (ATR)  $\nu$ , cm<sup>-1</sup>: 2990 – 2908 (C-H)<sub>sp3</sub>, 1315 (Py), 1236, 1215, 1157, 1027, 632 (CF<sub>3</sub>SO<sub>3</sub>). <sup>1</sup>H-NMR (400 MHz, CD<sub>2</sub>Cl<sub>2</sub>, 300 K)  $\delta$ , ppm: 182 (s), 117 (s), 76 (s), 51 (s), 32.3 (s), 28.8 (s), 21.8-17.4 (m), 7.9 to -6 (m), -8.3 (s), -20.6 (s). ESI-MS (m/z): 715.3 (100) [M-CF<sub>3</sub>SO<sub>3</sub>]<sup>+</sup>, 283.1 (50) [M-2CF<sub>3</sub>SO<sub>3</sub>]<sup>+2</sup>. UV(CH<sub>3</sub>CN):  $\lambda_{max}$ , nm ( $\epsilon$ , M<sup>-1</sup>cm<sup>-1</sup>): 256 (sh), 265 (sh) and 376 (6301). X-Ray analysis indicates that the complex adopts a  $\Lambda$  topological chirality.

**$\Delta$ -[FeCl<sub>2</sub>(L5)] (5Cl).** The same procedure as for complex 2Cl gave 5Cl as a yellow powder (52%). Anal. Calcd for C<sub>34</sub>H<sub>46</sub>Cl<sub>2</sub>FeN<sub>4</sub>·0.9 CH<sub>2</sub>Cl<sub>2</sub> (MW = 713.95 g/mol): N, 7.85; C, 58.71; H, 6.75%. Found: N, 8.23; C, 58.55; H, 6.64%. FT-IR (ATR)  $\nu$ , cm<sup>-1</sup>: 3051 – 2827 (C-H)<sub>sp3</sub>, 1739, 1615, 1560, 1488, 1468, 1421, 1357, 1270, 1214, 1103, 1023, 951, 912, 900, 863, 730, 696. <sup>1</sup>H-NMR (400 MHz, CD<sub>3</sub>CN, 300 K)  $\delta$ , ppm: 152 (s), 120 (s), 77.8 (s), 47.0 (s), 23.3 (s), 20.3 (s), 11.3 to -1.4 (m), -7.5 (s), -11.0 (s), -12.1 (s), -18 (s). ESI-MS (m/z): 601.2 (100) [M-Cl]<sup>+</sup>, 283.1 (33) [M-2Cl]<sup>+2</sup>. UV(CH<sub>3</sub>CN):  $\lambda_{max}$ , nm ( $\epsilon$ , M<sup>-1</sup>cm<sup>-1</sup>): 269 (5582), 327 (sh) and 420 (1168). CV: E<sub>1/2</sub> ( $\Delta E$ ): 67 mV (102).

**$\Delta$ -[Fe(CF<sub>3</sub>SO<sub>3</sub>)<sub>2</sub>(L5)] (5OTf).** The same procedure as for complex 1OTf gave 5OTf as yellow crystals (57%). Anal. Calcd for C<sub>36</sub>H<sub>46</sub>F<sub>6</sub>FeN<sub>4</sub>O<sub>6</sub>S<sub>2</sub>·1H<sub>2</sub>O (MW = 882.75 g/mol): N, 6.35; C, 48.99; H, 5.48; S, 7.25%. Found: N, 6.39; C, 48.88; H, 5.40; S, 7.10%. FT-IR (ATR)  $\nu$ , cm<sup>-1</sup>: 2987 – 2873 (C-H)<sub>sp3</sub>, 1312 (Py), 1235, 1216, 1158, 1029, 630 (CF<sub>3</sub>SO<sub>3</sub>). <sup>1</sup>H-NMR (400 MHz, CD<sub>2</sub>Cl<sub>2</sub>, 300 K)  $\delta$ , ppm: 176 (s), 118 (s), 79 (s), 49 (s), 33.7 (s), 28.3 (s), 18.3 (sa), 8.2 to -2 (m), -8.1 (s), -15.9 (s). ESI-MS (m/z): 715.3 (100) [M-CF<sub>3</sub>SO<sub>3</sub>]<sup>+</sup>, 283.1 (80) [M-2CF<sub>3</sub>SO<sub>3</sub>]<sup>+2</sup>. UV(CH<sub>3</sub>CN):  $\lambda_{max}$ , nm ( $\epsilon$ , M<sup>-1</sup>cm<sup>-1</sup>): 257 (sh), 265 (sh) and 378 (5550). X-Ray analysis indicates that the complex adopts a  $\Delta$  topological chirality.

**[FeCl<sub>2</sub>(L8)] (8Cl).** The same procedure as for complex 2Cl gave 8Cl as a yellow powder (79%). Anal. Calcd for C<sub>20</sub>H<sub>26</sub>Cl<sub>2</sub>FeN<sub>4</sub>·0.35 CH<sub>2</sub>Cl<sub>2</sub> (MW = 478.93 g/mol): N, 11.70; C, 51.04; H, 5.62%. Found: N, 11.45; C, 51.25; H, 5.47%. FT-IR (ATR)  $\nu$ , cm<sup>-1</sup>: 3053 – 2901 (C-H)<sub>sp3</sub>, 1601, 1569, 1475, 1439, 1376, 1299, 1263, 1096, 1021, 994, 979, 897, 784. ESI-MS (m/z): 413.1 (100) [M-Cl]<sup>+</sup>. UV(CH<sub>3</sub>CN):  $\lambda_{max}$ , nm ( $\epsilon$ , M<sup>-1</sup>cm<sup>-1</sup>): 258 (8951) and 426 (1556). CV: E<sub>1/2</sub> ( $\Delta E$ ): 125 mV (96).

**[Fe(CF<sub>3</sub>SO<sub>3</sub>)<sub>2</sub>(L8)] (8OTf).** The same procedure as for complex 1OTf gave 8OTf as yellow crystals (62%). Anal. Calcd for C<sub>22</sub>H<sub>26</sub>F<sub>6</sub>FeN<sub>4</sub>O<sub>6</sub>S<sub>2</sub> (MW = 676.43 g/mol): N, 8.28; C, 39.07; H, 3.87; S, 9.48%. Found: N, 8.46; C, 39.26; H, 3.87; S, 9.33%. FT-IR (ATR)  $\nu$ , cm<sup>-1</sup>: 2970 - 2897 (C-H)<sub>sp3</sub>, 1311 (Py), 1237, 1215, 1155, 1020, 630 (CF<sub>3</sub>SO<sub>3</sub>). <sup>1</sup>H-NMR (400 MHz, CD<sub>2</sub>Cl<sub>2</sub>, 300 K)  $\delta$ , ppm: 177 (s), 127.5 (s), 78 (s), 55 (s), 52 (s), 30 (s), 27 (s), 15 (m), -4.8 (s), -9.8 (s), -18 (s) ESI-MS (m/z): 527.0 (60) [M-CF<sub>3</sub>SO<sub>3</sub>]<sup>+</sup>, 188.9 (100) [M-2CF<sub>3</sub>SO<sub>3</sub>]<sup>+2</sup>. UV(CH<sub>3</sub>CN):  $\lambda_{max}$ , nm ( $\epsilon$ , M<sup>-1</sup>cm<sup>-1</sup>): 236 (15194), 250 (sh) and 378 (7072).



### III.5.5. UV-Vis spectra

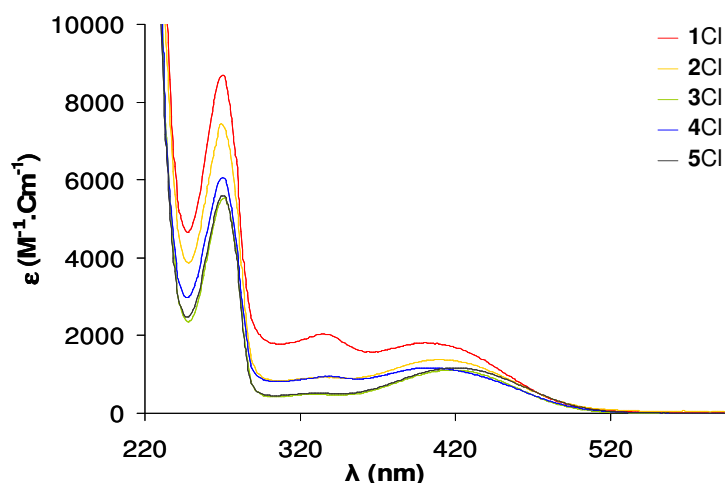


**Figure 13.** UV-Vis spectra of complexes 1-5Cl in CH<sub>3</sub>CN.

### III.5.6. Crystal data

Single crystals of **2Cl**, **3Cl**, **1OTf**, **2OTf**, **4OTf** and **5OTf** were mounted on a nylon loop and used for room temperature (**4OTf** and **5OTf**) or low temperature (100(2) K, **2Cl**, **3Cl**, **1OTf** and **2OTf**) X-ray structure determination. The measurements were carried out on a BRUKER SMART APEX CCD diffractometer using graphite-monochromated Mo K $\alpha$  radiation ( $\lambda = 0.71073 \text{ \AA}$ ) from an x-Ray Tube. Programs used: data collection, Smart version 5.631 (Bruker AXS 1997-02); data reduction, Saint + version 6.36A (Bruker AXS 2001); absorption correction, SADABS version 2.10 (Bruker AXS 2001). Structure solution and refinement was done using SHELXTL Version 6.14 (Bruker AXS 2000-2003).

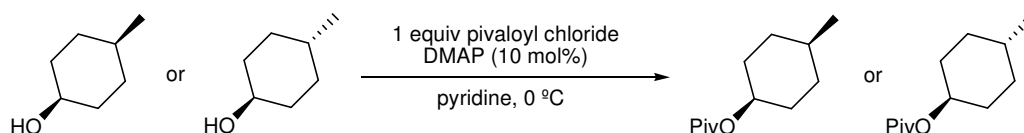
The structure was solved by direct methods and refined by full-matrix least-squares methods on  $F^2$ . The non-hydrogen atoms were refined anisotropically. The hydrogen atoms were placed in geometrically optimized positions and forced to ride on the atom to which they are attached. **2Cl** presented a considerable amount of electron density belonging to disordered CH<sub>2</sub>Cl<sub>2</sub> solvent molecule that was eliminated from the difference map with the SQUEEZE tool from the Platon program (Spek, A. L. (2005). PLATON, A Multipurpose Crystallographic Tool, Utrecht University, Utrecht, The Netherlands). **1OTf** showed spurious electron density peaks non attributable to any solvent molecule and **5OTf** exhibit electron density attributable to partially disordered solvent water molecule, in both cases SQUEEZE option in PLATON was used to remove them from the difference map. (Cambridge Crystallographic Data Center reference for **2OTf** is CCDC 726566).

**Table 12.** Crystal data and structure refinement for **2Cl**, **3Cl**, **1OTf**, **2OTf**, **4OTf** and **5OTf**.

| Compound                | 2Cl                                                                                           | 3Cl                                                                                    | 1OTf                                                                                          | 2OTf                                                                                          | 4OTf                                                                                          | 5OTf                                                                                          |
|-------------------------|-----------------------------------------------------------------------------------------------|----------------------------------------------------------------------------------------|-----------------------------------------------------------------------------------------------|-----------------------------------------------------------------------------------------------|-----------------------------------------------------------------------------------------------|-----------------------------------------------------------------------------------------------|
| Empirical formula       | C <sub>34</sub> H <sub>48</sub> Cl <sub>2</sub> FeN <sub>4</sub>                              | C <sub>36</sub> H <sub>52</sub> Cl <sub>6</sub> FeN <sub>4</sub>                       | C <sub>32</sub> H <sub>42</sub> F <sub>6</sub> FeN <sub>4</sub> O <sub>6</sub> S <sub>2</sub> | C <sub>36</sub> H <sub>48</sub> F <sub>6</sub> FeN <sub>4</sub> O <sub>6</sub> S <sub>2</sub> | C <sub>36</sub> H <sub>46</sub> F <sub>6</sub> FeN <sub>4</sub> O <sub>6</sub> S <sub>2</sub> | C <sub>36</sub> H <sub>46</sub> F <sub>6</sub> FeN <sub>4</sub> O <sub>6</sub> S <sub>2</sub> |
| Formula weight          | 639.51                                                                                        | 809.37                                                                                 | 812.67                                                                                        | 866.75                                                                                        | 864.74                                                                                        | 864.74                                                                                        |
| Temperature             | 100(2) K                                                                                      | 100(2) K                                                                               | 100(2) K                                                                                      | 100(2) K                                                                                      | 300(2) K                                                                                      | 300(2) K                                                                                      |
| Wavelength              | 0.71073 Å                                                                                     | 0.71073 Å                                                                              | 0.71073 Å                                                                                     | 0.71073 Å                                                                                     | 0.71073 Å                                                                                     | 0.71073 Å                                                                                     |
| Cristal system          | Monoclinic                                                                                    | Orthorhombic                                                                           | Monoclinic                                                                                    | Orthorhombic                                                                                  | Orthorhombic                                                                                  | Orthorhombic                                                                                  |
| Space group             | C2                                                                                            | P2(1)2(1)2(1)                                                                          | C2                                                                                            | P2(1)2(1)2(1)                                                                                 | P2(1)2(1)2(1)                                                                                 | P2(1)2(1)2(1)                                                                                 |
| Unit cell dimensions    | a = 12.928(4) Å<br>α = 90°<br>b = 14.089(4) Å<br>β = 96.535(4)°<br>c = 10.754(3) Å<br>γ = 90° | a = 11.853(2) Å<br>α = 90°<br>b = 13.953(3) Å<br>β = 90°<br>c = 23.885(5) Å<br>γ = 90° | a = 16.240(4) Å<br>α = 90°<br>b = 14.594(3) Å<br>β = 109.371°<br>c = 16.823(4) Å<br>γ = 90°   | a = 13.7437(17) Å<br>α = 90°<br>b = 16.5609(19) Å<br>β = 90°<br>c = 17.487(2) Å<br>γ = 90°    | a = 14.954(11) Å<br>α = 90°<br>b = 16.340(12) Å<br>β = 90°<br>c = 16.575(12) Å<br>γ = 90°     | a = 15.398(2) Å<br>α = 90°<br>b = 26.204(3) Å<br>β = 90°<br>c = 10.6011(14) Å<br>γ = 90°      |
| Volume                  | 1946.1(10) Å <sup>3</sup>                                                                     | 3950.1(14) Å <sup>3</sup>                                                              | 3761.4(14) Å <sup>3</sup>                                                                     | 3980.1(8) Å <sup>3</sup>                                                                      | 4050(5) Å <sup>3</sup>                                                                        | 4277.4(10) Å <sup>3</sup>                                                                     |
| Z                       | 2                                                                                             | 4                                                                                      | 4                                                                                             | 4                                                                                             | 4                                                                                             | 4                                                                                             |
| Density (calculated)    | 1.091 Mg/m <sup>3</sup>                                                                       | 1.361 Mg/m <sup>3</sup>                                                                | 1.435 Mg/m <sup>3</sup>                                                                       | 1.446 Mg/m <sup>3</sup>                                                                       | 1.418 Mg/m <sup>3</sup>                                                                       | 1.610 Mg/m <sup>3</sup>                                                                       |
| Absorption coefficient  | 0.549 mm <sup>-1</sup>                                                                        | 0.818 mm <sup>-1</sup>                                                                 | 0.588 mm <sup>-1</sup>                                                                        | 0.561 mm <sup>-1</sup>                                                                        | 0.551 mm <sup>-1</sup>                                                                        | 0.537 mm <sup>-1</sup>                                                                        |
| F(000)                  | 680                                                                                           | 1696                                                                                   | 1688                                                                                          | 1808                                                                                          | 1800                                                                                          | 2152                                                                                          |
| Reflections collected   | 11719                                                                                         | 60454                                                                                  | 28518                                                                                         | 82561                                                                                         | 63774                                                                                         | 67855                                                                                         |
| Independent reflections | 4497 [R(int) = 0.0428]                                                                        | 9732 [R(int) = 0.0468]                                                                 | 9156 [R(int) = 0.0900]                                                                        | 23809 [R(int) = 0.0347]                                                                       | 10101 [R(int) = 0.0808]                                                                       | 10554 [R(int) = 0.1084]                                                                       |
| Final R indices         | R1 = 0.0545,<br>[>2σ(I)]<br>wR2 = 0.1560                                                      | R1 = 0.0323,<br>wR2 = 0.0750                                                           | R1 = 0.0848,<br>wR2 = 0.2045                                                                  | R1 = 0.0443,<br>wR2 = 0.1290                                                                  | R1 = 0.0549,<br>wR2 = 0.1440                                                                  | R1 = 0.0596,<br>wR2 = 0.1301                                                                  |
| R indices (all data)    | R1 = 0.0566,<br>wR2 = 0.1600                                                                  | R1 = 0.0415,<br>wR2 = 0.0794                                                           | R1 = 0.1681,<br>wR2 = 0.2380                                                                  | R1 = 0.0497,<br>wR2 = 0.1330                                                                  | R1 = 0.0890,<br>wR2 = 0.1610                                                                  | R1 = 0.1112,<br>wR2 = 0.1467                                                                  |

### III.5.7. Synthesis of substrates

*Cis*-1,2-dimethylcyclohexane (*cis*-1,2-DMCH), cyclohexane, D<sub>12</sub>-cyclohexane, (1*R*)-(-)-menthyl acetate (**S1**), 2,6-dimethyloctane (**S2H**) and 1-bromo-3,7-dimethyloctane (**S2Br**), were purchased from Aldrich, TCI America or Cambridge Isotope and passed through an alumina plug before being used. 3,7-dimethyl-1-octanol, *cis*-4-methylcyclohexanol and *trans*-4-methylcyclohexanol were purchased from TCI America.



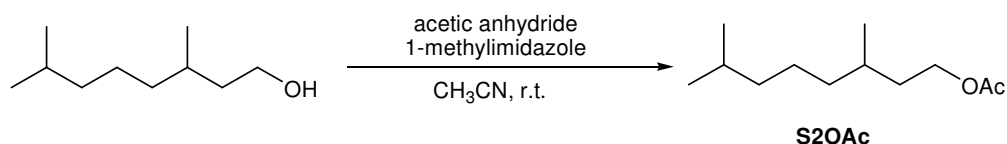
**Scheme 15.** Synthesis of *cis*-4-methylcyclohexyl-1-pivalate and *trans*-4-methylcyclohexyl-1-pivalate.

*cis*-4-methylcyclohexyl pivalate and *trans*-4-methylcyclohexyl pivalate were prepared by reaction of pivaloyl chloride with the commercially available *cis*-4-methylcyclohexanol and *trans*-4-methylcyclohexanol, respectively, following the procedure described below (scheme 15):

*Cis*-4-methylcyclohexanol or *trans*-4-methylcyclohexanol (5 mL, 40.0 mmol) and dimethylaminopyridine (0.49 g, 4.0 mmol) were dissolved in pyridine (65 mL). The mixture was cooled in an ice-bath and a solution of pivaloyl chloride (5.5 mL, 43.0 mmol) in pyridine (40 mL) was added dropwise. After stirring for 24 hours, the solvent was removed under reduced pressure and the resulting residue was treated with CHCl<sub>3</sub> (250 mL) and washed with water (100 mL), saturated NaHCO<sub>3</sub> aqueous solution (100 mL) and saturated NaCl aqueous solution (100 mL). The organic phase was dried over MgSO<sub>4</sub>, filtered and the solvent was removed under reduced pressure to yield a yellow oil. The product was purified by column chromatography over silica eluting with hexane which gave the desired compounds as colourless oils.

*Cis*-4-methylcyclohexyl pivalate (98.9% *cis* analyzed by GC): 63% yield. <sup>1</sup>H-NMR (400 MHz, CDCl<sub>3</sub>, 300 K) δ, ppm: 4.96 (m, 1H), 1.84 – 1.79 (m, 2H), 1.54 – 1.46 (m, 5H), 1.30 – 1.12 (m, 2H), 1.21 (s, 9H), 0.92 (d, J = 6.4 Hz, 3H). <sup>13</sup>C-NMR (100 MHz, CDCl<sub>3</sub>, 300 K) δ, ppm: 177.9, 69.1, 38.9, 32.1, 29.6, 29.5, 27.2, 22.3. FT-IR (ATR) ν, cm<sup>-1</sup>: 2950, 2925, 2870, 2836, 1725, 1479, 1371, 1283, 1161, 1130, 1033, 967, 887, 678, 630. ESI-MS (m/z): 221.1 [M+Na]<sup>+</sup>, 237.1 [M+K]<sup>+</sup>

*Trans*-4-methylcyclohexyl pivalate (98.9% *trans* analyzed by GC): 72 % yield. <sup>1</sup>H-NMR (400 MHz, CDCl<sub>3</sub>, 300 K) δ, ppm: 4.63 (m, 1H), 1.90 (m, 2H), 1.73 (m, 2H), 1.35 – 1.23 (m, 3H), 1.18 (s, 9H), 1.06 (m, 2H), 0.90 (d, J = 8.4 Hz, 3H). <sup>13</sup>C-NMR (100 MHz, CDCl<sub>3</sub>, 300 K) δ, ppm: 178.1, 72.9, 38.6, 32.9, 31.7, 31.4, 27.1, 21.8. FT-IR (ATR) ν, cm<sup>-1</sup>: 2949, 2931, 2868, 1725, 1480, 1454, 1366, 1283, 1166, 1152, 1086, 1033, 1021, 995, 686, 630. ESI-MS (m/z): 221.1 [M+Na]<sup>+</sup>.



**Scheme 16.** Synthesis of 3,7-dimethyloctyl acetate (**S2OAc**).

3,7-dimethyloctyl acetate (**S2OAc**) was prepared by acetylating the commercially available 3,7-dimethyl-1-octanol following the procedure described below (scheme 16):

3,7-dimethyl-1-octanol (0.8 g, 4.8 mmol), 1-methylimidazole (0.7 mL) and acetic anhydride (7 mL) were dissolved in CH<sub>3</sub>CN (12 mL) and stirred for 30 min at room temperature. Ice (20 mL) was added at this point. After stirring for 15 min, CHCl<sub>3</sub> (50 mL) was added. The organic layer was washed with H<sub>2</sub>SO<sub>4</sub> 1 M (20 mL), saturated NaHCO<sub>3</sub> solution (20 mL) and water (20 mL), dried over MgSO<sub>4</sub> and the solvent was removed under reduced pressure. The resulting crude product was purified by flash chromatography over alumina (100% hexanes) which afforded 0.81 g of the desired product (**S2OAc**) as a colourless liquid (4.1 mmol, 85%). <sup>1</sup>H-NMR (400 MHz, CDCl<sub>3</sub>, 300 K) δ, ppm: 4.10 (m, 2H), 2.05 (s, 3H), 1.64 (m, 1H), 1.53 (m, 2H), 1.47(m, 1H), 1.41 – 1.13 (m, 6H), 0.93 (d, J = 6.4 Hz, 3H), 0.88 (d, J = 6.4 Hz, 6H). <sup>13</sup>C-NMR (100 MHz, CDCl<sub>3</sub>, 300 K) δ, ppm: 171.2, 63.1, 39.2, 37.1, 35.5, 29.1, 28.0, 24.6, 22.7, 22.6, 21.0, 19.5. FT-IR (ATR) ν, cm<sup>-1</sup>: 2955, 2927, 2870, 1741, 1463, 1367, 1232, 1047, 686, 628. ESI-MS (m/z): 233.1 [M+Na]<sup>+</sup>.

## III.5.8. Reaction conditions for catalysis

### III.5.8.1. Alkanes

#### III.5.8.1.1. Standard conditions

**Substrate excess and room temperature conditions; catalyst:substrate:H<sub>2</sub>O<sub>2</sub>, 1:10:1000, 1:100:1000 and 1:100:100**

0.36 mL of a H<sub>2</sub>O<sub>2</sub> solution (diluted from 35% H<sub>2</sub>O<sub>2</sub>/H<sub>2</sub>O solution) with adequate concentration in CH<sub>3</sub>CN was delivered by syringe pump over 30 min at 25°C in air to a vigorously stirred CH<sub>3</sub>CN solution (2.14 mL) containing the iron catalyst (2.5 μmol) and the appropriate amount of alkane substrate (250 or 2500 μmols). For adamantane, due to low solubility, only 25 μmols of substrate were added. The final concentration of the mononuclear iron catalyst was 1 mM. The solution was stirred for another 10 min after syringe pump addition. Biphenyl was added as internal standard and the iron complex was removed by passing the solution through basic alumina followed by elution with 2 mL AcOEt. The solution was subjected to GC analysis. The organic products were identified by comparison with authentic compounds and GC-MS analysis. In the studies of kinetic isotope effects, a substrate mixture of cyclohexane/cyclohexane-D<sub>12</sub> of 1:3 mol/mol was used to improve the accuracy of the KIE values obtained.

**Reactions with AcOH as additive and substrate excess at 0°C, catalyst:substrate:H<sub>2</sub>O<sub>2</sub>:AcOH, 1:10:1000:50**

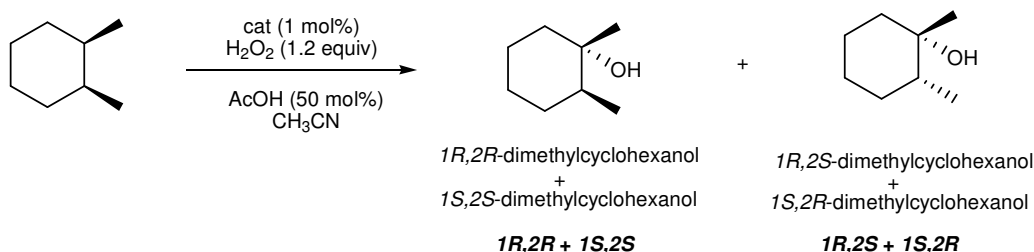
To a vigorously stirred solution of the iron catalyst (2.5 μmol) in CH<sub>3</sub>CN (2.14 mL) at 0°C, 72 μL of a 1.74 M solution of acetic acid in CH<sub>3</sub>CN and the appropriate amount of alkane substrate (2500 μmols; for adamantane, due to low solubility, only 25 μmols of substrate were added) were added. 0.36 mL of a 70 mM H<sub>2</sub>O<sub>2</sub> solution (diluted from 35% H<sub>2</sub>O<sub>2</sub>/H<sub>2</sub>O solution) in CH<sub>3</sub>CN was delivered by syringe pump over 30 min in air. The solution was stirred for another 10 min after syringe pump addition. Biphenyl was added as internal standard and the iron complex was removed by passing the solution through basic alumina followed by elution with 2 mL AcOEt. The solution was subjected to GC analysis. The organic products were identified by comparison with authentic compounds and GC-MS analysis. In the studies of kinetic isotope effects, a substrate mixture of cyclohexane/cyclohexane-D<sub>12</sub> of 1:3 mol/mol was used to improve the accuracy of the KIE values obtained.

**III.5.8.1.2. Conditions of limited substrate****Single addition**Cyclohexane oxidation

A 5 mL vial was charged with: Catalyst (1 μmol, 1 mol% or 5 μmol, 5 mol%), cyclohexane (100 μmol, 1 equiv), CH<sub>3</sub>CN (0.67 mL) and a magnetic stir bar. The vial was placed on an ice bath and stirred. A CH<sub>3</sub>CO<sub>2</sub>H solution in CH<sub>3</sub>CN with the appropriate concentration was added (29 μL of 1.74M, 50 μmol; 29μL of 7.0M, 200 μmol; 60μL of acetic acid glacial, 1000 μmol) and 80 μL or 100 μL of a 1.5 M (120 μmols, 1.2 equiv or 150 μmols, 1.5 equiv) H<sub>2</sub>O<sub>2</sub> solution (diluted from a 35% H<sub>2</sub>O<sub>2</sub> aqueous solution) were delivered by syringe pump over 6 min at 0 °C. After syringe pump addition, the solution was stirred for 10 min at 0°C. If a second additions is required a solution of catalyst (1 μmol, 1 mol%), CH<sub>3</sub>CN (0.67 mL) and CH<sub>3</sub>CO<sub>2</sub>H (29 μL 1.74M solution, 50 μmol or 60μL of acetic acid glacial, 1000 μmol) was added simultaneously with 80 μL of a 1.5 M (120 μmols, 1.2 equiv) H<sub>2</sub>O<sub>2</sub> solution via syringe pump over 6 min. After syringe pump addition, the solution was stirred for 10 min at 0°C. If a third additions is required a solution of catalyst (1 μmol, 1 mol%), CH<sub>3</sub>CN (0.67 mL) and CH<sub>3</sub>CO<sub>2</sub>H (29 μL 1.74M solution, 50 μmol or 60μL of acetic acid glacial, 1000 μmol) was added simultaneously with 80 μL of a 1.5 M (120 μmols, 1.2 equiv) H<sub>2</sub>O<sub>2</sub> solution via syringe pump over 6 min. After syringe pump addition the resulting solution was stirred for another 10 min. If a forth additions is required a solution of catalyst (1 μmol, 1 mol%), CH<sub>3</sub>CN (0.67 mL) and CH<sub>3</sub>CO<sub>2</sub>H (60μL of acetic acid glacial, 1000 μmol) was added simultaneously with 80 μL of a 1.5 M (120 μmols, 1.2 equiv) H<sub>2</sub>O<sub>2</sub> solution via syringe pump over 6 min. After syringe pump addition, the resulting solution was stirred for another 10 min. An internal standard was added at this point. The iron complex was removed by passing the solution through a short path of basic alumina followed by elution with 2 mL of AcOEt. Finally, the solution was subjected to GC analysis. GC analysis of the solution provided substrate conversions and product yields relative

to the internal standard integration. Calibration curves were obtained from commercially available cyclohexanol and cyclohexanone.

*cis*-1,2-dimethylcyclohexane oxidation (*cis*-1,2-DMCH)



**Scheme 17.** Catalytic oxidation of *cis*-1,2-dimethylcyclohexane.

A 5 mL vial was charged with: Catalyst (1  $\mu$ mol, 1 mol%), *cis*-1,2-DMCH (100  $\mu$ mol, 1 equiv), CH<sub>3</sub>CN (0.67 mL) and a magnetic stir bar. The vial was placed on an ice bath and stirred. A 1.74 M CH<sub>3</sub>CO<sub>2</sub>H solution in CH<sub>3</sub>CN was added (29  $\mu$ L, 50  $\mu$ mol, 50 mol%) and 80  $\mu$ L of a 1.5 M (120  $\mu$ mol, 1.2 equiv) H<sub>2</sub>O<sub>2</sub> solution (diluted from a 35% H<sub>2</sub>O<sub>2</sub> aqueous solution) were delivered by syringe pump over 6 min at 0 °C. After syringe pump addition, the resulting solution was stirred for another 10 min. An internal standard was added at this point. The iron complex was removed by passing the solution through a short path of basic alumina followed by elution with 2 mL of AcOEt. Finally, the solution was subjected to GC analysis. GC analysis of the solution provided substrate conversions and product yields relative to the internal standard integration. Calibration curves were obtained from pure isolated products obtained from a catalytic reaction (see below). Retention of configuration in the oxidation of the tertiary C-H bonds is expressed as the ratio of the tertiary alcohols:  $[(1R,2R + 1S,2S) - (1R,2S + 1S,2R)] / [1S,2R + 1R,2S + 1S,2S + 1R,2R]$  (For nomenclature see scheme 6). Notice that analysis of the substrate by GC revealed 1% of *trans*-dimethylcyclohexane, which was taken into account to calculate the retention of configuration. **1S,2R** and **1R,2S** were identified as described below<sup>2</sup> and by GC-MS (figure 13).

Isolation of pure **1S,2S** and **1R,2R**

A 50 mL round bottom flask was charged with: 16 mg of **6OTf** (25  $\mu$ mol, 1 mol%), *cis*-1,2-dimethylcyclohexane (0.37 mL, 2.5 mmol, 1 equiv), CH<sub>3</sub>CN (17 mL) and a magnetic stir bar. The vial was placed on an ice bath and stirred. A 1.74 M CH<sub>3</sub>CO<sub>2</sub>H solution in CH<sub>3</sub>CN was added (0.73 mL, 1.25 mmol, 50 mol%) and 2 mL of a 1.5 M (3 mmol, 1.2 equiv) H<sub>2</sub>O<sub>2</sub> solution (diluted from a 35% H<sub>2</sub>O<sub>2</sub> aqueous solution) were delivered by syringe pump over 6 min at 0 °C. After syringe pump addition, the resulting solution was stirred for another 10 min. The solvent from the crude mixture was removed under reduced pressure. The resulting residue was purified by flash chromatography on silica gel (hexanes:AcOEt 3:1) to afford 80 mg of **1S,2S** and **1R,2R** (6.2 mmol, 25% yield).

**1*S*,2*S*** and **1*R*,2*R*** were characterized by several spectroscopic techniques:  $^1\text{H-NMR}$  (400 MHz,  $\text{CDCl}_3$ , 300 K)  $\delta$ , ppm: 1.75 - 20 (m, 9H), 1.09 (s, 3H), 0.92 (d,  $J = 6.8$  Hz, 3H).  $^{13}\text{C-NMR}$  (100 MHz,  $\text{CDCl}_3$ , 300 K)  $\delta$ , ppm: 74.9, 42.4, 41.4, 32.1, 25.3, 24.2, 20.9, 15.4. FT-IR (ATR)  $\nu$ ,  $\text{cm}^{-1}$ : 3382, 2927, 2856, 1454, 1373, 1113, 988, 912, 631. GC-MS ( $m/z$ ): 128.2 [ $\text{M}$ ] $^+$ .

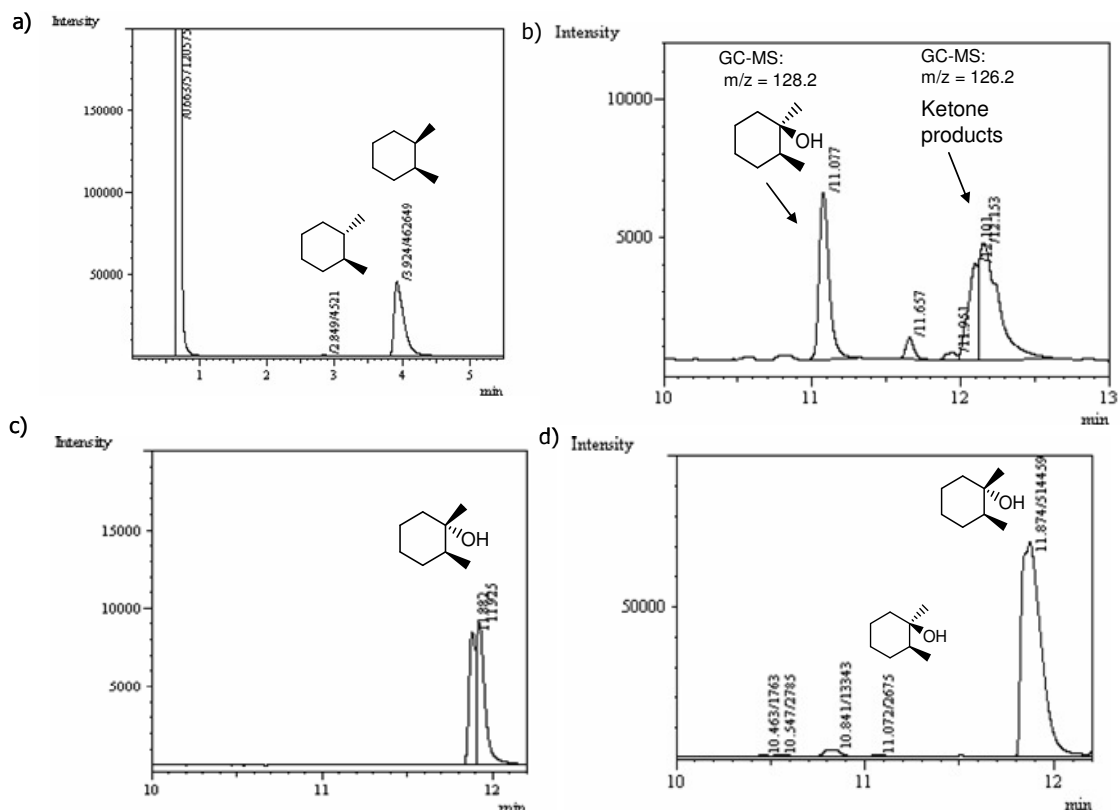


**Figure 13.** a) GC chromatogram (chiral column) of *cis*-1,2-dimethylcyclohexane (peaks: retention time/area). *Cis*-1,2-dimethylcyclohexane contains 1% of *trans*-1,2-dimethylcyclohexane. b) Chromatogram of the oxidation of *trans*-1,2-dimethylcyclohexane by **6OTf** with  $\text{H}_2\text{O}_2$  as described in the literature.<sup>2</sup> Identification of **1*R*,2*S*** and **1*S*,2*R*** alcohols. c) Pure **1*R*,2*S*** and **1*S*,2*R*** alcohols. d) GC-trace of the catalytic oxidation of *cis*-dimethylcyclohexane by **2OTf** (peaks: retention time/area), RC > 99%.

### 2,6-dimethyloctane oxidation

A 5 mL vial was charged with: Catalyst **2OTf** (1  $\mu\text{mol}$ , 1 mol%), 2,6-dimethyloctane **S2H** (100  $\mu\text{mol}$ , 1 equiv),  $\text{CH}_3\text{CN}$  (0.67 mL) and a magnetic stir bar. The vial was placed on an ice bath and stirred. A 1.74 M  $\text{CH}_3\text{CO}_2\text{H}$  solution in  $\text{CH}_3\text{CN}$  was added (29  $\mu\text{L}$ , 50  $\mu\text{mol}$ , 50 mol%) and 120  $\mu\text{L}$  of a 1.5 M (180  $\mu\text{mol}$ , 1.8 equiv)  $\text{H}_2\text{O}_2$  solution (diluted from a 35%  $\text{H}_2\text{O}_2$  aqueous solution) were delivered by syringe pump over 9 min at 0  $^\circ\text{C}$ . After syringe pump addition, the resulting solution was stirred for another 10 min. An internal standard was added at this point. The iron complex was removed by passing the solution through a short path of basic alumina followed by elution with 2 mL of  $\text{AcOEt}$ . Finally, the solution was subjected to GC analysis. The two alcohol products were identified by comparison of the GC and GC-MS spectra corresponding to commercially available tetrahydrolinalool (**O4H**) and tetrahydromyrcenol (**O3H**) with the spectra of the crude reaction mixture. GC analysis of the solution provided substrate

conversions and product yields relative to the internal standard integration. Calibration curves were obtained from commercially available tetrahydrolinalool and tetrahydromyrcenol. Regioselectivity was obtained by GC.

### Procedure using iterative addition protocol

#### a) Two additions

Substrates: cyclohexane, D<sub>12</sub>-cyclohexane, *trans*-4-methylcyclohexyl pivalate, **S1**, **S2H**, **S2Br** and **S2OAc**.

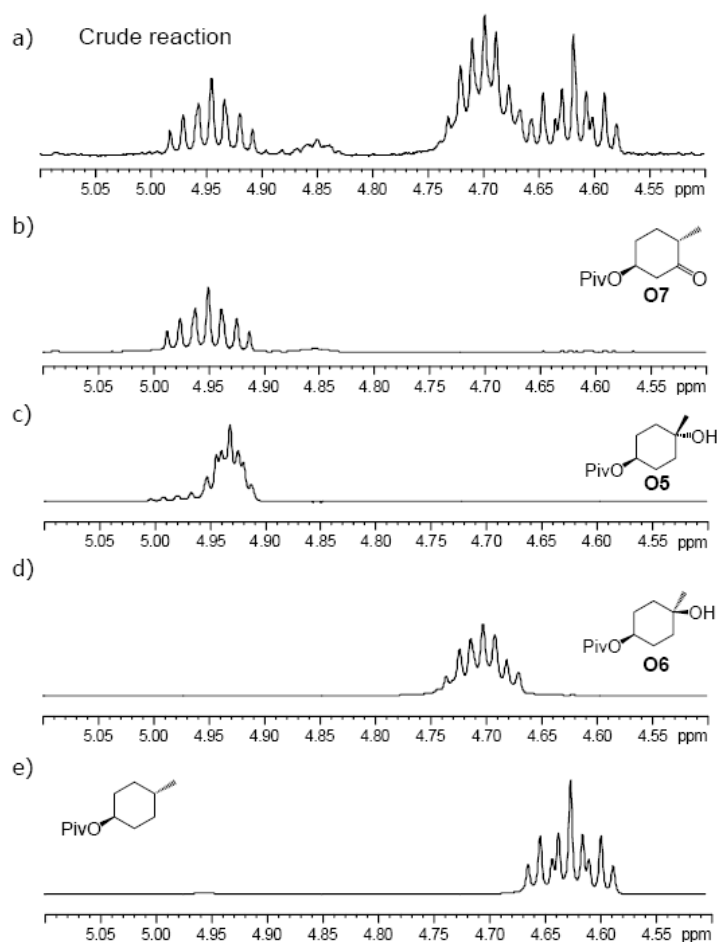


**Figure 14.** a) Portion of the <sup>1</sup>H-NMR spectrum of the crude mixture corresponding to the catalytic oxidation of *trans*-4-methylcyclohexyl pivalate (no epimerized tertiary alcohol product is detected). b) <sup>1</sup>H-NMR spectrum of isolated **O7** (see below) c) <sup>1</sup>H-NMR spectrum of isolated **O5**. d) <sup>1</sup>H-NMR spectrum of isolated **O6** (see below) (no **O5** is detected). e) <sup>1</sup>H-NMR spectrum of *trans*-4-methylcyclohexyl pivalate.

A 5 mL vial was charged with: Catalyst **2OTf** (1 μmol, 1 mol%), alkane (100 μmol, 1 equiv), CH<sub>3</sub>CN (0.67 mL) and a magnetic stir bar. The vial was placed on an ice bath and stirred. A 1.74 M CH<sub>3</sub>CO<sub>2</sub>H solution in CH<sub>3</sub>CN was added (29 μL, 50 μmol, 50 mol%) and 80 μL of a 1.5 M (120 μmols, 1.2 equiv) H<sub>2</sub>O<sub>2</sub> solution (diluted from a 35% H<sub>2</sub>O<sub>2</sub> aqueous solution) were delivered by syringe pump over 6 min at 0 °C. After syringe pump addition, the solution was stirred for 10 min at 0°C and a solution of catalyst (1 μmol, 1 mol%), CH<sub>3</sub>CN (0.67 mL) and



CH<sub>3</sub>CO<sub>2</sub>H (29  $\mu$ L 1.74M solution, 50  $\mu$ mol 50 mol%) was added simultaneously with 80  $\mu$ L of a 1.5 M (120  $\mu$ mol, 1.2 equiv) H<sub>2</sub>O<sub>2</sub> solution via syringe pump over 6 min. After syringe pump addition the resulting solution was stirred for another 10 min. An internal standard was added at this point. The iron complex was removed by passing the solution through a short path of basic alumina followed by elution with 2 mL of AcOEt. Finally, the solution was subjected to GC analysis. GC analysis of the solution provided substrate conversions and product yields relative to the internal standard integration. Cyclohexanone, D<sub>12</sub>-cyclohexanone, tetrahydrolinalool and tetrahydromyrcenol were purchased from Aldrich. For non-commercially available products, pure samples were synthesized, isolated and characterized following the experimental procedure described below. In the oxidation of *trans*-4-methylcyclohexyl pivalate the retention of configuration in the tertiary alcohol formed was determined by <sup>1</sup>H-NMR spectroscopy (Figure 14).

### b) Three additions

Substrate: *cis*-4-methylcyclohexyl pivalate.

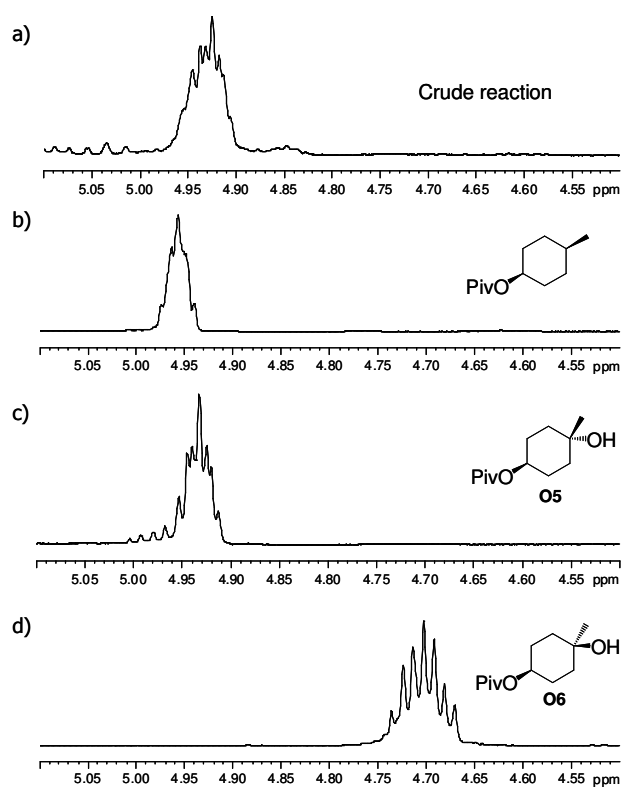


**Figure 15.** a) Portion of the <sup>1</sup>H-NMR spectrum of the crude mixture corresponding to the catalytic oxidation of *cis*-4-methylcyclohexyl pivalate (no epimerized tertiary alcohol product is detected). b) <sup>1</sup>H-NMR spectrum of *trans*-4-methylcyclohexyl pivalate. c) <sup>1</sup>H-NMR spectrum of isolated **O5** (see below) (no **O6** is detected). d) <sup>1</sup>H-NMR spectrum of isolated **O6**.

A 5 mL vial was charged with: Catalyst **2OTf** (1  $\mu$ mol, 1 mol%), *cis*-4-methylcyclohexyl pivalate (100  $\mu$ mol, 1 equiv), CH<sub>3</sub>CN (0.67 mL) and a magnetic stir bar. The vial was placed on an ice bath and stirred. A 1.74 M CH<sub>3</sub>CO<sub>2</sub>H solution in CH<sub>3</sub>CN was added (29  $\mu$ L, 50  $\mu$ mol, 50

mol%) and 80  $\mu\text{L}$  of a 1.5 M (120  $\mu\text{mol}$ s, 1.2 equiv)  $\text{H}_2\text{O}_2$  solution (diluted from a 35%  $\text{H}_2\text{O}_2$  aqueous solution) were delivered by syringe pump over 6 min at 0  $^\circ\text{C}$ . After syringe pump addition, the solution was stirred for 10 min at 0 $^\circ\text{C}$  and a solution of catalyst (1  $\mu\text{mol}$ , 1 mol%),  $\text{CH}_3\text{CN}$  (0.67 mL) and  $\text{CH}_3\text{CO}_2\text{H}$  (29  $\mu\text{L}$  1.74 M solution, 50  $\mu\text{mol}$ , 50 mol%) was added simultaneously with 80  $\mu\text{L}$  of a 1.5 M (120  $\mu\text{mol}$ s, 1.2 equiv)  $\text{H}_2\text{O}_2$  solution via syringe pump over 6 min. After syringe pump addition the resulting solution was stirred for another 10 min, then a solution of catalyst (1  $\mu\text{mol}$ , 1 mol%),  $\text{CH}_3\text{CN}$  (0.67 mL) and  $\text{CH}_3\text{CO}_2\text{H}$  (29  $\mu\text{L}$  1.74 M solution, 50  $\mu\text{mol}$ , 50 mol%) was added simultaneously with 80  $\mu\text{L}$  of a 1.5 M (120  $\mu\text{mol}$ s, 1.2 equiv)  $\text{H}_2\text{O}_2$  solution via syringe pump over 6 min. After syringe pump addition the resulting solution was stirred for another 10 min. An internal standard was added at this point. The iron complex was removed by passing the solution through a short path of basic alumina followed by elution with 2 mL of AcOEt. Finally, the solution was subjected to GC analysis. The calibration curve of the oxidation product was obtained from pure isolated product obtained from a catalytic reaction (see below). The retention of configuration in the tertiary alcohol formed was determined by  $^1\text{H-NMR}$  (figure 15).

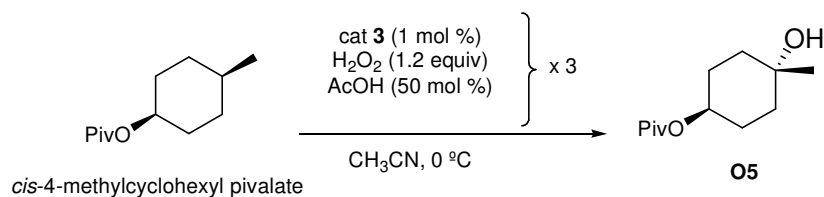
### III.5.8.1.3. Procedure for product isolation

Substrates: **S1** (scheme 20), **S2OAc** (scheme 22), **S2Br** (scheme 21), *trans*-4-methylcyclohexyl pivalate (scheme 19).

A 25 mL round bottom flask was charged with: catalyst **2OTf** (10  $\mu\text{mol}$ s, 1 mol%), alkane (1 mmol, 1 equiv),  $\text{CH}_3\text{CN}$  (6.7 mL) and a magnetic stir bar. The vial was placed on an ice bath and stirred. A 1.74 M  $\text{CH}_3\text{CO}_2\text{H}$  solution in  $\text{CH}_3\text{CN}$  was added (0.29 mL, 0.5 mmol, 50 mol%) and 0.8 mL of a 1.5 M (1.2 mmol, 1.2 equiv)  $\text{H}_2\text{O}_2$  solution (diluted from a 35%  $\text{H}_2\text{O}_2$  aqueous solution) were delivered by syringe pump over 6 min at 0  $^\circ\text{C}$ . After syringe pump addition, the solution was stirred for 10 min at 0  $^\circ\text{C}$  and a solution of catalyst (10  $\mu\text{mol}$ s, 1 mol%),  $\text{CH}_3\text{CN}$  (6.7 mL) and  $\text{CH}_3\text{CO}_2\text{H}$  (0.29 mL 1.74 M solution, 0.5 mmol, 50 mol%) was added simultaneously with 0.8 mL of a 1.5 M (1.2 mmol, 1.2 equiv)  $\text{H}_2\text{O}_2$  solution (diluted from a 35%  $\text{H}_2\text{O}_2$  aqueous solution) via syringe pump over 6 min. After syringe pump addition the resulting solution was stirred for another 10 min. The solvent from the crude mixture was removed under reduced pressure and the resulting residue was purified by flash chromatography on silica gel.

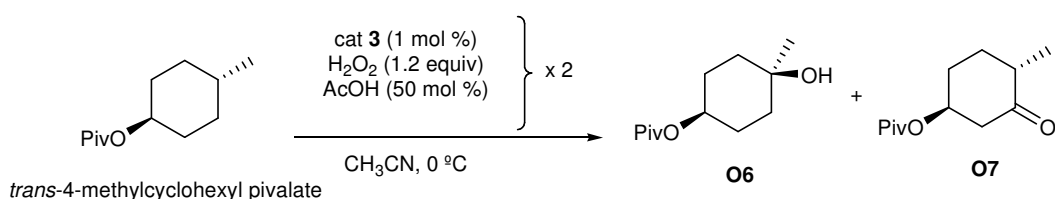
Substrate: *cis*-4-methylcyclohexyl pivalate (scheme 18).

For *cis*-4-methylcyclohexyl pivalate a third addition was done: after stirring for 10 min at 0  $^\circ\text{C}$ , a solution of catalyst **3** (10  $\mu\text{mol}$ s, 1 mol%),  $\text{CH}_3\text{CN}$  (6.7 mL) and  $\text{CH}_3\text{CO}_2\text{H}$  (0.29 mL 1.74 M solution, 0.5 mmol, 50 mol%) was added simultaneously with 0.8 mL of a 1.5 M (1.2 mmol, 1.2 equiv)  $\text{H}_2\text{O}_2$  solution (diluted from a 35%  $\text{H}_2\text{O}_2$  aqueous solution) via syringe pump over 6 min. After syringe pump addition the resulting solution was stirred for another 10 min. The solvent from the crude mixture was removed under reduced pressure and the resulting residue was purified by flash chromatography on silica gel.

cis-4-methylcyclohexyl pivalate:**Scheme 18.** Catalytic oxidation of *cis*-4-methylcyclohexyl pivalate.

Purification by flash chromatography over silica (hexanes:AcOEt 3:1) afforded 122 mg of product (0.57 mmol, 57% yield).

The oxidized product (**O5**) was fully characterized by several spectroscopic techniques:  $^1\text{H-NMR}$  (400 MHz,  $\text{CDCl}_3$ , 300 K)  $\delta$ , ppm: 4.93 (m, 1H), 1.91 – 1.85 (m, 2H), 1.72 – 1.63 (m, 4H), 1.54 – 1.50 (m, 2H), 1.27 (s, 3H), 1.20 (s, 9H).  $^{13}\text{C-NMR}$  (100 MHz,  $\text{CDCl}_3$ , 300 K)  $\delta$ , ppm: 178.3, 69.3, 69.2, 38.9, 34.5, 30.3, 27.0, 26.3. FT-IR (ATR)  $\nu$ ,  $\text{cm}^{-1}$ : 3461, 2960, 2933, 2872, 1725, 1480, 1370, 1284, 1259, 1231, 1217, 1168, 1031, 1011, 968, 795, 631. ESI-MS ( $m/z$ ): 237.1  $[\text{M}+\text{Na}]^+$ .

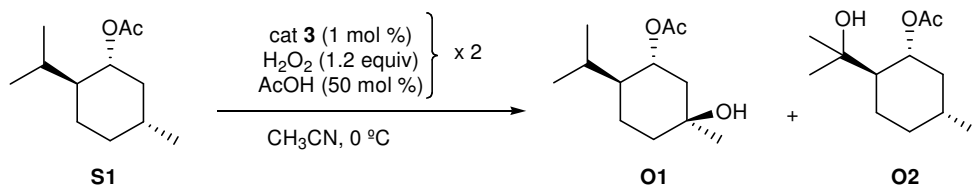
trans-4-methylcyclohexyl pivalate:**Scheme 19.** Catalytic oxidation of *trans*-4-methylcyclohexyl pivalate.

Purification by flash chromatography over silica (hexanes:AcOEt 3:1) afforded 85 mg of **O6** (0.39 mmol, 39% yield) and 34 mg of **O7** (0.16 mmol, 16% yield).

**O6** was fully characterized by several spectroscopic techniques:  $^1\text{H-NMR}$  (400 MHz,  $\text{CDCl}_3$ , 300 K)  $\delta$ , ppm: 4.70 (m, 1H), 1.78 – 1.68 (m, 6H), 1.54 – 1.47 (m, 2H), 1.25 (s, 3H), 1.19 (s, 9H).  $^{13}\text{C-NMR}$  (100 MHz,  $\text{CDCl}_3$ , 300 K)  $\delta$ , ppm: 178.1, 71.3, 68.7, 38.7, 36.5, 29.6, 27.1. FT-IR (ATR)  $\nu$ ,  $\text{cm}^{-1}$ : 3457, 2959, 2934, 2872, 1723, 1705, 1480, 1459, 1397, 1371, 1285, 1162, 1134, 1032, 996, 915, 681, 629. ESI-MS ( $m/z$ ): 237.2  $[\text{M}+\text{Na}]^+$ , 215.3  $[\text{M}+\text{H}]^+$ .

**O7** was fully characterized by several spectroscopic techniques:  $^1\text{H-NMR}$  (400 MHz,  $\text{CDCl}_3$ , 300 K)  $\delta$ , ppm: 4.95 (m, 1H), 2.78 - 2.73 (m, 1H), 2.44 - 2.32 (m, 2H), 2.21 – 2.17 (m, 1H), 2.11 - 2.05 (m, 1H), 1.81 - 1.72 (m, 1H), 1.41 – 1.31 (m, 1H), 1.19 (s, 9H), 1.07 (d,  $J = 6.8$  Hz, 3H).  $^{13}\text{C-NMR}$  (100 MHz,  $\text{CDCl}_3$ , 300 K)  $\delta$ , ppm: 209.0, 177.5, 71.3, 46.6, 44.1, 38.7, 29.9, 29.1, 27.1, 14.3. ESI-MS ( $m/z$ ): 235.2  $[\text{M}+\text{Na}]^+$ , 213.3  $[\text{M}+\text{H}]^+$ .

(-)-menthyl acetate:

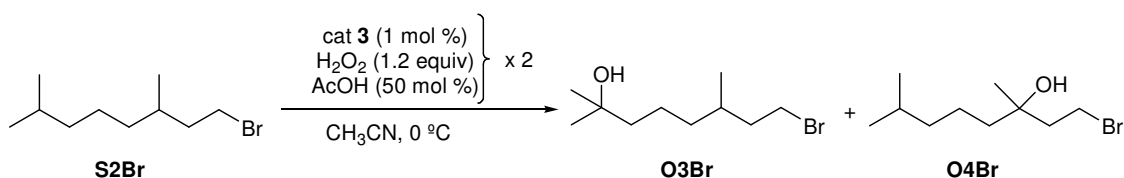


**Scheme 20.** Catalytic oxidation of **S1**.

Purification by flash chromatography over silica (hexanes:AcOEt 3:1) afforded 108 mg of **O1** product (0.50 mmol, 50% yield). Regioselectivity was determined by  $^1\text{H-NMR}$  spectroscopy of the crude reaction mixture by comparison of the hydrogen  $\alpha$  to the acetate group at 5.01 ppm for **O1** and 4.83 ppm for **O2** as reported in the literature.<sup>5</sup> The ratio of **O1:O2** was 17:1.

**O1** was fully characterized by several spectroscopic techniques:  $^1\text{H-NMR}$  (400 MHz,  $\text{CDCl}_3$ , 300 K)  $\delta$ , ppm: 5.01 (m, 1H), 2.08 (m, 1H) 2.03 (s, 3H), 1.89 (m, 1H), 1.68 (m, 1H), 1.50 – 1.33 (m, 5H), 1.26 (s, 3H), 0.93 (d,  $J = 7.2$  Hz, 3H), 0.81 (d,  $J = 6.8$  Hz, 3H).  $^{13}\text{C-NMR}$  (100 MHz,  $\text{CDCl}_3$ , 300 K)  $\delta$ , ppm: 170.6, 71.8, 71.1, 46.9, 44.6, 37.9, 31.4, 26.3, 21.3, 20.8, 19.3, 16.5. FT-IR (ATR)  $\nu$ ,  $\text{cm}^{-1}$ : 3449, 2958, 2931, 2872, 1735, 1714, 1449, 1370, 1241, 1161, 1025, 968, 907, 826, 668. ESI-MS ( $m/z$ ): 237.1  $[\text{M}+\text{Na}]^+$ .

**S2Br:**



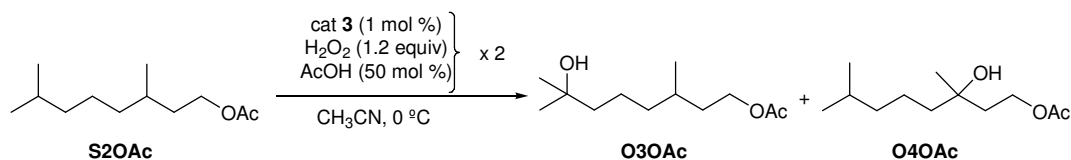
**Scheme 21.** Catalytic oxidation of **S2Br**.

Purification by flash chromatography over silica (hexanes:AcOEt 9:1) afforded 100 mg of **O3Br** (0.42 mmol, 42% yield) and 14 mg **O4Br** (0.06 mmol, 6% yield). The regioselectivity of the reaction was determined by GC analysis of the crude reaction mixture. The ratio of **O3Br:O4Br** was 7:1.

**O3Br** was fully characterized by several spectroscopic techniques:  $^1\text{H-NMR}$  (400 MHz,  $\text{CDCl}_3$ , 300 K)  $\delta$ , ppm: 3.50 – 3.38 (m, 2H), 1.89 (m, 1H), 1.66 (m, 2H), 1.44-1.17 (m, 6H), 1.22 (s, 6H), 0.91 (d,  $J = 6.4$  Hz, 3H).  $^{13}\text{C-NMR}$  (100 MHz,  $\text{CDCl}_3$ , 300 K)  $\delta$ , ppm: 71.0, 44.1, 40.0, 37.0, 32.2, 31.6, 29.3, 29.2, 21.6, 18.9. FT-IR (ATR)  $\nu$ ,  $\text{cm}^{-1}$ : 3390, 2964, 2933, 2870, 1738, 1711, 1463, 1378, 1260, 1080, 1011, 790. ESI-MS ( $m/z$ ): 260.2  $[\text{M}+\text{Na}]^+$ .

**O4Br** was fully characterized by several spectroscopic techniques:  $^1\text{H-NMR}$  (400 MHz,  $\text{CDCl}_3$ , 300 K)  $\delta$ , ppm: 3.51 (m, 2H), 2.09 (m, 2H), 1.58 (m, 1H), 1.47 – 1.17 (m, 6H), 1.20 (s, 3H), 0.90 (d,  $J = 6.8$  Hz, 6H).  $^{13}\text{C-NMR}$  (100 MHz,  $\text{CDCl}_3$ , 300 K)  $\delta$ , ppm: 73.1, 45.0, 42.6, 39.4, 28.3, 27.9, 26.7, 22.6, 22.5, 21.6. ESI-MS ( $m/z$ ): 260.2  $[\text{M}+\text{Na}]^+$ , 274.1  $[\text{M}+\text{K}]^+$ .

### **S2OAc:**



**Scheme 22.** Catalytic oxidation of **S2OAc**.

Purification by flash chromatography over silica (hexanes:AcOEt 7:3) afforded 80 mg of **O3OAc** (0.37 mmol, 37% yield) and 19 mg of **O4OAc** (0.09 mmol, 9% yield). Regioselectivity was determined by  $^1\text{H-NMR}$  by comparison of the hydrogen  $\alpha$  to the acetate group at 4.12 ppm for **O3OAc** and at 4.23 ppm for **O4OAc**. The ratio of **O3OAc**:**O4OAc** was 5:1.

**O3OAc** was fully characterized by several spectroscopic techniques:  $^1\text{H-NMR}$  (400 MHz,  $\text{CDCl}_3$ , 300 K)  $\delta$ , ppm: 4.12 (m, 2H), 2.07 (s, 3H), 1.68 – 1.19 (m, 10H), 1.22 (s, 6H), 0.94 (d,  $J = 6.4$  Hz, 3H).  $^{13}\text{C-NMR}$  (100 MHz,  $\text{CDCl}_3$ , 300 K)  $\delta$ , ppm: 171.1, 71.1, 63.0, 44.1, 37.4, 35.5, 29.8, 29.3, 29.2, 21.6, 21.1, 19.5. FT-IR (ATR)  $\nu$ ,  $\text{cm}^{-1}$ : 3453, 2963, 2932, 2872, 1738, 1724, 1462, 1366, 1235, 1160, 1048, 1033, 937, 680, 607. ESI-MS ( $m/z$ ): 239.1  $[\text{M}+\text{Na}]^+$ .

**O4OAc** was fully characterized by several spectroscopic techniques:  $^1\text{H-NMR}$  (400 MHz,  $\text{CDCl}_3$ , 300 K)  $\delta$ , ppm: 4.23 (t,  $J = 7.3$  Hz, 2H), 2.05 (s, 3H), 1.80 (m, 2H), 1.62 – 1.19 (m, 7H), 1.15 (s, 3H), 0.88 (d,  $J = 6.6$  Hz, 6H).  $^{13}\text{C-NMR}$  (100 MHz,  $\text{CDCl}_3$ , 300 K)  $\delta$ , ppm: 170.7, 72.0, 61.3, 42.8, 39.6, 39.4, 28.0, 27.1, 22.6, 21.7, 21.1. FT-IR (ATR)  $\nu$ ,  $\text{cm}^{-1}$ : 3459, 2954, 2933, 2870, 1740, 1724, 1465, 1366, 1239, 1168, 1149, 1049, 1032, 630, 609. ESI-MS ( $m/z$ ): 239.1  $[\text{M}+\text{Na}]^+$ .

### **III.5.8.2. Alkenes**

#### **catalyst:substrate:H<sub>2</sub>O<sub>2</sub>:AcOH, 3:110:100:30, 3:150:100:30, 1:110:100:10**

Olefin (67  $\mu\text{mol}$ , 1 equiv) was weighed directly into a 4 mL flask and dissolved in 0.4 mL anhydrous  $\text{CH}_3\text{CN}$ . Catalyst (2  $\mu\text{mol}$ , 3 mol% or 0.67  $\mu\text{mol}$ , 1 mol%) and acetic acid solution in anhydrous  $\text{CH}_3\text{CN}$  (0.17 M, 20  $\mu\text{mol}$  0.3 equiv or 6.7  $\mu\text{mol}$  0.1 equiv), were added and the resulting solution was cooled to  $0^\circ\text{C}$  and stirred vigorously. A 1.5 M  $\text{H}_2\text{O}_2/\text{CH}_3\text{CN}$  solution (73  $\mu\text{mol}$  for 1.1 equiv and 100  $\mu\text{mol}$  for 1.5 equiv, diluted from 35%  $\text{H}_2\text{O}_2/\text{H}_2\text{O}$  solution) was cooled to  $0^\circ\text{C}$  and added dropwise via syringe to the olefin solution (addition time 2 min). After 3 minutes, biphenyl was added as internal standard. The resulting solutions were treated with acetic anhydride (1 mL) together with 1-methylimidazole (0.1 mL), stirred for 15 minutes at RT

to esterify the diol products. Then 3-4 mL of ice were added and stirred for 10 minutes. Organic products were extracted with  $\text{CHCl}_3$  (5 mL). The organic layer was extracted and washed with  $\text{H}_2\text{SO}_4$  (2 mL, 1M), saturated aq.  $\text{Na}_2\text{CO}_3$  (2 mL) and water (2 mL). The organic layer was dried over  $\text{MgSO}_4$ , filtered and subjected to GC analysis. The products were identified by comparison of their GC retention times with authentic compounds and by GC-MS analysis.

### III.5.9. Kinetic studies

#### Profiles of the catalytic oxidation of (1*R*)-(-)-menthyl acetate (S1)

A 5 mL vial was charged with: Catalyst (7  $\mu\text{mol}$ , 1 mol%), **S1** (700  $\mu\text{mol}$ , 1 equiv),  $\text{CH}_3\text{CN}$  (4.7 mL) and a magnetic stir bar. The vial was placed in an ice bath and stirred. A 1.74 M  $\text{CH}_3\text{CO}_2\text{H}$  solution in  $\text{CH}_3\text{CN}$  was added (197  $\mu\text{L}$ , 350  $\mu\text{mol}$ , 50 mol%) and 560  $\mu\text{L}$  of a 1.5 M (840  $\mu\text{mol}$ , 1.2 equiv)  $\text{H}_2\text{O}_2$  solution (diluted from a 35%  $\text{H}_2\text{O}_2$  aqueous solution) were delivered by syringe pump over 6 min at 0  $^\circ\text{C}$ . After syringe pump addition, the resulting solution was stirred for another 10 min. 100  $\mu\text{L}$  samples of the crude reaction were taken at different times and immediately passed through a short alumina plug along with the internal standard, followed by elution with 0.5 mL of AcOEt. Finally, the solution was subjected to GC analysis.

#### Two-step addition of $\text{H}_2\text{O}_2$ to prove the relative stability of the catalysts in the presence of large excess of substrate.

A 5 mL vial was charged with: Catalyst (7  $\mu\text{mol}$ , 1 mol%), **S1** (700  $\mu\text{mol}$ , 1 equiv),  $\text{CH}_3\text{CN}$  (4.7 mL) and a magnetic stir bar. The vial was placed in an ice bath and stirred. A 1.74 M  $\text{CH}_3\text{CO}_2\text{H}$  solution in  $\text{CH}_3\text{CN}$  was added (197  $\mu\text{L}$ , 350  $\mu\text{mol}$ , 50 mol%) and 560  $\mu\text{L}$  of a 1.5 M (840  $\mu\text{mol}$ , 1.2 equiv)  $\text{H}_2\text{O}_2$  solution (diluted from a 35%  $\text{H}_2\text{O}_2$  aqueous solution) were delivered by syringe pump over 6 min at 0  $^\circ\text{C}$ . After syringe pump addition, the resulting solution was stirred for another 6 min. At this point 4 equiv of **S1** (2.8 mmol) were added and a second addition of  $\text{H}_2\text{O}_2$  (560  $\mu\text{L}$  of 1.5 M, 840  $\mu\text{mol}$ , 1.2 equiv, starting time of second addition: 12.5 min) were delivered by syringe pump over 6 min. After syringe pump addition, the resulting solution was stirred for another 6 min. 100  $\mu\text{L}$  samples of the crude reaction were taken at different times and immediately passed through a short alumina plug along with the internal standard, followed by elution with 0.5 mL of AcOEt. Finally, the solution was subjected to GC analysis.

### III.6. References

1. Chen, K.; Que Jr., L. *Chem. Commun.* **1999**, 1375-1376.
2. Chen, K.; Que Jr., L. *J. Am. Chem. Soc.* **2001**, *123*, 6327-6337.
3. White, M. C.; Doyle, A. G.; Jacobsen, E. N. *J. Am. Chem. Soc.* **2001**, *123*, 7194-7195.
4. Costas, M.; Que Jr., L. *Angew Chem. Int. Ed.* **2002**, *41*, 2179-2181.
5. Chen, M. S.; White, M. C. *Science* **2007**, *318*, 783-787.

6. Suzuki, K.; Oldenburg, P. D.; Que Jr., L. *Angew. Chem. Int. Ed.* **2008**, *47*, 1887-1889.
7. Dyker, G. *Handbook of C-H Transformations*; Wiley-VCH: Weinheim, 2005; Vol. 1-2.
8. Labinger, J. A.; Bercaw, J. E. *Nature* **2002**, *417*, 507-514.
9. Davies, H. M. L.; Manning, J. R. *Nature* **2008**, *451*, 417-424.
10. Bergman, R. G. *Nature* **2007**, *446*, 391-393.
11. Godula, K.; Sames, D. *Science* **2006**, *312*, 67-72.
12. Murray, R. W.; Jeyaraman, R.; Mohan, L. *J. Am. Chem. Soc.* **1986**, *108*, 2470-2472.
13. Mello, R.; Fiorentino, M.; Fusco, C.; Curci, R. *J. Am. Chem. Soc.* **1989**, *111*, 6749-6757.
14. Asensio, G.; González-Núñez, M. E.; Bernardini, C. B.; Mello, R.; Adam, W. *J. Am. Chem. Soc.* **1993**, *115*, 7250-7253.
15. Periana, R. A.; Taube, D. J.; Gamble, S.; Taube, H.; Satoh, T.; Fujii, H. *Science* **1998**, *280*, 560-564.
16. Lee, S.; Fuchs, P. L. *J. Am. Chem. Soc.* **2002**, *124*, 13978-13979.
17. Brodsky, B. H.; Bois, J. D. *J. Am. Chem. Soc.* **2005**, *127*, 15391-15393.
18. Ekkati, A. R.; Kodanko, J. J. *J. Am. Chem. Soc.* **2007**, *129*, 12390-12391.
19. Yiu, S.-M.; Man, W.-L.; Lau, T.-C. *J. Am. Chem. Soc.* **2008**, *130*, 10821-10827.
20. Jr., L. Q.; Tolman, W. B. *Nature* **2008**, *455*, 333-340.
21. Correa, A.; Mancheño, O. G.; Bolm, C. *Chem. Soc. Rev.* **2008**, *37*, 1108-1117.
22. Costas, M.; Chen, K.; Que Jr., L. *Coord. Chem. Rev.* **2000**, *200-202*, 517-544.
23. Joergensen, K. A. *Chem. Rev.* **1989**, *89*, 431-458.
24. Sheldon, R. A. *Applied Homogeneous Catalysis with Organometallic Compounds*; Wiley-VCH: Weinheim, 2002.
25. Bäckvall, J. E. *Modern oxidation Methods*; Wiley-VCH: Weinheim, 2004.
26. England, J.; Davies, C. R.; Banaru, M.; White, A. J. P.; Britovsek, G. J. P. *Adv. Synth. Catal.* **2008**, *350*, 883-897.
27. Company, A.; Gómez, L.; Fontrodona, X.; Ribas, X.; Costas, M. *Chem. Eur. J.* **2008**, *14*, 5727-5731.
28. England, J.; Britovsek, G. J. P.; Rabadia, N.; White, A. J. P. *Inorg. Chem.* **2007**, *46*, 3752-3767.
29. Company, A.; Gómez, L.; Güell, M.; Ribas, X.; Luis, J. M.; Que Jr., L.; Costas, M. *J. Am. Chem. Soc.* **2007**, *129*, 15766-15767.
30. Romakh, V. B.; Therrien, B.; Süss-Fink, G.; Shul'pin, G. B. *Inorg. Chem.* **2007**, *46*, 3166-3175.

31. Roelfes, G.; Lubben, M.; Hage, R.; Que Jr., L.; Feringa, B. L. *Chem. Eur. J.* **2000**, *6*, 2152-2159.
32. Meunier, B. *Chem. Rev.* **1992**, *92*, 1411-1456.
33. McLain, J. L.; Lee, J.; Groves, J. T. In *Biomimetic Oxidations Catalyzed by Transition Metal Complexes*; Meunier, B. Ed.; Imperial College Press: London, 2000; pp. 91-169.
34. Mas-Ballesté, R.; Costas, M.; Berg, T. v. d.; Que Jr., L. *Chem. Eur. J.* **2006**, *12*, 7489-7500.
35. Britovsek, G. J. P.; England, J.; White, A. J. P. *Dalton Trans.* **2006**, *11*, 1399-1408.
36. Aldrich-Wright, J. R.; Vagg, R. S.; Williams, P. A. *Coord. Chem. Rev.* **1997**, *166*, 361-389.
37. Knof, U.; von Zelewsky, A. *Angew. Chem. Int. Ed.* **1999**, *38*, 302-322.
38. Ryu, J. Y.; Kim, J.; Costas, M.; Chen, K.; Nam, W.; Que Jr., L. *Chem. Commun.* **2002**, *12*, 1288-1289.
39. Costas, M.; Tipton, A. K.; Chen, K.; Jo, D.-H.; Que Jr., L. *J. Am. Chem. Soc.* **2001**, *123*, 6722-6723.
40. Hagen, K. S. *Inorg. Chem.* **2000**, *39*, 5867.
41. Mialane, P.; Nivorojkine, A.; Pratviel, G.; Azéma, L.; Slany, M.; Godde, F.; Simaan, A.; Banse, F.; Kargar-Grisel, T.; Bouchoux, G.; Sinton, J.; Horner, O.; Guilhem, J.; Tchertanova, L.; Meunier, B.; Girerd, J.-J. *Inorg. Chem.* **1999**, *38*, 1085-1092.
42. Diebold, A.; Hagen, K. S. *Inorg. Chem.* **1998**, *37*, 215-223.
43. Blakesley, D. W.; Payne, S. C.; Hagen, K. S. *Inorg. Chem.* **2000**, *39*, 1979-1989.
44. Zang, Y.; Kim, J.; Dong, Y.; Wilkinson, E. C.; Appelman, E. H.; Que Jr., L. *J. Am. Chem. Soc.* **1997**, *119*, 4197-4205.
45. Mas-Balleste, R.; Que Jr., L. *J. Am. Chem. Soc.* **2007**, *129*, 15964-15972.
46. Nehru, K.; Kim, S. J.; Kim, I. Y.; Seo, M. S.; Kim, Y.; Kim, S.-J.; Kim, J.; Nam, W. *Chem. Comm.* **2007**, 4623-4625.
47. Das, S.; Incarvito, C. D.; Crabtree, R. H.; Brudvig, G. W. *Science* **2006**, *312*, 1941-1943.
48. Murphy, A.; Dubois, G.; Stack, T. D. P. *J. Am. Chem. Soc.* **2003**, *125*, 5250-5251.
49. Garcia-Bosch, I.; Company, A.; Fontrodona, X.; Ribas, X.; Costas, M. *Org. Lett.* **2008**, *10*, 2095-2098.
50. Garcia-Bosch, I.; Ribas, X.; Costas, M. *Adv. Synth. Catal.* **2009**, *351*, 348-352.
51. Marchi-Delapierre, C.; Jorge-Robin, A.; Thibon, A.; Ménage, S. *Chem. Commun.* **2007**, 1166-1168.
52. Company, A. *PhD Dissertation* **2008**, University of Girona.



53. Chen, K.; Costas, M.; Kim, J.; Tipton, A. K.; Que Jr., L. *J. Am. Chem. Soc.* **2002**, *124*, 3026-3035.
54. Halcrow, M. A. *Polyhedron* **2007**, *26*, 3523-3576.
55. Chen, K.; Eschenmoser, A.; Baran, P. S. *Angew. Chem. Int. Ed.* **2009**, *48*, 9705-9708.
56. Chen, M. S.; White, M. C. *Science* **2010**, *327*, 566-571.
57. Kirillov, A. M.; Kopylovich, M. N.; Kirillova, M. V.; Haukka, M.; Silva, M. F. C. G. d.; Pombeiro, A. J. L. *Angew Chem. Int. Ed.* **2005**, *44*, 4345-4348.
58. Trettenhahn, G.; Nagl, M.; Neuwirth, N.; Arion, V. B.; Jary, W.; Pöchlauer, P.; Schmid, W. *Angew. Chem. Int. Ed.* **2006**, *45*, 2794-2798.
59. Pavan, C.; Legros, J.; Bolm, C. *Adv. Synth. Catal.* **2005**, *347*, 703-705.
60. Retcher, B.; Sánchez Costa, J.; Tang, J.; Hage, R.; Gamez, P.; Reedijk, J. *J. Mol. Catal. A: Chem.* **2008**, *286*, 1-5.
61. Bautz, J.; Comba, P.; Lopez de Laorden, C.; Menzel, M.; Rajaraman, G. *Angew. Chem. Int. Ed.* **2007**, *46*, 8067-8070.
62. Chen, K.; Que Jr., L. *Angew. Chem. Int. Ed.* **1999**, *38*, 2227-2229.
63. Bukowski, M. R.; Comba, P.; Lienke, A.; Limberg, C.; Lopez de Laorden, C.; Mas-Ballesté, R.; Merz, M.; Que Jr., L. *Angew. Chem. Int. Ed.* **2006**, *45*, 3446-3449.
64. Bitterlich, B.; Anilkumar, G.; Gelalcha, F. G.; Spilker, B.; Grotevendt, A.; Jackstell, R.; Tse, M. K.; Beller, M. *Chem. As. J.* **2007**, *2*, 521-529.
65. Anilkumar, G.; Bitterlich, B.; Gelalcha, F. G.; Tse, M. K.; Beller, M. *Chem. Commun.* **2007**, 289-291.
66. Bitterlich, B.; Schröder, K.; Tse, M. K.; Beller, M. *Eur. J. Org. Chem.* **2008**, 4867-4870.
67. Schröder, K.; Enthaler, S.; Bitterlich, B.; Schulz, T.; Spannenberg, A.; Tse, M. K.; Junge, K.; Beller, M. *Chem. Eur. J.* **2009**, *15*, 5471-5481.
68. Yeung, H.-L.; Sham, K.-C.; Tsang, C.-S.; Lau, T.-C.; Kwong, H.-L. *Chem. Commun.* **2008**, 3801-3803.
69. Gelalcha, F. G.; Bitterlich, B.; Anilkumar, G.; Tse, M. K.; Beller, M. *Angew Chem. Int. Ed.* **2007**, *46*, 7293-7296.
70. Gelalcha, F. G.; Anilkumar, G.; Tse, M. K.; Brückner, A.; Beller, M. *Chem. Eur. J.* **2008**, *14*, 7687-7698.
71. Kim, C.; Chen, K.; Kim, J.; Que Jr., L. *J. Am. Chem. Soc.* **1997**, *119*, 5964-5965.
72. Sauers, A. L.; Ho, D. M.; Bernhard, S. *J. Org. Chem.* **2004**, *69*, 8910-8915.
73. Oishi, T.; Hiram, M.; Sita, L. R.; Masamune, S. *Synthesis* **1991**, 789-792.
74. Denmark, S. E.; Fu, J.; Lawler, M. J. *Org. Syn.* **2006**, *83*, 121128.



---

# Chiral Manganese Complexes with Pinene Appended Tetradentate Ligands as Stereoselective Epoxidation Catalysts

---

### Abstract

In this chapter, we take advantage of L2 and L3 ligands described in Chapter III, in which pinene rings have been fused to the 4<sup>th</sup>-5<sup>th</sup> position of the two pyridine groups of the bpmcn ligand, to synthesize two manganese(II) complexes (**Λ-2Mn** and **Δ-3Mn**, respectively), which have been tested as catalysts for the stereoselective epoxidation of olefins. The complexes are structurally related to [Mn(CF<sub>3</sub>SO<sub>3</sub>)<sub>2</sub>(bpmcn)], **7Mn**, recently reported as a very efficient epoxidation catalyst in combination with peracetic acid. In addition to exhibit comparable catalytic activity to **7Mn**, **Λ-2Mn** presents remarkable stereoselectivity (up to 46% ee (enantiomeric excess)) in the epoxidation of selected substrates.



# Contents

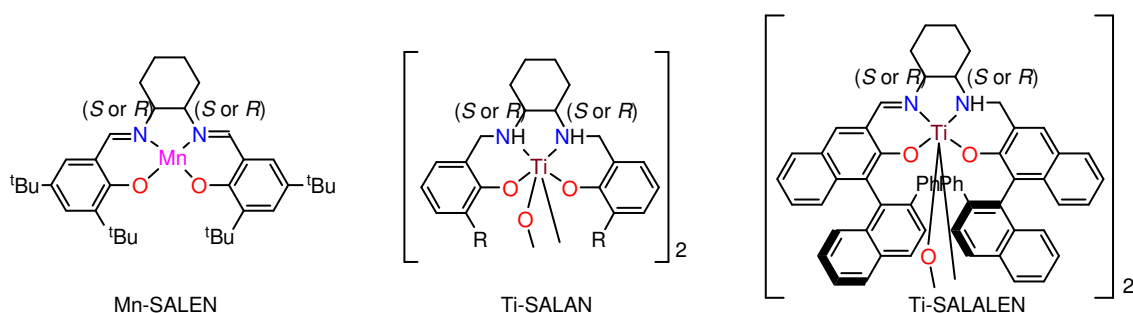
|                                                           |            |
|-----------------------------------------------------------|------------|
| <b>IV.1. INTRODUCTION .....</b>                           | <b>128</b> |
| <b>IV.2. RESULTS .....</b>                                | <b>129</b> |
| IV.2.1. SYNTHESIS OF COMPLEXES .....                      | 129        |
| IV.2.2. CHARACTERIZATION .....                            | 130        |
| IV.2.2.1. Solid state structure .....                     | 130        |
| IV.2.2.2. Solution Behavior .....                         | 132        |
| IV.2.2.2.1. ESI-MS .....                                  | 132        |
| IV.2.2.2.2. UV-Vis and CD spectroscopy .....              | 132        |
| VI.2.3. CATALYTIC STUDIES .....                           | 133        |
| <b>IV.3. DISCUSSION .....</b>                             | <b>135</b> |
| IV.3.1. SYNTHESIS AND CHARACTERIZATION OF COMPLEXES ..... | 135        |
| IV.3.2. CATALYTIC EPOXIDATION .....                       | 136        |
| <b>IV.4. CONCLUDING REMARKS .....</b>                     | <b>138</b> |
| <b>IV.5. EXPERIMENTAL SECTION .....</b>                   | <b>138</b> |
| IV.5.1. INSTRUMENTATION .....                             | 138        |
| IV.5.2. MATERIALS .....                                   | 138        |
| IV.5.3. SYNTHESIS OF COMPLEXES .....                      | 138        |
| IV.5.4. CRYSTAL DATA .....                                | 139        |
| IV.5.5. REACTION CONDITIONS FOR CATALYSIS .....           | 140        |
| <b>IV.6. REFERENCES .....</b>                             | <b>140</b> |

## IV.1. Introduction

Olefin epoxidation constitutes a very important reaction in organic synthesis because epoxides are excellent building blocks for a number of subsequent transformations.<sup>1-3</sup> Most common epoxidation methods still rely on the use of organic peroxides and/or *m*-chloroperbenzoic acid (mCPBA).<sup>2,3</sup> Extensive work has been done to identify metal catalyzed transformations using benign oxidants such as O<sub>2</sub> or H<sub>2</sub>O<sub>2</sub>.<sup>2-6</sup> Both of these oxidants exhibit excellent atom economy, are cheap and do not produce toxic byproducts. As a result of these studies, manganese complexes have emerged as very promising catalysts.<sup>7</sup>

Prominent examples were described by Stack and co-workers using manganese complexes bearing tridentate and tetradentate nitrogen based ligands that, in combination with peracetic acid (AcOOH), act as very fast and efficient epoxidation agents.<sup>8,9</sup> Peracetic acid is also an interesting oxidant because it is easily prepared from acetic acid and H<sub>2</sub>O<sub>2</sub>, it simply generates acetic acid as byproduct and it biases the rather common manganese-catalyzed peroxide disproportionation. From aforementioned complexes,  $\Delta$ -[Mn(CF<sub>3</sub>SO<sub>3</sub>)<sub>2</sub>((*R,R*)-bpmcn)] ( **$\Delta$ -7Mn**, scheme 2) stand out, unfortunately, this highly active manganese catalyst affords only marginal stereoselectivity ( $\leq 10\%$ ) in epoxidation reactions.

State of the art metal catalyzed asymmetric epoxidation of olefins include Mn-SALEN,<sup>10-14</sup> Mo-Bishydroxamic acid<sup>15</sup> and Ru-oxazine catalysts systems.<sup>16,17</sup> All of these systems afford excellent enantioselectivity for specific substrates, but suffer from a limited substrate scope and relatively high catalyst loadings (usually 2-5%).



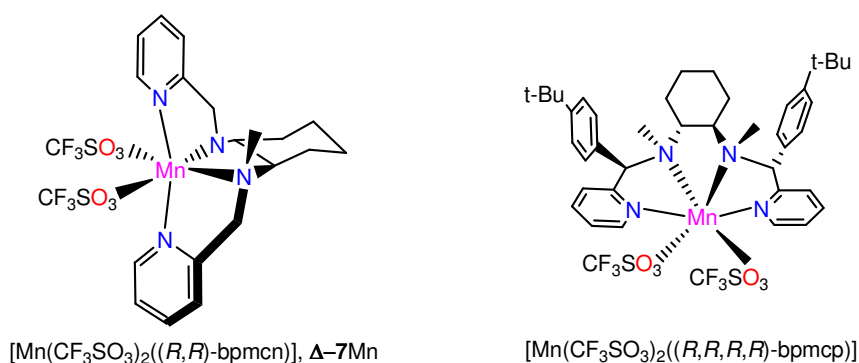
**Scheme 1.** Representative manganese and titanium complexes employed in oxidation of olefins.

A major breakthrough in the field has been done very recently by Katsuki and co-workers who reported highly enantioselective (up to 99% ee) epoxidation of olefins with H<sub>2</sub>O<sub>2</sub> catalyzed by Ti-SALAN and Ti-SALALEN complexes (scheme 1).<sup>18-21</sup> The latter systems have broader substrate scope than Mn-SALEN catalysts and they use H<sub>2</sub>O<sub>2</sub> as oxidant. However, the main limitation is still the relatively high catalyst-loading (1-5%) and a relatively complicated catalysts preparation.

Clearly, an ideal catalyst should combine the efficiency and substrate scope of Stack's catalysts and the stereoselectivity of SALAN/SALALEN systems.

As happened with iron catalysts, modification of the structure of the manganese

catalysts with the aim of enhancing their stereoselectivity has proven a challenging task. Pioneering studies by Stack and co-workers<sup>8,9</sup> demonstrated that small modifications on the structure of the ligand result in dramatic changes in the efficiency and selectivity of this class of catalysts. A clear example is the modification of the 6<sup>th</sup> positions of the pyridines by alkyl groups, which leads to non robust catalysts.<sup>9</sup> Encouraged by the good results of the introduction of the pinene in the 4<sup>th</sup>-5<sup>th</sup> positions of the pyridine rings in Chapter III for iron catalysts, we envisioned that the same strategy could be applied to obtain robust and more stereoselective manganese catalyst for the enantioselective epoxidation of olefins. In fact, pinene groups fused to bipyridine rings have been recently used in bioinspired iron catalyzed asymmetric olefin epoxidation reactions.<sup>22</sup>

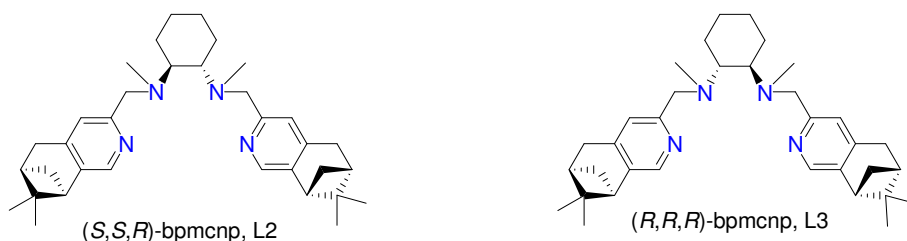


**Scheme 2.** bpmcn-based manganese(II) complexes employed in olefin epoxidation.

On the other hand, after the publication of the data presented in this chapter,<sup>23</sup> Xia and co-workers described a series of bpmcn's derivate ligands (*R,R,R,R*-bpmcp, see scheme 2) achieving relatively high enantiomeric excesses (70-80%) in the epoxidation of  $\alpha,\beta$ -enones.<sup>24</sup> This system exhibited particularly good enantioselectivity for  $\alpha,\beta$ -unsaturated ketones, but moderate enantiomeric excesses were obtained for other alkenes, similar to those reported by us.

## IV.2. Results

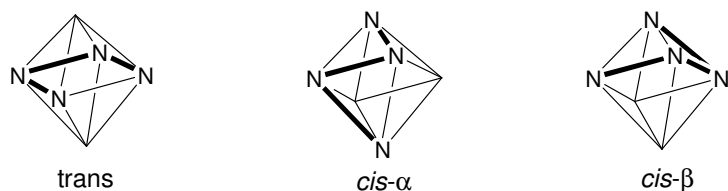
### IV.2.1. Synthesis of complexes



**Scheme 3.** Ligands employed in this work.

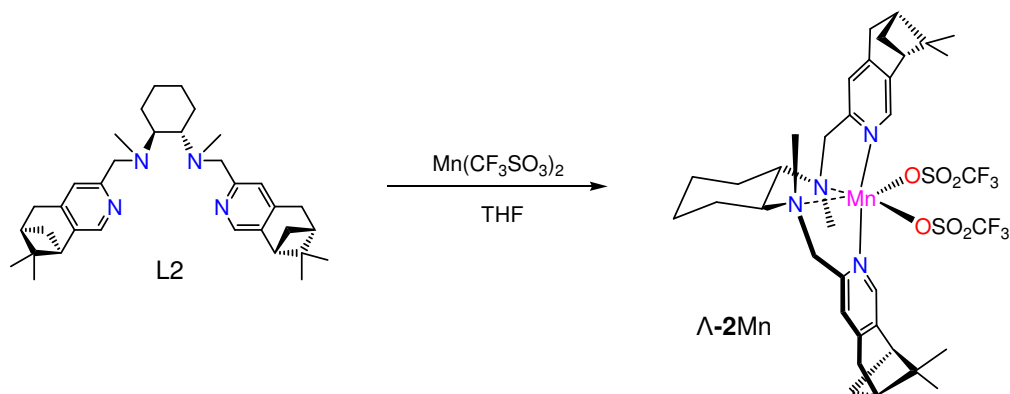
As described in Chapter III, linear tetradentate ligands can form three isomerically related octahedral complexes depending on the way they wrap around the metal centre: *cis*- $\alpha$ ,

*cis*- $\beta$  and *trans* (scheme 3 and 4).<sup>25,26</sup> Nevertheless, manganese complexes with *cis*- $\alpha$  topology  $\Lambda$ -[Mn(CF<sub>3</sub>SO<sub>3</sub>)<sub>2</sub>(L2)],  $\Lambda$ -2Mn, and  $\Delta$ -[Mn(CF<sub>3</sub>SO<sub>3</sub>)<sub>2</sub>(L3)],  $\Delta$ -3Mn, were stereoselectively prepared by reaction of Mn(CF<sub>3</sub>SO<sub>3</sub>)<sub>2</sub> with (*S,S,R*)-bpmcnp (L2) or (*R,R,R*)-bpmcnp (L3) in THF (scheme 5).



**Scheme 4.** Three different topologies that can be adopted by linear tetradentate ligands.

$\Lambda$ -2Mn and  $\Delta$ -3Mn were obtained as colorless crystals in good yield (75 and 67%, respectively) after slow ether diffusion to dichlorometane solutions of the complex.



**Scheme 5.** Preparation and structural drawing of  $\Lambda$ -2Mn.

## IV.2.2. Characterization

### IV.2.2.1. Solid state structure

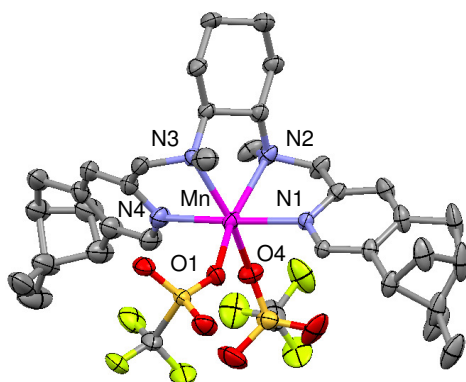


**Figure 1.** Ellipsoid diagram (50%) of  $\Lambda$ -2Mn. Hydrogen atoms omitted for clarity.

The solid state structure of  $\Lambda$ -2Mn was established by X-Ray analysis (see experimental section for crystallographic and refinement details). Figure 1 shows the ellipsoid diagram of the complex and table 1 gathers selected bond lengths and angles for the crystallographically



determined structure. X-ray analysis of  **$\Lambda$ -2Mn** reveals that the coordination geometry of the Mn center is distorted octahedral with the ligand adopting a *cis*- $\alpha$  topological structure. The nitrogen atoms of the two pyridine rings are disposed *trans* each other, while the two aliphatic nitrogen atoms are situated in a *cis* position. The Mn-N distances reflect the different chemical nature of the donor atoms: the distance to the pyridyl nitrogens [Mn-N ~ 2.24(1) Å] is noticeably shorter than to the amine nitrogens [Mn-N ~ 2.30(1) Å]. Mn-N distances measured in  **$\Lambda$ -2Mn** are in good agreement with those reported in the literature for related high spin Mn<sup>II</sup> complexes with N4 based ligands.<sup>27-29</sup>

**Table 1.** Selected Bond lengths [Å] and angles [°] for  **$\Lambda$ -2Mn**.

|       |          |          |            |          |            |
|-------|----------|----------|------------|----------|------------|
| Mn O1 | 2.140(2) | O1 Mn O4 | 91.97(18)  | N1 Mn N3 | 105.77(10) |
| Mn O4 | 2.162(6) | O1 Mn N1 | 86.19(9)   | N4 Mn N3 | 75.92(11)  |
| Mn N1 | 2.237(2) | O4 Mn N1 | 91.39(19)  | O1 Mn N2 | 159.63(10) |
| Mn N4 | 2.238(3) | O1 Mn N4 | 99.32(11)  | O4 Mn N2 | 97.19(19)  |
| Mn N3 | 2.304(3) | O4 Mn N4 | 86.0(2)    | N1 Mn N2 | 75.47(9)   |
| Mn N2 | 2.315(3) | N1 Mn N4 | 173.96(12) | N4 Mn N2 | 99.44(11)  |
|       |          | O1 Mn N3 | 99.41(9)   | N3 Mn N2 | 77.61(9)   |
|       |          | O4 Mn N3 | 159.90(18) |          |            |

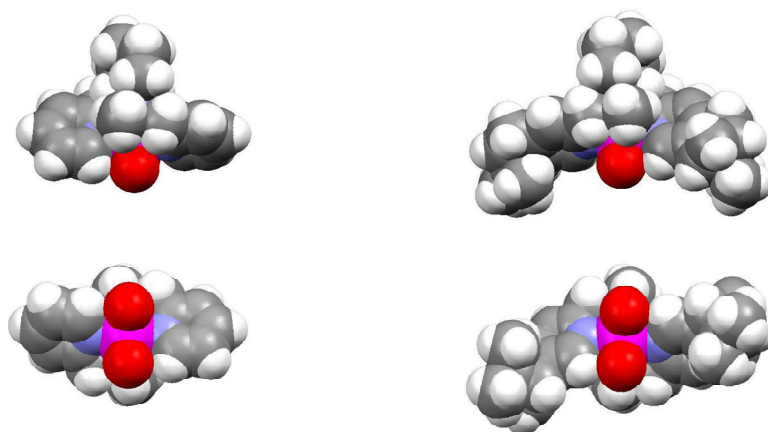


**Figure 2.** Space-filling diagram of  **$\Delta$ -7Mn** (left) and  **$\Lambda$ -2Mn** (right). Trifluoromethanesulfonate groups have been omitted for clarity, except for the oxygen atoms directly bound to the manganese centre. Color code; white (H), grey (C), red (O), blue (N) and pink (Mn).

Overall, the structural parameters are reminiscent to those of  $\Delta$ -[Mn(CF<sub>3</sub>SO<sub>3</sub>)<sub>2</sub>((*R,R*)-bpmcn)],  **$\Delta$ -7Mn**,<sup>12</sup> previously described by Stack and co-workers.<sup>12</sup> Space-filling structural analysis of the catalyst  **$\Delta$ -7Mn**, (figure 2) indicates that the two available binding sites in the manganese center are completely exposed to the bulk, and barely affected by the chiral topology of the ligand. As happened with the iron analogues (Chapter III), comparison between the solid state structures of  **$\Lambda$ -2Mn** and  **$\Delta$ -7Mn** shows for the former a deep well-defined cavity formed by the pyridine-pinene arms, surrounding the CF<sub>3</sub>SO<sub>3</sub> ligands, where presumably the substrate oxidation takes place (figure 2). This observation leads us to predict that, a priori, better stereodiscrimination should be accomplished by  **$\Lambda$ -2Mn** (notice though that we employ  $\Lambda$ -

[Mn(CF<sub>3</sub>SO<sub>3</sub>)<sub>2</sub>((S,S)-bpmcn)], **Λ-7Mn**, in the catalytic reactions described in this work; but the structural comparison is equally valid).

## IV.2.2.2. Solution Behavior

### IV.2.2.2.1. ESI-MS

ESI-MS analyses of **Λ-2Mn** and **Δ-3Mn** in acetonitrile show a peak at *m/z* 716.2 assigned to [Mn(CF<sub>3</sub>SO<sub>3</sub>)(L)]<sup>+</sup> (L = L2 and L3) cations. This strongly suggests that the complexes reported in this work retain in solution the mononuclear nature determined in the solid state.

### IV.2.2.2.2. UV-Vis and CD spectroscopy

The visible region of the electronic spectra of **Λ-2Mn** and **Δ-3Mn** in acetonitrile solution (figure 3) displays no bands consistent with the lack of d-d transitions expected for a high spin d<sup>5</sup> metal ion in an octahedral coordination environment.<sup>30</sup> On the other hand, the UV-vis spectra exhibit an intense band at 272 nm ( $\epsilon = 5700 \text{ M}^{-1} \text{ cm}^{-1}$  and  $5970 \text{ M}^{-1} \text{ cm}^{-1}$ , respectively) that is tentatively assigned to  $\pi\text{-}\pi^*$  transitions of the ligand.

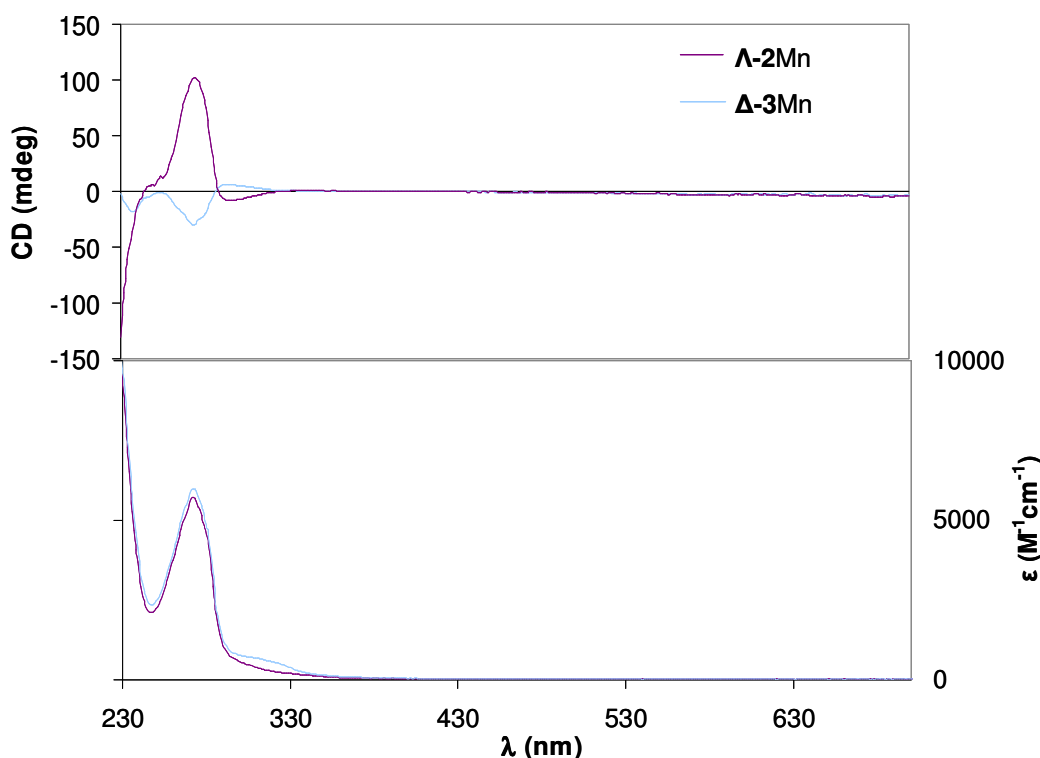
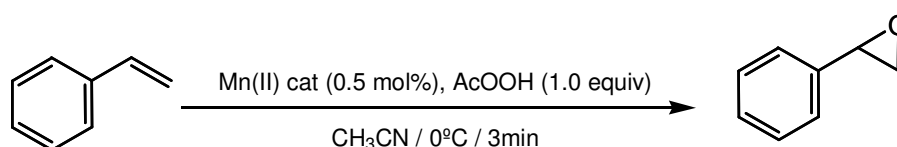


**Figure 3.** CD (top) and UV-vis (bottom) spectra of **Λ-2Mn** and **Δ-3Mn**.

CD spectra of **Λ-2Mn** and **Δ-3Mn** (figure 3) show a bisignate shape and exhibit an intense Cotton effect at 272 nm with opposite sign ( $\Delta\epsilon = + 98$  and  $- 36 \text{ M}^{-1} \text{ cm}^{-1}$ , respectively). The second band, also of respective opposite sign ( $\Delta\epsilon = - 7$  and  $+10 \text{ M}^{-1} \text{ cm}^{-1}$ , respectively) is broader and appears at 290 nm (see section IV.3.1 for further discussion).

### VI.2.3. Catalytic studies

Complexes  **$\Lambda$ -2Mn** and  **$\Delta$ -3Mn** were studied as epoxidation catalysts using peracetic acid (AcOOH) as oxidant. For comparative purposes,  **$\Lambda$ -7Mn** was also studied under analogous conditions. In a typical alkene oxidation experiment, 200 equiv of AcOOH (purchased as 32% solution in AcOH/H<sub>2</sub>O and directly used) were delivered via syringe pump during 3 min into an acetonitrile solution of the catalyst (1 equiv) and the substrate (200 equiv) at 0 °C. Initial tests were performed for the epoxidation of styrene (scheme 6, table 2 and 3).



**Scheme 6.** Styrene oxidation.

Under the reaction conditions employed (1:200:200 catalyst:styrene:AcOOH),  **$\Lambda$ -2Mn**,  **$\Delta$ -3Mn** and  **$\Lambda$ -7Mn** catalyze the quantitative oxidation of the substrate, but the selectivity of the reaction is dependent on the catalyst. Oxidations catalyzed by  **$\Lambda$ -2Mn** and  **$\Lambda$ -7Mn** afford the epoxide product with good selectivity (86 and 80%, respectively, table 2). Instead, the epoxide only accounts for 39% of the oxidized products in the case of  **$\Delta$ -3Mn**. Comparison between the epoxidation of styrene reactions catalyzed by  **$\Lambda$ -7Mn**,  **$\Delta$ -3Mn** and  **$\Lambda$ -2Mn** clearly indicate the impact of the pinene ring in the enantioselectivity of the reactions, which increase from 15% up to 35 and 40% ee's, respectively. Lower catalysts loadings (0.5 to 0.1%) were also tested and, although the efficiency was significantly diminished, the stereoselectivity on the epoxidation of styrene remained practically intact under these conditions.

**Table 2.** Asymmetric epoxidation of styrene with complexes  **$\Lambda$ -7Mn**,  **$\Delta$ -3Mn** and  **$\Lambda$ -2Mn**.<sup>a</sup>

| Complex                         | AcOOH (equiv)     | Conv. (%) | Yield (%) | Sel <sup>b</sup> (%) | ee     |
|---------------------------------|-------------------|-----------|-----------|----------------------|--------|
| <b><math>\Lambda</math>-7Mn</b> | 200               | 100       | 86        | 86                   | 15 (R) |
| <b><math>\Delta</math>-3Mn</b>  | 200               | 100       | 39        | 39                   | 35 (S) |
| <b><math>\Lambda</math>-2Mn</b> | 200               | 100       | 80        | 80                   | 40 (R) |
| <b><math>\Lambda</math>-2Mn</b> | 1200 <sup>c</sup> | 100       | 61        | 61                   | 38 (R) |

<sup>a</sup> Styrene (0.5 M in CH<sub>3</sub>CN, 200 equiv), 32% AcOOH in AcOH/H<sub>2</sub>O addition in 3 min, 0°C. Conversion and epoxide yields determined by GC relative to an internal Standard. <sup>b</sup> Selectivity for epoxide; (Yield/Conv) x 100. <sup>c</sup> 1000 equiv of substrate.

The encouraging efficiencies and ee's obtained for the epoxidation of styrene by  **$\Lambda$ -2Mn** prompted us to attempt the improvement of the enantioselectivity by optimizing the reaction conditions in terms of solvent, temperature and use of different additives (table 3). Different solvents were tested and acetonitrile proved to be the best choice, both in terms of efficiency and enantioselectivity. Increase of catalyst loading did not cause significant improvement on the

enantioselectivity. The use of different additives, including acids, bases and chloride salts at 0.5% level (1 equiv with respect to the catalyst) did not significantly improve reactions in terms of efficiency or stereoselectivity, either. Finally, lowering the temperature had an impact on the enantioselectivity, which increased up to 46% when the reaction was run at -40 °C (table 3). The use of H<sub>2</sub>O<sub>2</sub> as oxidant was also tested, affording styrene epoxide in poor yields and marginal stereoselectivity. On the view of the preceding results, we decided to evaluate the scope of **Λ-2Mn** over a series of substrates under optimized conditions (1:200:200 catalyst:styrene:AcOOH in acetonitrile); for practical results reactions were run at 0 °C.

**Table 3.** Effect of additives in the epoxidation of styrene by **Λ-2Mn**.<sup>a</sup>

| Solvent                         | Additive <sup>b</sup>                           | T (K) | Conv. (%) | Yield (%) | ee | Other                         |
|---------------------------------|-------------------------------------------------|-------|-----------|-----------|----|-------------------------------|
| CH <sub>3</sub> CN              | -                                               | 273   | 100       | 80        | 40 |                               |
| CH <sub>3</sub> CN              |                                                 | 273   | 84        | 63        | 41 | Under N <sub>2</sub>          |
| CH <sub>2</sub> Cl <sub>2</sub> | -                                               | 273   | 84        | 75        | 31 |                               |
| Acetone                         | -                                               | 273   | N. R.     | 0         | -  |                               |
| THF                             | -                                               | 273   | 4         | 4         | 34 |                               |
| 2-propanol                      | -                                               | 273   | 6         | 6         | 23 |                               |
| CH <sub>3</sub> CN              | -                                               | 273   | 100       | 82        | 35 | 1:100:100 <sup>c</sup>        |
| CH <sub>3</sub> CN              | 1-imidazol                                      | 273   | 100       | 80        | 35 |                               |
| CH <sub>3</sub> CN              | C <sub>6</sub> F <sub>5</sub> CO <sub>2</sub> H | 273   | 92        | 76        | 38 |                               |
| CH <sub>3</sub> CN              | 4- <i>t</i> Bu-py                               | 273   | 88        | 79        | 37 |                               |
| CH <sub>3</sub> CN              | Oxal. Acid <sup>f</sup>                         | 273   | 84        | 71        | 34 |                               |
| CH <sub>3</sub> CN              | Salic. Acid <sup>g</sup>                        | 273   | 94        | 71        | 37 |                               |
| CH <sub>3</sub> CN              | Et <sub>4</sub> NCl                             | 273   | 94        | 71        | 35 |                               |
| CH <sub>3</sub> CN              | Dipic. <sup>h</sup>                             | 273   | 92        | 81        | 41 |                               |
| CH <sub>3</sub> CN              | CF <sub>3</sub> CO <sub>2</sub> H               | 273   | 96        | 78        | 41 |                               |
| CH <sub>3</sub> CN              | H <sub>2</sub> O (70 μl)                        | 273   | 95        | 54        | 33 |                               |
| CH <sub>3</sub> CN              | Picol. Acid <sup>i</sup>                        | 273   | 95        | 74        | 32 |                               |
| CH <sub>3</sub> CN              | CH <sub>3</sub> CO <sub>2</sub> H <sup>d</sup>  | 273   | 85        | 70        | 40 |                               |
| CH <sub>3</sub> CN              |                                                 | 273   | 87        | 71        | 42 |                               |
| CH <sub>3</sub> CN              |                                                 | 253   | 90        | 71        | 44 |                               |
| CH <sub>3</sub> CN              |                                                 | 233   | 99        | 78        | 46 | 1:200:220 <sup>c</sup>        |
| CH <sub>3</sub> CN              |                                                 | 233   | 90        | 74        | 39 | 1:200:220 <sup>c,e</sup>      |
| CH <sub>3</sub> CN              | Acetone                                         | 273   | 33        | 26        | 4  | H <sub>2</sub> O <sub>2</sub> |

<sup>a</sup> Substrate (0.5 M in CH<sub>3</sub>CN, 200 equiv), 32% AcOOH in AcOH/H<sub>2</sub>O addition in 3 min. <sup>b</sup> 0.5 mol%. <sup>c</sup> Cat:substrate:oxidant. <sup>d</sup> 0.25 mol%. <sup>e</sup> Catalyst added over the reaction mixture. <sup>f</sup> Oxalic acid. <sup>g</sup> Salicylic acid. <sup>h</sup> Dipicolinic acid. <sup>i</sup> Picolinic acid.

Epoxidation of a wide range of aromatic and aliphatic olefins proceeds very fast (3 min) with high conversion and selectivity for the epoxide product in most of the cases (table 4). Enantiomeric excesses range from 5% (aliphatic olefins) to 46% (styrene). For example, the oxidation of *trans*- $\beta$ -methyl styrene is nearly quantitative (93% epoxide yield) and a moderate ee is achieved (36%).

## IV.3. Discussion

### IV.3.1. Synthesis and characterization of complexes

Two novel asymmetric Mn<sup>II</sup> complexes have been prepared and characterized in the solid state and in solution. They are based on the bpmcn ligand whose manganese complex has been reported as efficient epoxidation catalyst.<sup>8,9</sup> The introduction of pinene groups in the pyridine 4<sup>th</sup>-5<sup>th</sup> positions of the bpmcn ligand is expected to have an electron-donating ability which would favor the stabilization of putative high oxidation states, commonly invoked as active species in manganese-SALEN oxidative chemistry (see below).<sup>31</sup>

*cis*- $\alpha$  manganese(II) complexes of bpmcn-derivate ligands are easily obtained by reaction of Mn(CF<sub>3</sub>SO<sub>3</sub>)<sub>2</sub>, as manganese source, and the ligand in THF. The *cis*- $\alpha$  topology is inherently chiral and the complexes can, in principle, adopt  $\Lambda$  or  $\Delta$  helicity. This chirality is determined by the stereochemistry of the methine carbons of the cyclohexyl backbone. Thus L2 and L3 ligands give rise to metal complexes with exclusively  $\Lambda$  and  $\Delta$  respective helical chirality. No isolation of additional isomers was obtained, as evidenced by the crystalline form of  $\Lambda$ -2Mn. The stereochemical identity and purity of  $\Delta$ -3Mn was inferred from UV-Vis and CD studies, by comparison to  $\Lambda$ -2Mn.

X-ray analysis of  $\Lambda$ -2Mn reveals that the coordination geometry of the Mn center is distorted octahedral with the ligand adopting a *cis*- $\alpha$  topology, which results in a  $\Lambda$  helical chirality of the complex.

The spectroscopic study of both complexes shows similar extinction coefficient of the 272 and 290 nm bands in the UV-Vis spectra (figure 3). Otherwise, opposite sign bands are present in the CD spectrum (figure 3). The lack of symmetry in intensity between the CD spectrum of  $\Lambda$ -2Mn and  $\Delta$ -3Mn arises from the fact that the two compounds are not a pair of enantiomers. The spectra can be assigned to exciton-coupled circular dichroism which arises from the spatial arrangement of the chromophores defined by the chiral centre. In the present case, the sign of these features is proposed to origin from the helical chirality imposed by the metal centre in the tetradentate ligand;  $\Lambda$  isomer is positive while  $\Delta$  is negative. In conclusion, the UV-Vis and CD spectra of  $\Lambda$ -2Mn and  $\Delta$ -3Mn are in good accordance with the proposal that the two complexes adopt a *cis*- $\alpha$  structure, with inversely related helical chirality  $\Lambda$  and  $\Delta$ , respectively.

### IV.3.2. Catalytic epoxidation

The catalytic properties of **A-2Mn** and **A-3Mn** for the oxidation of olefins have been evaluated. Remarkably, only trace amounts of epoxide ring opening products, namely diols, are obtained even in the case of acid sensitive substrates. Presumably, the short reaction times and the low temperature used for these oxidations avoid epoxide ring opening reaction.

**A-2Mn** demonstrated good performance and provided, for the first time, a modest but remarkable stereoselectivity for this novel class of highly active epoxidation catalysts. While still far from satisfactory, the results enclosed herein constitute a significant step forward towards the development of a fast and efficient chiral epoxidation catalyst.

The level of chiral induction seems to be barely affected by the chirality of the pinene ring, but instead it is dictated by the chirality of the cyclohexyl backbone (table 2). Thus, **A-3Mn** affords preferentially (S)-styrene epoxide, while **A-2Mn** affords preferentially the (R)-epoxide enantiomer. This strongly indicates that the role of the pinene ring is just the expansion of the chiral pocket dictated by the cyclohexyl backbone.

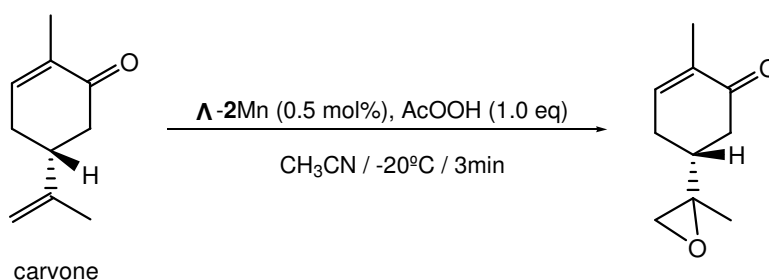
**Table 4.** Asymmetric epoxidation of different olefins with AcOOH using complex **A-2Mn**.<sup>a</sup>

| Substrate                             | Conv.(%)          | Yield(%) | Selectivity (%) | ee              |
|---------------------------------------|-------------------|----------|-----------------|-----------------|
| <i>trans</i> - $\beta$ -methylstyrene | 100               | 93       | 93              | 36              |
| Styrene <sup>b</sup>                  | 99                | 78       | 79              | 46              |
| 4-chlorostyrene                       | 85                | 85       | 100             | 45              |
| 4-methylstyrene                       | 81                | 49       | 61              | 34              |
| 3-nitrostyrene                        | 85                | 85       | 100             | 27              |
| <i>trans</i> -chalcone                | 93                | 45       | 48              | 37              |
| ethyl cinnamate                       | 70                | 41       | 59              | 6               |
| 1-phenyl-1-cyclohexene                | 99                | 37       | 38              | 37              |
| 1-octene                              | 76                | 60       | 79              |                 |
| vinyl cyclohexane                     | 85                | 85       | 100             | 17              |
| <i>cis</i> -cyclooctene               | 89                | 81       | 91              |                 |
| (-)-carvone <sup>d</sup>              | 99                | 71       | 72              | 42 <sup>c</sup> |
| <i>trans</i> -2-octene                | 82                | 65       | 79              |                 |
| <i>trans</i> -4-octene                | 76                | 58       | 76              |                 |
| <i>cis</i> -2-heptene                 | n.d. <sup>e</sup> | 51       |                 | 5               |

<sup>a</sup> **A-2Mn** (1 equiv), Olefin (0.5 M in CH<sub>3</sub>CN, 200 equiv), 32% AcOOH in AcOH/H<sub>2</sub>O (200 equiv) addition in 3 min, 0°C. Conversion and epoxide yields determined by GC relative to an internal standard. <sup>b</sup> -40°C, 220 equiv of AcOOH.<sup>c</sup> diastereomeric excess. <sup>d</sup> -20°C. <sup>e</sup> not determined.

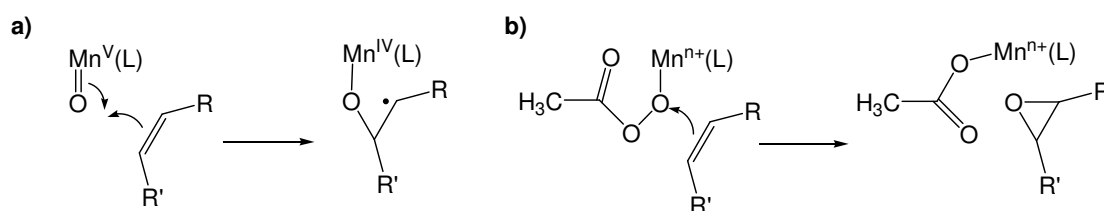
Styrene and most of its derivatives achieve good epoxide yields (styrene 78%, 4-chlorostyrene 85%, and 3-nitrostyrene 85%) and modest yet remarkable ee (46, 45 and 27%)

using  **$\Lambda$ -2Mn** as catalyst (table 4). However, the more electron-rich 4-methylstyrene is epoxidized with lower selectivity (61%). On the other hand, olefins bearing more bulky substituents or with electron-withdrawing groups are not suitable substrates for this system, resulting in poor yields (chalcone 45%, ethyl cinnamate 41% and 1-phenyl-1-hexene 37%). Aliphatic olefins are modest to good substrates, with conversions ranging from 76 to 99%, and selectivities up to 100%. The epoxidation of *cis* and *trans* olefins is stereospecific, affording epoxides with >99% retention of configuration in the three examples studied. Oxidation of carvone by  **$\Lambda$ -2Mn** is regioselective, affording almost exclusively (72% selectivity) the 8,9-monoepoxide (scheme 6). Most remarkably, the reaction exhibits a significant degree of diastereoselective excess (de) (42% at -20 °C). The de exhibited by  **$\Lambda$ -2Mn** is significantly better than the previously reported for  **$\Delta$ -7Mn** in the same conditions (15% de).<sup>8</sup> Clearly the introduction of the pinene ring has a profound impact on the diastereoselectivity of the reaction.



**Scheme 7.** Regioselective oxidation of carvone.

Insight into the reaction mechanism and the species involved in these highly active systems is specially complicated due to the paramagnetic nature of the metal species implicated and the lack of accumulation of any reaction intermediate, even when the reactions are run at very low temperature. Nevertheless, the lack of *cis-trans* epimerization in the epoxidation of *cis* and *trans* olefins suggests that the oxygen atom is transferred in a concerted step. Alternatively, any radical or carbocationic intermediate that may form must be very short-lived. At present we favor two possible mechanistic scenarios. By analogy to SALEN type of systems, we suggest that a high-valent  $\text{Mn}^{\text{V}}=\text{O}$  species is the final oxygen atom transfer agent in a concerted or nearly concerted step (scheme 8a). Alternatively, a high-valent Mn-oxo species may act as a Lewis acid activating the peracid molecule towards oxygen atom transfer via a transition state reminiscent of mCPBA oxidations (scheme 8b).<sup>32</sup> However, further studies are mandatory to explore these initial hypotheses.



**Scheme 8.** The two mechanistic scenarios proposed: a) oxygen atom transfer by high-valent Mn-oxo species; b) the oxidant is Lewis acid activated by a high valent  $\text{Mn}^{\text{IV}}$  or  $\text{Mn}^{\text{V}}$  species.

## IV.4. Concluding remarks

The present work describes a robust manganese catalyst which epoxidizes a wide range of olefins with modest yet remarkable enantiomeric excess. While the levels of enantiomeric induction should still be improved to reach state of the art SALEN's systems,  **$\Lambda$ -2Mn** constitutes the first modification of the highly active Stack's catalyst combining good efficiency and considerable enantioselectivity. Furthermore, the present study indicates that the modification of the pyridine ring at 4<sup>th</sup> and 5<sup>th</sup> positions in order to expand the chirality induced by the cyclohexyl backbone is a good strategy to improve the stereoselectivity of these novel systems and retaining their high catalytic ability. Studies on this regard are currently being pursued in our laboratory. The current work involves the extension of the family of complexes and the use of hydrogen peroxide as oxidant in combination with AcOH.

## IV.5. Experimental section

### IV.5.1. Instrumentation

IR spectra were taken in a Mattson-Galaxy Satellite FT-IR spectrophotometer using a MKII Golden Gate single reflection ATR system. UV-vis spectroscopy was performed on a Cary 50 Scan (Varian) UV-Vis spectrophotometer with 1 cm quartz cells. The ESI-MS experiments were performed on a Navigator LC/MS chromatograph from Thermo Quest Finnigan, and a Bruker Daltonics Esquire 3000 spectrometer, using acetonitrile as a mobile phase. Enantiomeric excess determined by HPLC using Chiralpak-IA(DAICEL) column or GC using Cyclodex-B 30 m or Chiraldex G-TA 30m x 0.25mm columns.

### IV.5.2. Materials

Reagents and solvents used were of commercially available reagent quality unless otherwise stated. Solvents were purchased from SDS and Scharlab. Solvents were purified and dried by passing through an activated alumina purification system (MBraun SPS-800) or by conventional distillation techniques. Preparation and handling of air-sensitive materials were carried out in a N<sub>2</sub> drybox (mBRAUN UNIlab) with O<sub>2</sub> and H<sub>2</sub>O concentrations < 1 ppm. Mn(CF<sub>3</sub>SO<sub>3</sub>)<sub>2</sub> and  $\Lambda$ -[Mn(CF<sub>3</sub>SO<sub>3</sub>)<sub>2</sub>((S,S)-bpmcn)],  **$\Lambda$ -7Mn**,<sup>8</sup> complexes, were prepared according to the literature. Experimental procedures for the preparation of (*R,R,R*)-bpmcnp (L3) and (*S,S,R*)-bpmcnp (L2) are described in Chapter III.

### IV.5.3. Synthesis of complexes

**$\Lambda$ -[Mn(CF<sub>3</sub>SO<sub>3</sub>)<sub>2</sub>(L2)],  $\Lambda$ -2Mn.** Under a N<sub>2</sub> atmosphere, a solution of Mn(CF<sub>3</sub>SO<sub>3</sub>)<sub>2</sub> (34 mg, 0.098 mmols) in THF (0.5 mL) was added to a stirred solution of L2 (50mg, 0.098 mmol) in THF (0.5 mL). The reaction mixture was stirred for 2 hours. The white solid was filtered and diethyl ether was added to the mother liquor. The new formed solid was filtered to achieve



quantitative precipitation of the complex. The two solid fractions collected were dissolved in  $\text{CH}_2\text{Cl}_2$  and filtered through Celite®. Slow diffusion of diethyl ether into this solution afforded 64.1 mg (0.074 mmols, 75%) of colorless crystals. Single crystals suitable for X-Ray analysis were obtained by slow diffusion of diethyl ether into a  $\text{CH}_3\text{CN}$  solution of the complex. Elemental Analyses Found: N, 6.4; C, 49.0, H, 5.2; S, 7.5%. Calcd for  $\text{C}_{36}\text{H}_{48}\text{F}_6\text{MnN}_4\text{O}_6\text{S}_2 \cdot \text{H}_2\text{O}$  (MW = 883.86 g/mol): N, 6.3, C, 48.9; H, 5.7; S, 7.3%. FT-IR (ATR)  $\nu_{\text{max}}/\text{cm}^{-1}$  2875-2930 (C-H) $\text{sp}^3$ , 1308 (py), 1214, 1156, 1029, 633 and 512 ( $\text{CF}_3\text{SO}_3$ ). ESI-MS (m/z): 716.2 ( $[\text{M}-\text{CF}_3\text{SO}_3]^+$ , 100%) 283.6 ( $[\text{M}-2\text{CF}_3\text{SO}_3]^{+2}$ , 54). UV( $\text{CH}_3\text{CN}$ ):  $\lambda_{\text{max}}$ , nm ( $\epsilon$ ,  $\text{M}^{-1}\text{cm}^{-1}$ ): 272 (5700).

**$\Delta$ -[Mn( $\text{CF}_3\text{SO}_3$ ) $_2$ (L3)],  $\Delta$ -3Mn.** The same procedure as for complex  **$\Lambda$ -2Mn** gave  **$\Delta$ -3Mn** as white crystals (57.1, 0.066 mmols, 67%). Elemental Analyses Found: N, 5.9; C, 50.9, H, 6.6. Calcd for  $\text{C}_{36}\text{H}_{48}\text{F}_6\text{MnN}_4\text{O}_6\text{S}_2 \cdot (\text{CH}_3\text{CH}_2)_2\text{O}$  (MW = 939.97 g/mol): N, 6.0, C, 51.1; H, 6.2. FT-IR (ATR)  $\nu_{\text{max}}/\text{cm}^{-1}$ : 2870-2930 (C-H) $\text{sp}^3$ , 1290 (py), 1217, 1159, 1027, 634 and 517 ( $\text{CF}_3\text{SO}_3$ ). ESI-MS (m/z): 716.2 ( $[\text{M}-\text{CF}_3\text{SO}_3]^+$ , 42%), 626.3(100). UV( $\text{CH}_3\text{CN}$ ):  $\lambda_{\text{max}}$ , nm ( $\epsilon$ ,  $\text{M}^{-1}\text{cm}^{-1}$ ): 272 (5970).

#### IV.5.4. Crystal data

**Table 5.** Crystal data and structure refinement for  **$\Lambda$ -2Mn**.

|                                         |                                                                        |                     |
|-----------------------------------------|------------------------------------------------------------------------|---------------------|
| Empirical formula                       | $\text{C}_{36}\text{H}_{48}\text{F}_6\text{MnN}_4\text{O}_6\text{S}_2$ |                     |
| Formula weight                          | 865.84                                                                 |                     |
| Temperature                             | 100(2) K                                                               |                     |
| Wavelength                              | 0.71073 Å                                                              |                     |
| Crystal system                          | Orthorhombic                                                           |                     |
| Space group                             | P2(1)2(1)2(1)                                                          |                     |
| Unit cell dimensions                    | a = 13.6695(14) Å                                                      | $\alpha = 90^\circ$ |
|                                         | b = 16.6450(17) Å                                                      | $\beta = 90^\circ$  |
|                                         | c = 17.5462(19) Å                                                      | $\gamma = 90^\circ$ |
| Volume                                  | 3992.3(7) Å <sup>3</sup>                                               |                     |
| Z                                       | 4                                                                      |                     |
| Density (calculated)                    | 1.441 Mg/m <sup>3</sup>                                                |                     |
| Absorption coefficient                  | 0.512 mm <sup>-1</sup>                                                 |                     |
| F(000)                                  | 1804                                                                   |                     |
| Crystal size                            | 0.5 x 0.3 x 0.2 mm <sup>3</sup>                                        |                     |
| Reflections collected                   | 63176                                                                  |                     |
| Independent reflections                 | 9930 [R(int) = 0.0796]                                                 |                     |
| Final R indices<br>[ $I > 2\sigma(I)$ ] | R1 = 0.0525, wR2 = 0.1349                                              |                     |
| R indices (all data)                    | R1 = 0.0673, wR2 = 0.1415                                              |                     |

Single crystals of  **$\Lambda$ -2Mn**, were mounted on a nylon loop and used for X-ray structure determination. The measurements were carried out on a BRUKER SMART APEX CCD diffractometer using graphite-monochromated Mo  $\text{K}\alpha$  radiation ( $\lambda = 0.71073$  Å). The

measurements were made in the range 2.25 to 28.40° for  $\theta$ . Full-sphere data collection was carried out with  $\omega$  and  $\phi$  scans. Programs used: data collection, Smart version 5.631 (Bruker AXS 1997-02); data reduction, Saint + version 6.36A (Bruker AXS 2001); absorption correction, SADABS version 2.10 (Bruker AXS 2001). Structure solution and refinement were done using SHELXTL Version 6.14 (Bruker AXS 2000-2003). The structure was solved by direct methods and refined by full-matrix least-squares methods on  $F^2$ . The non-hydrogen atoms were refined anisotropically. The H-atoms were placed in geometrically optimized positions and forced to ride on the atom to which they are attached. One of the triflate moieties is disordered. All the atoms except the Carbon atom were refined over two disordered positions. The ratio between the two disordered positions is 0.69. (Cambridge Crystallographic Data Center reference for  **$\Lambda$ -2Mn** is CCDC 657976).

### IV.5.5. Reaction conditions for catalysis

#### Catalyst:AcOOH:substrate 1:1200:1000

A CH<sub>3</sub>CN (4 mL) solution of alkene (2 mmol, 0.5 M) and catalyst (2  $\mu$ mol, 0.5 mM) was prepared in a 10 mL flask and cooled to 0°C in an ice bath. 1.2 equivalents of 32% AcOOH (2.4 mmol, 0.5 mL) were added via syringe pump over the course of 3 minutes with stirring. After an additional 10 minutes, the reaction flask was removed from the ice bath and allowed to warm to room temperature. Biphenyl was added as internal standard and the resulting solution was subjected to GC analysis, providing the substrate conversion and product yield relative to the internal standard integration. The epoxide product was identified by comparison of the GC retention time of an authentic sample.

#### Catalyst:AcOOH:substrate 1:200:200

A CH<sub>3</sub>CN (0.8 mL) solution of alkene (0.4 mmol, 0.5 M) and catalyst (2  $\mu$ mol, 2.5 mM) was prepared in a 10 mL flask and cooled to 0°C in an ice bath. 1.0 equivalents of 32% AcOOH (0.4 mmol, 84  $\mu$ L) were added via syringe pump over the course of 3 minutes with stirring. After an additional 10 minutes, the reaction flask was removed from the ice bath and allowed to warm to room temperature. Analogous work-up and GC analysis was performed to identify the epoxide product. ee was determined by chiral HPLC for the epoxides of the following olefins: *trans*- $\beta$ -methylstyrene, ethyl cinnamate, 4-methylstyrene, 4-chlorostyrene, 3-nitrostyrene.

## IV.6. References

1. Sundermeier, U.; Döbler, C.; Beller, M. In *Modern Oxidation Methods*; Ed. Wiley-VCH: Weinheim, 2004.
2. Lane, B. S.; Burgess, K. *Chem. Rev.* **2003**, *103*, 2457-2474.
3. Joergensen, K. A. *Chem. Rev.* **1989**, *89*, 431-458.

4. Punniyamurthy, T.; Velusamy, S.; Iqbal, J. *Chem. Rev.* **2005**, *105*, 2329-2364.
5. Noyori, R.; Aoki, M.; Sato, K. *Chem. Commun.* **2003**, 1977–1986.
6. Tanase, S.; Bouwman, E. *Adv. Inorg. Chem.* **2006**, *58*, 29-75.
7. Bäckvall, J. E. *Modern oxidation Methods*; Wiley-VCH: Weinheim, 2004.
8. Murphy, A.; Dubois, G.; Stack, T. D. P. *J. Am. Chem. Soc.* **2003**, *125*, 5250-5251.
9. Murphy, A.; Pace, A.; Stack, T. D. P. *Org. Lett.* **2004**, *6*, 3119-3122.
10. Zhang, W.; Loebach, J. L.; Wilson, S. R.; Jacobsen, E. N. *J. Am. Chem. Soc.* **1990**, *112*, 2801-2803.
11. Jacobsen, E. N.; Zhang, W.; Muci, A. R.; Ecker, J. R.; Deng, L. *J. Am. Chem. Soc.* **1991**, *113*, 7063-7064.
12. Palucki, M.; Pospisil, P. J.; Zhang, W.; Jacobsen, E. N. *J. Am. Chem. Soc.* **1994**, *116*, 9333-9334.
13. Palucki, M.; McCormick, G. J.; Jacobsen, E. N. *Tetrahedron Lett.* **1995**, *36*, 5457-5460.
14. Palucki, M.; Finney, N. S.; Pospisil, O. J.; Güler, M. L.; Ishida, T. T.; Jacobsen, E. N. *J. Am. Chem. Soc.* **1998**, *120*, 948-954.
15. Barlan, A. U.; Basak, A.; Yamamoto, H. *Angew. Chem. Int. Ed.* **2006**, *45*, 5849-5852.
16. Tse, M. K.; Bhor, S.; Klawonn, M.; Anilkumar, G.; Jiao, H.; Döbler, C.; Spannenberg, A.; Mägerlein, W.; Hugl, H.; Beller, M. *Chem. Eur. J.* **2006**, *12*, 1855-1874.
17. Tse, M. K.; Bhor, S.; Klawonn, M.; Anilkumar, G.; Jiao, H.; Spannenberg, A.; Döbler, C.; Mägerlein, W.; Hugl, H.; Beller, M. *Chem. Eur. J.* **2006**, *12*, 1875-1888.
18. Matsumoto, K.; Sawada, Y.; Saito, B.; Sakai, K.; Katsuki, T. *Angew. Chem. Int. Ed.* **2005**, *44*, 4935-4939.
19. Sawada, Y.; Matsumoto, K.; Kondo, S.; Watanabe, H.; Ozawa, T.; Suzuki, K.; Saito, B.; Katsuki, T. *Angew. Chem. Int. Ed.* **2006**, *45*, 3478-3480.
20. Sawada, Y.; Matsumoto, K.; Katsuki, T. *Angew. Chem. Int. Ed.* **2007**, *46*, 4559-4561.
21. Matsumoto, K.; Oguma, T.; Katsuki, T. *Angew. Chem. Int. Ed.* **2009**, 7432 -7435.
22. Marchi-Delapierre, C.; Jorge-Robin, A.; Thibon, A.; Ménage, S. *Chem. Commun.* **2007**, 1166-1168.
23. Gómez, L.; Garcia-Bosch, I.; Company, A.; Sala, X.; Fontrodona, X.; Ribas, X.; Costas, M. *Dalton Trans.* **2007**, 5539–5545.
24. Wu, M.; Wang, B.; Wang, S.; Xia, C.; Sun, W. *Org. Lett.* **2009**, *11*, 3622-3625.
25. Aldrich-Wright, J. R.; Vagg, R. S.; Williams, P. A. *Coord. Chem. Rev.* **1997**, *166*, 361-389.

26. Knof, U.; von Zelewsky, A. *Angew. Chem. Int. Ed.* **1999**, *38*, 302-322.
27. Hubin, T. J.; McCormick, J. M.; Collinson, S. R.; Buchalova, M.; Perkins, C. M.; Alcock, N. W.; Kahol, P. K.; Raghunathan, A.; Busch, D. H. *J. Am. Chem. Soc.* **2000**, *122*, 2512-2522.
28. Hureau, G. B. C.; Charlot, M.-F.; Philouze, C.; Nierlich, M.; Césarío, M.; Anxolabéhère-Mallart, E. *Inorg. Chem.* **2005**, *44*, 3669-3683.
29. Albela, B.; Carina, R.; Policar, C.; Poussereau, S.; Cano, J.; Guilhem, J.; Tchertanov, L.; Blondin, G.; Delroisse, M.; Girerd, J.-J. *Inorg. Chem.* **2005**, *44*, 6959-6966.
30. Greenwood, N. N.; Earnshaw, A.; Butterworth-Heinemann: Oxford, 1997; p. 1060.
31. Feichtinger, D.; Plattner, D. A. *Angew. Chem. Int. Ed. Engl.* **1997**, *36*, 1718-1719.
32. Yin, G.; Buchalova, M.; Dandy, A. M.; Perkins, C. M.; Kitko, D.; Carter, J. D.; Scheper, W. M.; Busch, D. H. *J. Am. Chem. Soc.* **2005**, *127*, 17170-17171.

---

# Self-Assembling of Nanoscopic Molecular Rectangles, Extended Helicates and Porous-like Materials Based on Macrocyclic Dicopper Building Blocks Under Fine Supramolecular Control

---

### Abstract

In this chapter, facile synthesis of self-assembled supramolecular structures is described. Two isomerically related macrocyclic dicopper complexes selectively encode, upon reaction with aromatic dicarboxylate linkers, the supramolecular self-assembly of nanoscopic molecular rectangles and a new class of extended helicates. Control over the rectangle shape and dimensions can also be tuned via anion- $\pi$ -aromatic interactions between a molecular rectangle and BArF anions (BArF = [B{3,5-(CF<sub>3</sub>)<sub>2</sub>-C<sub>6</sub>H<sub>3</sub>}<sub>4</sub>]). Finally, control over 3D organization of the structures leading to selective crystal engineering is attained via the judicious choice of ligands and counterions.



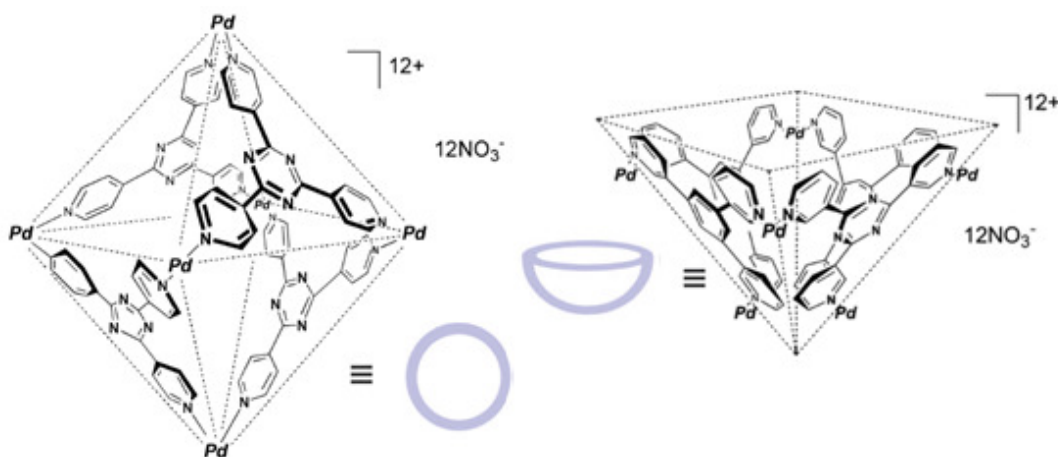
# Contents

|                                                                  |            |
|------------------------------------------------------------------|------------|
| <b>V.1. INTRODUCTION .....</b>                                   | <b>146</b> |
| <b>V.2. RESULTS AND DISCUSSION .....</b>                         | <b>148</b> |
| V.2.1. SYNTHESIS OF COMPLEXES .....                              | 148        |
| V.2.2. CHARACTERIZATION OF COMPLEXES .....                       | 149        |
| V.2.2.1. Solid state structures .....                            | 149        |
| V.2.2.2. Spectroscopic characterization.....                     | 153        |
| V.2.2.3. Integrity of the molecular rectangles in solution ..... | 154        |
| <b>V.3. CONCLUDING REMARKS .....</b>                             | <b>157</b> |
| <b>V.4. EXPERIMENTAL SECTION.....</b>                            | <b>157</b> |
| V.4.1. INSTRUMENTATION.....                                      | 157        |
| V.4.2. MATERIALS.....                                            | 157        |
| V.4.3. SYNTHESIS OF COMPLEXES .....                              | 158        |
| V.4.4. UV-VIS SPECTRA.....                                       | 159        |
| V.4.5. CRYSTAL DATA .....                                        | 160        |
| <b>V.5. REFERENCES .....</b>                                     | <b>162</b> |

## V.1. Introduction

Chemists have developed an extensive collection of protocols for making compounds with desirable properties or functions. It is often the case, however, that complex molecules require equally complex synthesis, which can be costly in terms of time, materials, atom economy and yield. In contrast, some biological structures and processes of impressive complexity are accomplished by natural systems in a relatively easy manner by exploiting the principles of non-covalent interactions.<sup>1</sup>

It is well known that self-assembly allows for the preparation of highly complex systems from relatively simple starting building blocks. One of the most rapidly developing tools for synthetic chemistry is supramolecular coordination chemistry. The greater directional control offered by metal-ligand coordinative bonding compared to weak electrostatic and  $\pi$ - $\pi$ -stacking interactions or even hydrogen bonding is one of the reasons for this rapid development. Moreover, the diversity of transition-metal complexes and multidentate ligands available as building blocks makes this strategy very versatile, allowing for the precise control over the shape of the assemblies and the regulation of their function and sizes.



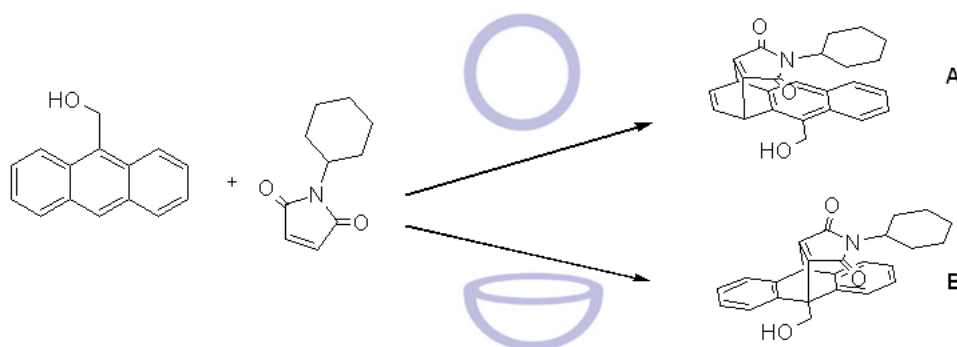
**Scheme 1.** Schematic representation of two supramolecular metal-driven assemblies by Fujita and co-workers: octahedral cage (up left) and bowl-shaped cage (up right).<sup>2</sup>

As a proof of concept, a tremendous variety of metal-coordination-based 2D (i.e. molecular grids), 1D (i.e. molecular ladders) and other high-dimensional structures, as well as discrete molecular structures (triangles, squares, pentagons, hexagons, rectangles, cubes, cylinders and more complex structures) have been obtained (scheme 1).<sup>3-5</sup> Furthermore, the applications, which generally are inspired in nature, are also diverse. Among them, molecular recognition, photophysics and catalysis stand out.<sup>4,6-17</sup>

For example, in natural systems, chemical conversions take place in a confined environment. Enzymes use binding and proximity effects to achieve astounding rate enhancements for specific reactions and substrates. Metal-containing assemblies have great potential to become artificial hosts due to their cage-like structure and cavities (scheme 1),



which are capable of interacting with guests. Many cage-like systems have been reported that, by means of hosting reactions, allow them to occur in conditions that usually do not take place, or enhance their rates and/or selectivities (scheme 2).<sup>18,19</sup>



**Scheme 2.** Diels-Alder reactions performed inside the cage and bowl-shaped molecules shown in scheme 1.<sup>2</sup>

Some prominent examples were reported by Fujita and co-workers.<sup>18</sup> In one of them, the Diels-Alder reaction between two highly hydrophobic reagents was performed in water making use of a supramolecular octahedral cage (scheme 1 and 2).<sup>2</sup> Inside the cage, the reagents are properly oriented to undergo a Diels-Alder reaction. Remarkably, the reaction is regioselective for the isomer A, thus contrasting with the isomer obtained when the reaction is performed without the cage (isomer B) or using a bowl-shaped macromolecule (isomer B).

Inspired by recent work on the self-assembly of calixarene-type of hosts into highly complex superstructures,<sup>20</sup> we envisioned that the preorganized structure of polyazamacrocyclic complexes will make them very attractive as sophisticated supramolecular building blocks, provided rational directed self-assembly could be applied. Indeed, molecular rectangles with a rather simple structure were recently described by our group as a proof of concept of this approach (figure 1).<sup>21,22</sup>

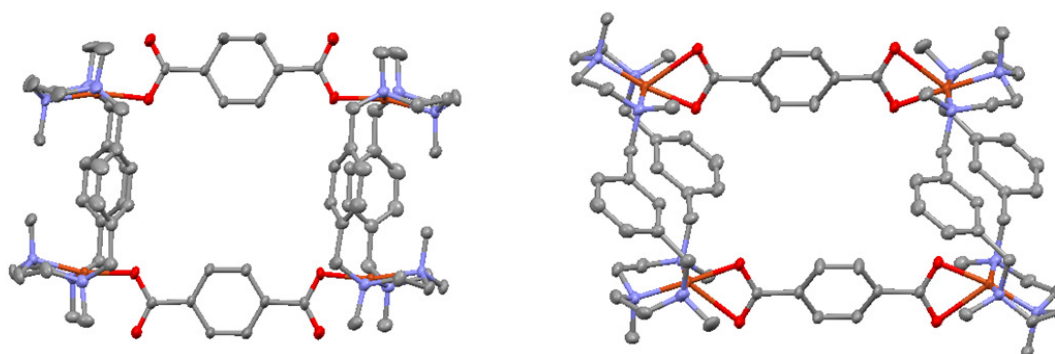


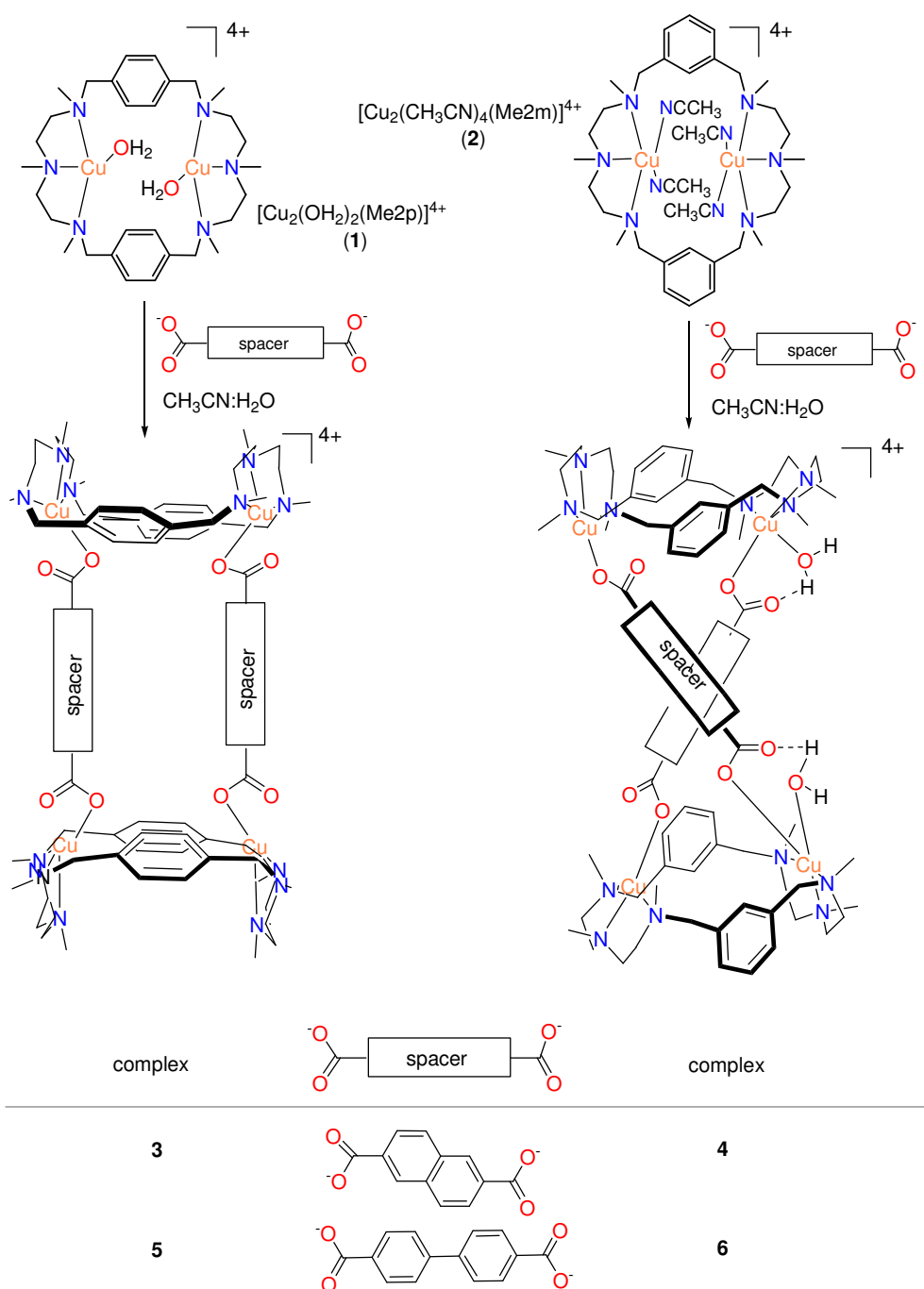
**Figure 1.** Molecular rectangles resulting from the self-assembling of dicopper complex of macrocyclic ligands with terephthalate linkers reported by our group.<sup>21</sup> Hydrogen atoms omitted for clarity.

Further exploration of this idea led us to discover unexpected subtleties in this chemistry that further expand the potential of this approach. In this chapter, the 2+2 self-assembly of dicopper hexaazamacrocyclic complexes with dicarboxylate spacers give rise to rectangle and

helicate structures. Fine tuning of the molecular structure is attained at three different levels: the design of the macrocyclic ligand, the length and nature of the dicarboxylate spacer and also the selected counteranion. The systems described in this chapter allowed us to develop a 3D cage-like assembly that is described in Chapter VI, in which catalytic centres based on porphyrins are embedded making possible its application in the catalytic oxidation of olefins.

## V.2. Results and discussion

### V.2.1. Synthesis of complexes



**Scheme 3.** Preparation and chemical structure diagram of the complexes described in this work.

Reaction between dicopper(II) precursor complexes  $[\text{Cu}_2(\text{OH}_2)_2(\text{Me2p})](\text{CF}_3\text{SO}_3)_4$ , **1OTf** or  $[\text{Cu}_2(\text{CH}_3\text{CN})_4(\text{Me2m})](\text{CF}_3\text{SO}_3)_4$ , **2OTf** (scheme 3, OTf = trifluoromethanesulfonate anion) with a diacid aromatic linker ( $\text{HO}_2\text{CC}_{12}\text{H}_8\text{CO}_2\text{H}$  or  $\text{HO}_2\text{CC}_{10}\text{H}_6\text{CO}_2\text{H}$ ) and triethylamine in acetonitrile:water 10:1 (v:v) mixtures at room temperature (typically overnight reaction) gives rise to tetranuclear copper complexes of general formula  $[(\text{Cu}_2\text{L})_2(\text{O}_2\text{CArCO}_2)_2](\text{CF}_3\text{SO}_3)_4$  (**3CF<sub>3</sub>SO<sub>3</sub>**, L = Me2p and Ar = C<sub>12</sub>H<sub>8</sub>; **4OTf**, L = Me2m, Ar = C<sub>12</sub>H<sub>8</sub>; **5OTf**, L = Me2p and Ar = C<sub>10</sub>H<sub>6</sub>; **6OTf** L = Me2m, Ar = C<sub>10</sub>H<sub>6</sub>, scheme 3). These compounds were obtained as crystalline materials in good yields (77 to 83 %) after diethyl ether diffusion over the reaction mixtures. Complexes of general formula  $[(\text{Cu}_2\text{L})_2(\text{O}_2\text{CArCO}_2)_2]\text{X}_4$ , **4ClO<sub>4</sub>** (L = Me2m, Ar = C<sub>12</sub>H<sub>8</sub>) and **5BArF** (L = Me2p, Ar = C<sub>12</sub>H<sub>8</sub>) were respectively prepared by crystallization of **4OTf** from acetonitrile:diethyl ether solutions containing NaClO<sub>4</sub>, and via anion metathesis of **5OTf** with NaBArF in CH<sub>2</sub>Cl<sub>2</sub>, followed by slow pentane diffusion.

## V.2.2. Characterization of complexes

### V.2.2.1. Solid state structures

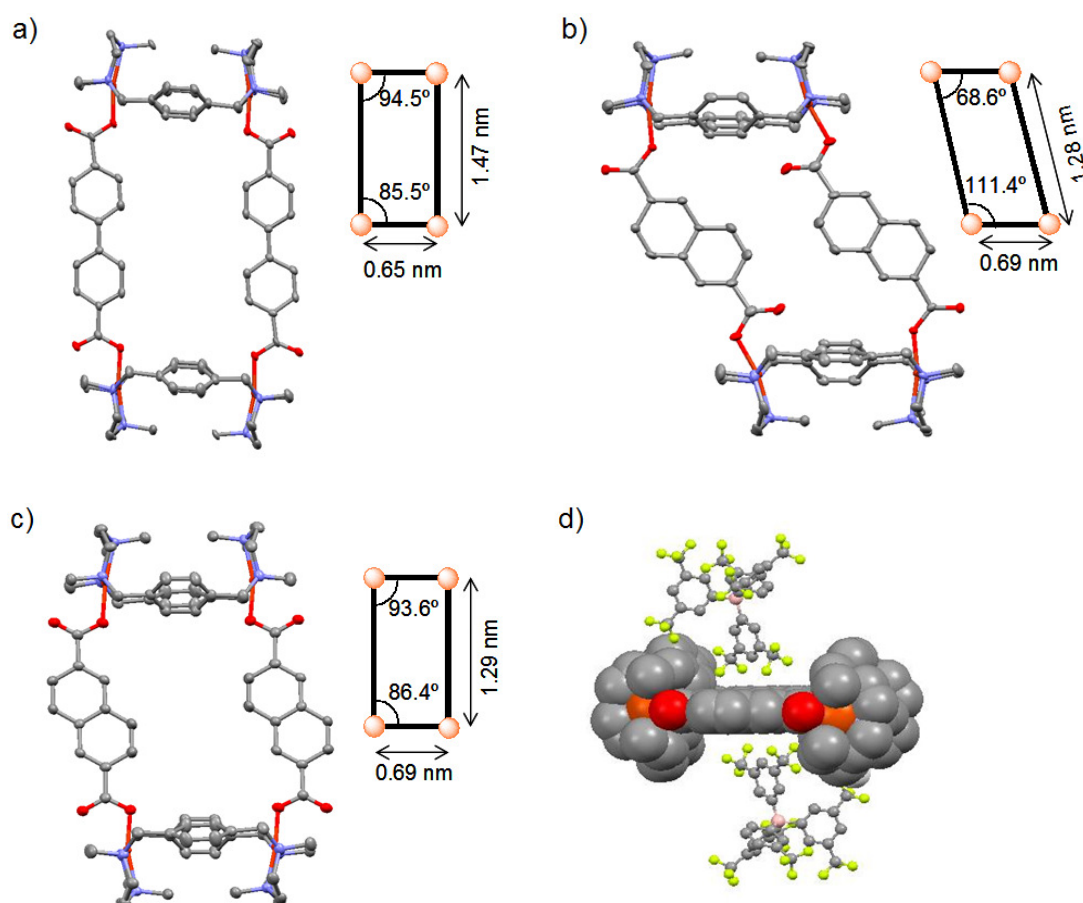


**Figure 2.** ORTEP diagrams (ellipsoids, 50%) of the cationic part of: a) **3OTf**, b) **5OTf** and c) **5BArF**; inset: the polyhedra angles and dimensions considering Cu ions as the hypothetical corners of the polyhedron. d) Space filling diagram of **5BArF** showing interaction with two BARF anions. Color code; orange (Cu), blue (N), red (O), yellow (F), pink (B), gray (C). Hydrogen atoms omitted for clarity.

The molecular structure of **3OTf**, **4ClO<sub>4</sub>**, **5OTf**, **5BArF** and **6OTf** were established by X-Ray diffraction analysis (XRD) (see experimental section for crystallographic and refinement details). Crystal structures of the cationic units of these complexes are displayed in figures 2 and 3. Crystal structure of **3OTf** and **5X** (X = OTf and BArF) showed that rectangle topologies resulted from a 2+2 self assembly processes when **1OTf**, containing *p*-phenyl substituted hexaazacyclophanes, is used as precursor (figure 2). Moreover, the copper ions adopt a square planar coordination environment formed by three N atoms of the macrocycle and an O atom of the carboxylate group, which coordinates in a monodentate mode. Nevertheless, **5OTf** and **5BArF** contain cavities with different geometric parameters which originate from the relative orientation of the two binding oxygen atoms of a carboxylate linker, being *anti* in **5OTf** and *syn* in **5BArF** (see figure 2, insets b and c, respectively). The molecular cavity generated within **5OTf** evidences a rhombohedral distortion that can be estimated by considering Cu ions as the hypothetical corners of a polyhedron. The polyhedral angles are 85.5(1)<sup>o</sup>/94.5(1)<sup>o</sup> (**3OTf**), 68.6(1)<sup>o</sup>/111.4(1)<sup>o</sup> (**5OTf**) and 86.4(1)<sup>o</sup>/93.6(1)<sup>o</sup> (**5BArF**). In addition, as a first approach to estimate the dimensions of the cavities, Cu...Cu distances in **3OTf**, **5OTf** and **5BArF** are 0.65 x 1.47 nm, 0.69 x 1.28 nm, and 0.69 x 1.29 nm, respectively. Interestingly, two BArF anions reside above and below of the hydrophobic pocket of the cavity generated in **5BArF** (figure 2d), and each of them contain five fluorine atoms at distances ≤ 3.5 Å from the centroid of aromatic rings of the hexaaza macrocyclic ligand and/or the naphthalene linkers, evidencing C-F...π and C-H...π aromatic interactions.<sup>23,24</sup> Despite the weak nature of this type of interactions, it is likely that they are at the origin of the more expanded rectangular structure of the cavity in **5BArF**, when compared with **5OTf**. Indeed, in the latter all CF<sub>3</sub>SO<sub>3</sub> anions reside outside of the cavity, suggesting negligible interactions. Overall, structural differences between **5OTf** and **5BArF** suggest that the walls of the cavity are flexible and may respond to the anionic guest's shape. Thus, the chemical nature of the anion allows suprastructural control on a primary level.

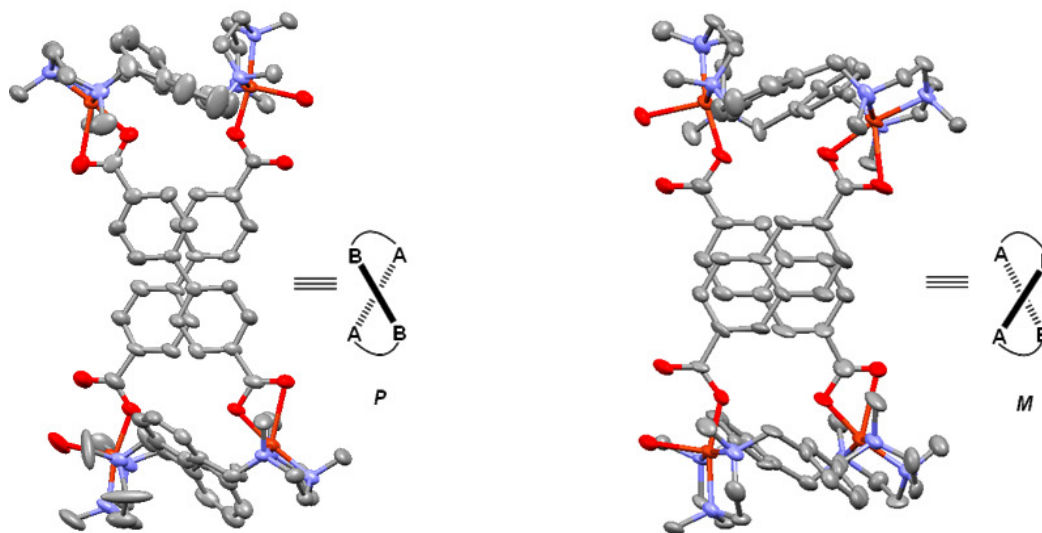


**Figure 3.** ORTEP diagrams (ellipsoids, 50%) of the cationic part of **4ClO<sub>4</sub>** (left), **6OTf** (right). Color code; orange (Cu), blue (N), red (O), yellow (F), pink (B), gray (C). Hydrogen atoms omitted for clarity.

Much to our surprise, the use of extended biphenyl-4,4'-dicarboxylate spacers and Me<sub>2</sub>m-containing dicopper complexes does not simply enlarge the dimensions of the rectangle,<sup>21,22</sup> but also gives double-stranded molecular helicates **4ClO<sub>4</sub>** and **6OTf**, as revealed by XRD analysis (figure 3). However, unlike the vast majority of such structures,<sup>14,15</sup> the chirality does not originate from the chiral topological orientation of the ligands in a tetrahedral or octahedral metal coordination geometry but from a helical twist of the two macrocyclic dicopper complexes. Because of this somewhat more complex architecture, **4ClO<sub>4</sub>** and **6OTf** constitute a new example of the recently described expanded molecular helicates.<sup>25</sup>

The coordination environment of the Cu ions in **4ClO<sub>4</sub>** and **6OTf** is also different from **3OTf** and **5OTf**. In the former cases, the Cu ions are five-coordinate; in two of the copper ions three coordination sites are occupied by N atoms of the macrocyclic ligand, and one oxygen atom from a water molecule and a monodentated carboxylate moiety fulfil the coordination environment. The water molecule is H-bonded to an O atom of the carboxylate group. However, there is no water molecule in the other two copper ions, in which the carboxylate binds in a bidentated asymmetric O,O:  $\eta^1:\eta^1$  binding mode. Nevertheless, in both cases the copper atoms adopt a distorted square pyramidal ( $\tau$  between 0.03 and 0.26) geometry.<sup>26</sup> In the first case, the coordinated water molecule occupies the apical position along an axially elongated axis, while in the other two copper ions one oxygen atom of the bidentate chelate carbonate occupy this position.

Careful analysis shows that the cationic units of **4ClO<sub>4</sub>** and **6OTf** are chiral. The chirality of the molecules is arbitrarily depicted in figure 3, showing that **4ClO<sub>4</sub>** and **6OTf** adopt *P* and *M* conformational chiralities, respectively. However, **4ClO<sub>4</sub>** and **6OTf** crystallize in non-chiral space groups *P*-1 and *Pna*2<sub>1</sub>, respectively, thus both *P* and *M* isomers are present in the crystal. A closer inspection of the structures also reveals a network of short interaromatic distances ( $\leq 3.5$  Å) between the two aromatic linkers, which indicate strong  $\pi$ -stacking interactions (see overlapping linkers in figure 3). Interestingly, these interactions are found neither in **3OTf**, **5OTf** and **5BARf**, nor in the previously described rectangle [(Cu<sub>2</sub>(Me<sub>2</sub>m))<sub>2</sub>(O<sub>2</sub>CC<sub>6</sub>H<sub>4</sub>CO<sub>2</sub>)<sub>2</sub>](ClO<sub>4</sub>)<sub>4</sub>.<sup>21</sup> Thus we conclude that these interactions play a major role in directing the assembly of the helicate structure. In conclusion, linker structure but, most remarkably, the nature of the hexaazamacrocyclic ligand allows a second level of control over the supramolecular structure by encoding for the selective formation of rectangles or helicates.

Besides the two structural levels already described, analysis of crystal packing evidences also dramatic differences in the three-dimensional supramolecular network. In one hand, the crystal packing of helicates **4ClO<sub>4</sub>** and **6OTf** does not reveal any unique extended supramolecular chirality and shows typical perchlorate and trifluoromethanesulfonate mediated hydrogen bonds.

On the other hand, compound **3OTf** shows hydrogen bonded interactions between the anions and also DMF solvent molecules from crystallization. It is interesting to observe one CF<sub>3</sub>SO<sub>3</sub> anion nicely placed inside a pocket depicted by the walls of adjacent macrocyclic moieties (figure 4). It is finally remarkable the different 3D packing in **5X** depending on the

counteranion used. BARf counteranion favors multiple C-F $\cdots\pi$  and C-H $\cdots\pi$  interactions that result in the isolation of the rectangle molecules surrounded by BARf anions in **5BARf**, thus excluding the possibility of guest encapsulation.

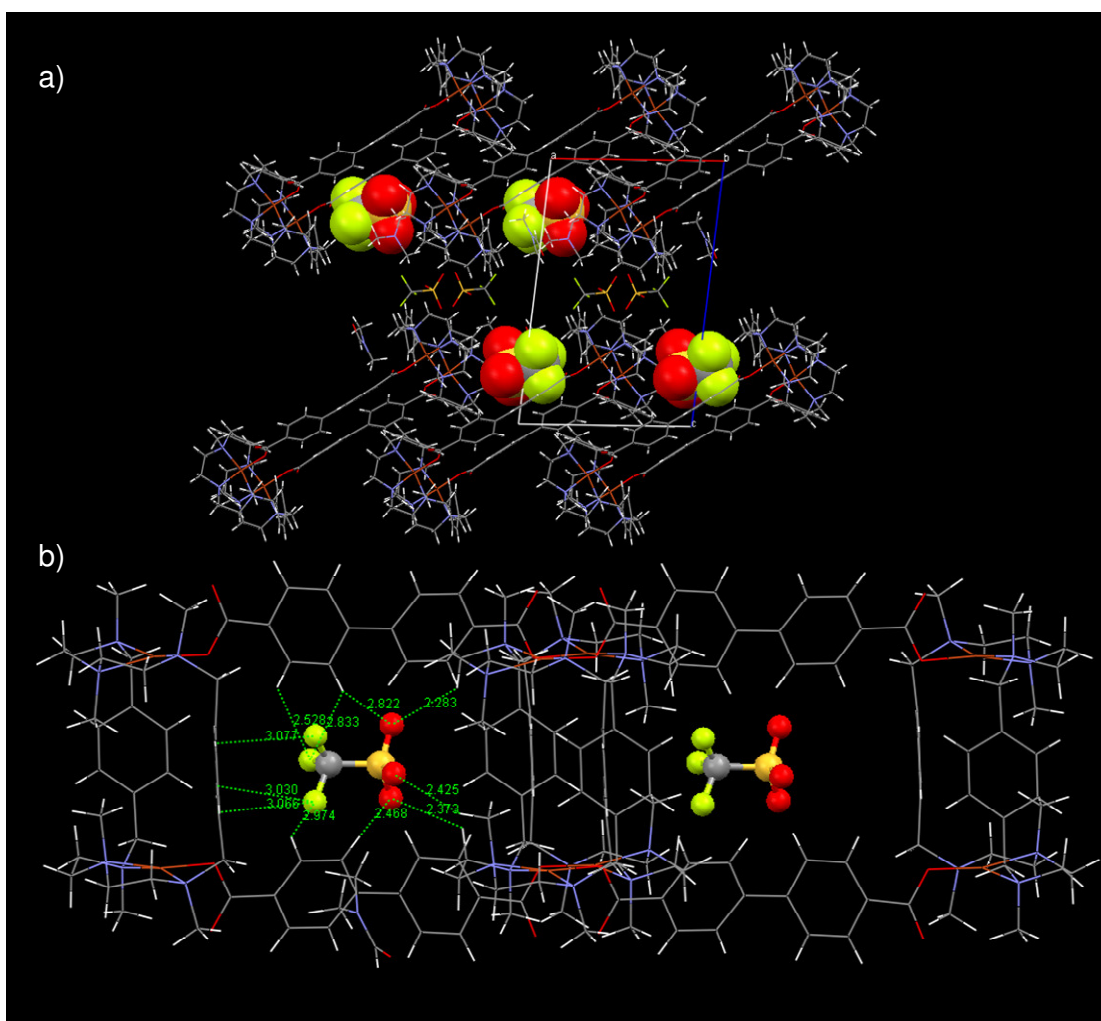


**Figure 4.** a) Crystal packing view perpendicular to *b* axis of compound [(Cu<sub>2</sub>(Me<sub>2</sub>p))<sub>2</sub>(O<sub>2</sub>CC<sub>12</sub>H<sub>8</sub>CO<sub>2</sub>)<sub>2</sub>](CF<sub>3</sub>SO<sub>3</sub>)<sub>4</sub> (**5OTf**) with one of the CF<sub>3</sub>SO<sub>3</sub> anions depicted in space-filling mode to highlight its encapsulation inside the pocket depicted by walls of two rectangular molecules; b) Detailed view of the encapsulated triflate anion with some C-H $\cdots$ F<sub>triflate</sub> and C-H $\cdots$ O<sub>triflate</sub> contact distances.

The crystal packing of **5OTf** does allow the formation of infinite monodimensional channels (approx. 1 nm of diameter) delimited by the aromatic moieties of spacer and macrocyclic ligands along the *c* axis, that host six DMF molecules per unit cell (figure 5). The latter is a direct consequence of the selection of CF<sub>3</sub>SO<sub>3</sub> as counteranion and constitutes the third supramolecular level control observed within this family of self-assembled metal-organic entities.

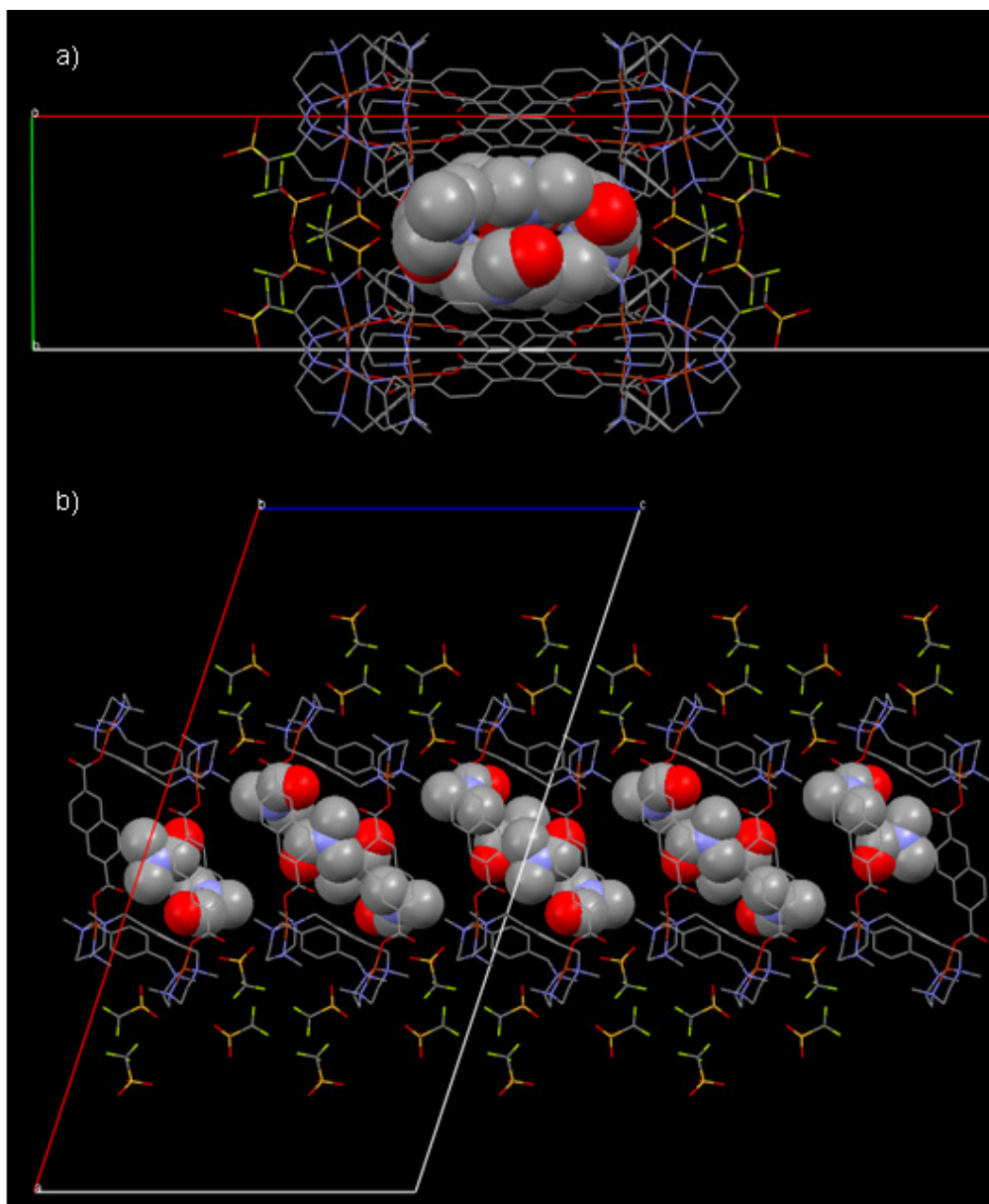


**Figure 5.** Crystal packing of **5OTf** showing (a) channels along *c* axis containing DMF solvent molecules and (b) a perpendicular view of the channels (DMF molecules depicted in space-filling mode for clarity). Hydrogen atoms omitted for clarity.

### V.2.2.2. Spectroscopic characterization

**3OTf-6OTf** were spectroscopically characterized by FT-IR and UV-Vis spectroscopy. The most distinctive features of their respective IR spectra are two strong bands corresponding to the COO stretching vibration. The high energy band/s (around  $1600\text{ cm}^{-1}$ ) are assigned to the  $\nu_{\text{asym}}$  COO stretching mode, while the lower energy component (around  $1350\text{ cm}^{-1}$ ) corresponds to the corresponding  $\nu_{\text{sym}}$  mode. ( $1614$  and  $1340\text{ cm}^{-1}$  for **3OTf**;  $1603$ ,  $1585$  and  $1370\text{ cm}^{-1}$  for **4OTf**;  $1623$  and  $1335\text{ cm}^{-1}$  for **5OTf**;  $1606$ ,  $1569$ ,  $1390$  and  $1360\text{ cm}^{-1}$ , for **6OTf**). The band assigned to the  $\nu_{\text{asym}}$  COO stretching mode is duplicated for **4OTf** and **6OTf**, showing two

different binding modes of the carboxylate ligand<sup>27</sup> in the same molecule as unambiguously ascertained by X-ray crystallography.

On the other hand, the UV-Vis spectra of the four copper complexes reported in this work are characterized by very intense absorptions around 300 nm that correspond to  $\pi$ - $\pi^*$  transition of the aromatic rings of the ligand and relatively weak features between 500-650 nm characteristic of ligand field transitions of  $d^9$  ions (figure 6 and 9 (in experimental section)).<sup>28</sup> The energy and number of these transitions convey information about the coordination geometry of the copper ions in the complexes. Square planar geometries present in **3OTf** and **5OTf** are characterized by a double hump at 502, 632 nm for **3OTf** and at 509, 630 nm for **5OTf**, responsible for the gray-blue color of their solutions. On the other hand, **4OTf** and **6OTf** present one broad band ( $\lambda_{max}$ ) 644 and 640 nm, respectively, that give rise to deep blue solutions. The energy of these d-d bands is relatively high compared with the spectrochemical behaviour observed in mononuclear trigonal bipyramidal copper complexes containing tripodal amine ligands which strongly suggests that the distorted square pyramidal coordination geometry adopted by the Cu ions in the solid state is retained in solution.<sup>29,30</sup>

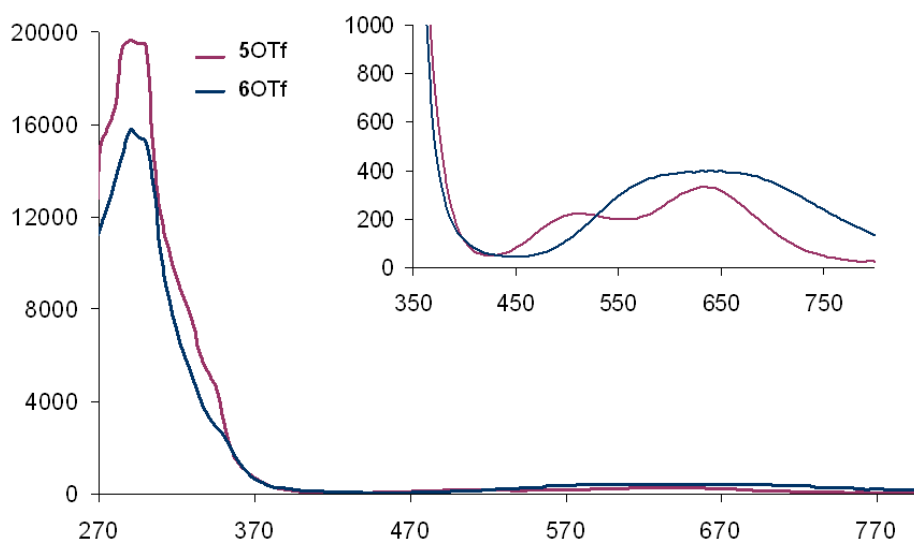


Figure 6. UV-Vis spectra of complexes **5OTf** and **6OTf** in acetonitrile.

### V.2.2.3. Integrity of the molecular rectangles in solution

Analytical evidence for the molecular composition of supramolecular structures in solution state was obtained by ESI-MS experiments of **3OTf**-**6OTf** in  $\text{CH}_3\text{CN}/\text{Et}_2\text{O}$  solutions (figure 7 and 8). Peaks corresponding to the expected 2+2 assemblies with systematic loss of counteranion molecules are found in all cases. The more intense  $m/z$  peaks and isotopic patterns could be satisfactorily simulated as the following cationic species:  $\{[\text{Cu}_4(\text{O}_2\text{C-spacer-CO}_2)_2\text{L}_2](\text{CF}_3\text{SO}_3)_2\}^{+2}$  ( $[\text{X}-2(\text{CF}_3\text{SO}_3)]^{+2}$ ),  $\{[\text{Cu}_4(\text{O}_2\text{C-spacer-CO}_2)_2\text{L}_2](\text{CF}_3\text{SO}_3)\}^{+3}$  ( $[\text{X}-3(\text{CF}_3\text{SO}_3)]^{+3}$ ) and  $\{[\text{Cu}_4(\text{O}_2\text{C-spacer-CO}_2)_2\text{L}_2]\}^{+4}$  ( $[\text{X}-4(\text{CF}_3\text{SO}_3)]^{+4}$ ) ( $\text{X} = \mathbf{3OTf}$ ,  $\text{L} = \text{Me2p}$  or  $\text{X} = \mathbf{4OTf}$ ,  $\text{L} = \text{Me2m}$ ) respective formulations. The isotopic pattern distribution excludes that these peaks could be attributed to ions containing a single macrocyclic complex, thus strongly



suggesting that the integrity of the macrocyclic tetrametallic boxes is retained in solution. In addition, cluster ions that could be identified as larger nuclearity assemblies were not observed.

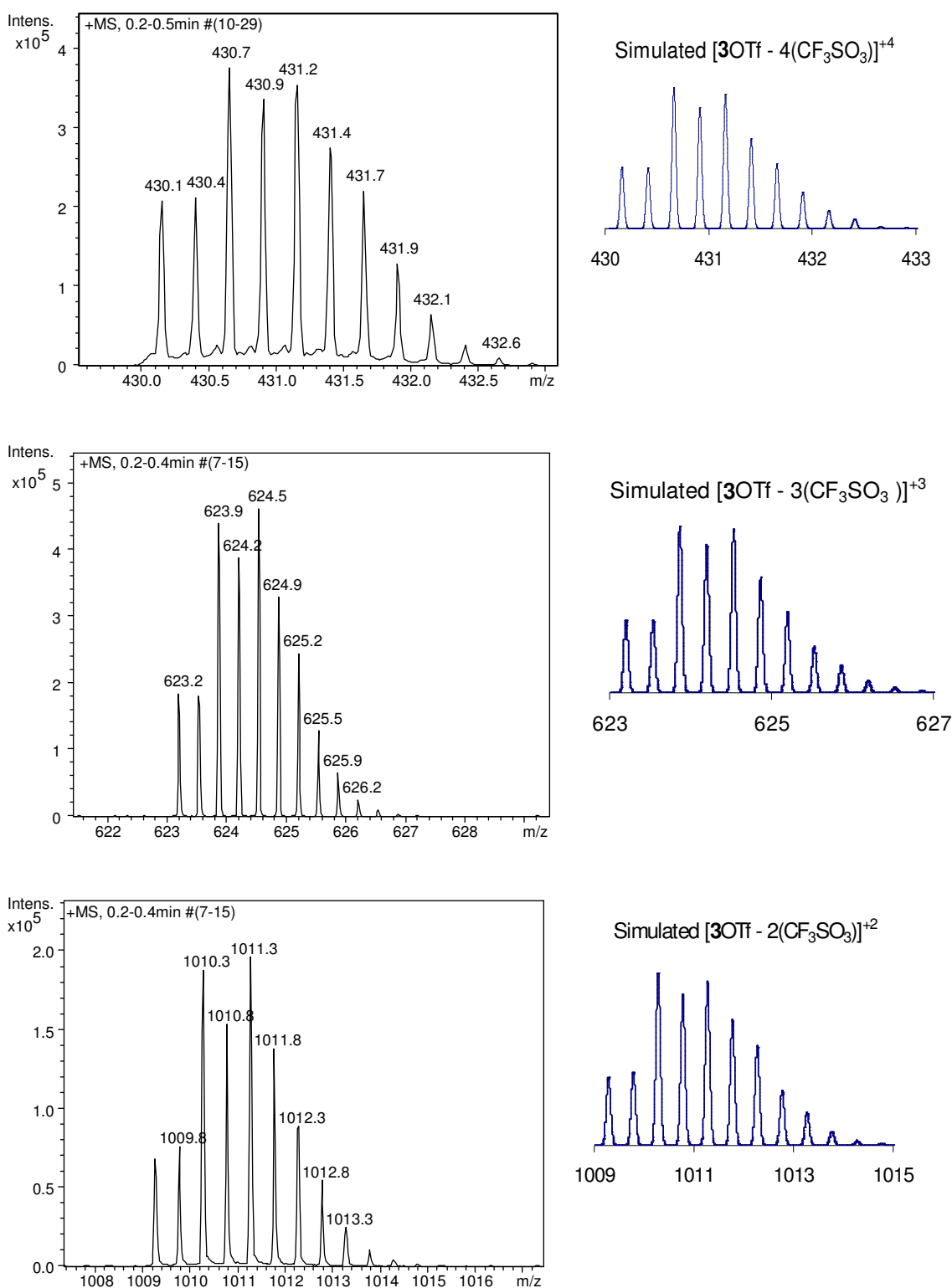


**Figure 7.** ESI-MS spectra of complex 3OTf (4OTf gave identical peaks and isotopic distribution ensuring the same composition). Simulated spectra of each selected peak are included.

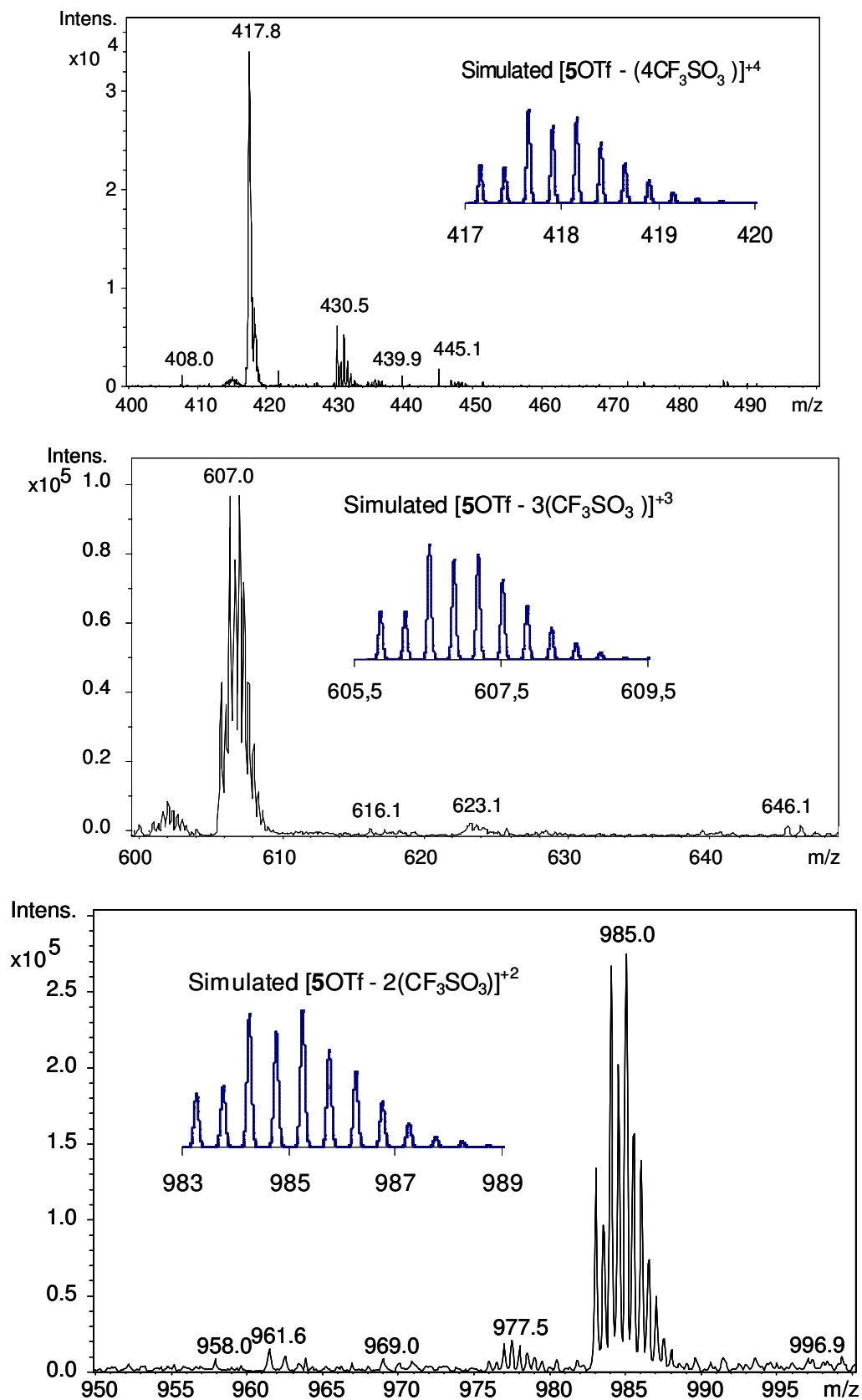


**Figure 8.** ESI-MS spectra of complex 5OTf (6OTf gave identical peaks and isotopic distribution ensuring the same composition). Simulated spectra of each selected peak are included.

### V.3. Concluding remarks

In conclusion, the supramolecular outcome of the present family of compounds can be controlled by the initial design of the macrocyclic ligand, the length and nature of the dicarboxylate spacer and also the selected counteranion. Combination of these parameters constitutes a set to design structurally diverse supramolecular structures that include differently sized rectangles and double-stranded helicates. Further subtle control on the 3D packing of these compounds allows, for instance, the creation of a nanosized monodimensional channel shown to host a large number of DMF molecules in the crystal structure of **5OTf**. Noteworthy, the non-restricted rotation of the  $-\text{COO}^-$  groups along with the possibility of mono or bidentation, allows for the richness of the supramolecular structures described, and it should be taken into account in the design of future self-assembled carboxylate-based metal-organic compounds. The structural versatility of our approach and its synthetic simplicity offers a powerful method to prepare complex suprastructures via the use of different polycarboxylate linkers, metal ions and counterions.

### V.4. Experimental section

#### V.4.1. Instrumentation

FT-IR spectra were taken in a Mattson-Galaxy Satellite FT-IR spectrophotometer containing a MKII Golden Gate Single Reflection ATR System. Elemental analyses were conducted in a Carlo Erba Instrument, Mod. CHNS 1108. UV-Vis spectroscopy was performed on a Cary 50 Scan (Varian) UV-vis spectrophotometer with 1 cm quartz cells. ESI-MS experiments were performed on a Navigator LC/MS chromatograph from Thermo Quest Finnigan or a Bruker Daltonics Esquire 3000 Spectrometer, using an acetonitrile/diethyl ether mixture as a mobile phase.

#### V.4.2. Materials

Solvents were purchased from SDS as reagent grade. Unless noted otherwise, all reagents were purchased from commercial sources and used as received. 3,6,9,16,19,22-hexamethyl-3,6,9,16,19,22-hexaazatricyclo[22.2.2.211,14]triaconta-(26),11(12),13,24,27,29-hexaene, Me2p, and 3,6,9,17,20,23-hexamethyl-3,6,9,17,20,23-hexaazatricyclo[23.3.1.111,15]triaconta-1(29),11(30),12,14,25,27-hexaene, Me2m, and NaBARf, BARf =  $[\text{B}\{3,5-(\text{CF}_3)_2-\text{C}_6\text{H}_3\}_4]$  were prepared according to or through slight modifications of the published procedures.<sup>31-34</sup>

**Caution!** Perchlorate salts of metal complexes with organic ligands are potentially explosive. While we have not encountered any problems, it is advisable to use only small amounts and handle the compounds with care.

### V.4.3. Synthesis of complexes

$[(\text{Cu}_2(\text{Me2p}))_2(\text{O}_2\text{CC}_{12}\text{H}_8\text{CO}_2)_2](\text{CF}_3\text{SO}_3)_4$ , **3OTf** and  $[(\text{Cu}_2(\text{Me2m}))_2(\text{O}_2\text{CC}_{12}\text{H}_8\text{CO}_2)_2](\text{CF}_3\text{SO}_3)_4$ , **4OTf** were prepared in analogous manners as exemplified for **3OTf**.

$[(\text{Cu}_2(\text{Me2p}))_2(\text{O}_2\text{CC}_{12}\text{H}_8\text{CO}_2)_2](\text{CF}_3\text{SO}_3)_4$ , **3OTf**. Me2p (50.0 mg, 0.10 mmol) and  $\text{Cu}(\text{CF}_3\text{SO}_3)_2$  (74.6 mg, 0.20 mmol) were charged in a 10 mL flask and dissolved in  $\text{CH}_3\text{CN}$  (2 mL) to form a reddish-blue solution. The mixture was stirred for 30 min and then, a suspension of biphenyl-4,4'-dicarboxylic acid (25.2 mg, 0.10 mmol) and triethylamine (28.3  $\mu\text{L}$ , 0.20 mmol) in  $\text{CH}_3\text{CN}$  (1 mL) was added dropwise to the stirred solution. The resulting dark blue solution was stirred for 10 h and then filtered through Celite. Diethyl ether diffusion after 5 days afforded blue needles. The solvent was decanted and the crystalline solids dried under vacuum. (89.0 mg, 0.038 mmol, 76.7%). Single crystals suitable for X-ray diffraction analysis were obtained by slow diethyl ether diffusion over a  $\text{CH}_3\text{CN}:\text{DMF}$  1:1 v:v solution of the complex. Elemental analysis calcd for  $\text{C}_{92}\text{H}_{116}\text{Cu}_4\text{F}_{12}\text{N}_{12}\text{O}_{20}\text{S}_4 \cdot 1.75\text{CH}_3\text{CN} \cdot 3\text{H}_2\text{O}$  (MW = 2446.15 g/mol): C, 46.90; N, 7.87; H, 5.24; S, 5.24%. Found: C, 47.10; N, 7.69; H, 5.44; S, 4.97%. FT-IR(ATR)  $\nu$ ,  $\text{cm}^{-1}$ : 3525, 1614, 1340, 1255, 1223, 1150, 1028 and 635  $\text{cm}^{-1}$ . UV( $\text{CH}_3\text{CN}$ ):  $\lambda_{\text{max}}$ , nm ( $\epsilon$ ,  $\text{M}^{-1}\text{cm}^{-1}$ ): 287(61500), 502 (578), 632 (774).

$[(\text{Cu}_2(\text{Me2m}))_2(\text{O}_2\text{CC}_{12}\text{H}_8\text{CO}_2)_2](\text{CF}_3\text{SO}_3)_4$ , **4OTf**. Blue needles. (92.4 mg, 0.04 mmol, 79.6%). Elemental analysis calcd for  $\text{C}_{92}\text{H}_{116}\text{Cu}_4\text{F}_{12}\text{N}_{12}\text{O}_{20}\text{S}_4 \cdot 0.75\text{CH}_3\text{CN} \cdot 2.5\text{H}_2\text{O}$  (MW = 2396.09 g/mol): C, 46.87; N, 7.45; H, 5.18; S, 5.35%. Found: C, 47.00; N, 7.17; H, 5.48; S, 4.98%. FT-IR(ATR)  $\nu$ ,  $\text{cm}^{-1}$ : 3463, 1585, 1370, 1248, 1224, 1156, 1028 and 636. UV( $\text{CH}_3\text{CN}$ ):  $\lambda_{\text{max}}$ , nm ( $\epsilon$ ,  $\text{M}^{-1}\text{cm}^{-1}$ ): 292 (80000) and 644 (1190). Single crystals of **4ClO<sub>4</sub>** suitable for X-ray diffraction analysis were obtained by slow diethyl ether diffusion into acetonitrile solutions of **4OTf** containing  $\text{NaClO}_4$  (**4ClO<sub>4</sub>**).

$[(\text{Cu}_2(\text{Me2p}))_2(\text{O}_2\text{CC}_{10}\text{H}_6\text{CO}_2)_2](\text{CF}_3\text{SO}_3)_4$ , **5OTf** and  $[(\text{Cu}_2(\text{Me2m}))_2(\text{O}_2\text{CC}_{10}\text{H}_6\text{CO}_2)_2](\text{CF}_3\text{SO}_3)_4$ , **6OTf** were prepared in analogous manners as exemplified for **5OTf**.

$[(\text{Cu}_2(\text{Me2p}))_2(\text{O}_2\text{CC}_{10}\text{H}_6\text{CO}_2)_2](\text{CF}_3\text{SO}_3)_4$ , **5OTf**. Me2p (60.0 mg, 0.125 mmol) and  $\text{Cu}(\text{CF}_3\text{SO}_3)_2$  (90.6 mg, 0.250 mmol) were charged in a 25 mL flask and dissolved in  $\text{CH}_3\text{CN}:\text{H}_2\text{O}$  20:1 (10 mL) to form a reddish-blue solution. The mixture was stirred during 30 minutes and then, 27 mg of 2,6-naphthalenedicarboxylic acid (0.125 mmol) were added directly as a solid to the stirred solution. 25.4 mg (0.250 mmol) of triethylamine were added via syringe over this suspension, causing the progressive dissolution of the solid diacid, while the solution turned dark blue. Water (1 mL) was added and the resulting dark blue-violet mixture was stirred for 48 hours and then filtered through Celite. Diethyl ether diffusion after a week affords large blue-violet rectangles. The solvent was decanted and the crystalline solids dried under vacuum (116 mg, 0.048 mmol, 76.8%). Single crystals suitable for X-ray diffraction analysis were obtained by slow diethyl ether diffusion over a  $\text{CH}_3\text{CN}:\text{DMF}$  1:1 v:v solution of the complex.

Elemental analysis calcd for  $C_{88}H_{112}Cu_4F_{12}N_{12}O_{20}S_4 \cdot CH_3CN \cdot 6H_2O$  (MW = 2417.47 g/mol): C, 44.71; N, 7.53; H, 5.30; S, 5.31%. Found: C, 44.45; N, 7.46; H, 5.22; S, 5.41%. FT-IR (ATR)  $\nu$ ,  $cm^{-1}$ : 3522, 1623, 1335, 1253, 1223, 1154, 1028, 769 and 635. UV( $CH_3CN$ ):  $\lambda_{max}$ , nm ( $\epsilon$ ,  $M^{-1}cm^{-1}$ ): 295 (19500), 509 (225), 630 (330).

**$[(Cu_2(Me_2m))_2(O_2CC_{10}H_6CO_2)_2](CF_3SO_3)_4$ , 6OTf.** Blue needles (144 mg, 0.057 mmol, 82.8%). Single crystals of 6OTf suitable for X-ray diffraction analysis were obtained by slow diethyl ether diffusion into acetonitrile solutions of the complex. Elemental analysis calcd for  $C_{88}H_{112}Cu_4F_{12}N_{12}O_{20}S_4 \cdot CH_3CN \cdot 12H_2O$  (MW = 2525.56 g/mol): C, 42.80; N, 7.21; H, 5.55; S, 5.08%. Found: C, 42.74; N, 7.24; H, 5.68; S, 5.52%. FT-IR(ATR)  $\nu$ ,  $cm^{-1}$ : 3476, 1606, 1569, 1463, 1390, 1360, 1248, 1224, 1155, 1028, 780 and 636. UV( $CH_3CN$ ):  $\lambda_{max}$ , nm ( $\epsilon$ ,  $M^{-1}cm^{-1}$ ): 291 (15750), 295 (15500), 620 (395).

**$[(Cu_2(Me_2p))_2(O_2CC_{10}H_6CO_2)_2](BARF)_4$ , 5BARf.** 5OTf (10.0 mg, 4.14  $\mu$ mol) was charged in a 25 mL flask and suspended in  $CH_2Cl_2$  (5 mL). The mixture was stirred while a  $CH_2Cl_2$  (5 mL) solution of NaBARf (15.6 mg, 17.6  $\mu$ mol) was added. The resulting mixture was stirred overnight, causing progressive dissolution of the copper complex and precipitation of a fine colorless solid. The resulting solution was filtered through Celite, and layered with pentane. Large blue-violet crystals suitable for X-ray analysis appeared over a week. The solvent was decanted and the solid dried under vacuum. (11.0 mg, 2.05  $\mu$ mol, 49.5%). Elemental analysis calcd for  $C_{88}H_{112}Cu_4F_{12}N_{12}O_{20}S_4 \cdot 2CH_2Cl_2 \cdot 3H_2O$  (MW = 5348.80 g/mol): C, 48.05; N, 3.14; H, 3.20%. Found: C, 47.75; N, 3.40; H, 3.33%. FT-IR(ATR)  $\nu$ ,  $cm^{-1}$ : 3522, 1611, 1353, 1307, 1272, 1231, 1112, 982, 886, 838, 712, 681 and 670.

#### V.4.4. UV-Vis spectra

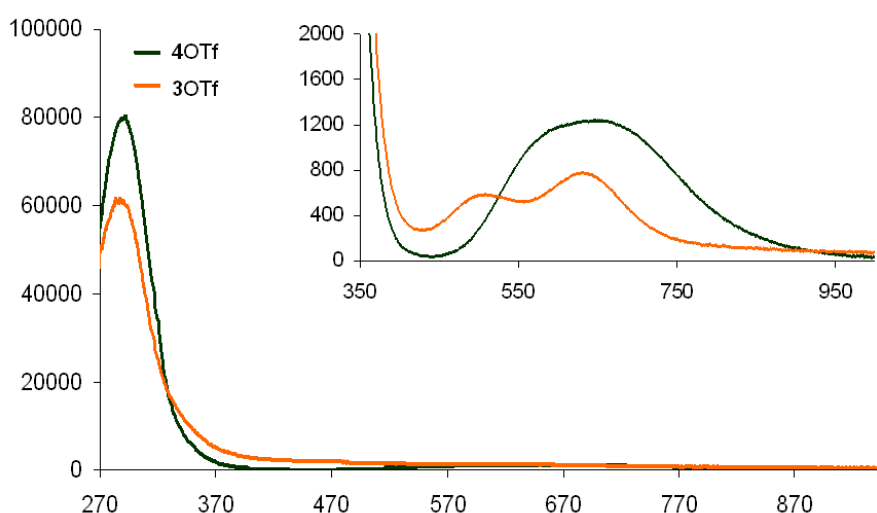


**Figure 9.** UV-Vis spectra of complexes 3OTf (in  $CH_3CN$ ) and 4OTf (in DMF).

### V.4.5. Crystal data

Crystals of **3OTf**, **4ClO<sub>4</sub>**, **5OTf**, **5BArF** and **6OTf** were mounted on a nylon loop and used for 300K (**3OTf**) or low temperature (100(2) K) (**4ClO<sub>4</sub>**, **5OTf**, **5BArF** and **6OTf**) X-ray structure determination. The measurements were carried out on a BRUKER SMART APEX CCD diffractometer using graphite-monochromated Mo K $\alpha$  radiation ( $\lambda = 0.71073 \text{ \AA}$ ). The measurements were made in the range 2.10 to 29.62 (**3OTf**), 1.92 to 28.52° (**4ClO<sub>4</sub>**), 1.93 to 28.39° (**5OTf**) 2.18 to 27.85° (**5BArF**), 1.94 to 28.55 (**6OTf**) for  $\theta$ . Full-sphere data collection was carried out with  $\omega$  and  $\varphi$  scans. A total of 46175 (**3OTf**), 87725 (**4ClO<sub>4</sub>**), 94392 (**5OTf**), 98561 (**5BArF**) 170433 (**6OTf**) reflections were collected of which 14726 [R(int) = 0.1348] (**3OTf**), 27652 [R(int) = 0.0845] (**4ClO<sub>4</sub>**), 15381 [R(int) = 0.1294] (**5OTf**), 29745 [R(int) = 0.0617] (**5BArF**), 27839 [R(int) = 0.1515] (**6OTf**) were unique. Programs used: data collection, Smart version 5.631 (Bruker AXS 1997-02); data reduction, Saint + version 6.36A (Bruker AXS 2001); absorption correction, SADABS version 2.10 (Bruker AXS 2001). Structure solution and refinement was done using SHELXTL Version 6.14 (Bruker AXS 2000-2003). The structures were solved by direct methods and refined by full-matrix least-squares methods on  $F^2$ . The non-hydrogen atoms were refined anisotropically. The H-atoms were placed in geometrically optimized positions and forced to ride on the atom to which they are attached. In all cases, the SQUEEZE option of the PLATON Program (Spek, A. L. (2005). PLATON, A Multipurpose Crystallographic Tool, Utrecht University, Utrecht, The Netherlands) was used to eliminate electron density from disordered solvent molecules.

The crystals used for structure determination contain in most of the cases solvent molecules which makes their manipulation extremely difficult and they have also disordered anions. Due to these difficulties some of the data sets are complicated to collect and not of best quality for refinement.

**5BArf**: A considerable amount of electron density attributable to CH<sub>2</sub>Cl<sub>2</sub> disordered solvent molecules was removed with the SQUEEZE option of PLATON (Spek, A. L. (2005). PLATON, A Multipurpose Crystallographic Tool, Utrecht University, Utrecht, THE Netherlands. (Cambridge Crystallographic Data Centre references are CCDC 648098 (**3OTf**), 648099 (**4ClO<sub>4</sub>**), 648100 (**5OTf**), 648101 (**5BArf**) and 648102 (**6OTf**)).

**Table 1.** Crystal Data for **3OTf**, **4ClO<sub>4</sub>**, **5OTf**, **5BArF** and **6OTf**.

| Compound                | 3OTf                                                                                                                                        | 4ClO <sub>4</sub>                                                                                                       | 5OTf                                                                                                                                 | 5BArF                                                                                                                                           | 6OTf                                                                                                                        |
|-------------------------|---------------------------------------------------------------------------------------------------------------------------------------------|-------------------------------------------------------------------------------------------------------------------------|--------------------------------------------------------------------------------------------------------------------------------------|-------------------------------------------------------------------------------------------------------------------------------------------------|-----------------------------------------------------------------------------------------------------------------------------|
| Empirical formula       | C <sub>92</sub> H <sub>116</sub> Cu <sub>4</sub> F <sub>12</sub> N <sub>12</sub> O <sub>20</sub> S <sub>4</sub>                             | C <sub>88</sub> H <sub>116</sub> Cl <sub>4</sub> Cu <sub>4</sub> N <sub>12</sub> O <sub>24</sub>                        | C <sub>88</sub> H <sub>112</sub> Cu <sub>4</sub> F <sub>12</sub> N <sub>12</sub> O <sub>20</sub> S <sub>4</sub>                      | C <sub>212</sub> H <sub>160</sub> B <sub>4</sub> F <sub>96</sub> Cu <sub>4</sub> N <sub>12</sub> O <sub>8</sub>                                 | C <sub>88</sub> H <sub>112</sub> Cu <sub>4</sub> F <sub>12</sub> N <sub>12</sub> O <sub>20</sub> S <sub>4</sub>             |
| Formula weight          | 2320.44                                                                                                                                     | 2122.01                                                                                                                 | 2268.37                                                                                                                              | 5124.98                                                                                                                                         | 2268.37                                                                                                                     |
| Temperature             | 300(2) K                                                                                                                                    | 100(2) K                                                                                                                | 100(2) K                                                                                                                             | 100(2) K                                                                                                                                        | 100(2) K                                                                                                                    |
| Wavelength              | 0.71073 Å                                                                                                                                   | 0.71073 Å                                                                                                               | 0.71073 Å                                                                                                                            | 0.71073 Å                                                                                                                                       | 0.71073 Å                                                                                                                   |
| Cristal system          | Triclinic                                                                                                                                   | Triclinic                                                                                                               | Monoclinic                                                                                                                           | Triclinic                                                                                                                                       | Orthorhombic                                                                                                                |
| Space group             | P-1                                                                                                                                         | P-1                                                                                                                     | C2/c                                                                                                                                 | P-1                                                                                                                                             | Pna21                                                                                                                       |
| Unit cell dimensions    | a = 11.882(18) Å<br>α = 70.93(3) <sup>o</sup><br>b = 13.44(2) Å<br>β = 79.53(3) <sup>o</sup><br>c = 18.78(3) Å<br>γ = 74.98(3) <sup>o</sup> | 14.585(4) Å<br>74.847(5) <sup>o</sup><br>19.674(6) Å<br>71.428(5) <sup>o</sup><br>22.666(7) Å<br>69.732(5) <sup>o</sup> | a = 47.459(6) Å<br>α = 90 <sup>o</sup><br>b = 10.8410(13) Å<br>β = 108.066(2) <sup>o</sup><br>c = 25.399(3) Å<br>γ = 90 <sup>o</sup> | a = 18.427(3) Å<br>α = 88.204(3) <sup>o</sup><br>b = 19.209(3) Å<br>β = 72.320(2) <sup>o</sup><br>c = 19.274(3) Å<br>γ = 76.923(2) <sup>o</sup> | a = 36.414(11) Å<br>α = 90 <sup>o</sup><br>b = 11.889(4) Å<br>β = 90 <sup>o</sup><br>c = 25.772(8) Å<br>γ = 90 <sup>o</sup> |
| Volume                  | 2722(7) Å <sup>3</sup>                                                                                                                      | 5699(3) Å <sup>3</sup>                                                                                                  | 12424(3) Å <sup>3</sup>                                                                                                              | 6326.4(17) Å <sup>3</sup>                                                                                                                       | 11158(6) Å <sup>3</sup>                                                                                                     |
| Z                       | 1                                                                                                                                           | 2                                                                                                                       | 4                                                                                                                                    | 1                                                                                                                                               | 1                                                                                                                           |
| Density (calculated)    | 1.594 Mg/m <sup>3</sup>                                                                                                                     | 1.255 Mg/m <sup>3</sup>                                                                                                 | 1.369 Mg/m <sup>3</sup>                                                                                                              | 1.459 Mg/m <sup>3</sup>                                                                                                                         | 1.420 Mg/m <sup>3</sup>                                                                                                     |
| Absorption coefficient  | 0.949 mm <sup>-1</sup>                                                                                                                      | 0.898 mm <sup>-1</sup>                                                                                                  | 0.831 mm <sup>-1</sup>                                                                                                               | 0.498 mm <sup>-1</sup>                                                                                                                          | 0.920 mm <sup>-1</sup>                                                                                                      |
| F(000)                  | 1360                                                                                                                                        | 2238                                                                                                                    | 5327                                                                                                                                 | 2818                                                                                                                                            | 4948                                                                                                                        |
| Θ range, deg            | 2.10 to 29.65                                                                                                                               | 1.92 to 28.52                                                                                                           | 1.93 to 28.39                                                                                                                        | 2.18 to 28.35                                                                                                                                   | 1.94 to 28.55                                                                                                               |
| Reflections collected   | 46175                                                                                                                                       | 87725                                                                                                                   | 94392                                                                                                                                | 100131                                                                                                                                          | 170433                                                                                                                      |
| Independent reflections | 14726 [R <sub>int</sub> = 0.1348]                                                                                                           | 27652 [R <sub>int</sub> = 0.0845]                                                                                       | 15381 [R <sub>int</sub> = 0.1294]                                                                                                    | 30760 [R <sub>int</sub> = 0.0620]                                                                                                               | 27839 [R <sub>int</sub> = 0.1515]                                                                                           |
| Final R indices         | R1 = 0.0836, wR2 =                                                                                                                          | R1 = 0.0910, wR2 =                                                                                                      | R1 = 0.0748, wR2 =                                                                                                                   | R1 = 0.0777, wR2 =                                                                                                                              | R1 = 0.0964, wR2 =                                                                                                          |
| [I>2σ(I)]               | 0.1930                                                                                                                                      | 0.2471                                                                                                                  | 0.1865                                                                                                                               | 0.2281                                                                                                                                          | 0.2450                                                                                                                      |
| R indices (all data)    | R1 = 0.1909, wR2 =<br>0.2266                                                                                                                | R1 = 0.1653, wR2 =<br>0.2790                                                                                            | R1 = 0.1410, wR2 =<br>0.2078                                                                                                         | R1 = 0.1128, wR2 =<br>0.2467                                                                                                                    | R1 = 0.1837, wR2 =<br>0.2962                                                                                                |

## V.5. References

1. Frieden, E. *J. Chem. Ed.* **1975**, *52*, 754-761.
2. Yoshizawa, M.; Tamura, M.; Fujita, M. *Science* **2006**, *312*, 251-254.
3. Northrop, B. H.; Zheng, Y.-R.; Chi, K.-W.; Stang, P. J. *Acc. Chem. Res.* **2009**, *42*, 1554-1563.
4. Leininger, S.; Olenyuk, B.; Stang, P. J. *Chem. Rev.* **2000**, *100*, 853-907.
5. Fujita, M.; Tominaga, M.; Hori, A.; Therrien, B. *Acc. Chem. Res.* **2005**, *38*, 369-378.
6. Thanasekaran, P.; Liao, R.-T.; Liu, Y.-H.; Rajendran, T.; Rajagopal, S.; Lu, K.-L. *Coord. Chem. Rev.* **2005**, *249*, 1085-1110.
7. Sun, S.-S.; Stern, C. L.; Nguyen, S. T.; Hupp, J. T. *J. Am. Chem. Soc.* **2004**, *126*, 6314-6326.
8. Dinolfo, P. H.; Williams, M. E.; Stern, C. L.; Hupp, J. T. *J. Am. Chem. Soc.* **2004**, *126*, 12989-13001.
9. Bélanger, S.; Hupp, J. T.; Stern, C. L.; Slone, R. V.; Watson, D. F.; Carrell, T. G. *J. Am. Chem. Soc.* **1999**, *121*, 557-563.
10. Oliveri, C. G.; Gianneschi, N. C.; Nguyen, S. T.; Mirkin, C. A.; Stern, C. L.; Wawrzak, Z.; Pink, M. *J. Am. Chem. Soc.* **2006**, *128*, 16286-16296.
11. Gianneschi, N. C.; Bertin, P. A.; Nguyen, S. T.; Mirkin, C. A.; Zakharov, L. N.; Rheingold, A. L. *J. Am. Chem. Soc.* **2003**, *125*, 10508-10509.
12. Papaefstathiou, G. S.; Zhong, Z.; Geng, L.; MacGillivray, L. R. *J. Am. Chem. Soc.* **2004**, *126*, 9158.
13. Merlau, M. L.; Mejia, M. d. P.; Nguyen, S. T.; Hupp, J. T. *Angew Chem. Int. Ed.* **2001**, *40*, 4239-4242.
14. Piguet, C.; Bernardinelli, G.; Hopfgartner, G. *Chem. Rev.* **1997**, *97*, 2005-2062.
15. Albrecht, M. *Chem. Rev.* **2001**, *101*, 3457-3498.
16. Sun, S.-S.; Lees, A. J. *Coord. Chem. Rev.* **2002**, *230*, 171-192.
17. Lee, S. J.; Hupp, J. T. *Coord. Chem. Rev.* **2006**, *250*, 1710-1723.
18. Yoshizawa, M.; Klosterman, J. K.; Fujita, M. *Angew. Chem. Int. Ed.* **2009**, *48*, 3418-3438.
19. Vriezema, D. M.; Comellas Aragomès, M.; Elemans, J. A. A. W.; Cornelissen, J. J. L. M.; Rowan, A. E.; Nolte, R. J. M. *Chem. Rev.* **2005**, *105*, 1445-1489.



20. Menozzi, E.; Busi, M.; Ramingo, R.; Campagnolo, M.; Geremia, S.; Dalcanale, E. *Chem. Eur. J.* **2005**, *11*, 3136-3148.
21. Company, A.; Gómez, L.; Lopez Valbuena, J. M.; Mas-Balleste, R.; Benet-Buchholz, J.; Llobet, A.; Costas, M. *Inorg. Chem.* **2006**, *45*, 2501-2508.
22. Company, A.; Jee, J.-E.; Ribas, X.; Lopez-Valbuena, J. M.; Gómez, L.; Corbella, M.; Llobet, A.; Mahía, J.; Benet-Buchholz, J.; Costas, M.; Eldik, R. v. *Inorg. Chem.* **2007**, *46*, 9098-9110.
23. Vangala, V. R.; Nangia, A.; Lynch, V. M. *Chem. Comm.* **2002**, 1304-1305.
24. Hayashi, N.; Mari, T.; Matsumoto, K. *Chem. Comm.* **1998**, 1905-1906.
25. Grote, Z.; Bonazzi, S.; Scopelliti, R.; Severin, K. *J. Am. Chem. Soc.* **2006**, *128*, 10382-10383.
26. Addison, A. W.; Rao, T. N.; Reedijk, J.; Van Rijn, J.; Verschoor, G. C. *J. Chem. Soc., Dalton Trans.* **1984**, *7*, 1349-46.
27. Nakamoto, K. *Infrared and Raman Spectra of Inorganic and Coordination Compounds*, 4th ed.; John Wiley: New York, 1986.
28. Hathaway, B. J.; Billing, D. E. *Coord. Chem. Rev.* **1970**, *5*, 143-207.
29. Schatz, M.; Becker, M.; Thaler, F.; Hampel, F.; Schindler, S.; Jacobson, R. R.; Tyeklar, Z.; Murthy, N. N.; Ghosh, P.; Chen, Q.; Zubieta, J.; Karlin, K. D. *Inorg. Chem* **2001**, *40*, 2312-2322.
30. Dittler-Klingemann, A. M.; Orvig, C.; Hahn, F. E.; Thaler, F.; Hubbard, C. D.; van Eldik, R.; Schindler, S.; Fabian, I. *Inorg. Chem.* **1996**, *35*, 7798-7803.
31. Menif, R.; Martell, A. E.; Squattrito, P. J.; Clearfield, A. *Inorg. Chem.* **1990**, *29*, 4723-4729.
32. Pietraszkiwicz, M.; Gasiorowski, R. *Chem. Ber.* **1990**, *123*, 405-406.
33. Clifford, T.; Danby, A. M.; Lightfoot, P.; Richens, D. T.; Hay, R. W. *J. Chem. Soc. Dalton. Trans.* **2001**, 240-246.
34. Brookhart, M.; Grant, B.; Volpe, A. F. J. *Organometallics* **1992**, *11*, 3920-3922.



---

# A Self-Assembled Nanoreactor with Porphyrinic Building Blocks as a Catalyst for the Selective Oxidation of Olefins

---

### Abstract

The synthesis, characterization and study of catalytic properties of a  $A_4B_2$ -type tetragonal prismatic cage, **1** (where  $A = [Cu_2(Me_2p)]^{+4}$ ;  $B = 5,10,15,20$ -tetrakis(4-carboxyphenyl)-porphyrin- $Mn^{III}$  chloride tetraanion; see scheme 4) are described. **1** constitutes one of the few examples of supramolecular structures that incorporate catalytic properties. Moreover, the very simple synthesis, not only of the supramolecular cage but also of the building blocks, represents a step forward for the development of polyfunctional supramolecular nanovessels. Preliminary results suggest that substrate shape selectivity in oxidation catalysis is achieved when the oxygen atom transfer is forced to occur inside of **1** by means of coordination of bulky N-coordinating ligands to porphyrinic Mn ions.

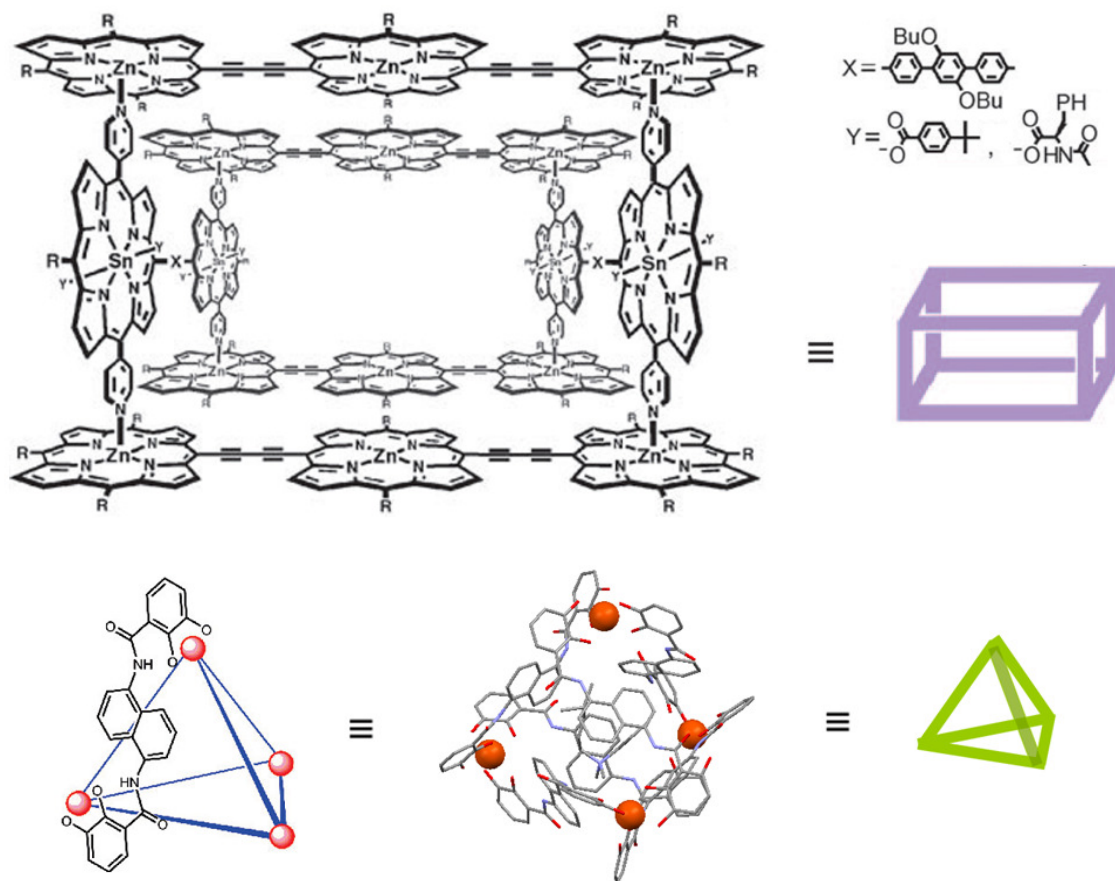


# Contents

|                                              |            |
|----------------------------------------------|------------|
| <b>VI.1. INTRODUCTION .....</b>              | <b>168</b> |
| <b>VI.2. RESULTS AND DISCUSSION .....</b>    | <b>170</b> |
| VI.2.1. SYNTHESIS OF COMPLEX 1 .....         | 170        |
| VI.2.2. SOLID STATE STRUCTURE.....           | 171        |
| VI.2.3. SPECTROSCOPIC CHARACTERIZATION ..... | 173        |
| VI.2.4. SOLUTION INTEGRITY .....             | 173        |
| VI.2.5. CATALYTIC BEHAVIOUR .....            | 174        |
| <b>VI.3. CONCLUDING REMARKS .....</b>        | <b>178</b> |
| <b>VI.4. EXPERIMENTAL SECTION.....</b>       | <b>178</b> |
| IV.4.1. INSTRUMENTATION.....                 | 178        |
| VI.4.2. MATERIALS.....                       | 178        |
| VI.4.3. SYNTHESIS OF COMPLEX 1 .....         | 179        |
| VI.4.4. CRYSTAL DATA .....                   | 179        |
| VI.4.5. CATALYTIC CONDITIONS .....           | 180        |
| <b>VI.5. REFERENCES .....</b>                | <b>181</b> |

## VI.1. Introduction

As shown in Chapter V, metal coordination-driven self-assembly is emerging as a very powerful tool to rationally construct large and chemically complex suprastructures, barely reachable by traditional covalent chemistry.<sup>1-6</sup>

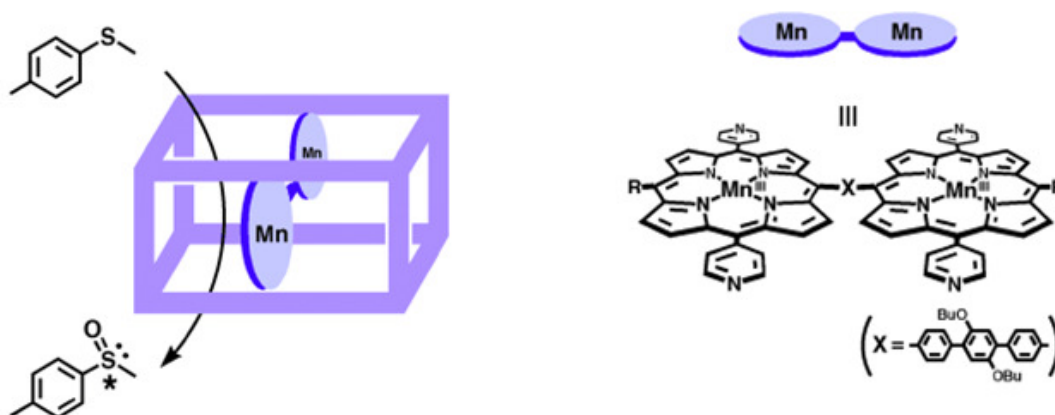


**Scheme 1.** Schematic representation of two supramolecular metal-driven assemblies: box-shaped multiporphyrin host reported by Nguyen, Hupp and co-workers;<sup>7</sup> tetrahedral coordination capsule reported by Raymond and co-workers.<sup>8</sup>

Particular notable examples have been the preparation of discrete metal containing cage-like nanostructures which hold potential use in catalysis.<sup>9</sup> In principle, the cavities in those structures could be used to bind and orient reactants selectively, control reaction stereochemistry or protect highly active catalytic sites from interaction with species other than intended substrates.

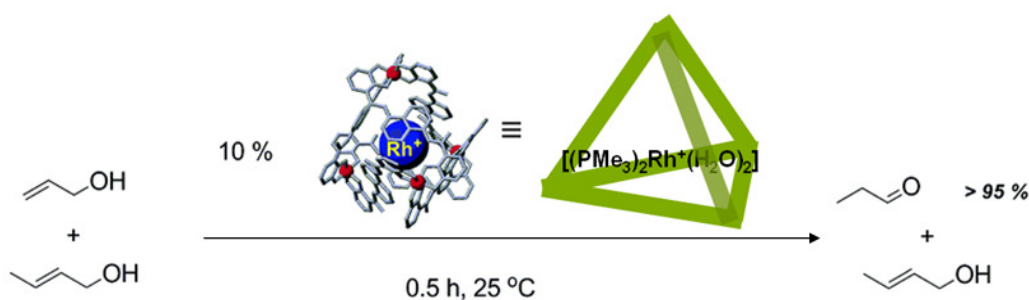
In the case of catalyzed reactions, the catalytic center has to be a component of the structure or be encapsulated. One prominent example was designed by Nguyen and co-workers, achieving enantioselectivity through space in the oxidation of sulfides and shape selectivity in the oxidation of alkenes by a totally self-assembled complex structure based on Mn-porphyrin reactive sites (scheme 1 and 2).<sup>7</sup> A different strategy was employed by Raymond and co-workers, who generated the active catalyst within a self-assembled capsule (scheme 1

and 3).<sup>8</sup> The system selectively isomerizes small and linear alcohols due to the restricted apertures in the host framework, being selective for allyl alcohol in a mixture of allyl and crotyl alcohol.



**Scheme 2.** Catalytic enantioselective oxidation of methyl *p*-tolyl sulfide by a manganese(III) porphyrin dimer within a box-shaped porphyrin-based host in toluene.<sup>7</sup>

As described in Chapter V, our group designed a strategy based on hexaaza macrocyclic dinuclear  $\text{Cu}^{\text{II}}$  complexes as directional bonding supramolecular entities that in combination with carboxylate linkers allows the self-assembly of small rectangles, extended helicates and porous like materials.<sup>10-12</sup> A step forward was the evolution from 2 D structures to 3D trigonal prisms with the use of tricarboxylate linkers.<sup>13</sup> Furthermore, the nature of tricarboxylate linkers introduced fluorescent or magnetic properties to the prismatic cages, thus constituting an important step towards the development of polyfunctional supramolecular nanovessels.



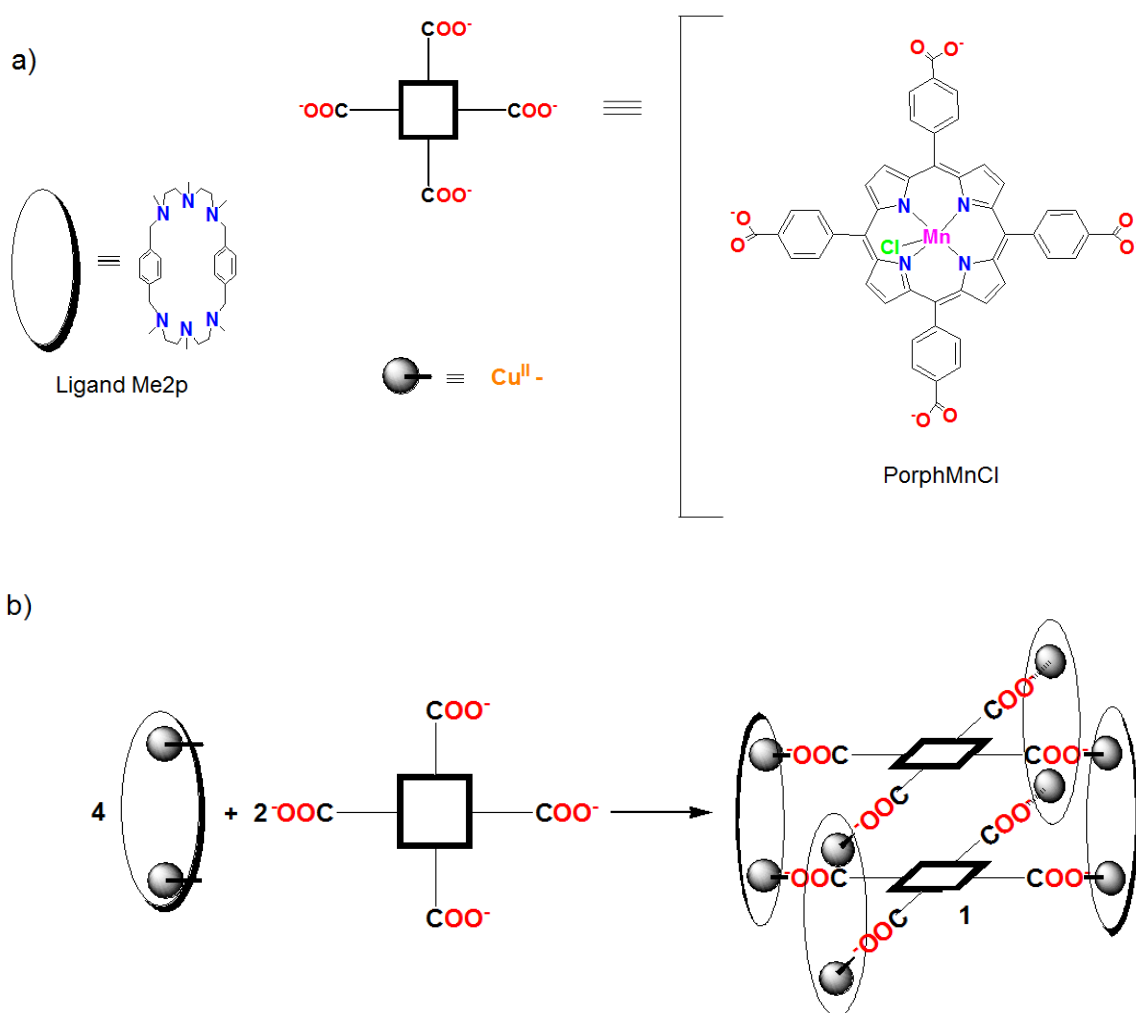
**Scheme 3.** Selective catalytic isomerisation of allylic alcohols by encapsulated rhodium catalyst in water.<sup>8</sup>

Taking in consideration the background of our group, the next challenge was to synthesize a supramolecular entity with catalytic properties in oxidation reactions. Porphyrins were the catalytic center of choice because their rigidity makes them convenient building blocks for planning supramolecular structures via directional coordination-driven interactions. Moreover, apart from been used for many years as models for P450 enzymes,<sup>14,15</sup> porphyrins have been also used as building blocks for many complex superstructures (scheme 1 and 2).<sup>1,16,17</sup>

## VI.2. Results and discussion

### VI.2.1. Synthesis of complex 1

Target cage compound  $[(\text{Cu}_2(\text{Me2p}))_4(\text{PorphMnCl})_2](\text{CF}_3\text{SO}_3)_8$ , **1**, was easily prepared at room temperature by reaction of 2 equivalents of the in situ prepared  $\text{HNEt}_3^+$  salt of the commercially available tetracarboxylate porphyrin linker PorphMnCl, **2**, (in  $\text{H}_2\text{O}/\text{CH}_3\text{CN}$  mixture) with four equivalents of the macrocyclic dicopper complex. The latter was previously prepared by 30 min stirring of a mixture of 4 equivalents of ligand Me2p and 8 equivalents of  $\text{Cu}(\text{CF}_3\text{SO}_3)_2$  in  $\text{CH}_3\text{CN}/\text{H}_2\text{O}$  (scheme 4). After overnight stirring, the solution was filtered and compound **1** was obtained in good yield (68%) upon slow diffusion of diethyl ether.



**Scheme 4.** Schematic representation of the building blocks (a) used in the synthesis of **1** (b).



## VI.2.2. Solid state structure

Single crystals suitable for X-ray diffraction were grown from slow diethyl ether diffusion over a DMF solution of **1**ClO<sub>4</sub> (same structure as **1** but ClO<sub>4</sub><sup>-</sup> instead of CF<sub>3</sub>SO<sub>4</sub><sup>-</sup> as counterion, for experimental details see section 4.3). The porosity of the 3D structure of **1**ClO<sub>4</sub> and the large amount of solvent and counterion residual density not easily assignable makes the crystal structure determination not straightforward. Even though the solution is provisional, X-Ray diffraction analysis served to ascertain the atom connectivity and 3D structure of the cage. It consists in two parallel porphyrins (Mn···Mn distance is 7.9 Å) linked by four macrocyclic dinuclear Cu<sup>II</sup> complexes (figure 1). Each porphyrin's carboxylate residue is linked by means of η<sup>1</sup>-O monodentate coordination to one Cu center. The metal center presents a rigid square-planar geometry as observed in 2D molecular rectangles and 3D trigonal prismatic cages already reported by us.<sup>10-13</sup> Altogether, the overall structure is defined as a tetragonal prismatic cage taking any set of eight equivalent atoms of the 4 carboxyphenyl moieties as vertices of the polyhedron. The overall dimensions of the supramolecular entity could be extracted by considering the eight copper ions as the hypothetical corners of a polyhedron (figure 1). Thus, the dimensions of the tetragonal prism are 6.8 x 17.3 x 15.8 Å<sup>3</sup> and the respective angles deviate slightly from 90°. The internal cavity is accessible to external molecules. Indeed, they are occupied by several distorted DMF molecules. A closer examination of the crystal packing of **1** shows the formation of nanosized one-dimensional channels along the *c* axis, and to a smaller degree, along *a* and *b* crystallographic axes (figure 2). Those channels are connected in the three dimensions and may allow for free diffusion of small molecules.

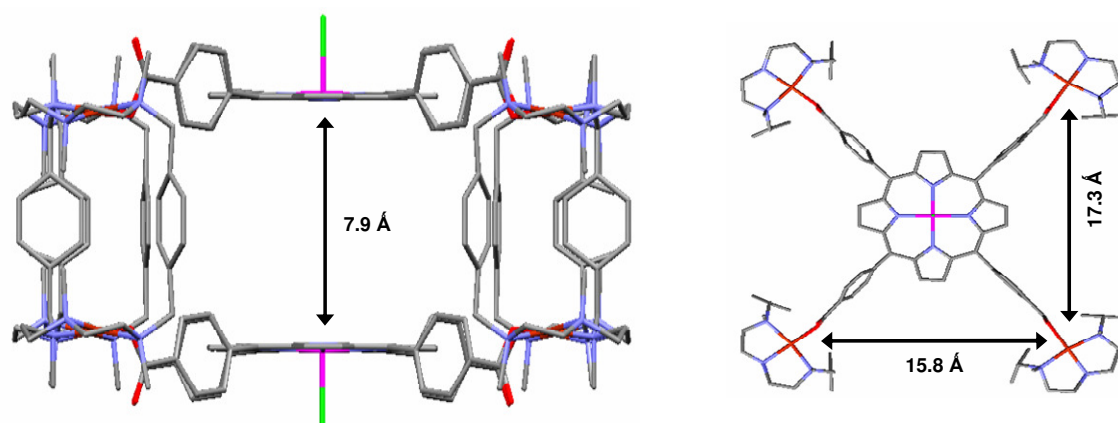


**Figure 1.** Side view (left) and up view (right) of the crystal structure of **1**ClO<sub>4</sub> along with the dimensions of the cage. Color code; orange (Cu), blue (N), red (O), pink (Mn), green (Cl), gray (C). Hydrogen atoms are omitted for clarity.

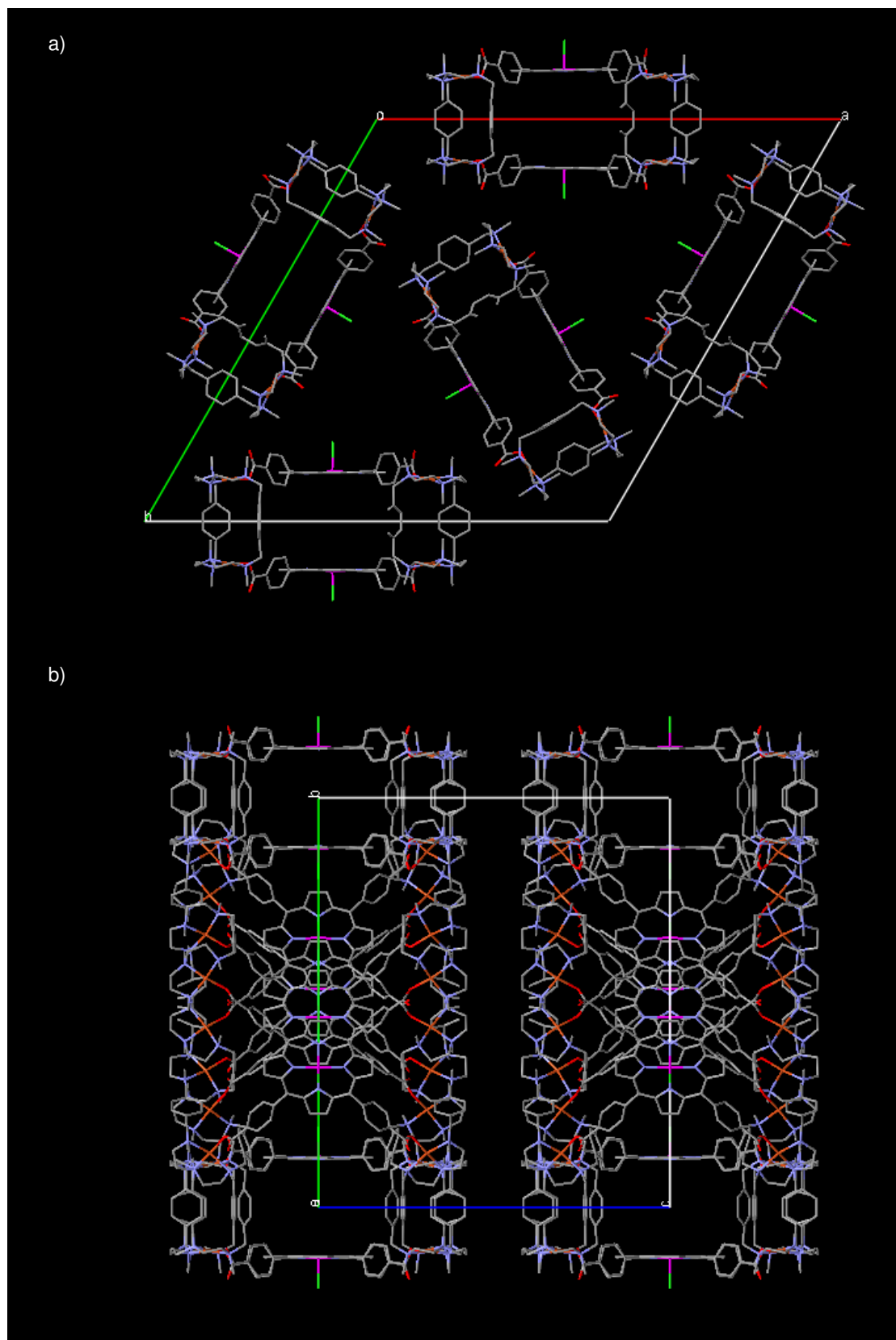


**Figure 2.** Crystal packing of  $1\text{ClO}_4$  showing (a) two kind of channels along  $c$  axis and (b) channels along axis  $a$ . Hydrogen atoms, solvent molecules and counterions are omitted for clarity. Color code; orange (Cu), blue (N), red (O), pink (Mn), green (Cl), gray (C).

### VI.2.3. Spectroscopic characterization

Cage **1** was spectroscopically characterized by FT-IR and UV-Vis spectroscopy. The most distinctive features of **1**'s IR spectra are two strong bands corresponding to the COO stretching. The high energy band is assigned to the  $\nu_{\text{asym}}$  COO stretching mode while the lower energy component corresponds to the  $\nu_{\text{sym}}$  mode (1622 and 1338  $\text{cm}^{-1}$ , respectively). Due to the low amount of characteristic IR peaks of metallo-porphyrin complexes, it was difficult to assign the rest of the observed peaks.

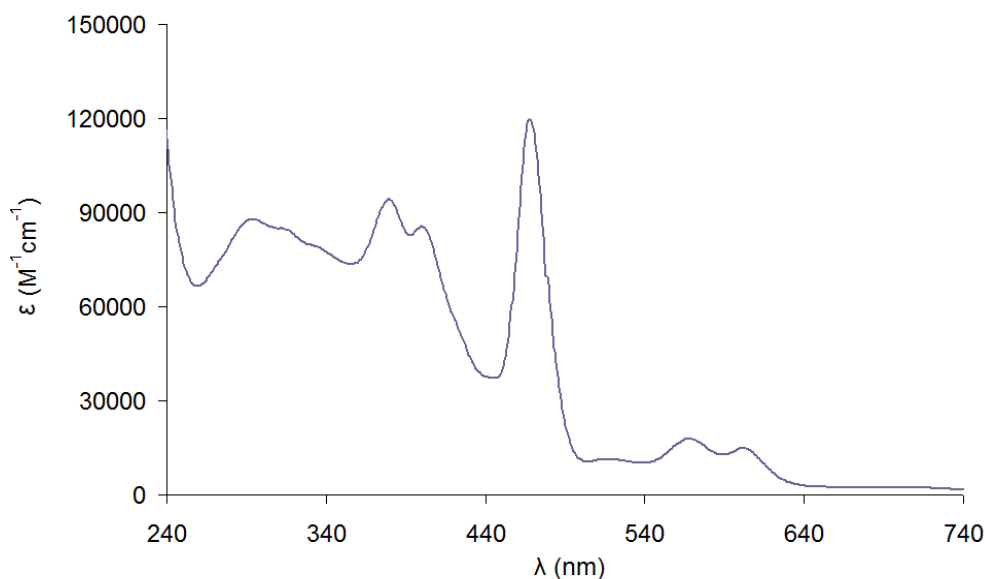


**Figure 3.** UV spectra of **1** in  $\text{CH}_3\text{CN}$ .

UV-Vis spectrum of **1** shows bands at  $\lambda = 468, 568$  and  $600$  nm characteristic of metalloporphyrins (Soret and Q bands, respectively) and around  $300$  nm corresponding to  $\pi\text{-}\pi^*$  transition of the aromatic rings of the macrocyclic ligands, indicating the presence of the both building blocks in the compound (figure 3). Furthermore, porphyrin's Soret and Q-bands do not shift noticeably in **1** with respect to **2**, confirming that the supramolecular structure in **1** entail minimal changes in the electronic properties of the manganese porphyrin.

### VI.2.4. Solution integrity

Analytical evidence for the molecular composition of **1** in solution was obtained by ESI-MS experiments in  $\text{CH}_3\text{CN}$  solution. Figure 4 shows the spectra recorded when  $100 \mu\text{M}$  solution of **1** in  $\text{CH}_3\text{CN}$  is subjected to analysis. The spectra is dominated by peaks assigned to  $[\mathbf{1} + 3\text{CH}_3\text{CN} - n(\text{CF}_3\text{SO}_3)]^{+n}$  suggesting that the structure observed in the X-Ray analysis is retained in solution in the catalytic conditions ( $[\mathbf{1}] = 0.5$  mM, see section VI.2.5).

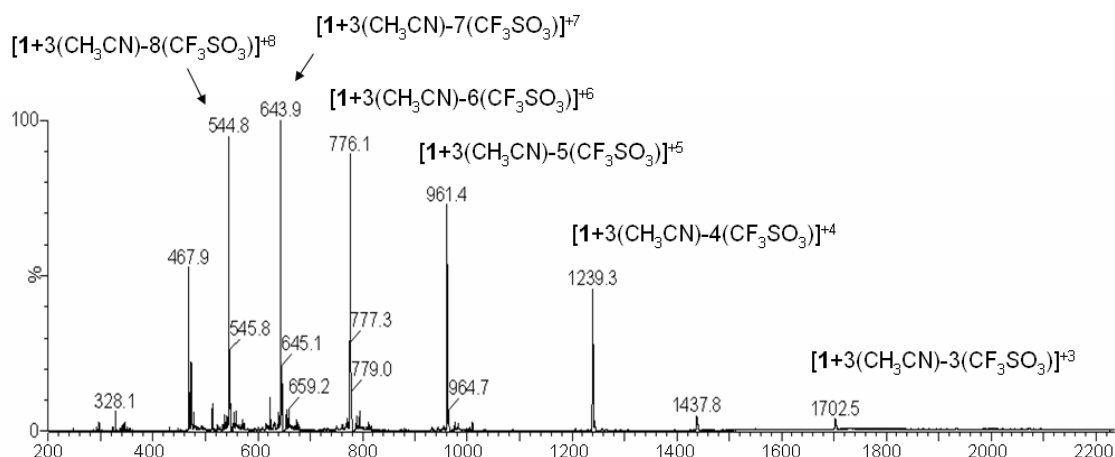


**Figure 4.** ESI-MS spectra of **1** along with the peak assignment. Experimental conditions:  $[1] = 100 \mu\text{M}$  in  $\text{CH}_3\text{CN}$ , cone voltage: 20 V.

### VI.2.5. Catalytic behaviour

The performance of the porphyrin-based nanostructure **1** in the catalytic oxidation of olefins was studied. Initial studies involved screening of different solvents and oxidants. Comparison between **1** and the porphyrin synthon **2** in the same conditions would give interesting clues about the influence of the 3D structure of **1** in catalysis. Unfortunately, solubility differences prevented those experiments. Typical reaction conditions with porphyrins as catalysts include monophasic or biphasic  $\text{CH}_2\text{Cl}_2$  layer as catalyst carrier. Presence of four carboxylate moieties in the phenyl rings in **2** and the supramolecular structure of **1** provide them special solubility properties. None of them are soluble in  $\text{CH}_2\text{Cl}_2$ . For this reason, other conditions were explored. **2** resulted insoluble in almost all solvents but water after addition of 5.4 equivalents of  $\text{K}_2\text{CO}_3$ . Moreover, addition of  $\text{CH}_3\text{CN}$  lowered the solubility of the porphyrin. The contrary happened with **1**, it was perfectly soluble in  $\text{CH}_3\text{CN}$  but insoluble in  $\text{H}_2\text{O}$ .

**Table 1.** Oxidation of *cis*-cyclooctene by **2** with different oxidants

| Oxidant                | Epoxide yield <sup>a</sup> |
|------------------------|----------------------------|
| PhIO                   | 80                         |
| mCPBA                  | 80                         |
| <sup>t</sup> BuOOH     | 27                         |
| $\text{H}_2\text{O}_2$ | 47                         |

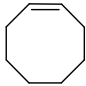
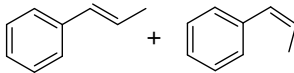
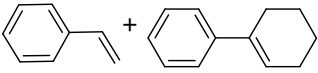
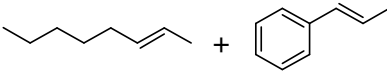
<sup>a</sup> **2**:oxidant *cis*-cyclooctene:imidazole 1:20:300:20 in water in presence of 5.4 equiv of  $\text{K}_2\text{CO}_3$ ,  $[2] = 0.5 \text{ mM}$ . PhIO and mCPBA were added at once, <sup>t</sup>BuOOH and  $\text{H}_2\text{O}_2$  were added dropwise over 10 minutes.

Oxidant screening was performed for **2** in the oxidation of *cis*-cyclooctene in water in presence of  $\text{K}_2\text{CO}_3$  (table 1), affording good yield and selectivity for the epoxide with PhIO and mCPBA as oxidants (80% epoxide yield in both cases). However, blank experiment with mCPBA in the same conditions but in absence of **2** afforded 65% yield, therefore this oxidant

was discarded. <sup>t</sup>BuOOH as oxidant afforded a mixture of products including 27% of epoxide, therefore it was also discarded. Finally, H<sub>2</sub>O<sub>2</sub> afforded a moderate yield of epoxide (47%).

On the other hand, **1** was tested in CH<sub>3</sub>CN using H<sub>2</sub>O<sub>2</sub> as oxidant obtaining 0.7 TN of epoxide (per porphyrin unit) showing possible cage decomposition. In contrast, PhIO converted *cis*-cyclooctene to its epoxide in 85% yield (account for 42 TN per porphyrin unit). Consequently, PhIO was the chosen oxidant for the rest of substrates.

**Table 2.** Comparison of yields and selectivities obtained by **1** and **2** in CH<sub>3</sub>CN and CH<sub>3</sub>CN/H<sub>2</sub>O solutions.<sup>a</sup>

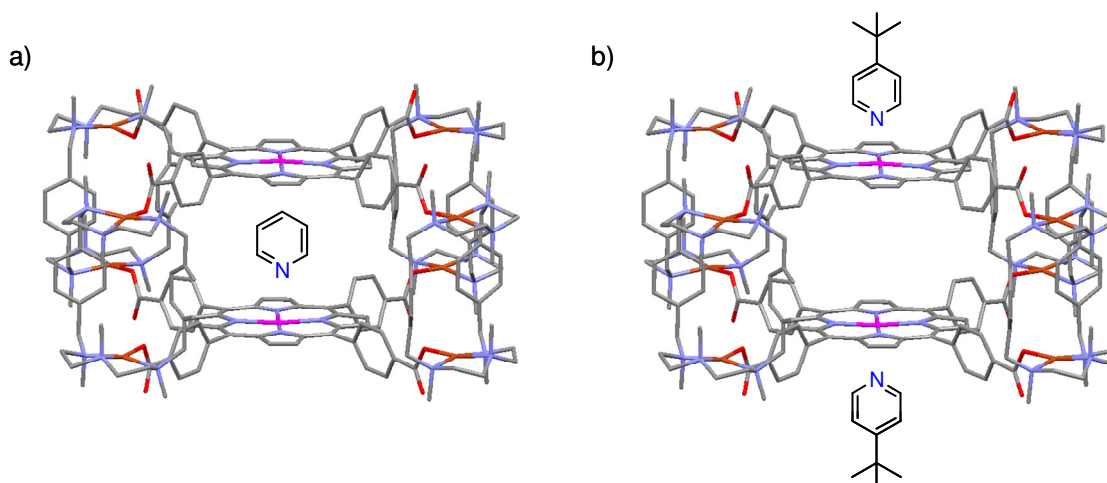
| substrate                                                                           | catalyst | solvent            |                                                  |
|-------------------------------------------------------------------------------------|----------|--------------------|--------------------------------------------------|
|                                                                                     |          | CH <sub>3</sub> CN | CH <sub>3</sub> CN/H <sub>2</sub> O <sup>b</sup> |
| Yield (%) <sup>c</sup>                                                              |          |                    |                                                  |
|    | <b>1</b> | 85                 | 20                                               |
|                                                                                     | <b>2</b> | 0                  | 80                                               |
| Selectivity                                                                         |          |                    |                                                  |
|    | <b>1</b> | 1 to 3             | 1 to 1.6                                         |
|                                                                                     | <b>2</b> | -                  | 1 to 1.4                                         |
|   | <b>1</b> | 1 to 2.9           | 1 to 1.9                                         |
|                                                                                     | <b>2</b> | -                  | 1 to 2.7                                         |
|  | <b>1</b> | 1 to 5             | 1 to 13                                          |
|                                                                                     | <b>2</b> | -                  | 1 to 26                                          |

<sup>a</sup> cat:PhIO:substrate, 1:100:1000 for catalyst **2** and 0.5:100:1000 for catalyst **1**. <sup>b</sup> CH<sub>3</sub>CN/H<sub>2</sub>O 2.3:1. <sup>c</sup> based on substrate converted to cyclooctene oxide.

Optimal solvent conditions for **1** and **2** are different. Comparison of **1** and **2** activities with CH<sub>3</sub>CN or CH<sub>3</sub>CN/H<sub>2</sub>O (2.3:1) as solvent showed that the solvent influence in the outcome of the reaction in terms of activity and selectivity prevent comparison of **1** and **2** in the same conditions (table 2). The low solubility of **2** in CH<sub>3</sub>CN resulted in no substrate conversion in those conditions; similarly, when **1** is used in a CH<sub>3</sub>CN/H<sub>2</sub>O mixture, a very low yield (20%) is obtained. That observation was corroborated in the competition of different olefins; selectivity strongly depends on the solvent and also on the catalyst (table 2).

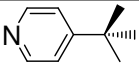
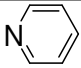
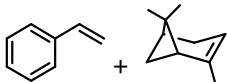
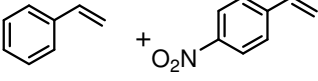
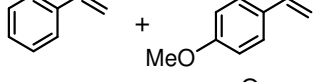
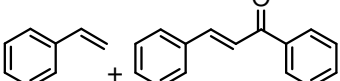
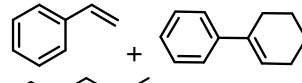
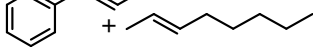
Therefore, another strategy was used to prove the influence of the supramolecular structure in **1**. Rowan, Nolte and co-workers described a system where control of the catalyst activity at the inner or outer side of the cavity is achieved through axial coordination of pyridine derivatives (scheme 26 in Chapter I).<sup>18,19</sup> In their work it is described that 1 equivalent of pyridine (py) is enough to ensure its coordination at the inner-cage face of the porphyrin units (scheme 5a), while 500 equivalents of <sup>t</sup>Bupy (4-*tert*-butylpyridine) are necessary to ensure coordination at the outer-cage face of the porphyrin (scheme 5b). In the latter case catalysis is forced to occur inside of the cavity. In addition, Collman and others reported “picnic basket” porphyrins (scheme 24 in Chapter I) to catalyze size selective and enantioselective epoxidation of olefins. In those

cases, 250 equivalents of bulky N-coordinating ligand per porphyrin unit were used to ensure the coordination at the outer-cage face of the porphyrin.<sup>20-23</sup>



**Scheme 5.** Drawing of the expected bonding of the auxiliary ligand at the inner-cage face of the porphyrin unit (a) or in the outer-cage face of the porphyrin unit for bulky ligands (b).

**Table 3.** Competitive oxidation of different pairs of olefins by **1**.<sup>a</sup>

| Entry | Substrate                                                                           | Selectivity                                                                                         |                                                                                                    |
|-------|-------------------------------------------------------------------------------------|-----------------------------------------------------------------------------------------------------|----------------------------------------------------------------------------------------------------|
|       |                                                                                     | Auxiliary ligand                                                                                    |                                                                                                    |
|       |                                                                                     | <br>(500 equiv) | <br>(5 equiv) |
| 1     |  | 15 to 1                                                                                             | 15 to 1                                                                                            |
| 2     |  | 10.3 to 1                                                                                           | 12.4 to 1                                                                                          |
| 3     |  | 1 to 2.1                                                                                            | 1 to 1.8                                                                                           |
| 4     |  | 2.3 to 1                                                                                            | 2.4 to 1                                                                                           |
| 5     |  | 1 to 2.3                                                                                            | 1 to 2.9                                                                                           |
| 6     |  | 1 to 6                                                                                              | 1 to 3.6                                                                                           |

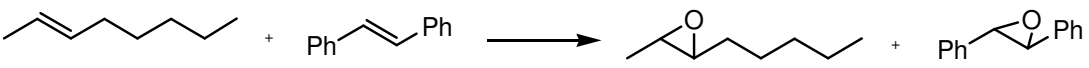
<sup>a</sup> **1**:PhIO:substrate, 0.5:100:1000 in CH<sub>3</sub>CN, yield in all cases is > 80%.

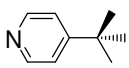
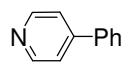
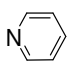
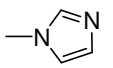
With the aim to force the catalysis to occur inside of the nanostructure, the addition of a bulky N-coordinating ligand such as <sup>1</sup>Bupy was explored. In principle, the bulkiness of this N-coordinating ligand prevents it to enter into the nanostructure, so it is forced to axially bind the metalloporphyrin at the outer-cage face. This was expected to force the oxidant-catalyst interaction to occur inside the cavity of the nanostructure. The contrary happens when smaller

N-coordinating ligands such as py or imidazole are used. Stabilizing cavity effects, which can be simply described as the entropically favorable filling of the empty cavity by the guest,<sup>24</sup> favor the coordination of those N-coordinating ligands at the inner-cage face, even at low concentrations, forcing the catalysis to occur at the outer-cage face. Selectivity in the competitive oxidation of several olefin pairs was evaluated in presence of 5 equivalents of py and 500 equivalents of <sup>t</sup>Bupy (table 3). Notably, in all studied cases 80-100% of conversion of oxidant into product was obtained.

Styrene derivatives were used to evaluate if electronic parameters play an important role in selectivity when the catalysis take place outside *versus* inside of the structure (entry 2 and 3, table 3). No selectivity change was observed and in both cases the more electron rich olefin is oxidized faster, indicating that electronic properties of the substrate are not important when inside/outside cage selectivities are compared. Other styrene derivatives, in this case with different steric properties, were evaluated (entry 4 and 5, table 3), however, no big changes in selectivity were observed. On the other hand, when aromatic flat olefins like styrene or stilbene compete with the aliphatic *trans*-2-octene noticeable changes in selectivity appeared (entry 6, table 3 and table 4). That indicates that probably drastic changes in shape and steric properties are needed in order to induce changes. In those cases, the selectivity for *trans*-2-octene is decreased when the reaction is forced to occur at the inner-cage face versus when reaction occurs at the outer-cage face of the porphyrin. A plausible interpretation of these observations is that the aromatic and flat structure of styrene and stilbene fits better in the cavity between the two porphyrins, increasing reactivity for those olefins.

**Table 4.** Competitive oxidation of different pairs of olefins by **1**.<sup>a</sup>



|                  | 500 equiv                                                                           |                                                                                     | 5 equiv                                                                             |                                                                                       | 0 equiv  |
|------------------|-------------------------------------------------------------------------------------|-------------------------------------------------------------------------------------|-------------------------------------------------------------------------------------|---------------------------------------------------------------------------------------|----------|
| Auxiliary ligand |  |  |  |  | --       |
| Selectivity      | 2.2 to 1                                                                            | 2.8 to 1                                                                            | 4.3 to 1                                                                            | 4.8 to 1                                                                              | 5.0 to 1 |

<sup>a</sup> **1**:PhIO:substrate, 0.5:100:1000 in CH<sub>3</sub>CN, [**1**] = 0.5 mM, yield in all cases is > 80%.

A more detailed study was done for the competition of *trans*-stilbene and *trans*-2-octene. Different N-coordinating ligands were evaluated; the selectivity in presence of 5 equivalents of small N-coordinating ligands like py or imidazole and 500 equivalents of bulkier N-coordinating ligands like <sup>t</sup>Bupy or *p*-phenylpyridine was compared with the selectivity obtained in absence of N-coordinating ligand (table 4). Two different behaviors were observed, *trans*-2-octene is oxidized about 4.5 times faster than stilbene when small N-coordinating ligands or none N-coordinating ligand are used. The use of bulkier N-coordinating ligands resulted in an increase of the oxidation of *trans*-stilbene (table 4). The more planar structure of this substrate

may be accommodated by weak interactions in the cavity formed between the two porphyrins, leading to an enhancement of the oxidation rate for this olefin.

### VI.3. Concluding remarks

The synthesis of a molecular nanocage constructed through metal self-assembly and its application in selective epoxidation of olefins is described. The synthesis is impressively facile, from commercially available porphyrin and easy to make dicopper complex. The catalytic properties of the system were studied in acetonitrile and using PhIO as the oxidant. In all studied cases epoxides were obtained in 80-100% yield respect to the oxidant. Moreover, the shape selectivity of the system could be easily tuned by the presence or absence of bulky N-coordinating ligands. The addition of those auxiliary ligands is supposed to force the catalysis to occur inside of the structure, facilitating the oxidation of those olefins with appropriate shape. More studies are required to understand the nature of these substrate-cage interactions.

### VI.4. Experimental section

#### IV.4.1. Instrumentation

IR spectra were recorded on a Mattson Satellite FT-IR using a MKII Golden Gate Single Reflection ATR System. UV-Vis spectroscopy was performed in a Cary 50 Scan (Varian) UV-Vis spectrophotometer. Elemental analyses were performed using a CHNS-O Elemental Analyzer EA-1108 from Fisons. The ESI-MS experiments were performed on a Micromass LCT mass spectrometer from Waters (UK) equipped with a Z-spray nanoelectrospray ionization source. Needles were made from borosilicate glass capillaries (Kwik-Fil, World Precision Instruments, Sarasota, FL) on a P-97 puller (Sutter Instruments, Novato, USA), coated with a thin gold layer by using an Edwards Scancoat (Edwards Laboratories, Milpitas, USA) six Pirani 501 sputter coater. Product analyses were performed on a Shimadzu GC-2010 gas chromatograph (Astec CHIRALDEXTM G-TA capillary column, 10 m x 0.25 mm) and a flame ionization detector.

#### VI.4.2. Materials

Solvents were purchased from SDS as reagent grade and used without further purification. Unless noted otherwise, all reagents were purchased from commercial sources and used as received. 5,10,15,20-tetra(4-carboxyphenyl)-porphyrin-Mn<sup>III</sup> chloride (PorphMnCl) was purchased from Porphyrin Systems. 3,6,9,16,19,22-hexamethyl-3,6,9,16,19,22-hexaazatricyclo[22.2.2.2<sup>11,14</sup>]triaconta-(26),11(12),13,24,27,29-hexaene, Me2p, was prepared according to the published procedure.<sup>25-27</sup>



### VI.4.3. Synthesis of complex 1

**[(Cu<sub>2</sub>(Me2p))<sub>4</sub>(PorphMnCl)<sub>2</sub>](CF<sub>3</sub>SO<sub>3</sub>)<sub>8</sub>, 1.** To a stirred suspension of 5,10,15,20-tetrakis(4-carboxyphenyl)-porphyrin-Mn<sup>III</sup> chloride (36.7 mg, 40.5 μmols) in H<sub>2</sub>O (2 mL), a solution of triethylamine (22.7 μL, 162 μmols) in CH<sub>3</sub>CN (0.4 mL) was added. The suspension was vigorously stirred for 30 min. Simultaneously, Me2p ligand (40 mg, 81 μmol) was dissolved in a CH<sub>3</sub>CN:H<sub>2</sub>O mixture (8:1, 9 mL) and a CH<sub>3</sub>CN solution (2 mL) of Cu(CF<sub>3</sub>SO<sub>3</sub>)<sub>2</sub> (61.2 mg, 162 μmol) was added dropwise under vigorous stirring forming a reddish-blue solution. The mixture was stirred for 30 min. Then, this solution was added dropwise to the porphyrin stirred suspension. After stirring overnight the green-brown solution was filtered through Celite ©. Ether diffusion over this solution afforded a brown solid. The solvent was decanted and the solid redissolved in CH<sub>3</sub>CN. Diethyl ether diffusion led to brown crystals (74.8 mg, 13.8 μmol, 68 %). Elemental analysis calcd for C<sub>224</sub>H<sub>248</sub>Cl<sub>2</sub>Cu<sub>8</sub>F<sub>24</sub>Mn<sub>2</sub>N<sub>32</sub>O<sub>40</sub>S<sub>8</sub>·13H<sub>2</sub>O: N, 7.91; C, 47.50; H, 4.88 %. Found: N, 8.34; C, 47.25; H, 4.59 %. FT-IR (ATR) ν, cm<sup>-1</sup>: 2926-2867 (C-H)<sub>sp3</sub>, 1622 (COO asym), 1340 (COO sym); 1250, 1223, 1156, 1028, 635 (CF<sub>3</sub>SO<sub>3</sub>); 1474, 770. ESI-MS (m/z): 1702.5 [1 + 3CH<sub>3</sub>CN - 3CF<sub>3</sub>SO<sub>3</sub>]<sup>+3</sup>, 1239.3 [1 + 3CH<sub>3</sub>CN - 4CF<sub>3</sub>SO<sub>3</sub>]<sup>+4</sup>, 961.4 [1 + 3CH<sub>3</sub>CN - 5CF<sub>3</sub>SO<sub>3</sub>]<sup>+5</sup>, 776.1 [1 + 3CH<sub>3</sub>CN - 6CF<sub>3</sub>SO<sub>3</sub>]<sup>+6</sup>, 643.9 [1 + 3CH<sub>3</sub>CN - 7CF<sub>3</sub>SO<sub>3</sub>]<sup>+7</sup> and 544.8 [1 + 3CH<sub>3</sub>CN - 8CF<sub>3</sub>SO<sub>3</sub>]<sup>+8</sup>. UV-Vis(CH<sub>3</sub>CN): λ<sub>max</sub>, nm (ε, M<sup>-1</sup>cm<sup>-1</sup>): 292 (sh), 377 (93400), 397 (sh), 468 (120000), 568 (18000) and 600 (15000).

Suitable crystals for X-Ray diffraction were grown from ether diffusion over a DMF solution of 1ClO<sub>4</sub>. This complex was prepared as described above but using Cu(ClO<sub>4</sub>)<sub>2</sub>·6H<sub>2</sub>O as copper source.

### VI.4.4. Crystal data

Crystals of 1ClO<sub>4</sub> were mounted on a nylon loop and used for low temperature (100(2) K) X-ray structure determination. The measurements were carried out using a Siemens *P4* diffractometer equipped with a SMART-CCD-1000 area detector, a MACScience Co rotating anode with graphite monochromated Mo Kα radiation (λ = 0.7173 Å) and a Siemens low-temperature device LT2 (T = -120°C). Full-sphere data collection using ω and φ scans was performed. The data collection was executed using SMART program. Absorption corrections were carried out using SADABS. Cell refinements and data reduction were made by the SAINT program. The structures were determined by direct methods using the SHELXTL program and refinement using full-matrix least-squares methods on F<sup>2</sup>. All non-hydrogen atoms were refined anisotropically.

1ClO<sub>4</sub> crystallizes in P-62m space group. Cell dimensions are: a = 36.9553 (11), b = 36.9553 (11), c = 27.5338 (18) Å, α = 90, β = 90 and γ = 90°. 14066 reflections were collected of which 7559 were unique. Final R indices [I > 2σ(I)] = R1 = 0.1288.

### VI.4.5. Catalytic conditions

#### *Oxidant screening (2:oxidant:cis-cyclooctene:imidazole, 1:20:300:20)*

0.5 mg of **2** (0.55  $\mu\text{mol}$ , 1 mol%) were weighted in a 4 mL vial. 25  $\mu\text{L}$  of an aqueous solution of  $\text{K}_2\text{CO}_3$  (19 mg/mL) were added along with 300  $\mu\text{L}$  of water and the solution was stirred until the complete solubilization of the porphyrin. Then, 0.75 mL of  $\text{CH}_3\text{CN}$  and imidazole (11  $\mu\text{mol}$ ) were added and the solution was stirred for 1 minute. *cis*-cyclooctene (0.17 mmols) was added at this point and the solution was stirred for another minute before starting the addition of the oxidant (11  $\mu\text{mol}$ ).  $^t\text{BuOOH}$  (1:10 solution in  $\text{CH}_3\text{CN}$  from 5-6 M solution commercially available) and  $\text{H}_2\text{O}_2$  (0.11 M  $\text{CH}_3\text{CN}$  solution from 35% commercially available) were added dropwise over 10 min; solid PhIO and mCPBA were added at once. The solution was stirred for 45 min at RT. The internal standard was added and the solution was passed through an alumina plug followed by elution with 0.5 mL of AcOEt. Finally the solution was subjected to GC analysis.

#### *Alkene oxidation with 2 as catalyst using PhIO in CH<sub>3</sub>CN/H<sub>2</sub>O. (2:PhIO:alkene, 1:100:1000).*

0.5 mg of **2** (0.55  $\mu\text{mol}$ , 1 mol%) were weighted in a 4 mL vial. 25  $\mu\text{L}$  of an aqueous solution of  $\text{K}_2\text{CO}_3$  (19 mg/mL) were added along with 300  $\mu\text{L}$  of water and the solution was stirred until the complete solubilization of the porphyrin. Then, 0.75 mL of  $\text{CH}_3\text{CN}$  and the appropriate N-coordinating ligand (pyridine, imidazole (1  $\mu\text{mol}$ ) or  $^t\text{Bupy}$ , 4-phenylpyridine (100  $\mu\text{mol}$ )) were added and the solution was stirred for 1 minute. The alkene/s (0.55 mmols 10 equiv) was/were added at this point and the solution was stirred for another minute before solid PhIO (55  $\mu\text{mol}$ , 1 equiv) was added. The solution was stirred for 45 min at RT. An internal standard was added and the solution was passed through an alumina plug followed by elution with 0.5 mL of AcOEt. Finally the solution was subjected to GC analysis. The formation of *trans*-stilbene epoxide was followed through  $^1\text{H-NMR}$  using mesitylene as internal standard: The solvent from the crude mixture was removed under reduced pressure, the internal standard and  $\text{CDCl}_3$  were added and the sample was analyzed by  $^1\text{H-NMR}$ .

#### *Alkene oxidation with 1 as catalyst using PhIO in CH<sub>3</sub>CN. (1:PhIO:alkene, 0.5:100:1000).*

A 4 mL vial was charged with 0.2 mL of a 0.5 mM  $\text{CH}_3\text{CN}$  solution of the catalyst **1** (0.1  $\mu\text{mol}$ , 1 mol%), the appropriate N-coordinating ligand (pyridine, imidazole (1  $\mu\text{mol}$ ) or  $^t\text{Bupy}$ , 4-phenylpyridine (100  $\mu\text{mol}$ )) and a magnetic stir bar were added. The solution was stirred for a minute and then the alkene/s (0.2 mmols 10 equiv) was/were added and the solution was stirred for another minute before solid PhIO (20  $\mu\text{mol}$ , 1 equiv each substrate) was added. The solution was stirred for 45 min at RT. The internal standard was added and the solution was passed through an alumina plug followed by elution with 0.5 mL of AcOEt. Finally the solution was subjected to GC analysis. The formation of *trans*-stilbene epoxide was followed through  $^1\text{H-NMR}$  using mesitylene as internal standard: The solvent from the crude mixture was removed

under reduced pressure, the internal standard and  $\text{CDCl}_3$  were added and the sample was analyzed by  $^1\text{H-NMR}$ . For reactions collected in table 4 the reactions were performed directly in  $\text{CD}_3\text{CN}$  and the selectivities and yields measured by  $^1\text{H-NMR}$ .

When reactions were done in  $\text{CH}_3\text{CN}/\text{H}_2\text{O}$  mixture, same experimental conditions as above were used but starting from 273  $\mu\text{L}$  of a 0.36 mM acetonitrile solution of **1** and adding 118  $\mu\text{L}$  of water leading to a catalyst **1** concentration of 0.25 mM and 0.5 mM concentration of porphyrin unit.

## VI.5. References

1. Leininger, S.; Olenyuk, B.; Stang, P. J. *Chem. Rev.* **2000**, *100*, 853-907.
2. Fujita, M.; Tominaga, M.; Hori, A.; Therrien, B. *Acc. Chem. Res.* **2005**, *38*, 369-378.
3. Holliday, B. J.; Mirkin, C. A. *Angew. Chem. Int. Ed.* **2001**, *40*, 2022-2043.
4. Fiedler, D.; Leung, D. H.; Bergman, R. G.; Raymond, K. N. *Acc. Chem. Res.* **2005**, *38*, 349-358.
5. Lehn, J. M. *Supramolecular Chemistry*; VCH: New York, 1995.
6. Caulder, D. L.; Raymond, K. N. *Acc. Chem. Res.* **1999**, *32*, 975-982.
7. Lee, S. J.; Cho, S.-H.; Mulfort, K. L.; Tiede, D. M.; Hupp, J. T.; Nguyen, S. T. *J. Am. Chem. Soc.* **2008**, *130*, 16828-16829.
8. Leung, D. H.; Bergman, R. G.; Raymond, K. N. *J. Am. Chem. Soc.* **2007**, *129*, 2746 – 2747.
9. Yoshizawa, M.; Klosterman, J. K.; Fujita, M. *Angew. Chem. Int. Ed.* **2009**, *48*, 3418-3438.
10. Company, A.; Jee, J.-E.; Ribas, X.; Lopez-Valbuena, J. M.; Gómez, L.; Corbella, M.; Llobet, A.; Mahía, J.; Benet-Buchholz, J.; Costas, M.; Eldik, R. v. *Inorg. Chem.* **2007**, *46*, 9098-9110.
11. Company, A.; Gómez, L.; Lopez Valbuena, J. M.; Mas-Balleste, R.; Benet-Buchholz, J.; Llobet, A.; Costas, M. *Inorg. Chem.* **2006**, *45*, 2501-2508.
12. Gómez, L.; Company, A.; Fontrodona, X.; Ribas, X.; Costas, M. *Chem. Commun.* **2007**, *42*, 4410-4412.
13. Company, A.; Roques, N.; Güell, M.; Mugnaini, V.; Gómez, L.; Imaz, I.; Datcu, A.; Solà, M.; Luis, J. M.; Veciana, J.; Ribas, X.; Costas, M. *Dalton Trans.* **2008**, *13*, 1679-1682.
14. Meunier, B. *Chem. Rev.* **1992**, *92*, 1411-1456.
15. Collman, J. P.; Zhang, X.; Lee, V. J.; Uffelman, E. S.; Brauman, J. I. *Science* **1993**, *261*, 1404-1411.

16. Beletskaya, I.; Tyurin, V. S.; Tsivadze, A. Y.; Guillard, R.; Stern, C. *Chem. Rev.* **2009**, *109*, 1659–1713.
17. Lee, S. J.; Hupp, J. T. *Coord. Chem. Rev.* **2006**, *250*, 1710-1723.
18. Elemans, J. A. A. W.; Bijsterveld, E. J. A.; Rowan, A. E.; Nolte, R. J. M. *Chem. Commun.* **2000**, 2443-2444.
19. Thordarson, P.; Bijsterveld, E. J. A.; Rowan, A. E.; Nolte, R. J. M. *Nature* **2003**, *424*, 915-918.
20. Collman, J. P.; Brauman, J. I.; Fitzgerald, J. P.; Hampton, P. D.; Maruta, Y.; Michida, T. *Bull. Chem. Soc. Jpn.* **1988**, *61*, 47-57.
21. Konishi, K.; Oda, K.-I.; Nishida, K.; Aida, T.; Inoue, S. *J. Am. Chem. Soc.* **1992**, *114*, 1313-1317.
22. Collman, J. P.; Lee, V. J.; Zhang, X.; Ibers, J. A.; Brauman, J. I. *J. Am. Chem. Soc.* **1993**, *115*, 3834-3835.
23. Collman, J. P.; Lee, V. J.; Kellen-Yuen, C. J.; Zhang, X.; Ibers, J. A.; Brauman, J. I. *J. Am. Chem. Soc.* **1995**, *117*, 692-703.
24. Reek, J. N. H.; Priem, A. H.; Engelkamp, H.; Rowan, A. E.; Elemans, J. A. A. W.; Nolte, R. J. M. *J. Am. Chem. Soc.* **1997**, *119*, 9956-9964.
25. Menif, R.; Martell, A. E.; Squattrito, P. J.; Clearfield, A. *Inorg. Chem.* **1990**, *29*, 4723-4729.
26. Pietraszkiewicz, M.; Gasiorowski, R. *Chem. Ber.* **1990**, *123*, 405-406.
27. Clifford, T.; Danby, A. M.; Lightfoot, P.; Richens, D. T.; Hay, R. W. *J. Chem. Soc. Dalton. Trans.* **2001**, 240-246.

## **CHAPTER VII**

---

### **General Conclusions**

---



## VII. General conclusions

- ◆ A new family of N<sub>4</sub>-tetradentate ligands (L1-L5) has been prepared. Their structure consists of an aliphatic diamine backbone from which two 2-methylpyridine-4,5-pinene arms are appended. Corresponding mononuclear iron(II) complexes [Fe(CF<sub>3</sub>SO<sub>3</sub>)<sub>2</sub>(L)], (**1OTf-5OTf**), have been synthesized and structurally and spectroscopically characterized. The performance of the prepared mononuclear iron(II) complexes as alkane and alkene oxidation catalysts has been evaluated. The high activity and robustness of this family of complexes is based in three key aspects: (1) the strong electron-donating nature of the ligand, (2) a *cis-α* octahedral topology that enforces two *cis* labile metal coordination sites available for exogenous ligands (substrate, oxidant, e.g.) and (3) the steric protection of the metal center by a hydrophobic cavity created by the ligand. Such robust character allows the catalysts to stand the harsh conditions used to oxidize alkanes and alkenes.
- ◆ In the oxidation of unactivated tertiary C-H bonds, **1OTf-5OTf** are remarkably efficient, and hydroxylation reactions proceed with high stereoretention (>99%). Those results compare favourably with state of the art iron catalysts for alkane oxidation. Moreover, oxidation of a chiral substrate shows that the topological chirality of the complex can be an important factor in the oxidation of chiral substrates, which opens the door to the development of stereoselective C-H hydroxylation Fe-based catalysts.
- ◆ The steric hindrance of the catalyst proves to be crucial for enhancing the stability of the catalysts, most likely by precluding bimetallic decomposition pathways and/or formation of catalytically non-competent oxo-bridged dimers.
- ◆ Mechanistic studies concluded that metal based oxidants instead of long lived radicals are involved in the reaction mechanism.
- ◆ In Alkene oxidation moderate to good yields were obtained for the corresponding epoxide with stereoretention. The reactions are performed using low catalyst loading and show high efficiencies in the conversion of the H<sub>2</sub>O<sub>2</sub> into products.
- ◆ Manganese(II) analogue complexes (**Λ-2Mn** and **Δ-3Mn**) with pinene-containing ligands L2 and L3 have been synthesised and characterized (Chapter IV). The performance of these manganese catalysts was evaluated in asymmetric alkene oxidation using peracetic acid as oxidant. A broad range of olefins were oxidized in moderate to good yields to the corresponding epoxide using low catalyst loadings (down to 0.1%) of catalyst **Λ-2Mn**. The ee's obtained, even though moderate, are remarkable for a non-SALEN manganese complex.
- ◆ Self-assembled molecular rectangles and helicates were prepared via the self-assembly of macrocyclic dicopper clips with carboxylate linkers (Chapter V). The supramolecular outcome of this family of compounds can be controlled by the initial design of the macrocyclic ligand, the

length and nature of the dicarboxylate spacer and also the selected counteranion, giving the possibility of obtaining structures ranging from differently sized rectangles to double-stranded helicates. Further subtle control on the 3D packing of these compounds allows, for instance, the creation of nanosized monodimensional channels. The structural versatility of our approach and its synthetic simplicity offers a powerful method to prepare complex suprastructures via the use of different polycarboxylate linkers, metal ions and counterions.

◆ We have taken advantage of the above supramolecular strategy to construct supramolecular nanovessels with catalytic properties in oxidation processes. As a proof of concept, a catalytic nanoreactor was constructed using a tetracarboxylic metalloporphyrin group as both linker and catalytic centre, in combination with macrocyclic dicopper complexes as structural units to define the dimensions and shape of the cavities. Modest shape selectivity was achieved in catalytic oxidation reactions of alkenes when the catalysis is forced to occur in the inside of the cavity. This study serves as a basis for an in-depth exploration of the catalytic activity of differently shaped nanoreactors.



---

## **Annex**

---



# Table of contents

|                                    |           |
|------------------------------------|-----------|
| <b>ANNEX.1 – CHAPTER III .....</b> | <b>5</b>  |
| <b>ANNEX.2 – CHAPTER IV .....</b>  | <b>77</b> |
| <b>ANNEX.3 – CHAPTER V .....</b>   | <b>81</b> |
| <b>ANNEX.4 – CHAPTER VI .....</b>  | <b>87</b> |



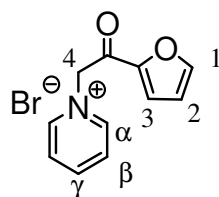
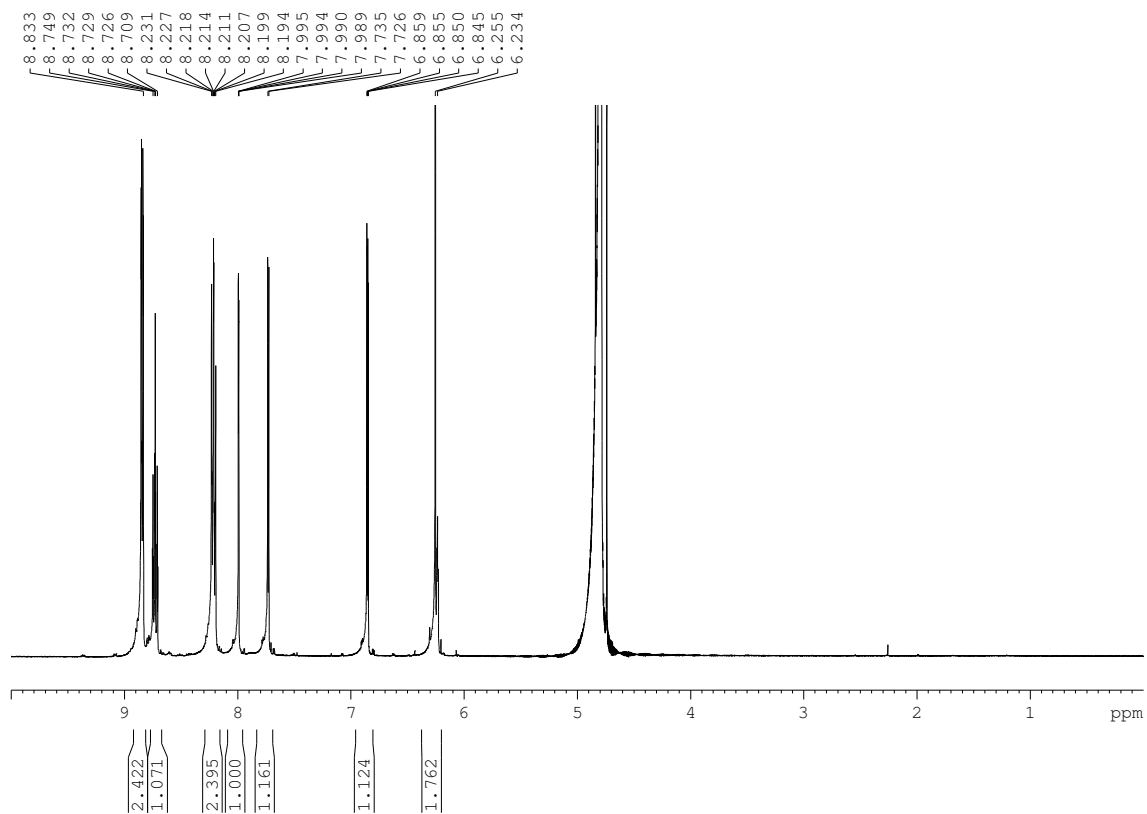
---

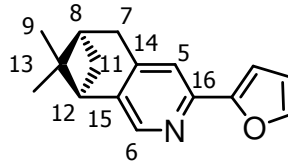
## **Annex.1 – Chapter III**

---

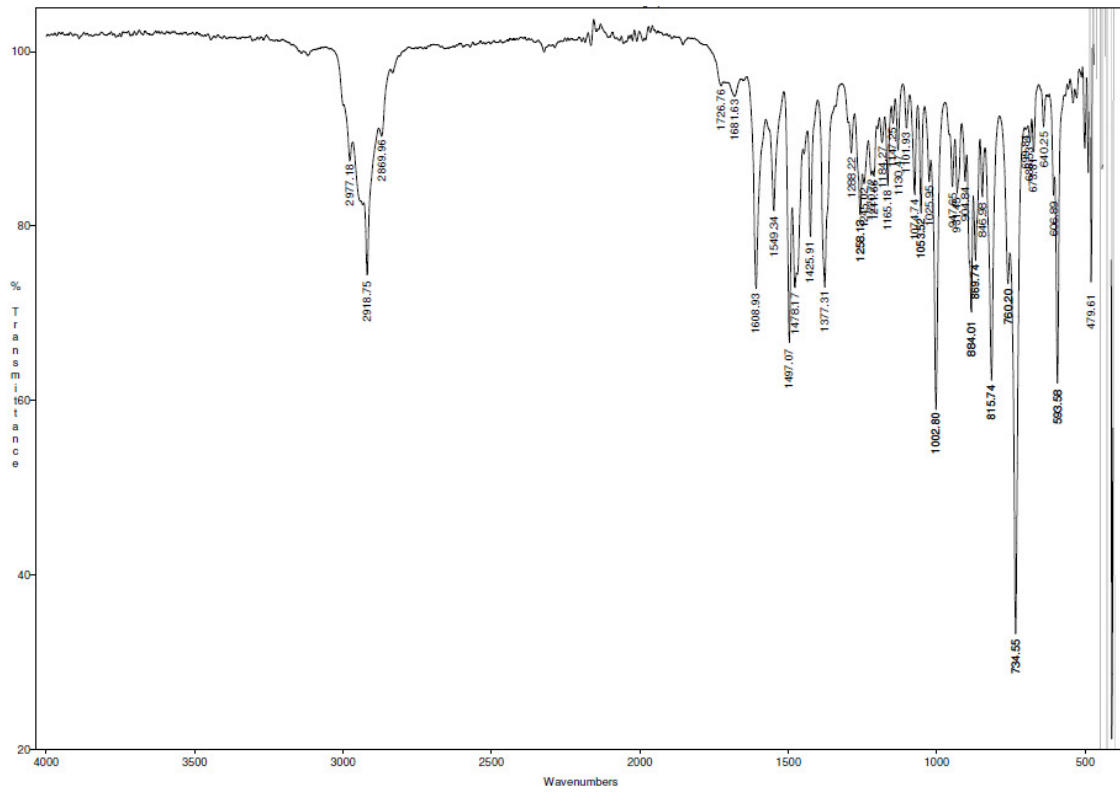


## Pyridinium Salt

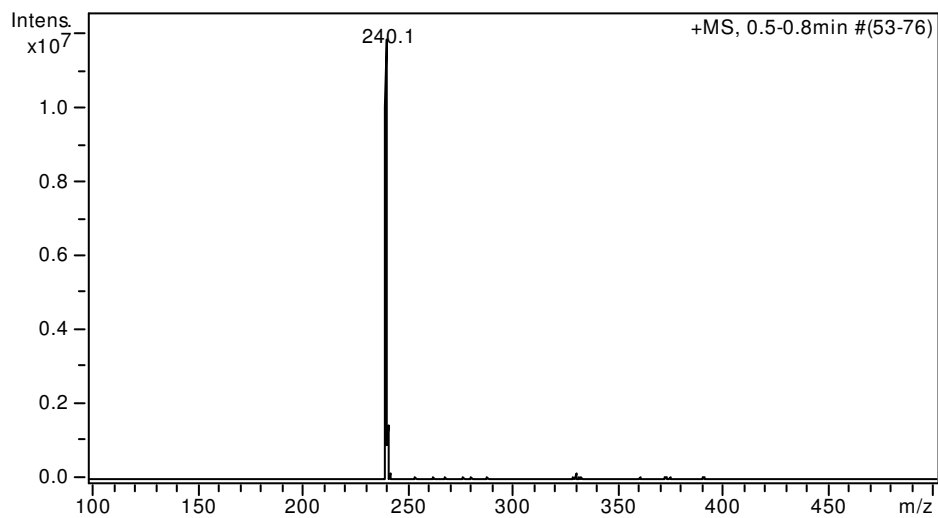
**<sup>1</sup>H-NMR (D<sub>2</sub>O, 400 MHz, 300K)**

*(R)*-4,5-pinene-2-(furan-2-yl)-pyridine, *(R)*-pinene-Pyfuran

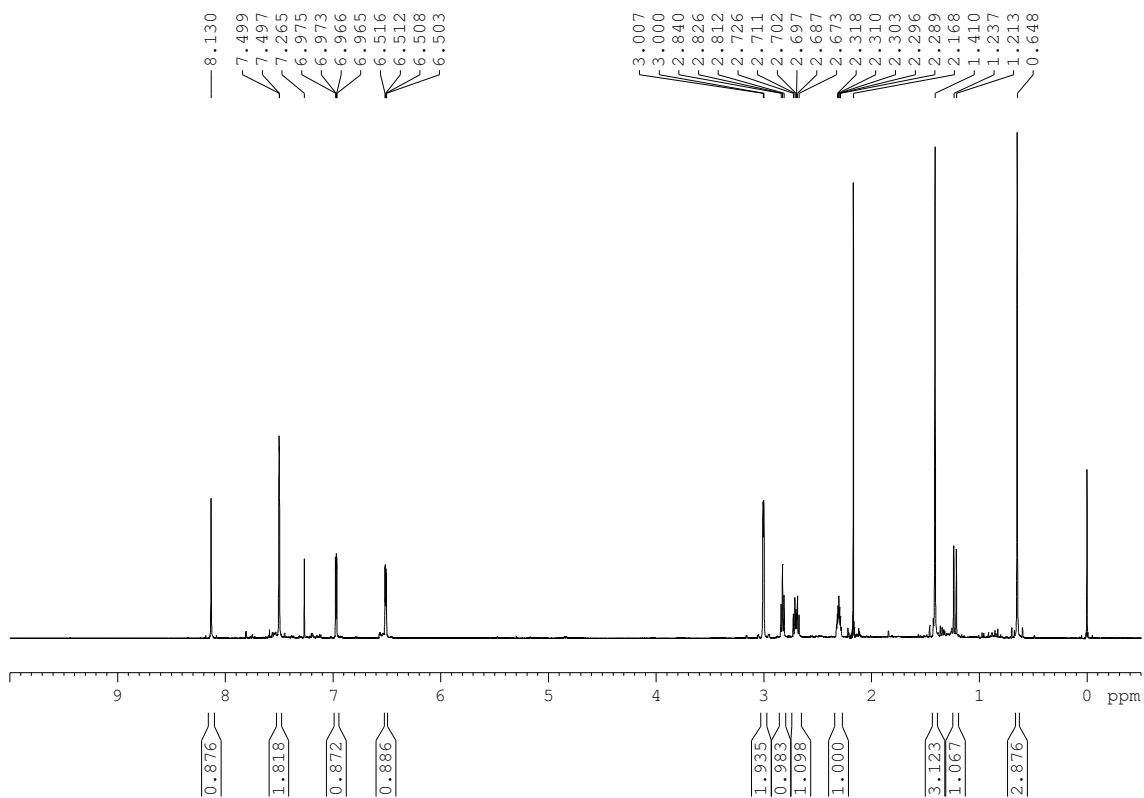
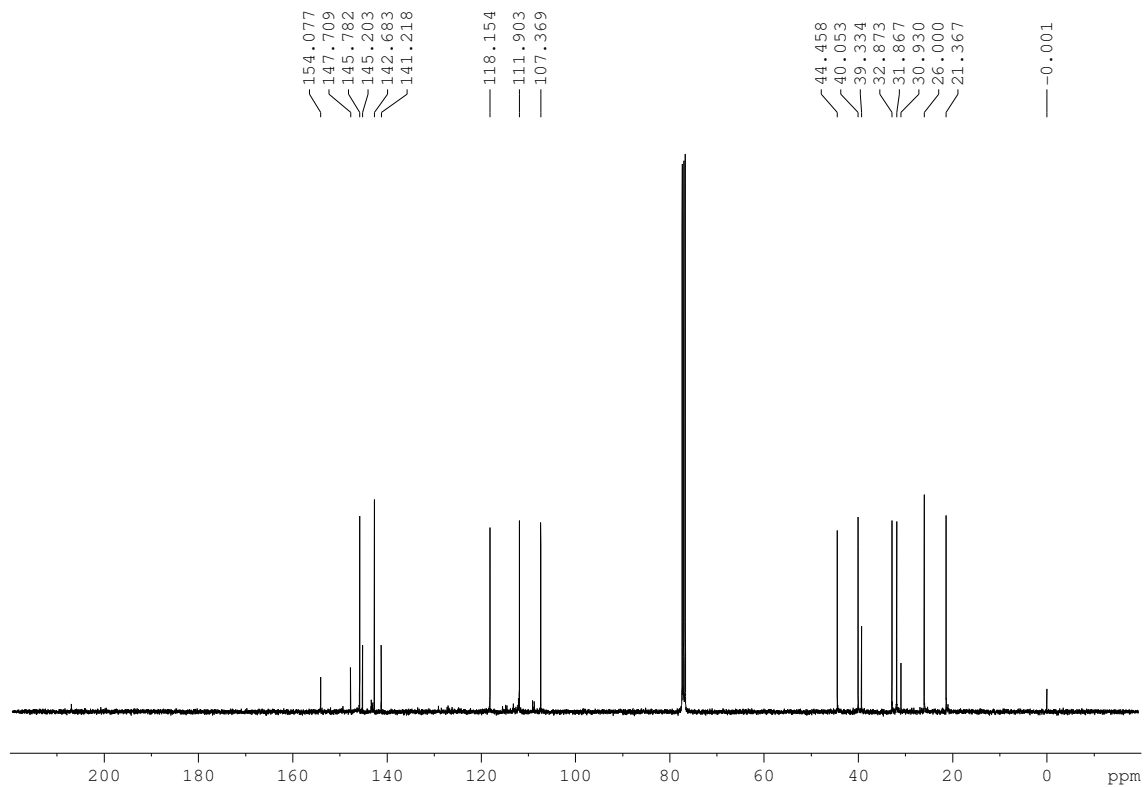
## FT-IR (ATR)



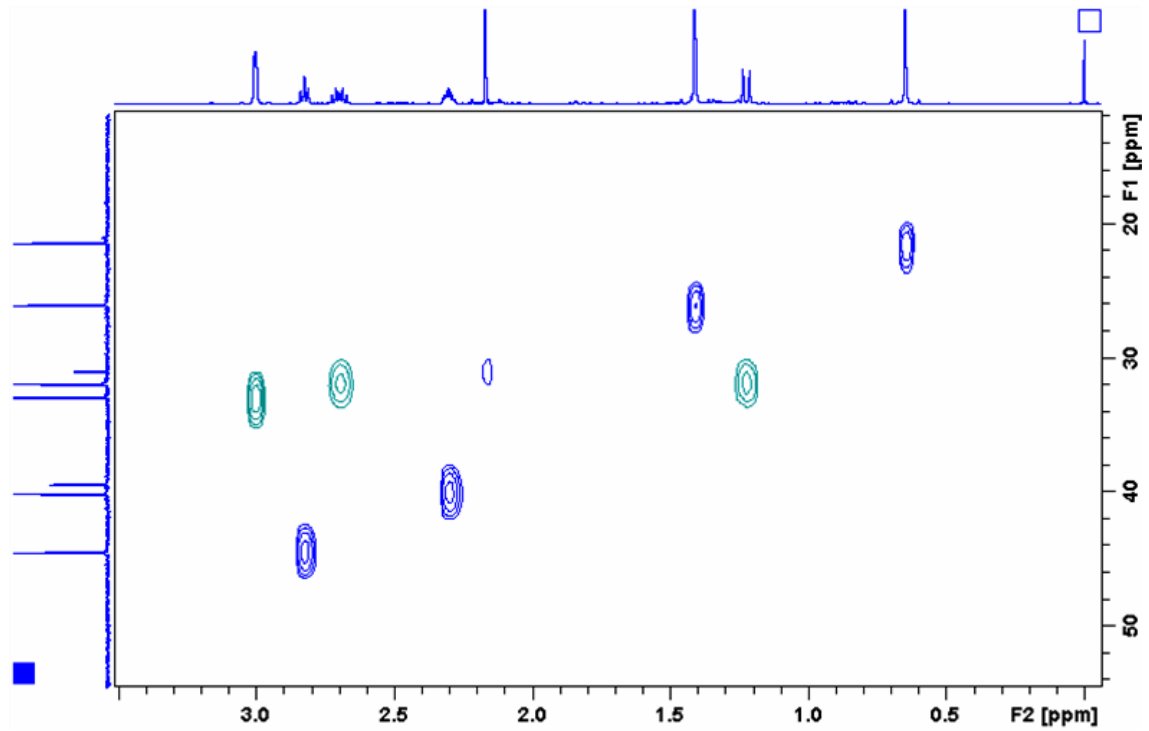
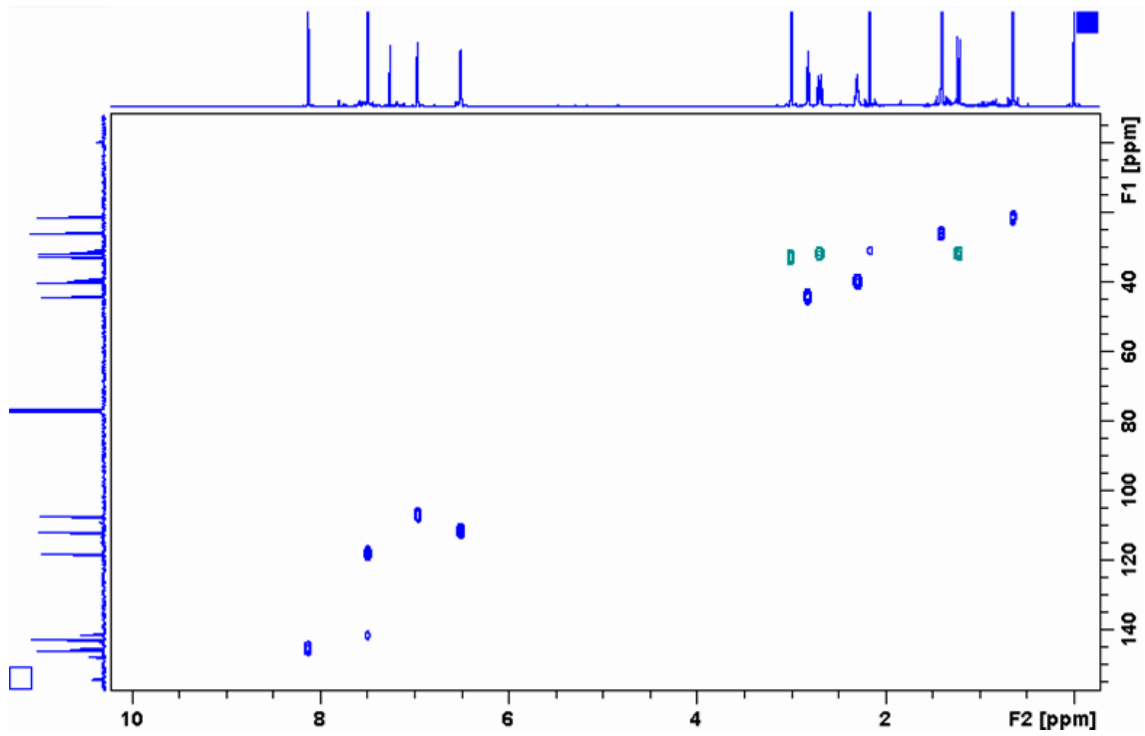
## ESI-MS

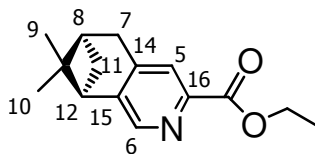
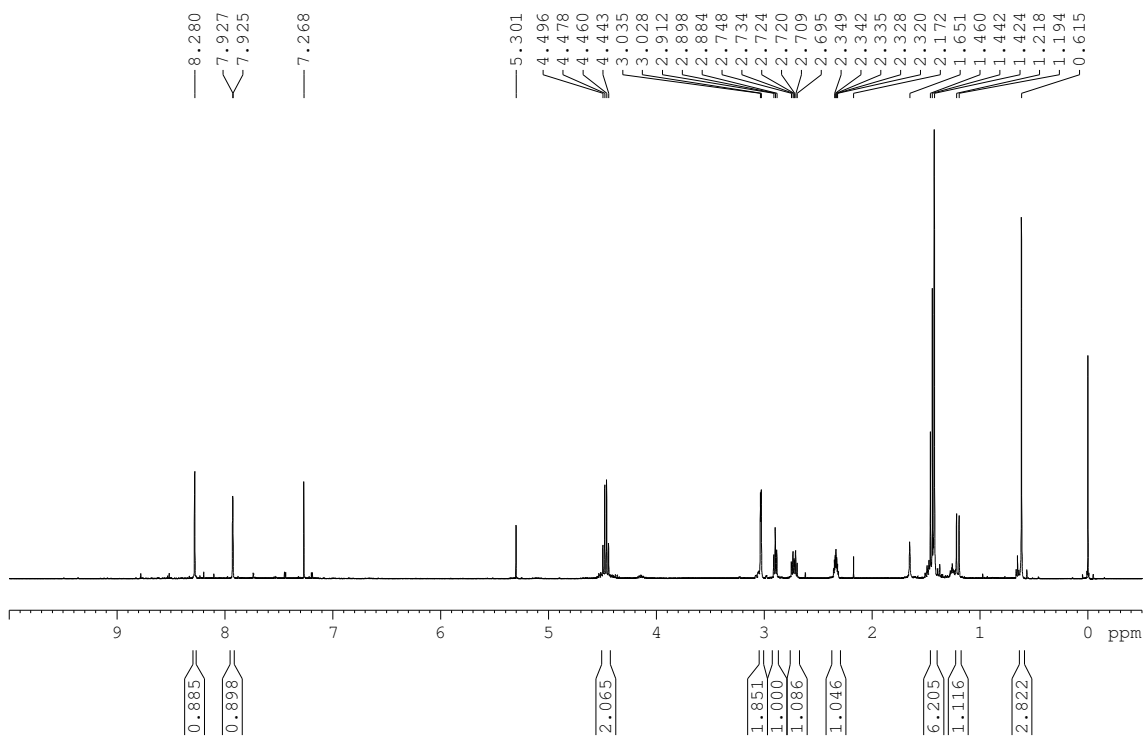
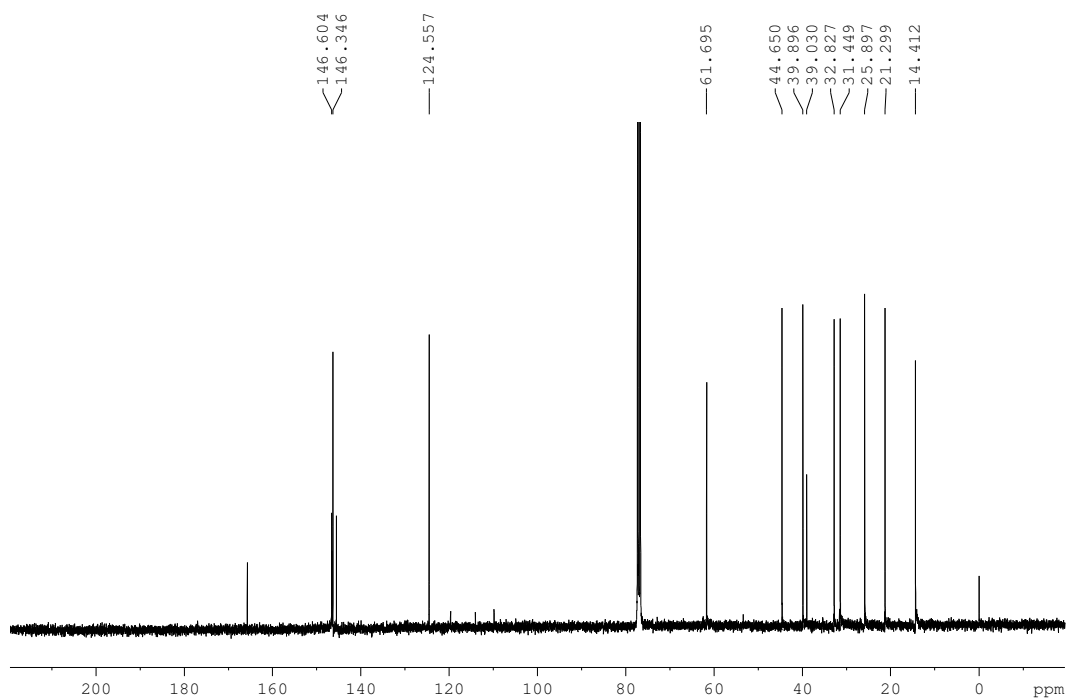




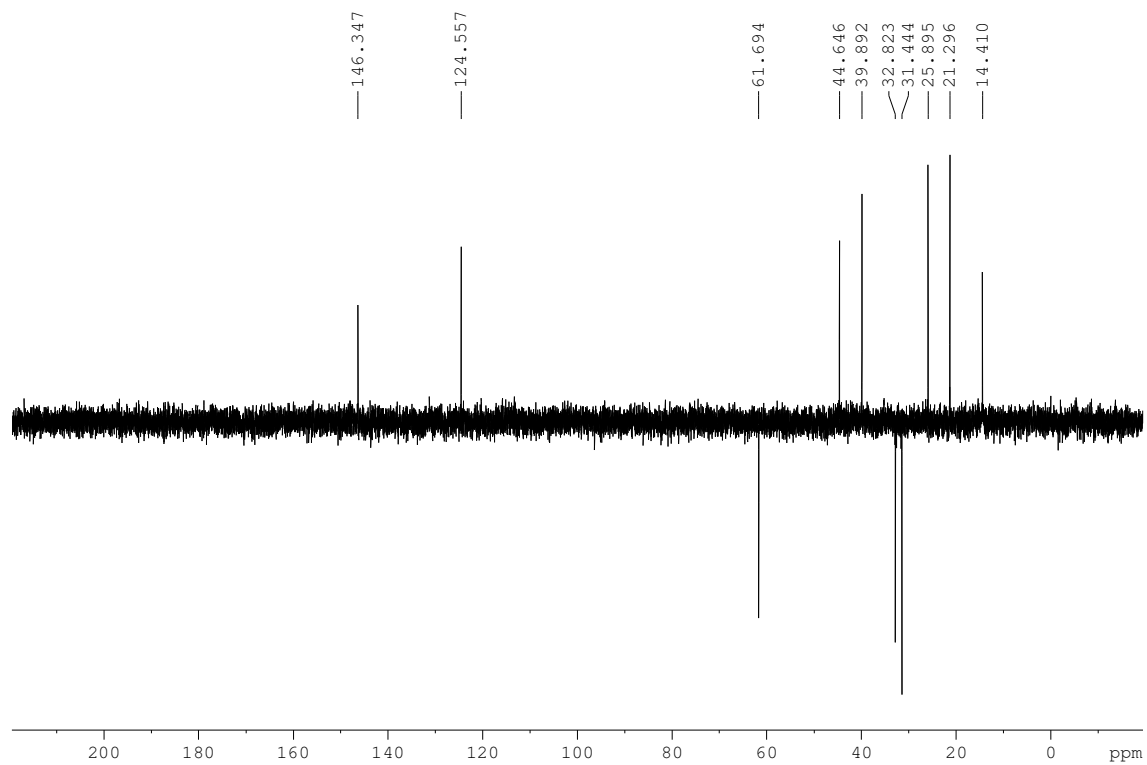
**$^1\text{H-NMR}$  ( $\text{CDCl}_3$ , 400 MHz, 300K)** **$^{13}\text{C-NMR}$  ( $\text{CDCl}_3$ , 100 MHz, 300K)**

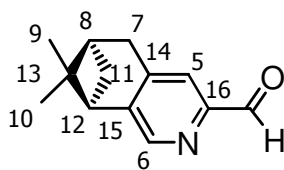
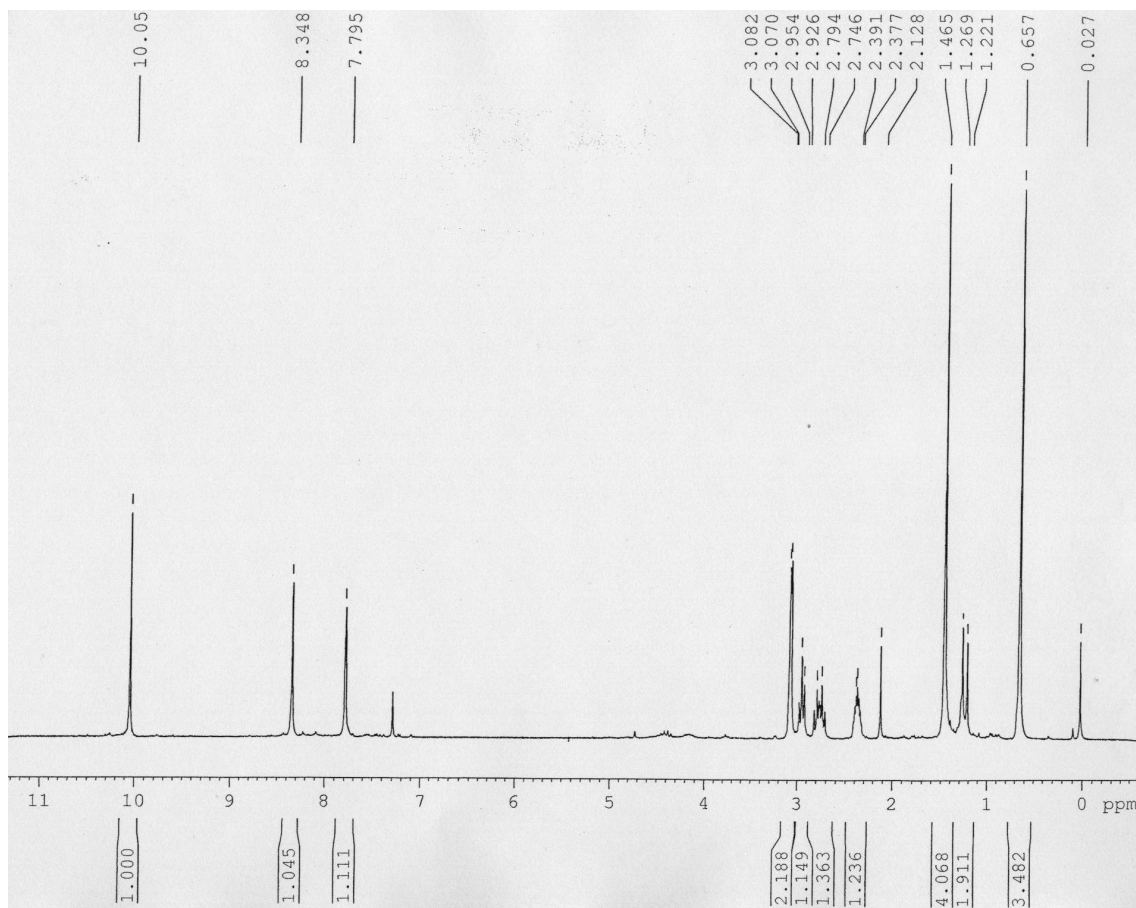
**HSQCed (CDCl<sub>3</sub>, 400 Mz, 300K)**

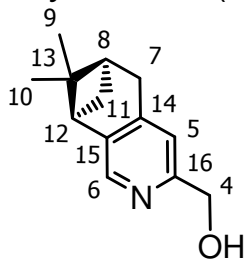
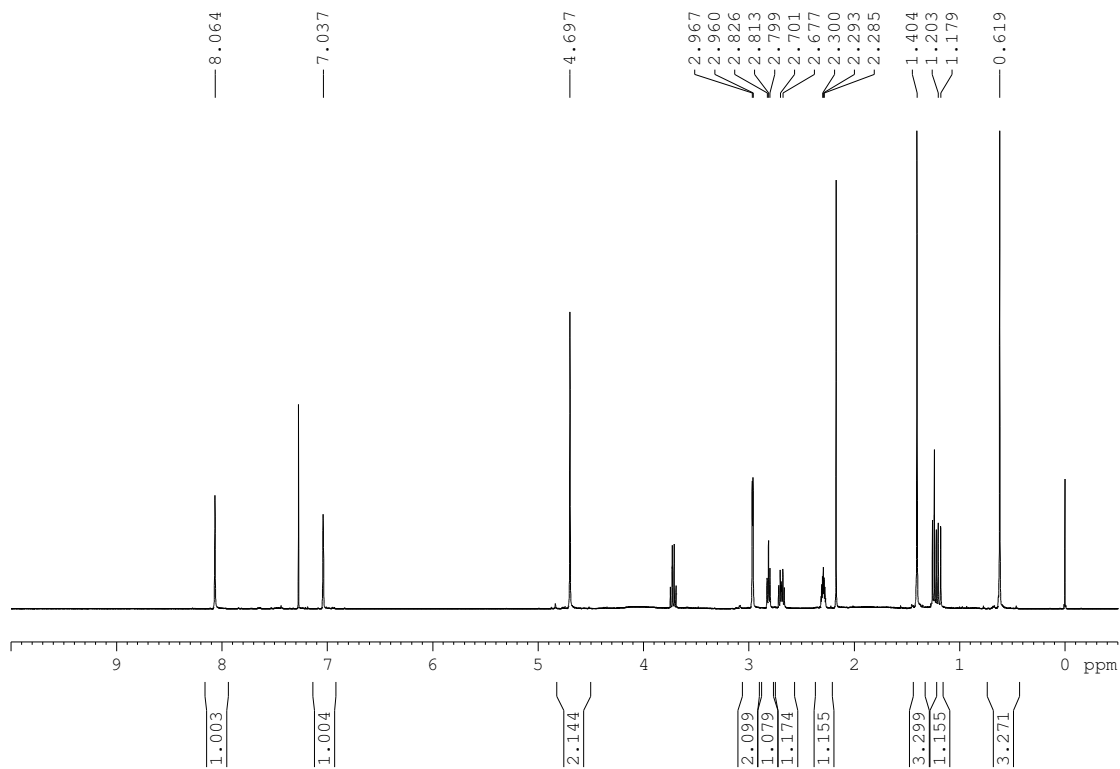
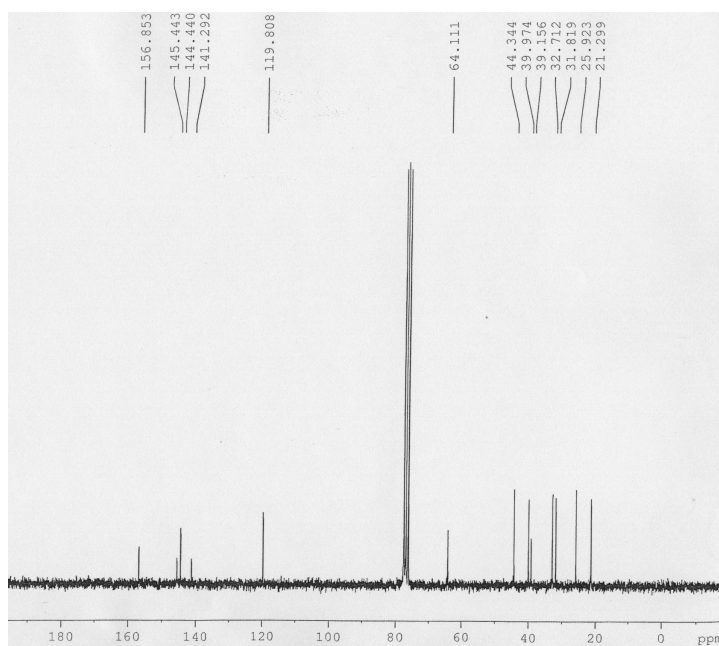


*(R)*-4,5-pinene-2-picolyl ethyl ester, *(R)*-pinene-PyCOOEt<sup>1</sup>H-NMR (CDCl<sub>3</sub>, 400 MHz, 300K)<sup>13</sup>C-NMR (CDCl<sub>3</sub>, 100 MHz, 300K)

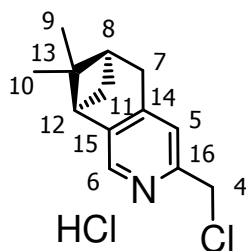
**DEPT 135 (CDCl<sub>3</sub>, 1000 MHz, 300K)**



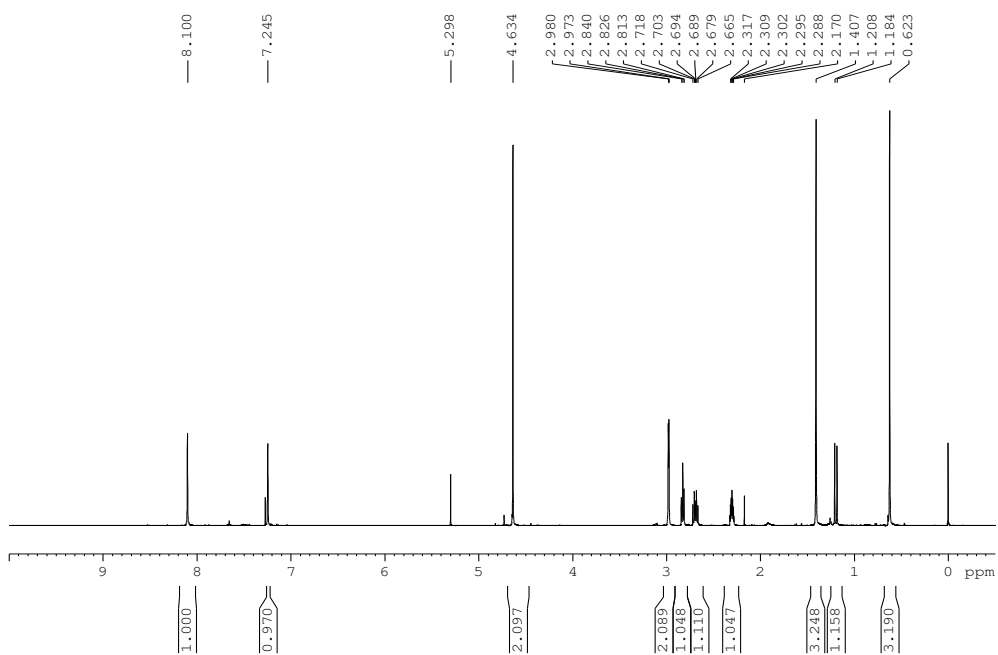
*(R)*-4,5-pinene-2-picolylaldehyde, *(R)*-pinene-PyCOH**<sup>1</sup>H-NMR (CDCl<sub>3</sub>, 200 MHz, 300K)**

*(R)*-4,5-pinene-2-picolylalcohol, *(R)*-pinene-PyCH<sub>2</sub>OH<sup>1</sup>H-NMR (CDCl<sub>3</sub>, 400 MHz, 300K)<sup>13</sup>C-NMR (CDCl<sub>3</sub>, 50 MHz, 300K)

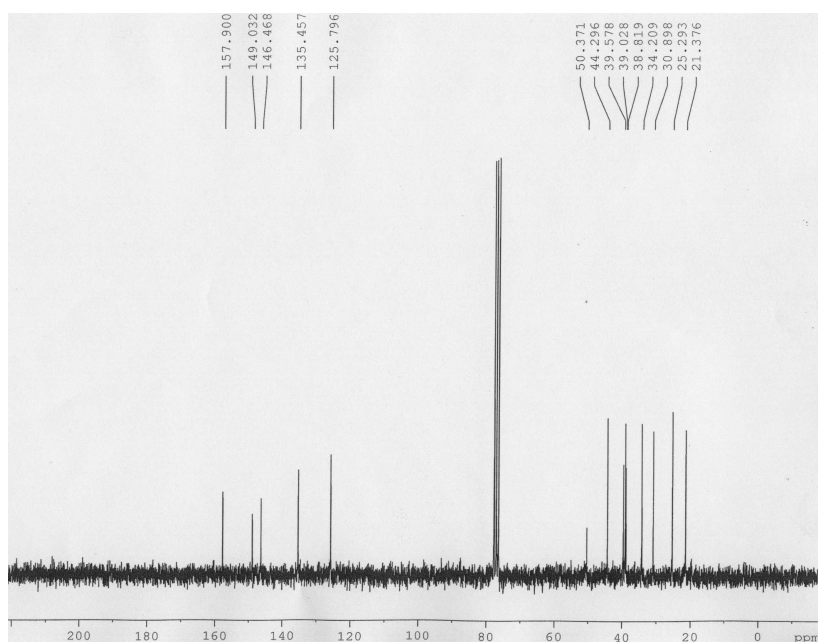
(*R*)-4,5-pinene-2-picolylchloride hydrochloride,  
(*R*)-pinene-PyCH<sub>2</sub>Cl·HCl



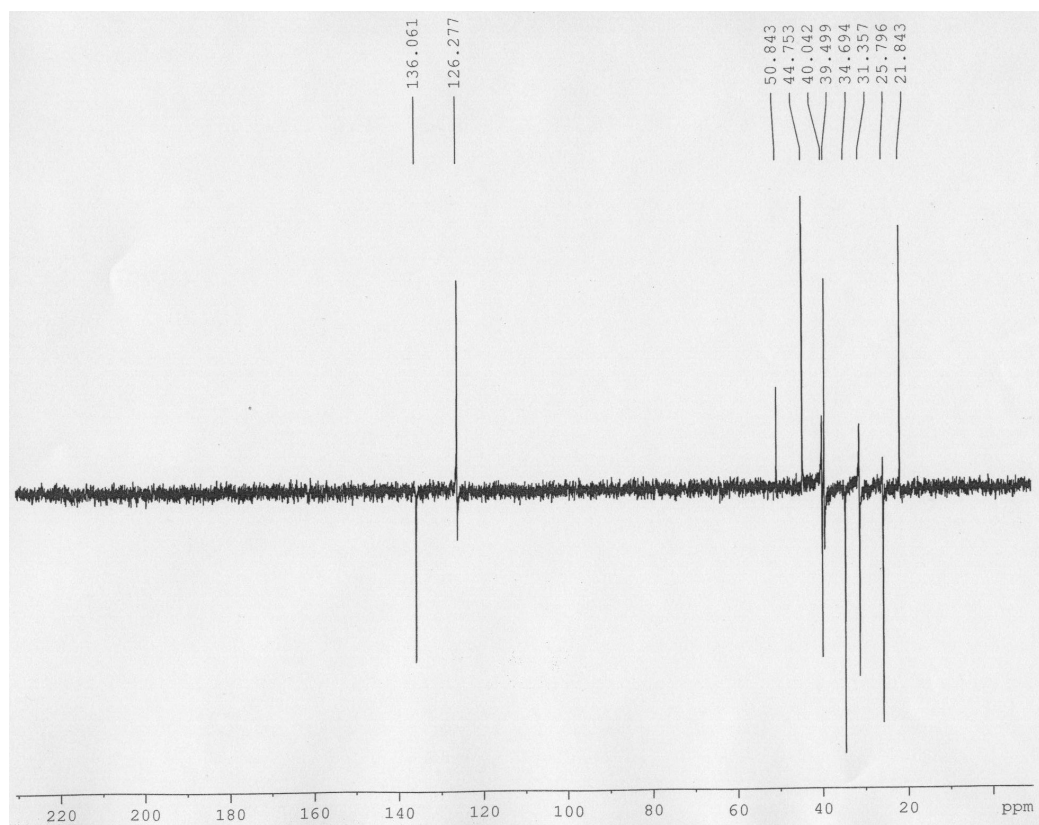
**<sup>1</sup>H-NMR (CDCl<sub>3</sub>, 400 MHz, 300K)**



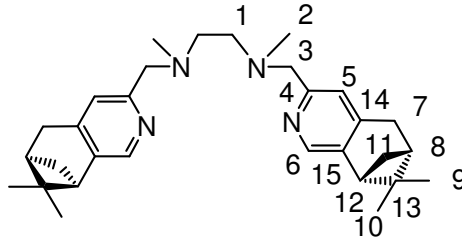
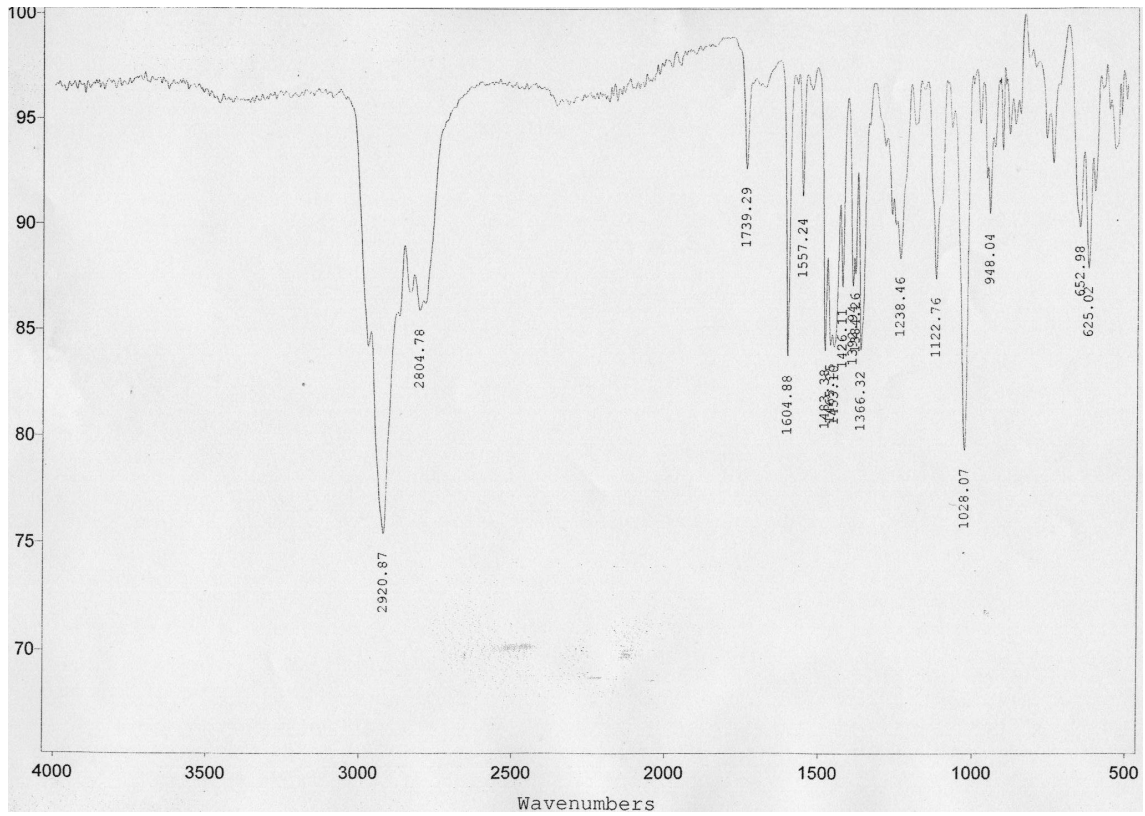
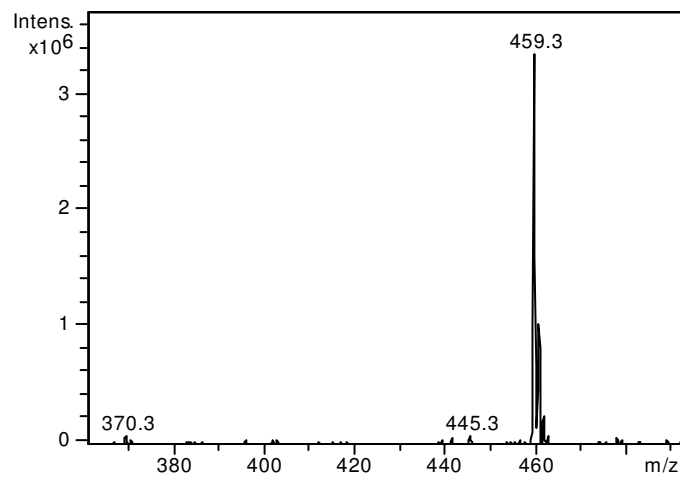
**<sup>13</sup>C-NMR (CDCl<sub>3</sub>, 50 MHz, 300K)**

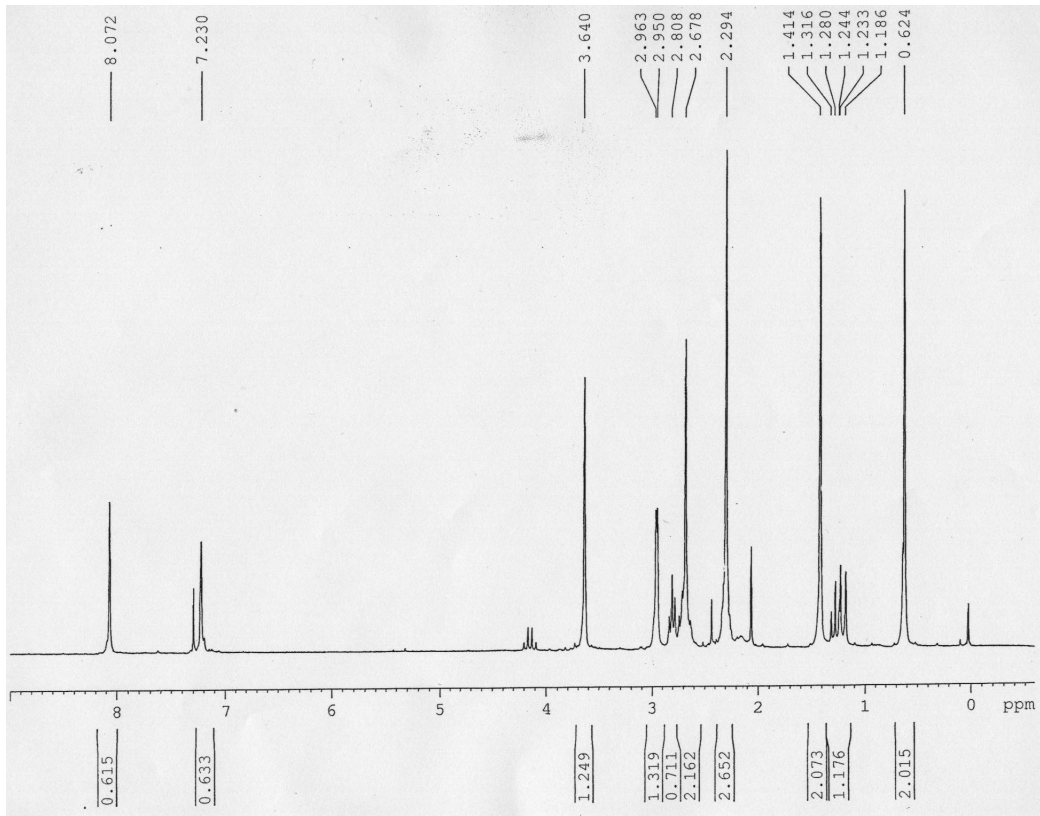
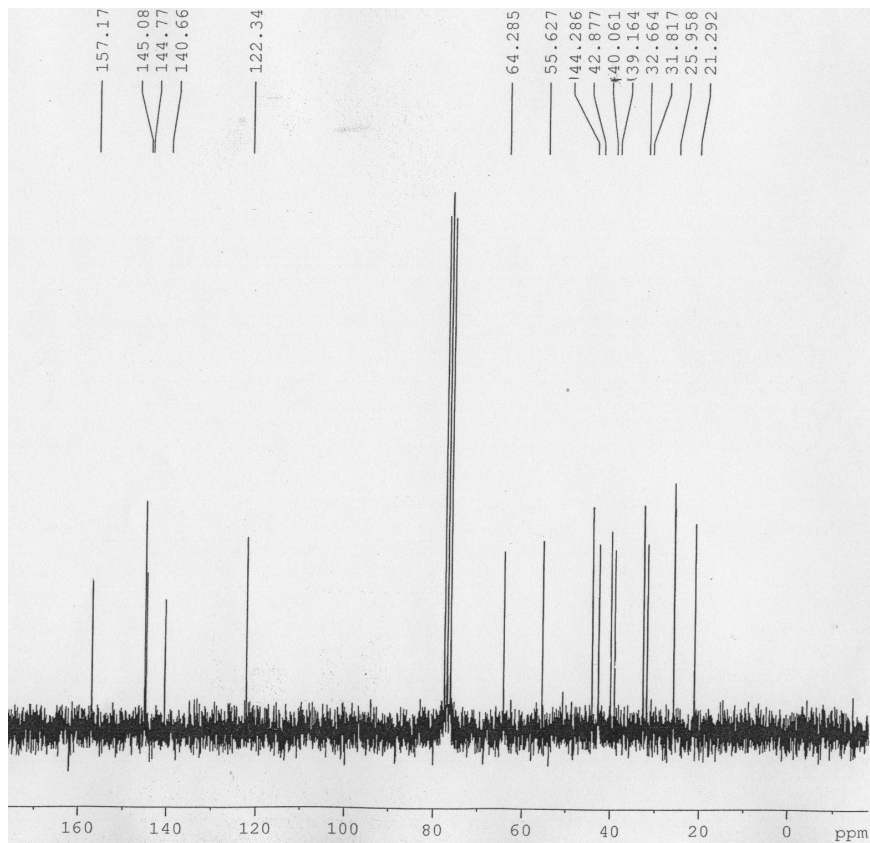


**DEPT 135 (CDCl<sub>3</sub>, 50 MHz, 300K)**

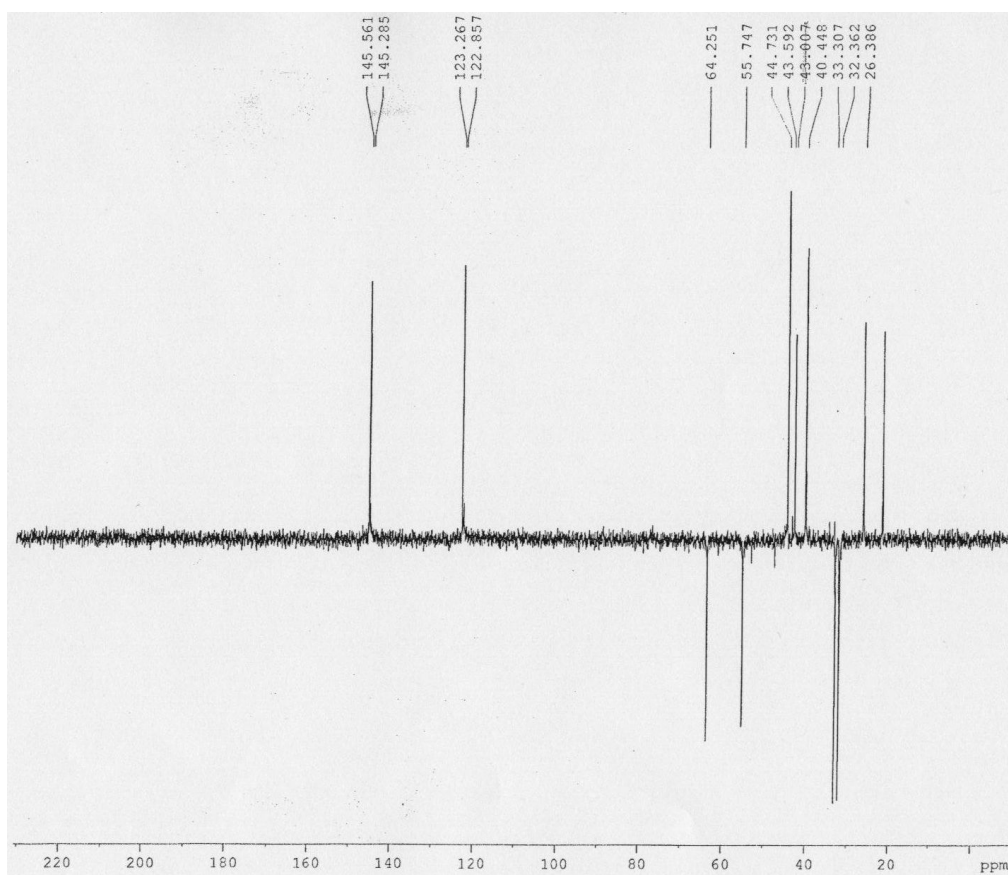




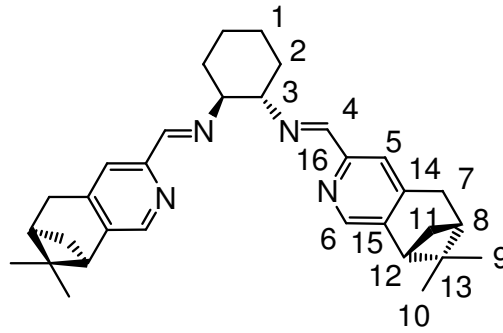
**(R)-bpmenp, L1****FT-IR (ATR)****ESI-MS**

**$^1\text{H-NMR}$  ( $\text{CDCl}_3$ , 200 MHz, 300K)** **$^{13}\text{C-NMR}$  ( $\text{CDCl}_3$ , 50 MHz, 300K)**

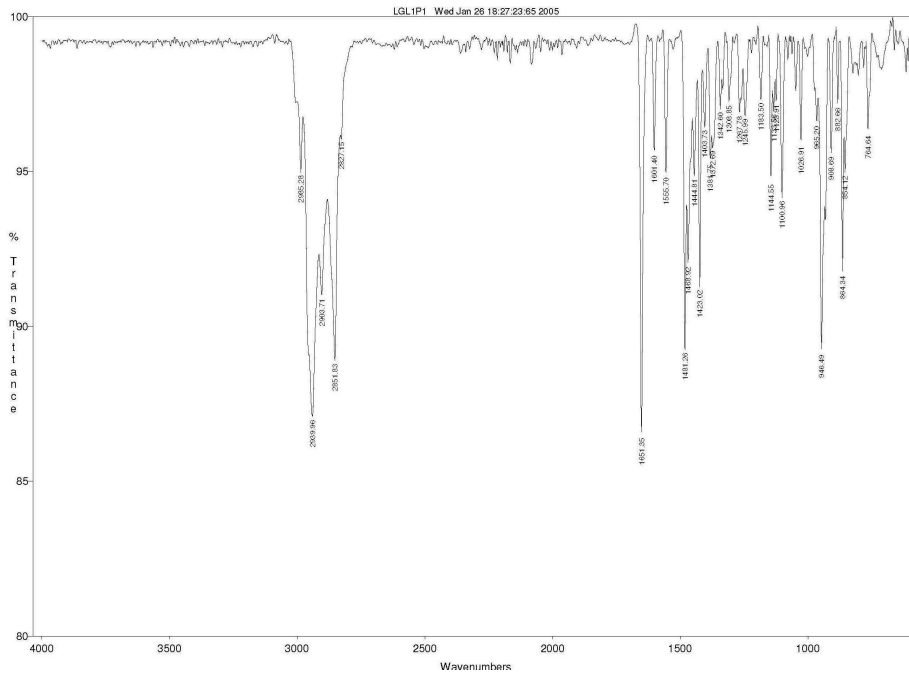
**DEPT 135 (CDCl<sub>3</sub>, 50 MHz, 300K)**



(*S,S,R*)-bpscnp

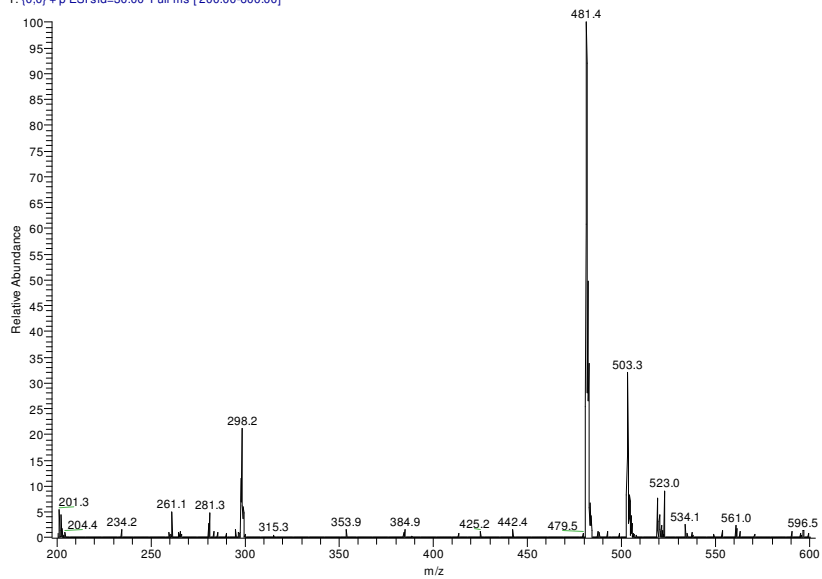


FT-IR (ATR)

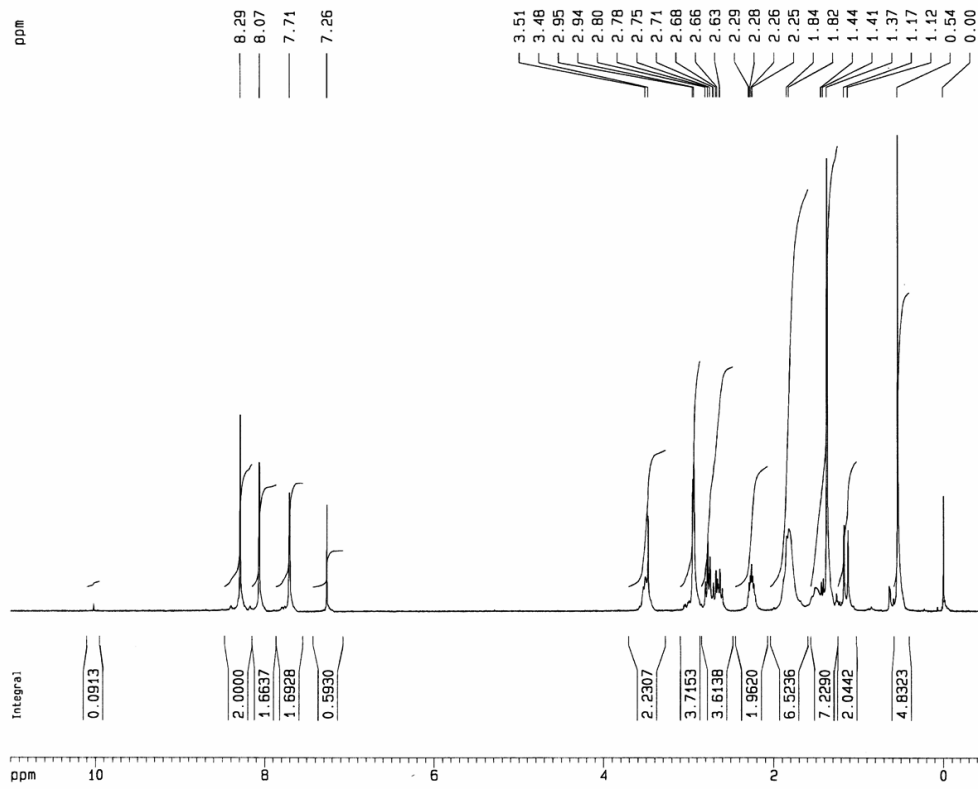


ESI-MS

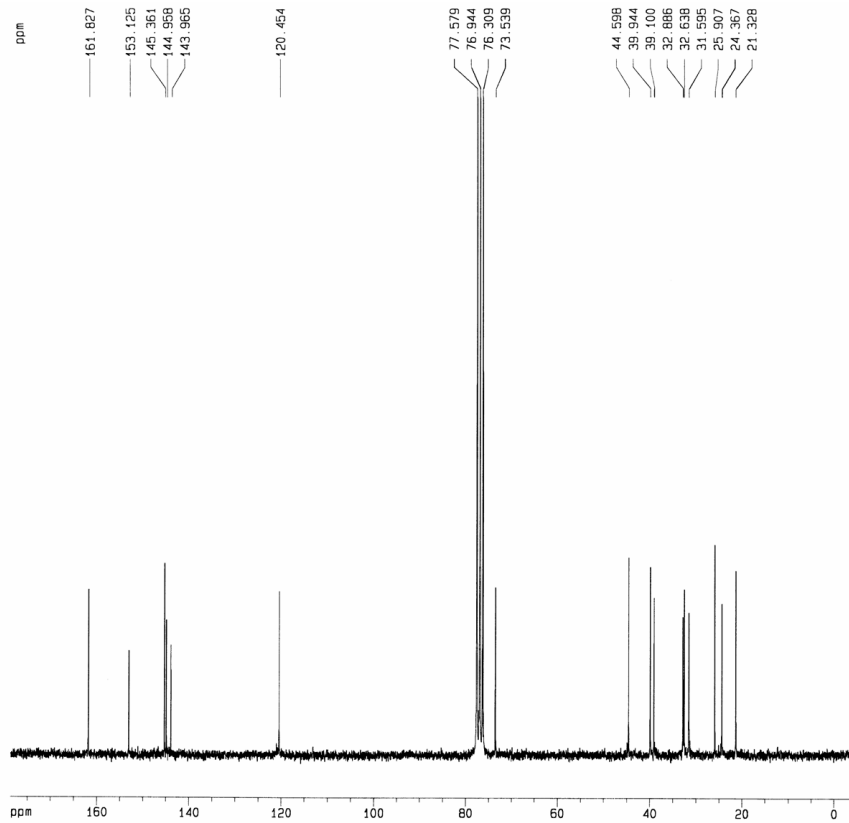
050127LGL1P1\_01#64-74 RT: 0.96-1.10 AV: 11 NL: 2.44E5  
 T: [0.0] +p ESI: sid=30.00 Full ms [200.00-600.00]

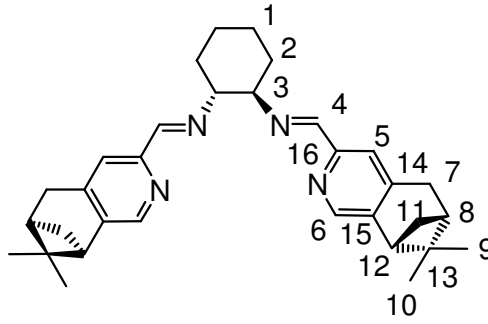
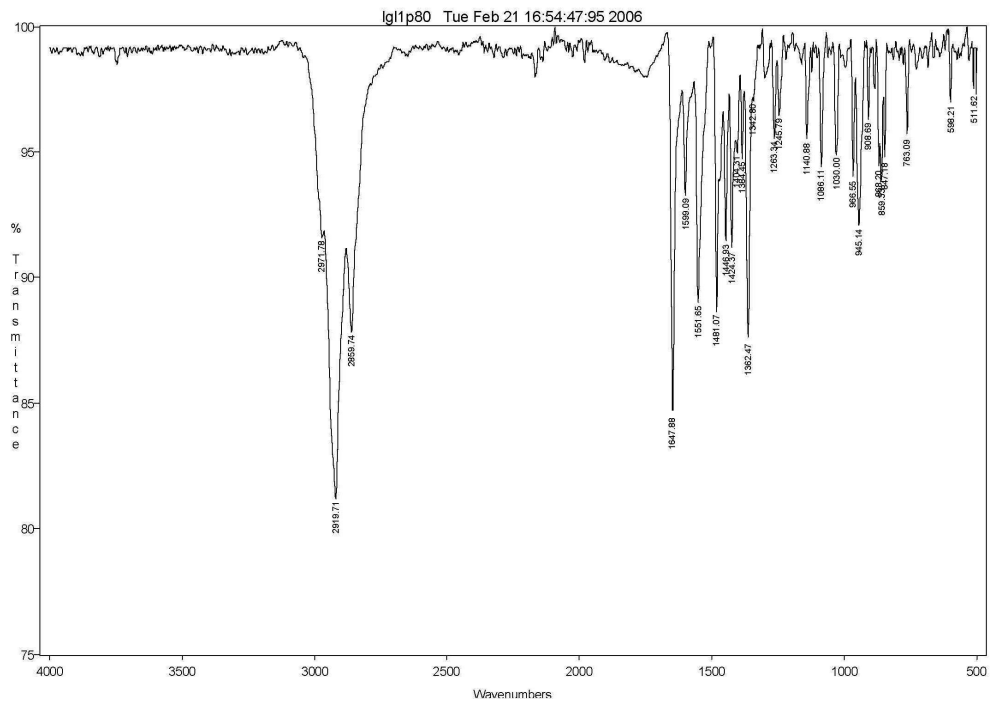
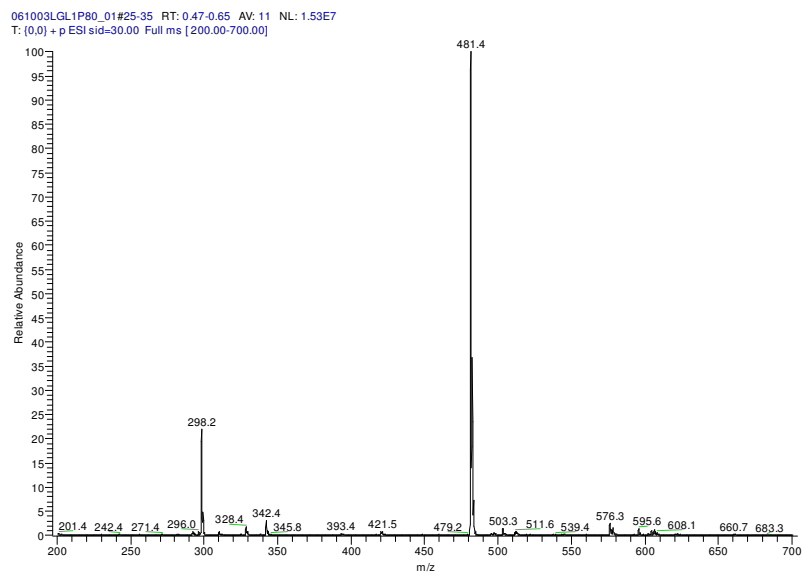


**<sup>1</sup>H-NMR (CDCl<sub>3</sub>, 200 MHz, 300K)**

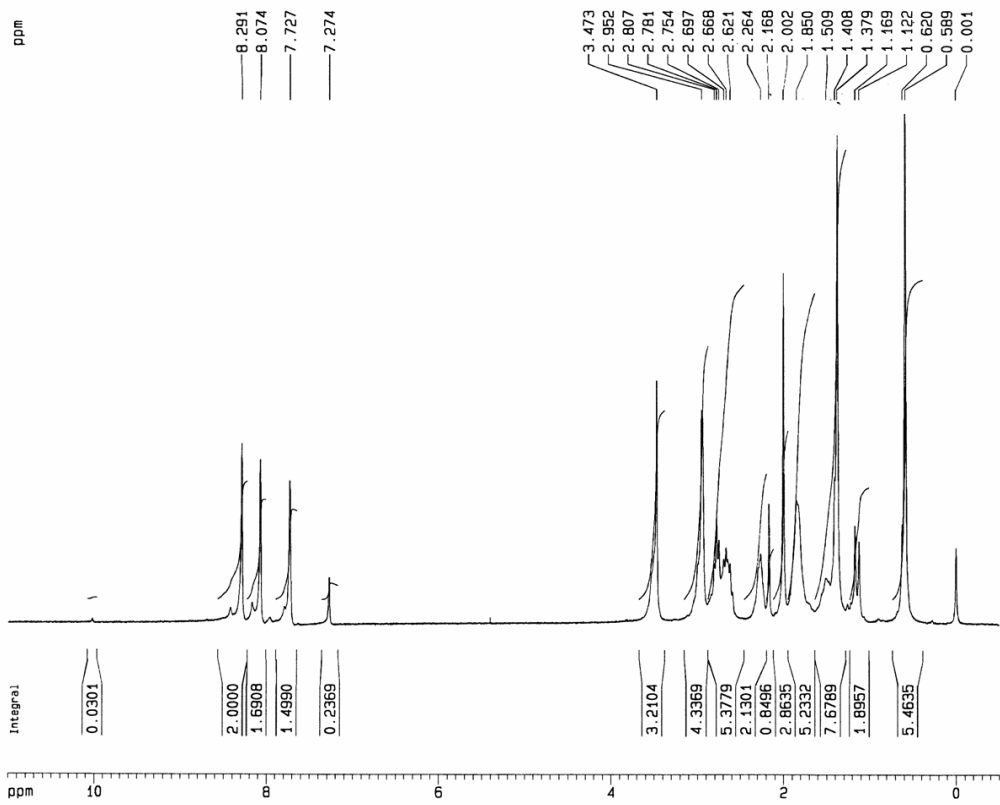


**<sup>13</sup>C-NMR (CDCl<sub>3</sub>, 50 MHz, 300K)**

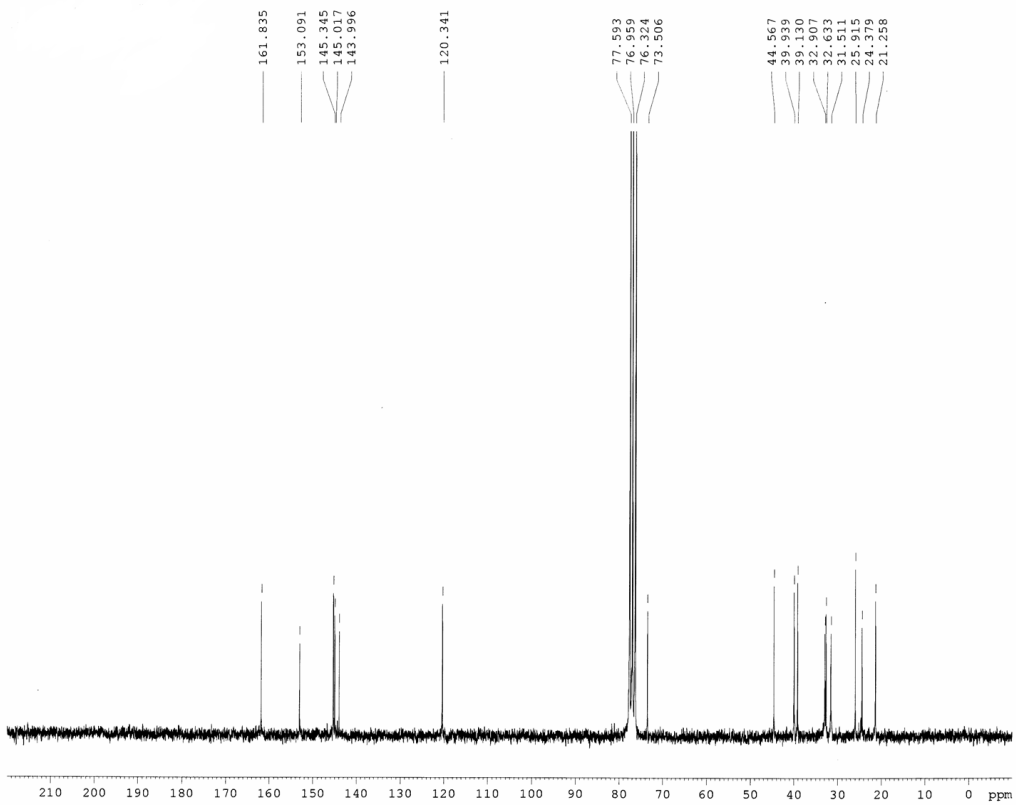


**(R,R,R)-bpscnp****FT-IR (ATR)****ESI-MS**

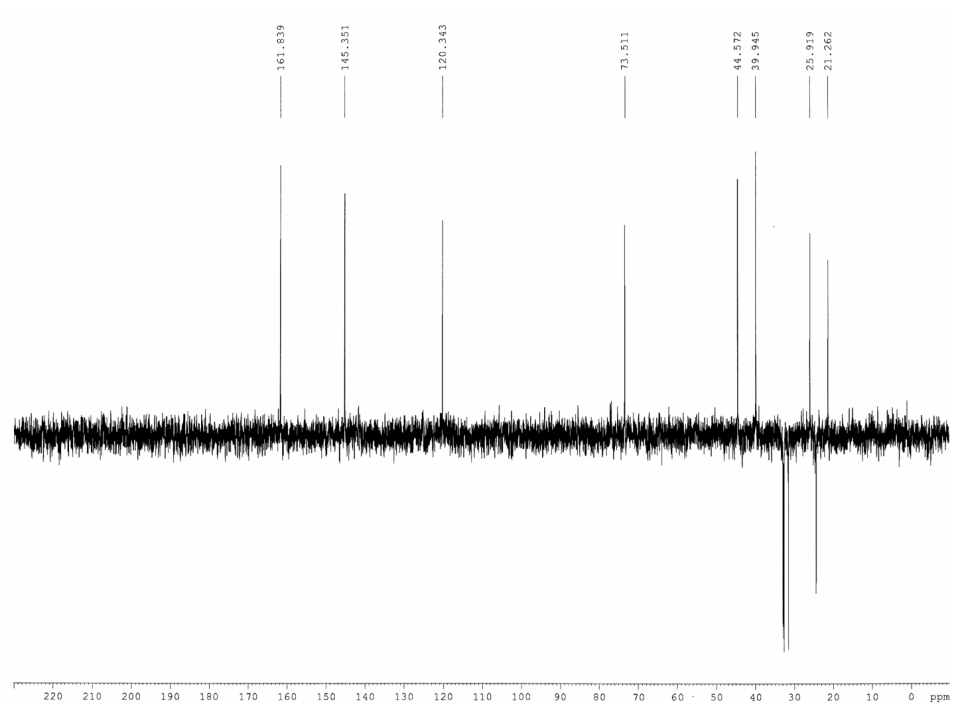
**<sup>1</sup>H-NMR (CDCl<sub>3</sub>, 200 MHz, 300K)**



**<sup>13</sup>C-NMR (CDCl<sub>3</sub>, 50 MHz, 300K)**

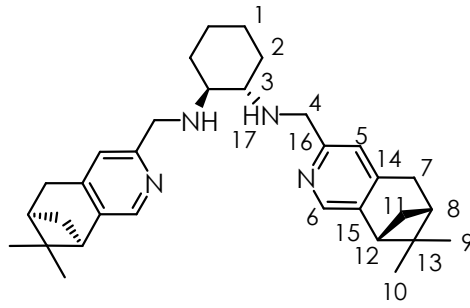


**DEPT 135 (CDCl<sub>3</sub>, 50 MHz, 300K)**

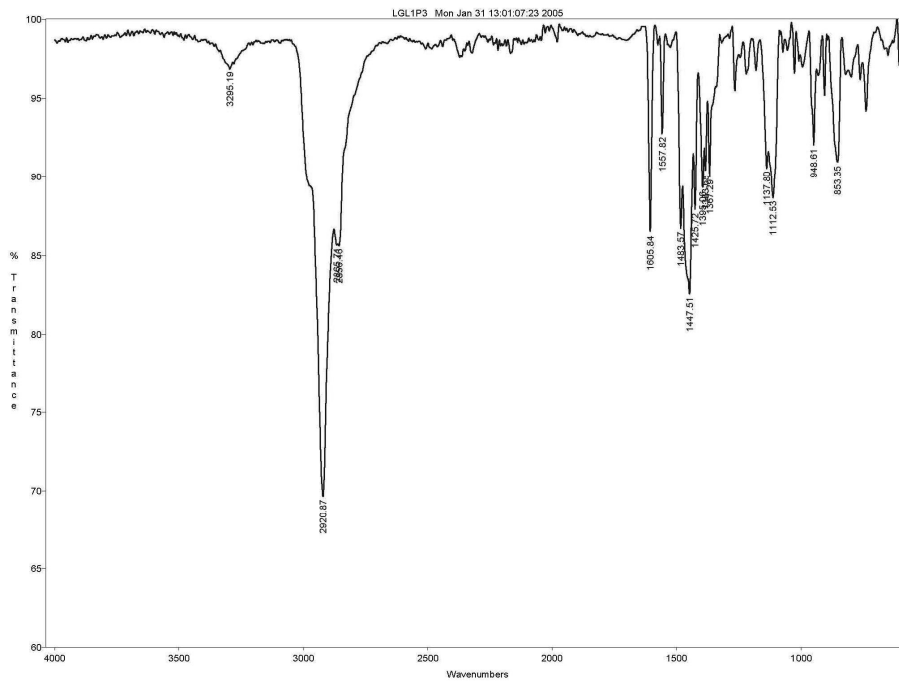




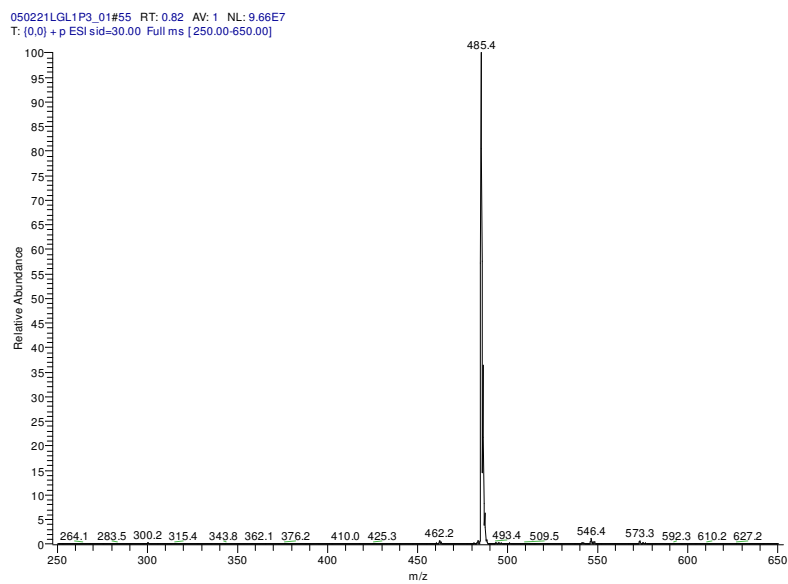
(*S,S,R*)-bphcnp



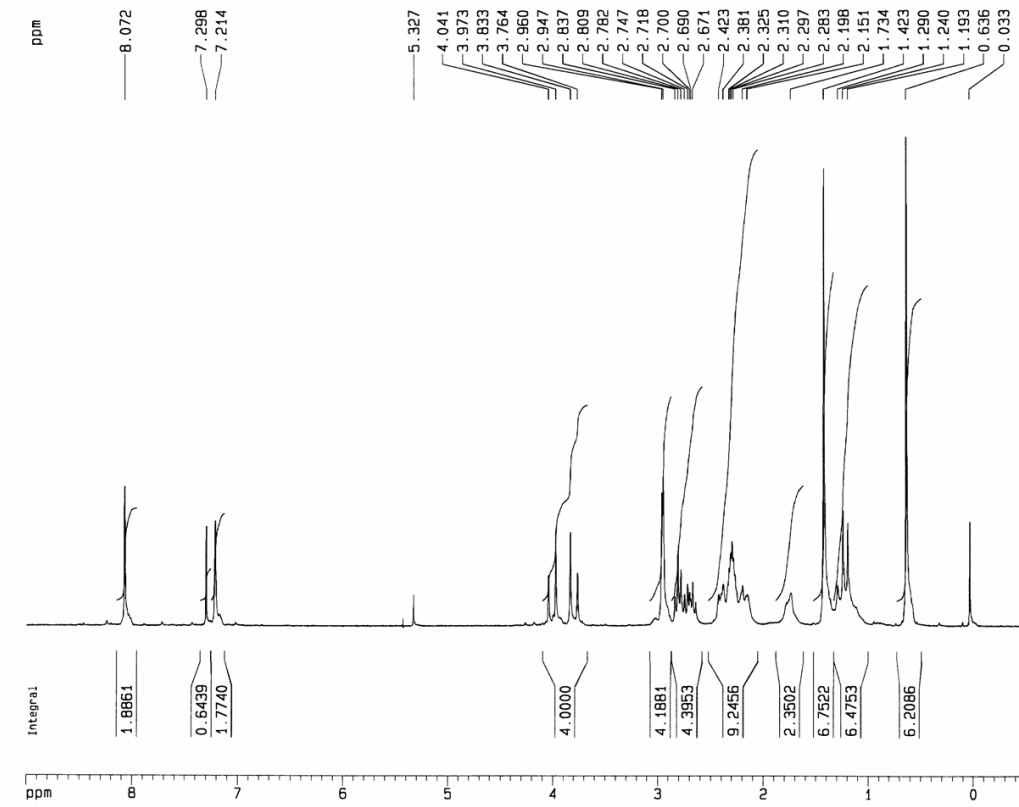
FT-IR (ATR)



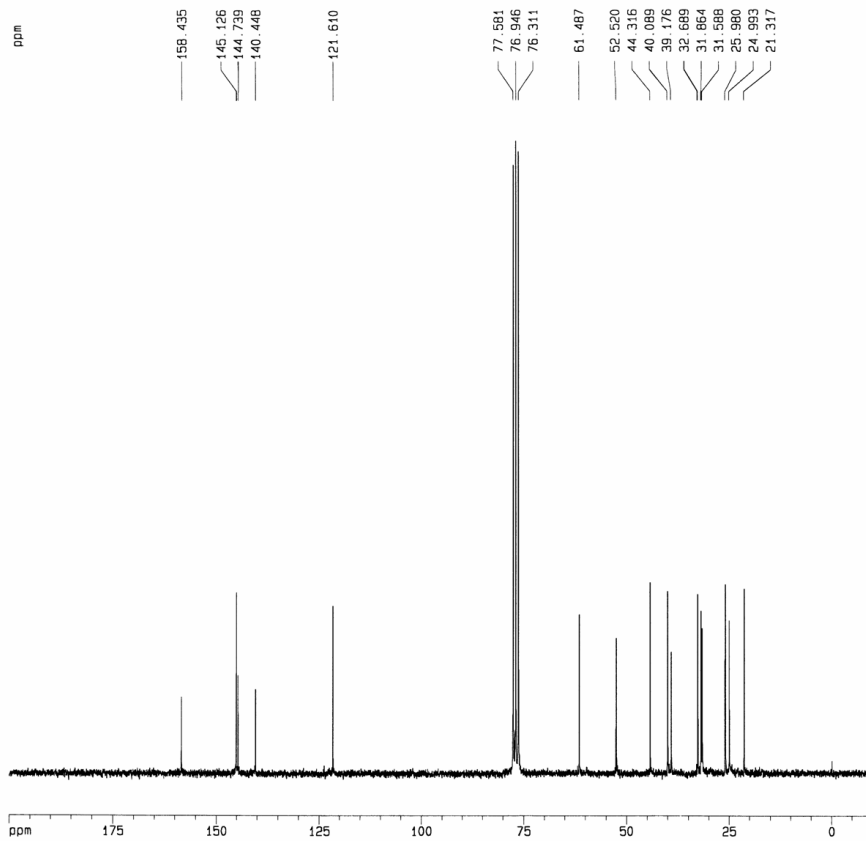
ESI-MS

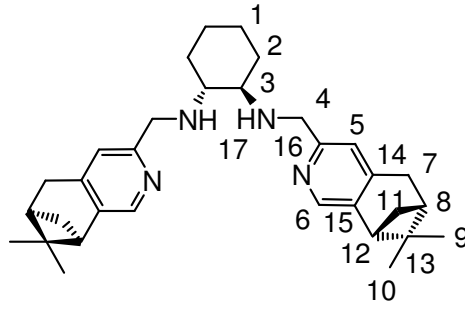
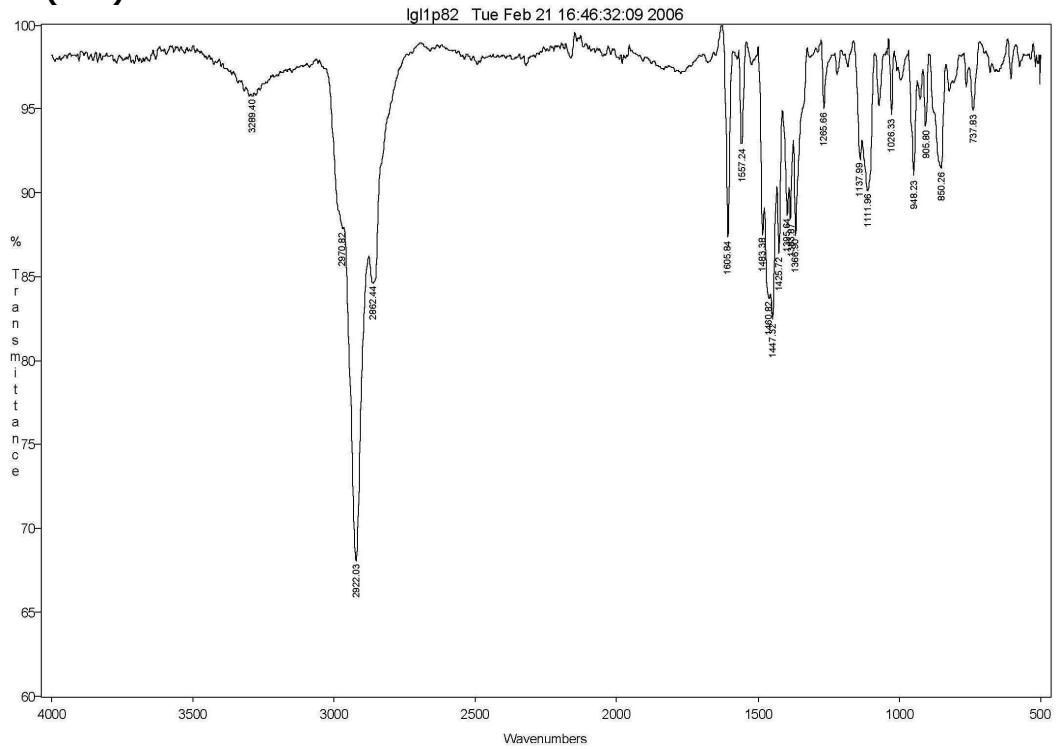


**<sup>1</sup>H-NMR (CDCl<sub>3</sub>, 200 MHz, 300K)**

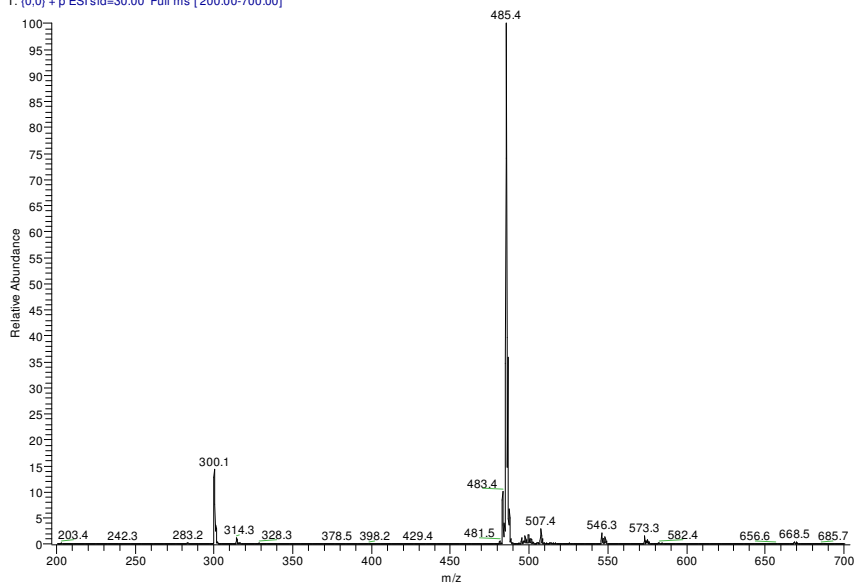


**<sup>13</sup>C-NMR (CDCl<sub>3</sub>, 50 MHz, 300K)**

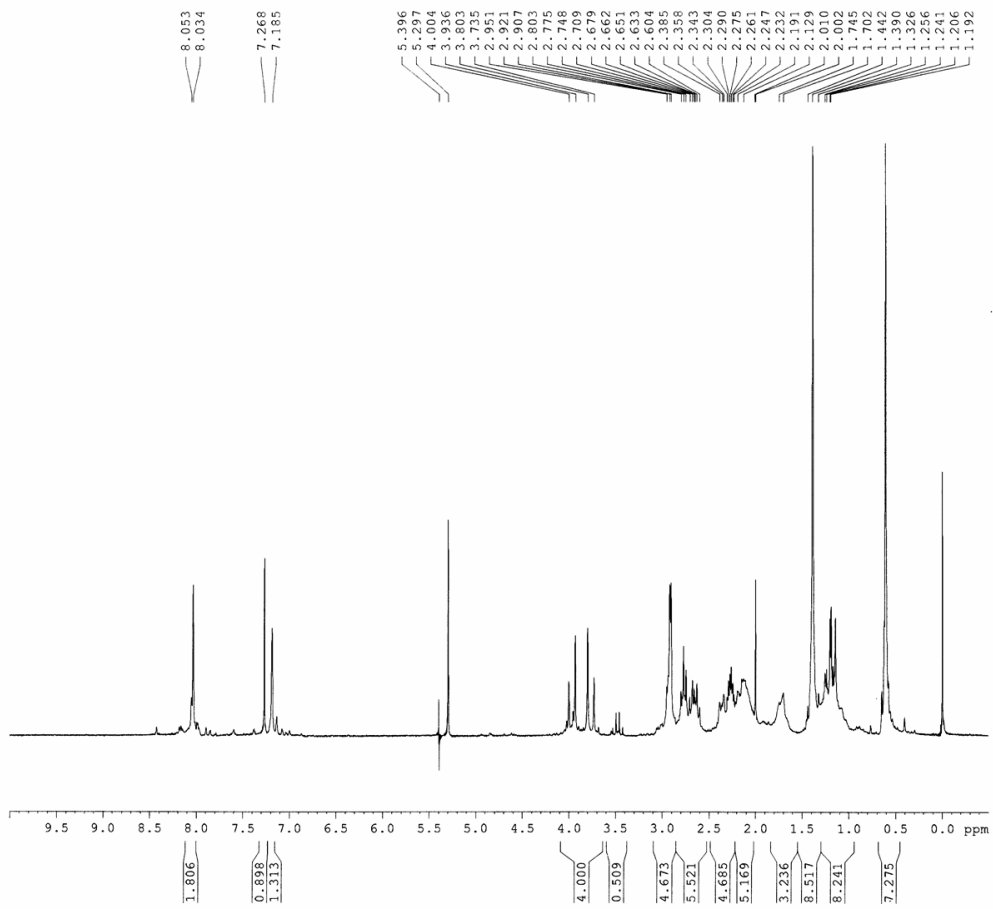


**(R,R,R)-bphcnp****FT-IR (ATR)****ESI-MS**

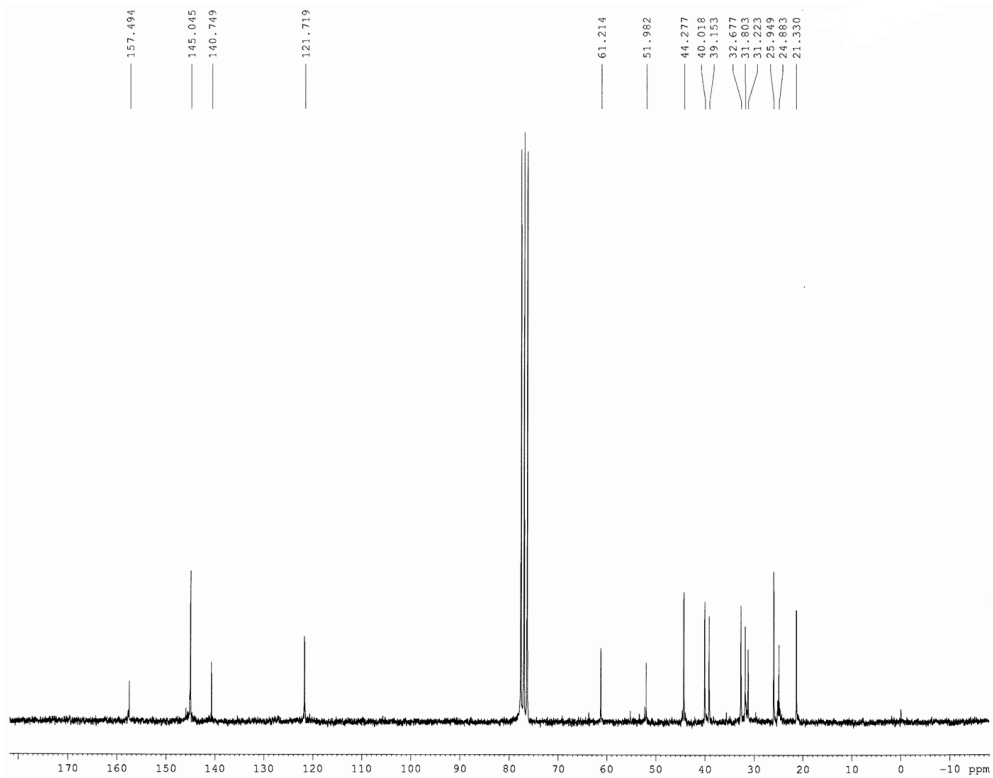
061003LGL1P82\_01#19-43 RT: 0.36-0.79 AV: 25 NL: 1.04E7  
T: (0,0) + p ESIsid=30.00 Full ms [200.00-700.00]



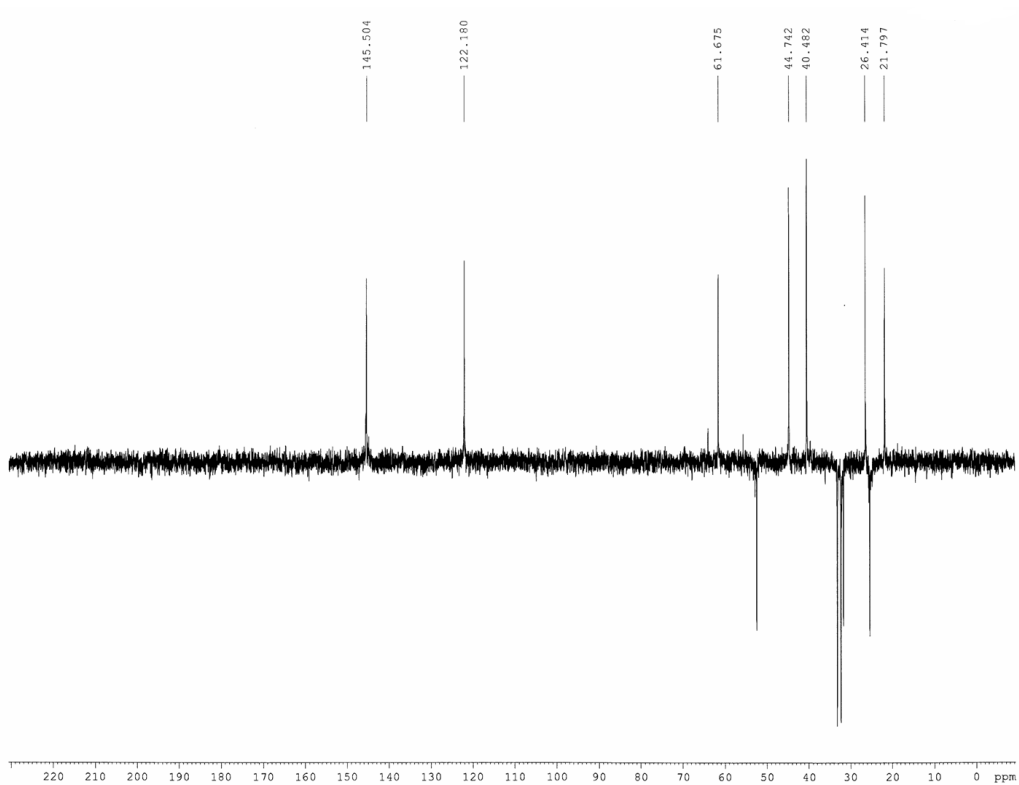
**<sup>1</sup>H-NMR (CDCl<sub>3</sub>, 200 MHz, 300K)**

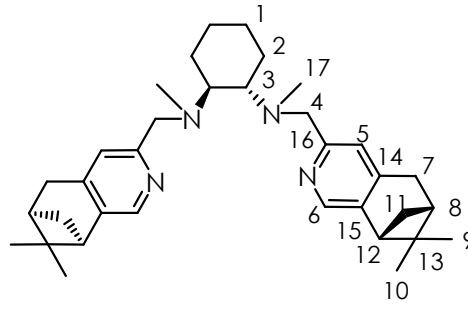
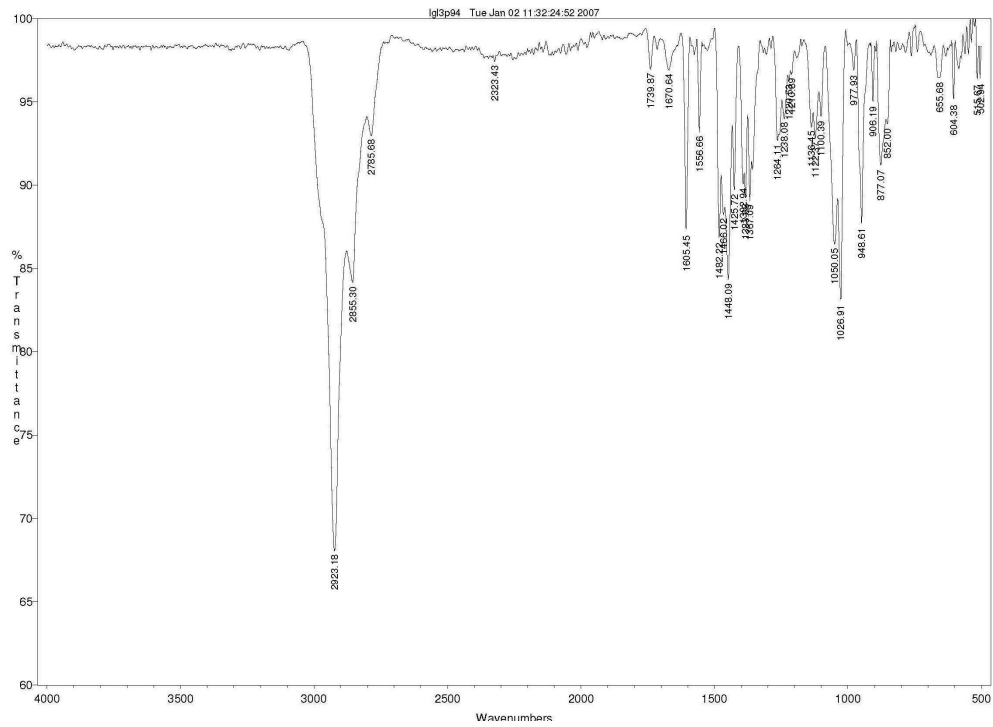


**<sup>13</sup>C-NMR (CDCl<sub>3</sub>, 50 MHz, 300K)**

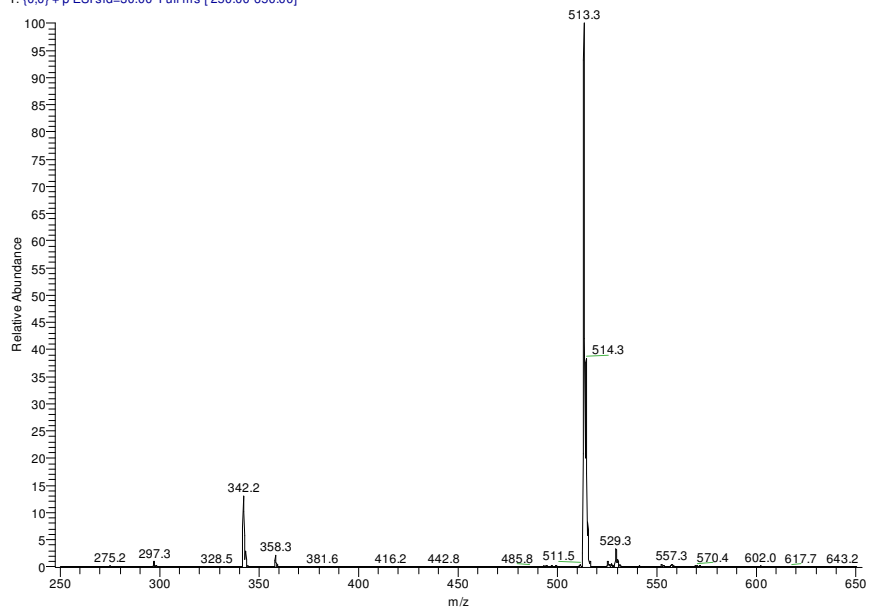


**DEPT 135 (CDCl<sub>3</sub>, 50 MHz, 300K)**

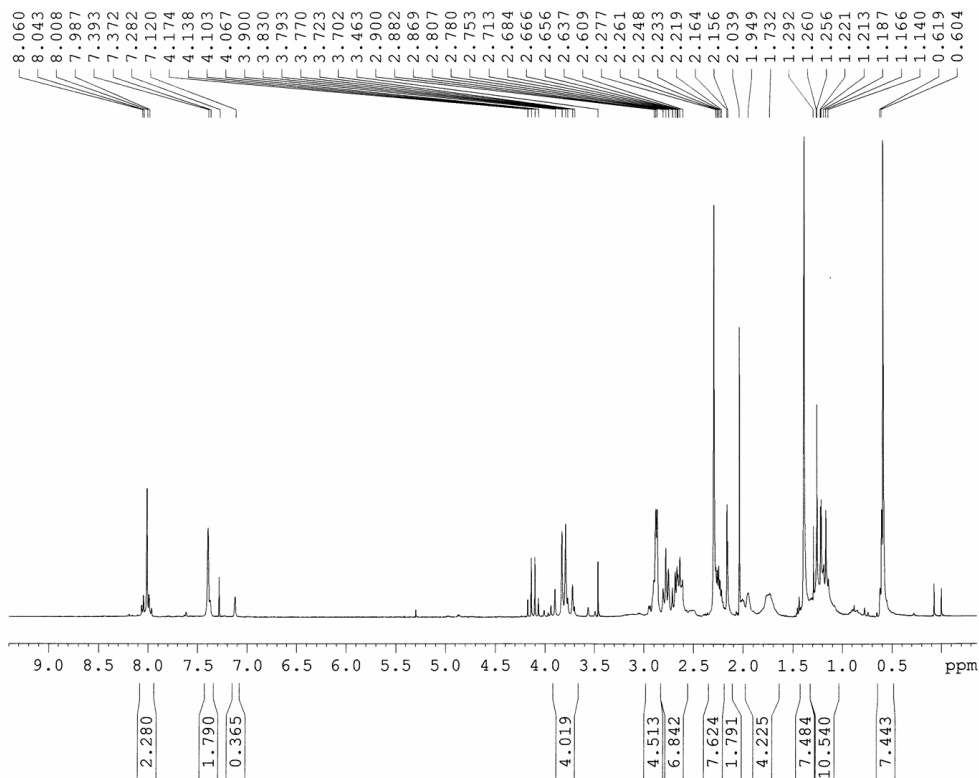


**(S,S,R)-bpmcnp, L2****FT-IR (ATR)****ESI-MS**

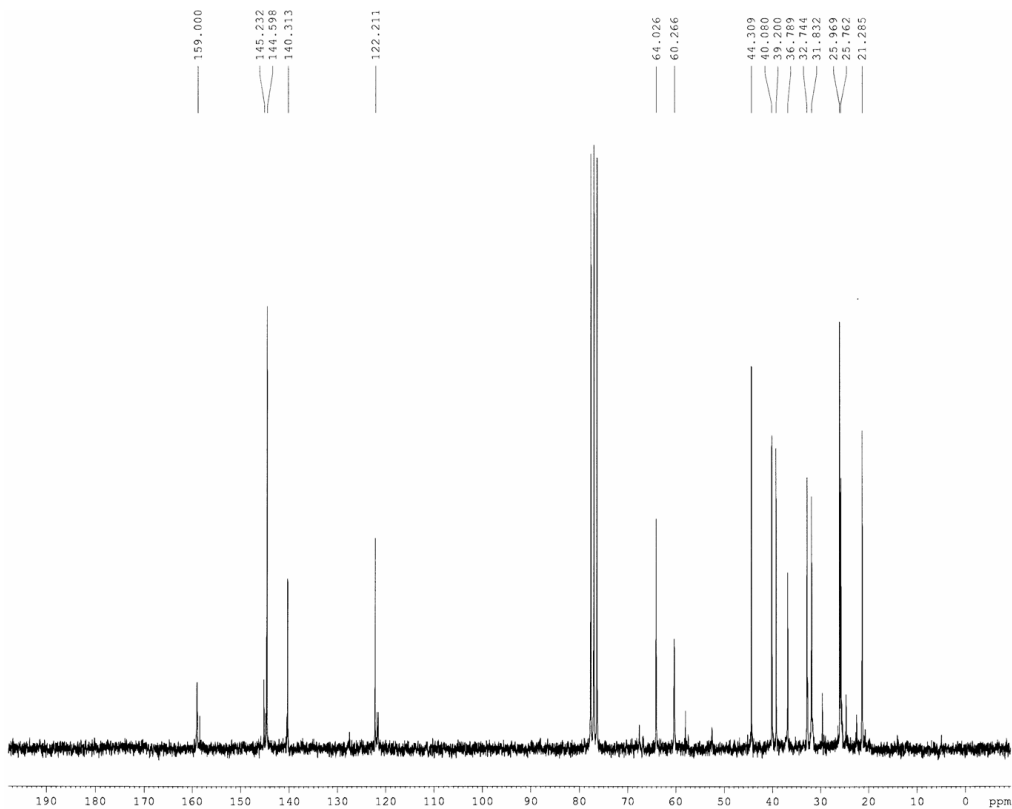
050221LGL1P7\_01#55 RT: 0.82 AV: 1 NL: 1.19E8  
T: {0,0} + p ESI: sid=30.00 Full ms [250.00-650.00]



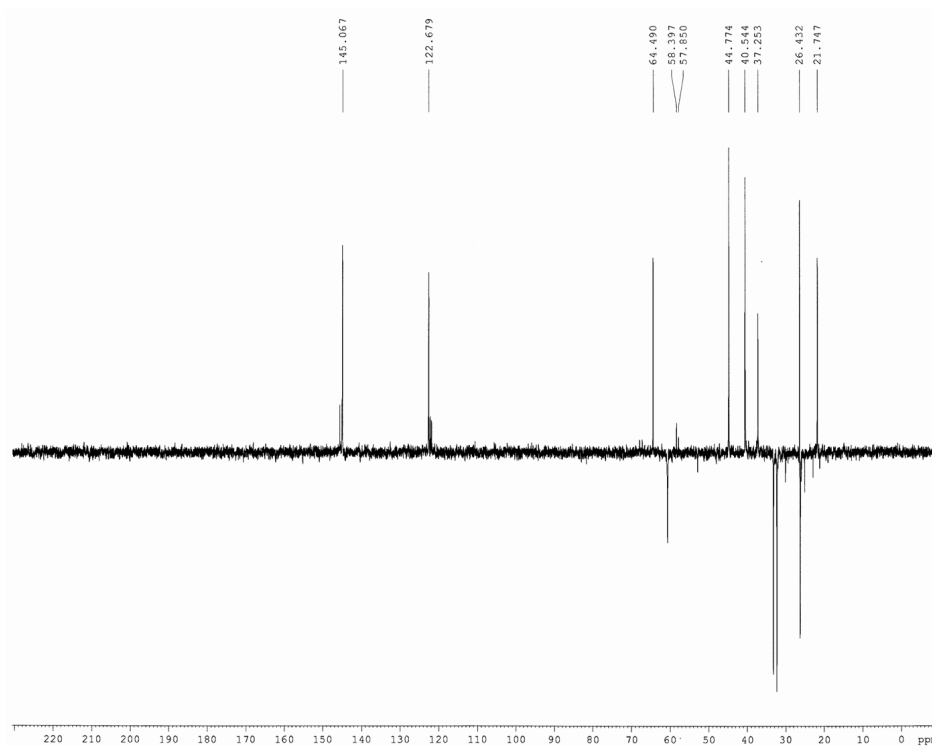
**<sup>1</sup>H-NMR (CDCl<sub>3</sub>, 200 MHz, 300K)**



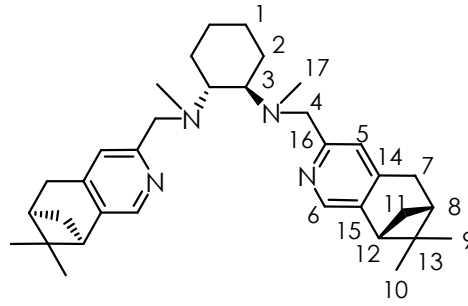
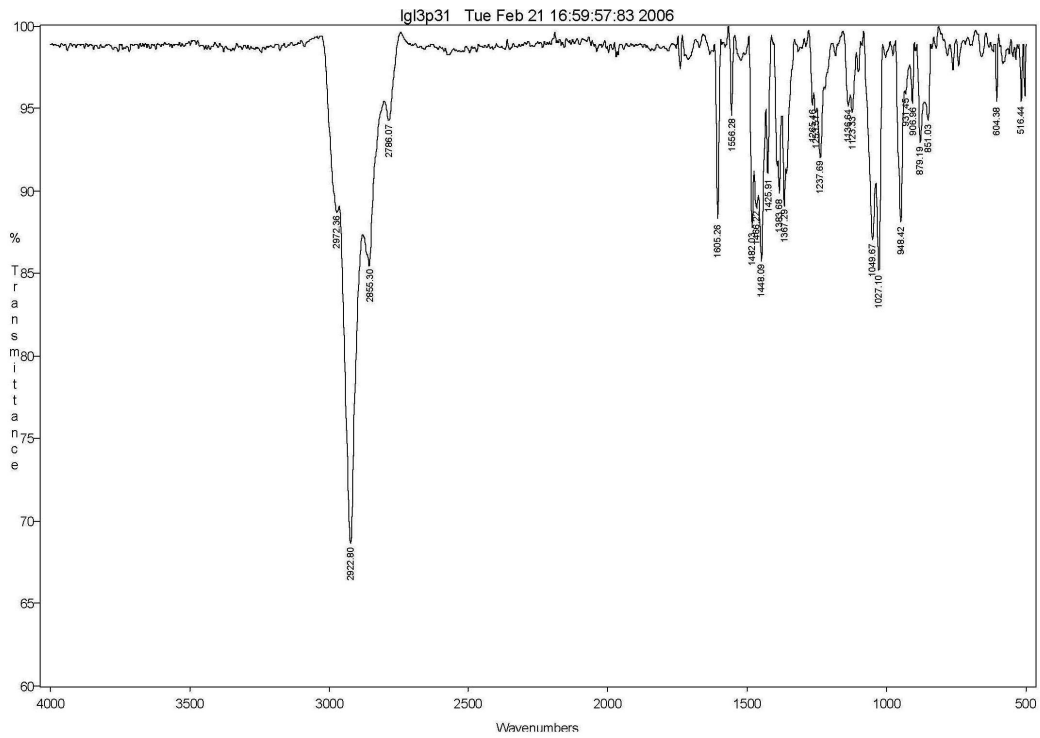
**<sup>13</sup>C-NMR (CDCl<sub>3</sub>, 50 MHz, 300K)**



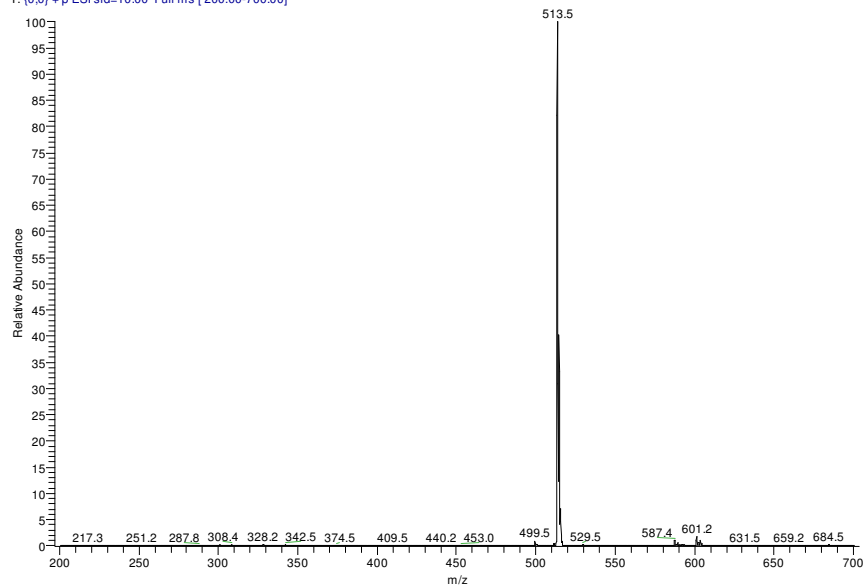
**DEPT 135 (CDCl<sub>3</sub>, 50 MHz, 300K)**



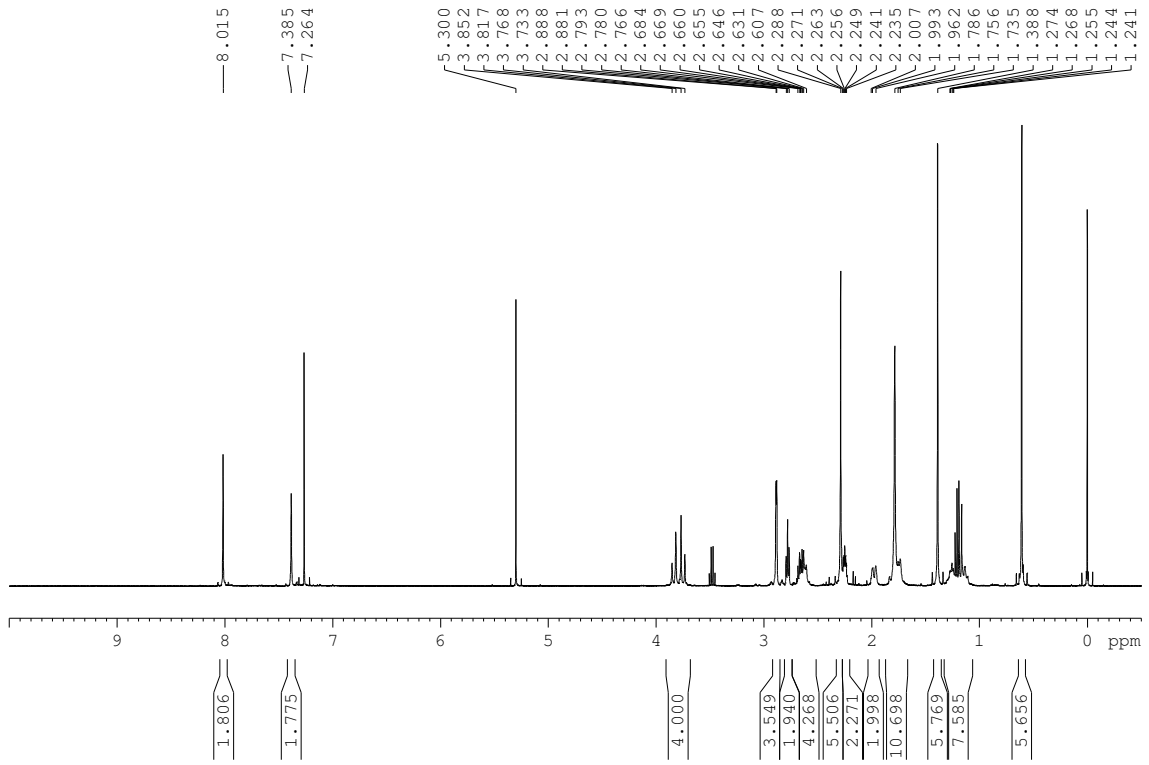


**(R,R,R)-bpmcnp, L3****FT-IR (ATR)****ESI-MS**

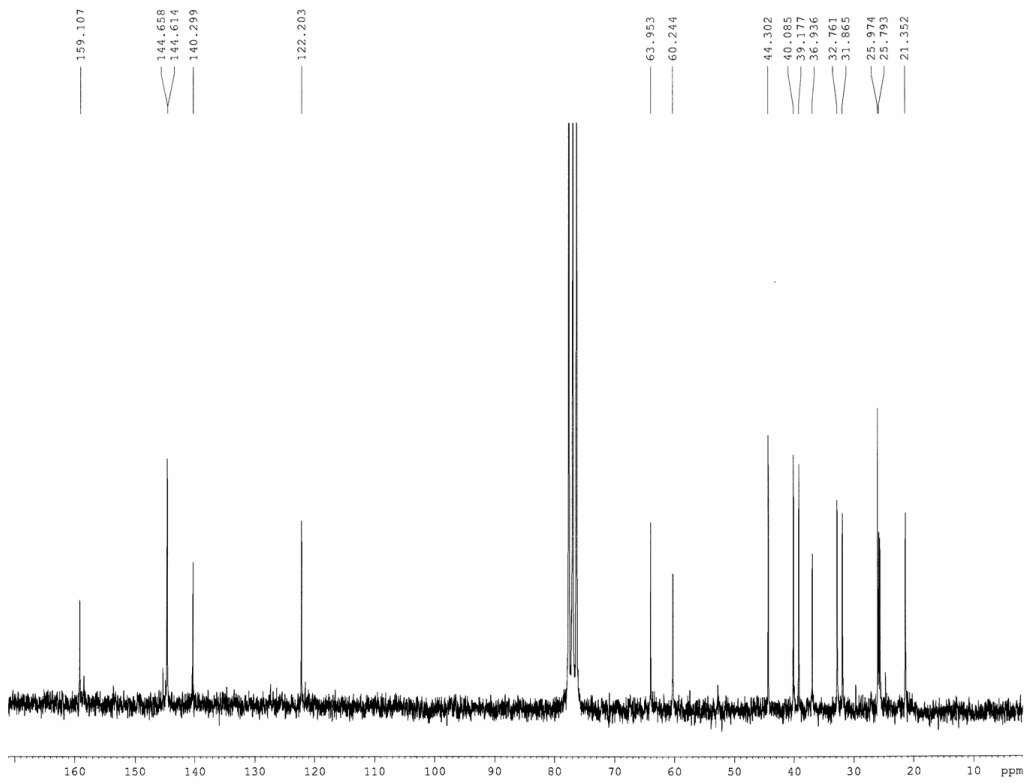
060921LGL3P31\_01#19-20 RT: 0.36-0.38 AV: 2 NL: 1.33E8  
T: (0,0) +p ESI: sid=10.00 Full ms [200.00-700.00]



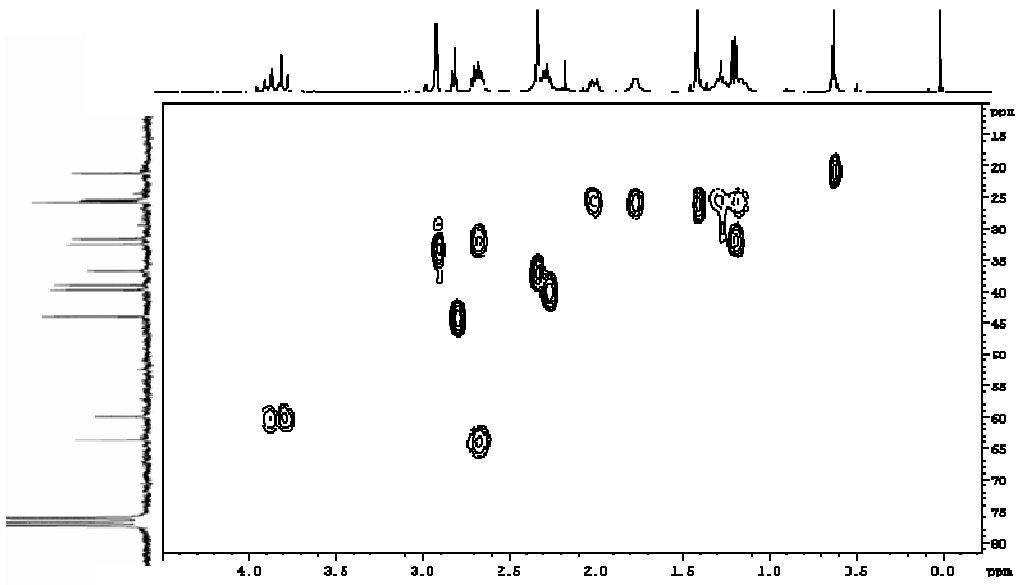
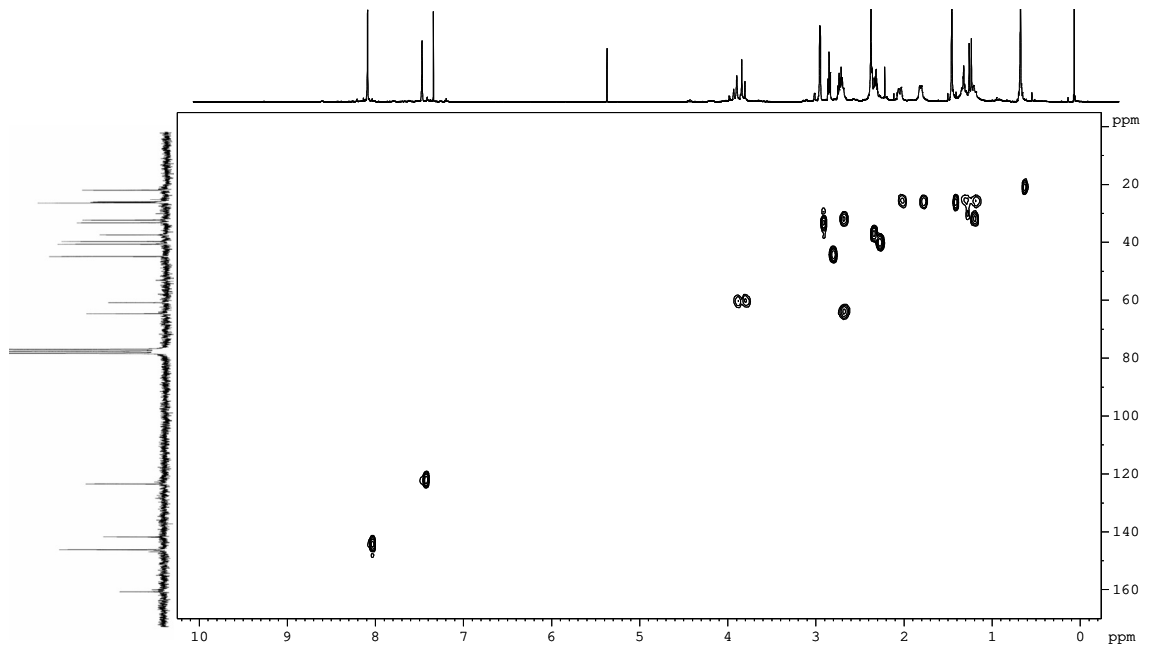
**<sup>1</sup>H-NMR (CDCl<sub>3</sub>, 400 MHz, 300K)**



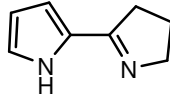
**<sup>13</sup>C-NMR (CDCl<sub>3</sub>, 50 MHz, 300K)**



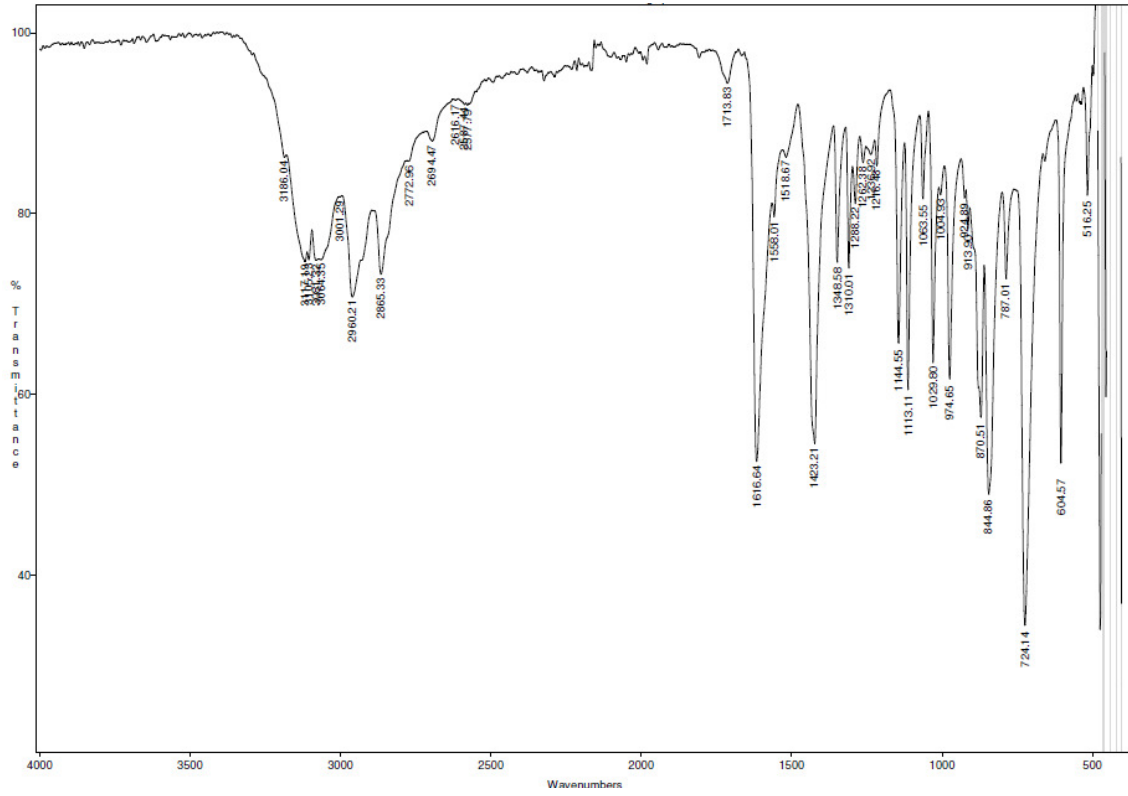
**HSQCed (CDCl<sub>3</sub>, 400 MHz, 300K)**



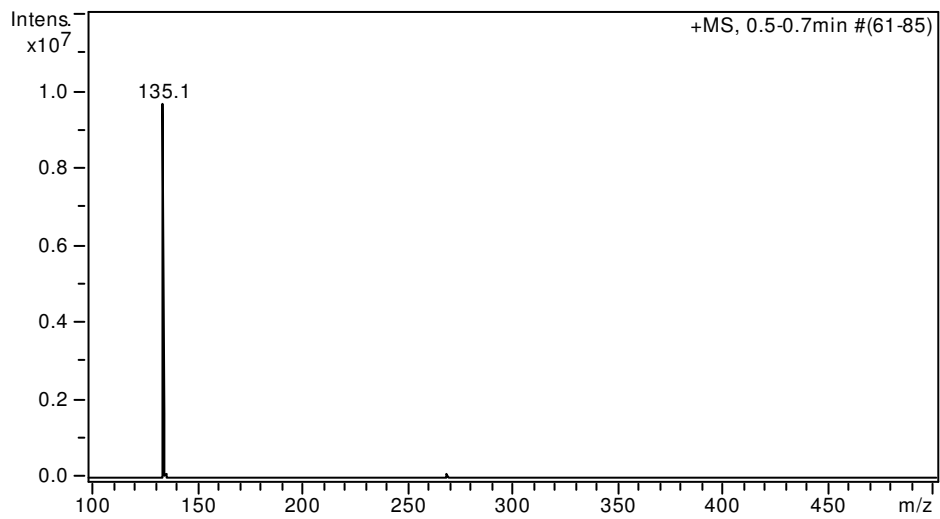
## 2-(3,4-dihydro-2H-pyrrol-5-yl)pyrrole

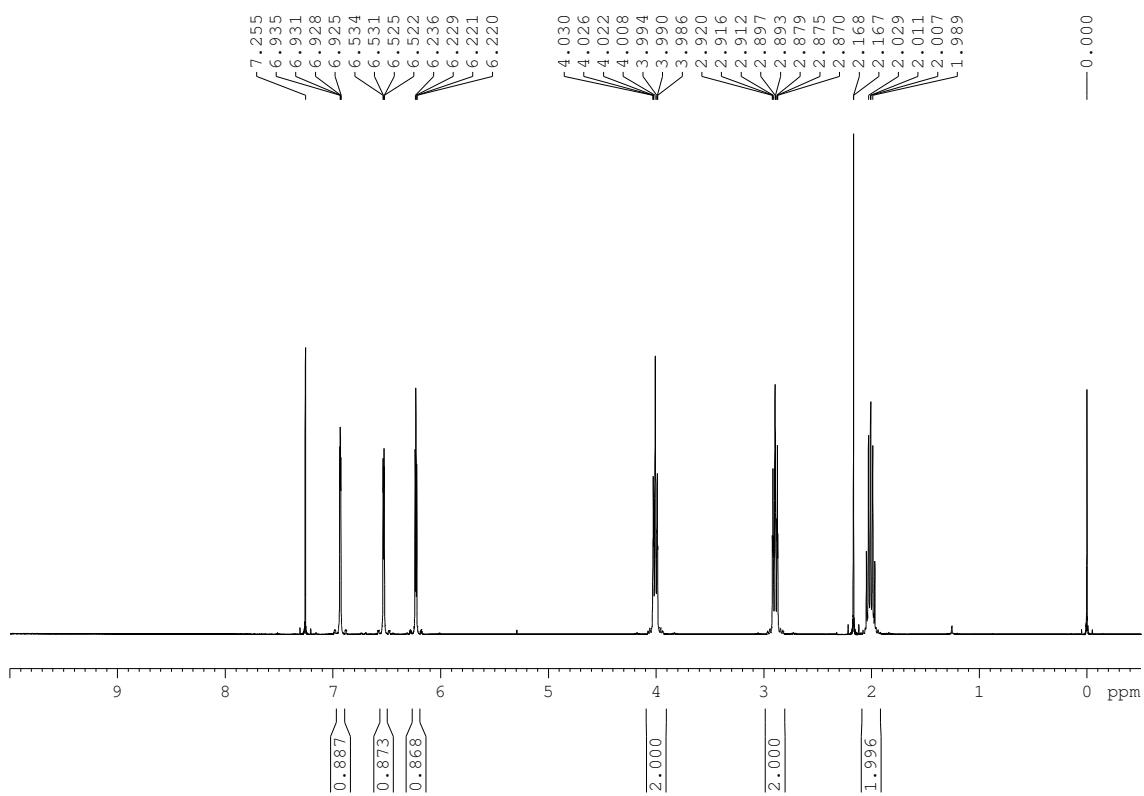
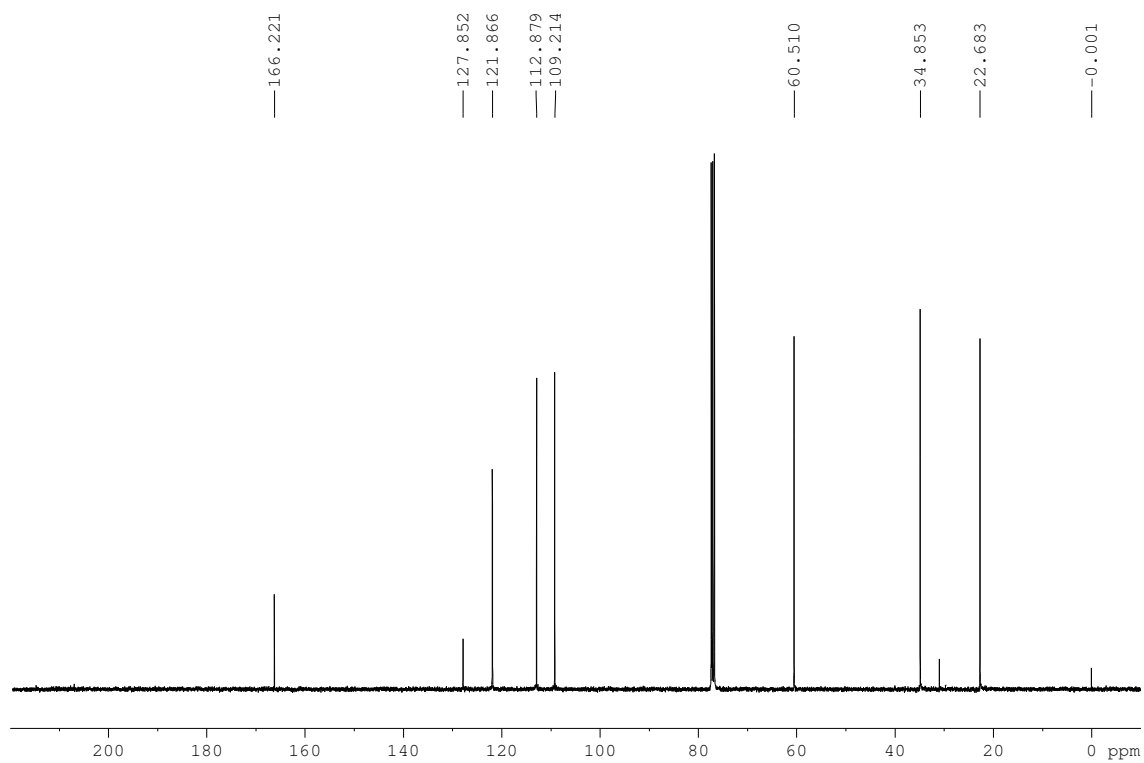


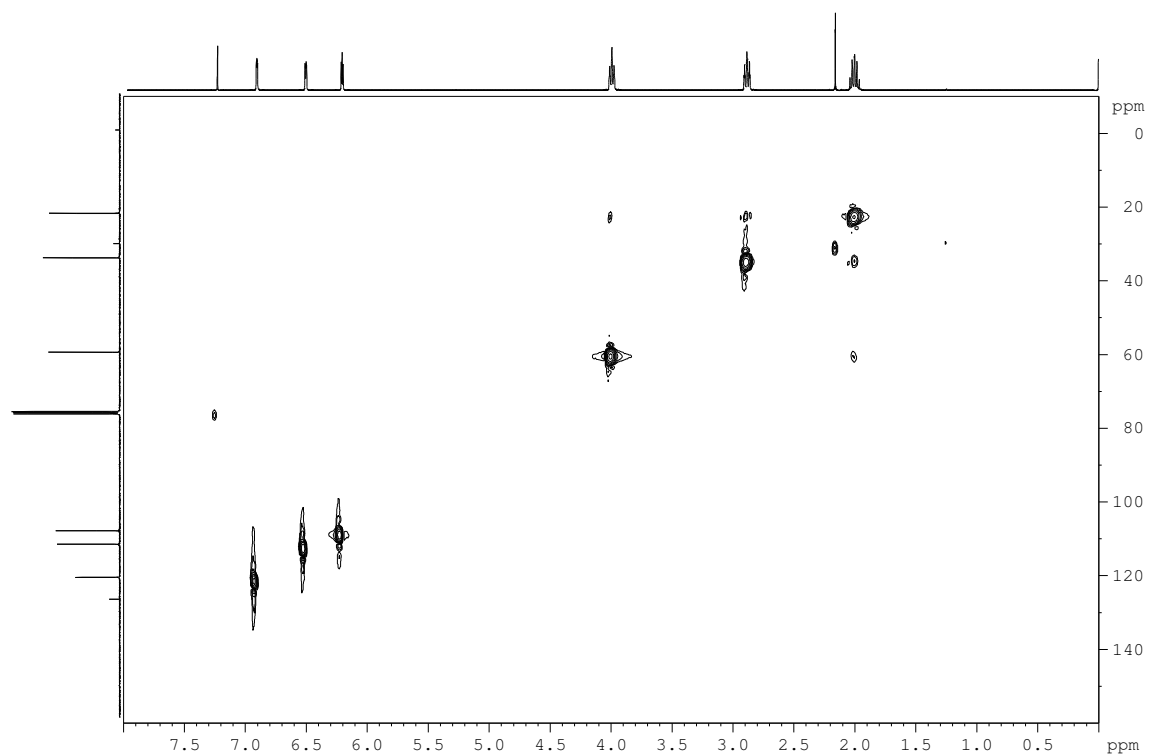
## FT-IR (ATR)

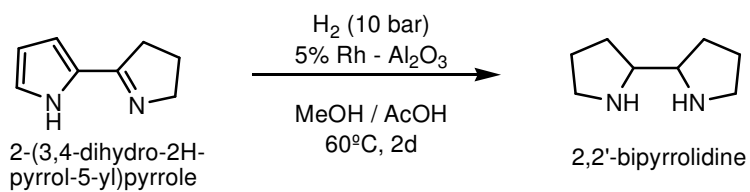
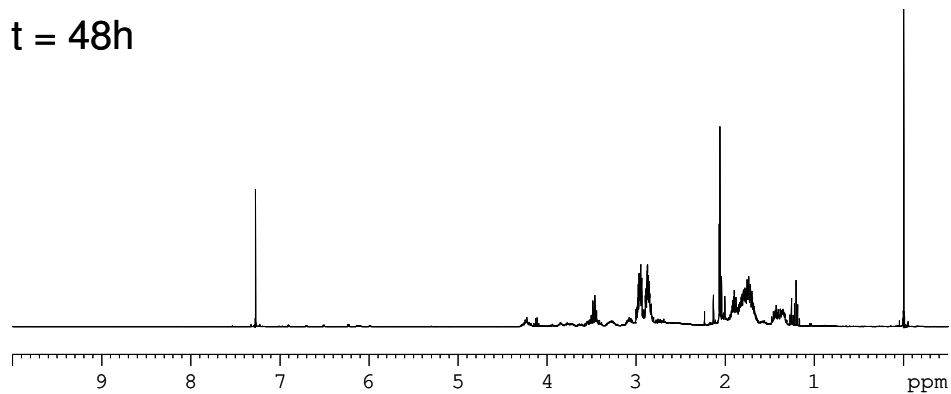
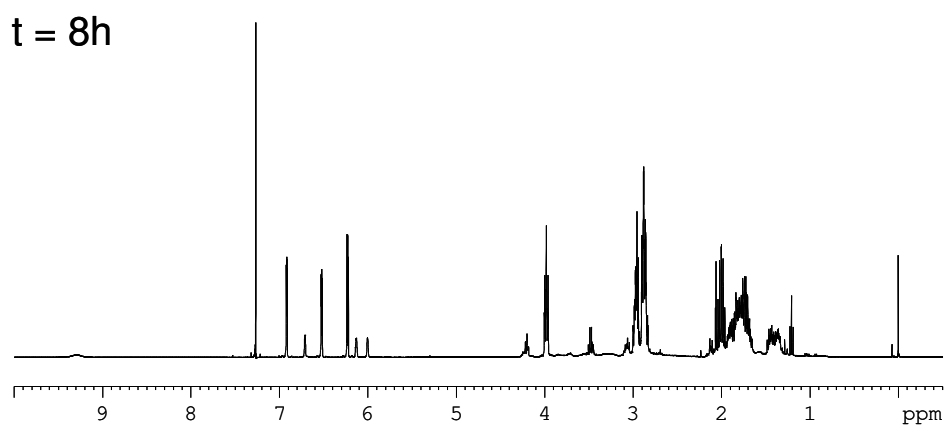
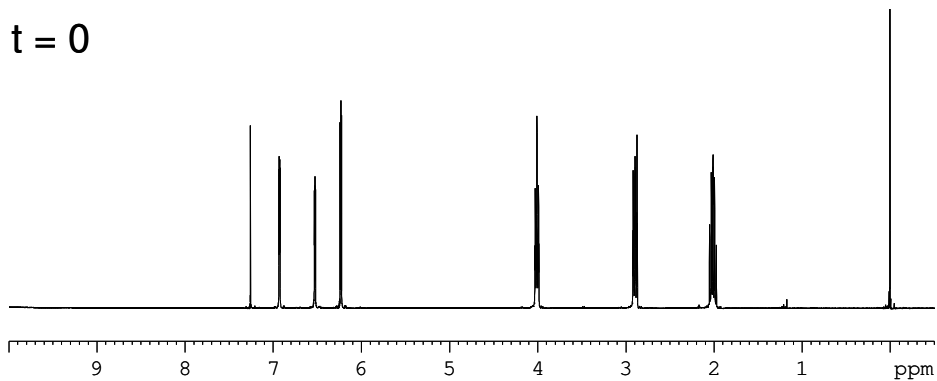


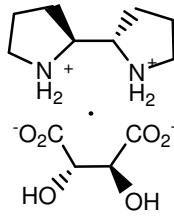
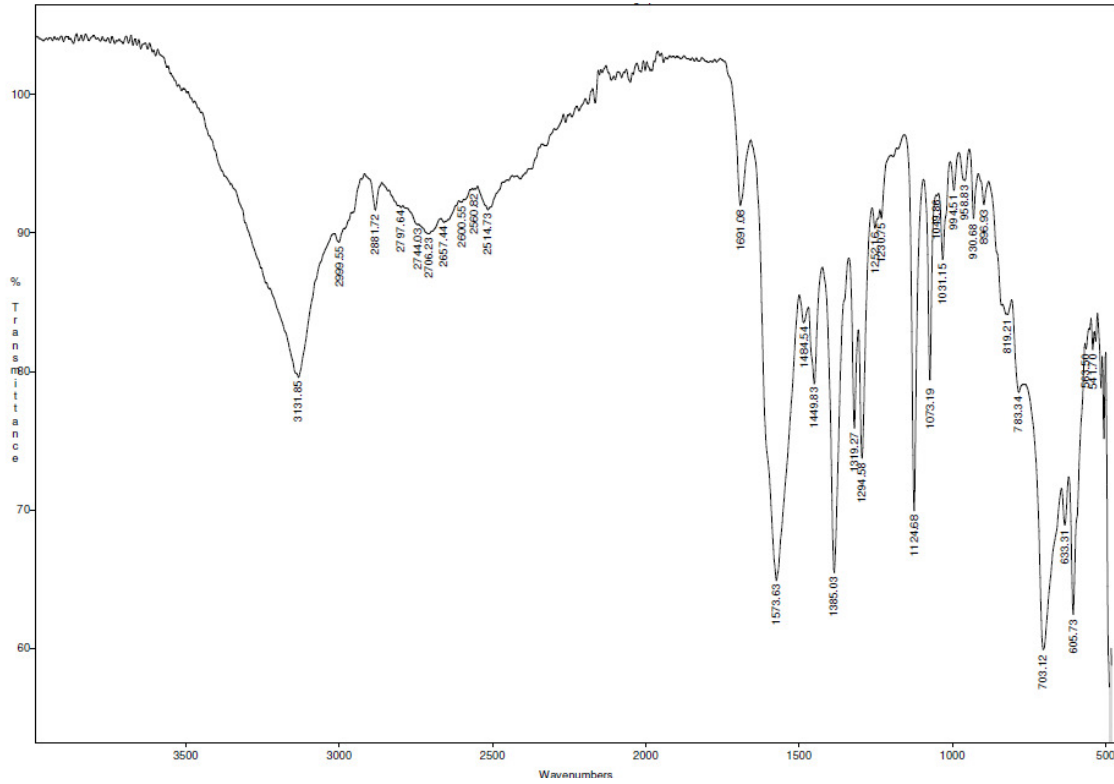
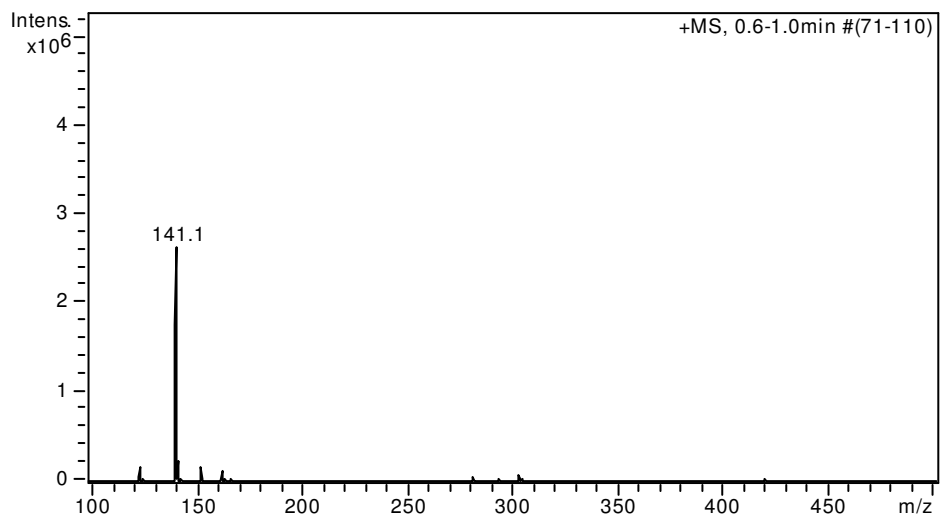
## ESI-MS



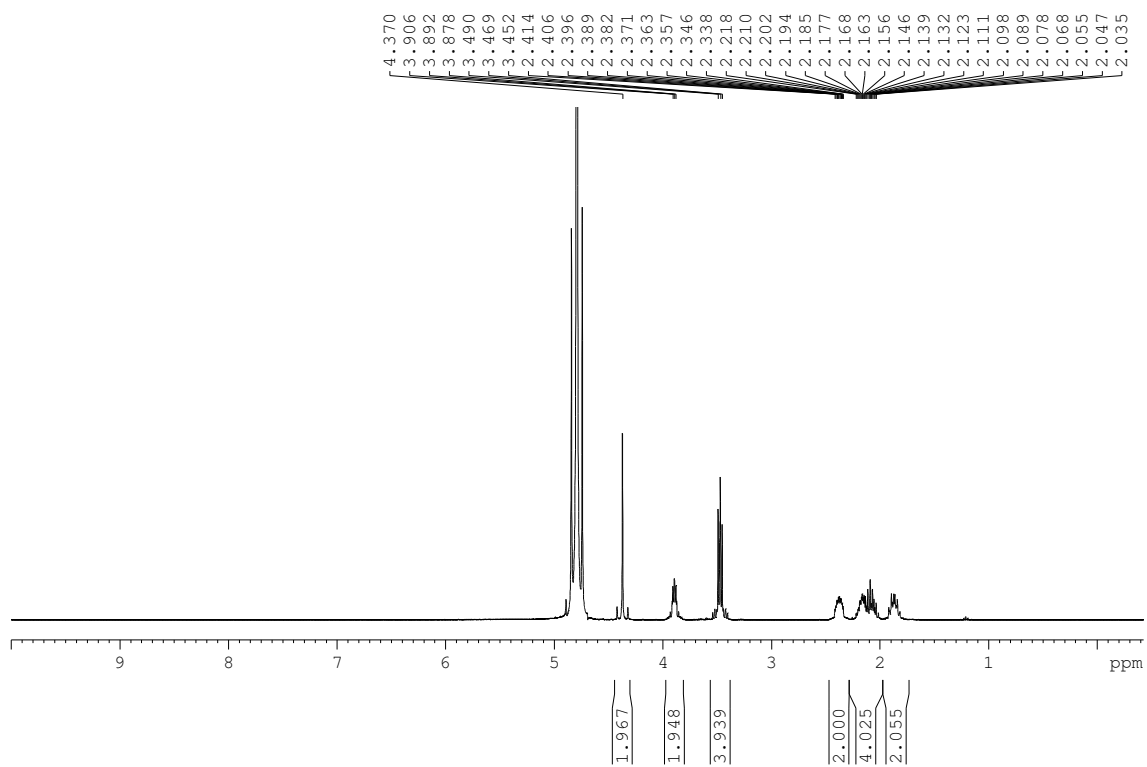
**$^1\text{H-NMR}$  ( $\text{CDCl}_3$ , 400 MHz, 300K)** **$^{13}\text{C-NMR}$  ( $\text{CDCl}_3$ , 100 MHz, 300K)**

**HSQCed (CDCl<sub>3</sub>, 400 MHz, 300K)**

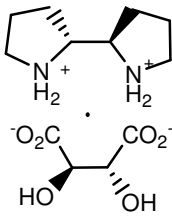
Reaction monitoring by  $^1\text{H-NMR}$  $^1\text{H-NMR}$  ( $\text{CDCl}_3$ , 400 MHz, 300K)

**(S,S)-2,2'-bipyrrolidine D-tartrate****FT-IR (ATR)****ESI-MS**

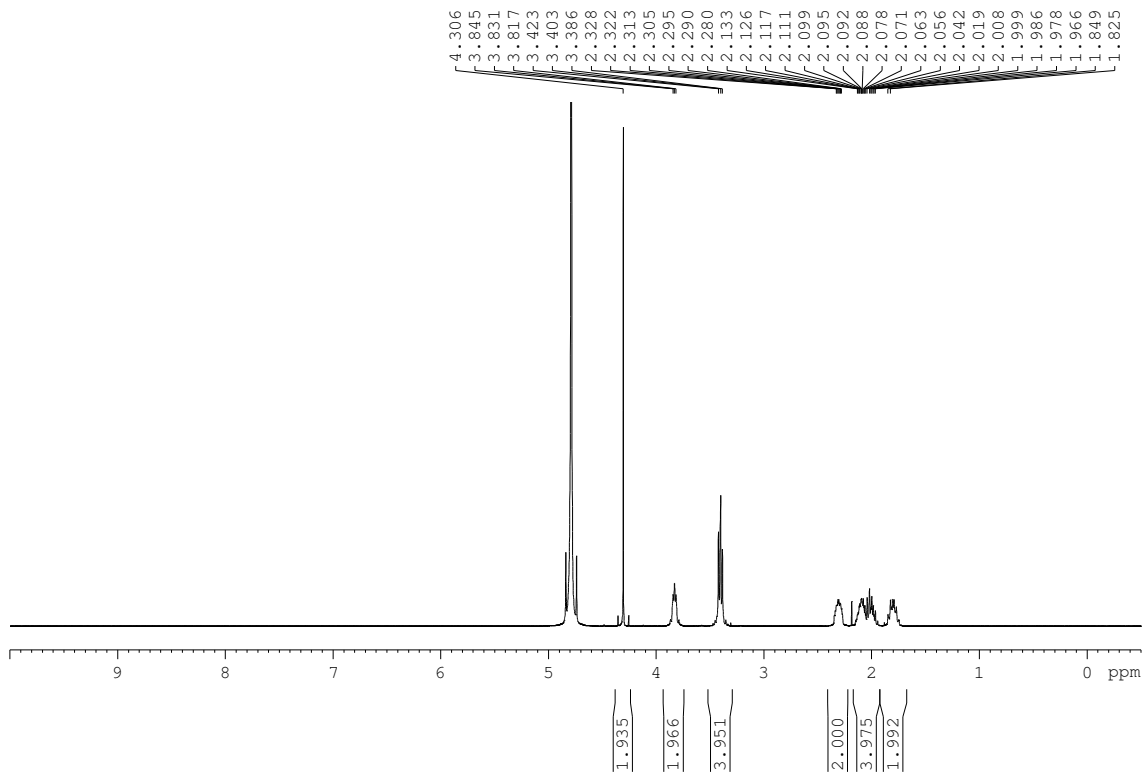


**$^1\text{H-NMR}$  ( $\text{D}_2\text{O}$ , 400 MHz, 300K)**

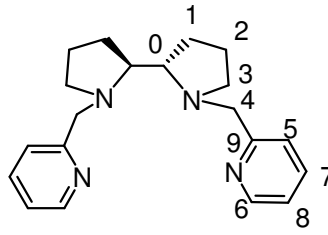
(*R,R*)-2,2'-bipyrrolidine L-tartrate



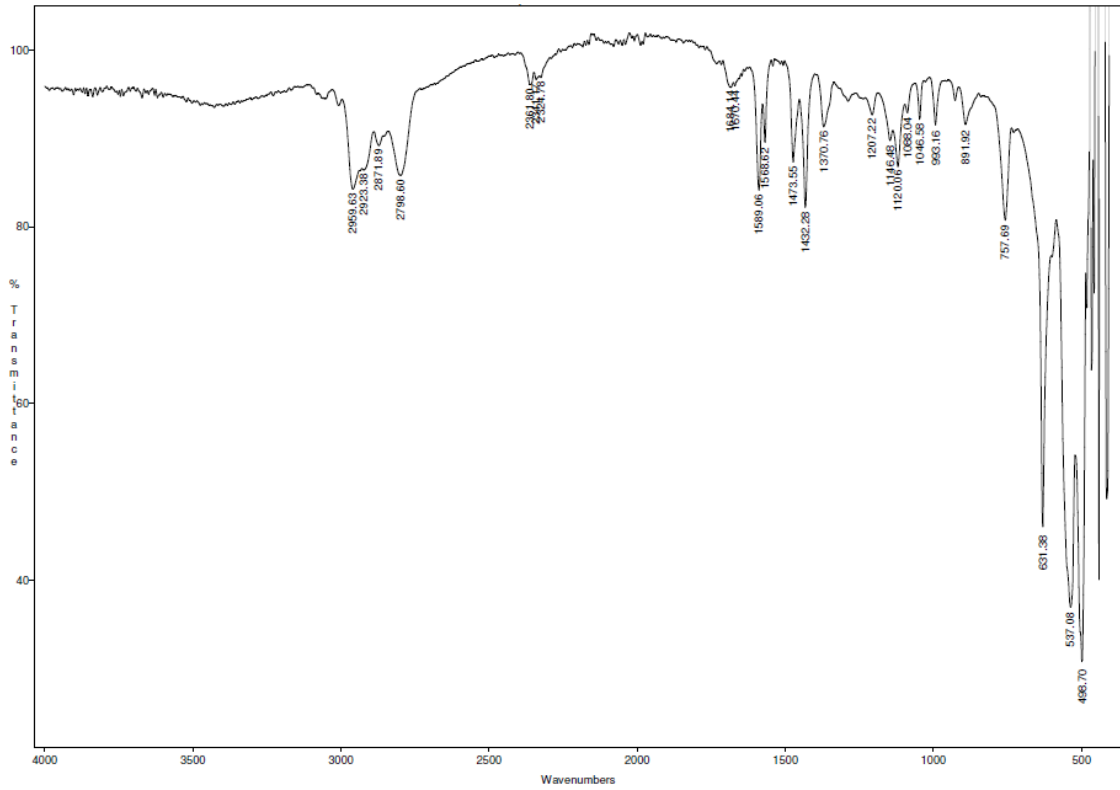
<sup>1</sup>H-NMR (D<sub>2</sub>O, 400 MHz, 300K)



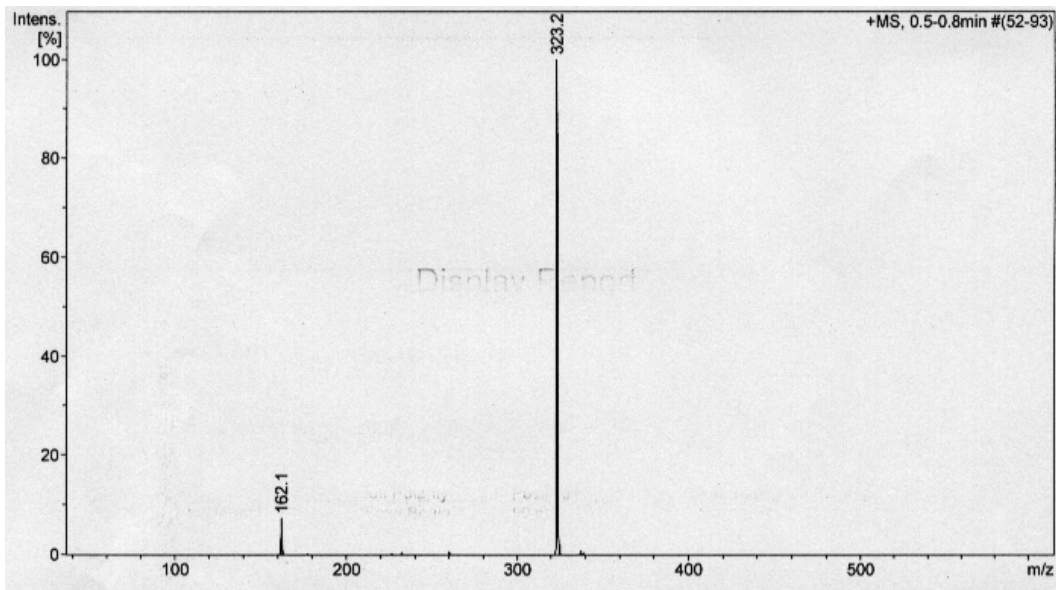
(S,S)-bpbp, L8



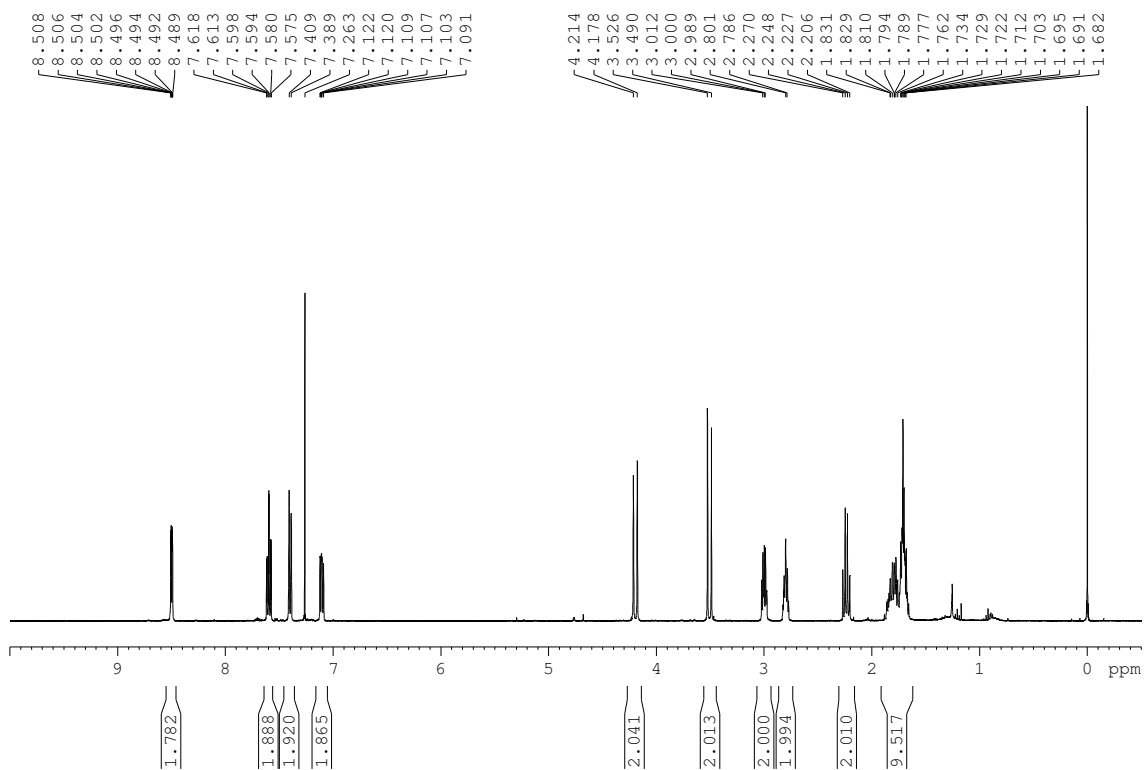
FT-IR (ATR)



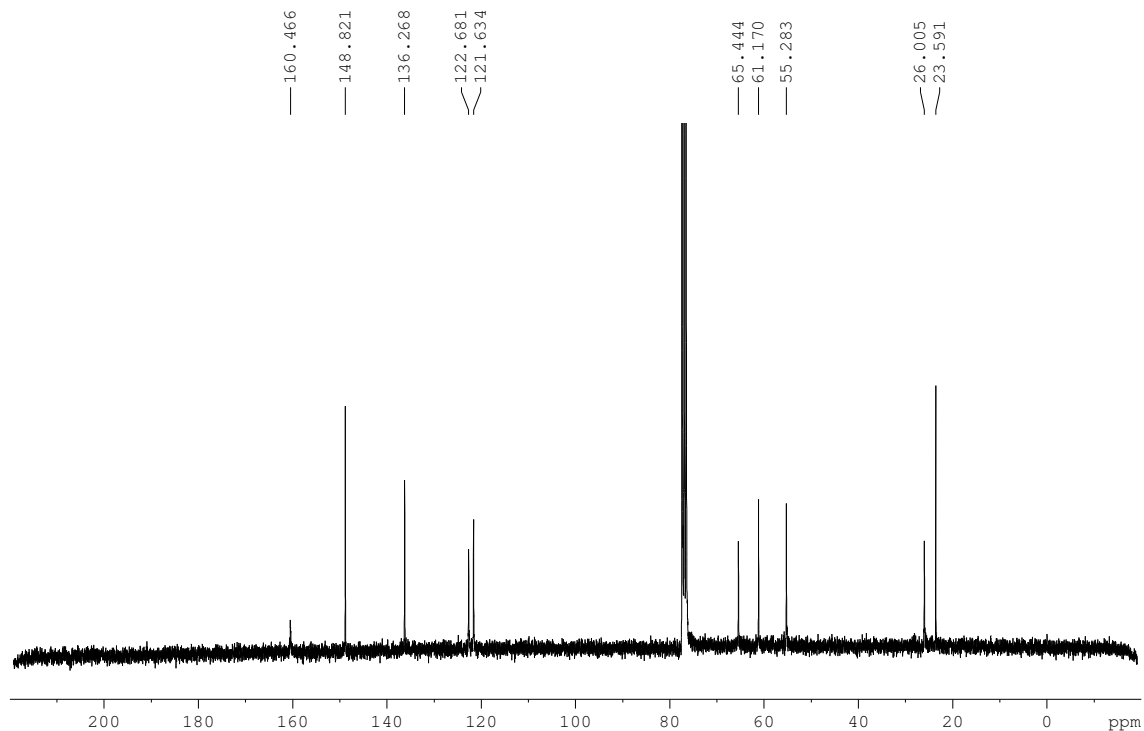
ESI-MS



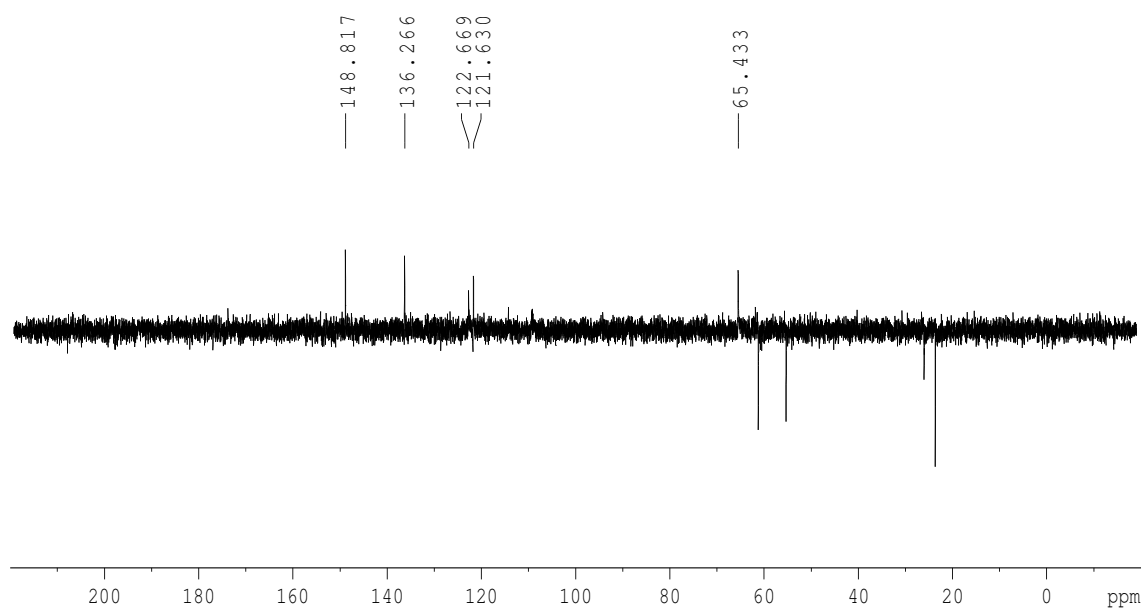
**<sup>1</sup>H-NMR (CDCl<sub>3</sub>, 400 MHz, 300K)**

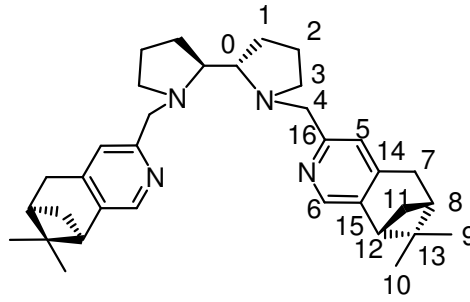
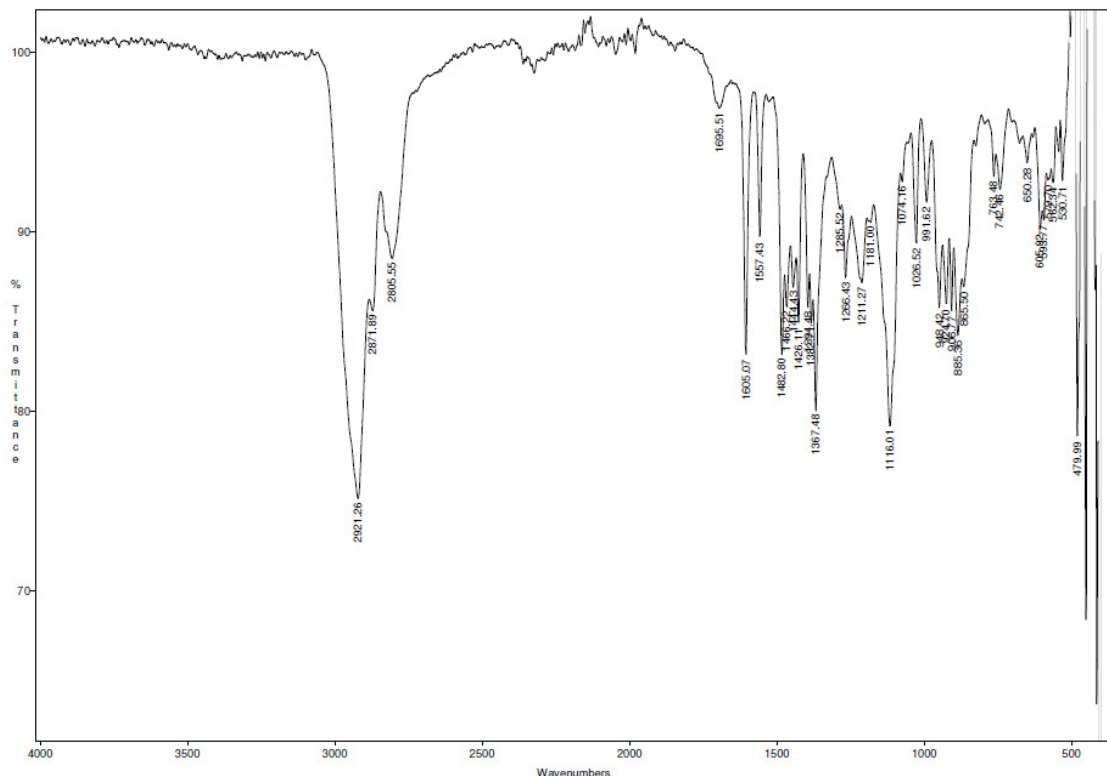
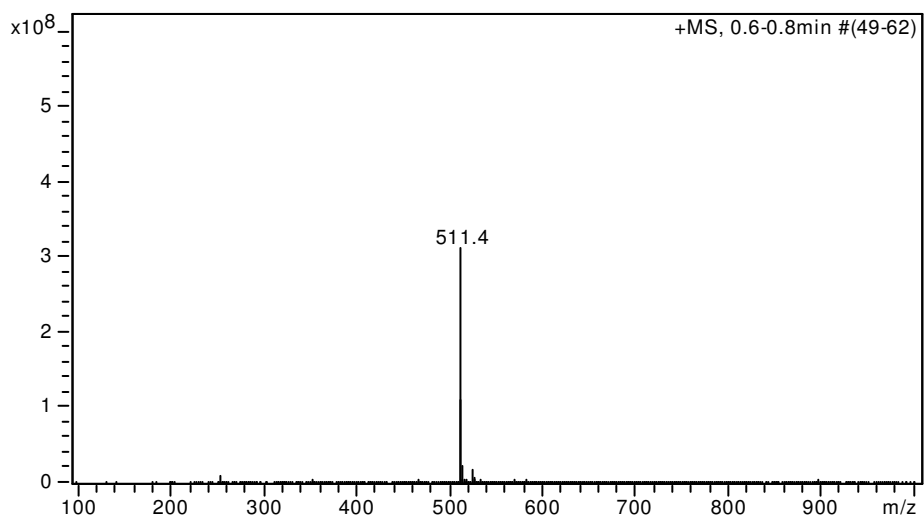


**<sup>13</sup>C-NMR (CDCl<sub>3</sub>, 75 MHz, 300K)**

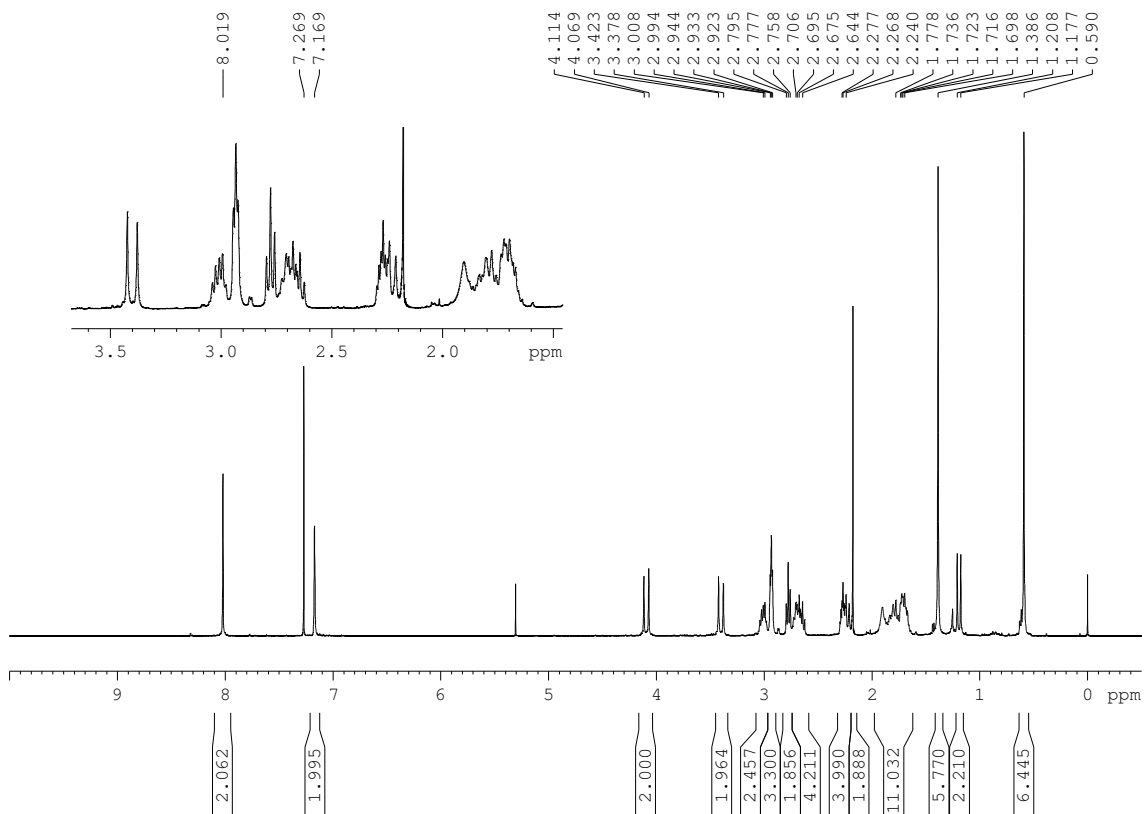


**DEPT 135 (CDCl<sub>3</sub>, 75 MHz, 300K)**

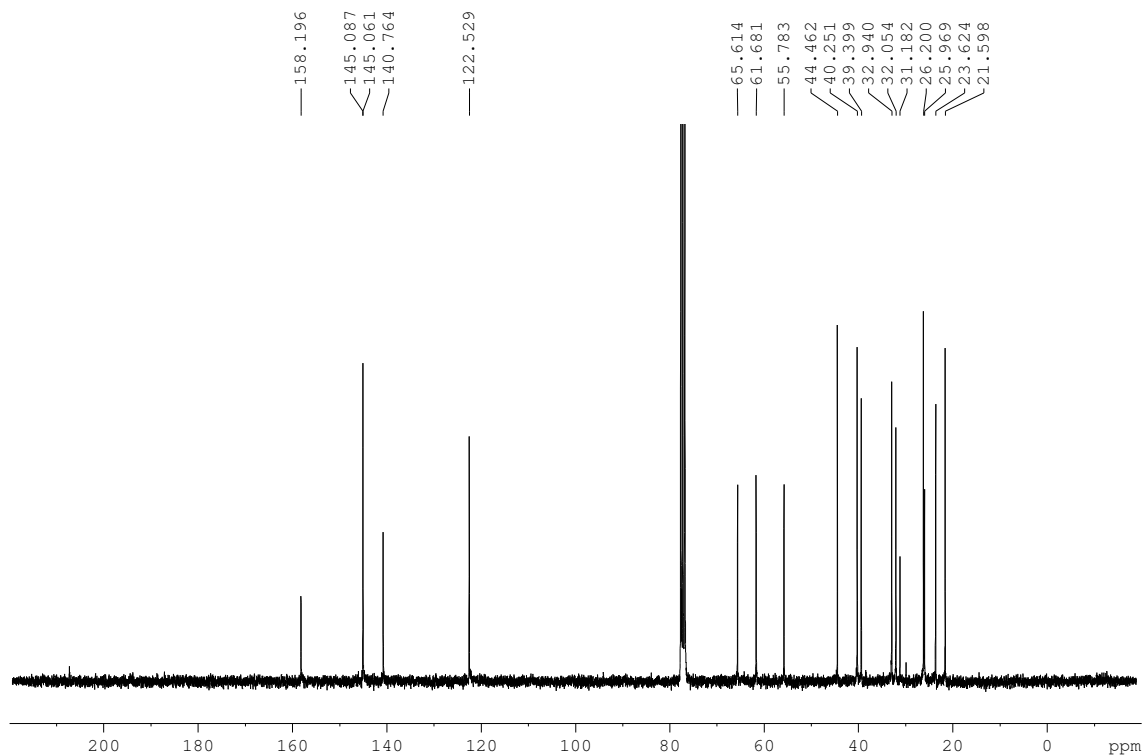


**(S,S,R)-bpbpp, L4****FT-IR (ATR)****ESI-MS**

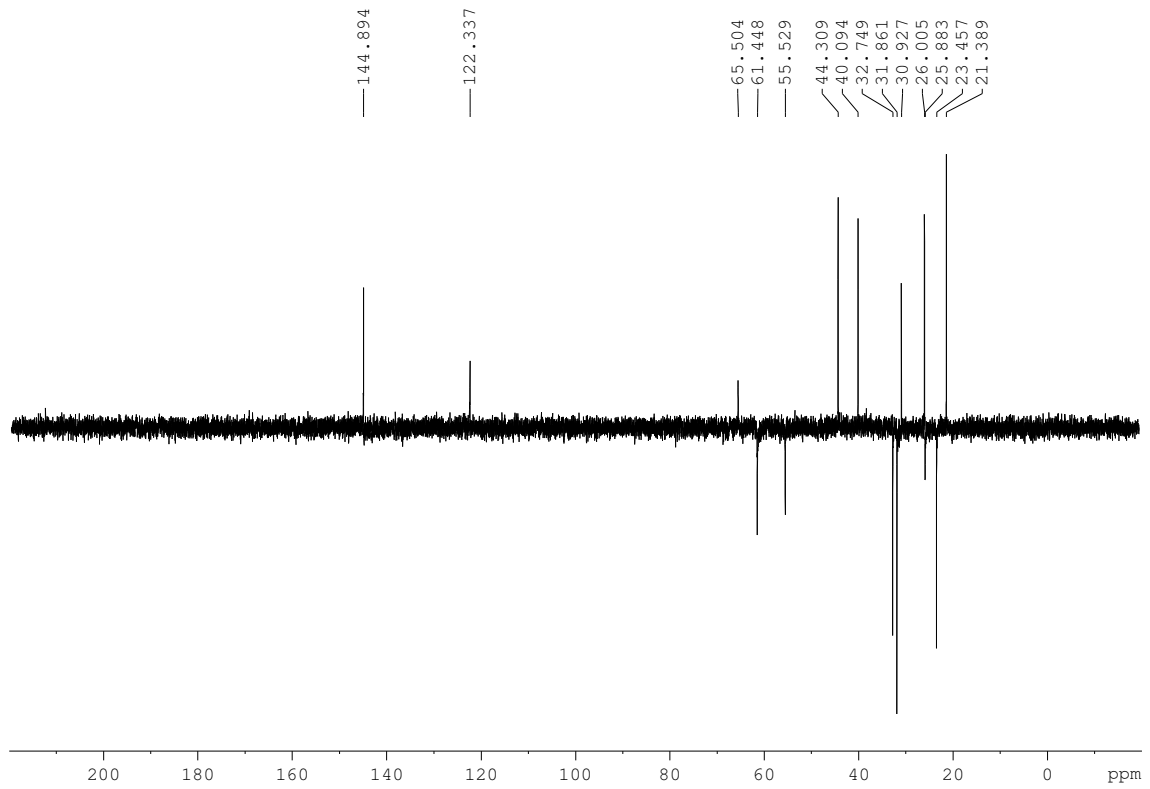
**<sup>1</sup>H-NMR (CDCl<sub>3</sub>, 300 MHz, 300K)**



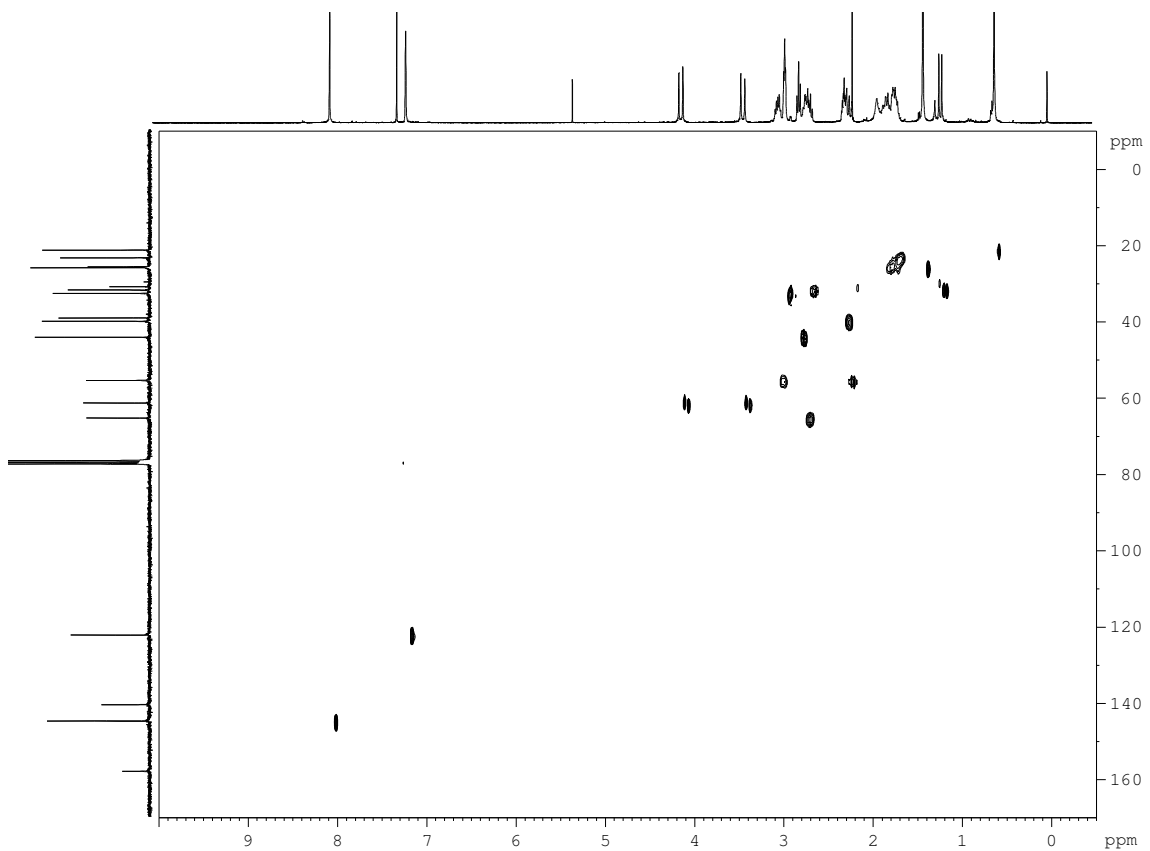
**<sup>13</sup>C-NMR (CDCl<sub>3</sub>, 75 MHz, 300K)**



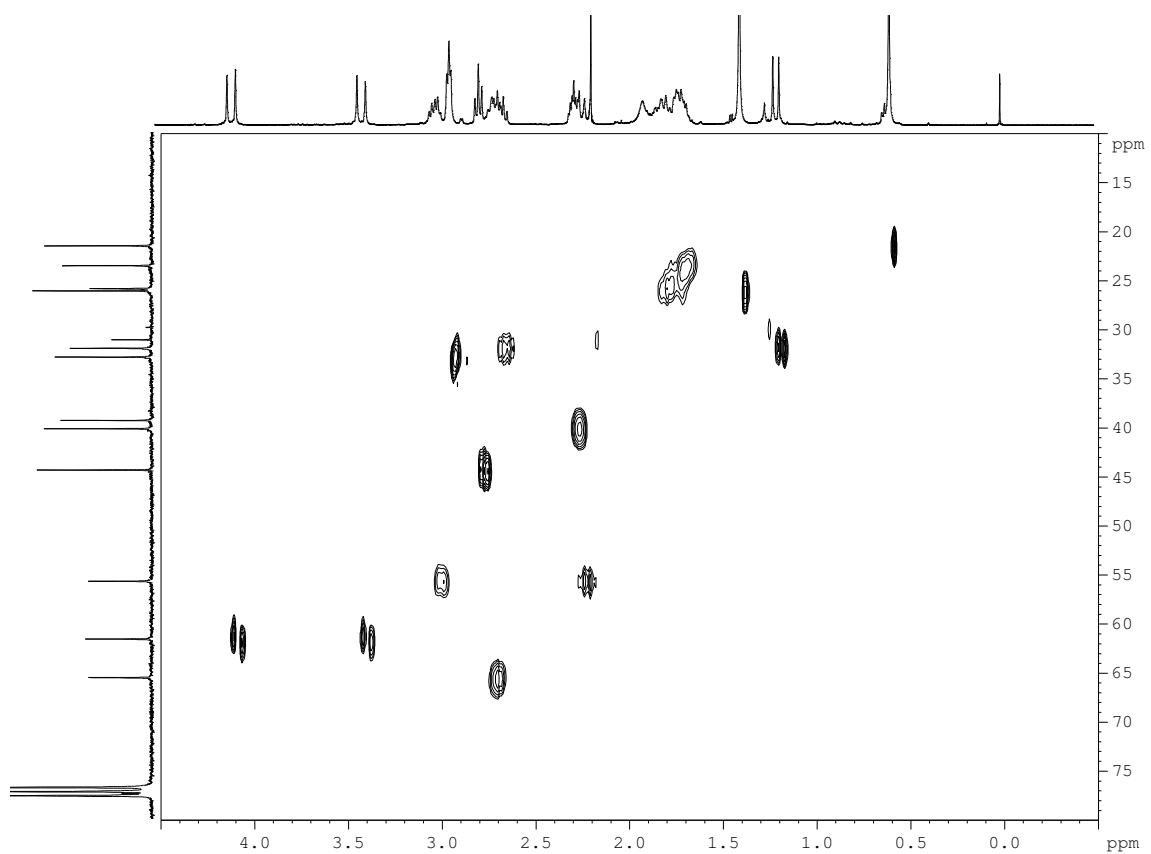
**DEPT 135 (CDCl<sub>3</sub>, 100 MHz, 300K)**

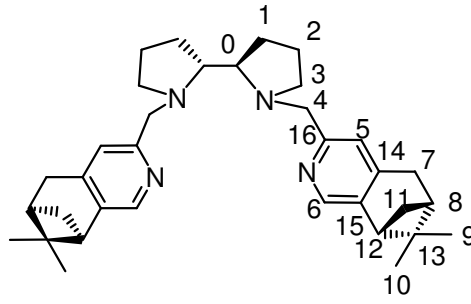
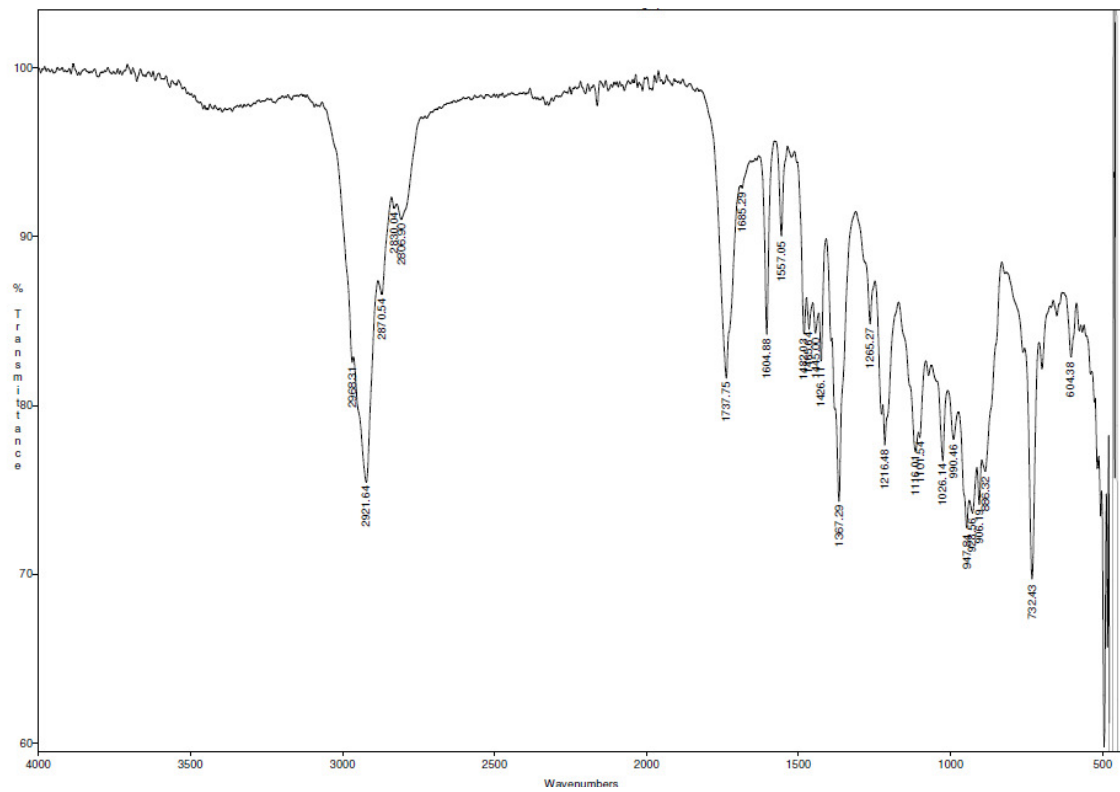
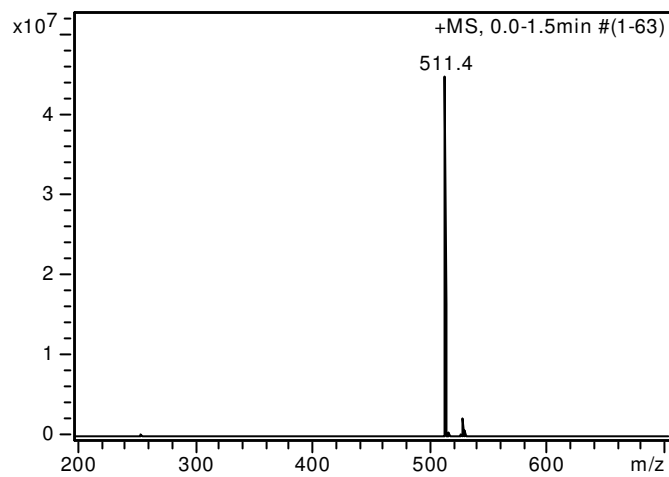


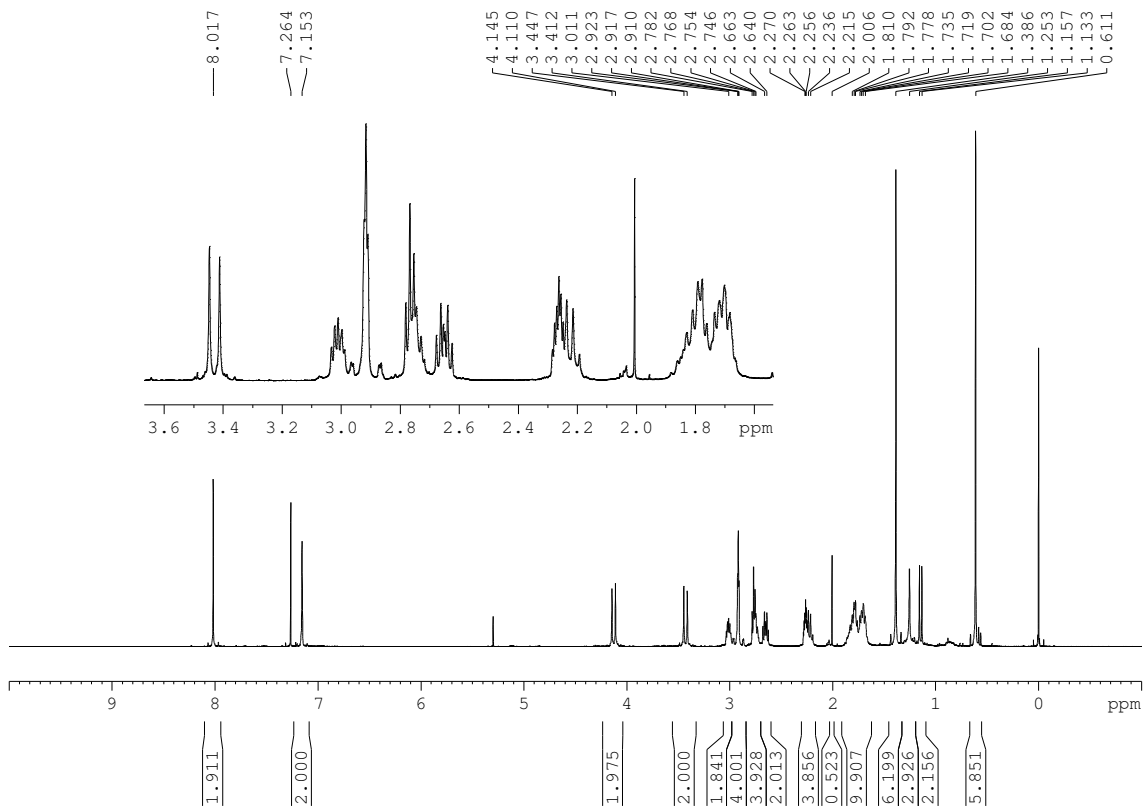
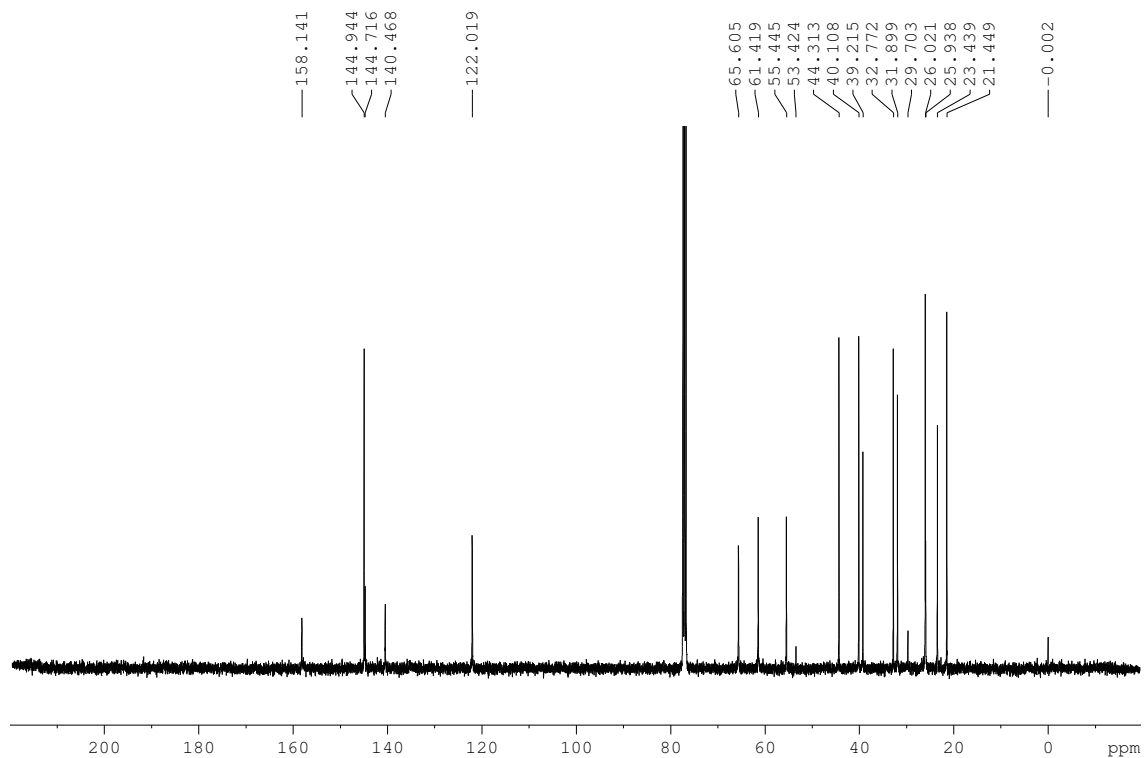
**HSQCed (CDCl<sub>3</sub>, 75 MHz, 300K)**



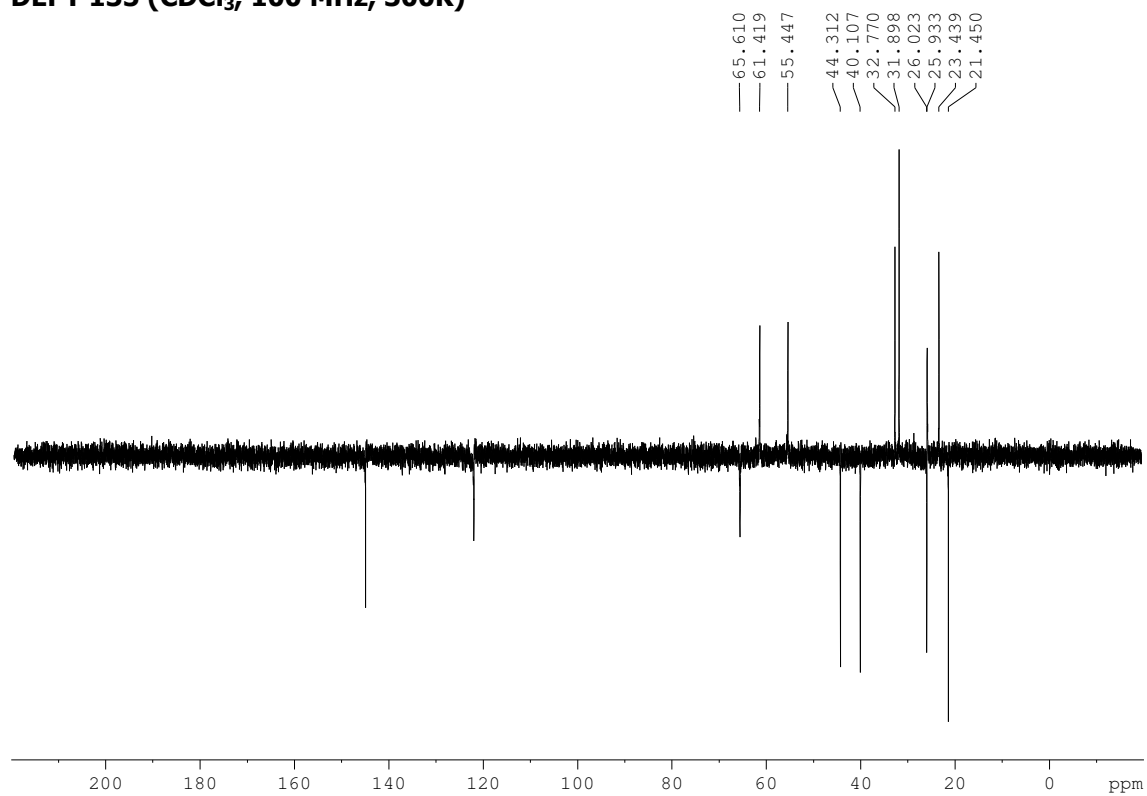


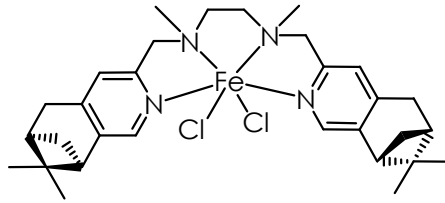


**(R,R,R)-bpbpp, L5****FT-IR (ATR)****ESI-MS**

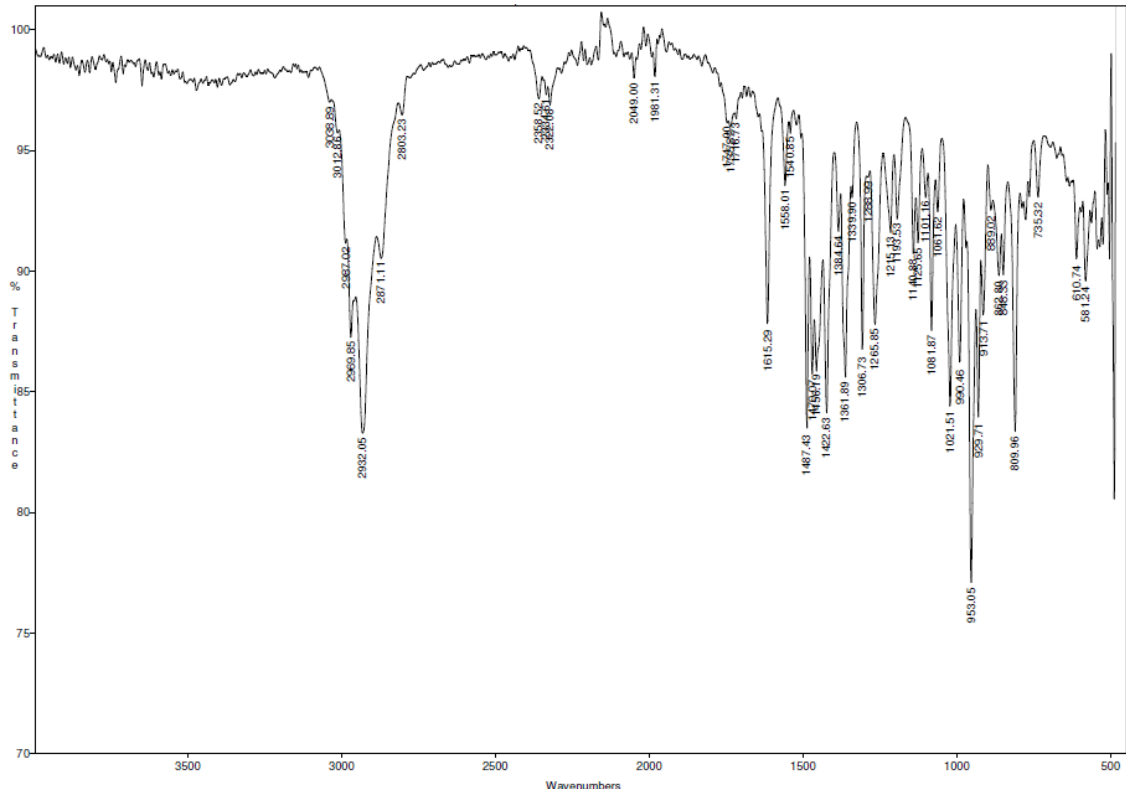
**$^1\text{H-NMR}$  ( $\text{CDCl}_3$ , 400 MHz, 300K)** **$^{13}\text{C-NMR}$  ( $\text{CDCl}_3$ , 100 MHz, 300K)**

**DEPT 135 (CDCl<sub>3</sub>, 100 MHz, 300K)**

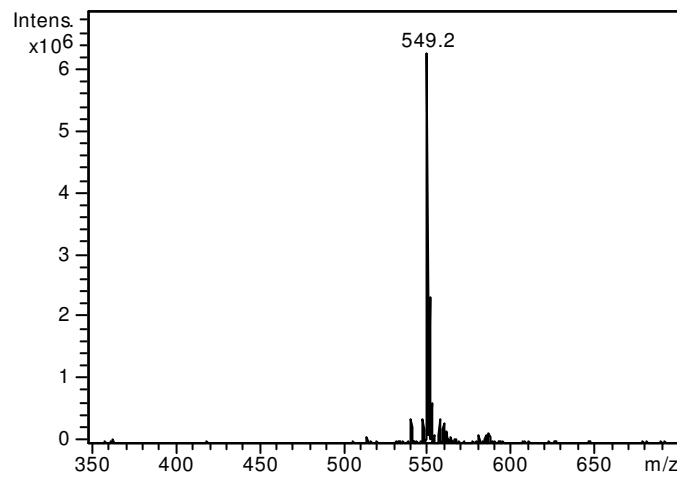


$\Delta$ -[FeCl<sub>2</sub>(L1)], 1Cl

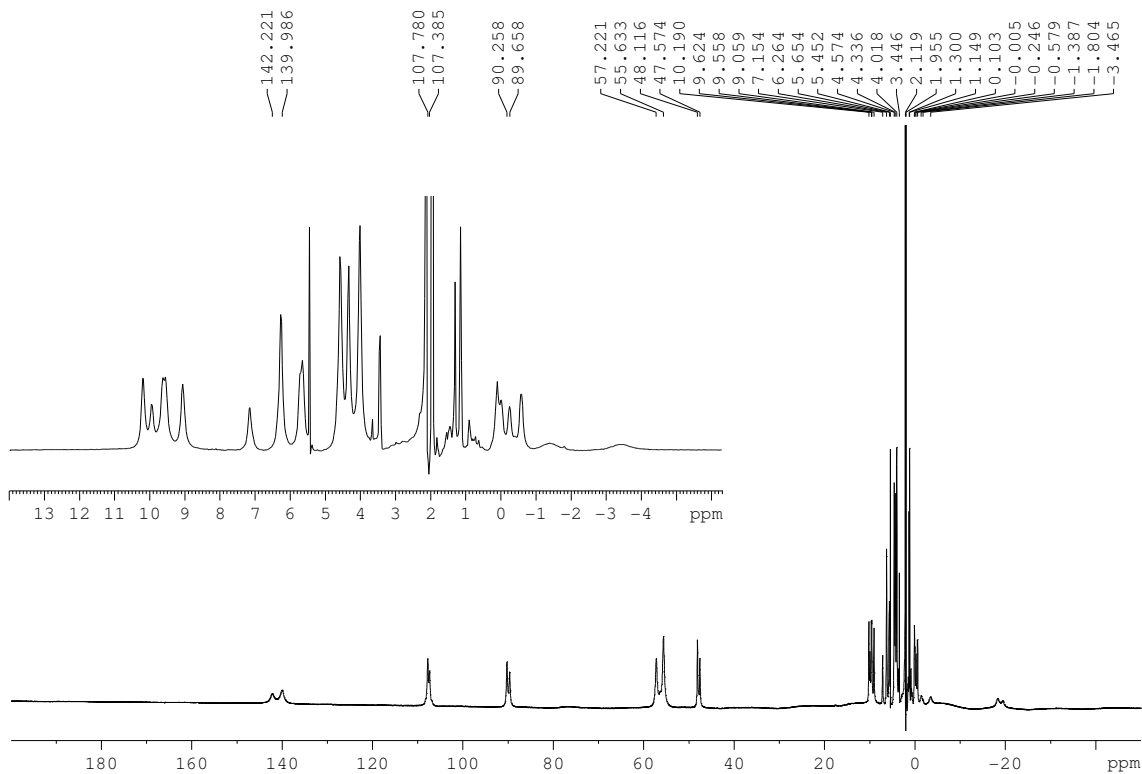
## FT-IR (ATR)



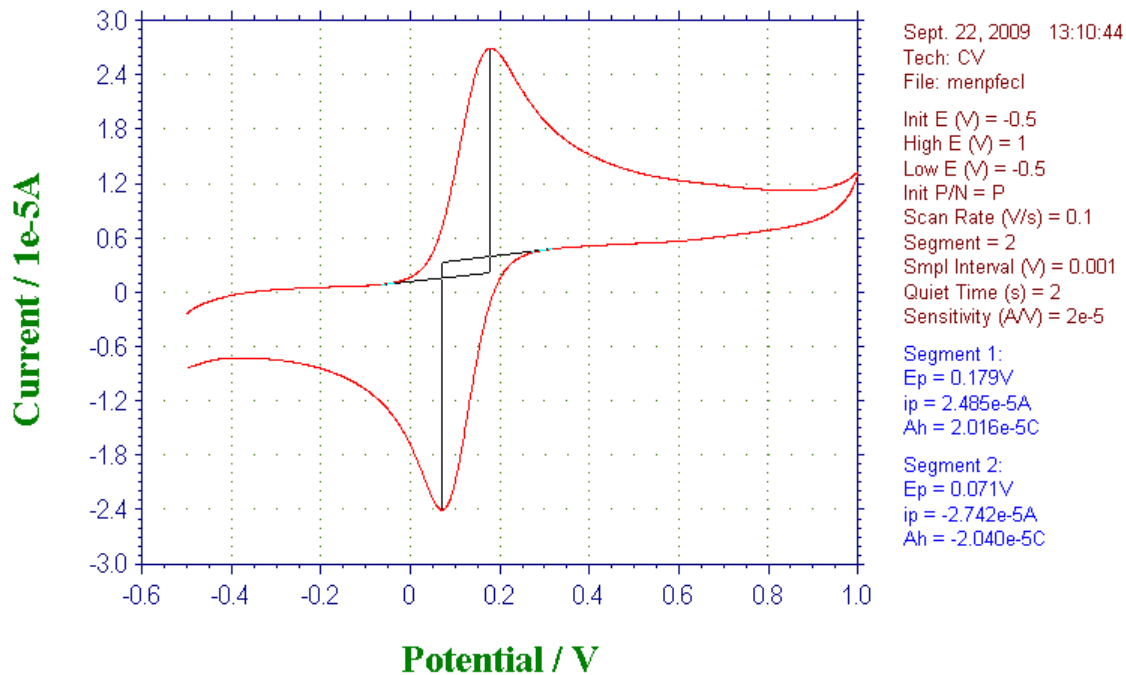
## ESI-MS

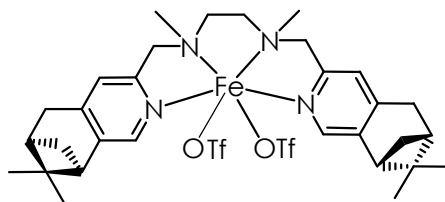
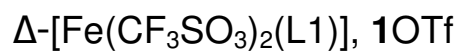
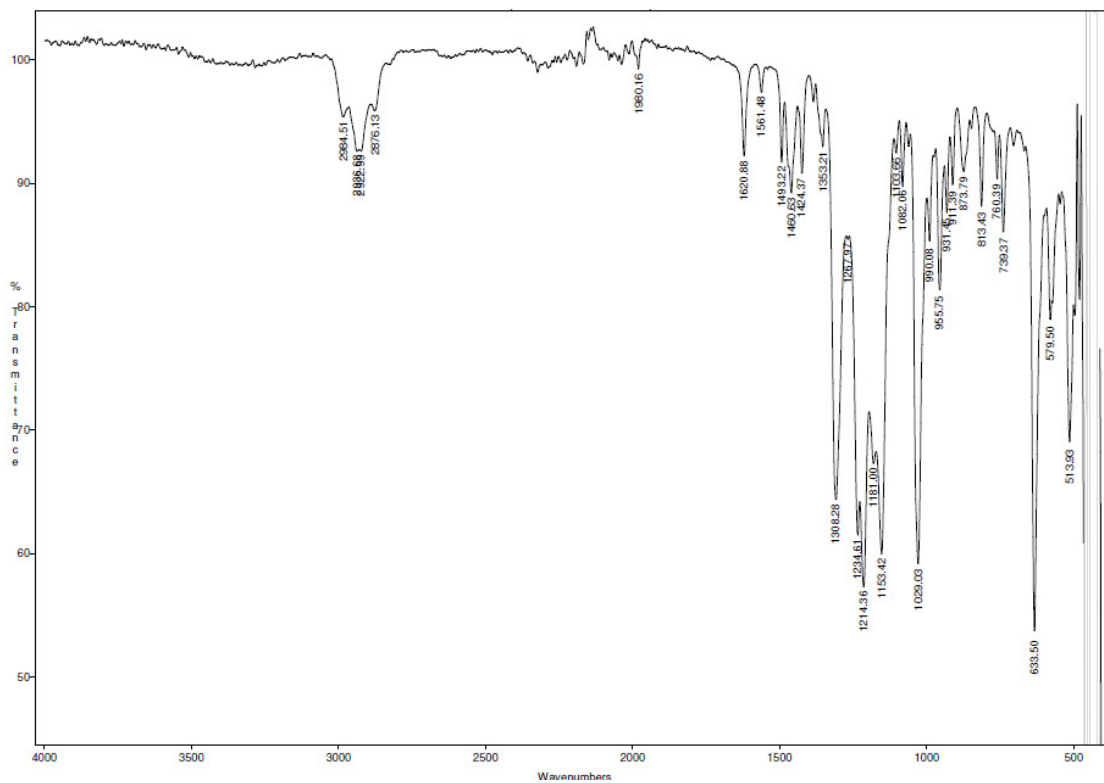
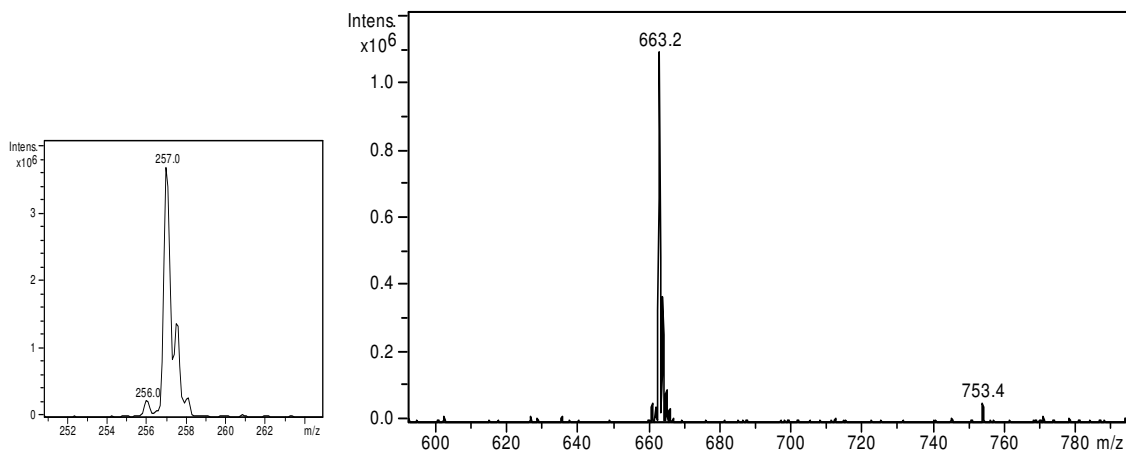


**<sup>1</sup>H-NMR (CD<sub>3</sub>CN, 400 MHz, 300K)**

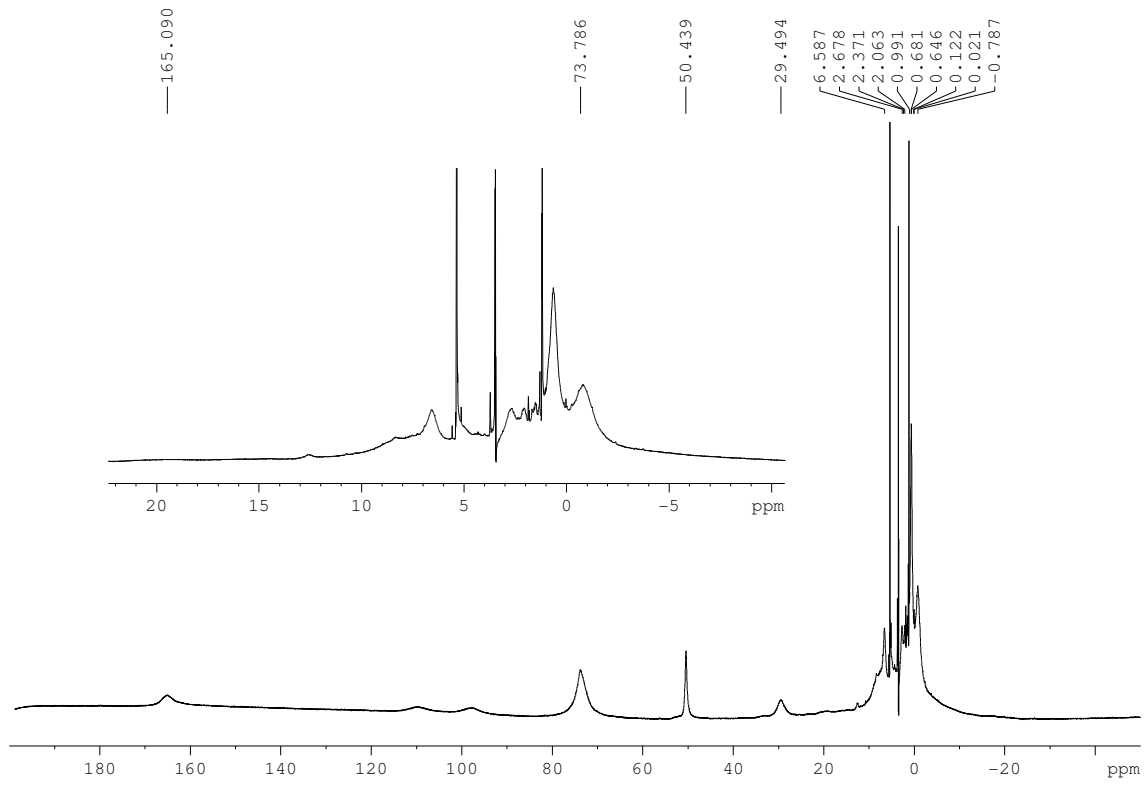


**CV**

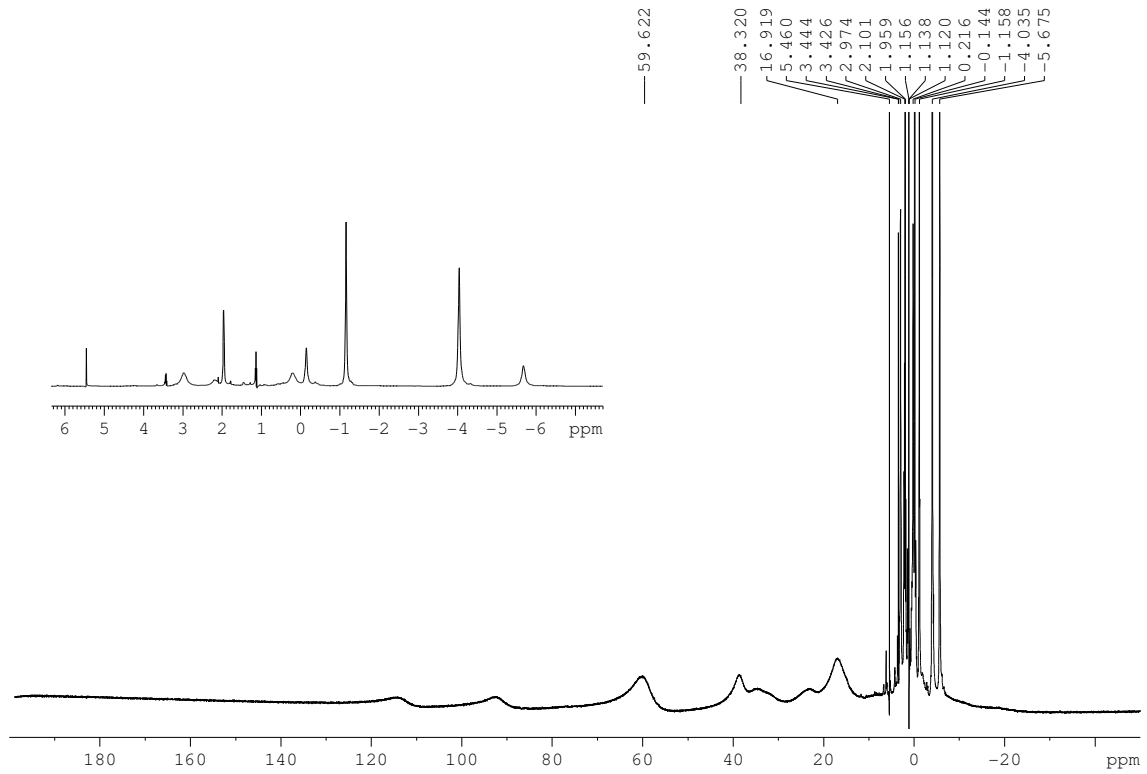


**FT-IR (ATR)****ESI-MS**

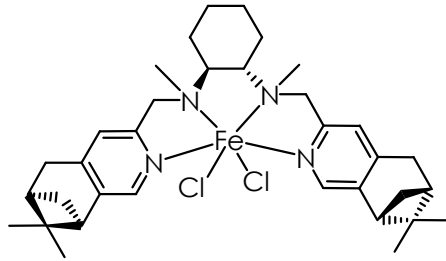
**$^1\text{H-NMR}$  ( $\text{CD}_2\text{Cl}_2$ , 400 MHz, 300K)**



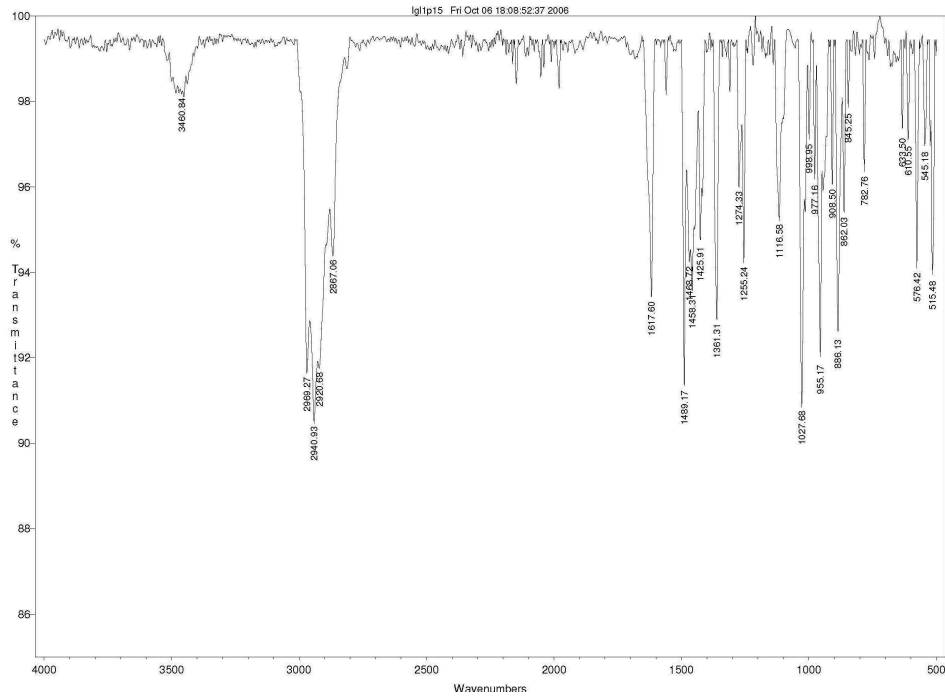
**$^1\text{H-NMR}$  ( $\text{CD}_3\text{CN}$ , 400 MHz, 300K)**



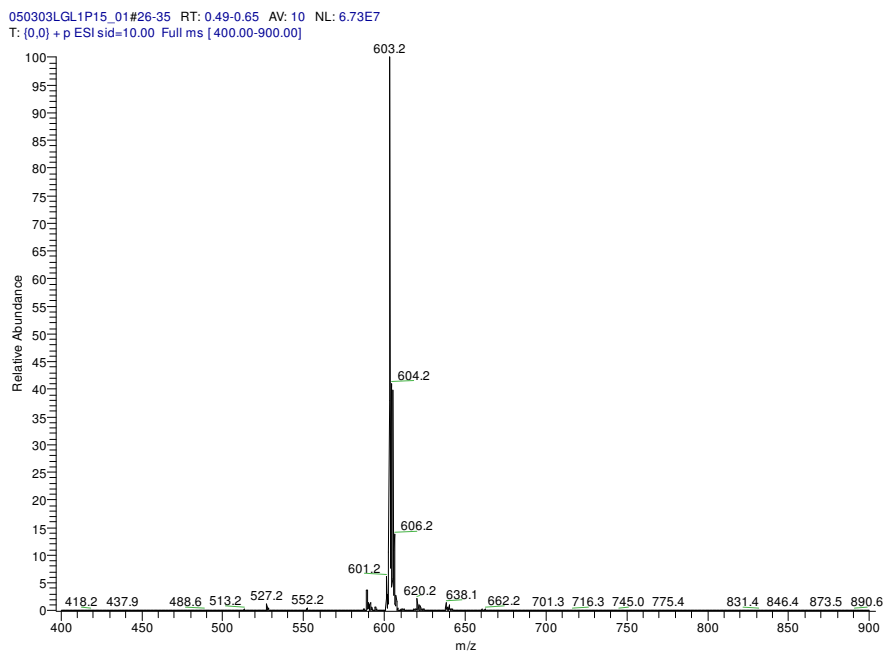


$\Lambda$ -[FeCl<sub>2</sub>(L2)], 2Cl

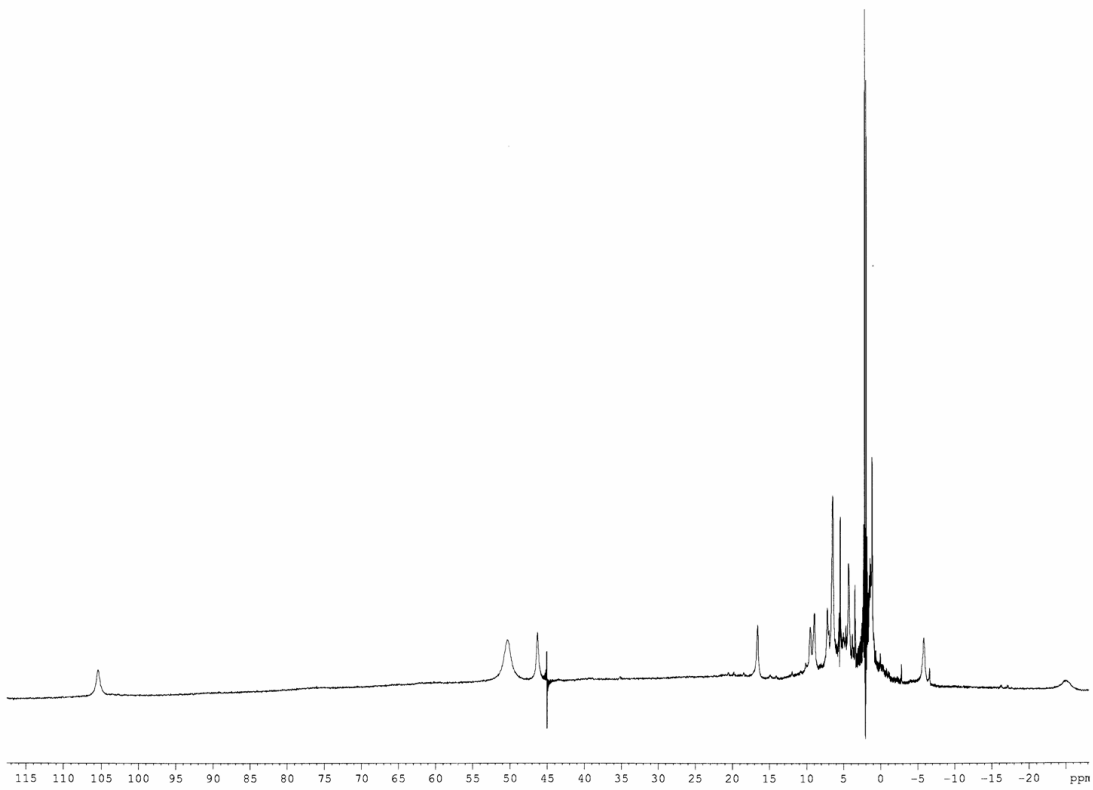
## FT-IR (ATR)



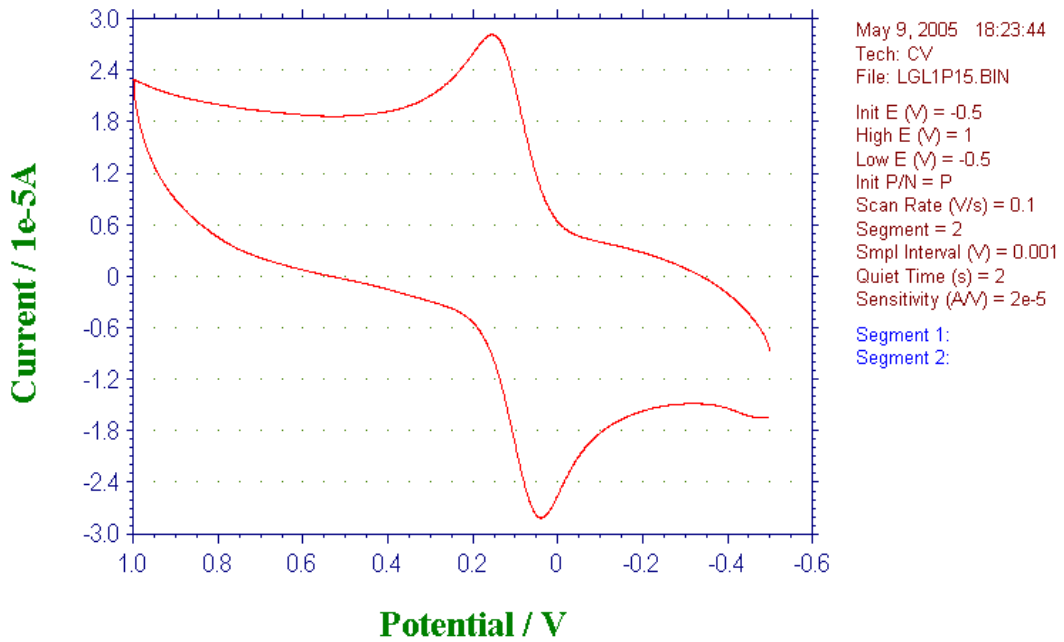
## ESI-MS

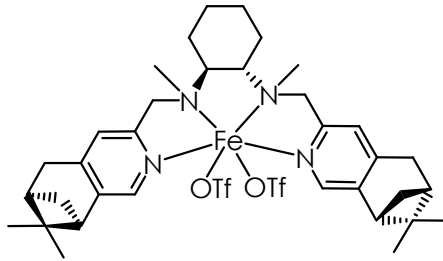


**$^1\text{H-NMR}$  ( $\text{CD}_2\text{Cl}_2$ , 200 MHz, 300K)**

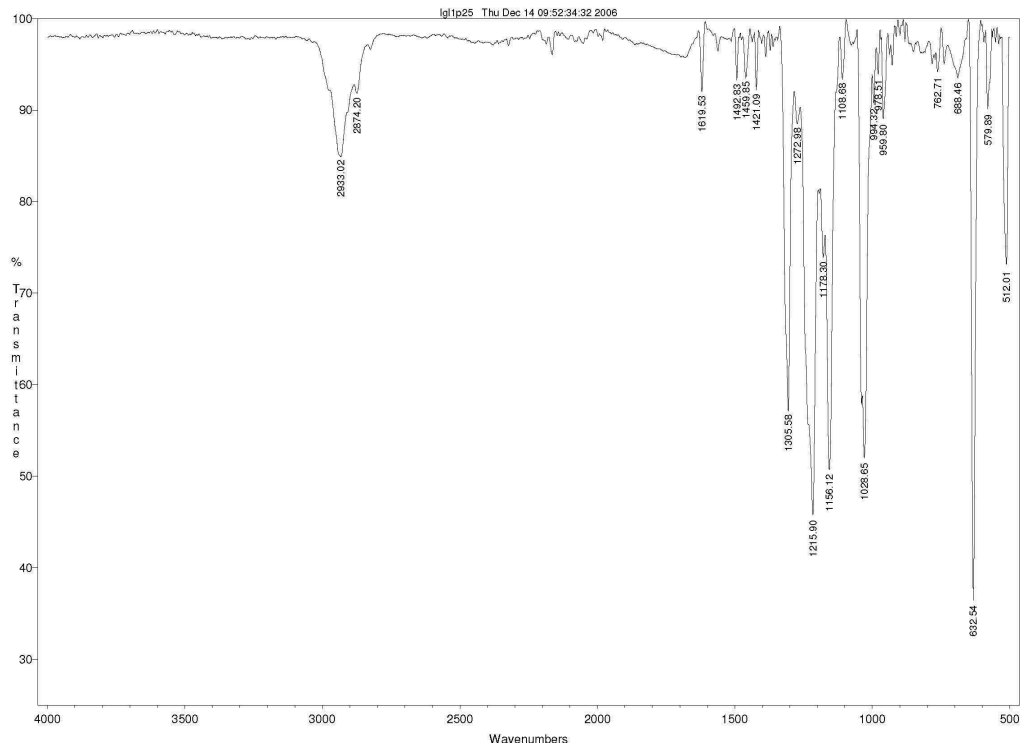


**CV**



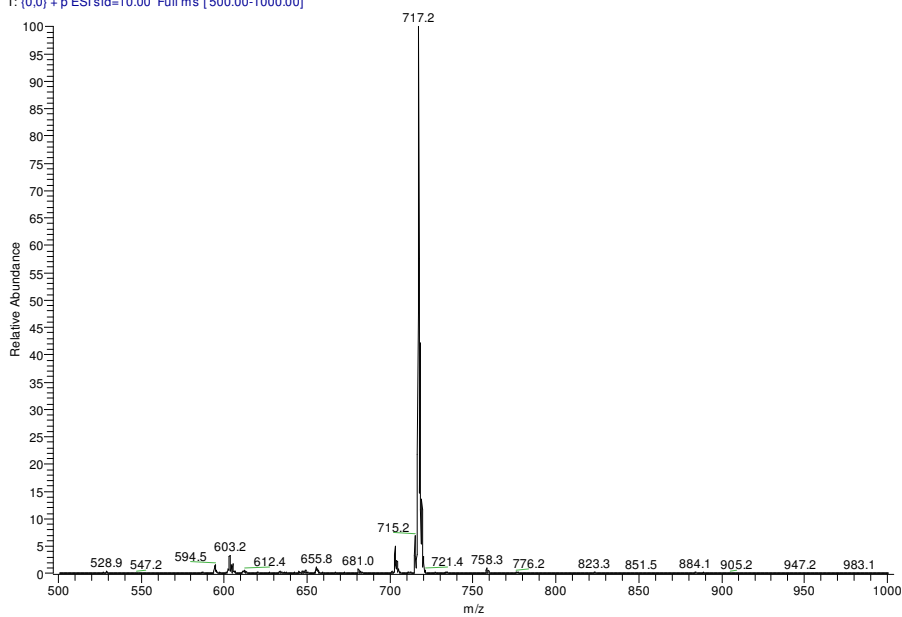
$\Lambda$ -[Fe(CF<sub>3</sub>SO<sub>3</sub>)<sub>2</sub>(L2)], 2OTf

## FT-IR (ATR)

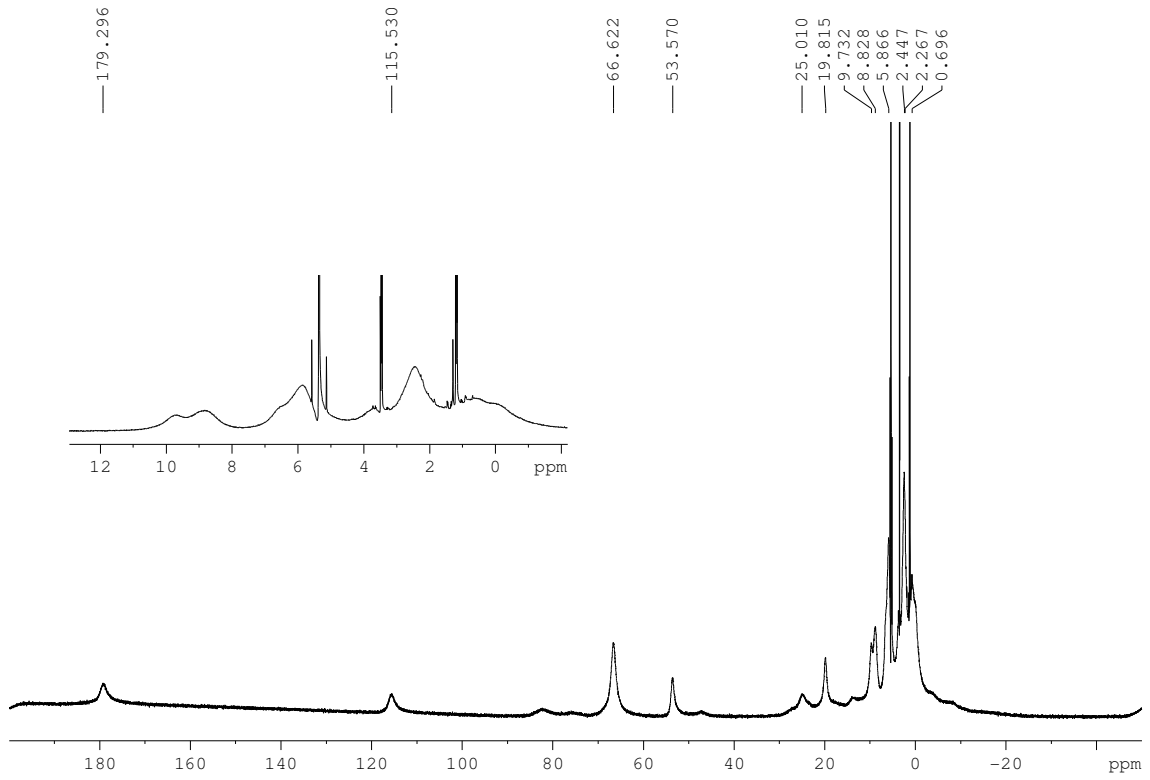


## ESI-MS

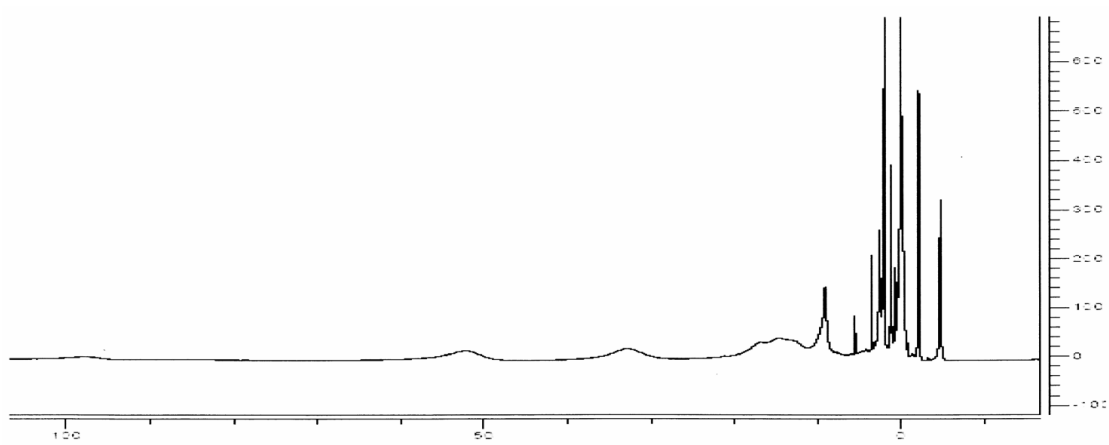
060112LGL1P25\_01#21-28 RT: 0.40-0.52 AV: 8 NL: 1.64E7  
T: [0.0] + p ESI: sid=10.00 Full ms [500.00-1000.00]

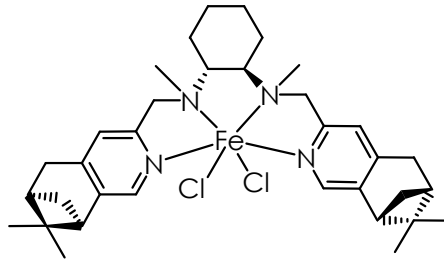


**$^1\text{H-NMR}$  ( $\text{CD}_2\text{Cl}_2$ , 200 MHz, 300K)**

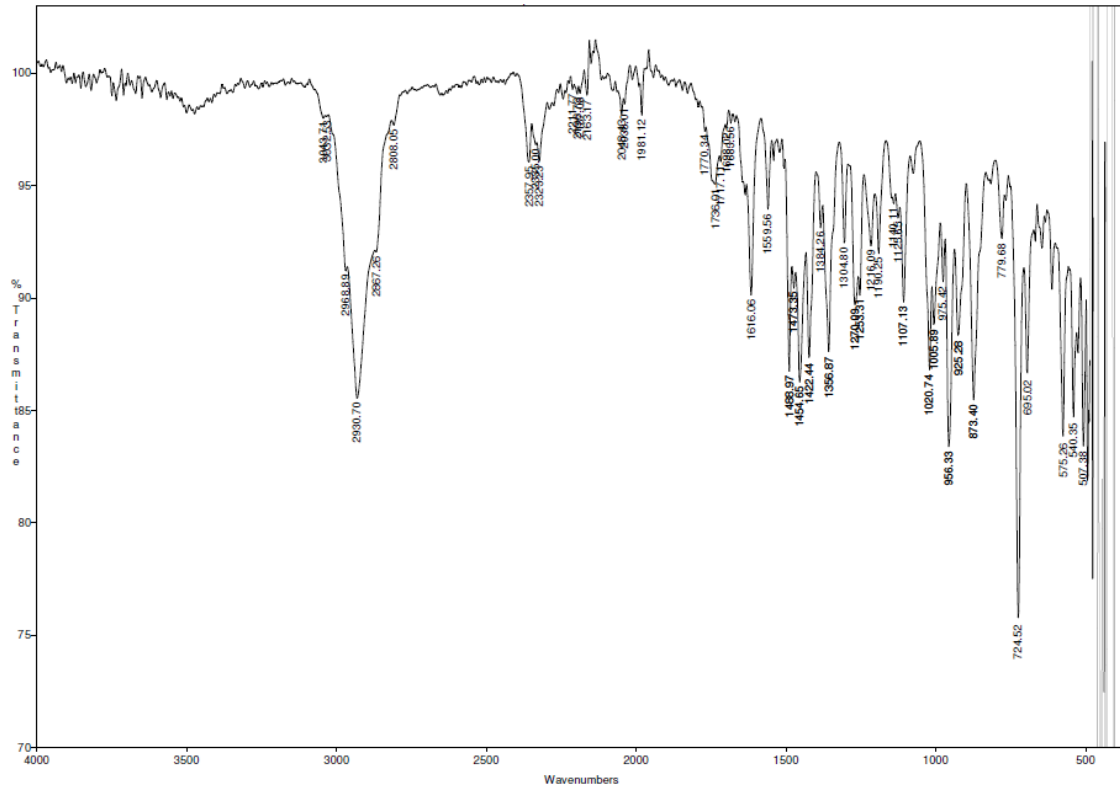


**$^1\text{H-NMR}$  ( $\text{CD}_3\text{CN}$ , 200 MHz, 300K)**

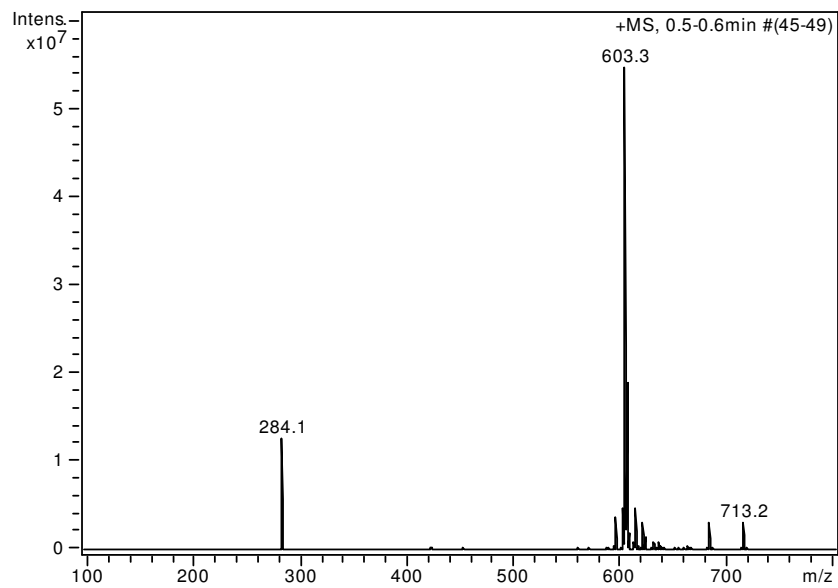


$\Delta$ -[FeCl<sub>2</sub>(L3)], 3Cl

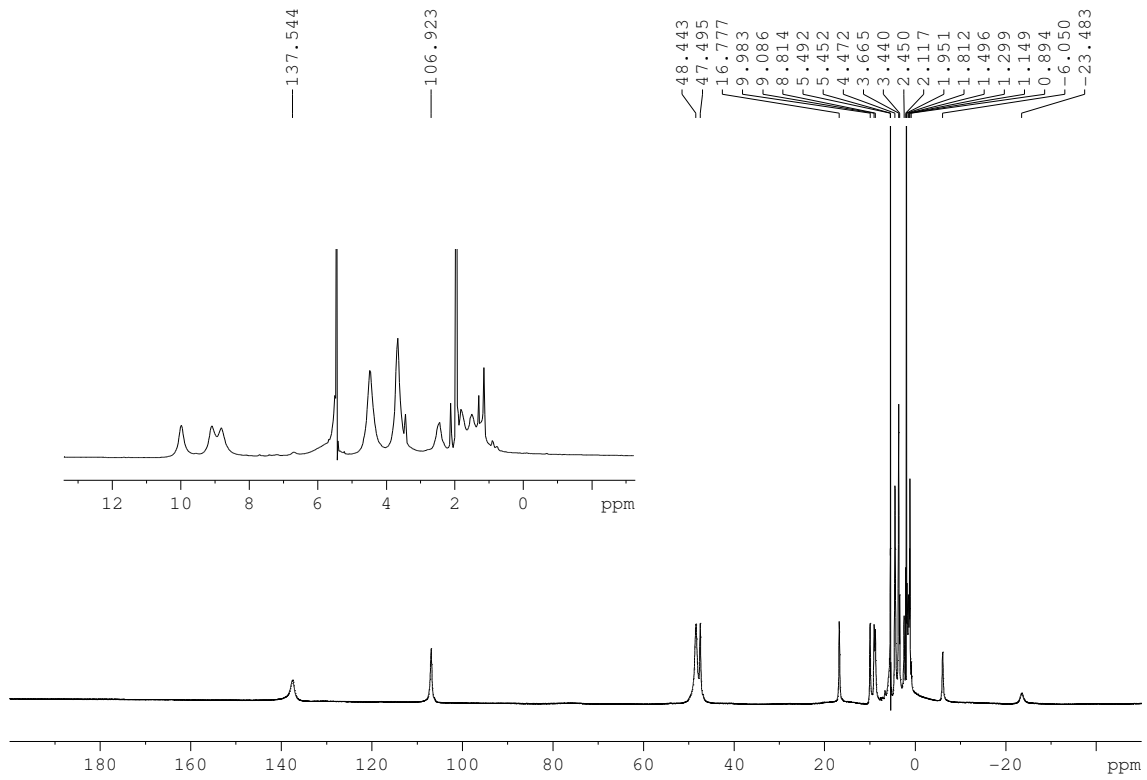
## FT-IR (ATR)



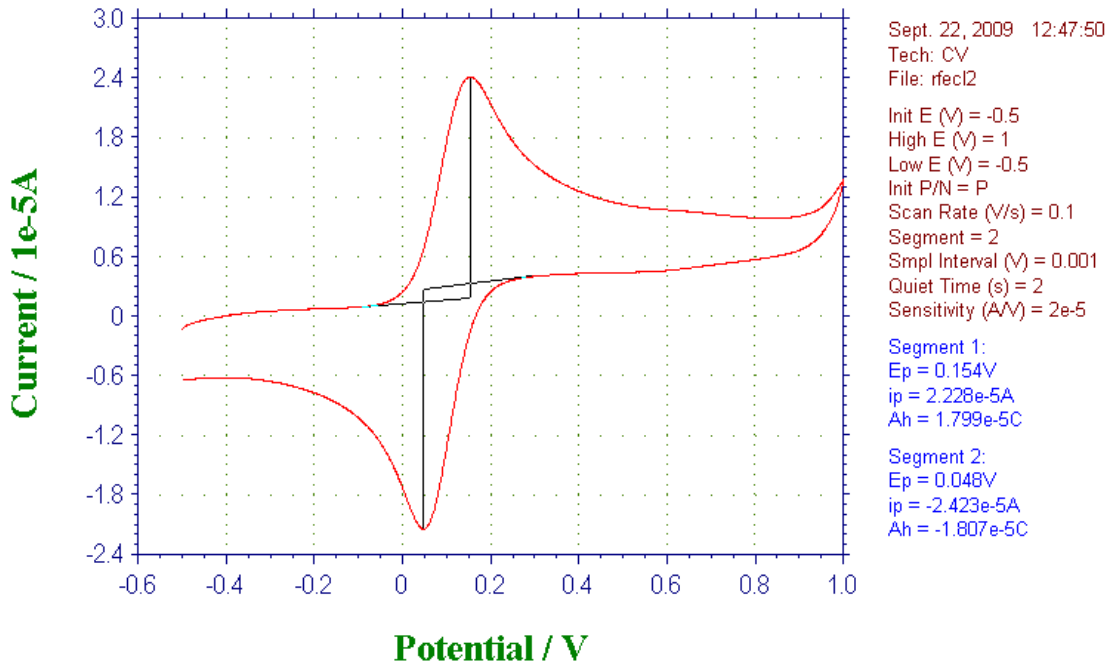
## ESI-MS

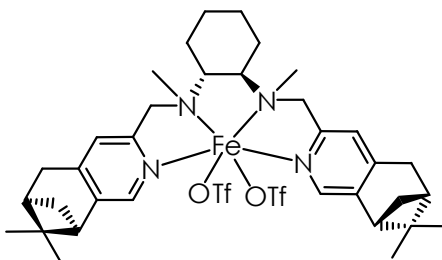


**<sup>1</sup>H-NMR (CD<sub>3</sub>CN, 200 MHz, 300K)**

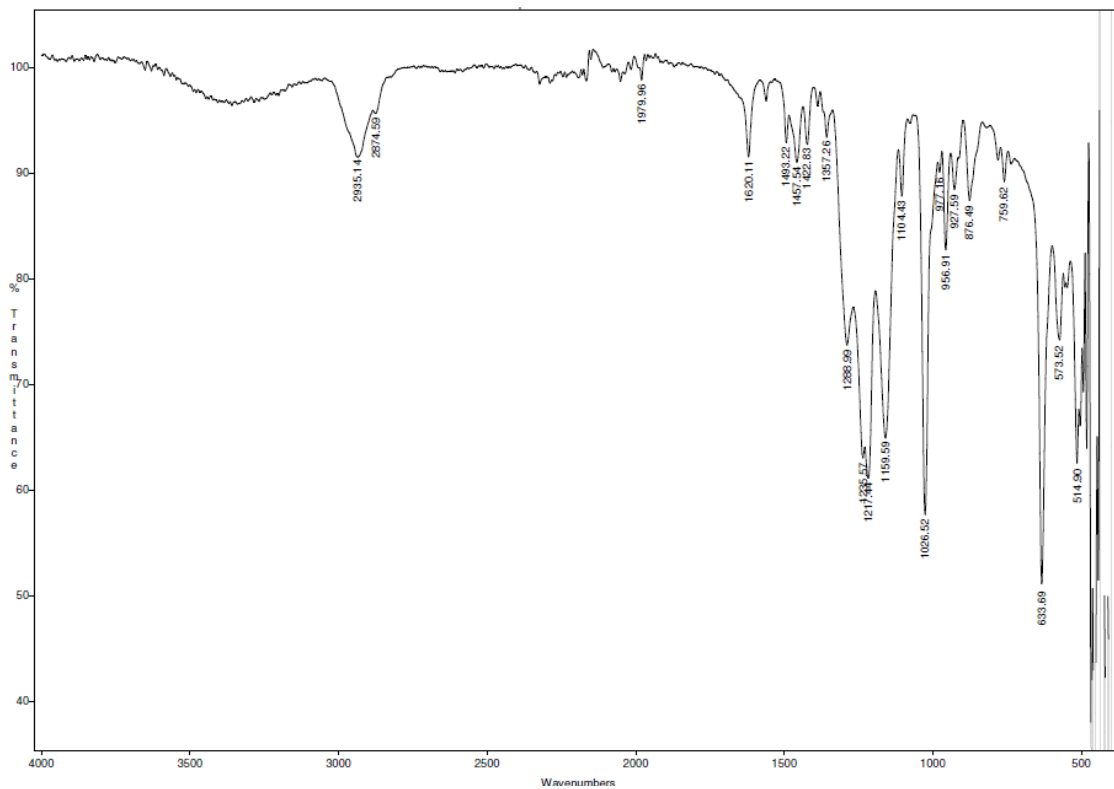


**CV**

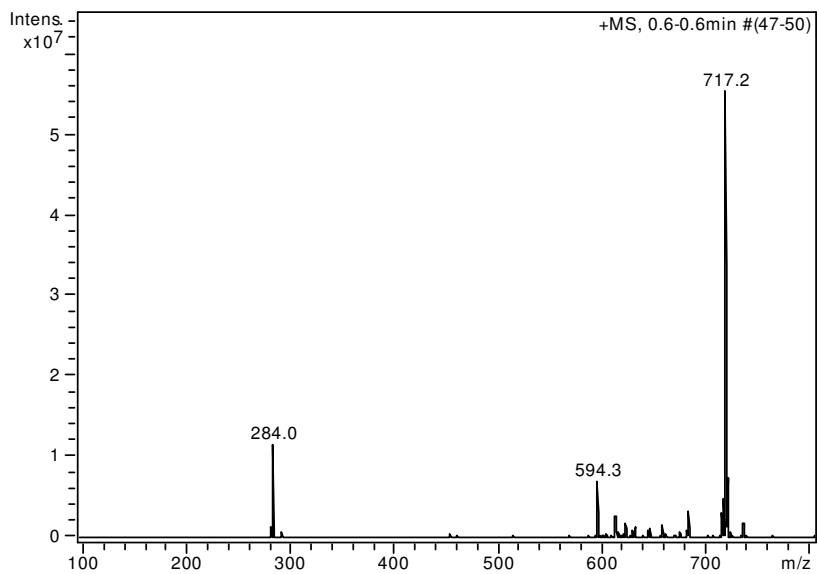


$\Delta$ -[Fe(CF<sub>3</sub>SO<sub>3</sub>)<sub>2</sub>(L3)], 3OTf

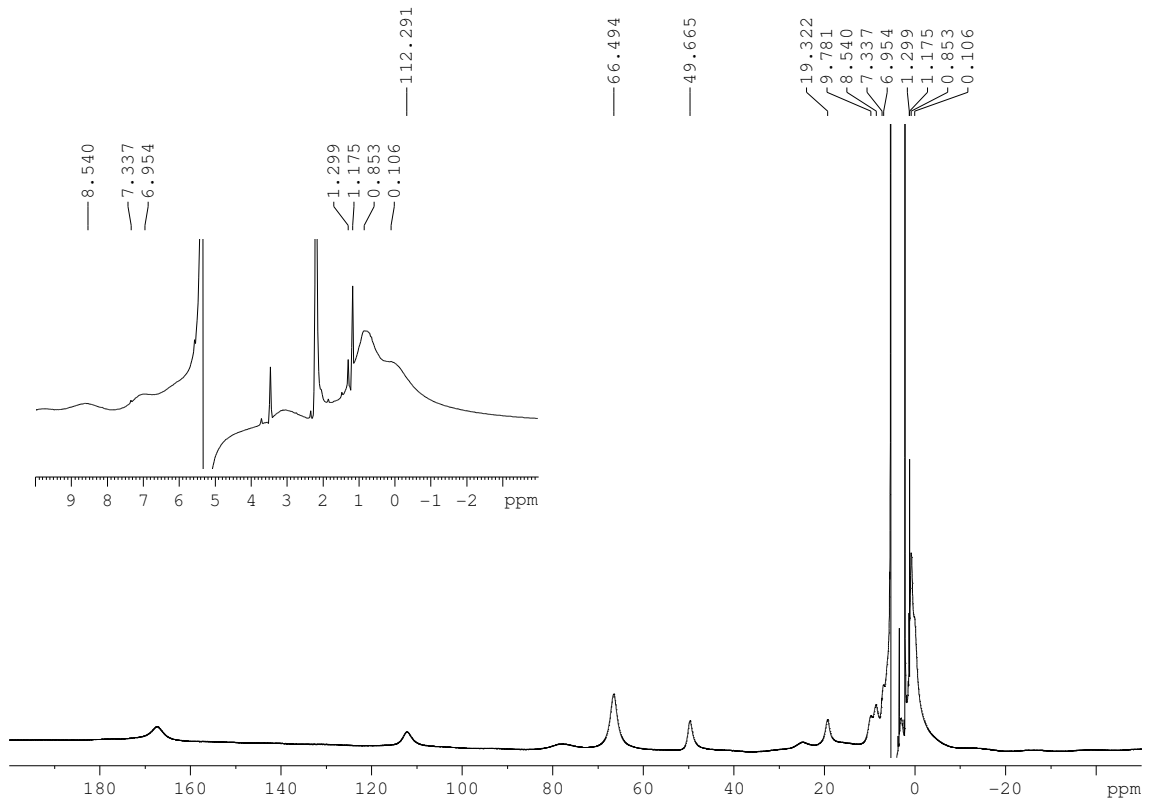
## FT-IR (ATR)



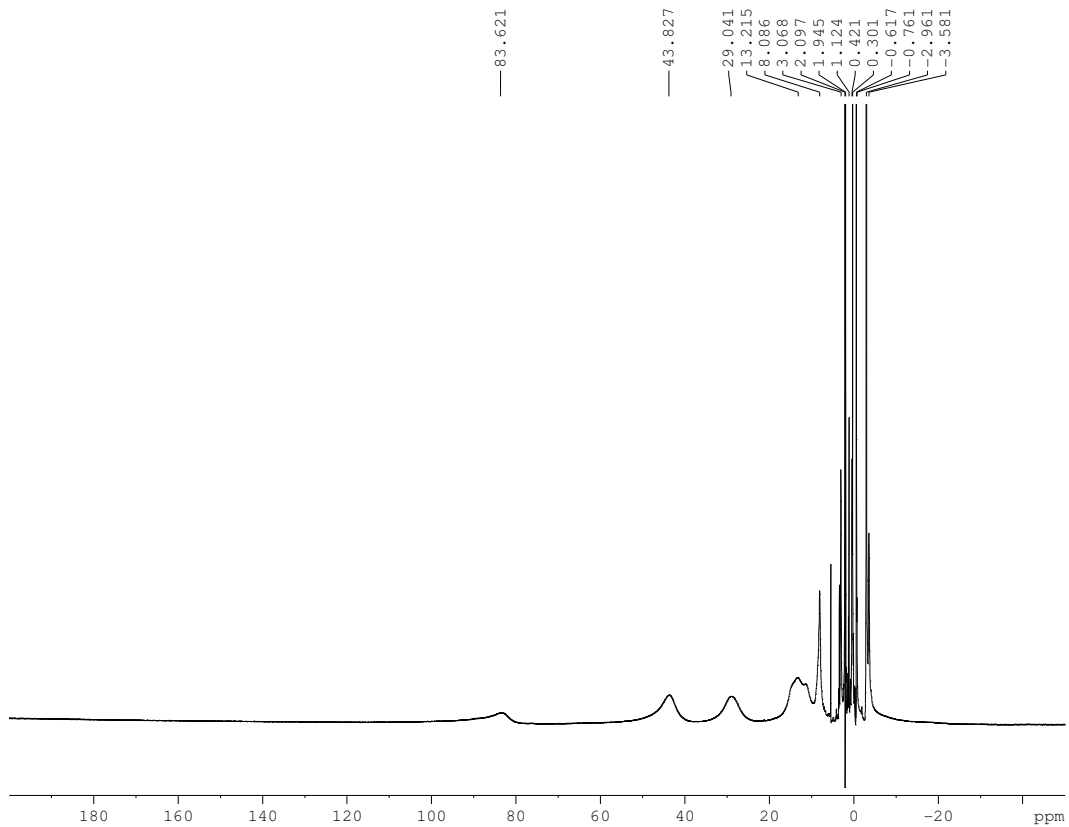
## ESI-MS



**$^1\text{H-NMR}$  ( $\text{CD}_2\text{Cl}_2$ , 400 MHz, 300K)**

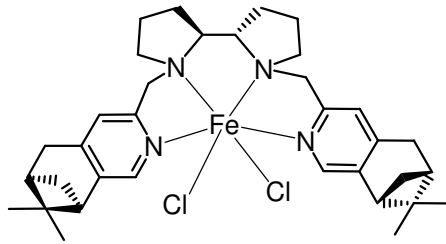


**$^1\text{H-NMR}$  ( $\text{CD}_3\text{CN}$ , 400 MHz, 300K)**

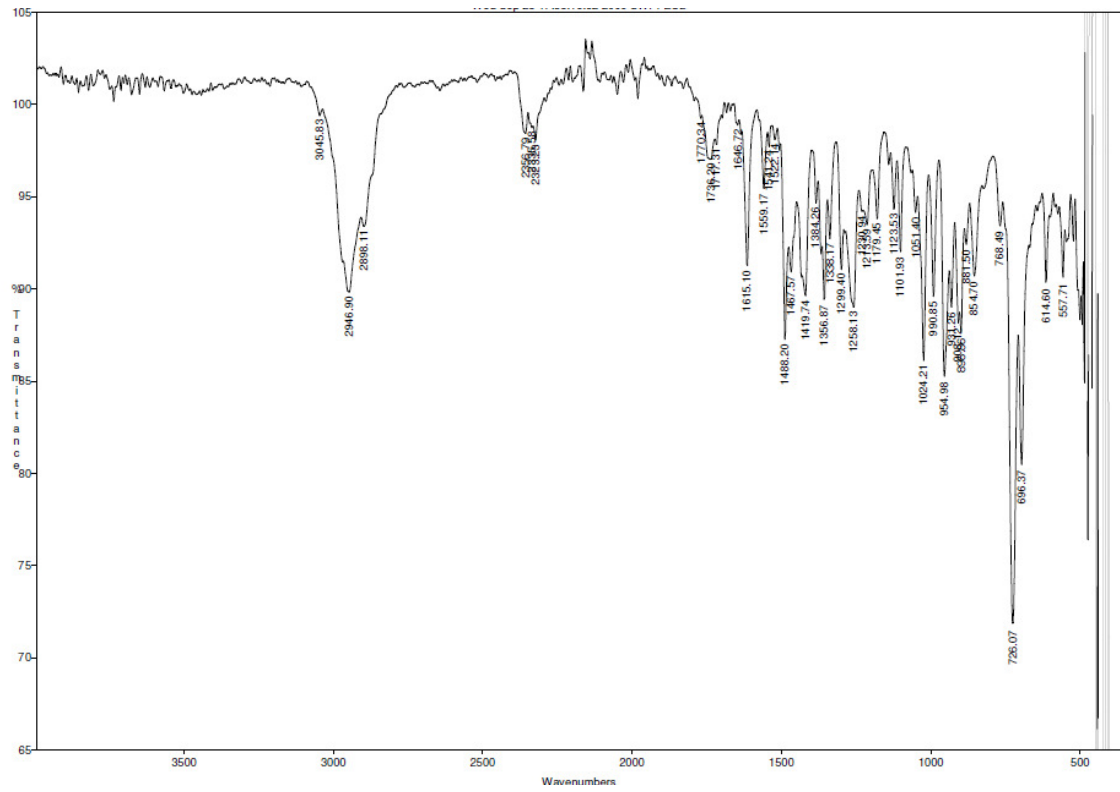




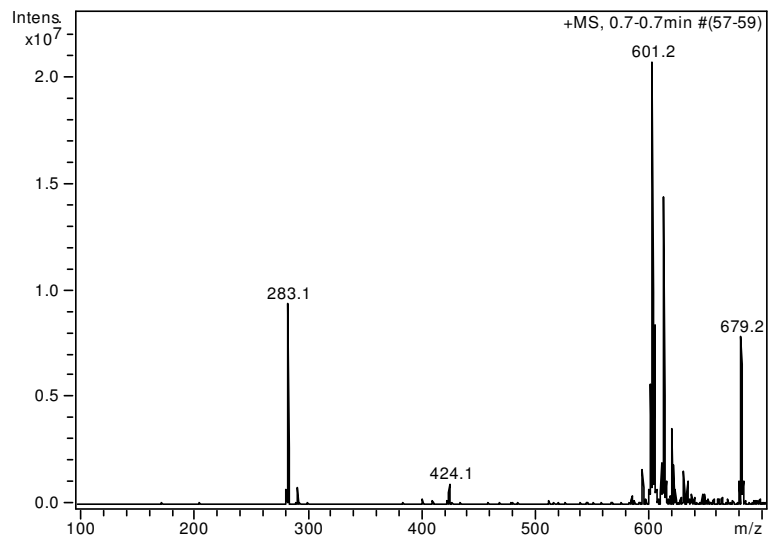
$\Lambda$ -[FeCl<sub>2</sub>(L4)], 4Cl



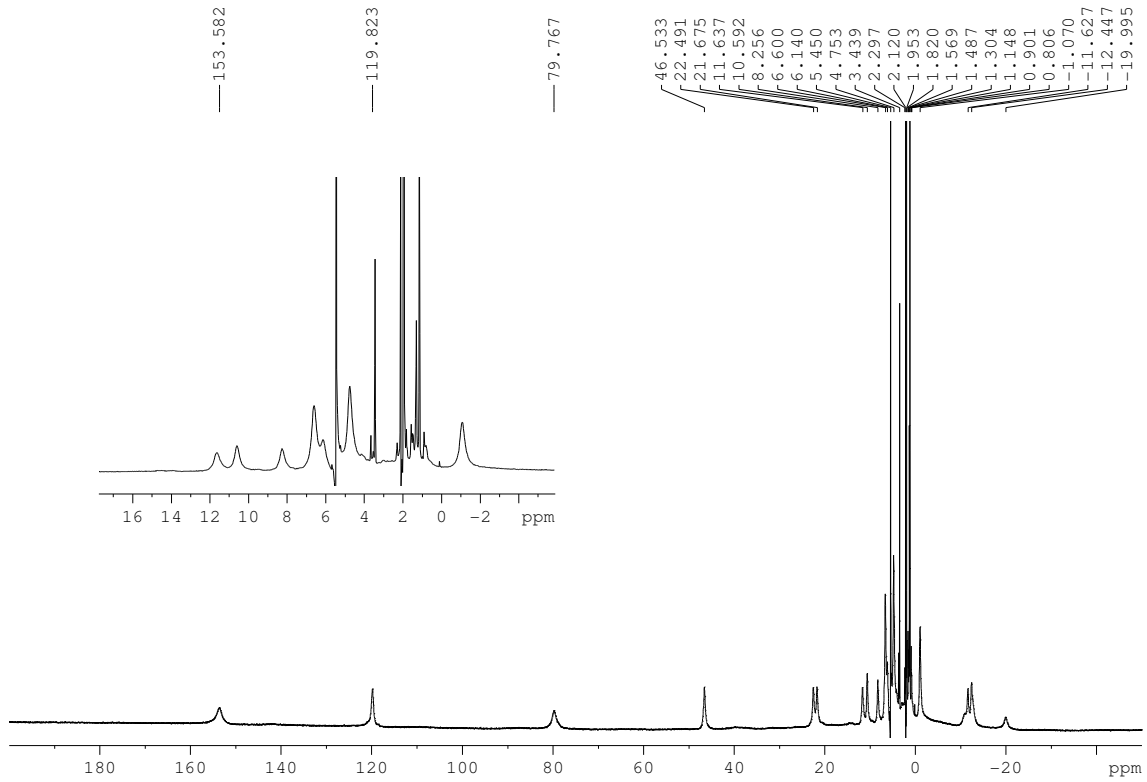
FT-IR (ATR)



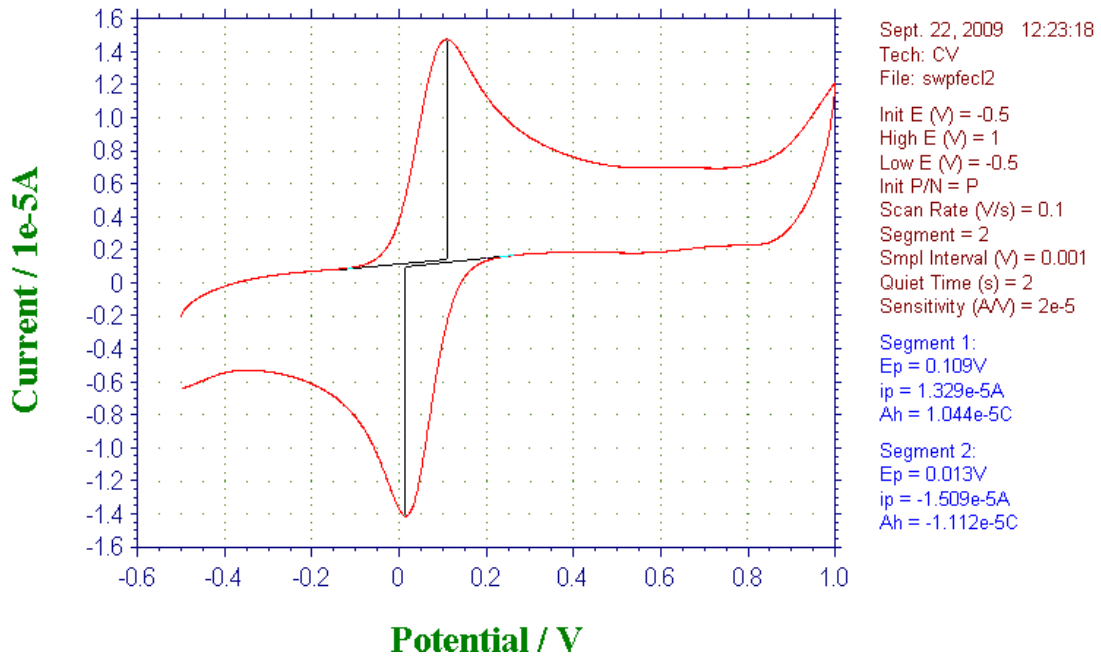
ESI-MS

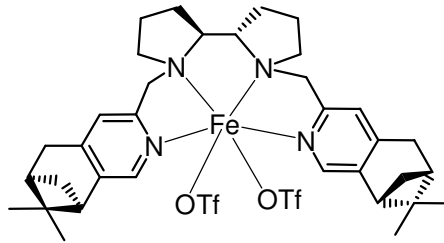


**<sup>1</sup>H-NMR (CD<sub>3</sub>CN, 400 MHz, 300K)**

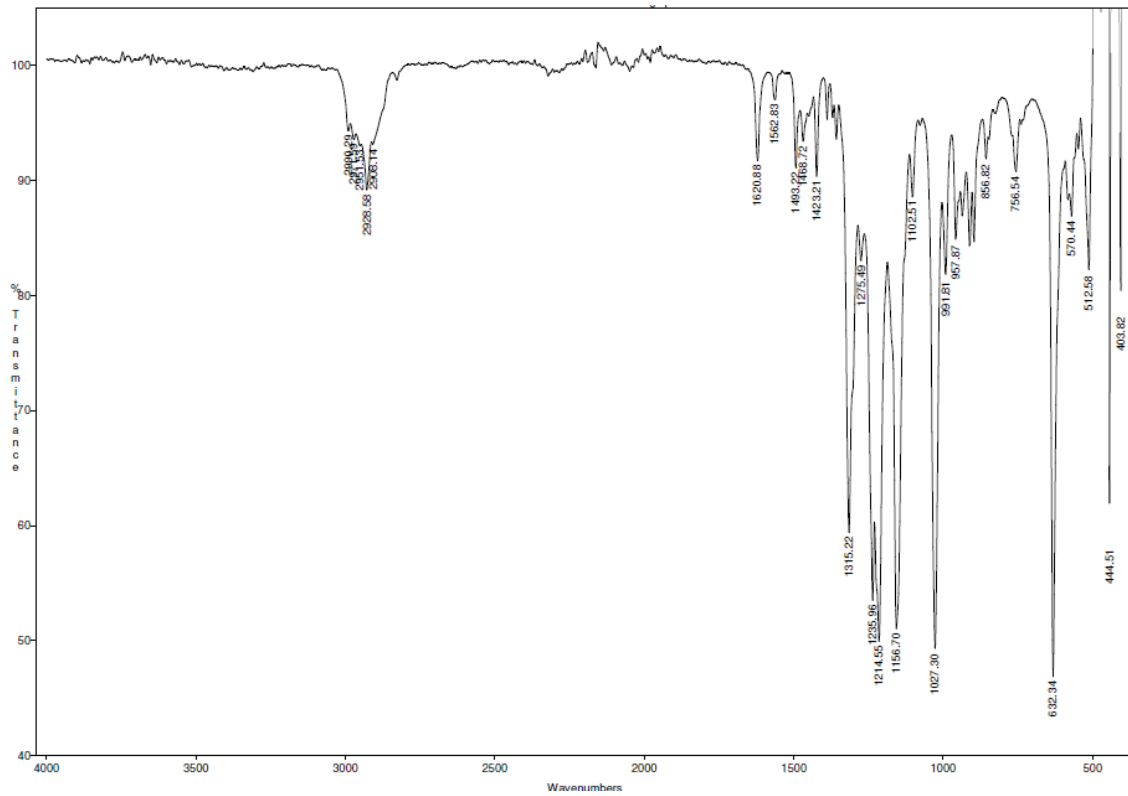


**CV**

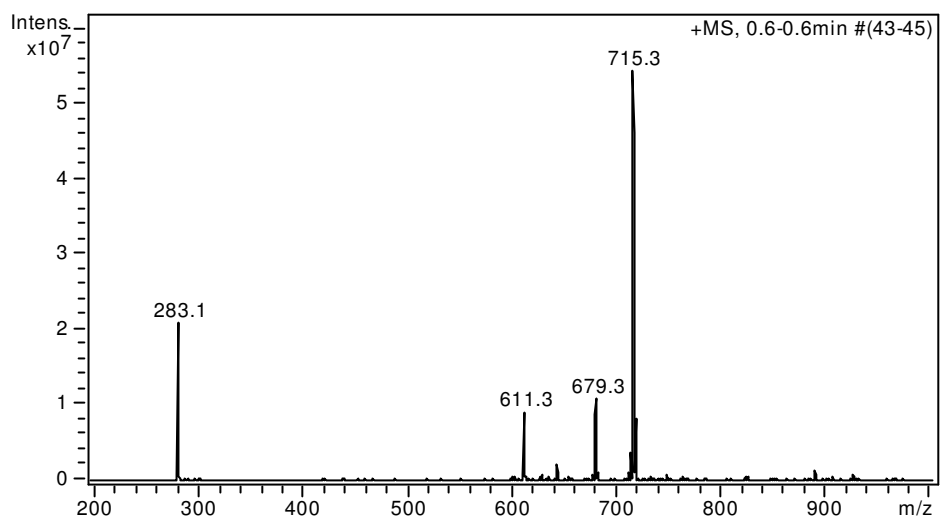


$\Lambda$ -[Fe(CF<sub>3</sub>SO<sub>3</sub>)<sub>2</sub>(L4)], 4OTf

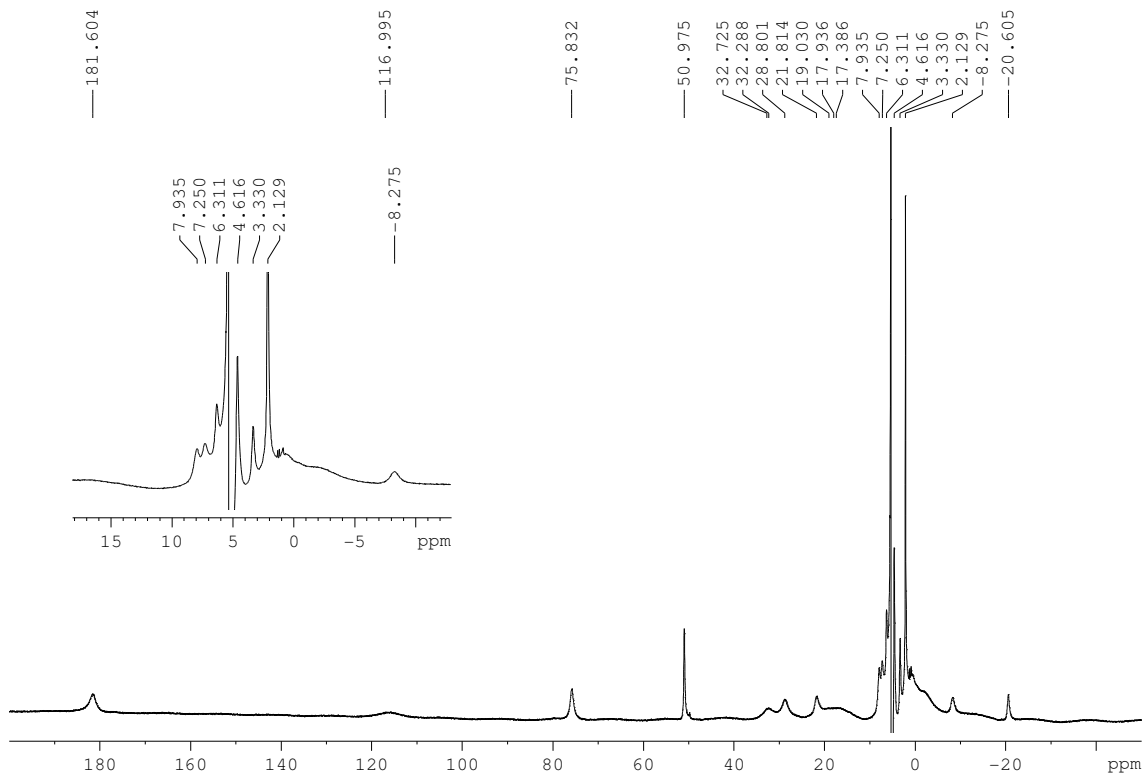
## FT-IR (ATR)



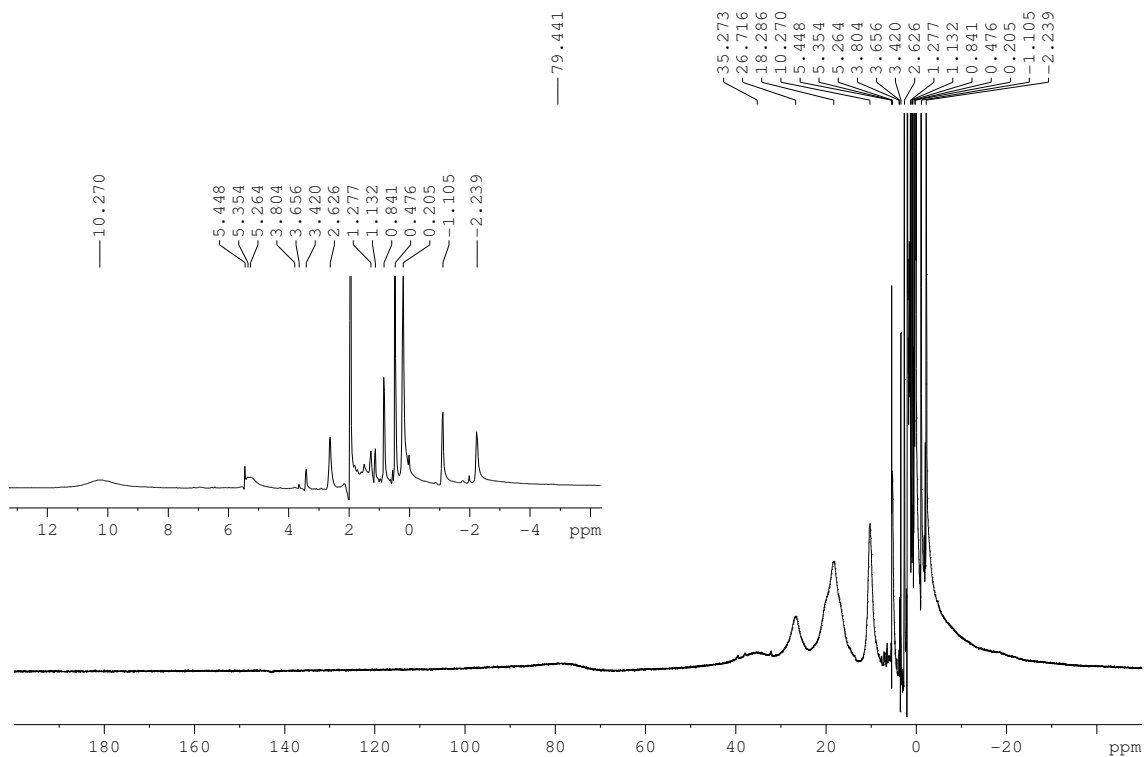
## ESI-MS

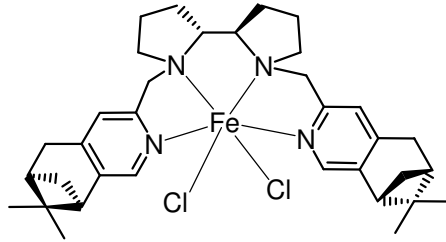


**$^1\text{H-NMR}$  ( $\text{CD}_2\text{Cl}_2$ , 400 MHz, 300K)**

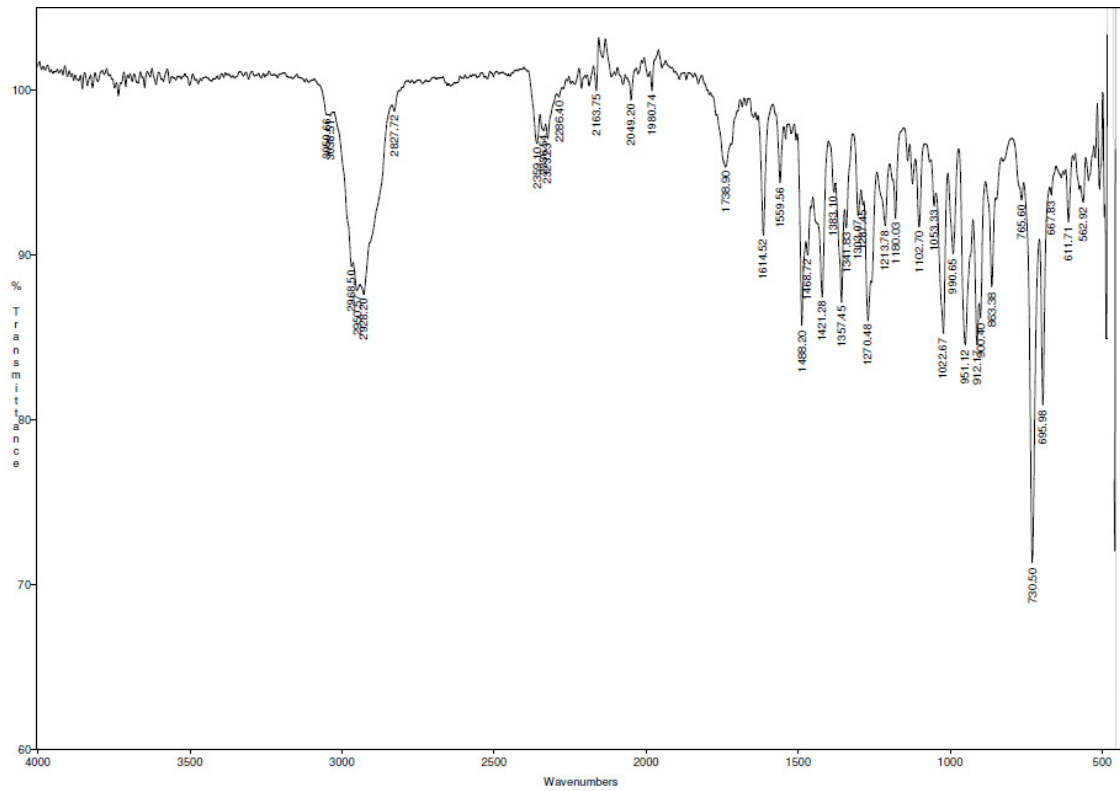


**$^1\text{H-NMR}$  ( $\text{CD}_3\text{CN}$ , 400 MHz, 300K)**

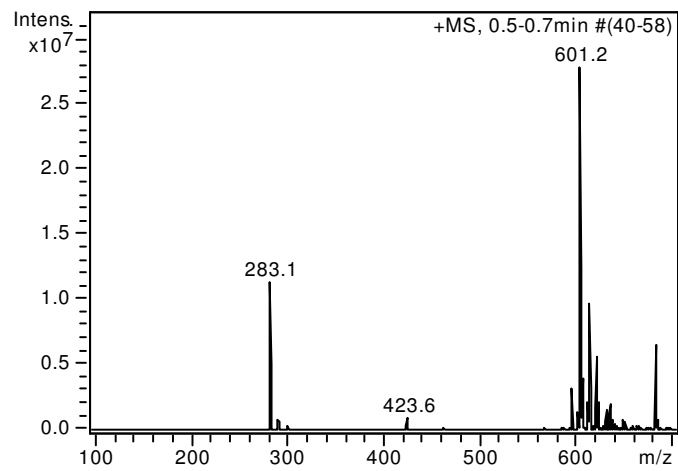


$\Delta$ -[FeCl<sub>2</sub>(L5)], 5Cl

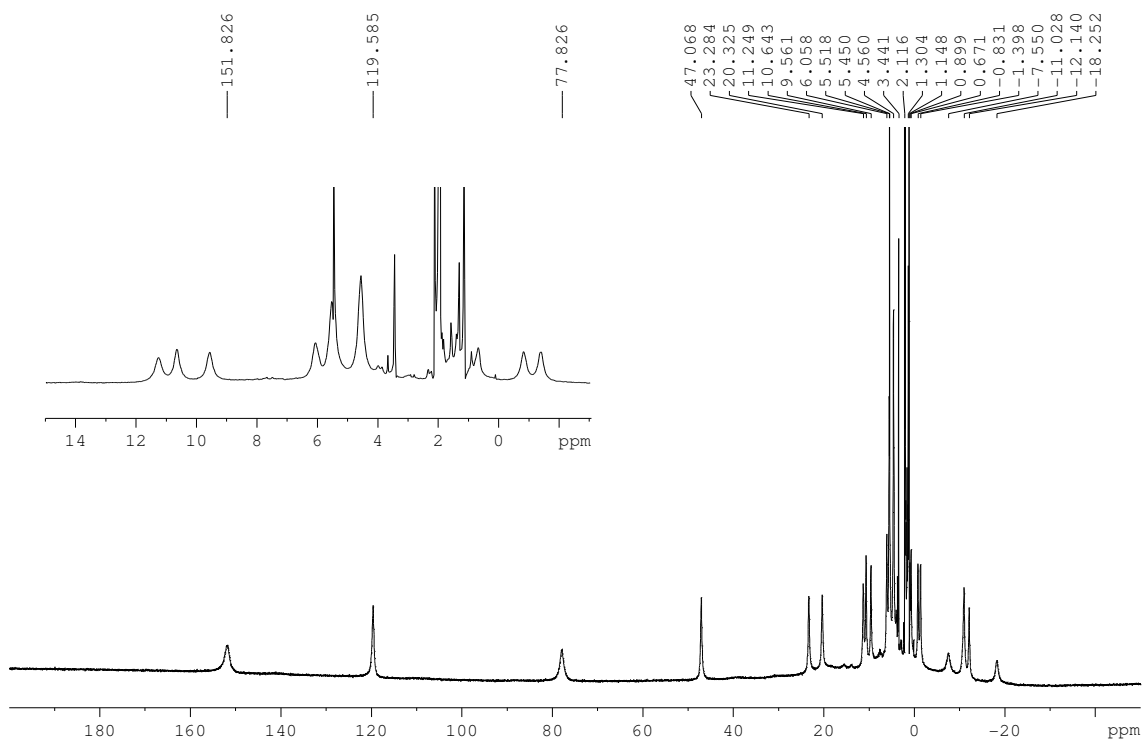
## FT-IR (ATR)



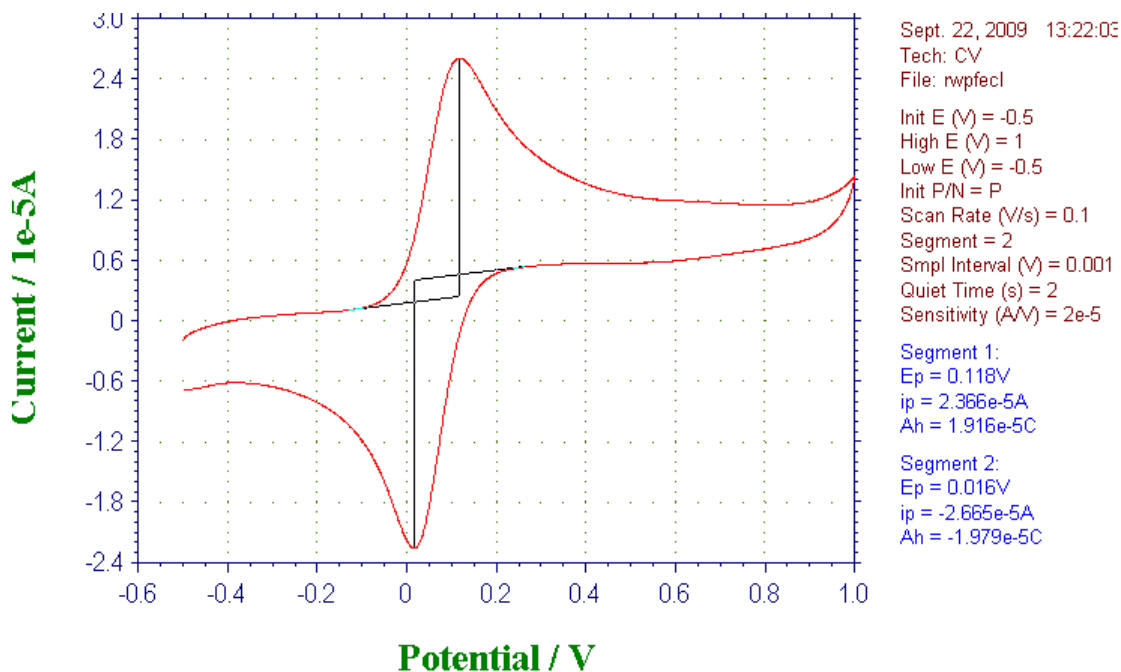
## ESI-MS

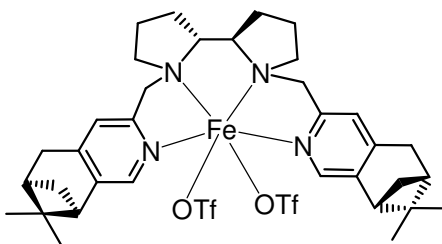


**<sup>1</sup>H-NMR (CD<sub>3</sub>CN, 400 MHz, 300K)**

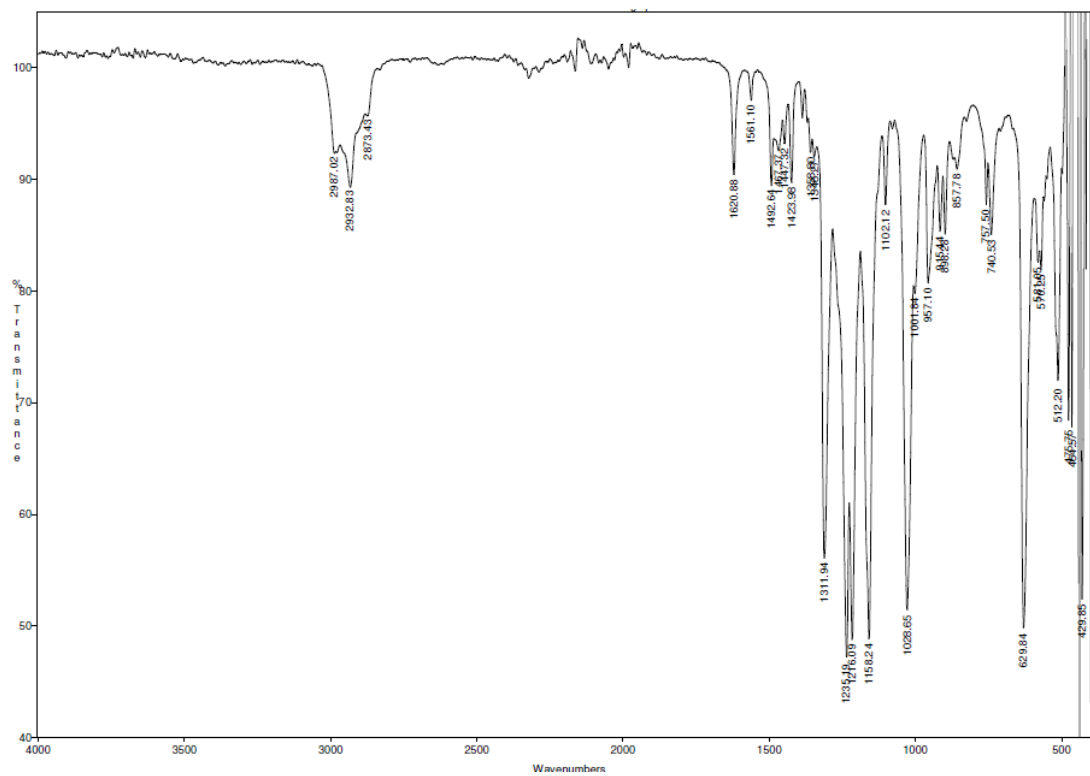


**CV**

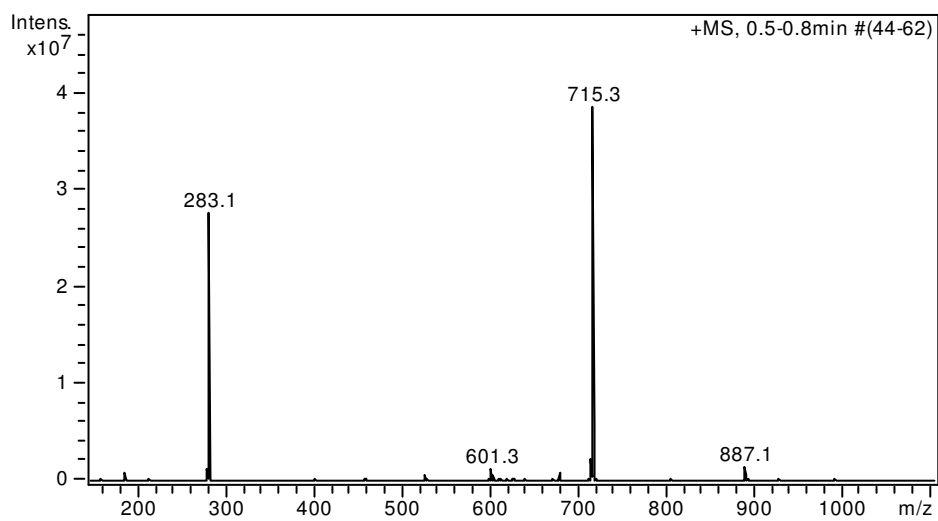


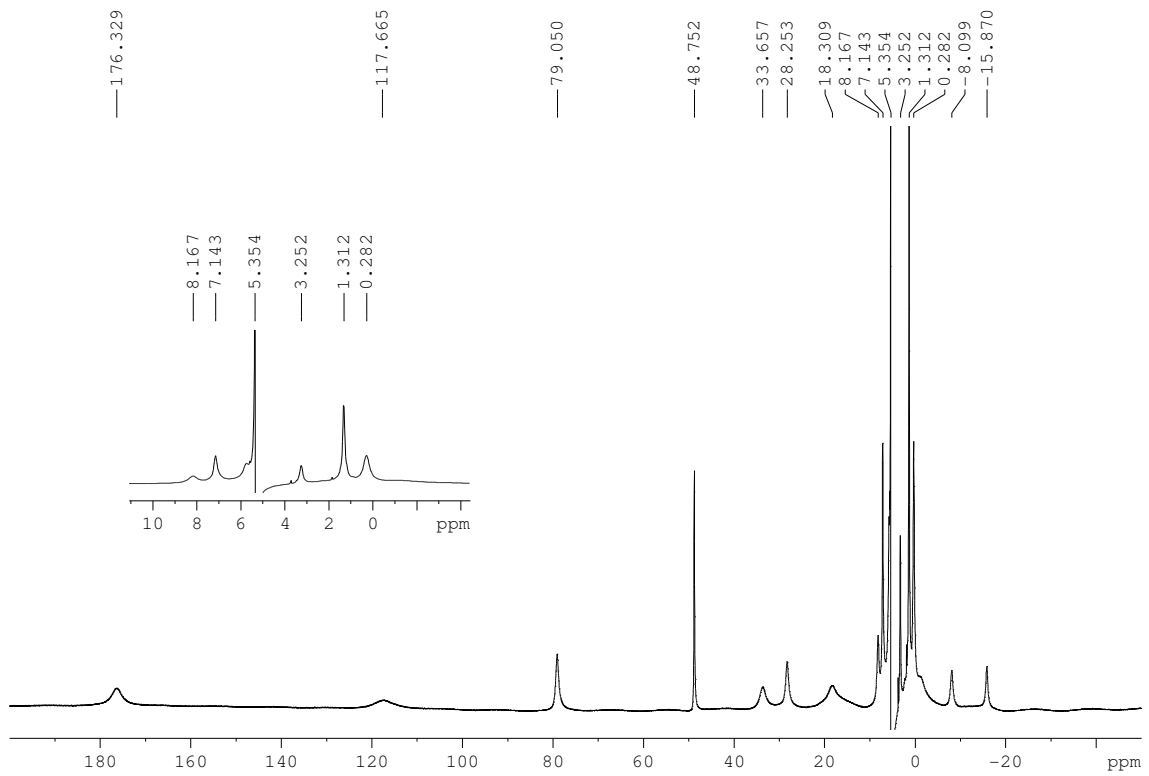
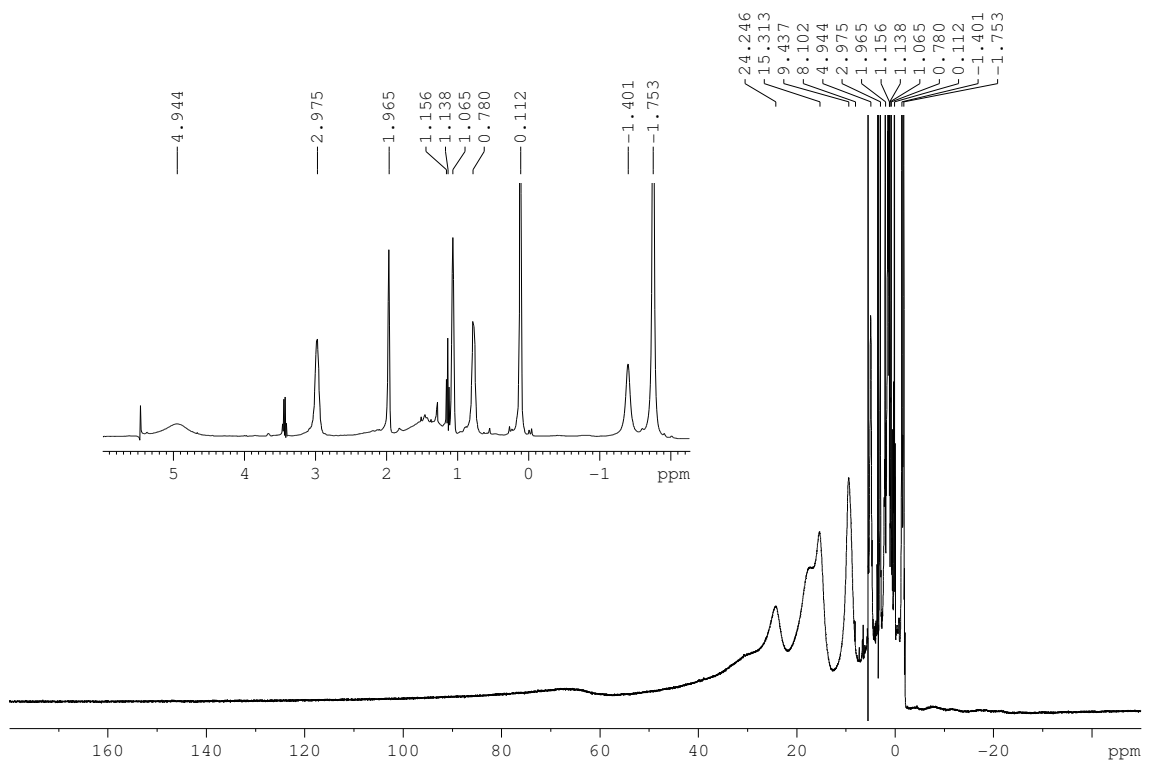
$\Delta$ -[Fe(CF<sub>3</sub>SO<sub>3</sub>)<sub>2</sub>(L5)], 5OTf

## FT-IR (ATR)

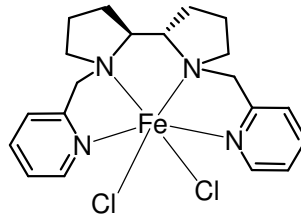
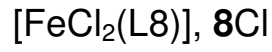
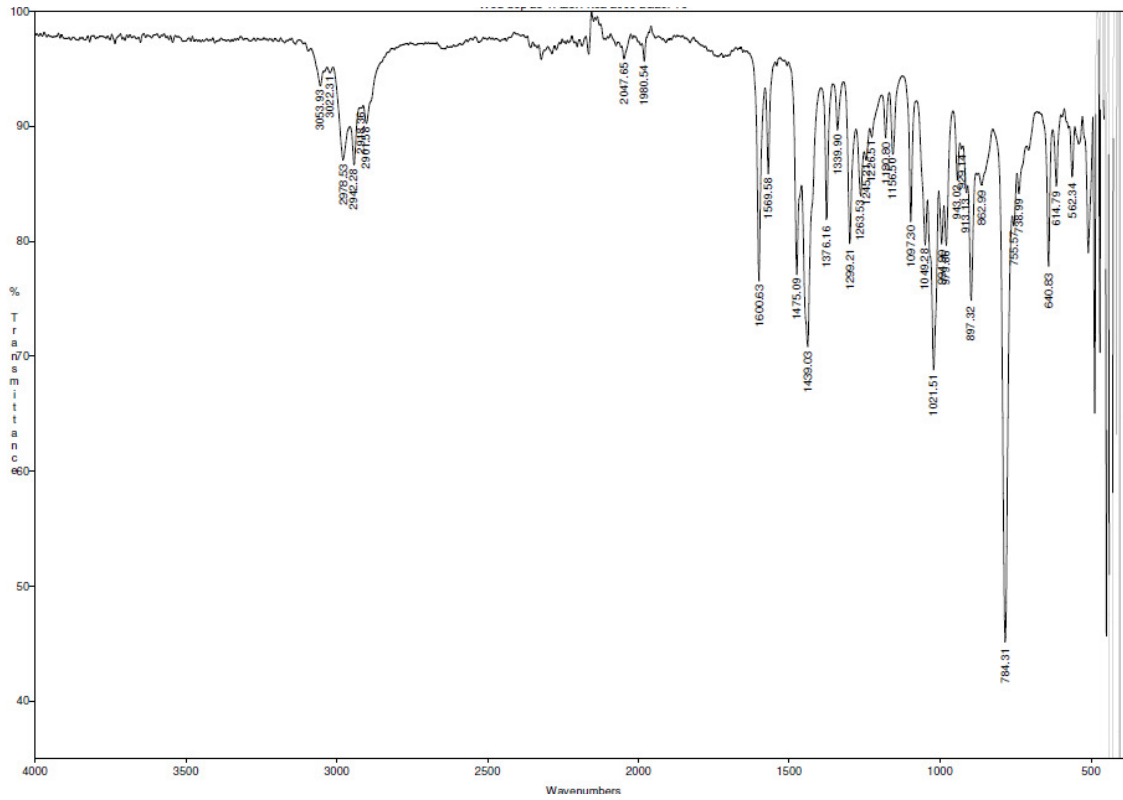
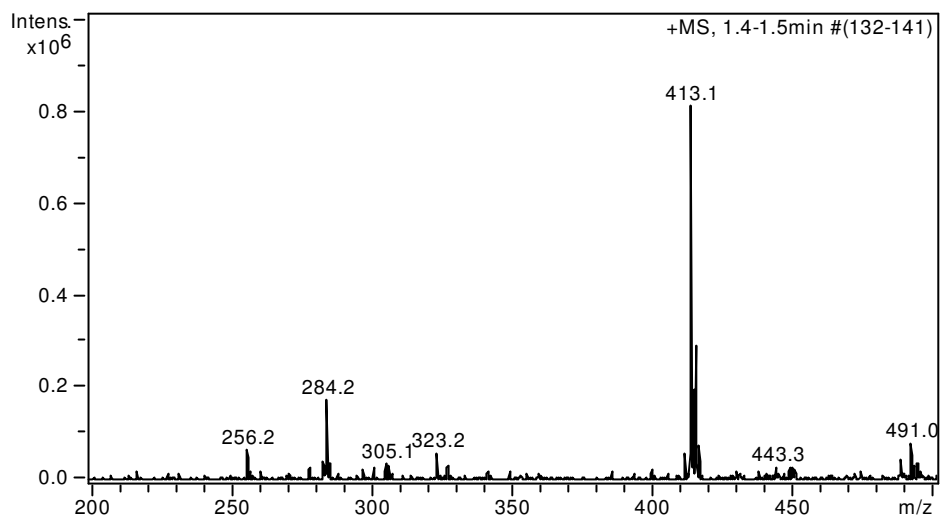


## ESI-MS

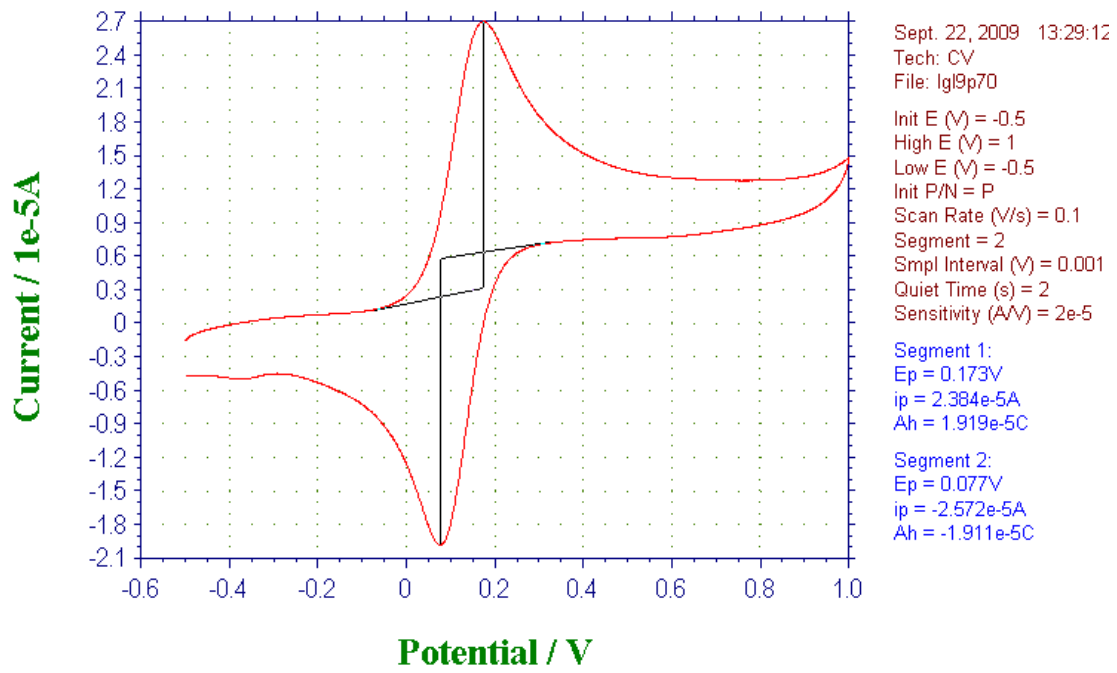


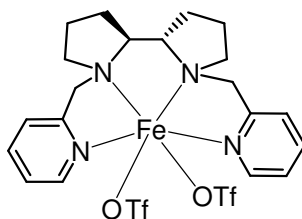
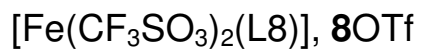
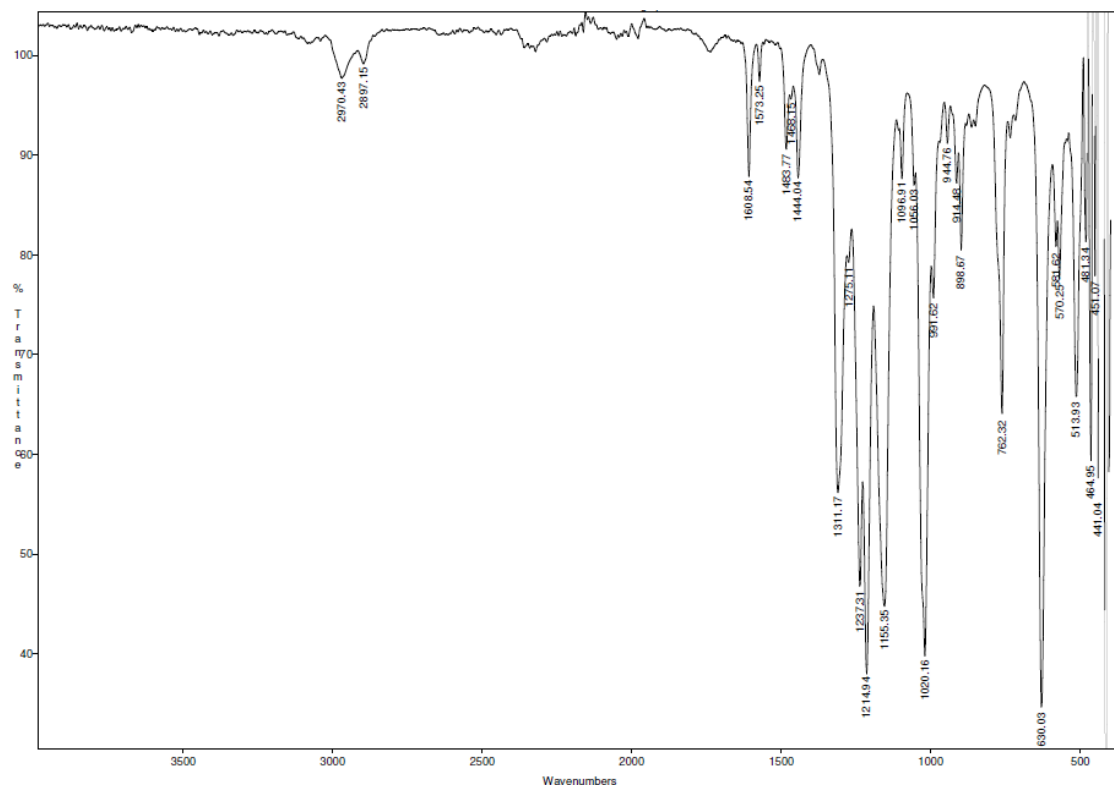
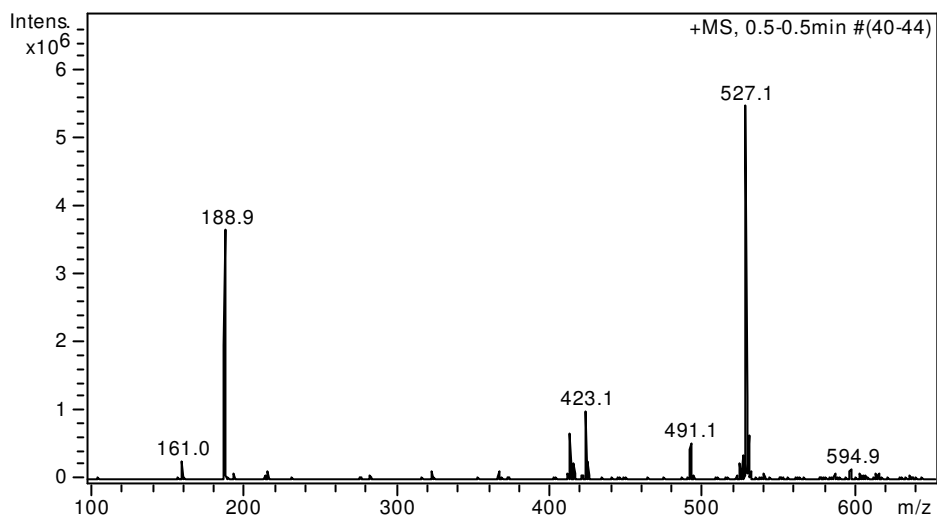
**$^1\text{H-NMR}$  ( $\text{CD}_2\text{Cl}_2$ , 400 MHz, 300K)** **$^1\text{H-NMR}$  ( $\text{CD}_3\text{CN}$ , 400 MHz, 300K)**



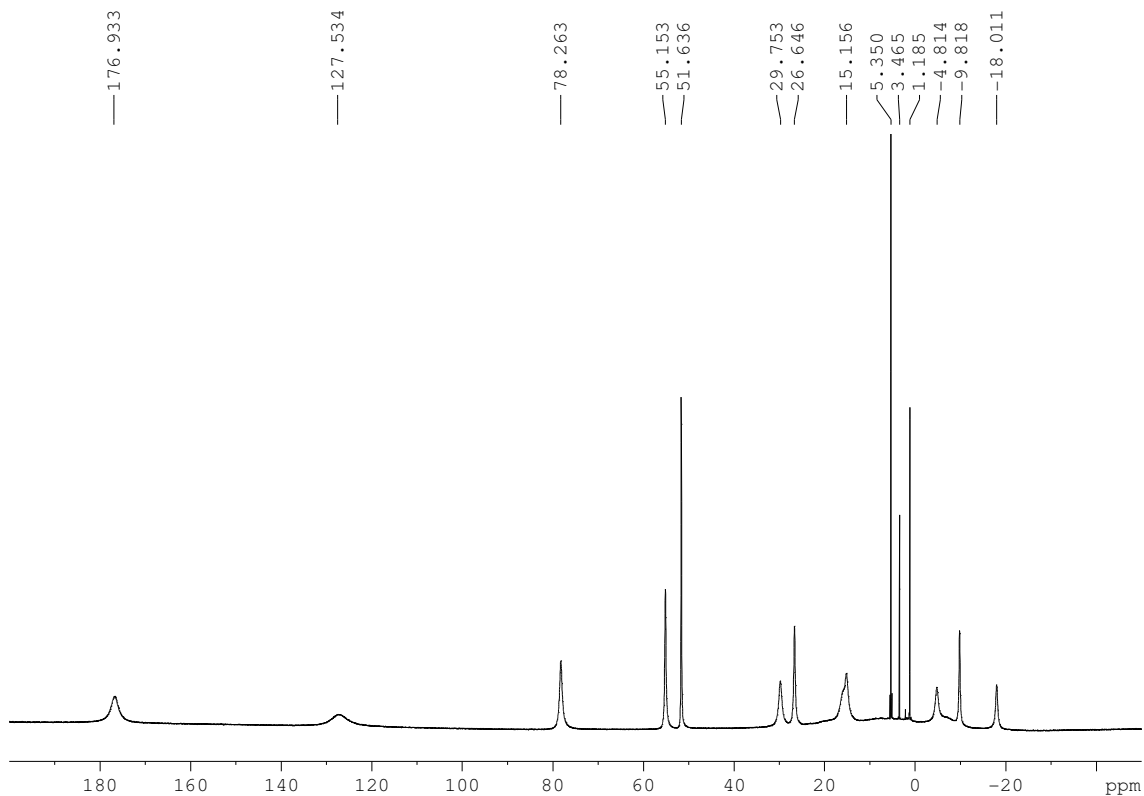
**FT-IR (ATR)****ESI-MS**

CV

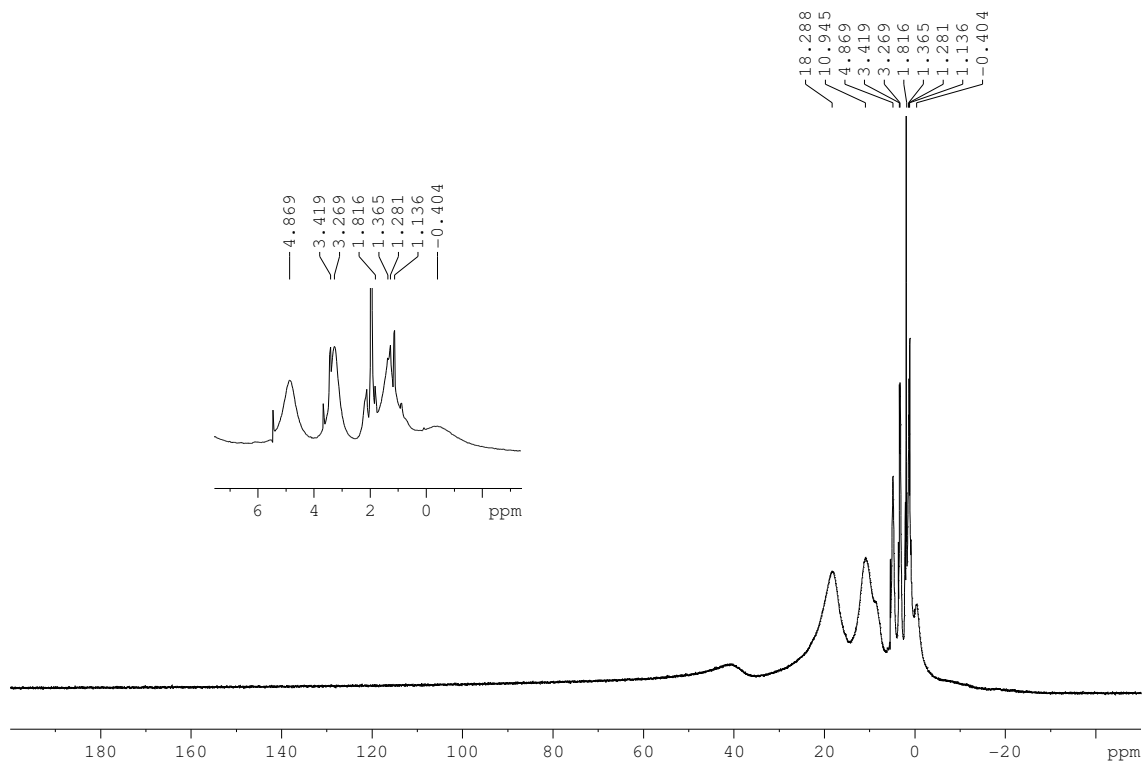


**FT-IR (ATR)****ESI-MS**

**$^1\text{H-NMR}$  ( $\text{CD}_2\text{Cl}_2$ , 400 MHz, 300K)**



**$^1\text{H-NMR}$  ( $\text{CD}_3\text{CN}$ , 400 MHz, 300K)**

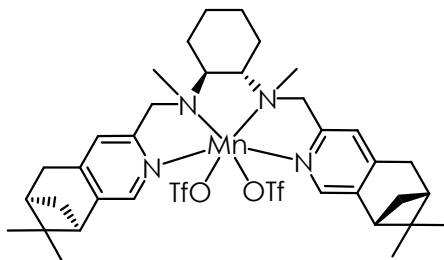


---

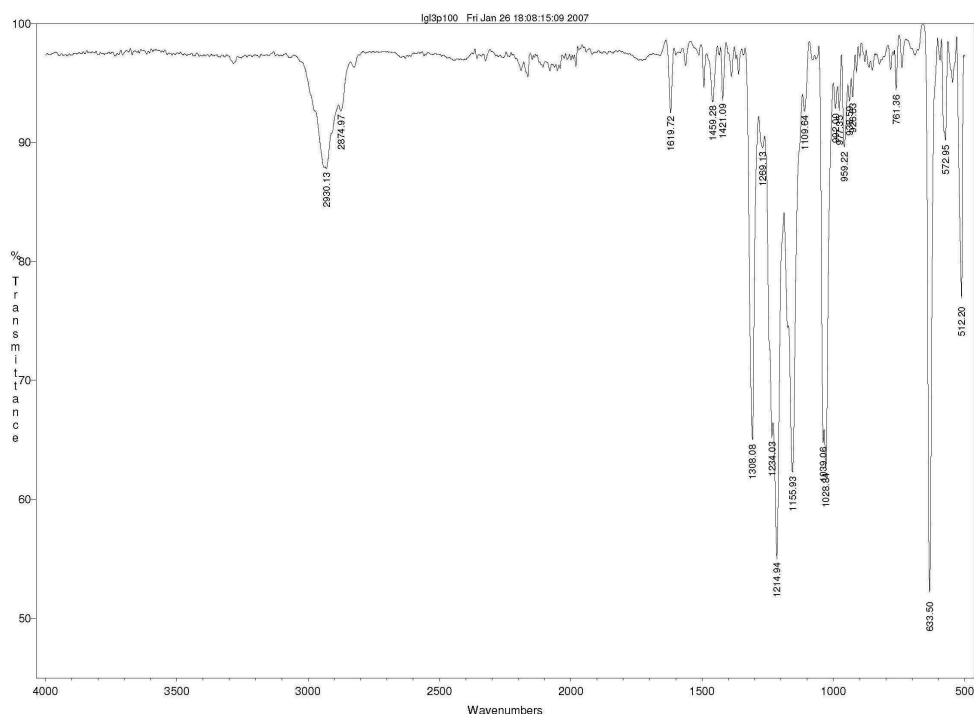
## **Annex.2 – Chapter IV**

---

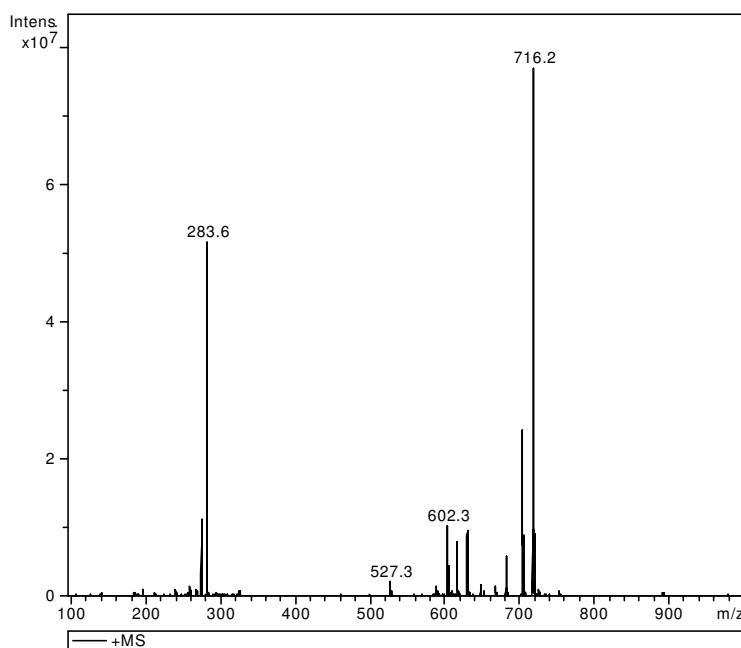


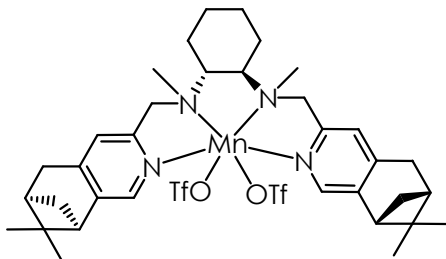
$\Lambda$ -[Mn(CF<sub>3</sub>SO<sub>3</sub>)<sub>2</sub>(L2)],  $\Lambda$ -2Mn

## FT-IR (ATR)

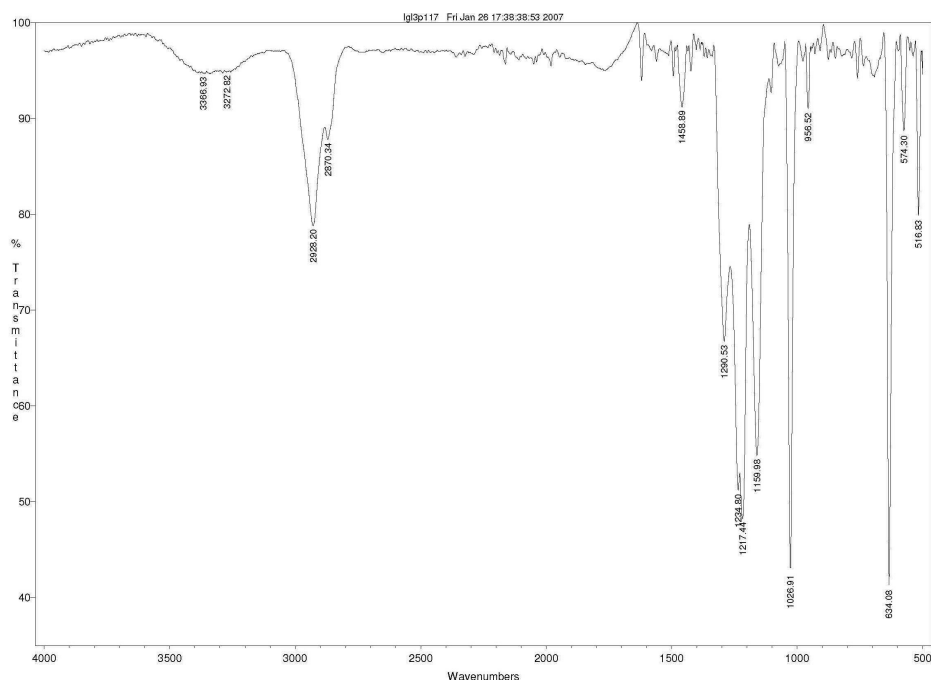


## ESI-MS

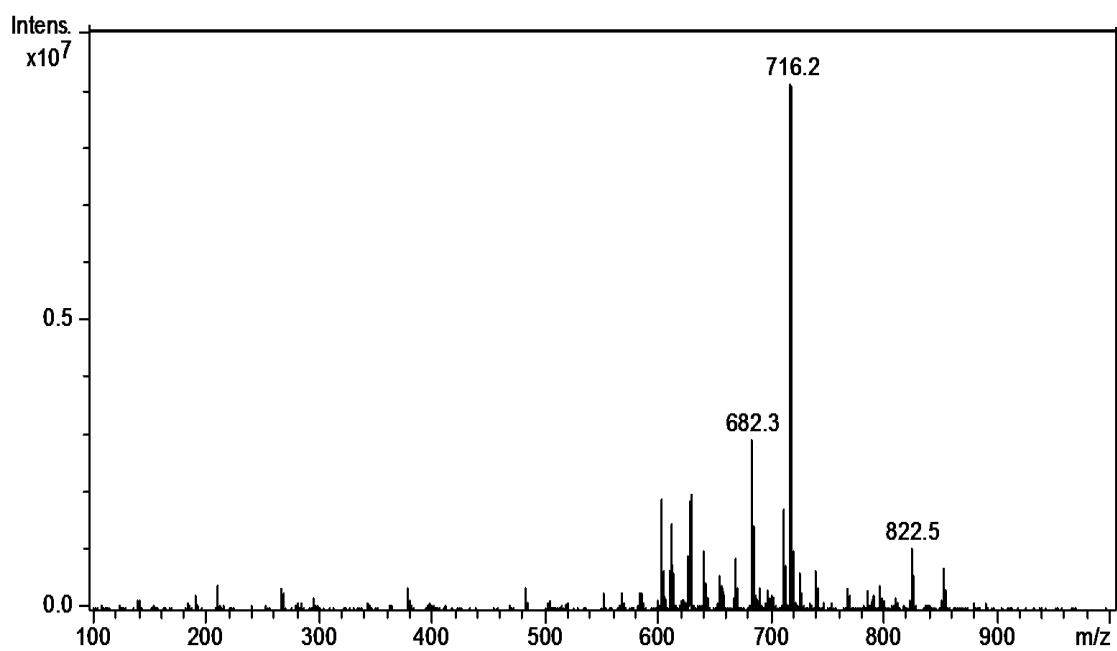


$\Delta$ -[Mn(CF<sub>3</sub>SO<sub>3</sub>)<sub>2</sub>(L3)],  $\Delta$ -3Mn

## FT-IR (ATR)



## ESI-MS



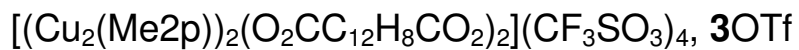


---

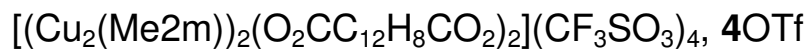
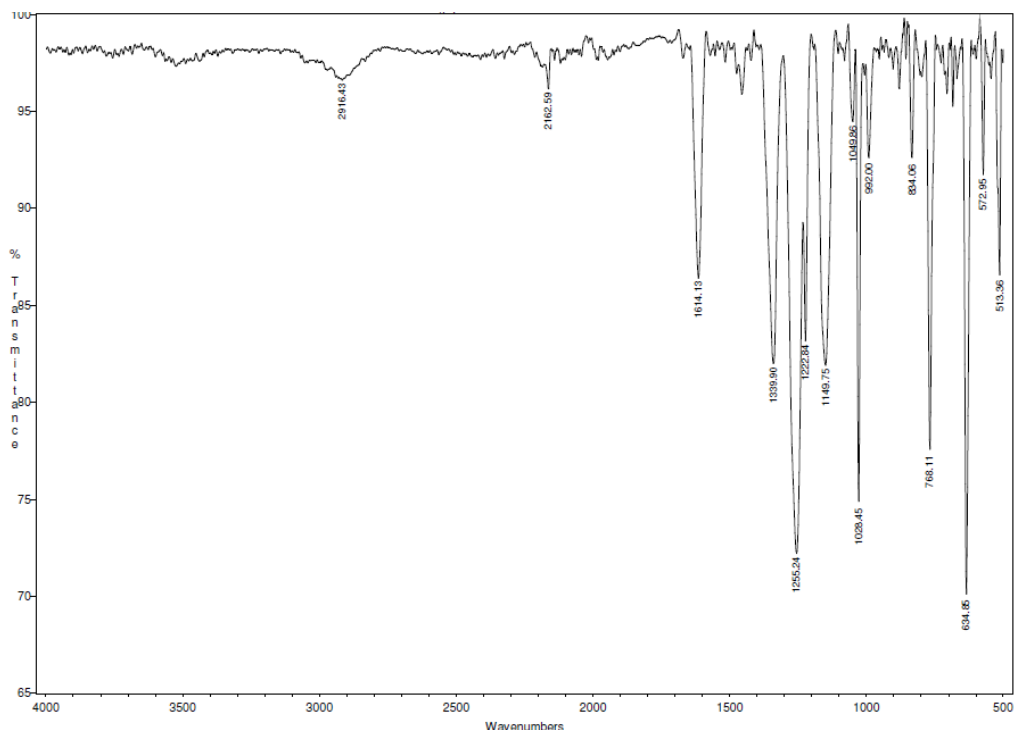
## **Annex.3 – Chapter V**

---

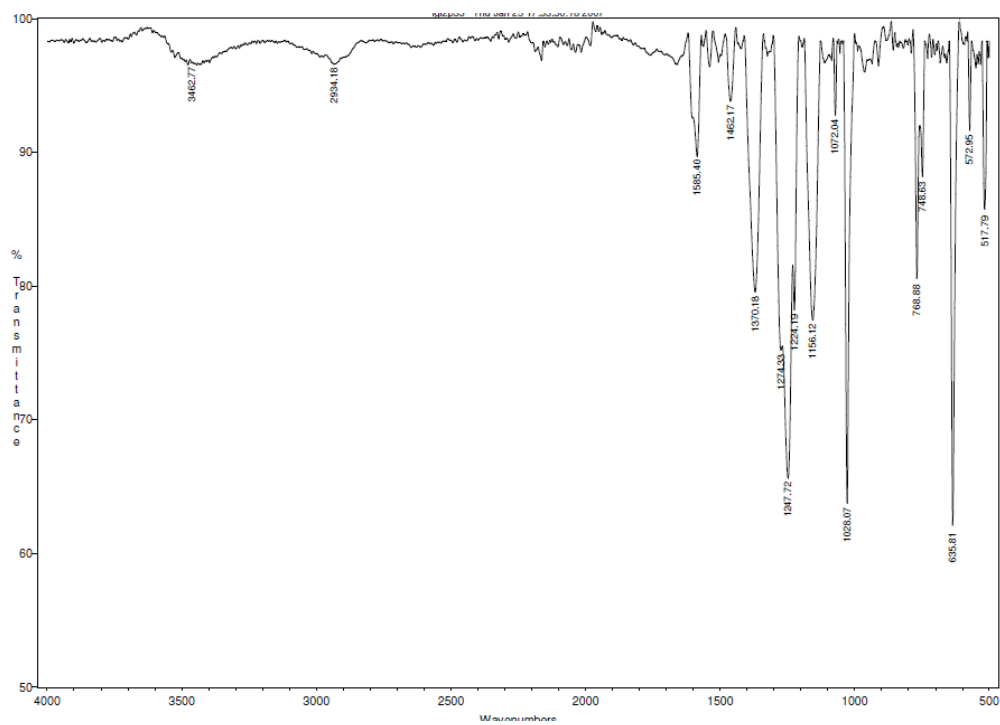


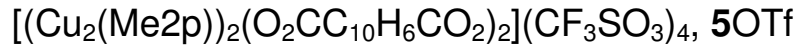


FT-IR (ATR)

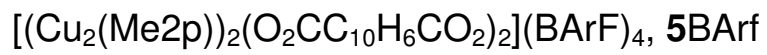
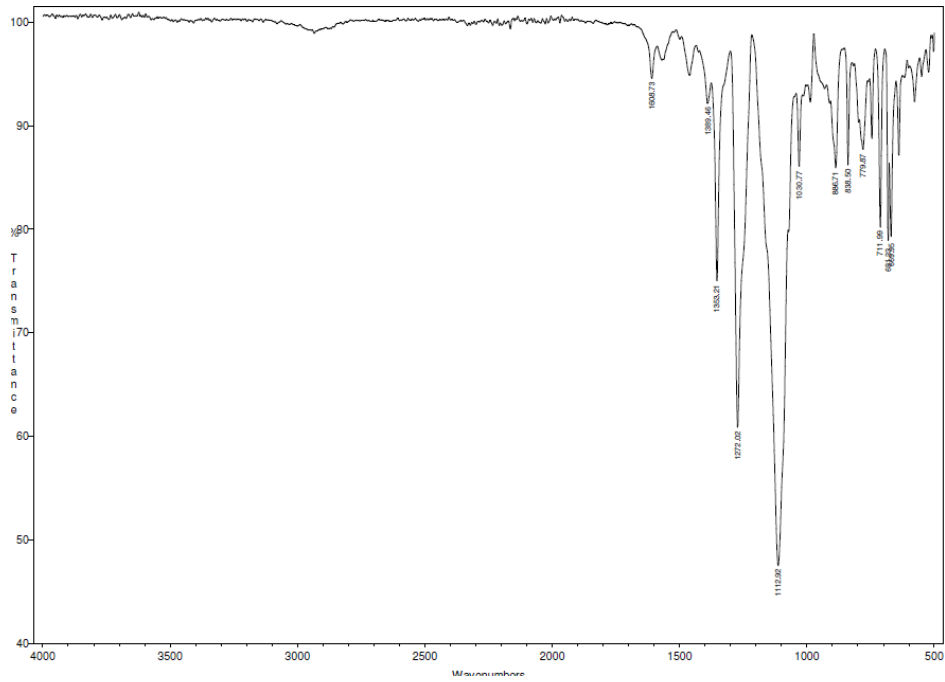


FT-IR (ATR)

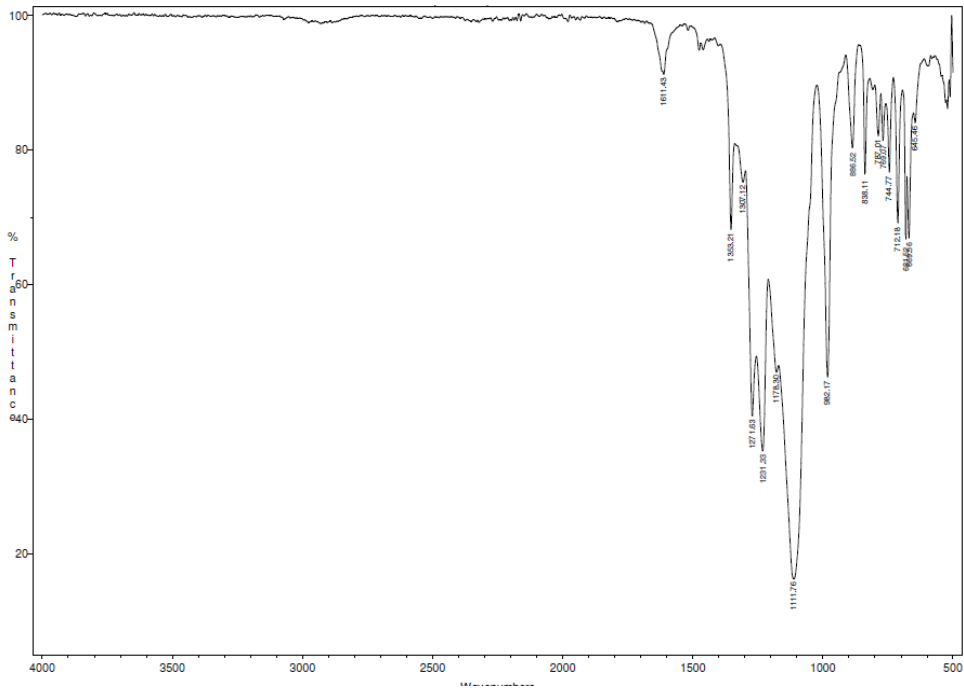


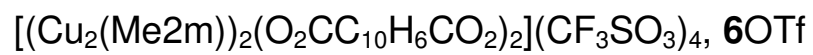
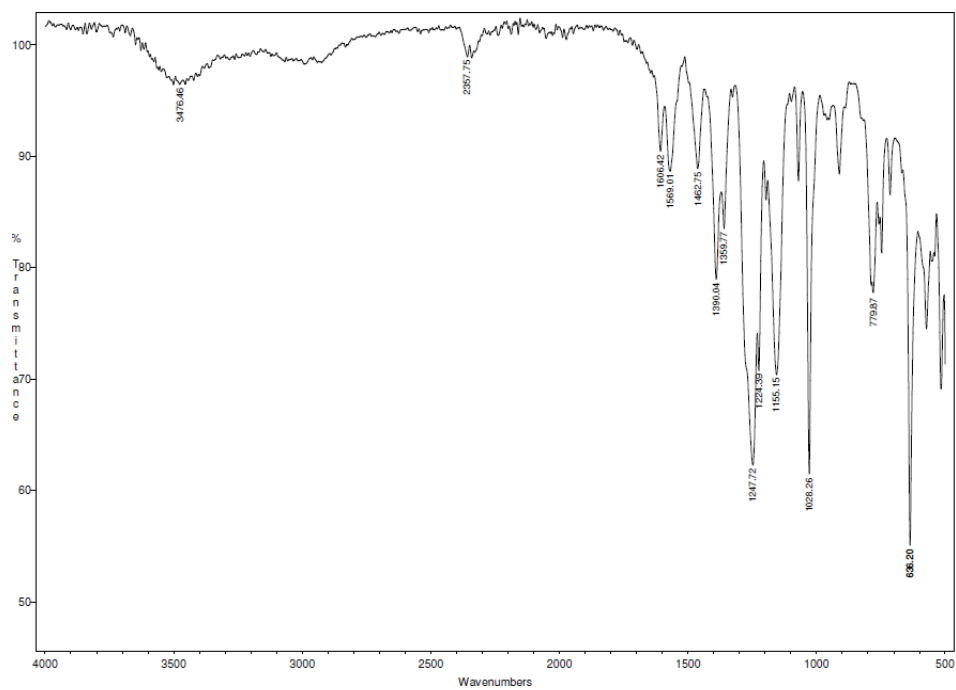


**FT-IR (ATR)**



**FT-IR (ATR)**



**FT-IR (ATR)**



---

## **Annex.4 – Chapter VI**

---





**FT-IR (ATR)**